NASA TM X-58075

NASA TECHNICAL MEMORANDUM

THE GEMINI PROGRAM

PHYSICAL SCIENCES EXPERIMENTS SUMMARY

Compiled by Edward O. Zeitler and Thomas G. Rogers
Manned Spacecraft Center
Houston, Texas 77058

September 1971

NATIONAL AERONAUTICS AND SPACE ADMINISTRATION

THE GEMINI PROGRAM

PHYSICAL SCIENCES EXPERIMENTS SUMMARY

Compiled by
Edward O. Zeitler
Manned Spacecraft Center
and
Thomas G. Rogers
ITT Federal Electric Corporation
Houston, Texas 77058
September 1971

FOREWORD

The Gemini Program Experiments Summaries are a compilation of the experiments that were performed on the Gemini III to XII missions. These results have been amended and annotated to include updated information. Therefore, this summary is not just a rewrite of the original information. The summaries are arranged according to experiment, rather than according to mission.

Fundamentally, two major divisions have been established: biomedical sciences experiments and physical sciences experiments. Within these major divisions, several subdivisions have been established, and, within these subdivisions, the individual experiments have been arranged in an order that emphasizes the interrelationships of many of the experiments. No rank of importance is expressed or implied by the sequence of the experiments.

Just as the Gemini Program was amplified by the knowledge and techniques that were developed during Project Mercury, the Apollo Program is being augmented by the achievements that were made during the Gemini Program. It is hoped that this document results in an augmented awareness of the tremendous importance of the Gemini Program Experiments and the effect of these experiments on the manned space-flight program.

THE GEMINI PROGRAM EXPERIMENTS

By Robert O. Piland* and Paul R. Penrod*

INTRODUCTION

During Project Mercury, it was proven that man can function as a pilot-engineer-experimenter for as many as 34 hours in weightless flight. Therefore, it was a primary objective of the Gemini Program to explore the capabilities of man in situations of longer duration and more complex missions. The proven effectiveness of man as a scientific observer in orbital flight was supported by the capabilities of the Gemini spacecraft with respect to scientific-equipment accommodation, fuel budget, attitude-control system, and habitability for extended missions. All of these factors, in context with the planned mission profiles, afforded an unprecedented opportunity for the performance of a comprehensive program of inflight experiments. Therefore, from the beginning of the Gemini Program, there was a parallel and concerted effort by NASA to support the generation of suitable experiments from all sources. Among others, these sources included educational institutions, U.S. Government agencies, NASA field centers, the Department of Defense, and industrial laboratories. Experiments of significance to the life sciences and the physical sciences were developed.

It is apparent that the concentration of experiments has been on the long-duration missions. This was done because of the inherent influence of time, which facilitates a larger data yield for time-sensitive parameters, repetitious contacts with selected subjects, and increased potential for objects of opportunity. However, the increased crew time that was available for the operation of equipment and participation in experimental protocol was of great significance. Also, it should be emphasized that planning on a programwide basis permitted the scheduling of experiments on multiple flights if these additional data points (with the associated continuity in time and procedures) were significant. Finally, more ambitious mission objectives (such as crewmember extravehicular activities and rendezvous and docking) facilitated the programing of experiments that extended beyond the confines of a single spacecraft, and even beyond the limitations of a single mission.

*NASA Manned Spacecraft Center, Houston, Texas.

PROCEDURES

To take most effective advantage of the capabilities that have been described, the following procedures were used. Experiment proposals were evaluated by NASA personnel within the framework of the following major considerations.

1. Life-science or physical-science merit
2. Effect on flight safety
3. Extent of spacecraft changes required
4. Mission compatibility
5. Readiness and qualification of equipment
6. Extent of crewmember participation
7. Attitude-control fuel budget
8. Weight and volume
9. Instrumentation and electrical power

After the selection of experiments that were in concert with these criteria, the principal investigators for the proposed experiments were contracted by NASA to design, develop, qualify, and deliver flight equipment in accordance with the Gemini Program management and design criteria. Also included was the requirement to establish the necessary experimental protocol and support the preflight, inflight, and postflight activities that were associated with the particular experiment.

Activities in the immediate preflight interval were variable and were unique to each experiment. Crewmember familiarization with objectives and training in procedures were the responsibility of the principal investigators, and each principal investigator was required to define and to assist as required in procedure implementation. Similarly, when base-line data on crewmember physiological parameters were required, the principal investigator had an equivalent responsibility. Preparation and the state of readiness of special ground-based targets or ground-located participating equipment was a principal investigator task. Participation in final crewmember briefings, equipment checks, and NASA-sponsored press conferences was required.

During the mission, availability of the principal investigator for consultation on real-time adjustment of experimental procedures was essential. Also, the manning and operation of ground-based targets and participating equipment sites were required.

Postflight activities included participation in the scientific debriefing of the crewmen. A summary compilation of experimental results was required for incorporation in the mission report during the immediate postflight interval. It is NASA policy to sponsor, within 90 days after a mission, a public report of the experimental results to

the extent of reduction and analysis that exists at the time. A final publication of results is required when data analysis is complete and when conclusions are established firmly.

CONCLUSION

The inflight experiments that were completed were successful, and these experiments are indicative of the desirability of full use of the capabilities of subsequent spacecraft designs and missions for the performance of an experiments program. The results of these experiments and similar experimental programs should contribute immeasurably to the related technologies and to the basic and applied sciences.

CONTENTS

INTRODUCTION TO THE GEMINI PROGRAM

PHYSICAL SCIENCES EXPERIMENTS

By Edward O. Zeitler*

The Gemini Program Physical Sciences Experiments Summary is based on the results and findings of experiments in the physical sciences. These experiments were selected to help answer questions in the fields of astronomy, navigation, radiation, geophysics, meteorology, photography, and communications. A flight summary of the experiments is given in table I. The answers to these questions aided in the completion of Apollo Program design and operational procedures.

The experiments were proposed by universities, laboratories, industry, governmental agencies, and other sources. Often, several investigators that had different affiliations were associated with a single experiment. The selected experiments were integrated into the spacecraft on a minimum interference basis, based on the participation of the crewmen. Although the direct effects of these experiments on Apollo systems are difficult to isolate, the general store of background data and available information is invaluable.

*NASA Manned Spacecraft Center, Houston, Texas.

TABLE I. - THE GEMINI PROGRAM PHYSICAL SCIENCES EXPERIMENTS FLIGHT SUMMARY

Experiment number	Gemini Mission										Experiment title
	III	IV	V	VI	VII	VIII	IX	X	XI	XII	
S001			X			X	X	X			Zodiacal Light Photography
S011							X		X	X	Airglow Horizon Photography
D009		X			X						Simple Navigation
D005					X			X			Star Occultation Navigation
T002										X	Manual Navigation Sightings
S029										X	Libration Regions Photography
M412					X			X			Landmark Contrast Measurement
S013								X	X	X	Ultraviolet Astronomical Camera
M411		X									Two-Color Earth Limb Photography
M403		X	X								Electrostatic Charge
M404		X			X						Proton-Electron Spectrometer
M408								X		X	Beta Spectrometer
M405		X			X			X		X	Tri-Axis Flux-Gate Magnetometer
M409								X		X	Bremsstrahlung Spectrometer
S026								X	X		Ion-Wake Measurement
D010								X		X	Ion-Sensing Attitude Control
S009						X			X		Nuclear Emulsion
D008		X		X							Radiation in Spacecraft
D004 and D007			X		X						Celestial and Space-Object Radiometry
S010						X	X	X		X	Agena Micrometeorite Collection
S012							X	X		X	Micrometeorite Collection
S005		X	X	X	X			X	X	X	Synoptic Terrain Photography
S006		X	X	X	X			X	X	X	Synoptic Weather Photography
S007			X			X					Cloud-Top Spectrometer
S051										X	Daytime Sodium Cloud
D015						X			X		Night Image Intensification
S030									X		Dim-Sky Photography/Orthicon
D001, D002, and D006			X								Basic Object, Nearby Object, and Surface Photography
M410								X			Color Patch Photography
T001	X										Entry Communications
D014						X	X				UHF/VHF Polarization
M406					X						Optical Communication
D016						X					Power Tool Evaluation
D012							X		X		Astronaut Maneuvering Unit
D003						X			X		Mass Determination

EXPERIMENT S001

ZODIACAL-LIGHT PHOTOGRAPHY

By E. P. Ney* and W. F. Huch*

INTRODUCTION

The light of the moonless night sky, as viewed from the surface of the earth, principally consists of scattered light from cities, twilight and starlight, zodiacal light, airglow, and aurora. Although lightning is an important contributor, and although Cerenkov light from cosmic-ray air showers is a detectable source, this report will be confined to slowly varying sources of light. All these contributing sources vary either with time, or with position in the sky, or with both. Quantitative observation of any of these phenomena from the surface of the earth is complicated further by the effects of light scattering and absorption within the atmosphere. For several years, a program has been in progress in an effort to separate and understand the individual contributions to the night sky brightness. In this study, balloon-borne photometers, polarimeters, and special camera techniques were used. More recently, special photographs, exposed during earth-orbital missions (Mercury-Atlas 9 and Gemini V), have been acquired.

The principal purpose of this report is to describe observations made during the Gemini V, IX, and X missions in the context of their relation to ground-based and balloon-based experiments on dim-light phenomena. Zodiacal light is the visible manifestation of dust grains in orbit around the sun. The brightness of the light at 20° elongation from the sun and on the ecliptic is approximately 2×10^{-12} of the surface brightness of the sun, or approximately the same brightness as the zenith sky observed from the surface of the earth at the time of full moon. At 60° elongation from the sun, the brightness is approximately 2×10^{-13} of the surface brightness of the sun, or approximately one-half the brightness of the Milky Way. At larger elongation angles, the zodiacal light becomes obscured by the terrestrial continuum airglow, which has an average surface brightness of approximately 2×10^{-14} of the surface brightness of the sun. In the direction approximately opposite to the sun, the phenomenon of the gegenschein occurs. The gegenschein is believed to be approximately 2×10^{-14} of the surface brightness of the sun. Before the Gemini V mission, no attempts to photograph the gegenschein were successful.

*University of Minnesota, Minneapolis, Minnesota.

As observed from the surface of the earth, the zodiacal light is distorted grossly by the effects of atmospheric extinction. From balloons at 100 000 feet, the effects of atmospheric extinction essentially may be eliminated, even in the horizontal direction. A photograph of the zodiacal light is shown in figure 1. The photograph was made with Ansco film 529, an f/0.8 lens, and a 1-minute exposure. The solar elongation in the horizontal direction was 21°. The star field, the horizontal, and the ecliptic appropriate for figure 1 are shown in figure 2. The photograph was made from a balloon over Texas to eliminate aurora. The airglow appears as a diffuse light increasing in brightness toward the horizontal, according to the Van Rijn variation of brightness with zenith angle. No twilight is evident in figure 1; however, because of twilight, measurement of the zodiacal light from balloons is impossible at elongation angles of less than 19°. One of the objectives of the experiment, as performed during earth-orbital missions, was to determine the minimum angle from the sun at which the zodiacal light could be studied without degradation by twilight.

To estimate airglow degradation of zodiacal light measurements in the visible region of the spectrum, an experiment was performed during the Mercury-Atlas 9 (MA-9) mission (ref. 1). A crewman carried a camera that had an f/1 lens, and he photographed the airglow in profile from above, using exposures of 10 seconds, 30 seconds, and 120 seconds on Ansco film 529. One of these photographs is shown in figure 3. The moon had not risen (so the earth is dark), the horizon is delineated by very distant lightning strokes, and the airglow layer is shown with a sharp line on top and a rather diffuse illumination below. The majority of the light in the visible region of the spectrum arises in a layer 20 kilometers thick and at an altitude of approximately 95 kilometers, as shown in these photographs. Although this result was not unexpected, it had not been demonstrated previously because height measurements of the airglow have been made for selected lines and for small regions of the continuum. However, the principal brightness is throughout the continuum, and broadband spectral observations with the MA-9 photographs are indicative that all the important illumination within the film bandwidth arises in a thin layer. Of course, this statement cannot be taken to include the 6300-angstrom line of oxygen or the infrared radiation to which the film is not sensitive. Sensitometric analysis of the negatives exposed on the MA-9 mission proved that only 10 percent of the light was reaching the film and that only third-magnitude stars could be identified because of the low transmission of the spacecraft window.

OBJECTIVES

Gemini V Mission

It had been proven conclusively by the experiment that was performed during the MA-9 mission that experiments on extraterrestrial light could be performed without airglow contamination at altitudes above 90 kilometers. The experiment performed during the Gemini V mission was designed to result in answers to the following questions.

1. What is the smallest elongation angle at which zodiacal light measurements can be made from an earth-orbital spacecraft above the airglow layer?

2. Can the gegenschein be detected and measured from above the airglow layer?

Gemini IX and X Missions

The purpose of Experiment S001 on the Gemini IX and X missions was to obtain 30-second exposures, with a lens setting of f/1, of the airglow (viewed in profile from above), the zodiacal light, and the Milky Way.

EQUIPMENT

Gemini V Mission

The camera that was designed for the experiment had an f/1 lens, was used with Eastman Kodak Tri-X film, and was programed with transistor circuits to take doubling exposures in sequence, starting at 0.50 second and concluding at 3 minutes. Between successive exposures, 20 seconds of shutter-closed time were allowed for spacecraft maneuvering. The field of view of the camera was 50° by 130°, obtained by rotation of the optical system during the exposure. With the camera mounted in the pilot-side window, a photosensitive eye was arranged to start the programed sequence at sunset. In the experiment, the photosensitive eye was not used because the camera was turned on by a crewmember precisely at sunset.

Gemini IX Mission

The camera was designed to view a wide-angle field (approximately 50° by 130°). Mechanically, it was the same kind of camera as the one flown on the Gemini V mission. The exposure sequence was automatic, and it alternated 30-second exposures with 10-second-off periods. During the off periods, thrusters could be fired without exposing the film. The film was 35-millimeter black and white and had a speed of 400 ASA.

Gemini X Mission

The camera was designed to view a wide-angle field of approximately 50° by 130°. Mechanically, it was the same kind of camera as that flown on the Gemini V and Gemini IX missions. The exposure sequence was automatic and alternated 30-second exposures with 10-second-off periods. During these off periods, thrusters could be fired for attitude-hold without exposure of the film. High-speed, 35-millimeter, black and white film was used.

PROCEDURE

Gemini V Mission

The experiment, performed on August 24, 1965, during orbit 46 of the Gemini V mission, was composed of two parts. Before sunset, the command pilot acquired a definite spacecraft orientation, using the reticle and the Southern Cross as

a reference. This placed the pilot-side window and the camera in the correct position to photograph the twilight and the zodiacal light. After 5 minutes of stepped exposures, the spacecraft was maneuvered toward the constellation Grus as a reference, with α and β Grus and Fomalhaut as the reference field for the reticle. The position opposite the sun was centered in the field of the camera. In this orientation, spacecraft motions were stopped as much as possible (by the use of reference stars) to attempt an inertial fix. Seventeen exposures were taken, three of which are of special interest.

Gemini IX Mission

The original Gemini IX flight plan was for the camera to be hand held during extravehicular activity (EVA), and to be used on the nightside pass just before ingress from EVA. However, because of visor fogging, the extravehicular operation of the camera was abandoned. Subsequently, the crewmen performed the experiment from inside the spacecraft, photographing through the pilot-side window. The pilot held the camera in the window during the exposures, sighting past the camera and directing the command pilot to maneuver the spacecraft to the appropriate position. The pilot turned the camera off between successive exposures. The astronomical objects were not in view of the command pilot, and his task was to null the spacecraft rotation rates.

Gemini X Mission

The flight plan was that the camera be hand held on night passes, with the pilot taking photographs through the pilot-side window. As was done on the Gemini IX mission, the pilot held the camera against the window during the exposure periods, sighting past the camera and directing the command pilot to maneuver the spacecraft to appropriate positions. Astronomical objects were not in the field of view of the command pilot, and his task was to null the spacecraft rotation rates. The planned procedure was that photographs be taken with the following camera orientations.

1. Horizontal toward the west
2. Alined along the Milky Way to include the southwest horizon
3. Alined along the Milky Way in the zenith
4. Alined along the Milky Way to include the northeast horizon
5. Horizontal toward the northeast
6. Horizontal toward the east
7. Horizontal toward the south

RESULTS

Gemini V Mission

Frames 1 to 5 were exposed properly, but the twilight was so bright that it obscured the zodiacal light. Frame 7, made with an 81-second exposure, is of the zodiacal light. The illuminated horizon, with the airglow layer showing in profile above it, also may be seen. The frame represents approximately the smallest elongation (16°) at which zodiacal light may be studied without external occultation. This photograph may be studied quantitatively for airglow brightness and zodiacal light characterization, but such study would be very difficult because of a photographic artifact. A print of frame 7, which shows the zodiacal light, is shown in figure 4; figure 5 is a sketch of the star field shown in figure 4. The top portion of frame 7 was printed with 40 times more exposure than was the bottom portion. This ratio improves the view of the earth limb and the airglow layer, which showed despite the artifact. The airglow layer, viewed in profile, had approximately the same surface brightness as did the zodiacal light at 16° elongation. The zodiacal light at this elongation (ref. 2) was 4×10^{-12} of the surface brightness of the sun. The ratio of profile brightness to zenith brightness of the airglow was approximately 40; thus, the inferred zenith-airglow brightness was 10^{-13} of the surface brightness of the sun. This was approximately three times brighter than the average nighttime airglow, but was within the range of variation commonly observed.

Frames 8 and 9 reveal exposure of the film by thruster light, and frames 10 to 14 reveal excessive motion of the star field. However, frames 15 and 16 represent good celestial holds, and both of these negatives appear to show the gegenschein. The center of the gegenschein is approximately halfway between θ and ι Aquarii, and it appears to have an angular size of approximately 10°. It is within a few degrees of the direction opposite the sun. Its brightness is estimated to be in the range of 1×10^{-14} to 9×10^{-14} of the surface brightness of the sun. The star field photographed in the gegenschein experiment is shown in figure 6. Stars up to the sixth magnitude may be identified. A drawing, which represents the star field shown in figure 6, is shown in figure 7. The direction opposite the sun should be the direction of the gegenschein, if this phenomenon was produced by the backscattering of sunlight by dust. There was no evidence of the westerly displacement which might have been expected if the gegenschein resulted from a comet-like dust tail of the earth.

Gemini IX Mission

The procedure adopted by the crewmen resulted in the acquisition of 17 very good photographs, which are listed in table I. Exposure 9 is shown in figure 8. This figure is a copy of a photograph of the Milky Way with Cygnus in the center. The airglow layer shows to the right of the spacecraft. The bright spot at the upper right was caused by moonlight. Exposure 15 is shown in figure 9. This figure is a copy of an overexposed print used to emphasize the zodiacal light, airglow, and stars.

The 20 photographs obtained are listed in table II. The spacecraft attitude held by the crewmen during the exposures was adequate. However, a combination of the following three factors make the pictures difficult to use quantitatively.

1. The film was only one-half as sensitive as the film that was used on the Gemini IX mission.

2. Observations of the same star field in various exposures proved that light transmission through the dirty spacecraft window varied by a factor of at least six.

3. The earth horizon was not seen in any of the pictures.

DISCUSSION

The negatives that were exposed on the Gemini IX mission were studied by the use of an isodensitracer to produce intensity isophotes. Data on the following factors were obtained.

1. Intensity distribution of the zodiacal light, both morning and evening

2. The height and intensity of the airglow at various geographic positions

3. Intensity distribution of the Milky Way in the region of the sky near Cygnus

Also, a previously unreported phenomenon was discovered. This phenomenon appeared as an upward extension of the normal 90-kilometer airglow layer. The extension was in the form of wisps or plumes approximately 5° wide and extending upward approximately 5°. The plumes appeared in the east and probably were not caused by aurora. The phenomenon is believed to be in the sky.

The experiment is considered an unqualified success, and the crewmen must be given credit for making an excellent program for the experiment after the extravehicular performance was terminated. The results obtained from pictures exposed on the Gemini X mission were of qualitative or geometrical value only. For example, the airglow heights were measurable in two pictures showing the earth horizon. One picture confirmed the existence of a higher airglow layer at 200 to 300 kilometers. This layer also was seen in photographs exposed on the Gemini IX mission. One picture showed the presence of wisps extending upward from the lower airglow layer. These wisps had been seen for the first time on photographs made during the Gemini IX mission.

REFERENCES

1. Gillett, F. C.; Huch, W. F.; Ney, E. P.; and Cooper, G.: Photographic Observations of the Airglow Layer. J. Geophys. Res., vol. 69, no. 13, July 1, 1964, pp. 2827-2834.

2. Gillett, F. C.; Stein, W. A.; and Ney, E. P.: Observations of the Solar Corona from the Limb of the Sun to the Zodiacal Light, July 20, 1963. Astrophys. J., vol. 140, no. 1, July 1, 1964, pp. 292-305.

TABLE I. - PHOTOGRAPHS TAKEN DURING THE GEMINI IX MISSION

Exposure number	Orientation	Object
1	North	Horizon airglow
2, 3	West	Horizon airglow
4, 5	South	Horizon airglow and aurora
6, 7	East	Horizon airglow
8, 9, 10, 11	Northeast	Milky Way
12, 13, 14	East	Horizon airglow
15, 16, 17	East	Airglow, zodiacal light, twilight

TABLE II. - PHOTOGRAPHS TAKEN DURING THE GEMINI X MISSION

Exposure number	Camera orientation	Object
1, 2, 3	Horizontal toward the west	--
4	--	Spacecraft thruster plumes
5, 6	Along the Milky Way	α and β Centauri centered in the field of view
7, 8, 9	Along the Milky Way	Galactic center in the upper right
10, 11, 12	Along the Milky Way	Northeastern sectors
13, 14	Along the Milky Way	From stars Vega to Cassiopeia
15, 16, 17, 18, 19, 20	Horizontal toward the east	Orion star field centered

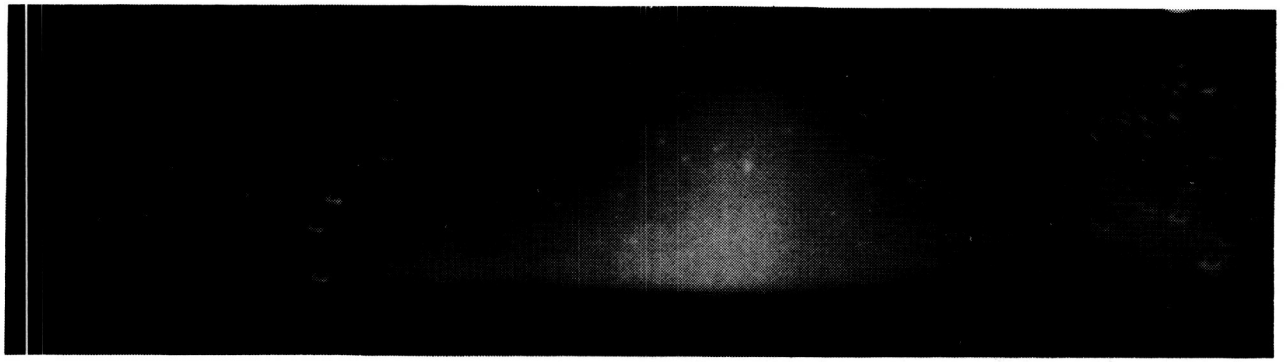

Figure 1. - A photograph of the zodiacal light rising in the east, taken on September 30, 1962, by the use of a balloon-borne camera.

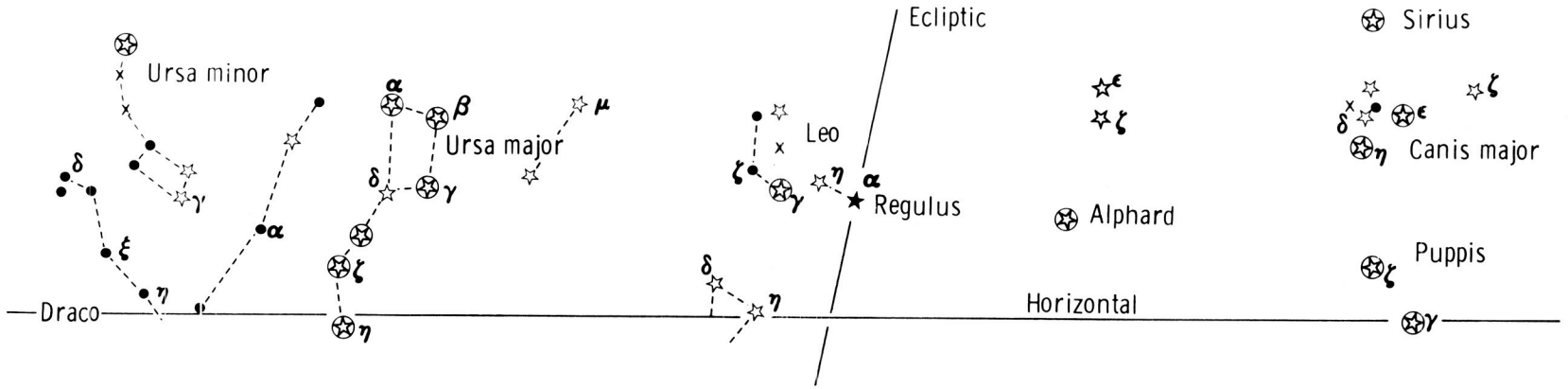

Figure 2. - A drawing of the star field shown in figure 1.

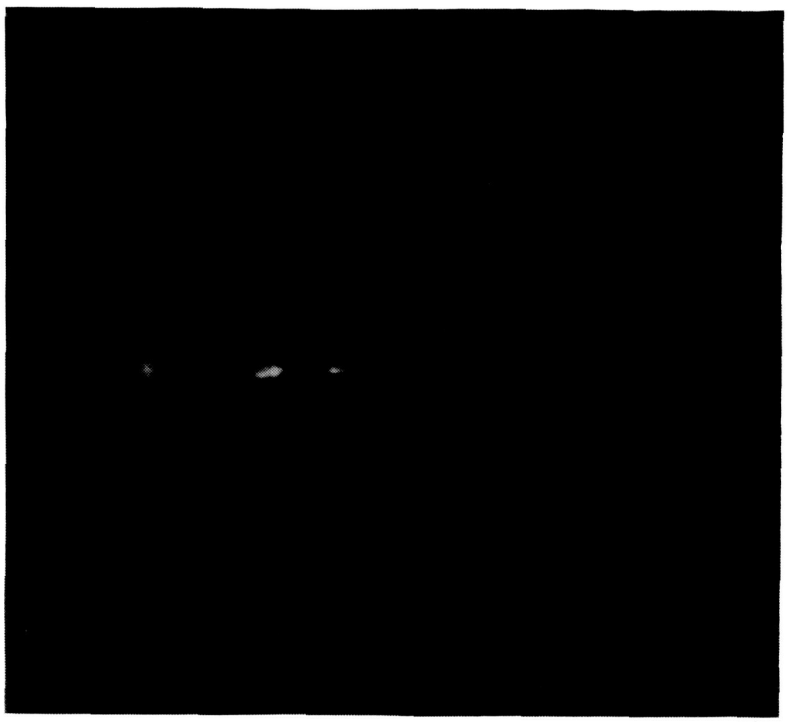

Figure 3. - A photograph (from the MA-9 mission) of the airglow viewed in profile from above.

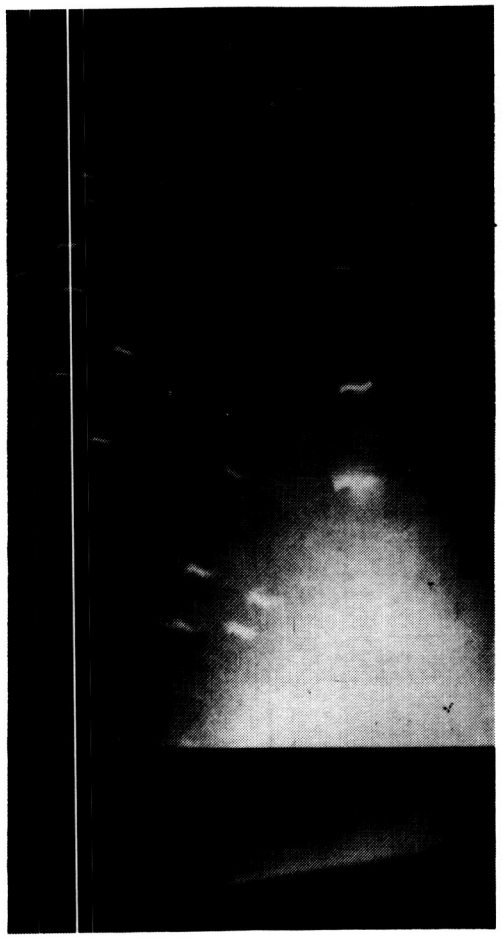

Figure 4. - A print of frame 7.

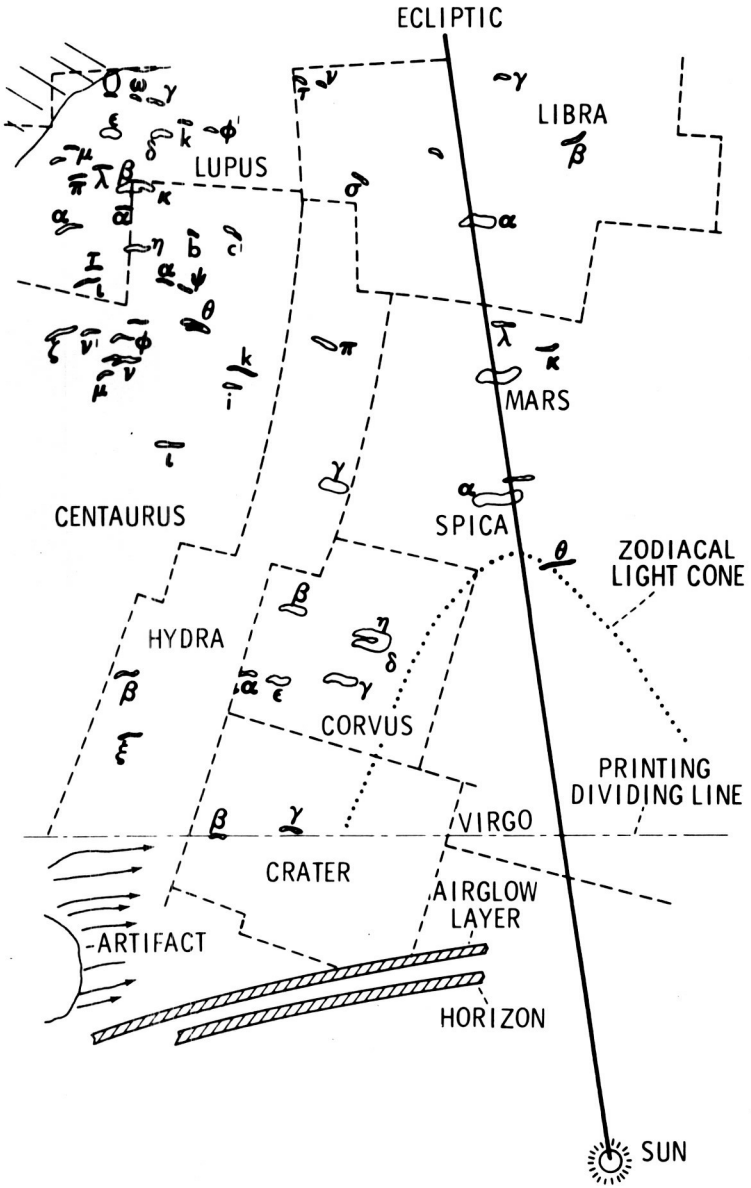

Figure 5. - A sketch of the pertinent features of figure 4.

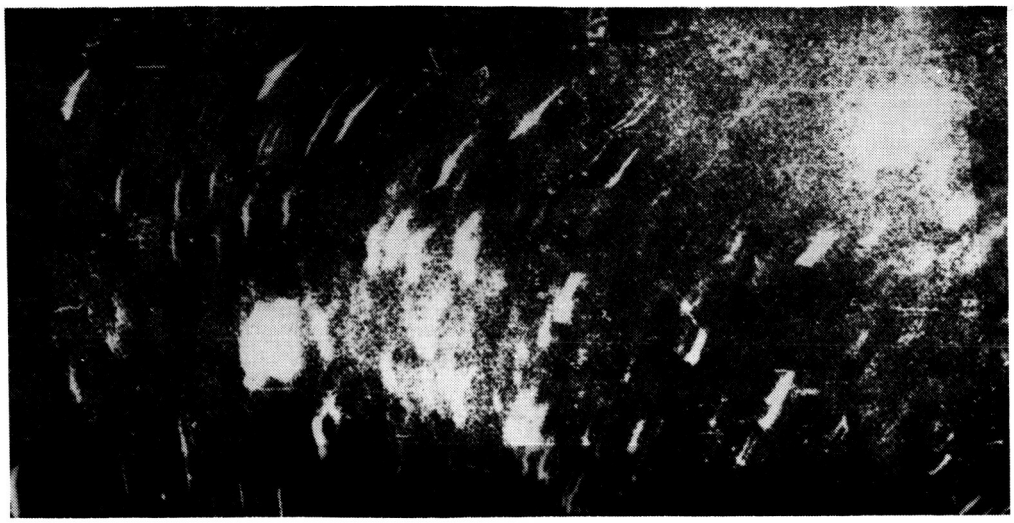

Figure 6. - A print of frame 15.

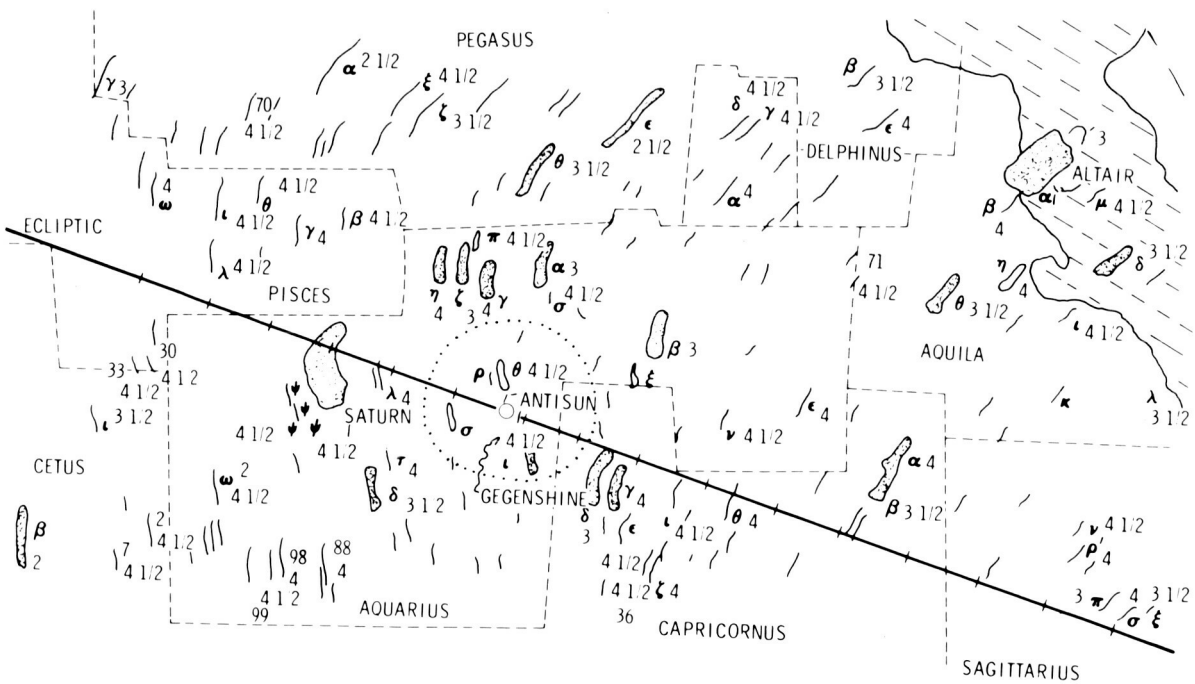

Figure 7. - A drawing of the star field shown in figure 6.

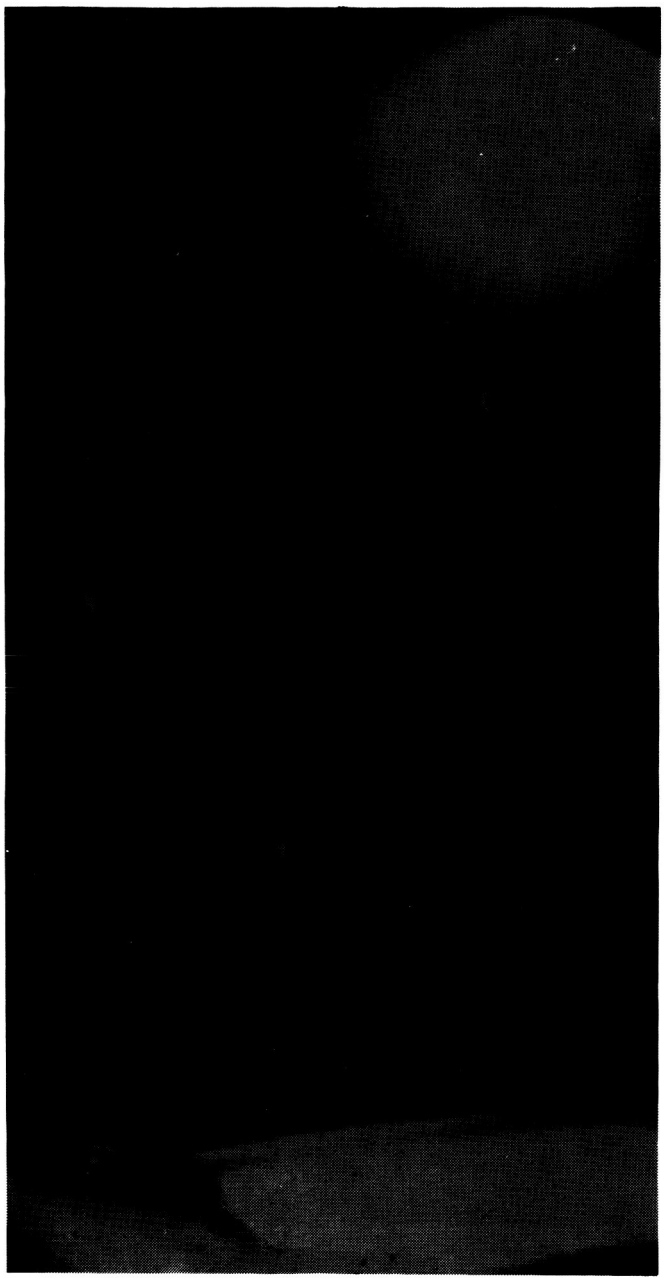

Figure 8. - A photograph of the Milky Way.

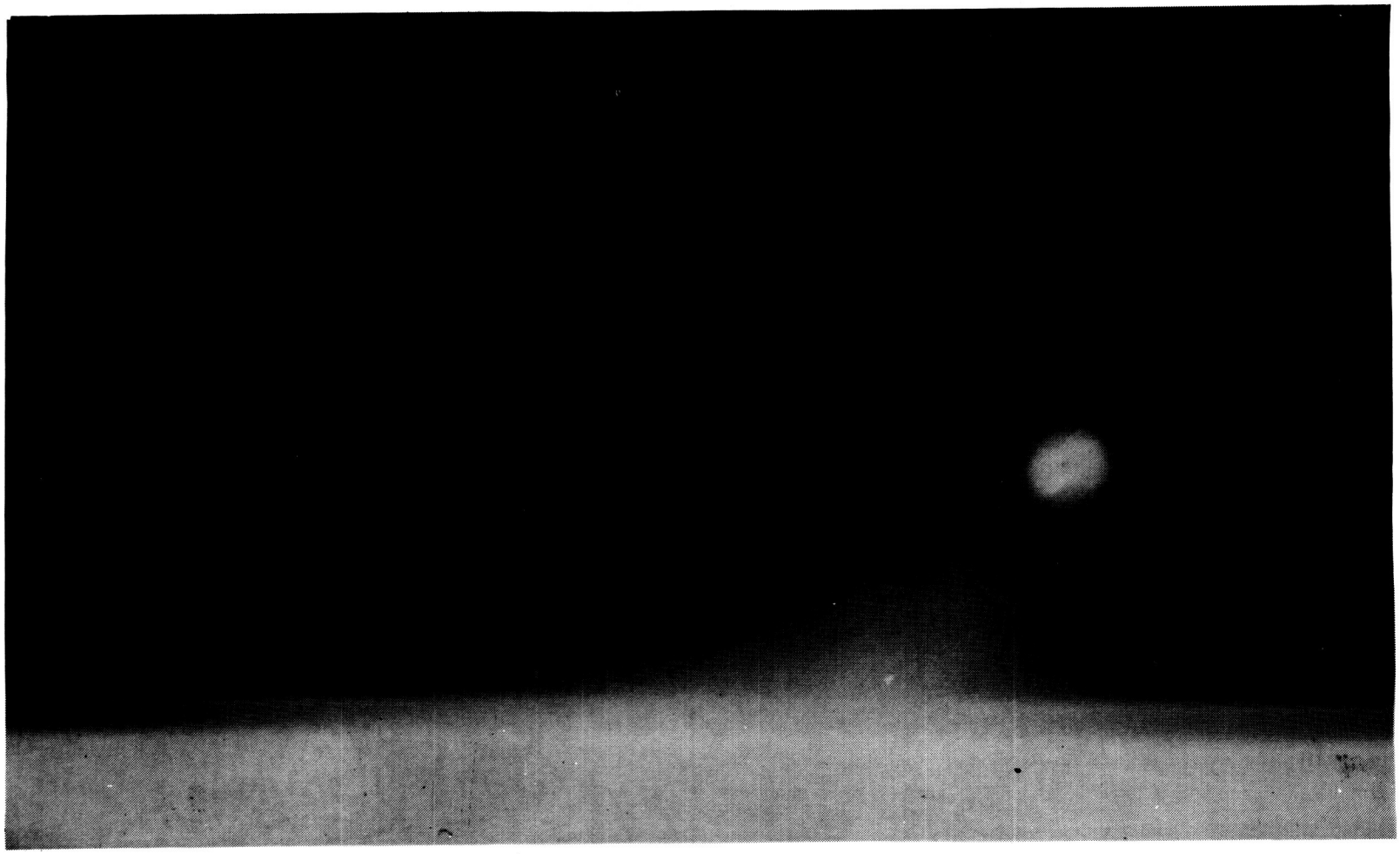

Figure 9. - A photograph of the zodiacal light.

EXPERIMENT S011

AIRGLOW HORIZON PHOTOGRAPHY

By M. J. Koomen,* R. T. Seal, Jr.,* and J. Lintott**

OBJECTIVE

Experiment S011, which was flown on the Gemini IX, XI, and XII missions, was designed so that the night airglow, which lies in a thin layer 70 to 100 kilometers (40 to 60 miles) above the earth, could be studied. Although the surface brightness is low when observed through this layer from below, brightness of the airglow is augmented by a factor of approximately 35 when the airglow is viewed tangentially from the vantage point of the Gemini orbit. This augmentation phenomenon, which makes the airglow observable easily, plus the worldwide coverage established by orbital vehicles, is an effective means of synoptic airglow study.

The Mercury and Gemini crewmembers have had no difficulty in observing the night airglow in the form of a relatively bright band above the nighttime horizon. During the Mercury-Atlas 9 mission, the pilot was able to photograph the layer by the use of high-speed color film and an f/1.0 hand-held camera at 10- and 30-second exposures (refs. 1 and 2). The photographs revealed geographical variations in altitude and intensity.

The objective of Experiment S011, flown on the Gemini IX, XI, and XII missions, was to extend and refine the photographic method. The following techniques were used to achieve this goal.

1. The camera was equipped with a filter to photograph the two prominent line emissions at 5577 and 5893 angstroms; these emissions are caused by atomic oxygen and sodium, respectively.

2. An illuminated camera sight and an aiming camera mount were used in an attempt to reduce the number of blurred photographs that had occurred during the longer exposures. Therefore, Experiment S011 on the Gemini IX mission was a feasibility test for the two components.

3. The number of photographs taken and the amount of the earth photographed were as large as possible.

---

*U.S. Naval Research Laboratory, Washington, D.C.
**NASA Manned Spacecraft Center, Houston, Texas.

4. Attempts were made to photograph the twilight horizon to reveal a sunlit dayglow layer.

EQUIPMENT DESCRIPTION

Because of equipment variation among the three missions, the discussion will be divided according to mission.

Gemini IX Mission

The Maurer 70-millimeter general-purpose camera with an f/0.95, 50-millimeter lens and a focal-plane filter was used on the Gemini IX mission. This configuration was designed especially for airglow and other dim-light photography. Eastman 103-D emulsion on 2.5-mil Estar base was used to ensure maximum film speed in the 5577- to 5893-angstrom region. Development time was 6 minutes in Eastman D-19. A camera lens filter and a focal-plane filter were used to perform the function shown in figure 1. The lens filter was of the multilayer interference type and had a steep-sided band pass that admitted wavelengths of 5577 and 5893 angstroms at short-wavelength and long-wavelength ends, respectively, of the band. The focal-plane filters, mounted side by side over the film, divided this band into two bands that were centered at 5577 and 5893 angstroms. Band half-widths (HW) were 270 and 380 angstroms, respectively. Thus, light in these two wavelength bands could be photographed so that the bands appeared side by side in the picture plane, in a split-field arrangement with a vertical dividing line. The extreme edges of the focal-plane filter were made of clear glass for admission of the entire lens-filter band. The system was designed to attempt the detection of small altitude differences in the airglow-emission wavelengths. The effect of the filter combination that has been discussed could not be achieved by the use of narrow-band filters in the focal plane alone because these filters would not perform in the convergent light of the f/0.95 lens. The filter bands were rather wide and admitted considerable contamination in addition to the wanted lines. The condition was particularly unfavorable for the 5893-angstrom sodium filter, which admitted a large amount of hydroxyl (OH) radiation. Continuum airglow radiation was admitted by the green (5577 angstrom) filter. However, it was expected that the photographs would yield significant results that would be indicative of the direction of refinements for subsequent missions.

The camera sight was designed and built specifically for the experiment, and it contained a reflex element molded in the shape of a parabolic toroid. The camera operator sighted through this element at the horizon and saw the images of three small pinlights arranged in a horizontal line superimposed on the horizon by reflection. The reflex element folded down for storage. The camera lens filter, and focal-plane filter are shown in figure 2. The sight is shown in the folded position; the cable release with event timer was not used. Because relatively long exposure times were used, the camera could not be hand held. A bracket of adjustable pitch held the camera to the right-hand spacecraft window. The bracket configuration is shown in figure 3. Two fluted knobs were used to fasten the bracket to the lower part of the window frame. The large knob adjusted the camera aim in the elevation (pitch) direction; the limits of motion

were slightly more than ±6° from the center position. The center position was marked by a visible grove in the knob shaft, and the groove could be felt manually when the cabin was dark. When not in use, the bracket could be removed from the window and folded into the storage configuration, which is shown in figure 4.

Gemini XI Mission

The camera was identical to that used on the Gemini IX mission. Eastman S0166 film (now designated number 2485) was used because of its high sensitivity in the spectral region from 5577 and 6300 angstroms. The camera lens filter and focal-plane filter were identical to those used on the Gemini IX mission. However, band half-widths were 250 and 300 angstroms, respectively. As with the Gemini IX filter system, short exposures could be taken with the lens filter removed and with only the focal-plane filter in place to record the red, orange, and yellow wavelengths on one side of the center line, while the didymium glass on the other side of the line admitted almost the entire visible spectrum except sodium yellow. For the planned high orbit, an interference-type lens filter that had a 150-angstrom half-width band (centered at 6330 angstroms) was used to photograph the red oxygen doublet. The focal-plane filters were left in place because they had a high-transmittance red leak at that wavelength.

The camera had a newly designed reflex sight that was characterized by better optical performance than the Maurer sight that was used on the Gemini IX mission. Aiming marks were two small points of light (on a horizontal line) that could be superimposed upon the horizon. The brightness of these lights was adjustable. The camera, with reflex sight and lens filter in place, is shown in figure 5. The camera bracket was identical to that which was used on the Gemini IX mission.

Gemini XII Mission

The camera was identical to that which was used on the Gemini IX and XI missions. Two film magazines were loaded with Eastman S0166 (now number 2485) film and were shared with Experiments S029 and S051. The split-field focal-plane filter arrangement that was used on the Gemini IX and XI missions was not used on the Gemini XII mission. A circular mask at the focal plane resulted in a total field of 45°. The focal-plane filter was omitted, and three narrow-band interference filters were used separately over the camera lens to isolate airglow emission lines with greater purity than was done on previous missions. These filters had peak transmittances at wavelengths of 5577 angstroms (green), 5893 angstroms (yellow), and 6330 angstroms (red). The green and yellow filters had half-widths of 45 and 55 angstroms, respectively. The red filter had a half-width of 150 angstroms, which was necessary to photograph the 6300- to 6364-angstrom doublet emission bands that were caused by atomic oxygen.

The camera sight and bracket were identical to those used in the Gemini XI mission. The Gemini XI flight resulted in proof that these items helped the operator to hold the camera steady on the horizon for time exposures of 20 seconds, in spite of normal spacecraft motions.

EXPERIMENTAL PROCEDURE

Gemini IX Mission

Camera components (including the window bracket) were stored in the spacecraft cabin and assembled onto the right-hand window when needed. Essentially, the camera axis was perpendicular to the spacecraft window and was, therefore, not boresighted to the spacecraft. To acquire the horizon at any particular azimuth, the spacecraft attitude was adjusted until the appropriate part of the horizon appeared "right side up" in the camera sight. This attitude adjustment required activity by the command pilot and the pilot. Then, spacecraft drift rates were damped as much as possible, and the exposure was begun. The pilot compensated for drifts in pitch during exposure by fine-pointing the camera at the horizon with the aid of the camera sight and the adjustable bracket. The spacecraft thrusters were not used during the exposure because they produced a large amount of light. Night exposures were taken in series of three; one exposure of 20-second duration with the lens filter in place, and two exposures with the filter removed for durations of 2 and 5 seconds. The series was taken to the east, west and south, and again toward the east at the beginning of twilight.

Gemini XI Mission

Generally, the procedure was the same as for the Gemini IX mission, except that all exposures were made with the spacecraft docked to the Agena vehicle. This proved to be a desirable configuration, particularly for long exposures, because of the increased stability and the improved attitude control.

Night photographs were taken in two sequences. The first sequence was taken during revolution 11, when sets of horizon exposures were taken successively toward the north, south, south, and north. The sets were taken 4 minutes apart, and each set consisted of a 10-second exposure with the lens filter in place and 2- and 5-second exposures with the lens filter removed. The second sequence was taken during revolution 19; the sequence consisted of four sets of exposures, spaced 4 minutes apart, but all exposures were taken in an easterly direction. The two sequences were a crude attempt, within mission constraints, to observe the effects of latitude and of local time. Eastward-looking photographs were the most difficult to take, because the horizon undergoes a maximum amount of blurring during a time exposure from an inertially stabilized vehicle. The pitch-adjustable camera bracket and sight were provided to compensate for the apparent horizon motion. However, the crewmembers learned that an appropriate pitch rate could be introduced into the spacecraft to make adjustment of the bracket almost unnecessary.

Gemini XII Mission

Experiment activities were designed to photograph the sunlit airglow layer as often as possible by the use of the three narrow-band camera lens filters which isolated the sodium yellow and the oxygen red and green emissions. The technique was to photograph the airglow layer from the nightside of the earth, but looking toward the twilight zone where the upper atmosphere was completely or partly sunlit.

Activities were planned for three revolutions, the first two of which were to be high orbits, where the red filter was to be used in an attempt to record the red oxygen emission that originates above an altitude of 200 kilometers. Because of a change in flight plan, no high-apogee photographs were obtained, and all data were taken from the normal orbital height (260 to 288 kilometers). During the first sequence, which began at 24:13 g.e.t., five exposures were made (using the red filter) of the western sunlit airglow after sunset. Exposure times ranged from 4 to 40 seconds, increasing with the time from sunset. Seven exposures were made during the night portion of the same revolution. These exposures included three photographs made without any filter, two photographs made with the red filter, and two photographs made with the green filter. The second sequence began at 25:43 g.e.t.; the procedures were the same as for the first sequence, except that the yellow filter replaced the red filter. The third sequence began at 70:45 g.e.t., and consisted of three twilight exposures made using the yellow filter, succeeded by eight 3-second exposures of the night airglow made without any filter. For the 3-second exposures, the spacecraft was yawed 50° between exposures.

RESULTS AND CONCLUSIONS

Gemini IX Mission

Forty-four photographs were obtained of the horizon airglow layer. Four photographs of the sunlit airglow on the eastern horizon represented the first photographic record of partly sunlit airglow. Typical examples of the night photographs are shown in figures 6 to 8. In figure 6, the strip to the left of the central vertical line was recorded in the sodium wavelength band (Na D) centered at 5893 angstroms, with a 380-angstrom half-width. The strip to the right of the central line was recorded in the oxygen green-emission band at 5577 angstroms, with a 270-angstrom half-width. Regions of the photograph at the extreme right and left were exposed through the clear portions of the focal-plane filter; thus, the band from 5577 to 5893 angstroms is included. Streaks in the sky were caused by stars that were rising while the camera was centered on the horizon. The most prominent streak above the airglow is α Ophiuchus. Five- and 2-second exposures, each made with the broadband (5893 to 5577 angstroms) filter removed from the camera lens, are shown in figures 7 and 8. The strip to the left of center recorded transmission through the orange section of the focal-plane filter (Corning 3480), which transmitted wavelengths of 5893 angstroms and longer; the strip to the right of center recorded transmission through the didymium glass section of the focal-plane filter, and included most of the visible spectrum except Na D. Sectors at the extreme right and left were exposed through the clear part of the focal-plane filter. The bright stars in and below the airglow in figures 7 and 8 are γ and ß Ursa Minor. The moonlit earth is visible in all the photographs. The photographs are indicative of global variations in the altitude and intensity of the airglow. The crewmembers reported variations in thickness and sharpness of the layer. This report is confirmed by the photographs.

Some of the photographs contained rich star fields, and stars of approximately the 7th magnitude were recorded. Sometimes, these stars were recorded through the airglow. These facts support the suggestion that the layer was transparent and did not

contain dust, as was suggested originally (ref. 3). There was no evidence that the moon, which was full at the time of the flight, contributed light to the airglow layer.

Airglow-layer heights were computed from measurements of the angular distance between the airglow layer and the moonlit horizon on the original negative. The horizon appeared sharpest through the orange section of the focal-plane filter; this was used for all measurements. The horizon line is not the earth limb, but an effective top of the atmosphere. The position of the true earth limb relative to the recorded star field was computed for several photographs for which spacecraft altitudes, positions, and times were known accurately. It was found that for the orange focal-plane filter, the moonlit horizon line was at a stable altitude of 20 kilometers above the true earth limb, and this value was included in computation of the true height of the layer. The airglow heights for all filters were 91 kilometers above the earth limb, within the remarkably small limits of ±3 kilometers, except for six measurements in the region 20° S 10° E. These resulted in an altitude of 87 ± 2.5 kilometers, which is within the overall experimental error. The thickness of the airglow layer, measured at half-intensity points, was a minimum of 18 kilometers for the yellow band and 20 kilometers for the green band. The maximum thickness for both was 30 kilometers, although it was difficult to judge the effect of possible small camera motions.

The intensities, which were specified in terms of a flat continuum entering the filter bands, varied between 0.5 and 1.0 Rayleigh per angstrom for both green and yellow bands; the values were computed for a vertical column through the layer. The filter bands were too wide to make estimates of the emission-line intensity in each. No geographical pattern in layer thickness or intensity was discernible from the photographs. The samples taken near the South Atlantic radiation anomaly showed no significant brightness enhancement.

Gemini XI Mission

Twelve good photographs of the night airglow layer were obtained on revolution 11 over the South Pacific Ocean. Twelve more photographs were taken on revolution 19 over the South Atlantic Ocean and South Africa. The measured airglow height was 90 ± 6 kilometers; there was no significant dependence on latitude, color, or geographical location.

No height variations as large as those observed on the Mercury 9 mission have been detected. However, there were easily observable changes of intensity, as illustrated in figures 9 and 10, which are, respectively, north- and south-looking photographs taken from the South Pacific Ocean. Each photograph is of the airglow layer with the dark earth below and with the star field above. The green wavelengths in the 5577-angstrom region are registered on the left side of the picture, and the yellow wavelengths spanning the sodium emission are registered on the right side. The extreme right and left edges recorded a spectral band that included both wavelength regions. To the north, the yellow wavelengths are slightly more intense than are the green wavelengths, whereas to the south, the yellow radiations are very faint. Another conspicuous feature is that the green and yellow radiations arise at the same altitude. Rocket measurements (ref. 4) from White Sands, New Mexico (106° W 33° N), usually locate the yellow wavelengths (Na D lines and OH bands) at a measurably lower altitude than the green wavelengths (oxygen 5577 angstroms and continuum).

An eastward-looking photograph of South Africa, taken from a point over the South Atlantic Ocean and with the camera lens filter removed, is shown in figure 11. The strip to the right of center recorded transmission through the focal-plane orange filter (Corning 3480) of wavelengths of 5893 angstroms and longer, whereas the strip to the left recorded transmission through the focal-plane didymium glass, which included most of the visible spectrum except the Na D line. Regions at the extreme right and left were exposed with no filter. The rich star field in Taurus, with the Pleiades in the airglow layer at the left, was rising because of the spacecraft orbital motion. A study of the star trails resulted in no evidence of atmospheric attenuation above approximately 25 kilometers. Therefore, there was no evidence of a high absorbing layer at the 100- to 150-kilometer region, which has been suggested (ref. 3) to explain the anomaly in the size of the shadow of the earth during eclipses. All photographs were taken at the time of the new moon; therefore, they do not show the earth limb. The position of the earth limb and an accurate layer altitude were deduced from the star field, time, and orbital position of the spacecraft.

Gemini XII Mission

The crewmembers obtained 23 good pictures of the sunlit and night airglow in the narrow wavelength bands that have been described under "Equipment Description." The average of all photographs, including several at twilight, yielded an airglow altitude of 88 ± 5 kilometers with no geographical dependence. The two emissions (5577 and 5893 angstroms) were within the same altitude range. Experiment S011 on both the Gemini XI and XII missions gave a greater spread in measured airglow heights than it did on the Gemini IX mission. This may reflect a smaller experimental error in the latter experiment, in which the moonlit earth and atmosphere were a stable reference point.

Typically, the airglow photographs from the Gemini XI and XII missions are like that of figure 12, which is a 3-second exposure taken to the west over South Africa. The earth was dark, except for the light from cities or lightning flashes, and the top of the atmosphere was defined, not by the moonlight horizon line, but by the attenuation of stars and airglow background. Also, this photograph is indicative that the atmospheric attenuation had an extremely steep gradient. Effectively, the top of the atmosphere for attenuation was at 25 kilometers. This value was used in the computation of the airglow heights in the cases wherein data were insufficient to compute the true position of the earth limb.

In the oxygen green and sodium yellow photographs, there is evidence that mostly the primary emission line was recorded on the film (because of the narrow band) with negligible radiation contamination. A typical 20-second exposure for the narrow-band green filter centered at 5577 angstroms is shown in figure 13. The image of the airglow layer does not extend to the edges of the frame because the interference filter characteristically does not transmit the 5577-angstrom emission at oblique angles.

No high-apogee orbits were attained during the Gemini XII mission; however, the twilight photographs that were taken using the 6300-angstrom filter contain a low-layer emission band, presumably caused by the OH radical, which emits in the red wavelengths (fig. 14). Its altitude was the same as the yellow and green emissions. This

was the first photograph from a spacecraft of the OH emission, and the photograph represents an interesting and useful addition to airglow observations.

It should be noted that the airglow altitudes just quoted were calculated by simple geometric methods from knowledge of the angular separation of the earth limb and the airglow layer seen in projection. Because of the curvature, the true vertical height is approximately 6 kilometers higher than the projected heights just given (ref. 5).

REFERENCES

1. Anon.: Mercury Project Summary. NASA SP-45, 1963.

2. Gillett, F. C.; Huch, W. F.; Ney, E. P.; and Cooper, G.: Photographic Observations of the Airglow Layer. J. Geophys. Res., vol. 69, no. 13, July 1964, pp. 2827-2834.

3. Link, F.: Thèorie photomètrique des èclipses de Lune. Comp. Rend., vol. 196, Jan. 1933, pp. 251-253.

4. Packer, Donald M.: Altitudes of the Night Airglow Radiations. Ann. Geophys., vol. 17, 1961, pp. 67-75.

5. Koomen, M. J.; Seal, R. T.; and Lintott, J.: Photography of the Night Airglow from the Gemini Series of Manned Spacecraft. Space Research VIII, Proceedings of the 10th Plenary Meeting of COSPAR (London), 1967. North Holland Publishing Co. (Amsterdam), 1968, pp. 684-691.

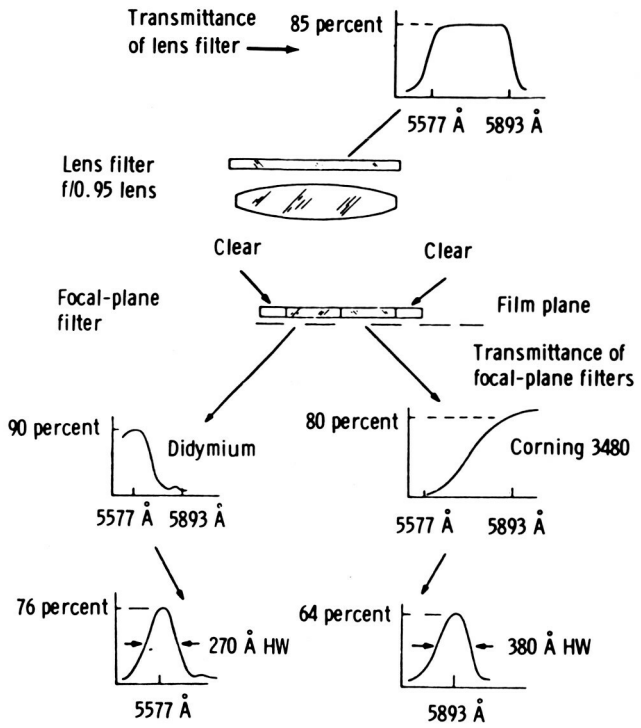

Figure 1. - A summary of the combined transmittance, lens, and focal-plane-filter characteristics.

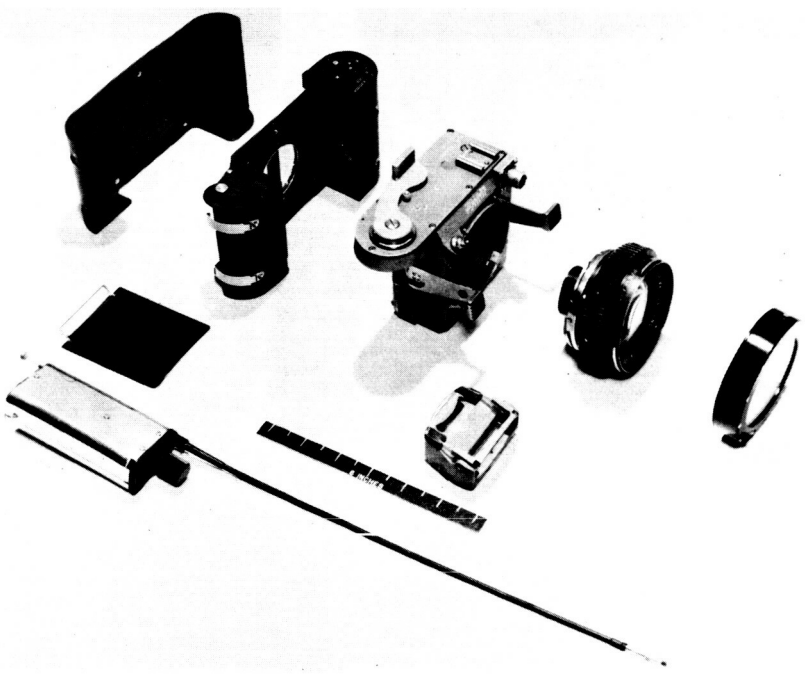

Figure 2. - The Experiment S011 camera system.

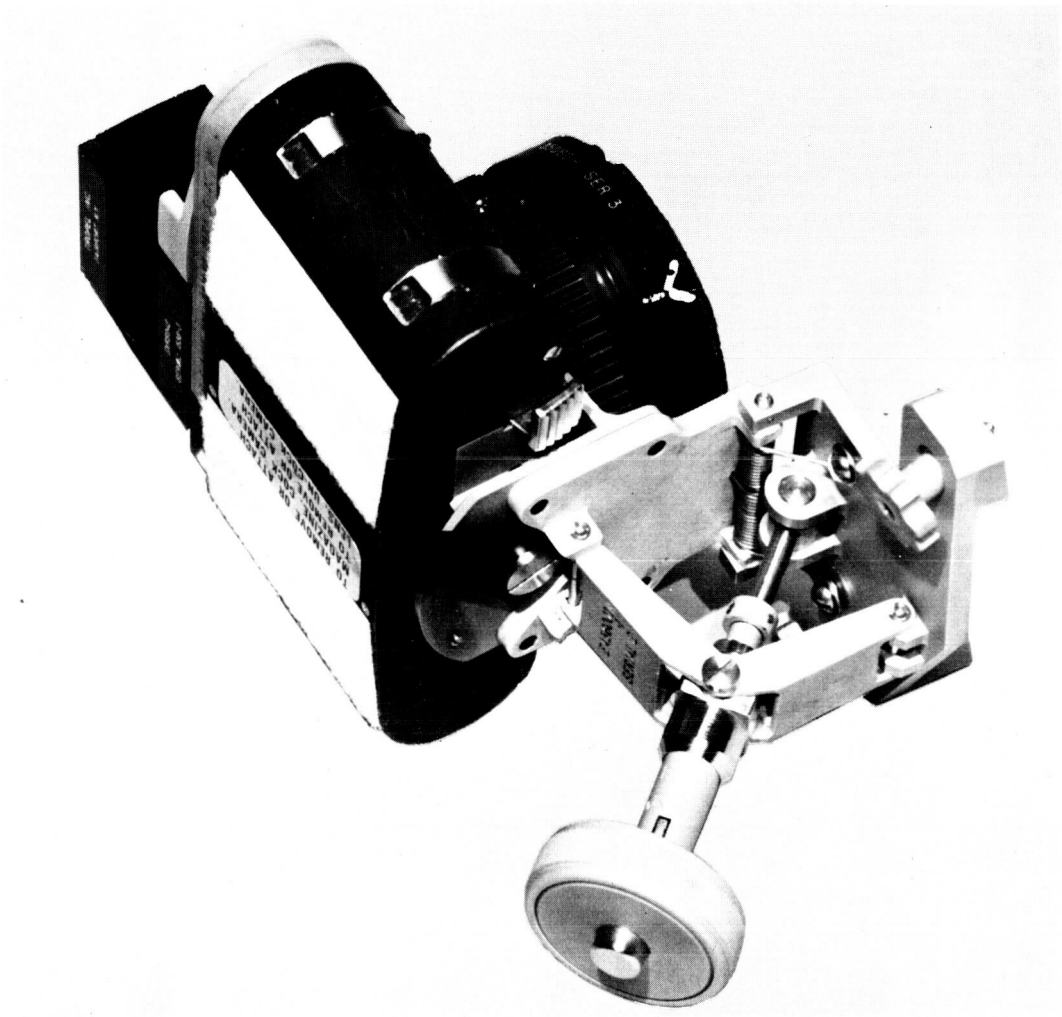

Figure 3. - The camera-mounting bracket.

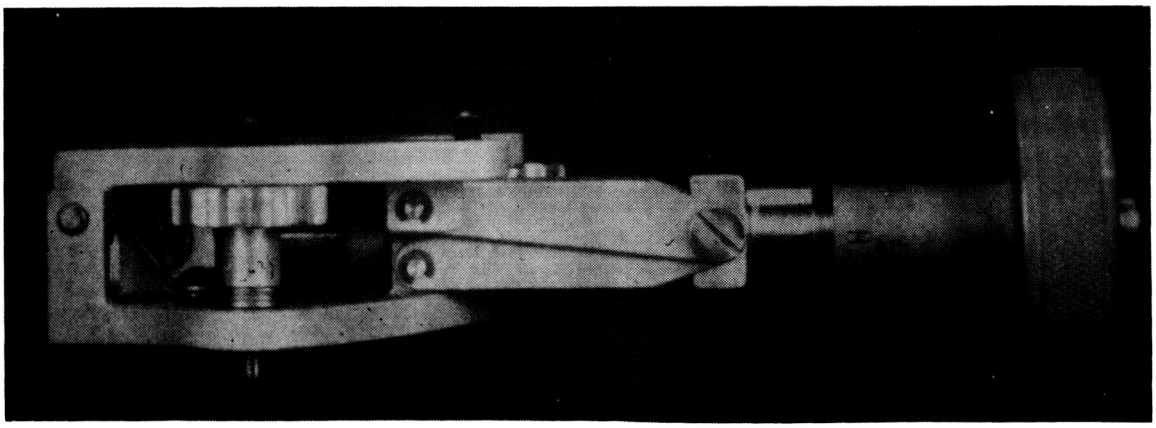

Figure 4. - The camera bracket folded for storage.

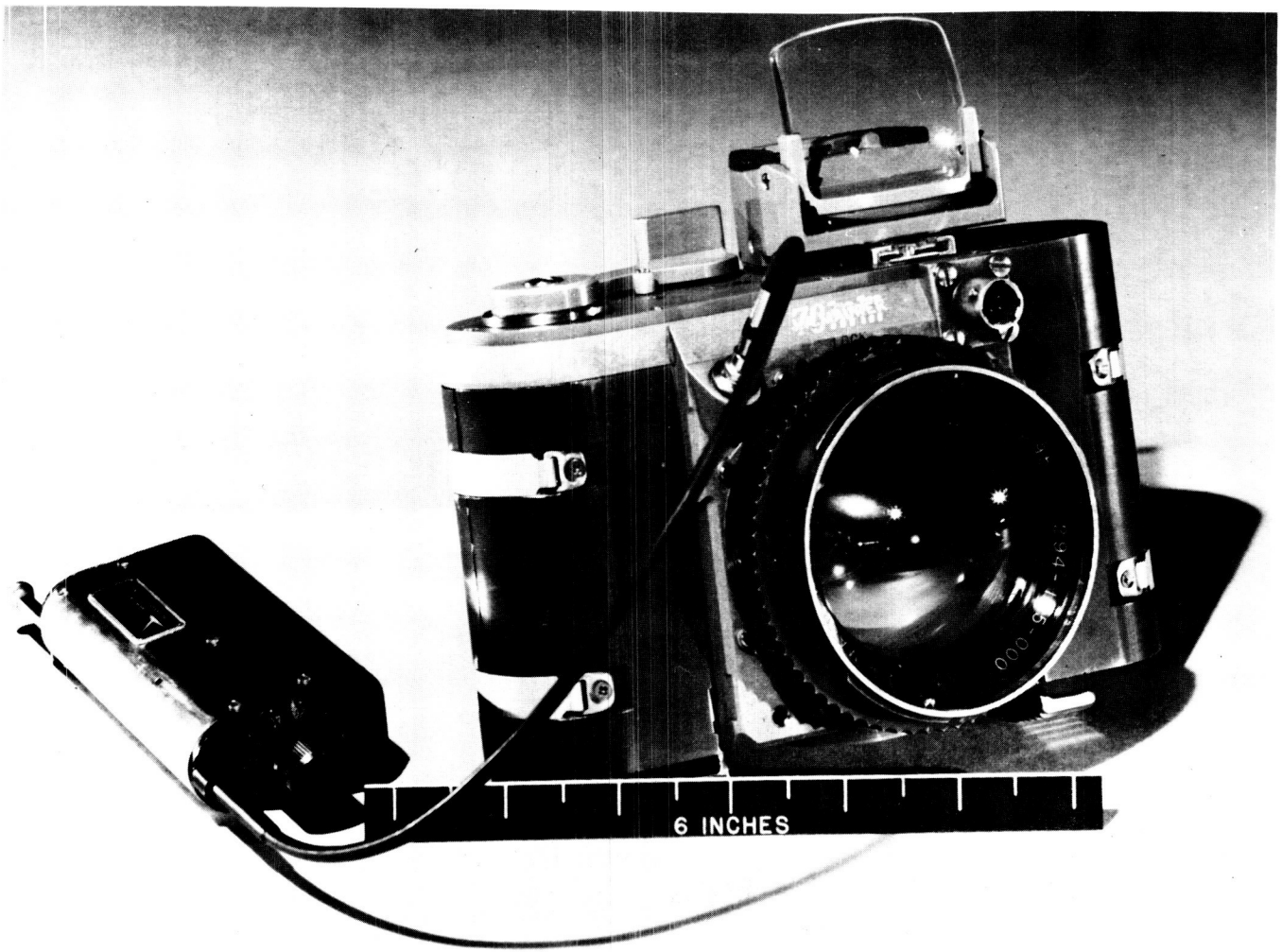

Figure 5. - The Maurer camera in the f/0.95 configuration with the reflex sight.

Figure 6. - Exposure 1, looking east during revolution 19; 20-second exposure at f/0.95 (Gemini IX).

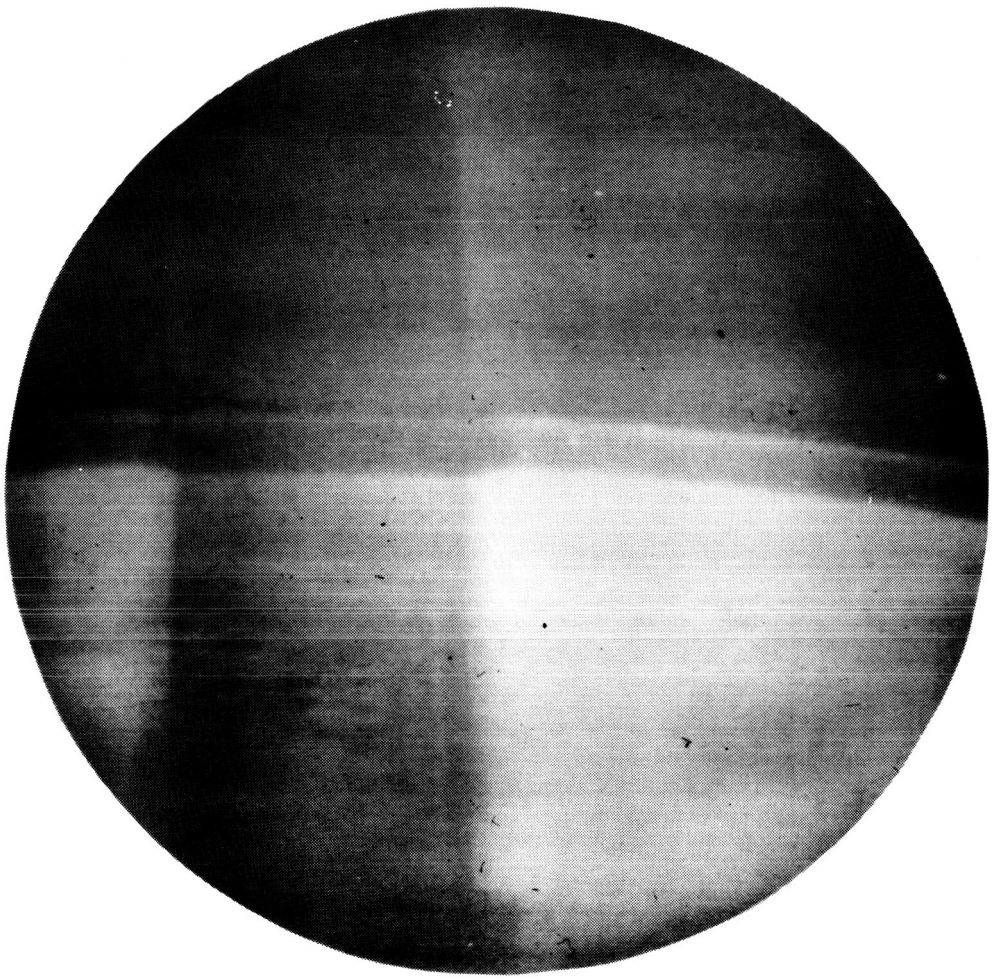

Figure 7. - Exposure 5, looking north during revolution 19; 5-second exposure at f/0.95 (Gemini IX).

Figure 8. - Exposure 18, looking north during revolution 20; 2-second exposure (Gemini IX).

Figure 9. - A 10-second exposure, northward view; the horizon is approximately 15° S and 170° W, and parts of Draco, Cepheus, and Cassiopeia are shown from left to right (Gemini XI).

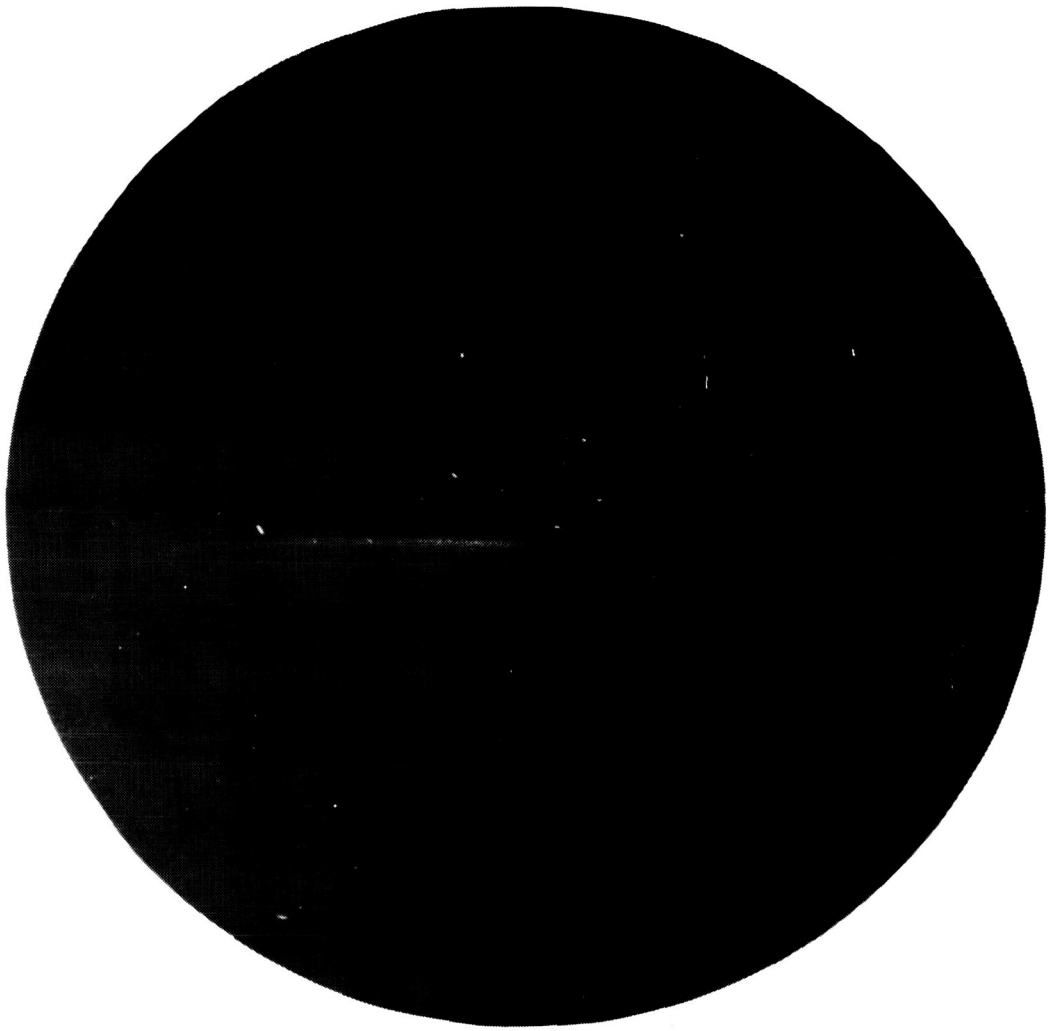

Figure 10. - A 10-second exposure, southward view; the horizon is approximately 40° S and 130° W, and Vela is near the horizon, Carina is above the horizon, and γ Velorum is at the left near the airglow layer (Gemini XI).

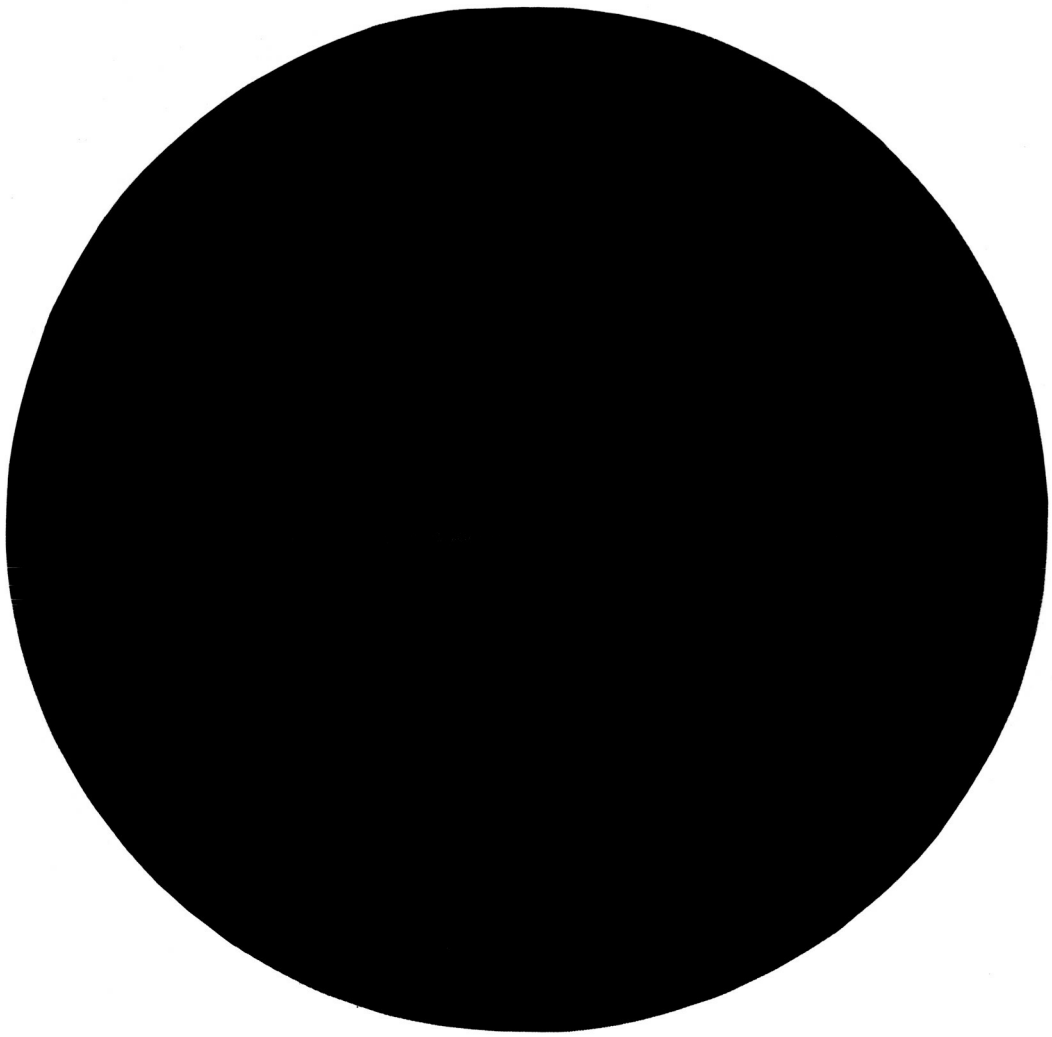

Figure 11. - A 4-second exposure, eastward view over South Africa, made without a lens filter; the horizon is approximately 25° S and 23° E, and Taurus is to the left of center and Pleiades is at the far left (Gemini XI).

Figure 12. - A 3-second exposure (made without filters) of the night airglow (Gemini XII).

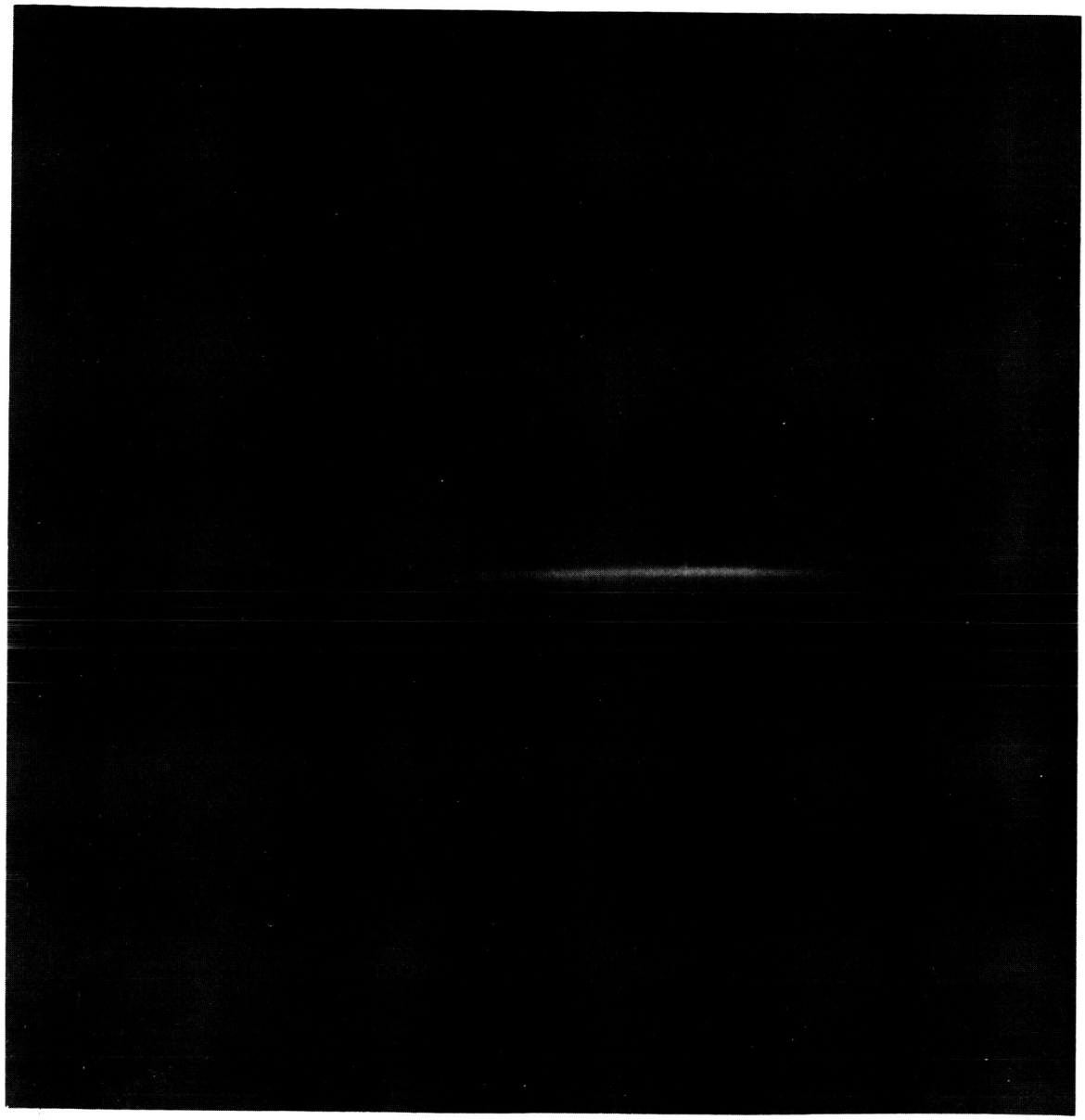

Figure 13. - A 20-second exposure (made with a green interference filter); the airglow does not extend the entire width of the frame, because its emission wavelength is not transmitted obliquely through the interference filter.

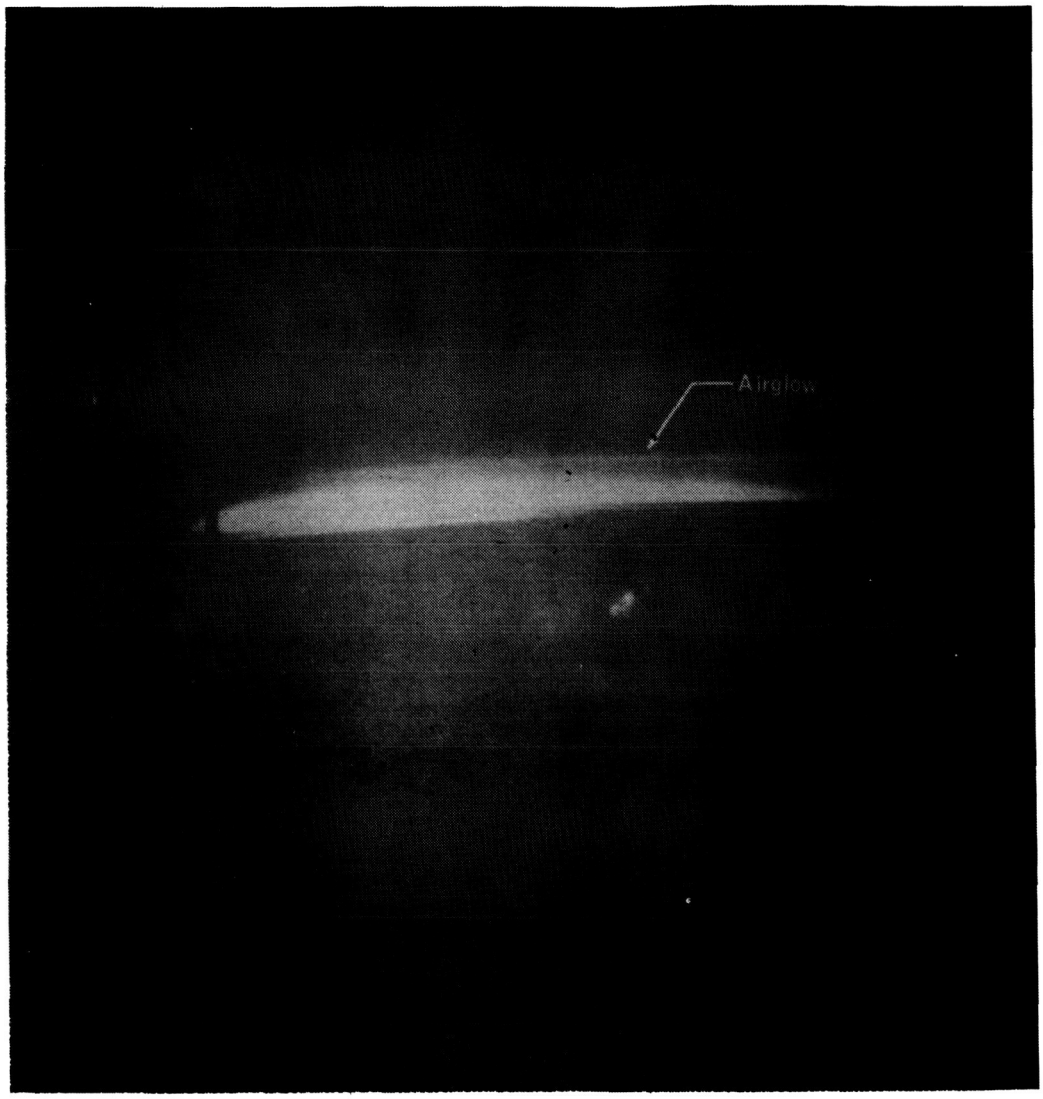

Figure 14. - A 20-second exposure (made with a red filter) taken 4 minutes after sunset; the emission layers probably were caused by the OH radical.

EXPERIMENT D009

SIMPLE NAVIGATION

By Robert M. Silva,* Terry R. Jorris,* and Eugene M. Vallerie III**

INTRODUCTION

Space position-fixing techniques had been investigated by the U.S. Air Force for more than 4 years prior to the flight of Gemini IV. A review of space-navigation and guidance-development programs indicated that most techniques were based on automated systems that had no manual capability. If the automatic space-navigation and guidance equipment or the communications equipment did not function correctly, the man in the spacecraft would have no tools to aid in a safe return to earth. The staff of the U. S. Air Force Avionics Laboratory, Wright-Patterson Air Force Base, Ohio, decided to develop an autonomous manual navigation and guidance technique. The technique offers a backup in case of complete power failure; but the technique can be merged and interfaced with primary automatic systems.

The objective of Experiment D009, flown on the Gemini IV and VII missions, was to collect data on the observable phenomena of space flight that could be used to solve the problem of autonomous navigation by the use of optical data and manual computations to calculate the position of a spacecraft. After completion of the developmental and test phases, the product of the experiment would be a manual-optical technique of orbital space navigation that could be used as a backup to onboard and ground-based spacecraft-navigation systems.

*U.S. Air Force Avionics Laboratory, Wright-Patterson Air Force Base, Dayton, Ohio.

**NASA Manned Spacecraft Center, Houston, Texas.

EQUIPMENT

Navigational instrumentation is shown in figure 1. Interfaced functions in a total-navigation system are shown in figure 2. The experimental equipment consisted of a sextant that had the following general characteristics.

Size, in.	6-11/16 by 5-27/32 by 5-9/16
Weight, lb:oz	5:13
Magnification	×4.5
Field of view, deg	14
Exit pupil, mm	7
Eye relief, mm	21
Diopter adjustment	-2 to +2
Resolution, arc sec	10
Image	Erect
Range, deg	74

EXPERIMENTAL PROCEDURE

The development of a manual space-navigation technique was both classical and logical. Development included the following phases.

Mathematical Analysis and Test

Mathematical analysis was used to reduce the extremely complex orbital-determination mathematics, which were used in automatic systems, to a very simple scheme that could be computed easily by hand (with the use of tables or graphs). One solution involved division of the normal sixth-dimensional problem (fig. 3) into two separate and distinct three-dimensional problems. The first three-dimensional solution would facilitate simple determination of the orbit size and shape; the second three-dimensional solution would facilitate calculation of orbit orientation.

The measurements that are requisite for implementation of this mathematical solution are quite simple. The first measurement needed is the altitude above the earth, and from this value, the angle from the center of the earth to the horizon can be computed. The second measurement needed is the coaltitude of a star; that is, the angle from the spacecraft zenith to the star (fig. 4). If the altitude above the

earth can be determined, the angle between the local vertical and the horizon can be determined. Combine knowledge of the altitude above the earth with an angular measurement from horizon to star, and the coaltitude may be determined simply.

Before the instruments were designed, the mathematical procedure was tested on board a KC-135 aircraft (fig. 5). It may seem strange that an aircraft was used in the solution of an orbital problem, but the manner in which the flight test was accomplished makes this somewhat more logical. The aircraft was flown from South America to Africa along the equator at a constant altitude of 35 000 feet. Thus, it could be assumed that the size and shape of the orbit was known exactly. With a circular orbit 35 000 feet above the earth, the calculated orientation could be tested against the known orientation of the equator. A standard aircraft sextant (fig. 6) was used for coaltitude measurements.

From these coaltitude measurements, the trace of the aircraft zenith on the celestial sphere was related to the earth; and this trace was compared with the equator (fig. 7). The results were much better than were predicted. The best results indicated an angular deviation of only 1 minute of arc, whereas the maximum angle deviation was only 14 minutes of arc. After the successful completion of this developmental phase, work was begun on the development of a space sextant and space stadimeter (optical altimeter).

Instrument Development and Construction

The field of view necessary for the crewmember to identify stars readily was a prime concern. A crewmember does not have the directional and attitudinal reference that aircraft or ship navigators have on earth. To simulate this situation, a navigator was placed in a test facility, and the attitude variations were simulated by movement of a star field relative to the navigator. This resulted in disorientation (fig. 8). If a field of view less than 14° were used, it took an inordinately long time for the navigator to identify stars. Identification was extremely difficult when the field of view was less than 20°. The first hand-held space sextant (fig. 9) weighed 8 pounds, was extremely rugged, and was similar to the standard sextant that is used on board all naval vessels. However, the field of view was larger and the light-gathering power was greater for the space sextant. Design of the stadimeter was more difficult. A classical way to measure the altitude above the earth would be to make angular measurements from one earth limb to the other earth limb. Half this angle could then be used to determine the angle from the horizon through the spacecraft to the center of the earth. Of course, this is extremely difficult for the near-earth orbit. When the angle subtended by the earth limb approximates 180°, the observations through a window become impractical for the hand-held instrument because of the infringed field of view. Therefore, it was decided that a unit should be developed which generates an angular measurement when three cardinal points on the horizon are alined by adjustment of instrument controls.

Flight Test

The next developmental phase was the actual test of the instruments during the Gemini Program. It was decided to fly the hand-held sextant on the Gemini IV and VII missions to acquire the needed information.

Gemini IV and VII Missions

The first portion of the experiment was the evaluation of the operational suitability of the space sextant and the acquisition of quantitative data for determination of the accuracy limits of the sextant for optical rendezvous measurements. This portion of the experiment was of primary interest to persons involved in the Apollo Program. It was predicted that the objective could be obtained by making angular measurements between known stars and by making angular measurements between a known star and the Titan booster during the planned rendezvous with the booster.

The second portion of the experiment involved the study of various star and horizon phenomena and specific star-to-horizon measurements to obtain data for postflight calculations and accuracy determinations of navigational position. This portion of the experiment was of primary interest to Air Force personnel. There were two basic space phenomena that appeared to be most stable and useful for space-navigation purposes. These were the blue haze and the 5577-angstrom green emission line. Also, there was the normal day horizon and the nightshade differentiation between the black of the dark earth and the black of space behind the earth. The sextant was equipped with neutral-density, blue-haze, and 5577-angstrom filters so that the horizons could be accentuated during specific sightings.

RESULTS

A large number of measurements were made. The results are divided according to mission, for convenience of discussion.

Gemini IV Mission

There were 160 scheduled star-to-horizon measurements with the 5577-angstrom green emission line at night, and with both the natural and blue-haze horizons during the day. Real-time flight-plan changes necessitated that these sextant sightings be performed later in the mission than was scheduled orginally. On the first daylight sequence, it was noted that the selected stars were not visible on the daylight side of the orbits. Thus, all sextant sightings were made on the nightside of the orbits, and no evaluation of the blue filter and blue-haze horizon could be made. The change created other problems, because the stars that were selected for the original star-to-horizon measurements were not all time phased for the nightsides of the orbits. This required the crewmembers to deviate to a real-time sighting. There were 45 star-to-horizon sightings accomplished to the natural night horizon and to the 5577-angstrom green emission line. Measurements to the green emission line airglow layer were made

with and without the special filter. The green emission line was more defined when the filter was used. Measurements were made to the top, middle, and bottom of this layer. However, failure of a timing device, external to the instrument, precluded obtaining any useful navigation measurements.

Rendezvous with the booster was not accomplished; therefore, the scheduled star-to-launch vehicle sightings were not performed. Of the 50 scheduled star-to-star measurements that were programed, 47 measurements were recorded. An evaluation criterion of the man-sextant operational capability was the accuracy with which the measured angle between two stars could be repeated. The repeatability of these star-to-star measurements was limited only by the read-out accuracy (30 arc seconds) of the sextant. Significant data are summarized in table I.

Valuable qualitative information was obtained on the availability of the observable phenomena. This information is summarized as follows.

1. Stars to the fifth magnitude were visible at night; constellations were identified easily.

2. Although stars were not visible during the day portion of the orbit, the Gemini IV crewmen predicted that stars would be visible by the use of a dark-adapted eye and a shaded window.

3. The launch-vehicle lights were visible at night and in daylight (when within range).

4. Observation of the thickness and number of the horizons that were used for sightings made it possible to determine the best horizon-filter combination for particular conditions.

Gemini VII Mission

The spacecraft was stabilized small-end forward, stars were acquired and identified, and two star-to-horizon angles were measured. Then, a left yaw was established, and upon alinement of the spacecraft in a position 90° to the orbital path, two additional measurements were made on the same star pair. The final measurements on the two stars were made with the spacecraft positioned blunt-end forward. Each measurement consisted of a selected set of two stars (called a sequence) and the use of a particular filter (called a mode). Five measurement sequences were planned for the flight. To adapt the work schedule for ease of real-time flight planning, all selected stars were time phased; launch time was used as a base.

During the flight, sequences and modes were called up as desired. The time allotted for each sextant measurement (based on the Gemini IV mission experience) was in excess of that required. As a result, the crewmen were provided time for additional measurements, and they gathered a large amount of additional data.

Experiment D009 was successful from a procedural standpoint. The sextant operated flawlessly, and measurements of angles as large as 51.155° were obtained

easily. Eight to 10 measurements were made per pass, whereas only six measurements per pass had been requested. The total number of measurements that were obtained is as follows: 37 star-to-horizon, five planet-to-moon limb (or star-to-moon limb), six star-to-star, and eight zero measurements on stars. Crewmember performance was excellent.

Interesting variations in the observations were recorded. The bright moon caused problems with star acquisition and identification when stars were near the moon. The 5577-angstrom airglow horizon was not as distinct as was recorded on the Gemini IV mission, and neither crewmember was able to see a 5577-angstrom horizon with the green filter. This was the first inspection of seasonal variations in the 5577-angstrom horizon. Most horizon measurements were made to the moonlit natural earth horizon, which presented a more distinct line than did the airglow.

The procedures used, the operation of the sextant, and the performance by the crewmen under orbital conditions were successful. Examination of the raw data is indicative that a sufficient number of navigation measurements can be made with the sextant. However, horizon determination still is a problem. During the Gemini IV mission, a definite 5577-angstrom horizon was found and used. No such horizon appeared during the Gemini VII mission. The stability of the observables, which establish system accuracy, needs further investigation. Additionally, the stadimeter, which was built and qualified but was never flown, should be used in space prior to integration with other manual space-navigation-system components. Thus far, experiment results are indicative of successful integration; total system operation can be expected.

BIBLIOGRAPHY

Silva, Robert M.; Jorris, Terry R.; and Vallerie, Eugene M., III: The Air Force Space Navigation Experiment on Gemini (DOD/NASA Gemini Experiment D-9, Gemini IV and VII Flights). AFAL-TR-66-289, 1966.

Bazhinov, I. K.: Method of Autonomous Guidance During Flights in Near-Planet Orbits. NASA TT F-9542, May 1965, p. 1191.

Lampkin, Bedford A.: Sextant Sighting Performance for Space Navigation Using Simulated and Real Celestial Targets. Navigation, vol. 12, winter 1965-66, pp. 312-320.

Anon.: Space Position Fixing Techniques Phase I. AFSC, Wright-Patterson AFB, Ohio, Rept. no. ASD-TDR-63-521, Apr. 1963.

Silva, R. M.; and Jorris, T. R.: The USAF Manned Space Navigation Experiment on Gemini and Its Implications on MOL. In Navigation for Manned Space Flight, 1964 Space Navigation Conference, St. Petersburg, Florida, April 30 and May 1, 1964, pp. 109-132.

TABLE I. - SIMPLE NAVIGATION DATA FROM GEMINI IV

Apollo Program interest sightings (star to star)	47
Repeatability, arc sec	30
Stars used	6
Maximum angle, deg:min	21:36
Air Force interest sightings (star to horizon)	45
Useful horizons, natural earth, and 5577-angstrom emission line	2
Stars used	11
Maximum angle, deg:min:sec	31:3:30
Number of green horizon layers observed	2
Thickness of 5577-angstrom layer, deg:min	2:42
Star transit time through green layer, sec	49.5
Star transit time, from first appearance to top of green layer, min:sec	3:23

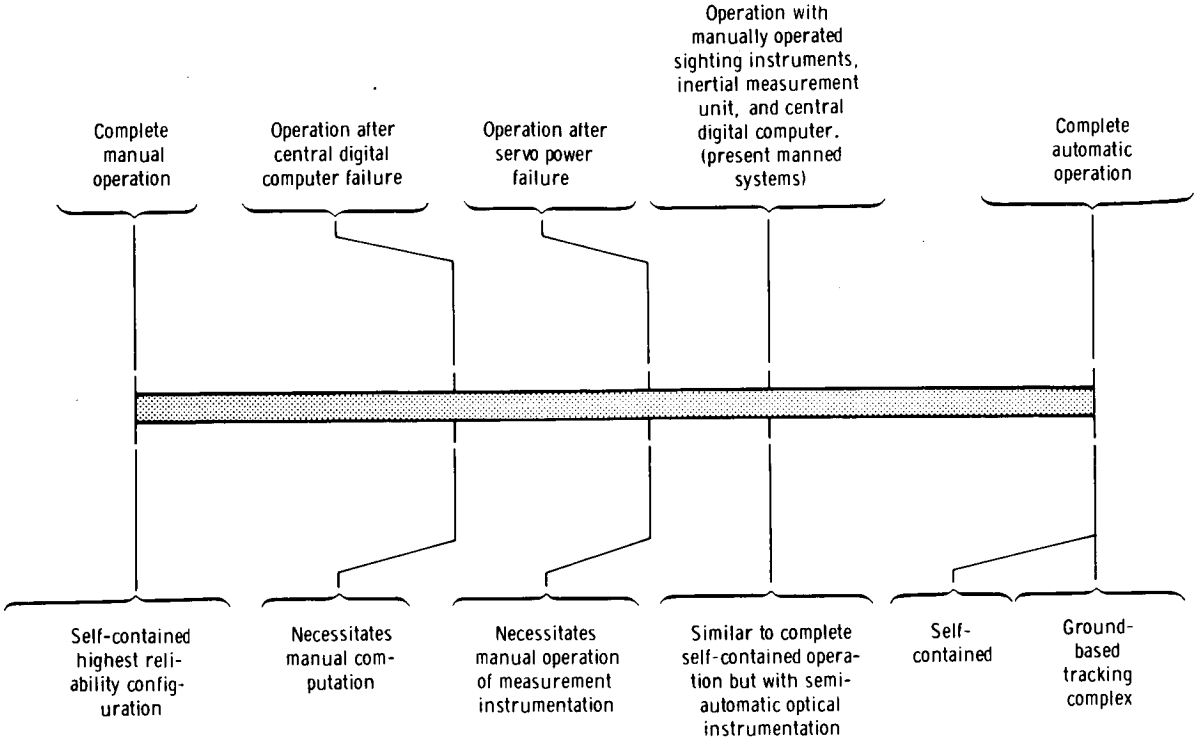

Figure 1. - Functional diagram of navigation instrumentation.

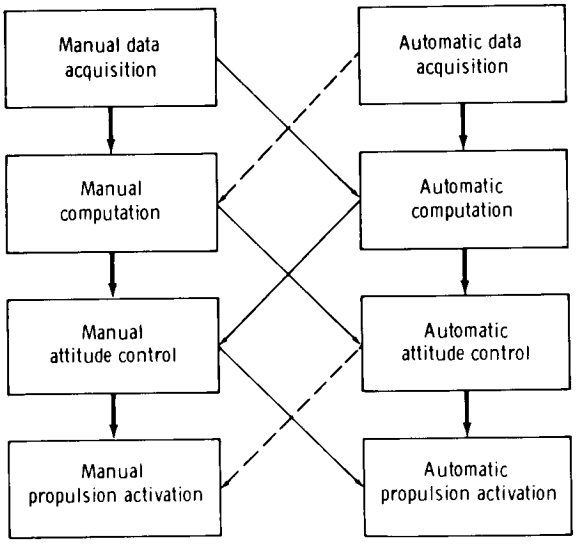

Figure 2. - Interfaced functions in a total-navigation system.

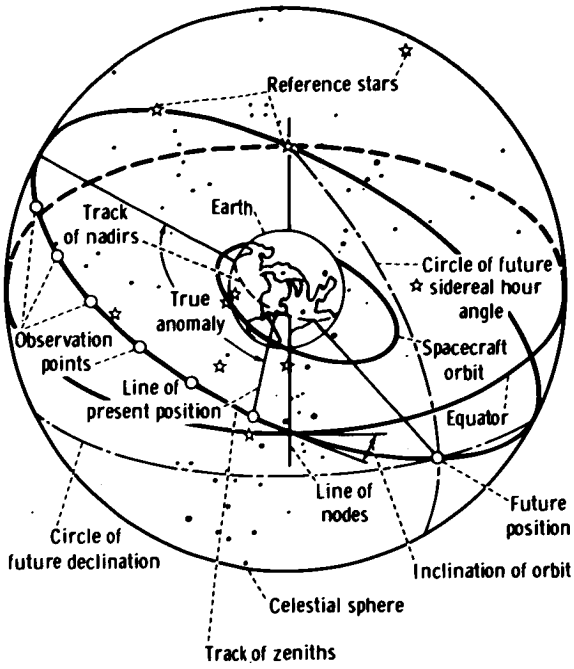

Figure 3. - The geometry of the orientation-parameters problem.

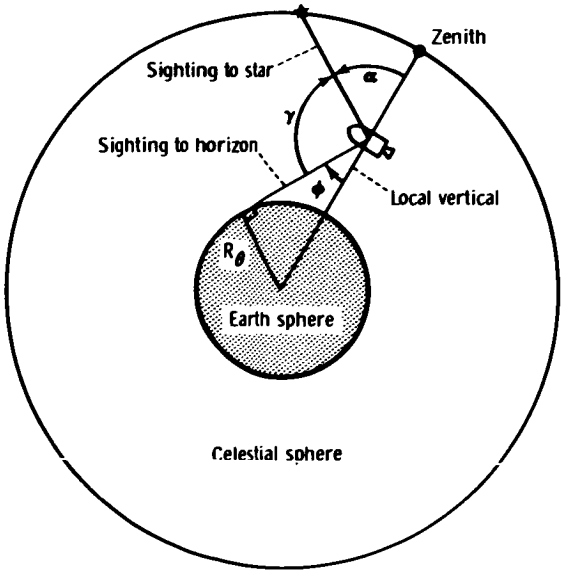

Figure 4. - Star-coaltitude-determination geometry.

Figure 5. - The KC-135 aircraft that was used to simulate the orbital problem.

Figure 6. - The standard aircraft sextant used to simulate the orbital problem.

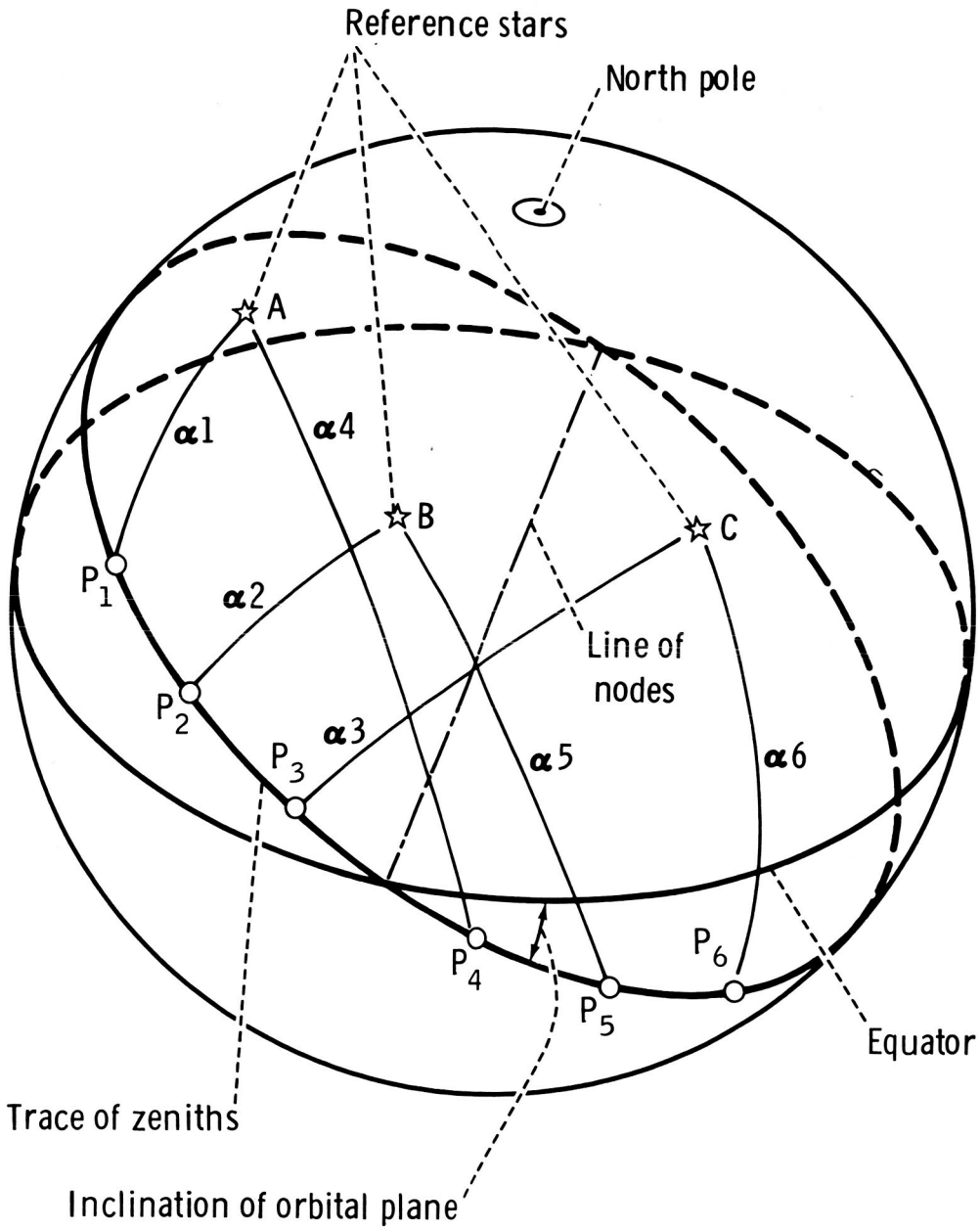

Figure 7. - The geometry of the graphical solution.

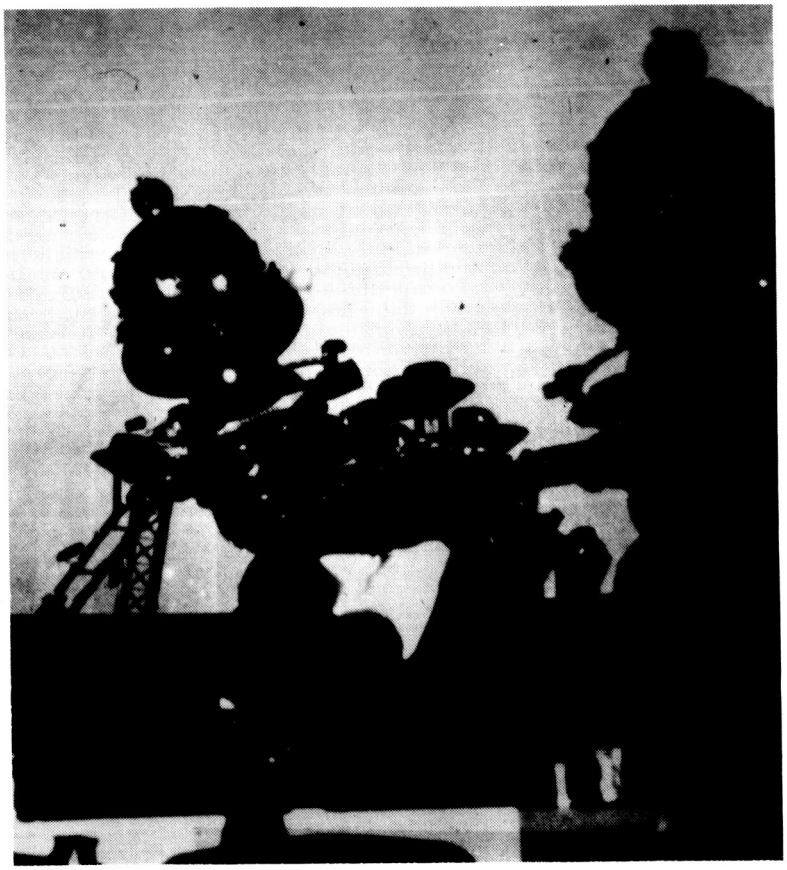

Figure 8. - The disorientation equipment.

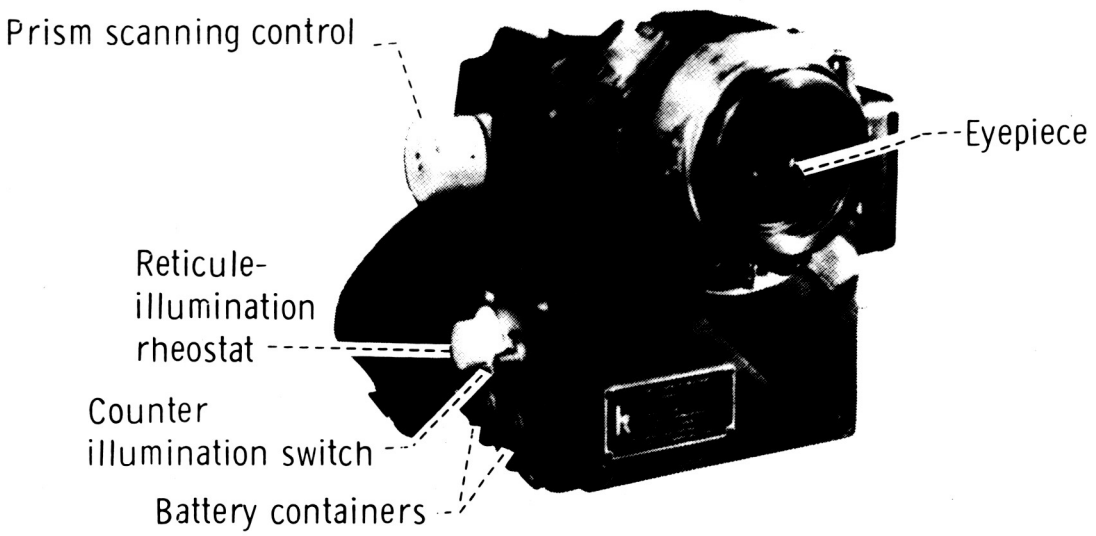

Left side-rear view

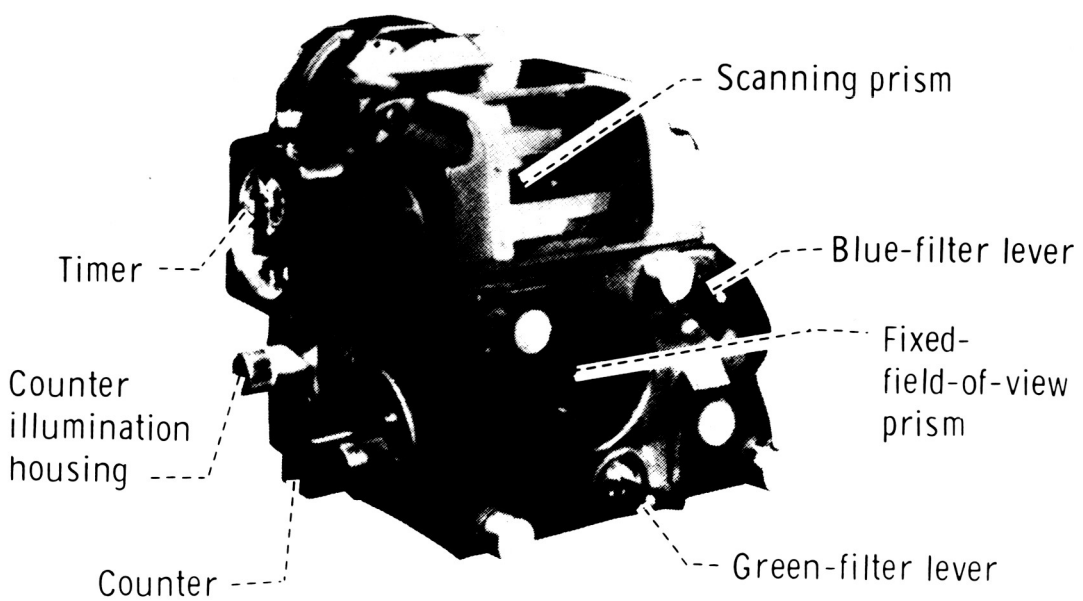

Right side-front view

Figure 9. - The Mod-1 space sextant.

EXPERIMENT D005

STAR-OCCULTATION NAVIGATION

By Robert M. Silva,* Terry R. Jorris,* and Eugene M. Vallerie III**

The objectives of Experiment D005, which was flown on the Gemini VII and X missions, were to determine the usefulness of star-occultation measurements for space navigation and to determine a horizon density profile which could be used to update atmospheric models for horizon-based measurement systems. The time of occultation of a known star by a celestial body, as seen by an orbiting observer, determines a cylinder of position, the axis of which is the line through the star and the body center, and the radius of which is equal to the occulting-body radius. The times of six occultations are used to determine uniquely all orbital parameters of the orbiting body. Determination of these occultation times from the earth is difficult because of atmospheric attenuation of the starlight. The star does not disappear abruptly but dims gradually into the horizon. The dimming percentage, with respect to the altitude of this grazing ray from the star to the observer, is a percentage altitude for occultation. That is, the star can be assumed to be occulted when it reaches a predetermined percentage of its unattenuated value. The procedure used in Experiment D005 would be the means of measuring this attenuation with respect to time to determine the usefulness of the measurements for autonomous space navigation. Also, the measurements would facilitate determination of an atmospheric-density profile, which could be used to update the atmospheric model for this system and to refine models used for other forms of horizon-based navigation, orbit predictions, and missile firings. Instrumentation for Experiment D005 was designed to gather experimental data on star occultations over the entire attenuation phenomena. This experiment was designed to make maximum use of human capabilities in orbit, the result of which would be the simplest and most reliable systems. In this experiment, the crewmembers had to accomplish star acquisition, identification, calibration, and tracking. Instrumentation was required only for measurement of the relative intensity of the star as it set into the atmosphere.

EQUIPMENT

The star-occultation photometer was a single-unit, dual-mode, hand-held, externally powered instrument that was used for electronic determination of the extent to which the sight line to a selected star penetrated a planetary atmosphere. The contrast of a sun-illuminated ground target also was measured with the photometer. Data from

*U. S. Air Force Avionics Laboratory, Wright Patterson Air Force Base, Dayton, Ohio.

**NASA Manned Spacecraft Center, Houston, Texas.

the instrument, when calibrated correctly and plotted against time, result in the attenuation curve of a star (passing through the earth atmosphere) relative to an unattenuated intensity. The general characteristics of the equipment are as follows.

Size, in.	5 by 5 by 3
Weight, lb	2.5
Volume, in^3	30
Magnification	× 6
Image	Erect

The optical system of the star-occultation photometer was a dual-path-type system, separated on a wavelength basis by a dichroic reflector. One path conducted the short-wavelength star spectrum (0.4 to 5 microns) to the photomultiplier cathode; the remainder of the starlight continued into the eye of the operator. The electronic system consisted of a photomultiplier detector, preamplifier, active bandpass-filter amplifier, and postfilter-amplifier demodulator in the carrier-signal section. A unijunction oscillator and flip-flop were used to generate two-phase 100-hertz power for the size-5 hysteresis-synchronous modulator motor. Input power was regulated to the motor, and additional voltage supplied an isolated lower voltage to the signal circuitry and supplied a high voltage to the photomultiplier. The output of the low-pass filter was conducted to the input of the Schmitt trigger-level detector, which was biased at approximately 1 volt. Depression of the CALIBRATE button inserted a nominal 5 to 1 attenuator in both the day and the night signal paths and lowered the full-signal amplitude from 5 volts to 1 volt for calibration. The photometer was readied for use by plugging in one cable for power and one cable for high-level telemetry, and by placing the mode switch to NIGHT. The optical characteristics of the instrument are summarized as follows.

Lens system	Aperture	Focal length, in.	Wavelength, Å	Magnification
Objective	32 mm	4.6	3500 to 7000	--
Eyepiece	0.788 in.	.73	5000 to 7000	× 6
Path 1	.2 in.	.33	3500 to 5000	× 1/16
Path 2	.4 in.	.277	--	--

The photometer is shown in figure 1. The photometer that was used on the Gemini X mission was an instrument which had been refurbished and recalibrated after inflight

failure during the Gemini VII mission. The failure was caused by loose particles in the photomultiplier tube. A stringent quality-control program, designed to facilitate identification and enumeration of all loose particles, was instituted in preparation for the Gemini X mission. Each photomultiplier tube considered for use was examined microscopically, and all particles were sized to ensure that the aggregate was not larger than the smallest element spacing in the photomultiplier tube. Because the equipment functioned as designed on the Gemini X mission, these quality-control measures apparently had the desired effect.

EXPERIMENTAL PROCEDURE

Star-occultation measurements were made by identification, acquisition, and tracking selected stars in the 0.5° reticle of the 10° field of view of the photometer. The light intensity of the star was normalized to the 5-volt telemetry output by depression of a CALIBRATE button and adjustment of the gain to drive the reticle light to an alternating red-green condition. When the light intensity had been normalized, the button was released, and the star was tracked as it disappeared into the horizon. The star intensity was measured, recorded, and time-correlated on the onboard high-level telemetry tape for postflight analysis. On any night pass, four to six stars were to be acquired, calibrated, and tracked to occultation; and the star name and approximate time of occultation were to be recorded in the flight log for postflight correlation with tape data and ground-track information. Timing marks were recorded on the telemetry (by use of the CALIBRATE button) on some runs to time special selected observations, such as the time a star passes through the top of the airglow. A mode-D procedure was established before printing of the final Gemini X mission plan. This mode necessitated use of the spacecraft computer and photometer data for real-time orbit navigation determination. This solution was to be compared with ground-track data to determine how well the orbit was established by the onboard technique.

RESULTS

Gemini VII Mission

The photometer collected no useful data because of a malfunction. Subsequent to the initial failure report from the Gemini VII mission, a photometer check was performed by the crewmembers; all light was occluded from the instrument. The results were inconclusive. A second test on two bright stars was indicative that the instrument was operating in a degraded mode. However, tests using Venus and Jupiter were indicative that no data could be obtained from the night mode of operation, even with all spacecraft radio equipment turned off to eliminate possible radio-frequency interference. When the results of a day test confirmed the conclusion that no data could be obtained, all photometer operations were suspended. During the Gemini VII mission, the backup photometer was obtained from Cape Kennedy, Florida, and tests were performed to determine the nature of the flight problem and to duplicate the failure modes. Generally, these tests were inconclusive, but they resulted in some possibilities which were forwarded to the Gemini VII crewmen. Some photometer damage could have occurred if it had been passed through direct sunlight; however, corrections for this had

no effect on the Gemini VII photometer. The possibility of radio-frequency interference from a frequency not carried on board the spacecraft (possibly because of harmonics) was investigated on the ground, and a correction was attempted in space by silencing all radio equipment for one test. There was no effect on the Gemini VII instrument. Ground-based test of the backup photometer, performed during the mission, did not result in isolation of the failure mode nor did the test result in proper corrective action. When this was determined, the backup-instrument tests were abandoned. Postflight analysis of the Gemini VII photometer was performed initially at the NASA Manned Spacecraft Center (MSC). The problems were isolated in the phototube. A direct short existed between a 900-volt line and the signal line. This explained the total saturation indication of all successive stages of signal amplification and accounted for the inflight malfunction indication. Because facilities were not available for complete analysis of the phototube at the MSC, the equipment was flown to contractor test facilities for a detailed analysis. Roentgenograms and photographs were taken at each stage of the examination. Microscopic analysis revealed a piece of metal between the cathode shield and dynode 9 (at -900 volts), which caused the short to the signal line (fig. 2). The metal particle was photographed in position; then current was applied through the short. When the metal was removed, the shorted condition no longer existed. Analysis of the tube was indicative that similar material existed in the welded lead connections. Vibrations or normal usage could have dislodged a small piece of the weld spatterings, which normally would have fallen harmlessly to the bottom of the tube. However, in a zero-g environment, the piece would float and be drawn into a region of high potential. If the element spacing were approximately the same size as the particle, a short would occur. If dislodged, the particle probably would float back into the same high-potential region. After determination of the exact cause of the phototube malfunction, an examination was made to establish a means for elimination of problems of this type. The following procedures were established.

Manufacturer quality control. - Additional specifications and procedures were developed to minimize the possibility of foreign particles in the tubes.

Factory examination. - The tube was to be examined microscopically for evidence of small particles and the possible source of particles.

Special environmental testing. - A special operating vibration test, that involved turning the tube in three axes, was conducted on each tube to dislodge any loose particles and to drop any such particles through the tube elements. Voltage variation across the elements during the test, or discovery of particles after the tests, disqualified a tube.

Gemini X Mission

The photometer was used twice during the Gemini X mission. The first time was at 26:30 g. e. t. while the spacecraft was docked with the Gemini Agena target vehicle (GATV); the second time was at 64:46 g. e. t. after the spacecraft and the GATV had separated. During the first attempt to perform the experiment in mode A (calibration), difficulty was encountered in vehicle-attitude control because of the docked configuration. Because of control problems, only five stars were tracked to total occultation. Because a minimum of six stars was required for complete computation, a total solution was not obtained.

A problem was encountered in tracking stars through the airglow. As the stars passed through the green-glow layer, they disappeared momentarily. When acquisition was lost, the pilot discontinued sighting through the photometer until the stars reappeared below the green glow; then tracking was resumed until the stars disappeared into the lower, dark horizon. Excessive attitude-control gas expenditure during this procedure resulted in cancellation of further experimentation until after undocking.

The second experiment attempt was a mode-D sequence in the undocked configuration. No difficulties were encountered on this run regarding acquisition and tracking of seven stars to occultation. However, procedural difficulties were encountered in introduction of the visual occultation data into the computer. Computation of an orbit solution was precluded because of improper entry of the right ascension and declination of the last star and because of computer workload problems encountered after measurement of the fourth star. A calibration check on three stars in Cygnus was not accomplished properly on either attempt. An attempt was made to calibrate on each star independently, rather than to retain one gain setting. This did not affect the use of the occultation technique for navigation but was included to aid in data analysis and reduction.

Visual occultations through the photometer reported by the pilot were somewhat different from occultations reported by the command pilot. The command pilot could still observe some stars visually after the pilot had reported their disappearance. The phenomenon probably was caused by the selective reflection within the instrument, which was designed to pass maximum blue light to the photomultiplier tube.

Representative telemetry plots of normalized starlight intensity are given in figures 3 to 5. A considerable amount of information can be derived from a visual analysis. In figure 3, the constant-output portion of the Vega curve can be seen clearly; this flat portion of the curve corresponds to the time the line of sight to the star remained above the earth atmosphere. As the line of sight to the star began to pass through the upper portion of the atmosphere, the apparent intensity of the star began to diminish (point A). In the lower portions of the atmosphere, the downward slope approximated a straight line (point B to C), until the star seemed to disappear into the background. In the straight-line portion, a time of percentage attenuation (accuracy of approximately ±0.5 second) can be discerned visually. The visual method of occultation-time determination would limit the accuracy of the navigation solution to 2.5 nautical miles; however, if computer smoothing techniques were used (as is anticipated for operational use), greater accuracies are achievable. Initial results of introduction of the occultation voltages into a computer for smoothing prior to calculation indicate time determination accurate to 0.1 to 0.2 second. Orbit solutions, based on these Gemini X timing accuracies and star occultation sequences (as outlined in the Gemini X mission plan) would have provided navigation accuracies of approximately 1 nautical mile root mean square.

Procedures for occultation measurements are visible in traces from Arcturus, shown in figure 4. The photometer was turned on at point 1. Calibration began at point 2 by depression of the calibration button. Between points 2 and 3, calibration was being accomplished; when calibration was complete (point 3), the button was released, and the photometer output jumped to the normalized 5-volt level. Sixty seconds later, the intensity began to decrease rapidly. The noise apparent on the intensity

signal was greater for the measurements to Arcturus than to Vega, although both stars were of the same approximate magnitude. The effect was anticipated because the photometer was constructed to be sensitive only to the 0.4 to 0.5 micron (or blue visual) light, and Arcturus was a predominantly red star. With the existing photometer, stars of second magnitude and slightly lower can be used easily, as shown in figure 5. The trace from Denebola was well defined and showed a clear slope for time of occultation determination. The equipment functioned properly, which was indicative that the stringent quality-control procedures established after failure of the photomultiplier tube on the Gemini VII mission were justified. The compact design of the equipment facilitated exhibition of the versatility of the instrument when used during the docked configuration. The possibility of using the photometer, suitably modified for direct inputs into the spacecraft computer, for onboard orbit determination was verified. The use of direct inputs into the spacecraft has advantages of simpler programing, no analog-to-digital conversion in the computer, and simpler system integration. However, some accuracy would be sacrificed. The star-occultation technique is accurate and flexible, and is a useful technique for automatic (for example, incorporation with star trackers), semiautomatic, or aided manual-navigation applications.

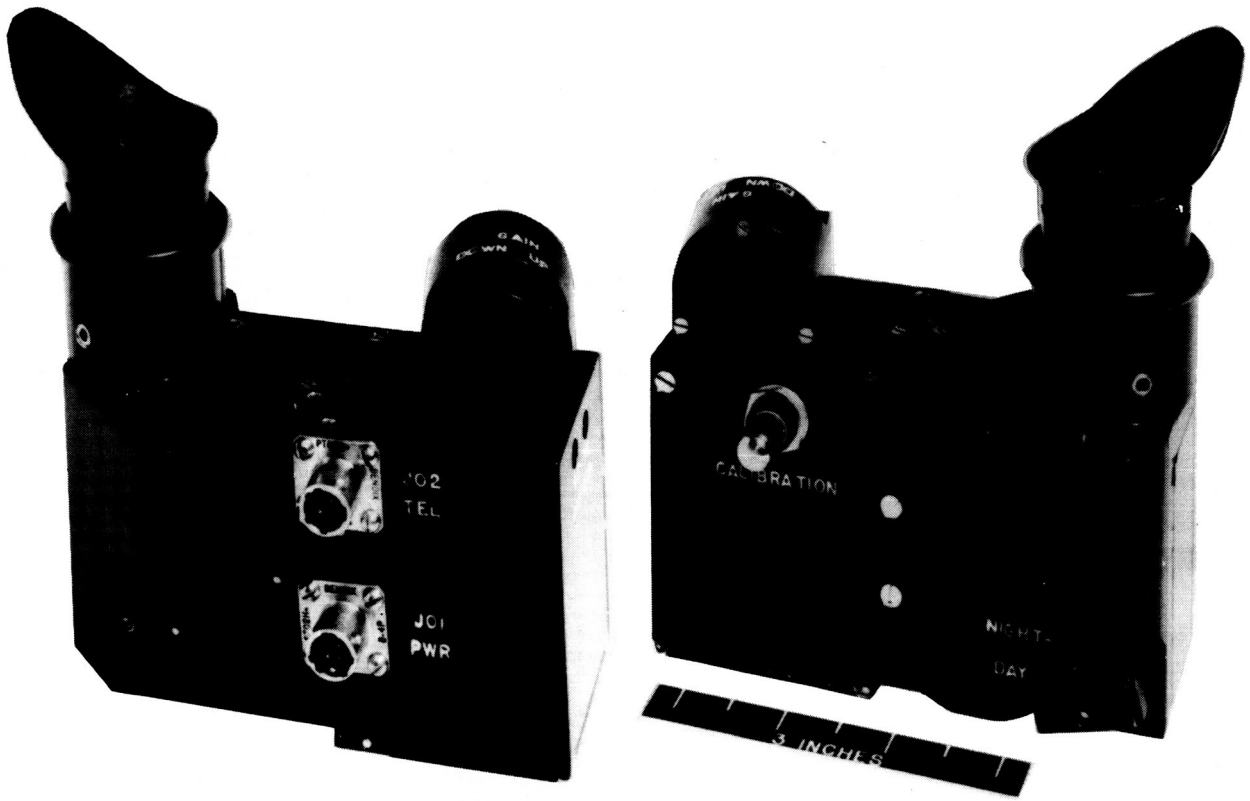

Figure 1. - The star-occultation photometer.

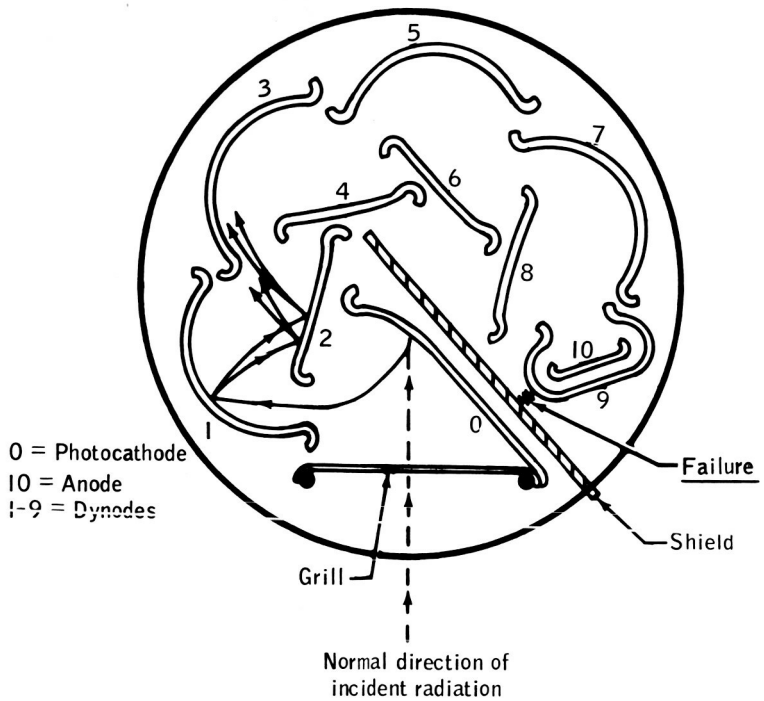

Figure 2. - The location of the photomultiplier-tube failure.

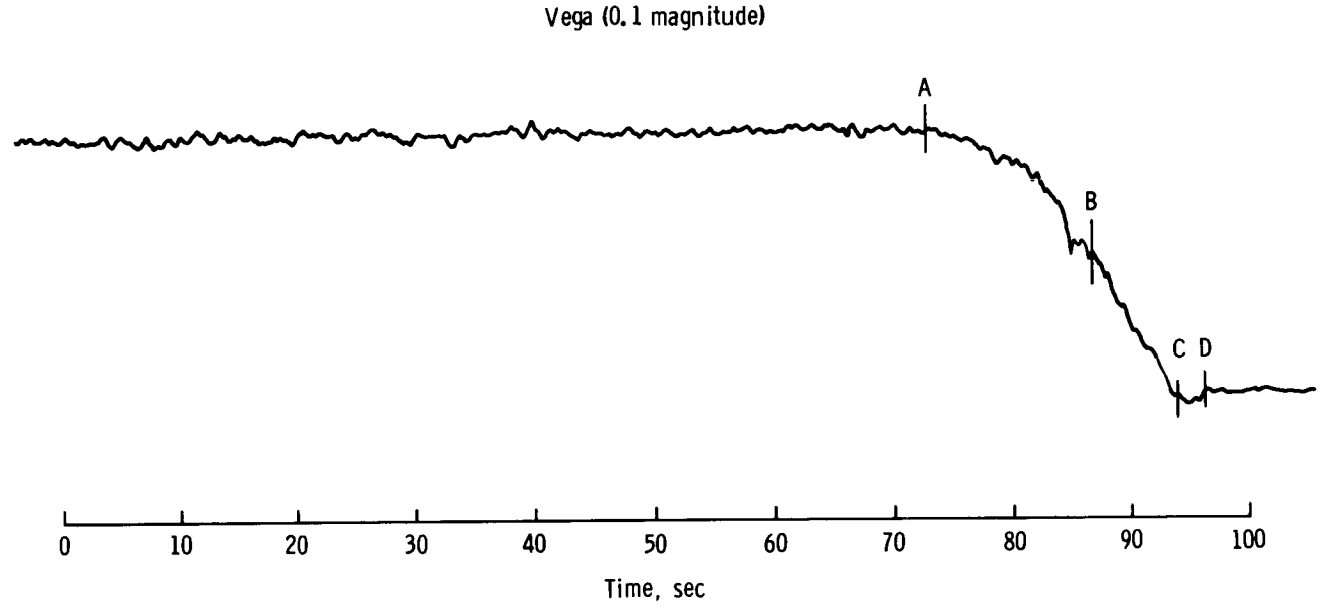

Figure 3. - The telemetry-intensity profile of Vega.

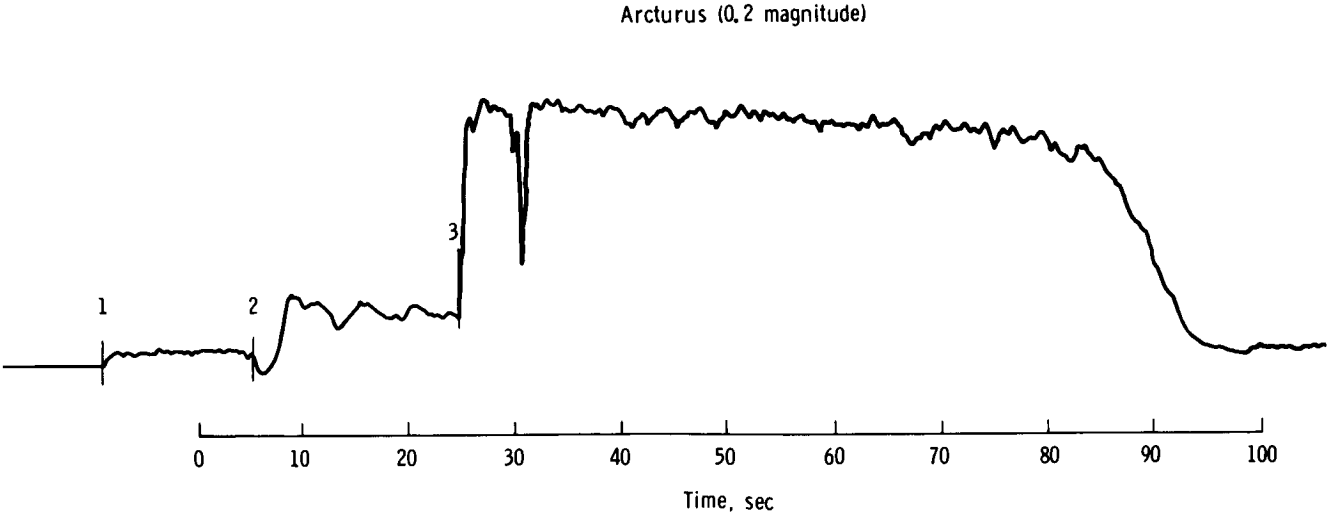

Figure 4. - The telemetry-intensity profile of Arcturus.

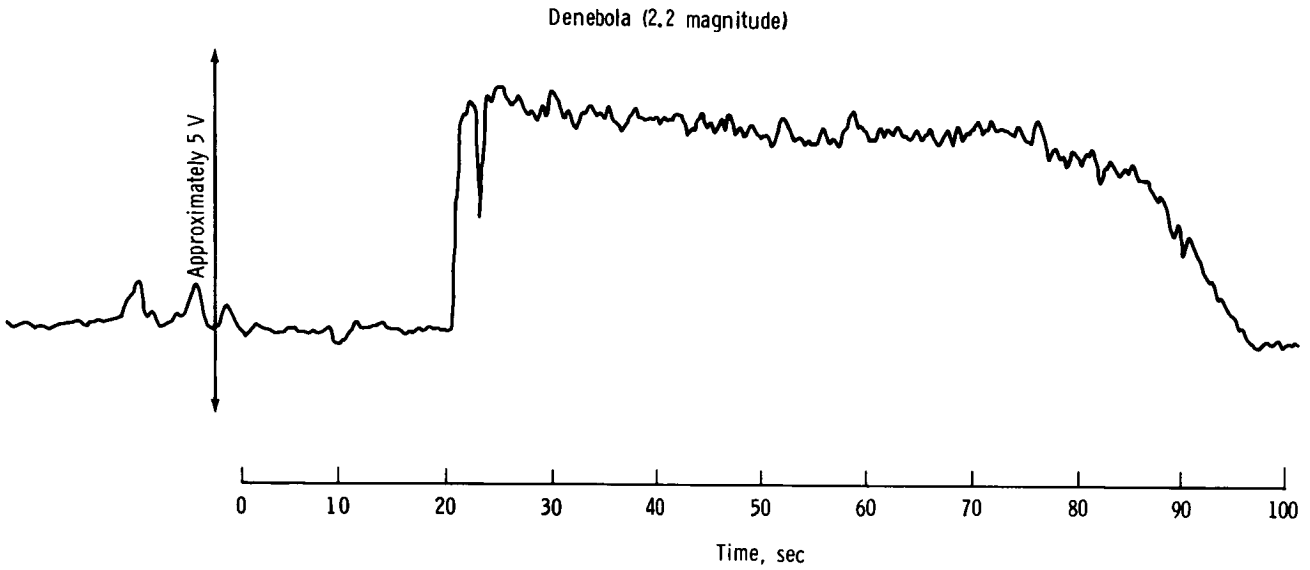

Figure 5. - The telemetry-intensity profile of Denebola.

EXPERIMENT T002

MANUAL NAVIGATION SIGHTINGS

By Donald Smith*

INTRODUCTION

The general objective of Experiment T002 was to make navigation-type measurements, through the window of the stabilized Gemini XII spacecraft, by the use of a hand-held sextant. The major objectives were as follows.

1. To evaluate the ability of the crewmen to make accurate navigational measurements by the use of simple instruments in an authentic space-flight environment

2. To evaluate the operational feasibility of the measurement techniques by the use of the pressure suit with the helmet off and with the helmet on and the visor closed

3. To evaluate operational problems associated with the spacecraft environment

4. To validate ground-based simulation techniques by comparison of the inflight results with base-line data obtained by the pilot by the use of simulators and celestial targets from ground-based observatories

EQUIPMENT

The equipment used in this experiment was a two-line-of-sight optical sextant (fig. 1). The sextant was designed to measure accurately the angle between various types of celestial targets. The view through the fixed line of sight of the sextant was imaged in the focal plane through a plate beam splitter, an objective lens, and a prism-mirror erecting system (fig. 2). The view through the scanning field was reflected from an articulated scanning mirror; then the view was combined with the fixed field in the beam splitter and was imaged in the focal plane by the same objective lens and erecting system. By observation of the focal plane through the eyepiece and adjustment of the scanning fields of view, the operator could superimpose the selected targets in the fixed and scanning fields of view, and thus could establish the angular separation of the targets. The angular rotation of the scanning mirror was controlled by means of the two-speed scanning control knobs, which provided target optical motions of 1° and 5° per revolution of the knobs.

*NASA Ames Research Center, Moffett Field, California.

The sextant was equipped with two removable eyepieces, one which had normal eye relief and one which had long eye relief. The normal-relief eyepiece was used when the sextant could be brought directly to the eye for viewing, whereas the long-relief eyepiece facilitated the use of the sextant with the pressure suit helmet on and the helmet visor down.

Data read-out was accomplished by direct reading of a mechanical counter located below the instrument eyepiece. The measured angle between the fixed and the scanning line of sight was indicated on the counter in degrees and thousandths of a degree, the smallest count being 0.001° (3.6 arc seconds). A dual-cell rechargeable nickel-cadmium 2.5-volt battery was contained within the sextant, and was used for illumination of the data read-out and the reticle.

An event-timer button and switch were located on the right side of the instrument. The event-timer switch was connected to the spacecraft telemetry recorder by means of the utility cord. Depression of the event-timer button placed a time-correlated signal on the onboard pulse-code-modulation recorder tape for use in the data analysis.

Two filters of different density were provided in each line of sight to reduce the amount of transmitted light. The filters facilitated viewing images of widely varying intensities, such as a star and a lunar landmark. The general characteristics of the sextant are shown in table I, and the preflight calibration of the instrument is shown in figure 3.

PROCEDURES

The experiment was performed during the dark periods of revolutions 40, 48, 54, 55, and 56 on the Gemini XII mission. The sextant was removed from its stowed location, and the event-timing-system connector was hooked to the spacecraft utility cord by the pilot. The command pilot installed his reticle on the left-hand window, started his elapsed timeclock on an even minute, and noted the time; then, the spacecraft lights were extinguished. The command pilot established spacecraft orientation with respect to selected stars by the use of the reticle, and he stabilized the spacecraft about all three axes within ±2° in pitch and yaw and within ±10° in roll, with very low-limit cycle rates (<0.25° per second). After the stabilization of the spacecraft, the pilot focused the sextant, set the reticle illumination to a comfortable level, and acquired the star Aldebaran in both lines of sight. Then, the pilot superimposed the two images and marked the time of superposition by depression of the event-timer button. "MARK" was called out by the pilot, and the command pilot read his elapsed time and noted the time and the measured angle (read off the sextant by the pilot) in the experiment log. This procedure was repeated five times for the same star to provide an indication of the zero bias of the sextant-operator combination.

Then, the spacecraft was reoriented and stabilized by the command pilot, and the pilot acquired the prescribed target pair for the sighting period. A procedure similar to that just described was followed for at least 10 consecutive measurements of the angle between the target pair. A selected number of the sextant measurements were transmitted to a ground-based station for real-time evaluation of the performance of the pilot in making the prescribed measurements.

RESULTS

The results of the experiment consisted of learning-curve data obtained during the initial period of familiarization and training with the sextant, base-line data for comparison with flight results, and inflight data obtained during the Gemini XII flight.

Initial Training and Familiarization

The initial training of the pilot was performed in the docking simulator at the NASA Manned Spacecraft Center during the period from August 5 to 10, 1966. Two simulated star targets were installed in the simulator room. These targets consisted of 12-inch parabolic mirrors that projected toward the sighting station the collimated light of a small source placed at the focal point of the mirror. A second-magnitude star was simulated. By the use of the hand-held sextant in the darkened docking simulator, the pilot made 15 consecutive measurements of the angle between the simulated stars and 10 consecutive measurements of the sextant angle when sighting on one star with both sextant lines of sight. These measurements were repeated in 15 sighting sessions over a period of 4 days. The standard deviation of the 15 measurements of the angles between the two stars from their mean value was used as a measure of the proficiency of the pilot. The standard deviation varied throughout the training period from a maximum value of approximately 13 arc seconds (near the beginning of the training period) to a minimum of approximately 4 arc seconds (near the end). These data are indicative that the pilot had achieved a high degree of proficiency during the 4 days of training.

Base-Line Data

All base-line data were obtained at the Ames Research Center, Moffett Field, California, during the period from September 7 to 9, 1966. The majority of these data were obtained in the midcourse navigation and guidance simulator. The basic components of the simulator are a visual scene that simulates a moon-star field and a movable cab that simulates a manned space vehicle. The two simulated stars that were used in the initial training were used in collection of the base-line data. By the use of the hand-held sextant, the pilot made five consecutive measurements of the angle obtained when viewing the same simulated star through both sextant lines of sight to establish an instrument-operator measured zero bias. Subsequently, 10 consecutive measurements of the angle between the selected sighting targets were made. Measurements were made with the helmet off (normal eye-relief eyepiece) and with the helmet on and the visor down (long eye-relief eyepiece). The standard deviation of the measurements from the mean value and the mean measurement error for all sessions are summarized in table II. Additional base-line data obtained by the use of real targets are summarized in table III.

The standard deviation of the measurement obtained, both in the simulator and by the use of actual stars, is substantially below the ±10-arc second level and is consistent for both helmet configurations. Also, the mean measurement errors are small, except for the helmet-on visor-down configuration.

Inflight Data

The Gemini XII inflight sextant-measurement data were obtained by the pilot on November 14 and 15, 1966. The measurements were made from the stabilized spacecraft in which the pilot looked through the right-side window. A summary of the standard deviation of the measurements and the mean measurement error is presented in table IV. The standard deviation of the measurements for all sighting conditions is less than ±9 arc seconds, which is consistent with the base-line data. Generally, the mean measurement errors of the inflight data are small, except for the helmet-on visor-down configuration. This is consistent with base-line data. The mean measurement error was uncorrected for window-induced measurement errors, for errors caused by the difference in the refractive index of the light-transmitting media within and outside the spacecraft, and for measured zero bias.

CONCLUSIONS

The standard deviation of the inflight measurements was ±9.0 arc seconds or less, which was indicative that the hand-held sextant may be suitable for making navigational measurements during the midcourse phase of lunar or interplanetary space flight. The hand-held sextant with a long eye-relief eyepiece can be used to make accurate navigational measurements ($1\sigma < 10$ arc seconds) with the pressure suit helmet on and with the visor down.

The performance of the pilot, as indicated by the base-line data obtained both in a simulator and by use of real stars from earth-based observatories, was approximately the same as that obtained in the space-flight environment. Thus, the usefulness of simulators and earth-based observatories in evaluation of space navigation-measurement techniques was validated. No operational difficulties were encountered that were associated with the space environment.

TABLE I. - SEXTANT CHARACTERISTICS

Size, in.	7 by 7-1/4 by 6-1/16
Weight, lb	6.25
Magnification:	
Normal eye-relief eyepiece	× 8
Long eye-relief eyepiece	× 4.6
Field of view, deg	7
Exit pupil:	
Normal eye-relief eyepiece, mm	4
Long eye-relief eyepiece, mm	7
Diopter adjustment	-3 to +3
Resolution, arc sec	7
Image	Erect
Range, deg	76

TABLE II. - PILOT BASE-LINE DATA FROM THE AMES SIMULATOR

Sighting target	Helmet configuration	Number of sighting sessions	Number of measurements per session	Standard deviation of measurements, arc sec	Mean measurement error, arc sec (a)
Star/star	Helmet off	7	10	±5	+3
Star/star	Helmet on, visor down	3	10	±7	-2

[a]The mean measurement error is the mean measured target angle minus the calibrated target angle. The mean measured target angle is the mean measured angle corrected for instrument calibration and measured zero bias.

TABLE III. - PILOT BASE-LINE DATA (REAL TARGET)

Sighting target	Helmet configuration	Number of sighting sessions	Number of measurements per session	Standard deviation of measurements, arc sec	Mean measurement error, arc sec (a)
Altair/Vega	Helmet off	1	10	±5	0
Altair/δ Cygni	Helmet off	1	10	±3	+1
Altair/δ Cygni	Helmet on, visor down	1	10	±8	-5

[a]The mean measurement error is the mean measured target angle minus computed target angle. The mean measured target angle is the mean measured angle corrected for instrument calibration and measured zero bias. The computed target angle is the angle between the targets corrected for annual aberration and atmospheric refraction.

TABLE IV. - PILOT INFLIGHT DATA

Sighting target	Pressure-suit configuration	Revolution	Approximate g.e.t., hr:min	Time, sec	Number of measurements	Standard deviation of measurements, arc sec	Mean measurement error, arc sec (a)
Betelgeuse/ Rigel	Helmet off, gloves off	40	63:15 to 63:47	32	13	±9	-2
Betelgeuse/ Rigel	Helmet off, gloves off	48	75:17 to 75:50	33	14	±5	0
Betelgeuse/ Bellatrix	Helmet off, gloves off	54	85:45 to 86:20	35	15	±8	-4
Betelgeuse/ Bellatrix	Helmet off, gloves off	55	87:15 to 87:48	33	15	±5	-2
Betelgeuse/ Rigel	Helmet on, visor down, gloves off	56	88:45 to 89:20	35	15	±8	-11

[a]The mean measurement error is the mean measured target angle minus computed target angle. The computed target angle is the angle between the targets corrected for annual aberration.

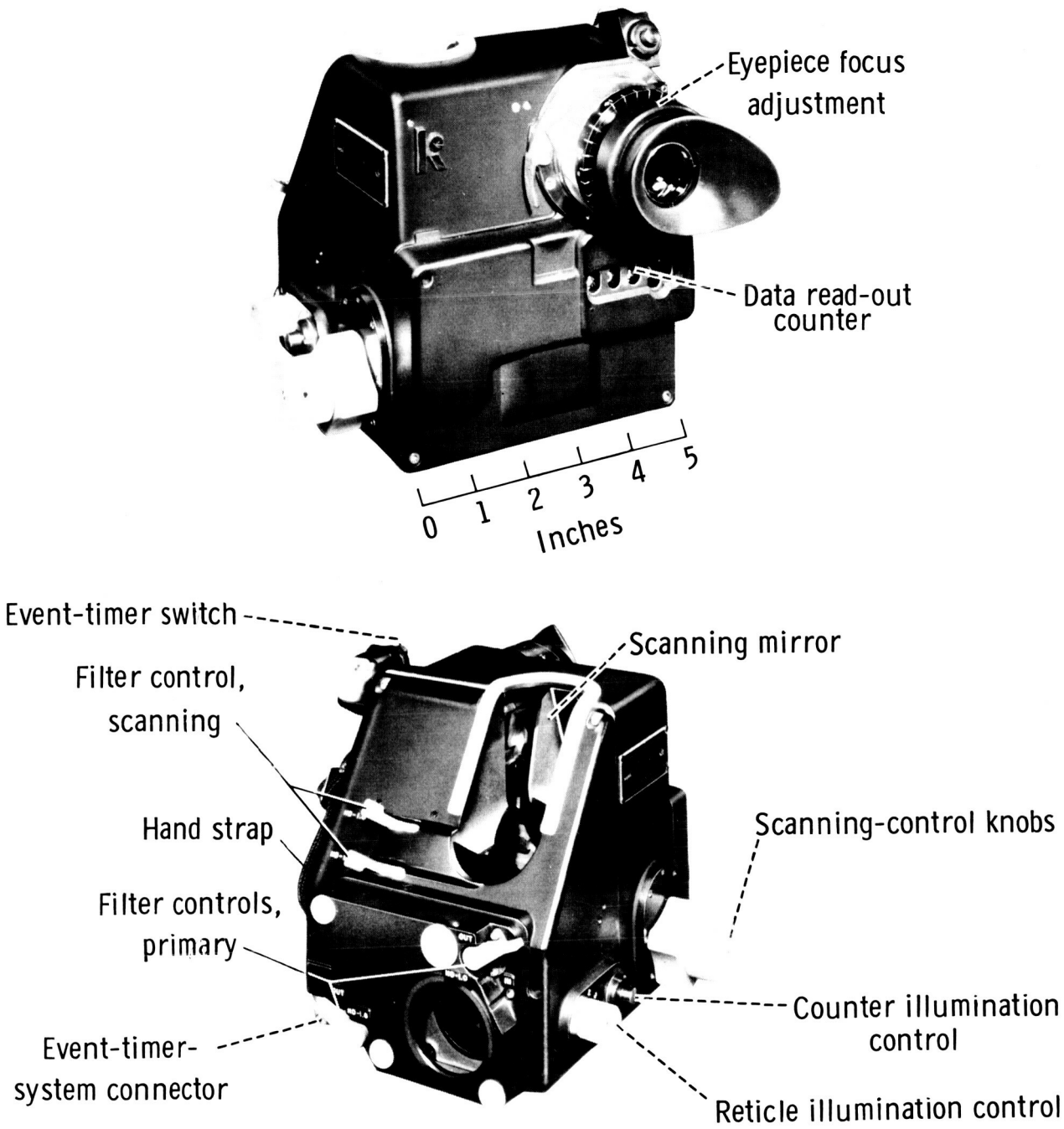

Figure 1. - The sextant configuration and controls.

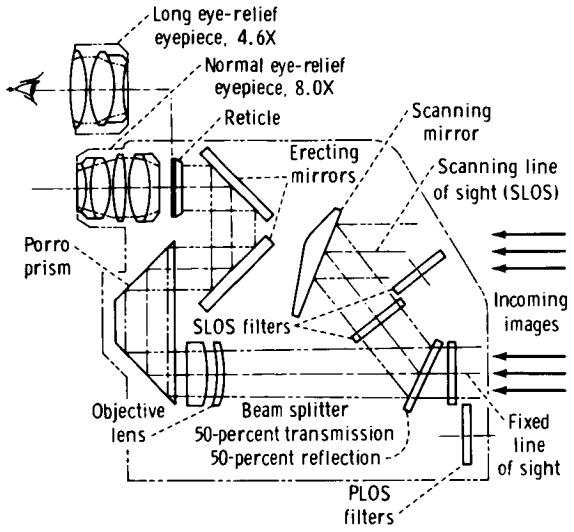

Figure 2. - The optical schematic of the sextant.

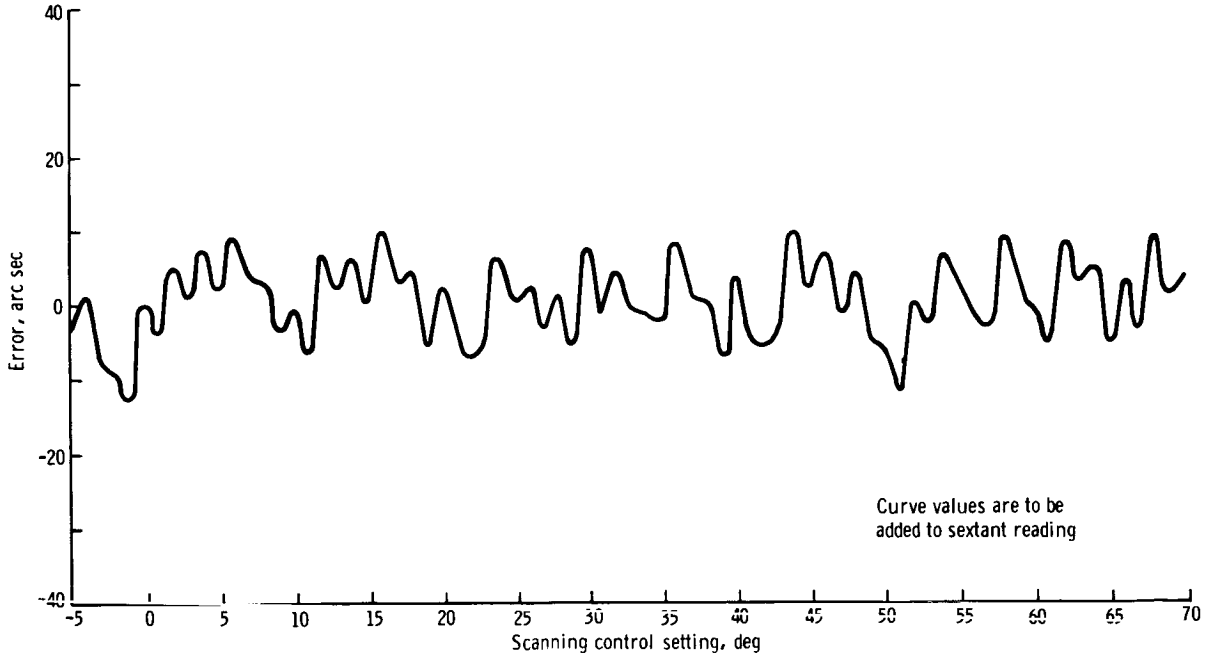

Figure 3. - The preflight sextant-calibration data (readings were taken in a positive direction).

EXPERIMENT S029

EARTH-MOON LIBRATION REGIONS PHOTOGRAPHY

By Elliott C. Morris*

INTRODUCTION

Eleven photographs were taken of the L_4 earth-moon libration region during the Gemini XII mission. The objective of Experiment S029 was to investigate the possible existence of clouds or particles of dust orbiting the earth in the L_4 and L_5 libration regions by the use of photographic techniques. The L_4 and L_5 libration points are in the orbital path of the moon, 60° ahead of and 60° behind the moon, respectively. Dust clouds in these regions may be visible in reflected sunlight.

EQUIPMENT

The following equipment was used for Experiment S029.

1. A 70-millimeter general-purpose camera equipped with an f/0.95 lens
2. One film magazine equipped with black and white, high-sensitivity film
3. Camera-mounting brackets similar to those that were used on Experiments T002 and S011

PROCEDURE

During the night pass on the 17th orbit, the camera was mounted on the pilot-side window by the use of the bracket that was used on Experiment T002; the bracket alined the camera with the spacecraft axis. In accordance with ground-based operational procedures, the spacecraft was oriented toward the constellation Capricornus, the star-field region in which the L_4 libration region would be passing 45 hours later.

---

*U.S. Geological Center, Flagstaff, Arizona.

Five photographs were taken of this region; a series of exposures of approximately 30 seconds, 1 minute, and 2 minutes was taken. The photographs were taken while the spacecraft was docked with the Gemini Agena target vehicle (GATV).

During the night pass on the 46th orbit, six exposures were taken of the L_4 libration point in Capricornus. The photographs were taken with the camera mounted on the mounting bracket that was used in Experiment S011; this bracket alined the camera perpendicular to the pilot-side window but not parallel to the spacecraft axis. The spacecraft, which was not docked with the GATV, was oriented so that the camera would be pointed at the libration point. Exposure times for the second set of photographs were 30 seconds, 1 minute, and 2 minutes.

RESULTS

Of the 11 photographs that were taken of the L_4 libration point, three were exposed properly. Mechanical failure of the shutter mechanism in the red-lens assembly resulted in overexposure of many of the photographs. Failure of the film to advance at the end of the first roll caused an unknown number of double exposures. No identifiable data were found in the first sequence of five photographs. Star-field images could be recognized in two photographs of the second sequence of pictures (figs. 1 and 2). However, the images were smeared badly because of camera motion that resulted from difficulty in stabilization of the spacecraft. A light flare, of unknown source but possibly caused by light refraction from the window of the spacecraft, was recorded in both pictures. A reconstructed star-field region (as photographed) is shown in figure 3. Isodensitraces of the two recognizable star fields were made; however, no conclusive results were obtained.

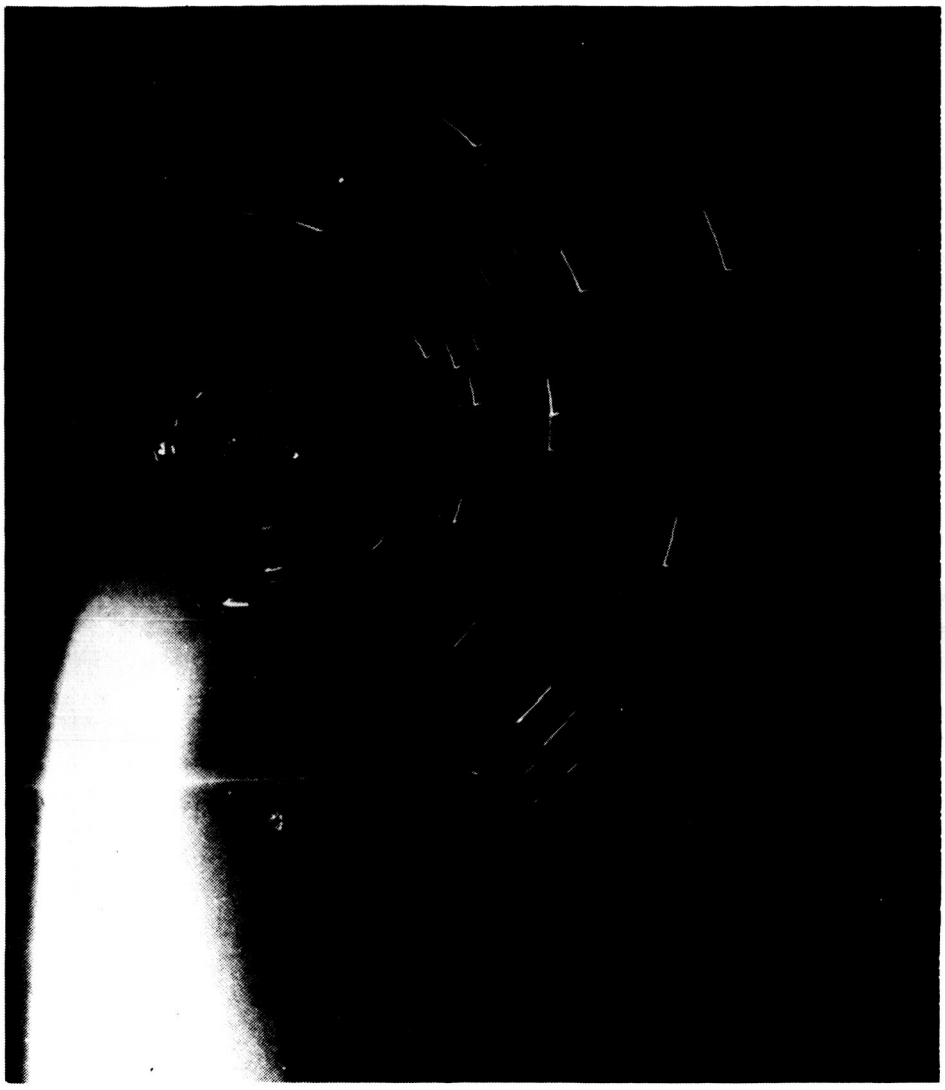

Figure 1. - A photograph of the L_4 libration region, taken at approximately 73:45 g.e.t. with an exposure time of 30 seconds.

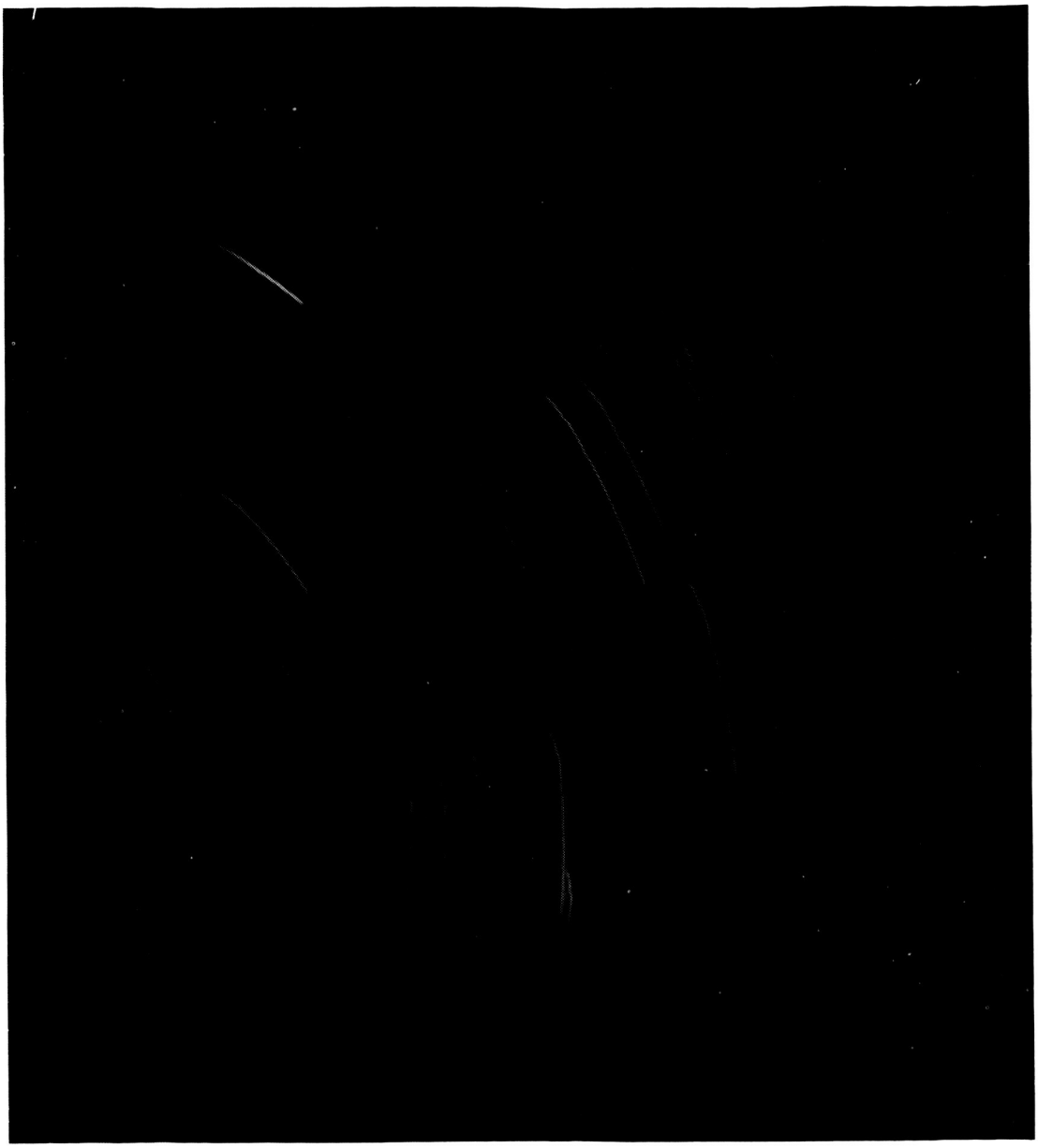

Figure 2. - A photograph of the L_4 libration region, taken at approximately 73:45 g.e.t. with an exposure time of 60 seconds.

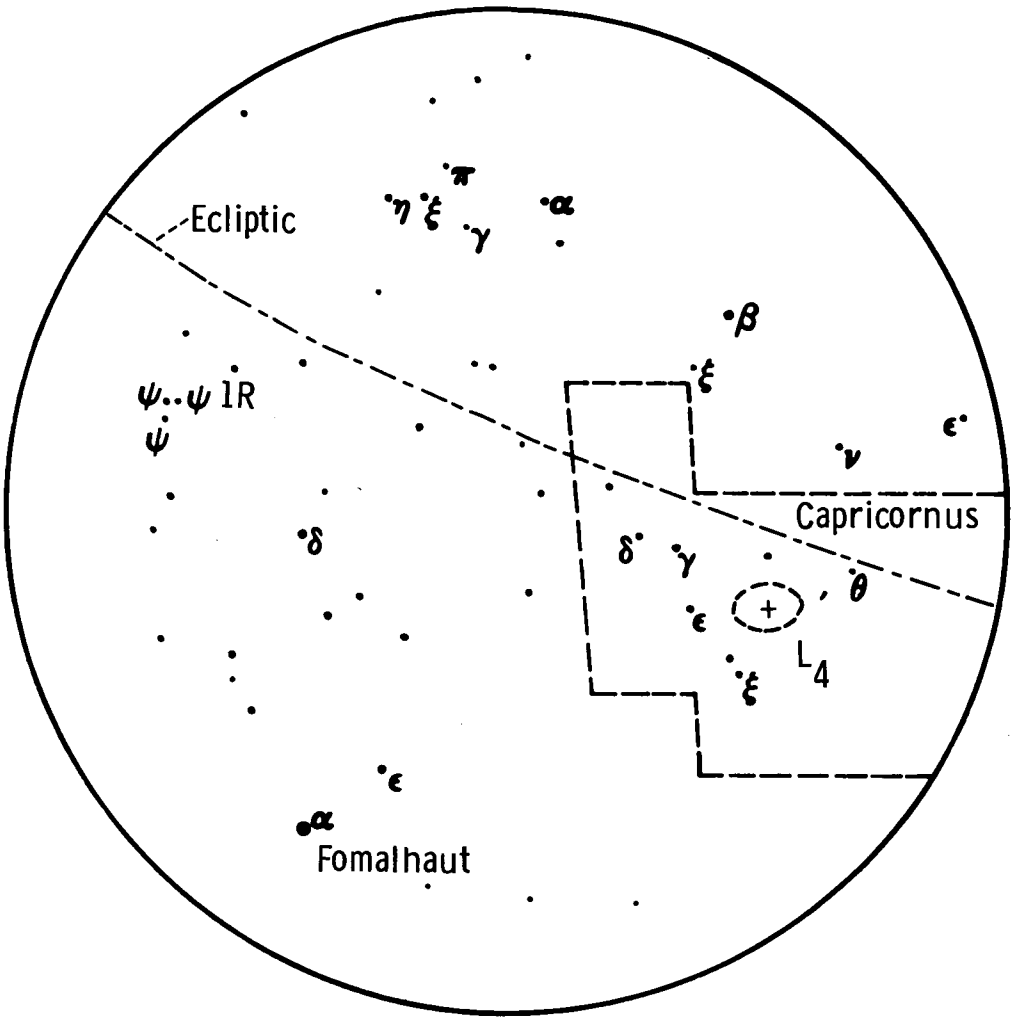

Figure 3. - Identification of the stars shown in figure 1, showing the position of the L_4 libration point on November 14, 1966, at 73:45 g.e.t.

EXPERIMENT M412

LANDMARK-CONTRAST MEASUREMENTS

By Charles E. Manry*

OBJECTIVE

The objective of Experiment M412, which was flown on the Gemini VII and X missions, was to measure the visual contrast of landmarks with the surroundings to determine the relative visibility of terrestrial landmarks from positions outside the atmosphere. These landmarks could be a source of navigational data for Apollo onboard guidance and navigation systems.

The ability to perceive, identify, and aline on landmarks is related closely to luminance of the landmarks and to the contrast of the landmarks with the surrounding regions. The visual contrast of a terrestrial feature with its surroundings is diminished according to the amount of atmosphere between the feature and the observer. Therefore, the visual contrast of ground targets, as seen from outside the atmosphere, will be diminished considerably from the contrast of the targets observed at close range. The measured parameter required during the missions was the visual contrast of landmarks; contrast is defined as follows.

$$\text{Contrast} = \frac{(\text{luminance of landmark}) - (\text{luminance of surroundings})}{\text{luminance of surroundings}}$$

This value can be positive or negative. The measured contrast value of a light-colored landmass viewed against a darker ocean might be more than 10. However, the contrast of a dark object viewed against lighter colored surroundings never can exceed unity.

As defined, visual contrast is a useful criterion for target visibility because of the constancy of threshold values through several orders of magnitude of luminance levels. Because contrast is a ratio, the measurement of contrast is independent of long-term photometric-equipment gain stability, a predominant source of error in devices that involve photomultiplier sensors. The effect of scattered light entering a photometer also is lessened because of the measured ratio.

*NASA Manned Spacecraft Center, Houston, Texas.

EXPERIMENTAL EQUIPMENT

Gemini VII Mission

The equipment consisted of the Experiment D005 photometer, equipped with an optical filter that was positioned in front of the objective lens. This filter attenuated the light in the blue region of the spectrum. Thus, the spectral response of the photometer was adjusted approximately to be equal to that of the standard Commission Internale de l'eclairage (CIE) observer. For details of the operation of the photometer and data read-out, reference should be made to the Experiment D005 report.

Gemini X Mission

The photometer that was provided for Experiment D005, with the addition of two optical filters that fit over the photometer lens, was used on Experiment M412. The instrument consisted of an objective lens that received landmark-reflected sunlight radiation and optically transferred the radiation to a field stop and then to a photomultiplier sensor. The amplified output from the photomultiplier was sampled 10 times per second, and the resultant signal was recorded on board the spacecraft by means of the standard Gemini telemetry system.

Typically, the linearity of the photomultiplier and the associated circuitry was better than 1 percent of full scale. The dynamic range of the instrument, designed to cover the expected luminance range of sunlit terrain, was 2.4 c/cm^2 (7000 ft-L) for maximum landmark luminance and was 0.02 c/cm^2 (58 ft-L) for minimum landmark luminance. The signal-to-noise ratio of the photometer was estimated to be in excess of 800: 1 for the minimum landmark luminance by the use of the sample rate of 10 per second.

The probable error of measurement was expected to be approximately 3 percent after adjustment for near-maximum signal level. Error caused by scattered light in the photometer during an observation could not be assessed accurately, except that the error would tend to diminish measured contrast.

Landmark-contrast data for use in guidance and navigation design in the Apollo Program have been calculated by extrapolation of airborne spectrophotometric measurements of photographs taken during Gemini and other orbital missions. A comparison of these data with direct measurements obtained in this experiment was expected to result in verification of the correctness of calculated contrasts and to reduce the present uncertainty of landmark-contrast variance with change of sun-aspect angle.

PROCEDURES

Gemini VII Mission

The photometer was to be hand held and aimed through the right-hand window of the spacecraft, as it was for Experiment D005. Several minutes before the appearance of the target landmark, the observer was to turn on the photometer power source. The spacecraft was to be turned so that the photometer could be pointed at the landmark. The spacecraft was to be positioned so that the sun was behind the observer, thus the spacecraft window would be shaded from direct sunlight.

It was anticipated that the landmark would be recognizable at approximately 60° from the nadir. This would have allowed time for the observer to aim the photometer and to adjust the instrument gain so that target-area luminance would provide a strong signal level to the telemetry system. As the command pilot tracked the landmark, the pilot was to have directed the photometer alternately at the landside and at the water-side of the landmark. Approximately eight to 12 measurements of each side were expected during each pass over a landmark. The pilot was to have described (verbally) the landmark, cloud cover, weather, sun aspect, and filter that was used. If available, operational camera film was to be used to photograph a few landmarks to assist in data validation.

Gemini X Mission

Observations were to include sightings of nine landmarks at each of three sun elevations. All landmarks were established at land and sea boundaries. The observation method involved tracking the landmark for approximately 80 seconds as the landmark passed through the nadir. Data were to have been taken continuously as the pitch angle to the landmark from the spacecraft ranged from 30° to 150°. The photometer was to have been alined alternately on the land and then on the sea for periods of 4 seconds and 2 seconds, respectively. The data were to have been stored in the onboard tape recorder and later telemetered to the ground station. A photograph was to have been taken of the landmark at the nadir to aid in identification and to provide photographic contrast. Measurement of the photograph would afford a rough correlation with the visual contrast measured by the photometer.

RESULTS

Gemini VII Mission

Because of a malfunction of the Experiment D005 photometer, no photometric data were obtained. A trial sighting run was performed at 163: 19: 40 ground elapsed time (g. e. t.), in which a landmark on the western African coast was sighted, tracked through the nadir, and photographed. The telemetry record of the photograph was examined. Because telemetry data were inconsistent with the known conditions of the

measurement, no further fuel usage seemed warranted for Experiment M412. The photograph of the landmark was used for practice identification of the exact geographic region observed.

Gemini X Mission

This experiment was not performed by the crewmen on the Gemini X mission because of fuel-usage constraints and time limitations. Therefore, no results are presented.

EXPERIMENT S013

ULTRAVIOLET ASTRONOMICAL CAMERA

By Karl G. Henize,* Lloyd R. Wackerling,*
and Albert Boggess III**

OBJECTIVE

The objective of Experiment S013, which was flown on the Gemini X, XI and XII missions, was to record the stellar ultraviolet (uv) radiation in the wavelength region from 2000 to 4000 angstroms. An analysis of the surface temperatures of the stars, the absorption effects occurring in the atmospheres of the stars, and the absorption effects of the interstellar dust was to be made from the photographic data obtained. It was predicted that the high-resolution photographs would reveal absorption and emission lines, which would facilitate the study of atomic excitation and ionization processes in the wavelength region from 2000 to 4000 angstroms. In addition to the acquisition of basic astronomical data, it would be possible to study and to evaluate the techniques by which objective-prism spectra can be obtained from manned spacecraft. The practical experience gained with this experiment will be useful in planning similar astronomical observations that will involve larger telescopes.

EQUIPMENT

A Maurer 70-millimeter camera was used to obtain the spectra. The uv lens had a 22-millimeter aperture, a 73-millimeter focal length, and a 30° diameter field. The film magazine contained 50 frames of Kodak spectroscopic I-O emulsion on an Estar base. Grating spectra with a dispersion of 184 angstroms per millimeter were produced by a 600-line per millimeter objective grating blazed for 2000 angstroms. Prism spectra with a dispersion of 1400 Å/mm at 2500 angstroms were produced by a quartz objective prism that had a 10° prism angle.

*Dearborn Observatory, Northwestern University, Chicago, Illinois.
**NASA Goddard Space Flight Center, Greenbelt, Maryland.

EXPERIMENTAL PROCEDURE

Gemini X Mission

Because Gemini windows do not transmit uv light, observations were made through the opened hatch. The camera was fastened on a bracket so that it pointed 5° above the roll axis of the spacecraft. One night orbit was added to the experiment, and the objective grating used as the dispersing element.

The original operating plan called for the command pilot to point the undocked Gemini at the desired star field and to nullify the angular motions of the spacecraft by using the pulse-control system. With the craft stabilized, the pilot was to make 10 exposures on each field, ranging in length from 10 to 60 seconds, for three separate fields.

During the Gemini X mission, the operating plan was altered because of shortage of fuel for maneuvering. The observations were made while the Gemini spacecraft was docked with the Agena, so that the Agena stabilization system could be used. Because the Agena could not be reoriented once the hatch was opened, it was decided to point at the Southern Cross, which was near the pole of the orbit and would remain in the camera field all night. However, by mischance during assembly of the equipment, the grating was turned 17° counterclockwise, which caused the orbital motion of the horizon-stabilized spacecraft to produce a migration of the field center from near β Crucis to near γ Velorum. After the basic pointing had been accomplished and the Agena stabilization had been activated, the pilot opened the hatch, mounted the camera on its bracket, and took 22 exposures. All exposures were approximately 20 seconds in length.

Gemini XI Mission

The observations were performed with the right-hand hatch open and with the spacecraft docked to the Agena. The camera (fig. 1) was mounted on the spacecraft frame by a bracket which positioned the field center 5° above the spacecraft roll axis. To operate the camera, the pilot stood up in the open hatch, while the command pilot remained in his seat to control the pointing of the spacecraft and to time the length of exposures. Each field was located visually by the astronauts, and the Gemini attitude-control system was used to point the spacecraft at the region. The automatic stabilizing system of the Agena was then activated in flight control mode 2. The pilot operated the camera, controlling both the opening and closing of the shutter and the film-advance mechanism. Six exposures were taken for each star field: two exposures at 20 seconds, two exposures at 60 seconds, and two exposures at 2 minutes. The experiment was performed during two successive night passes. The first night pass was used for objective-grating spectroscopy purposes, and the second night pass was used for objective-prism spectroscopy purposes.

Gemini XII Mission

The operating procedures for the Gemini XII mission were identical to the operating procedures that were used on the Gemini XI mission. However, a different set of star fields was observed.

RESULTS

Gemini X Mission

One of the most interesting regions of the Milky Way was scanned, and spectra were obtained for many more stars than was expected. However, the displacement of the grating caused trailing in the direction of dispersion for most stars, thus degrading the wavelength resolution. This degradation prevented the resolution of line spectra, but did not interfere with the measurement of uv energy curves.

In preliminary examinations of the film, the spectra of 57 stars have been identified (table I) with approximately 10 of the stars being bright enough for quantitative analysis of the uv energy curves. The only absorption feature visible in the spectra was the Balmer continuum. The limiting uv magnitude (effective wavelength 2500 angstroms) on frames with little or no widening is approximately +3.5.

One of the better frames is shown in figure 2; figure 3 is a key chart for figure 2.

The following is a list of four equipment problems that occurred during the mission.

1. Twelve frames were marred by a vertical streak that did not appear to be caused by ordinary light leaks. Static electricity, rising from camera operation under vacuum conditions, was the probable cause of the effect.

2. Preflight and postflight calibration exposures with the flight camera showed images of good quality at the center of the field. The inflight exposures showed poor image quality at the center of the field, but good image quality away from the center. The shape of the images indicated that the film was too close to the lens, apparently caused by film bowing towards the lens in vacuum conditions.

3. The cable release was broken during camera assembly. A more suitable cable release was provided for the Gemini XI mission.

4. One of the screws in the bracket assembly backed out and prevented proper insertion in the ways. According to the pilot, difficulty was encountered during bracket insertion.

Nearly 10 percent of the field of first-order star spectra was obscured by the Gemini Agena Target Vehicle (GATV) when in the docked configuration, and nearly 40 percent of the field of zero-order star images also was obscured. The masking of zero-order images prevented interference with most of the first-order spectra.

Extraneous light was not observed either originating in or reflected from the GATV. Stabilization of the GATV, achieved during the second portion of the night exposure period, appeared to have been adequate for the purpose of Experiment S013. Operation of the experiment while in a docked configuration now is recommended to use the greater inertia of the combined masses of the two vehicles and to provide an increased sensitivity of the pulse-control mode in attitude-hold.

In addition to gathering basic astrophysical data about hot, young stars, the experiment was used to clarify the problems and techniques of uv photography of stars from manned spacecraft. Such problems and techniques had to be explored in order to lay the technical foundation for the large manned orbiting telescopes. The amount of data gathered by the crewmen of the Gemini X mission with very simple equipment and in the face of unexpected difficulties indicated the value of man in such research programs. The experiment can be considered successful in that it resulted in the collection of useful scientific data and established needs for better equipment and procedures on subsequent missions.

Gemini XI Mission

No apparent problems occurred in the assembly and operation of the camera equipment during the mission. The use of a carbon dioxide cartridge eliminated all traces of static electricity markings on the film, a condition that had been noticed on the film from the Gemini X mission. There was no evidence of a light leak from the venthole drilled in the film magazine immediately prior to launch.

The stabilization supplied by the GATV was somewhat erratic. One-third of the exposures showed excellent stabilization, indicated by the smooth image motion in the yaw direction. The remaining exposures showed jumpy motion in both yaw and pitch, with a resulting degradation of wavelength resolution.

Six star fields were photographed. Grating spectra were obtained in fields that were centered on λ Scorpii and i Orionis. A log of the flight film is given in tables II and III. The single deviation from the flight plan was the observation of Canopus, an F0 supergiant, instead of Achernar, a B5 star. The deviation was fortunate in that the spectrum of Canopus between 2000 and 3000 angstroms showed more detail than was expected from the Achernar spectrum.

Excellent spectra were produced with both the grating and the prism. For the grating spectra, a limiting magnitude in the 2200- to 2600-angstrom region of early B-type stars on unwidened 2-minute exposures was $V = 4.5$. In prism spectra with a widening of 0.5 millimeter, the corresponding limiting magnitude was $V = 6.0$.

Grating spectra contained resolved absorption lines in the middle uv spectra of Canopus and Sirius and marked the first time that lines had been observed in this wavelength region in stars other than the sun. The spectrum of Canopus (fig. 4) showed the very strong Mg II resonance doublet at 2799 angstroms, the weaker Mg I resonance line at 2852 angstroms, the 2882 line of Si I, and several broad features which were identifiable as blended features of Fe I and Fe II. A blended feature, caused by the ultimate lines of Fe II near 2400 angstroms, was especially strong. These identifications were confirmed by the close similarity between the uv spectra of Canopus and the sun.

The spectrum of Sirius showed the Mg II doublet and the lines of the hydrogen Balmer series. As expected, no lines were resolved in the middle uv spectra of the B-type stars observed in Scorpius and Orion, except that the Mg II doublet at 2799 angstroms is visible faintly in the overexposed spectra of Rigel (fig. 5).

Grating spectra of 99 stars were identifiable in the three regions photographed. The film had a photometric calibration, and it is expected that energy curves may be derived for approximately 20 stars.

The prism spectra (fig. 6) contain two absorption features of interest, in spite of their low dispersion. The hydrogen Balmer discontinuity was very prominent in A-type stars, and in F-type stars, the metal multiplets seen in the grating spectrum of Canopus blended into two broad absorption features visible in the 2400- to 2800-angstrom region. A break in the prism spectra at 2800 angstroms, initially identified as being possibly caused by the He 2^3S continuum, has been identified as a break in emulsion sensitivity at that wavelength.

Three stars showed features of special interest. In the Wolf-Rayet star HD 156385 (spectral class WC7), an emission line was visible at a wavelength of about 2300 angstroms and was identified tentatively as the 2297-angstrom line of C III caused by the $2p^2\ ^1D - 2p\ ^1P^0$ transition. In the B-type shell star 48 Libra, the absorption features caused by iron multiplets appeared, even though these features are not expected in the spectra of normal B stars. Therefore, these bands must be features arising in the shell of the star. The spectrum of the M-type supergiant star Antares showed a uv extension of greater than expected strength. It appears that this uv radiation arose from the B-type companion to Antares and that measures of the intensity distribution in the spectrum could give an improved value of the visual magnitude and spectral type of the companion star.

A 2-minute prism exposure in the region of Orion (fig. 7) showed the region centered on the Orion Nebula to be surrounded by a uv haze. The structure of this nebulosity in uv light was slightly different from the structure seen in visible light, and the conclusion is that the structure arose from starlight scattered from dust particles in the region. A study of the intensity distribution of this phenomenon is suggestive that the interstellar dust in the Orion region forms a hollow shell that is centered on the Orion nebula.

Gemini XII Mission

Four star fields were photographed; two with the grating and two with the prism. The grating fields were centered on γ Cassiopeiae and Sirius. The prism fields were centered on Deneb and γ Velorum. Expected observations of grating spectra in the γ Velorum field and prism spectra in the α Persei field were not obtained because of workloads on the Gemini crewmen. The decision not to use platform orientation required the Gemini crewmen to use planned observation time at the beginning of each night in order to acquire the first star field.

No major problems were apparent in the assembly and operation of the camera. However, problems do remain concerning focus, static marks, and light leaks. The

image quality produced by the camera (as judged by zero-order grating images) was considerably better than the quality obtained during previous Gemini missions. In particular, the central region of poor focus was eliminated, which indicated that the increased tension of the film-retaining spring used in the Gemini XII camera prevented warping of the film. The worst image diameter on the Gemini XII photographs was approximately 100 microns; whereas, the worst image diameter on the Gemini XI photographs was approximately 200 microns. The superb resolution (approximately 5 angstroms) in the spectrum of Sirius (fig. 8) is illustrative of the improved image quality with the grating.

The best prism spectra do not appear as sharp as those of the Gemini XI mission. The reason for the discrepancy between the performance with the grating and that with the prism is not apparent.

All the frames showed the effects of static electricity. The carbon dioxide cartridge was less effective in eliminating this effect than it had been during previous Gemini missions. Possibly, the difference was the result of gas loss by a greater-than-expected venting rate through the film back. The static marks did not interfere with the study of lines and bands in the spectra, but the marks could reduce the accuracy of photometric measures on the film.

A log of the flight film is given in table IV. The 2-minute exposures on Cassiopeia (fig. 9) gave point images for the stars, which indicated that spacecraft stabilization remained accurate to $\pm 0.05^{\circ}$. The star γ Cassiopeiae was of particular interest, having ejected a shell that subsequently dissipated. The spectrum in recent years has been that of an ordinary, rapidly rotating B-type star; but, indications of hydrogen emission lines have appeared. These observations resulted in negative evidence for the return of a shell spectrum at this time.

The spectra of δ Cassiopeiae and β Cassiopeiae showed resolved absorption lines in the uv region, while the middle-uv spectrum of ϵ Cassiopeiae was devoid of strong features.

The middle-uv spectrum of Sirius (fig. 8) had a resolution of about 5 angstroms and showed six or more fine absorption lines. The 2795.5- and 2802.7-angstrom lines of Mg II were resolved for the first time in a photograph of a stellar spectrum. Preliminary measures of the wavelengths of the remaining lines indicate that the lines were probably caused by Fe II. Lines were also seen in the spectra of α Leporis and, possibly, υ Orionis. Prism spectra of hundreds of stars were recorded in the region of Deneb and Velorum. On most frames, little detail was apparent in the spectra.

The grating spectra from the Gemini XII mission were of high quality. The stronger grating spectra are listed in table V. In both fields, the presence of very many weak spectra was suspected on the long exposures. The spectra listed in table V were well exposed to yield measures of energy curves. The failure to obtain grating spectra of the γ Velorum-ζ Puppi star field was unfortunate, because they were well placed for observation during the mission.

TABLE I. - REVISED CENSUS OF STARS ON THE GEMINI X FILM

Star	Frame	Maximum intensity (a)	Spectral type	V (b)	B-V (c)	Predicted 2200-Å magnitude	BS (d)	HD (e)
β Cru	5	3	B0.5 IV	1.50	-0.24	-0.82	4853	111123
α Cru	8	4	B1 IV + B3m	1.05	-.26	-1.14	4730/1	108248/9
β Mus	11	3	B2.5 V	3.26	-.19	1.45	4844	110879
α Mus	14	4	B3 IV	2.94	-.20	1.12	4798	109668
β Cen	7	3	B1 II	.86	-.22	-1.42	5267	122451
α Cen	6	1	G2 V + dK1	.06	--	--	5459/60	128620/1
ϵ Cen?	1	1	B1 V	2.56	-.23	.33	5132	118716
γ Mus	4	2	B5 V	4.04	-.16	2.76	4773	209026
ζ Cru	3	1	B3 IV	4.26	-.18	2.54	4679	106983
β Cha	3	1	B6 V	4.38	-.13	3.41	4674	106911
δ^2 Cha	3	1	B3 V	4.62	-.19	2.85	4234	93845
ω Car	11	2	B7 IV	3.56	-.08	3.00	4037	89080
β Car	13	3	A1 IV	1.80	.00	2.04	3685	80007
E Car	8	1	B2 Ve	4.86	-.16	3.16	3642	78764
θ Car	13	4	09.5 V	3.03	-.22	.62	4199	93030
HR 4205+	7	2	B5 Vn	5.09	-.14	3.91	4205	93194
HR 4222			B3 IV	5.10	-.15	3.53	4222	93607
M Car	1	1	Am	5.15	+.22	5.60:	4025	88981
ν Car	2	1	A9 II	3.15	--	4.95:	3890/1	85123/4
i Car	8	2	B3 IV	4.18	-.19	2.41	3663	79447
χ Vol?	1	1	B9 + Ap	4.74	-.06	4.49	3301/2	71046/66
p Car	8	3	B5 Ve	3.58	-.12	2.50	4140	91465
c Car	7	2	B8 II	3.98	-.11	3.48	3571	76728
d Car	5	2	B1 III	4.42	-.12	2.74	3457	74375
ϵ Car	3	2	K0 II + B	1.85	+1.30	--	3307	71129
γ Vel	8	4	WC7 + 0	2.22	-.26	-.16	3207	68273
l Car	7	2	F0 Ib	2.24	+.18	4.04	3699	80404
a Car	7	3	B2 IV	3.56	-.19	1.71	3659	79351
δ Vel	7	3	A0 V	2.01	+.04	2.21	3485	74956

[a] 1 - barely visible, 2 = weak, 3 = medium, 4 = strong, 5 = overexposed.

[b] Photoelectric visual magnitude (yellow).

[c] Photoelectric visual magnitude (blue) minus photoelectric visual magnitude (yellow).

[d] Serial numbers for stars from the Yale Catalogue of Bright Stars.

[e] Serial numbers for stars from the Henry Draper Catalogue of Stellar Spectra.

TABLE I. - REVISED CENSUS OF STARS ON THE GEMINI X FILM - Concluded

Star	Frame	Maximum intensity (a)	Spectral type	V (b)	B-V (c)	Predicted 2200-Å magnitude	BS (d)	HD (e)
o Vel	6	3	B3 III	3.68	-0.19	1.91	3447	74195
χ Car	4	2	B2 IV	3.60	-.19	1.75	3117	65575
HR 4188+	4	1	WN7	6.48	+.08	5.82	4188	92740
HR 4198			B3 Ia	5.44	+.24	5.47	4198	92964
χ Vel	5	4	B2 IV	2.63	-.20	.73	3734	81188
NGC 3293	2	1	B0 Ib[f]	6.51	+.01	4.24	--	91969
J Vel	3	2	B3 IV	4.65	-.13	3.18	4074	89890
φ Vel	4	3	B5 II	3.70	-.09	2.67	3930	86440
f Car	3	1	B2 Vne	4.63	-.17	2.87	3498	75311
L Vel	3	2	B3 n	5.16	-.20	3.34	3819	83058
H Vel	1	1	B5 V	4.77	-.13	3.64	3574	76805
I Vel	2	2	B5 n	5.22	-.12	4.14	3753	81848
HR 3467	2	2	B4 IV	5.04	-.18	3.49	3467	74560
D Vel	4	1	B0 Vn	5.19	-.22	2.93	3476	74753
E Vel?	1	1	B9 si	5.79	-.14	5.54	3413	73340
f Vel	4	1	B0 III	4.89	-.22	2.63	3527	75821
n Vel	3	1	A5 II	4.76	+.13	5.93	3452	74272
B Vel	3	1	B1 V	4.90	-.16	3.02	3294	70930
J Pup	3	2	B1 Ib	4.32	-.15	2.14	3090	64760
h Car	2	1	B5 II	4.20	+.01	3.67	3825	83183
HR 3453?	1	1	B2 Vn	6.14	-.22	4.14	3453	74253
V Pup	2	1	B2 n	4.40	-.18	2.60	3129	65818
HR 3142/3?	2	1	B5	6.43	--	4.50	3142/3	66005/6
b^2 Car	1	1	B3 IV	5.08	--	3.26	3582	77002
e^2 Car	1	1	B3 Vn	5.40	-.15	3.83	3415	73390
HR 3330	1	1	B3 n	5.23	--	3.41	3330	71510
A Vel	1	1	B4	6.50	--	4.50	3375	72485
P Pup	1	2	B0.5 III	4.25	-.20	2.13	3055	63922

[a] 1 = barely visible, 2 = weak, 3 = medium, 4 = strong, 5 = overexposed.

[b] Photoelectric visual magnitude (yellow).

[c] Photoelectric visual magnitude (blue) minus photoelectric visual magnitude (yellow).

[d] Serial numbers for stars from the Yale Catalogue of Bright Stars.

[e] Serial numbers for stars from the Henry Draper Catalogue of Stellar Spectra.

[f] The data given are for the brightest star in the cluster.

TABLE II. - GRATING EXPOSURES FROM EXPERIMENT S013 INFLIGHT EXPOSURES

[Gemini XI mission]

Frame	Field	Vehicle attitude control	Remarks
S66-53091	Wasted frame	--	Light struck
S66-53092	Scorpius	Poor	Spectra wide, streaked; no lines
093		Fair	Spectra double; Balmer lines in Shaula
094		Poor	Spectra wide, streaked; no lines
095		Poor	Spectra side, streaked; lines in Shaula, θ Sco
096		Poor	Spectra wide, streaked; lines in Shaula, Sco, θ Sco, Ara
S66-53097	Canopus	Good	Lines rather wide, uv well exposed
098		Excellent	Lines rather wide; uv a bit weak
099		Excellent	Lines, uv well exposed
100		Excellent	Lines, uv well exposed; spectrum streaked
101		Good	Lines, spectrum double
102		Excellent	Lines, spectrum double
S66-53103	Orion	Bad	Spectra extremely wide; no lines
104		Fair	3727-Å emission (O II) in nebula; lines in Sirius
105		Poor	Spectra wide, streaked; probably no lines
106		--	Grossly underexposed; no spectra
107		Good	Strongly exposed; 3727-Å emission in nebula, lines in Sirius
108		--	Light struck, ruined

TABLE III. - PRISM EXPÓSURES FROM EXPERIMENT S013 IN FLIGHT EXPOSURES

[Gemini XI mission]

Frame	Field	Vehicle attitude control	Remarks
S66-53109	Wasted frame	--	Light struck
110	Scorpius head	Poor	Spectra streaked; focus poor; no lines
111		Good	Spectra smooth; lines visible
112		Poor	Spectra streaked; focus poor; no lines
113		Good	Spectra double, smooth; lines visible
114		Poor	Spectra streaked; focus poor; no lines
115		Poor	Spectra streaked; focus poor; some lines
S66-53116	Scorpius tail	Fair	Spectra very wide, streaked; lines visible
117		Fair	Spectra wide, streaked; lines visible
118		Good	Spectra wide, smooth; focus poor; lines visible
119		Poor	Motion mainly in pitch; no lines
120		Fair	Spectra streaked; focus poor; some lines
121		Poor	Spectra streaked; focus poor; some lines
122		Bad	Spectra very wide; focus poor; no lines
S66-53123	Orion	Fair	Spectra streaked; some lines
124		Fair	Spectra streaked; some lines
125		Excellent	Spectra smooth; lines visible
126		Poor	Motion in pitch; no lines
127		Fair	Spectra smooth; focus poor; some features
128		Poor	Spectra streaked; no lines
129	Wasted frame	--	Spectra streaked; no lines

TABLE IV. - EXPERIMENT S013 GEMINI XII INFLIGHT EXPOSURES — GRATING ATTACHED

Frame[a]	Field	Vehicle attitude hold	Remarks
S66-63557	Wasted frame	--	Light struck
58	Cassiopeia	Fair	Images triple; spectra streaked; no lines
59	Cassiopeia	Excellent	Spectra smoothly widened; no lines
60	Cassiopeia	Good	Spectra unevenly widened; lines in β Cassiopeiae, δ Cassiopeiae
61	Cassiopeia	Fair	Spectra unwidened, slightly trailed in wavelength direction; lines β Cassiopeiae, δ Cassiopeiae, ζ Cassiopeiae
62	Cassiopeia	Good	Spectra rather narrow; lines in β Cassiopeiae, ϵ Cassiopeiae, ζ Cassiopeiae, λ Cassiopeiae
63	Cassiopeia	Good	Spectra rather narrow; lines in β Cassiopeiae, ϵ Cassiopeiae, ζ Cassiopeiae, λ Cassiopeiae
64	Canis Major	Excellent	Spectrum rather wide; many fine lines below 3000 Å
S66-63565	Canis Major	Fair	Spectrum rather narrow; Balmer lines in Sirius
66	Canis Major	Fair	Spectra unevenly widened; lines of Mg II, Fe II
67	Canis Major	Good	Spectra smoothly widened; many lines below 3000 Å
68	Canis Major	Excellent	Spectra smoothly widened; lines below 3000 Å
69	Canis Major	Good	Spectra smoothly widened; lines around 2400 Å; lines in α Lep, υ Ori
S66-63570	Canis Major	Good	Sirius ultraviolet superposed on sunlit GATV

[a]All frames were marred by static marks or light leaks.

TABLE V.- EXPERIMENT S013 GEMINI XII INFLIGHT EXPOSURES — PRISM ATTACHED

Frame[a]	Field	Vehicle attitude hold	Remarks
S66-63571	Wasted frame	--	Grossly overexposed; positive image of GATV and sunlit earth
72	Cygnus	Fair	Spectra streaked; no detail
73	Cygnus	Poor	No detail
74	Cygnus	Poor	Some detail
75	Cygnus	Fair	Some detail
76	Cygnus	Poor	No detail in spectra
77	Puppis-Vela	Poor	Spectra very wide; possible detail
78	Puppis-Vela	Poor	No detail
79	Puppis-Vela	Poor	No detail
80	Puppis-Vela	Fair	Spectra streaked; apparent line in 3817 Å
81	Puppis-Vela	Poor	No detail
82	Puppis-Vela	Good	Spectra smoothly widened; some detail
83	Puppis-Vela	Poor	Spectra streaked; no detail
84	Puppis-Vela	Fair	Spectra streaked; apparent detail in γ Vel, ζ Puppi
85	Puppis-Vela	Fair	Spectra streaked; no detail
S66-63586	Wasted frame	--	Light struck

[a]All frames were marred by static marks or light leaks.

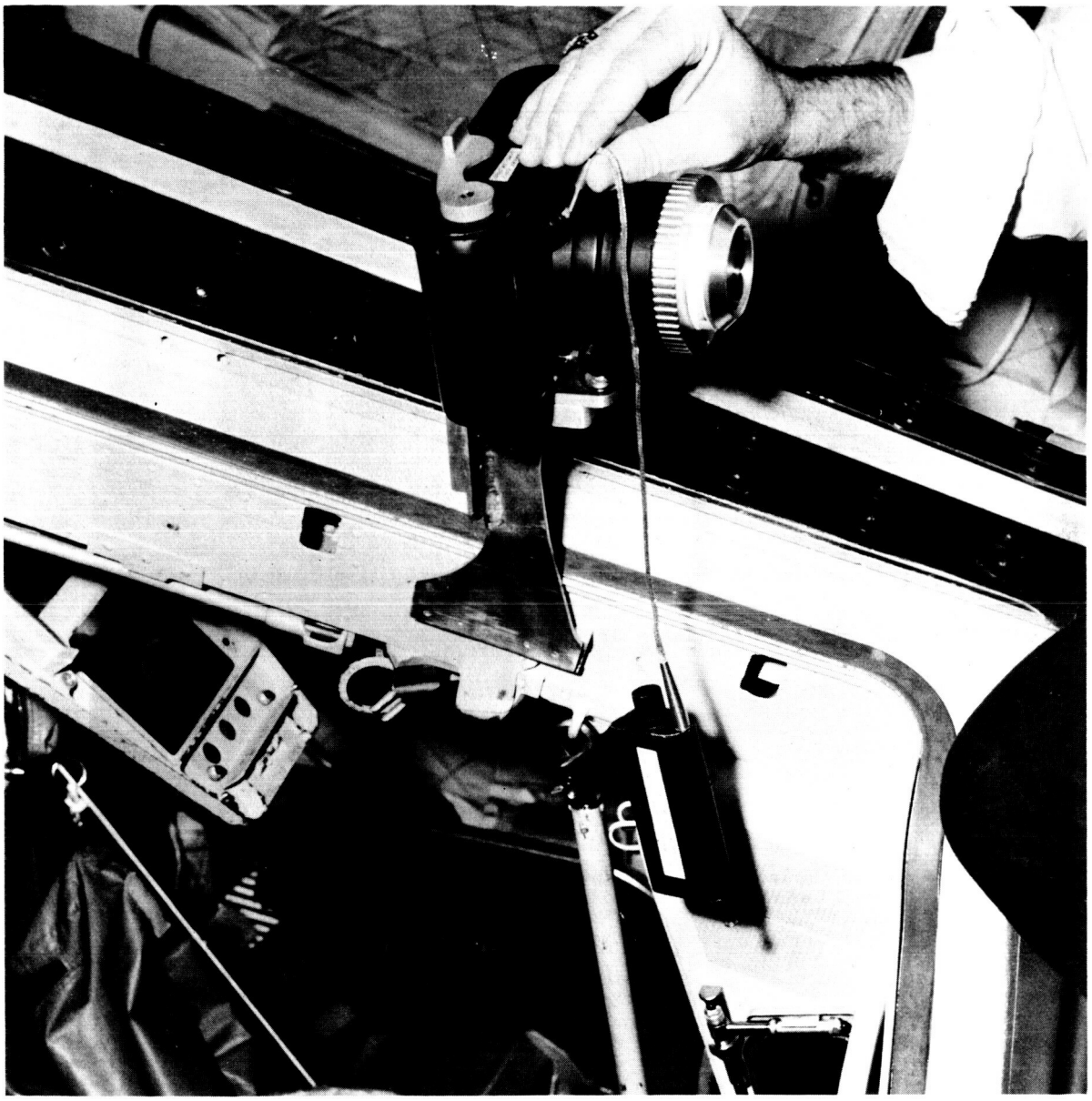

Figure 1. - The astronomical camera assembly.

Figure 2. - The ultraviolet spectra of stars in the Carina-Vela region of the southern Milky Way (Gemini X).

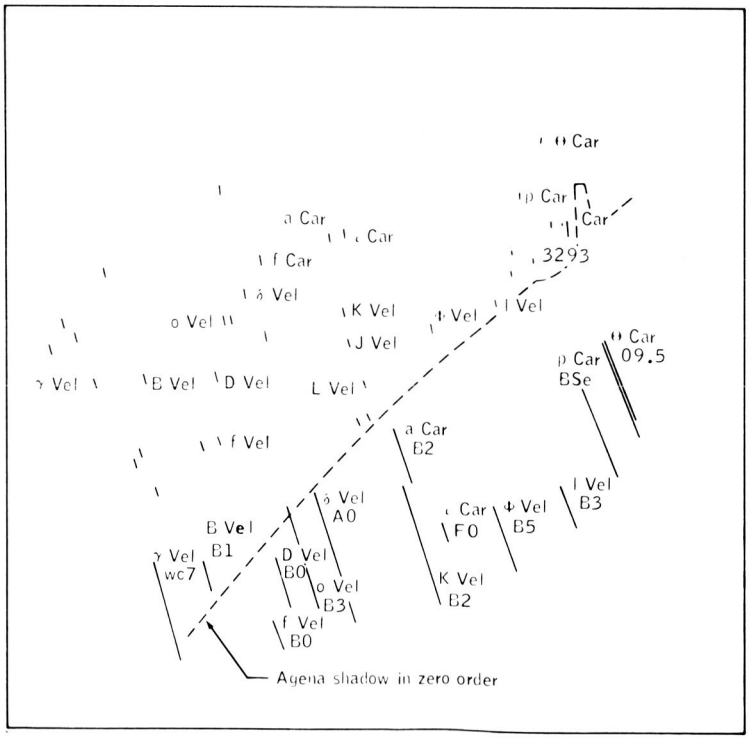

Figure 3. - Key chart for figure 2.

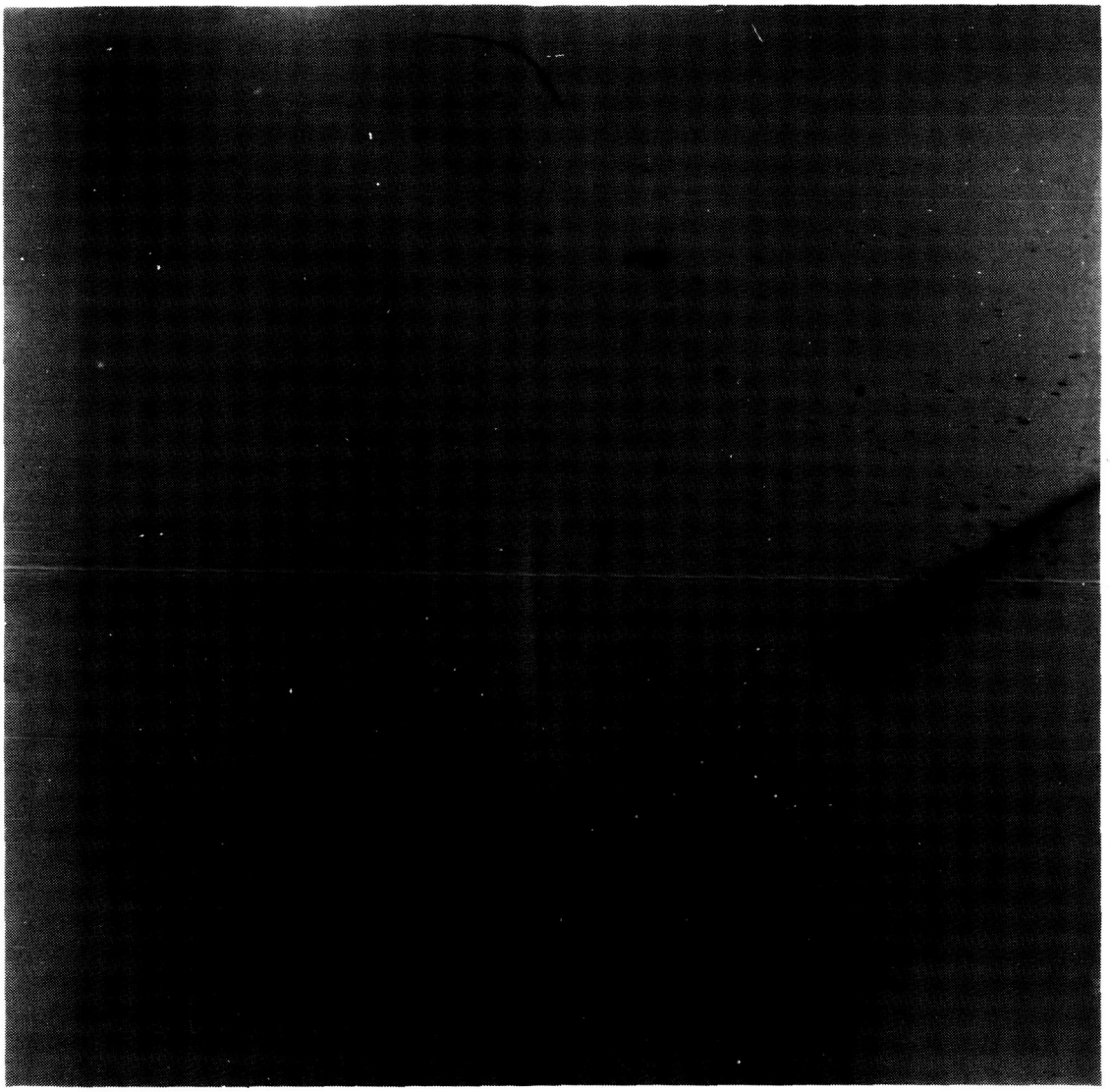

Figure 4. - The middle-uv spectrum of Canopus (Gemini XI).

Canopus was photographed from the Gemini XI spacecraft.

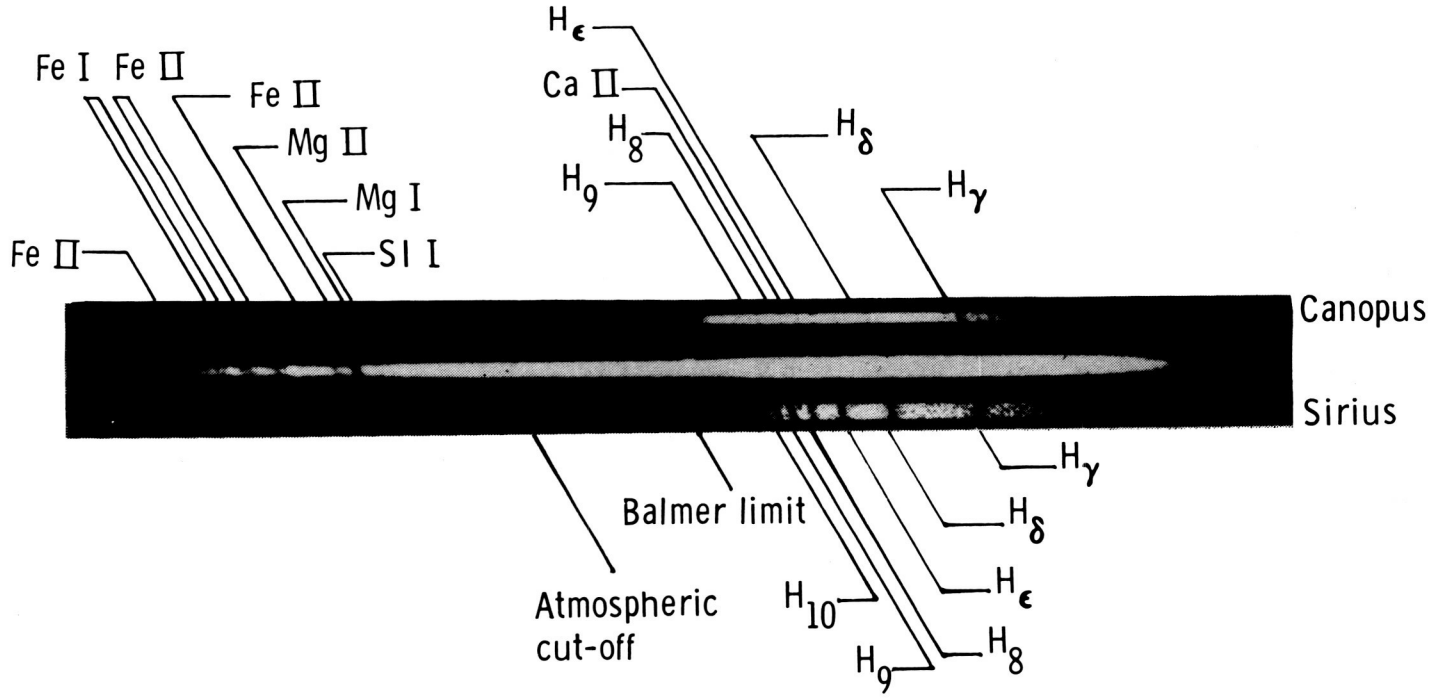

Sirius photographed from surface of the earth.

The opaqueness of the earth atmosphere is shown clearly
by the lack of spectral data in the ultraviolet band from Sirius.

Figure 5. - The comparative spectra of Canopus and Sirius.

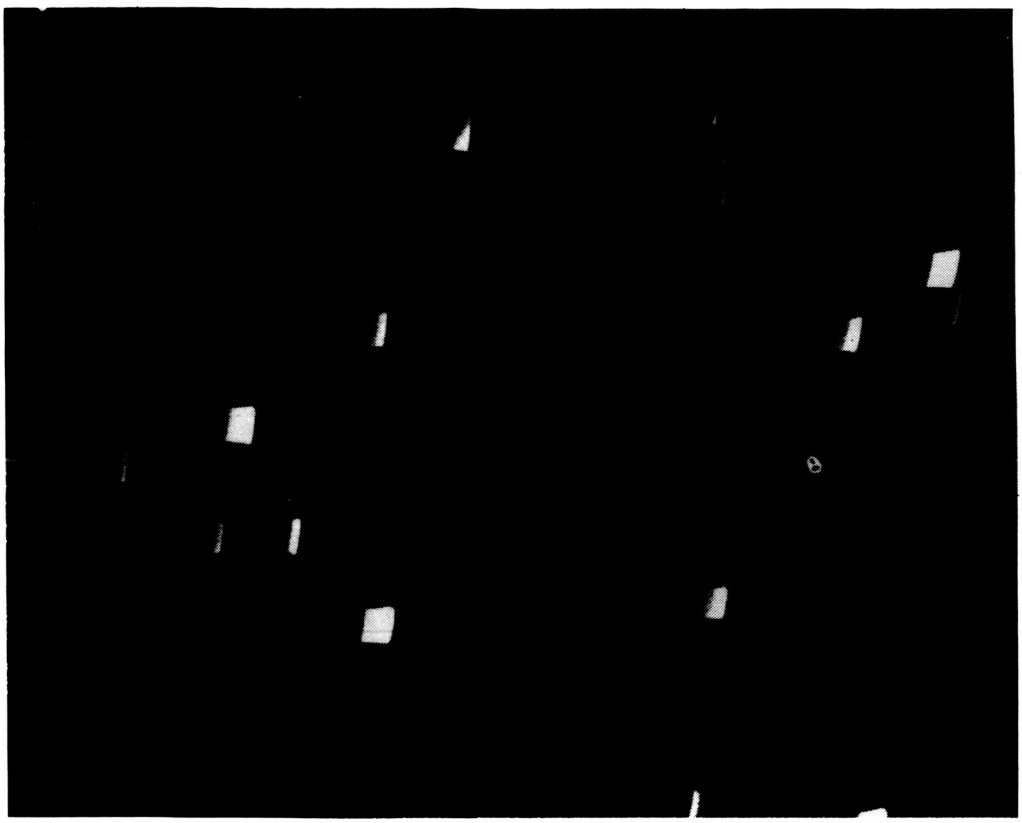

Figure 6. - The ultraviolet spectra of hot stars in Scorpius (Gemini XI).

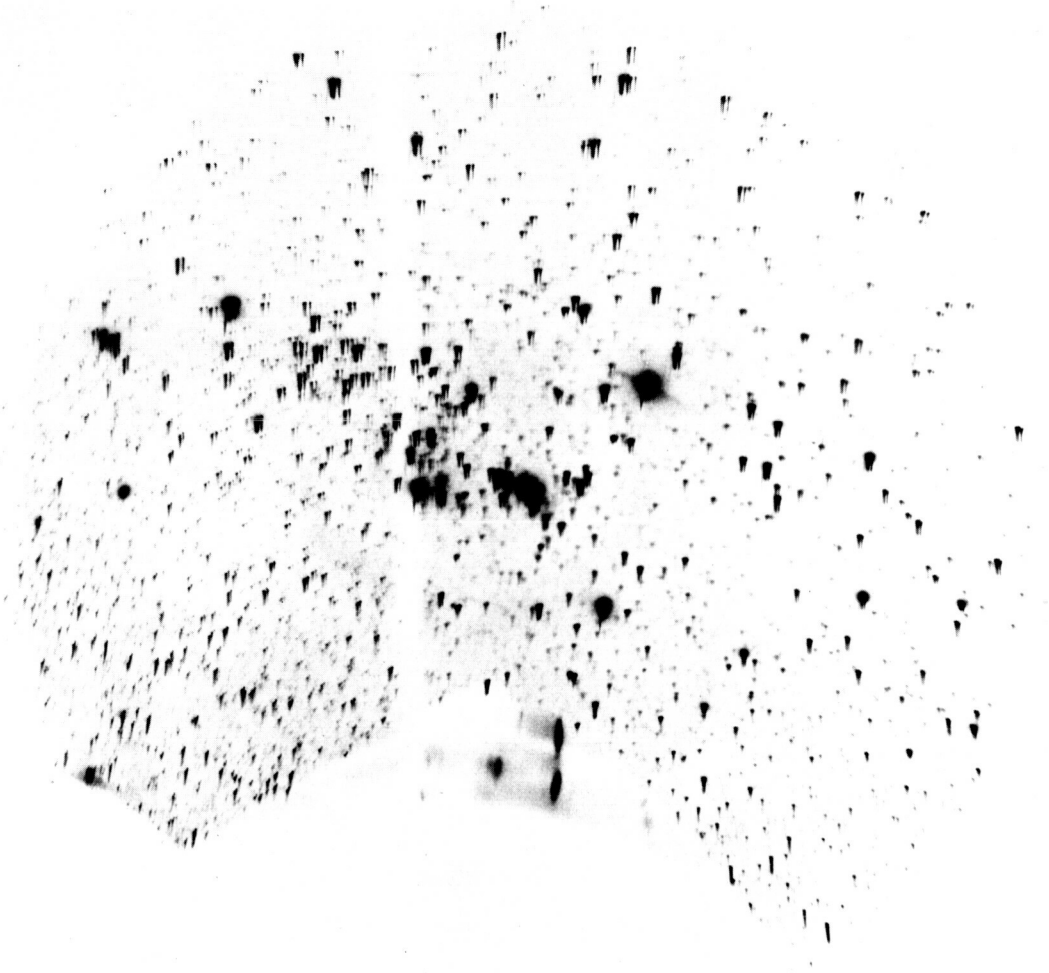

Figure 7. - The ultraviolet objective-prism spectra of stars in Orion (Gemini XI).

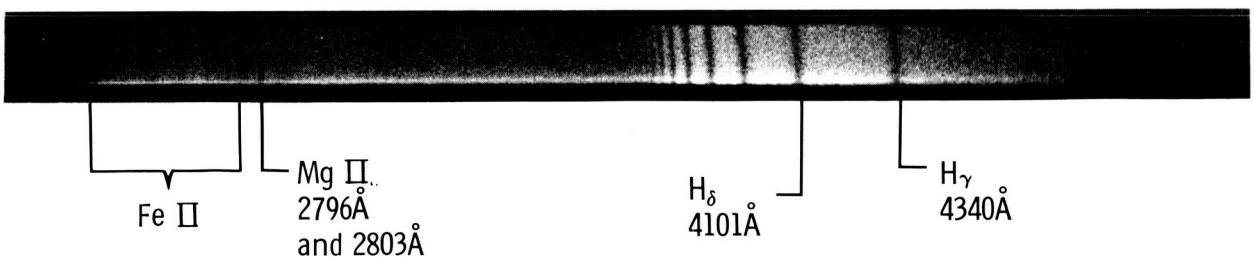

Figure 8. - The ultraviolet spectrum of Sirius; 20-second exposure (Gemini XII).

Figure 9. - The grating spectra in the region of Cassiopeia; 2-minute exposure (Gemini XII).

EXPERIMENT M411

TWO-COLOR EARTH LIMB PHOTOGRAPHY

By Max Petersen*

INTRODUCTION

Experiment M411 was a sequel to the photography that was performed on the Mercury 7 flight. The photographs taken on the Mercury 7 flight raised questions that could be answered, in part, only by a new series of pictures, extended with respect to the involved scattering angle of the sunlight. The general plan of the experiment proposed for the Gemini IV mission was similar to that used on the Mercury 7 flight. Therefore, it is useful to review the considerations that prompted the performance of these two experiments. The plans for guidance and navigation of the Apollo missions necessitate observation of the earth, presumably the limb, to make a navigational fix. Precise definition of the observable limb is essential. The uncertain condition of the lower atmosphere (with its tropospheric storms) and the accompanying clouds prompt consideration of observation of higher levels of the atmosphere, which scatter the shorter wavelengths of light in a manner that may approximate Rayleigh scattering (if so, there is satisfactory predictability).

Some simple, slightly tedious, calculations were made regarding the scattered-light phenomenon of a sunlit earth limb. It was assumed that the light was to be scattered by an atmosphere (defined in the U.S. Standard Atmosphere) irradiated by a zenith sun. Calculations were made with several different scattering coefficients assignable to various wavelengths of the extended visual region. The wavelength assignments need not be made initially; they depend on whether simple Rayleigh scattering prevails. The relation of the total attenuation of incident radiation (entering the atmosphere and passing through it) to light scattered in a particular direction (as, for example, at 90° to the incidence) is a well-known integral relation for Rayleigh scattering.

CALCULATIONS

A comparison of observed extinction coefficients for the extended visual spectrum with calculated coefficients for an atmosphere of pure air is given as follows (cited from ref. 1).

*Massachusetts Institute of Technology, Cambridge, Massachusetts.

Wavelength, Å	Observed τ	Pure air τ
3 530	0.488	0.474
4 220	.268	.226
4 880	.166	.125
5 700	.126	.066
7 190	.053	.026
10 300	.028	.006

The differences between the coefficients for the several wavelengths are indicative that these curves can have only provisional wavelength ascription until they are compared with some observed limb profiles. Calculations that proceed in terms of the numerical values of the extinction coefficients can yield relative profile curves of significance. Initially, therefore, such wavelength ascription will not be made.

The variable τ is defined by the equation for the observed brightness of a star at zenith distance ζ

$$b = b_0 e^{-\tau \sec \zeta} \tag{1}$$

where b = observed brightness, irradiance units

b_0 = brightness outside the atmosphere, irradiance units

e = base of natural logarithm

τ = optical thickness of the atmosphere

ζ = observed zenith distance

The optical thickness of the atmosphere may be related to a local extinction coefficient β by the relation

$$\tau = \int_0^\infty \beta \, dh \tag{2}$$

where h = atmospheric height. For a clear sky, β depends only on the density of the atmosphere. Thus,

$$\tau = \beta_0 h_1 \tag{3}$$

In this equation, β_0 is the coefficient for the density at sea level, and h_1 is the reduced height of the atmosphere, the total mass of air in a unit-cross-section column above the observer divided by the sea-level density. The numerical values for observed τ apply to the atmosphere above Mount Wilson Observatory (h = 6.44 kilometers). The pure air values corresponded to 6.44 kilometers of pure air (ref. 1).

In the calculations considered, a plane lamina of atmosphere is thought of as having, at its closest point to the earth, a perigee altitude h_0. Normally, it is irradiated by the sun. The various scattering elements of this lamina vary in density with their altitude, from the density at h_0 to a negligible density. The scattering elements vary slightly in solar irradiance because of the air above them and because of its extinction. More importantly, they vary in the transmission of their locally scattered light toward the observer because of the light scattering along that path. Secondary scattering has not been included. The variables were evaluated in terms of the pertinent goemetry and the density profile of the atmosphere (ref. 2). Whereas, the choice of extinction coefficients and (tentatively) the specific 90° scattering function were intended to involve the extended visual spectrum, wavelength ascription is not necessitated. However, pure Rayleigh scattering cannot be ascribed to the lowest perigee height involved.

Consider a lamina of atmosphere that, normal to the radius at its perigee point, has a terrestrial altitude h_0 (fig. 1). The several small segments of the lamina, such as that centered at P_i, are more distant from the center of the earth by the sagitta S_i that is given closely enough by $D_i^2 = S_i \times 2R_\oplus$. The density of the scattering air in the element at P_i is that for the altitude $h_0 + S_i$. The scattering mass per unit cross-sectional area is equal to that density multiplied by the element of length. The chosen elements of length subtended 20 minutes of arc around the center of the earth, and ranged from 37.11 to 37.64 kilometers. The sagittae, calculated on the diameter of the earth (6357 × 2 kilometers), ranged from 0.108 to 48.04 kilometers. Given a spectral density of solar flux outside the atmosphere of the earth, $f\lambda$, the flux falling on a unit area of a scattering element at P_i in a spectral interval $\Delta\lambda$ will be measured by $f\lambda\,\Delta\lambda \exp(-\tau H_i)$, in which H_i is the reduced height of the atmosphere above P_i at the level $h_0 + S_i$. The light scattered by the element at P_i will be proportional to the mass $\rho_i \Delta D_i$ and to the scattering coefficient, of which the solid angle integral defines τ. The scattering coefficient used here was that for 90° scattering. The

light scattered in the direction of the observer will be attenuated by the airmass between P_i and the observer. This can be obtained as $\sum_{i}^{z} \rho_i \ \Delta D_i$, in which sum the zth element has no significant atmosphere beyond the zth element. The total transmitted light from all elements in the lamina from the far side to the near side of the observer, for a unit exterior solar flux density and spectral range, may be calculated by use of the sum

$$\sum_{-z}^{+z} c\tau\rho_i \ \Delta D_i \exp\left[-\tau\left(H_i + \sum_{i}^{z} \rho_i \ \Delta D_i\right)\right]$$

The use of $c\tau$ for the 90° scattering coefficient, where τ is a measured or observed attenuation coefficient, necessitates comment. The initial brightness per unit of solar irradiance of the 90° scattered radiation from an element of the lamina is given by a scattering function, the solid angle integral of which is the attenuation coefficient. In the application of these concepts to the current problem, it is assumed that the scattering coefficient for a 90° angle is proportional to the attenuation coefficient because only the relative brightness for various laminae of different h_0 values is sought. For Rayleigh scattering, the scattering function is of the form

$$\beta(\phi, \lambda) = a\lambda^{-4}\left(1 + \cos^2\phi\right)$$

This is related to the attenuation coefficient of the equation for flux depletion for flux crossing a path differential $dr(dF/F = -b\ dr)$ by the relation

$$b = 2\pi\int_0^{\pi} B(\phi)\sin\ \phi\ d\phi$$

The hazard involved in substitution of the attenuation coefficient for the specific scattering coefficient is that, for any given wavelength of light, the ratio of the two will be significantly different at the different altitudes pertinent to the applicable results (namely, 10 kilometers and higher). Evidence in this matter (which extends to 9200 meters) is presented in reference 3. This point, which is tantamount to the assumption of a Rayleigh atmosphere, may not be overlooked. The detailed calculations that are involved in the assembly of the summations for several points of a limb profile, given any one scattering coefficient, are somewhat tedious and will not be described. For a given scattering coefficient, light transmission sums were calculated for h_0 values of 5, 10, 15, 20, 25, 30, and 40 kilometers. This was done for each of five scattering coefficients: 0.00641, 0.0106, 0.0175, 0.0358, and 0.0543 per

kilometer air at normal temperature and pressure (NTP). The results of these calculations are displayed in the curves of figure 2. Certain features of these curves are discussed as follows.

1. The maximum slopes of the several curves do not differ much. Contrary to a sometimes-expressed notion that the blue horizon is less sharp than the red, recent photographs (obtained in two-color frames with a camera mounted in an X-15 aircraft) help to confirm the Gemini IV mission results, that the blue and red horizons do not differ much in relative appearance.

2. At terrestrial levels lower than 10 kilometers, the curves for larger scattering coefficients are indicative of a falloff brightness. The source of this is evident from the curves of figure 2 that describe the relative contributions from the successively more remote elements of a given lamina for the scattering coefficient 0.0175 per kilometer NTP. It reasonably might be expected that because secondary scattering has been ignored here, the recession of brightness will not be observed. However, the blue-limb photographs do not support this supposition.

3. Insofar as any particular scattering coefficient results in a curve with an inflection point significantly below the tropopause, these calculated results may be considered unobservable, or unreal. This is because these calculations involved single scattering only; multiple scattering and the influence of the albedo of the earth or clouds was neglected. In reference to these effects, the brightness of the zenith sky is cited (ref. 1) as 0.0427 for single scattering alone, 0.0515 for multiple scattering, and 0.0559 for a ground albedo of 0.1.

EXPERIMENTAL PROCEDURE

The experimental procedure on the Gemini IV mission was simply to use a handheld camera to take a series of groups of three photographs of the limb of the earth, at intervals of approximately 5 minutes during the sunlit part of one revolution. These photographs necessitated installation of a two-color (red in the center and blue on the sides) Wratten filter mosaic in the camera magazine, mounted closely in front of the focal plane behind the dark slide. The thin frame of the filter mosaic reduced the picture area to approximately 44 by 43 millimeters with a narrow vertical center mullion. Thus, the margins beyond the filter panel made edge strips of the film available for densitometric exposures. The magazine could be loaded with sufficient film for approximately 40 exposures. Extended panchromatic film was used. The filters used, numbers 92 and 47B, had transmission regions of 400 to 470 nuclear magnetons centered at approximately 432 nuclear magnetons, and 640 to 710 nuclear magnetons centered at approximately 675 nuclear magnetons.

The method used for taking the pictures, in consideration of spacecraft and power exigencies, was to take the pictures forward, in the direction of the orbit as judged by the crewmember. This caused the loss of the early morning pictures when the sun was just to the right of straight ahead and was shining on the window. The pictures were measured with the microdensitometer of the Harvard University Physics Laboratory. The microdensitometer records directly the transmission data by transversing the limb image across a fine slit that is set parallel to the limb. It travels across the back once,

normal to the limb, in the blue part of the image and then again in the red, each time close to the filter joint. Repetition of the procedure on the other side of the picture was a check on the parallelism of an artificial reference line (a fine ink line drawn on the negative parallel and close to the limb at an arbitrary and convenient distance from the limb profile). The reference line is a satisfactory means to establish the difference of location of the limbs in the radial direction of the earth. The hand-held camera had no means for recording the terrestrial limb.

The radiance profile of the limb could be drawn, in arbitrary units, by reference to a step-wedge calibration exposure. Because the sharpness or definition of the limb was the principal feature available from these photographs for use in Apollo Program navigation observations, such profiles have been investigated. For this purpose, the film prepared for the Gemini IV mission had, on each edge, a series of densitometric exposures made in a flashlamp sensitometer, by use of a step-wedge (21 steps). The exposures on one edge were made through a number 92 red filter and those on the other edge were made through a number 47B blue filter. Each earth-limb photograph could be interpreted by reference to the adjacent step-wedge exposures. The film was developed in a machine in the Manned Spacecraft Center (MSC) photographic laboratory.

RESULTS

The initial inspection of the pictures on the microdensitometer was indicative that the limb profiles in the blue generally were not as sharp as those recorded in the red. This resulted in the need to adopt a useful feature of a limb profile for designation of its terrestrial elevation in the red image compared with the blue, both with respect to the arbitrarily located reference line. The point that was chosen with regard to the gamma values for red and blue was that which had four times the transmission of the limb brightness peak on the negative; these points, in consideration of the difference of λ values for red and blue images, represented a local limb brightness of approximately one-third that at the peak. In terms of this designation, the values of the excess elevation of the blue limb over the red in the measured photographs is shown in table I. These photographs were taken in groups of three, each such group taken in prompt succession and succeeded by another group after almost 5 minutes, until sunset. The picture numbering is indicative that the first two groups were useless because the window was sunlit.

The measurements, complemented by ephemeris data for the orbit and for the sun, resulted in the blue-limb excess elevation over the red and the relevant scattering angles that are tabulated in table I. Regarding the data in table I, note that the scale of the microdensitometer charts was approximately 1.5 millimeters per kilometer; the variation of repeated measurements of a single picture was approximately 0.5 millimeter. The measurement of two sides of each photograph was used as a check for any ill-drawn reference line. Positives of several typical photographs, one printed to show the aspect of the limb primarily and the other to show the face of the atmosphere of the earth (or ground appearance), are shown in figure 3.

Detailed measurements of a blue-limb profile and its red limb will result in unequal peak values of the brightness gradient. The ratios that may represent the

sharpness of the limb are fairly, but not entirely, constant. This means that what is reported as the excess elevation would be different if another feature were the criterion. If the point of half-peak brightness were chosen, rather than the one that was used, the excess elevation would be less. Inasmuch as the several limb-brightness gradients among the different photographs maintain a nearly constant ratio of the red limb to the blue, the excess elevations would retain the same relative aspects. This concept underlies the conclusion that the correlation between the blue-limb excess elevation and the scattering angle was not as good as had been thought based on the Mercury 7 photographs. Also, it is pertinent to note that in those photographs the blue-limb gradients more nearly equaled those of the same limits observed in the red.

The presence in the blue-limb elevation of factors other than scattering angle is obvious. The variable albedo of the lower atmosphere surely is involved, because of its effect on the importance of secondary scattering (which has not been included in the analysis of a Rayleigh atmosphere). As to the terrain itself, the flight log was indicative of which groups of photographs were taken of limbs over land (groups 5, 6, and 7). Three of the groups disclose land in the foreground. The flight passed over Africa, from Morocco to Saudi Arabia. Two of the groups over Africa were not as consistent internally as were others; however, from so few pictures, any generalization is hazardous.

One feature of the data that were evaluated was related to the values of the limb gradients in the several pictures, in which first attention went to the arbitrarily defined excess blue-limb elevation. The limb profiles did not show well-defined inflection points. The details of the limb gradients were indicative of an unexpectedly long gradient far out into space, having, at a distance of 200 kilometers, a density as great as 0.4; this is compared with a peak brightness density of 2.5, which corresponded to a radiance ratio of nearly 1.5 percent, because the gamma value was approximately 1.25. The red image tail was only one-third of this value. This predominantly blue far-out scatter has been found most significant on the photographs taken late in the series. In the fourth group, the far-out scatter was almost equal in the red and in the blue; in the earliest groups, it was stronger in the red. Such was not observed in the pictures from the Mercury 7 and 9 missions. The blue far-out scatter was thought to be artificial, either because of the dirty window surface or because of some stray light. The reason for its variance with the time of day was not obvious. The scatter was without pattern, being bounded by the filter frame alone.

To obtain a concise survey of the peak value of gradients of the earth-limb radiance, attention has been confined primarily to an arbitrary feature available from the many microdensitometer traces. The definition of the gradient chosen has been the difference in terrestrial elevation that occurred between points on the limb which had one-half and one-fourth, respectively, of the peak image densities of that limb. In the red limb, these differences (which corresponded to a brightness ratio of $\log^{-1} 0.20$ for $\lambda = 1.5$) average 4.8 kilometers, the greatest was 6.0 kilometers and the least was 4.0 kilometers. In the blue limb, they corresponded to a ratio of $\log^{-1}$ of 0.24, λ being approximately 1.26. They averaged 7.2 kilometers, being 8.6 and 5.2 kilometers (greatest and least). These numbers were indicative that, with a limb-sensing device this is capable of measuring to 2 percent, the red-limb accuracy would be approximately 0.2 kilometer, and a blue-limb accuracy of approximately 0.27 kilometer.

Referring to the analytically derived curves for a Rayleigh scattering atmosphere, a difference of 8.1 kilometers was found for the ratio of $\log^{-1} 0.300$, which was between the estimated values for the blue-limb and the red-limb gradients for the Gemini IV negatives. These numbers are assembled in slightly revised form in table II. It is not now possible to give any appraisable numbers regarding peak values of the limb radiances. Comparative values between the blue and red limbs, which were frequently obtained when two parts of the same limb were scanned without any change in the microdensitometer slit, varied nearly 50 percent; the two opposite sides of the same limb were significantly different repeatedly. Traces of outer aerosol scatter seemed to occur several times, but these were too fragmentary to discuss. The 28- to 30-kilometer dust maximum also was not obvious.

CONCLUSIONS

The dependence of the excess blue-limb elevation was less obviously determined by the scattering angle than was suspected from an examination of the Mercury 7 photographs. In several cases, various factors cause three photographs (taken as one group in rapid succession) to vary as much as one group varied from the next. Generally, the blue limbs were less sharp than were the red limbs (the worst case was in the ratio of 2 to 3). Consequently, the measured excess blue-limb elevation usually depended on the feature chosen to define it. Concerning the practical matter of the precision of observation of the blue earth limb, a sensor of 2-percent accuracy could result in a limb-sensing accuracy of about 0.27 kilometer for a limb distance of 1600 kilometers. It is reasonable to surmise that the variation of the values of excess blue-limb elevation originated principally from the red-limb variance, because the form of the blue-limb profiles (at least in their upper part) was more regular than was that of the red-limb profiles.

REFERENCES

1. Van de Hulst, H. C.: Scattering in the Atmosphere of the Earth and Planets. Ch. 3, Atmospheres of the Earth and Planets, G. P. Kuiper, Ed., Univ. Chicago Press, 1952.

2. Minzner, R. A.; Champion, K. S. W.; and Pond, H. L.: The ARDC Model Atmosphere, 1959. Air Force Surveys in Geophysics No. 115 (AFCRC-TR-59-267), Air Force Cambridge Res. Center, Aug. 1959. cf. NASA, U.S. Air Force, and U.S. Weather Bureau: U.S. Standard Atmosphere, 1962, U.S. Government Printing Office, Dec. 1962.

3. Middleton, W. E.K.: Vision Through the Atmosphere. Univ. Toronto Press, 1952.

TABLE I. - EXCESS ELEVATION OF THE BLUE LIMB OVER THE RED LIMB

Photograph number	Elevation difference, blue over red		Scattering angle, deg
	Difference, km	Average, km	
7	4.4		
8	4.0	4.2	53
9	4.3		
10	7.2		
11	7.0	6.7	68
12	6.0		
13	7.3		
14	8.5	7.3	83
15	6.1		
16	4.5		
17	5.4	4.8	99
18	4.5		
19	5.2		
20	5.0	5.1	113
21	5.2		
22	5.5		
23	5.7	5.8	125
24	6.3		
25	5.7		
26	6.9	6.4	133
27	6.6		
28	7.8		
29	8.7	7.7	138
30	6.5		

TABLE II. - DATA FROM THE GEMINI IV NEGATIVES

Limb gradient, log radiance ratio/km	Limb	Precision of observing with 2-percent sensor, km
0.042	Average red	0.21
.033	Poorest red	.27
.050	Best red	.18
.033	Average blue	.27
.027	Poorest blue	.33
.046	Best blue	.20
.037	Rayleigh, calculator, single scatter	.24

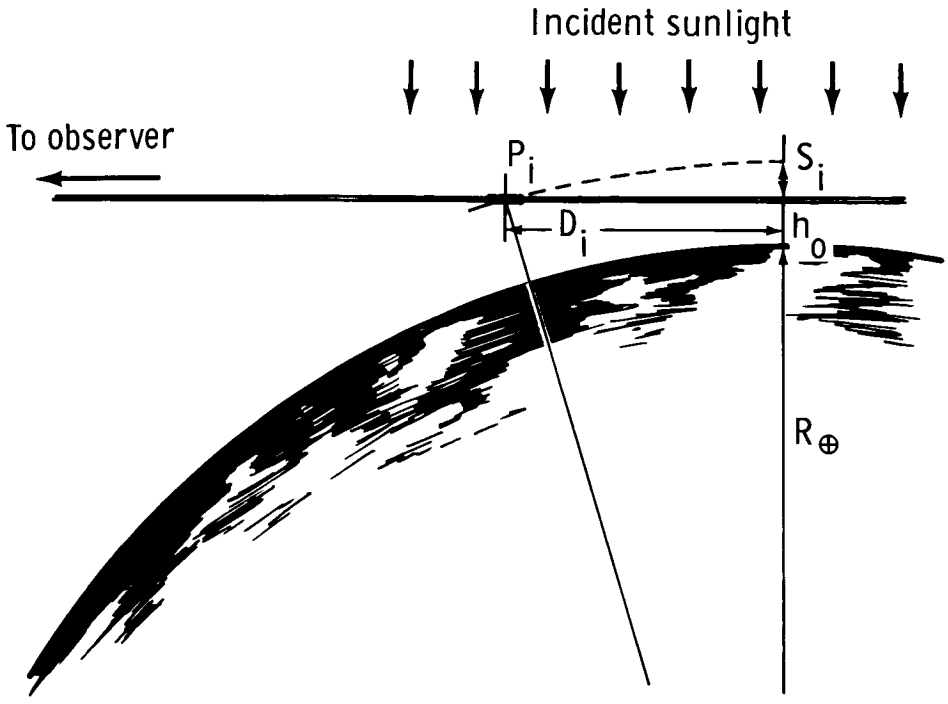

Figure 1. - The lamina of the atmosphere of the earth.

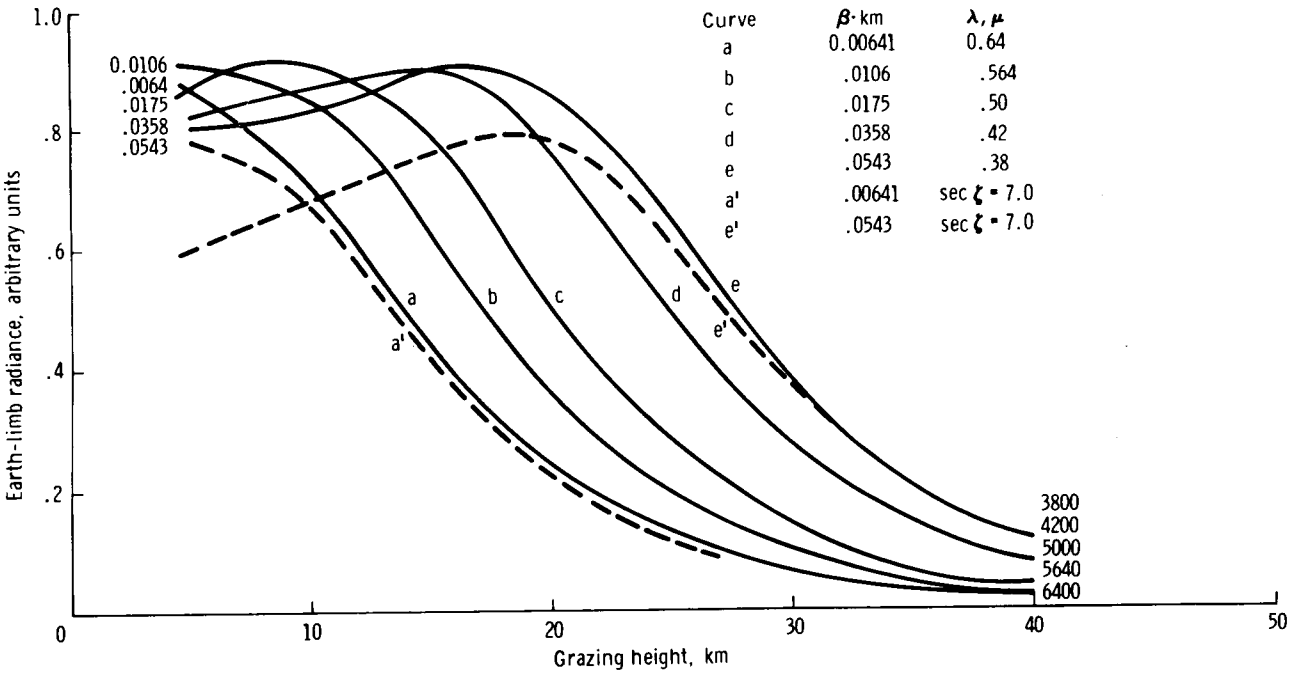

Figure 2. - The radiance of the limb of the earth referred to solar radiance.

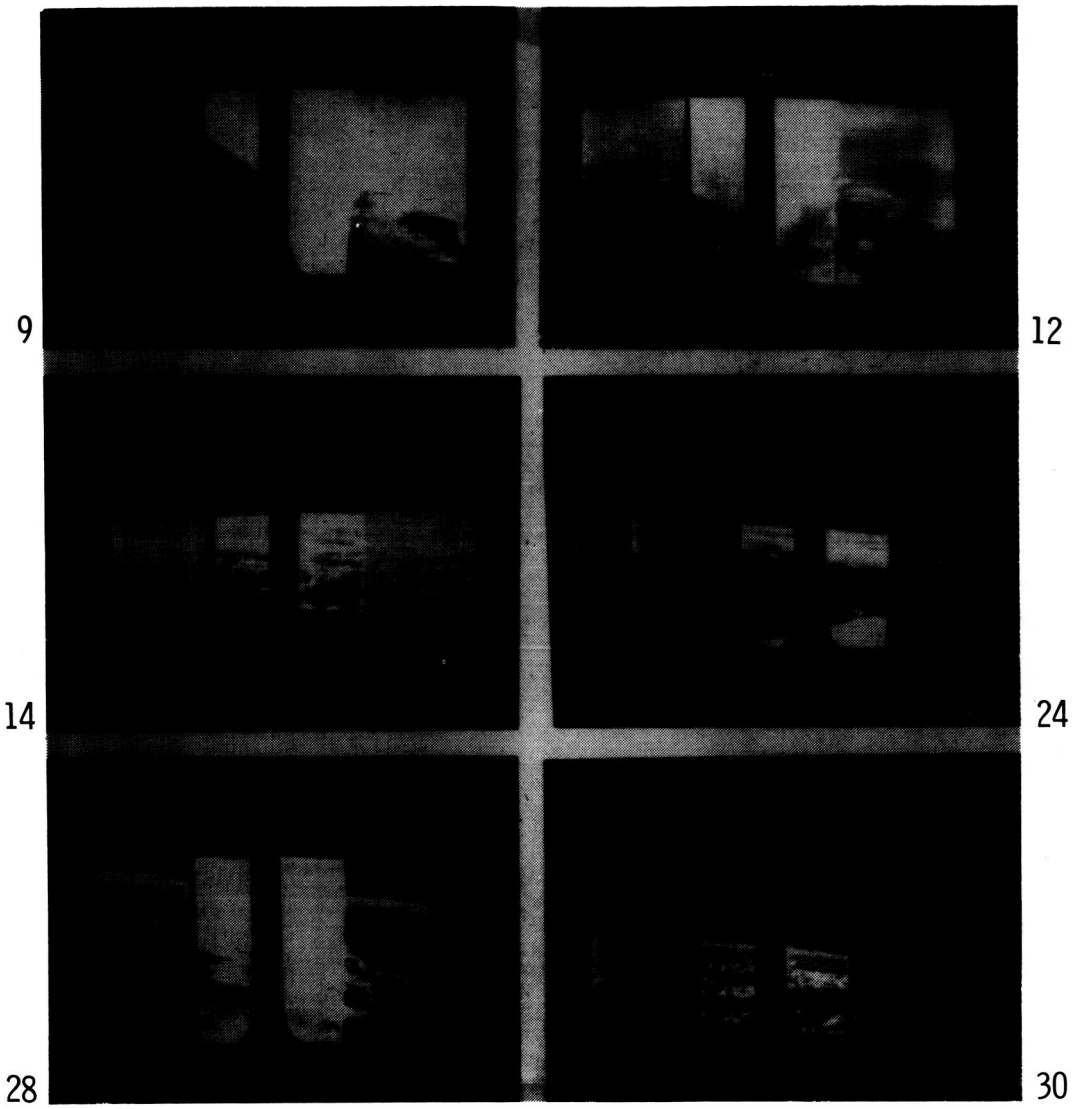

(a) Frames 9, 12, 14, 24, 28, and 30.

Figure 3. - Two-color earth limb photographs.

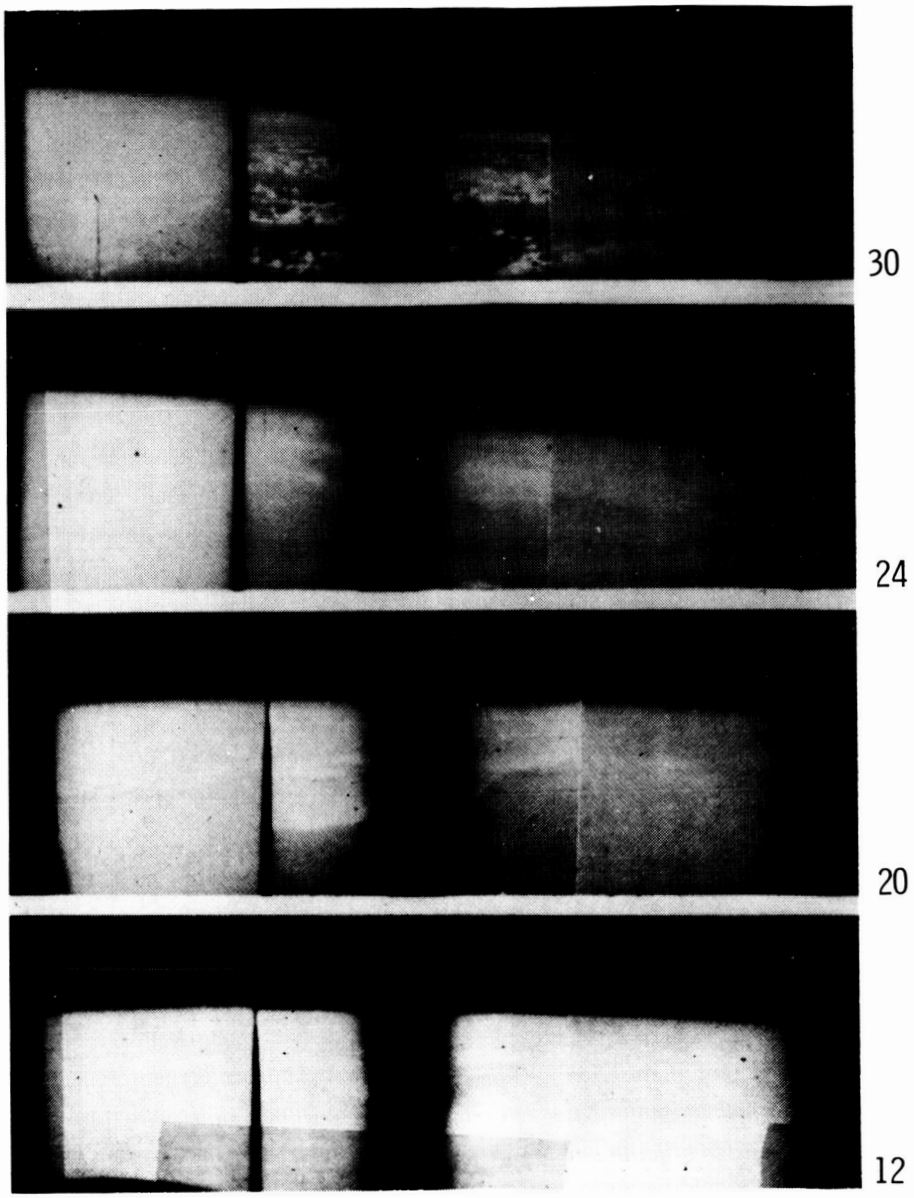

(b) Frames 12, 20, 24, and 30.

Figure 3. - Concluded.

EXPERIMENT M403

ELECTROSTATIC CHARGE

By Patrick E. Lafferty*

OBJECTIVE

Experiment M403 was flown on the Gemini IV and V spacecraft in an effort to discover whether the spacecraft could accumulate sufficient excess electric charge to constitute a hazard for later Gemini-Agena rendezvous missions. An attempt was made to measure the electric field terminating on a small area of the spacecraft retrograde adapter section. Then, an attempt was made to calculate the total spacecraft charge from this measured field value.

EQUIPMENT

The experimental instrument was called an electrostatic potential meter (EPM); the EPM is shown in figure 1. The EPM consisted of two packages, the sensor and the electronics unit. The two packages were mounted in the spacecraft retrograde adapter section, and were interconnected by electrical wiring (fig. 2). The electronics unit was wired to spacecraft power and telemetry equipment.

The sensor contained a sensing head assembly and a variable-gain amplifier. The electronics unit contained logic and power-conditioning circuitry. The EPM had two outputs that were monitored by two analog telemetry channels that had a sample rate of 1.25 samples per second. The experimental instrument controls consisted of a power-circuit breaker and an on-off power switch; these controls were operated by the pilot.

With the exception of an external modification, the Gemini V experimental equipment was the same as that used on the Gemini IV mission. The modification consisted of a screen assembly mounted in front of the sensor unit. The purpose of the screen was to inhibit the electric field that was incident on the face of the sensor unit.

*NASA Manned Spacecraft Center, Houston, Texas.

INSTRUMENT SENSING PRINCIPLE

When a conducting surface in an electric field is deformed locally, the surface charge density will be altered. When the deformed region is isolated electrically, a potential difference will appear between the region and the remainder of the surface. This difference is a linear function of the electric field. For the EPM, the deformed region was in the form of a disk, and the deformation was a sinusoidal motion normal to the spacecraft surface. The disk was connected to the surface through a resistance. The motion of the disk produced an alternating current (ac) through the resistance. The magnitude of this current was proportional to the diameter of the disk, the frequency at which the disk oscillated, the amplitude of the oscillations, and the electric-field strength. That is,

$$I = -\left(4\pi f a \epsilon_o E_o\right) d$$

where I = current

f = disk oscillation frequency

a = disk radius

ϵ_o = permittivity of free space

E_o = field at conductor surface

$d = d_o \cos(2\pi)$ = distance between the outer surface of the disk and the conducting surface

A block diagram of the Gemini IV EPM is shown in figure 3. As indicated in the figure, the sensor faces away from the spacecraft (toward space). The spacecraft charge distributes itself on the surface of the spacecraft and the sensor disk. As the disk is vibrated by the driver, which is excited by the oscillator output current, an ac voltage is developed across the input of the variable-gain amplifier. The amplifier output is converted into a direct current (dc) signal by the demodulator, and is routed to the spacecraft telemetry system through the buffer and telemetry clamps.

The amplitude of the channel 1 output signal is proportional to the field that is incident on the spacecraft. When the amplifier output varies to values that are greater than or less than the operating range of the level detectors, the automatic ranging logic alters the gain of the amplifier to stabilize the outputs. Voltages that represent the operating range of the amplifier and the polarity of the input field are summed by the digital-to-analog converter and are routed to the telemetry system through channel 2. The squaring circuit, buffer amplifier, and phase detector supply a polarity signal to the digital-to-analog converter.

The instrument outputs, as they would appear if the input electric field varied from the maximum detectable negative value to the maximum detectable positive value, are shown in figure 4.

EXPERIMENTAL PROCEDURE

The EPM was turned on periodically throughout the course of the Gemini IV mission. Because of its low power consumption, the experiment was powered continuously during the Gemini V mission.

RESULTS

The electric-field readings that were made on the Gemini IV mission were extremely large compared with what was expected, based on measurements of potential on satellites and compared with the short discharge times that were expected for a vehicle in the ionosphere. The telemetered data gave no reason to suspect any electrical or mechanical malfunction of the instrument. Consequently, investigations were made to determine whether the apparent electric field was caused by something other than an electric field at the surface of the spacecraft. It was revealed in postflight tests that the instrument was responsive to radiated radio-frequency energy and to streams of charged particles incident on the sensing face of the sensor unit.

The time available between the conclusion of Gemini IV postflight tests and the launch of the Gemini V mission precluded any internal modification of the Gemini V instrument. However, the external screen was incorporated to shield the sensor from electric fields terminating on the spacecraft. From a comparison of the outputs obtained on the Gemini V mission with those obtained on the Gemini IV mission, it was anticipated that an estimate could be obtained of the contribution of the electric field to the output levels that were observed on the Gemini IV mission.

A comparison plot of the data obtained during the first three orbits of the Gemini IV and V missions is shown in figure 5. The preflight calibrations of both instruments were in terms of electric field. The unit that was used for the ordinate of figure 5 is volts per centimeter, as determined in preflight calibrations.

Because the instrument was responsive to charged-particle fluxes, it is possible that the high readings that were made during the initial orbits of both missions were, in part, caused by augmented ionospheric charged-particle concentrations that resulted from outgassing of the spacecraft. There is some evidence to support this hypothesis. Because heating of the spacecraft would have accelerated outgassing, it would be expected that the ionosphere would be enhanced during the daylight portions of the initial orbits. During the first three orbits of the Gemini V spacecraft, sustained high readings occurred during daylight. A dropoff of one to two orders of magnitude occurred during a period of approximately 5 minutes preceding total darkness, succeeded by lower readings during the subsequent period of total darkness. The Gemini V data were indicative that the output began to increase upon exit from total darkness.

The total darkness periods early in the Gemini V mission (fig. 5) were from 00: 42: 00 to 01: 21: 00 g. e. t., from 02:12: 00 to 02: 50: 00 g. e. t., and from 03: 50: 00 to 04: 20: 00 g. e. t.

Additional support for the enhanced-ionosphere hypothesis was obtained from the Gemini V air-to-ground communications log. The Gemini V crewmen reported a slight yawing of the spacecraft because of operation of the water boiler before 00: 45: 00 g. e. t. An enhanced ionosphere, caused by the ejection of steam, may have contributed toward the high readings from 00: 25: 00 to 00: 37: 00 g. e. t. Also, the Gemini V crewmen reported fuel-cell purging in progress at 01: 50: 00 g. e. t. A significant and abrupt increase in instrument output occurred at 01: 45: 00 g. e. t.

Additional support for the enhanced-ionosphere idea was noted from a comparison of the outputs during the initial orbits of the Gemini IV spacecraft with outputs later in the mission. Gemini IV data from 46: 05: 00 to 47: 10: 00 g. e. t. are shown in figure 6. These outputs were comparatively steady; the maximum output was two orders of magnitude lower than the highest readings taken in the initial orbits. Perhaps this was an indication that outgassing was no longer taking place. The Gemini V instrument ceased to function properly after 04: 05: 00 g. e. t.

CONCLUSIONS

The Gemini V instrument was inhibited from responding to electric fields that corresponded to a charge on the spacecraft. However, readings were obtained on the Gemini V mission that were of as great or greater magnitude than those obtained on the Gemini IV mission. This could be interpreted as an indication that the contribution of a net spacecraft charge to the Gemini IV measurements was negligible. An operational measurement that was performed on a later rendezvous mission was indicative of a very small exchange of charge between the Gemini spacecraft and the Agena vehicle.

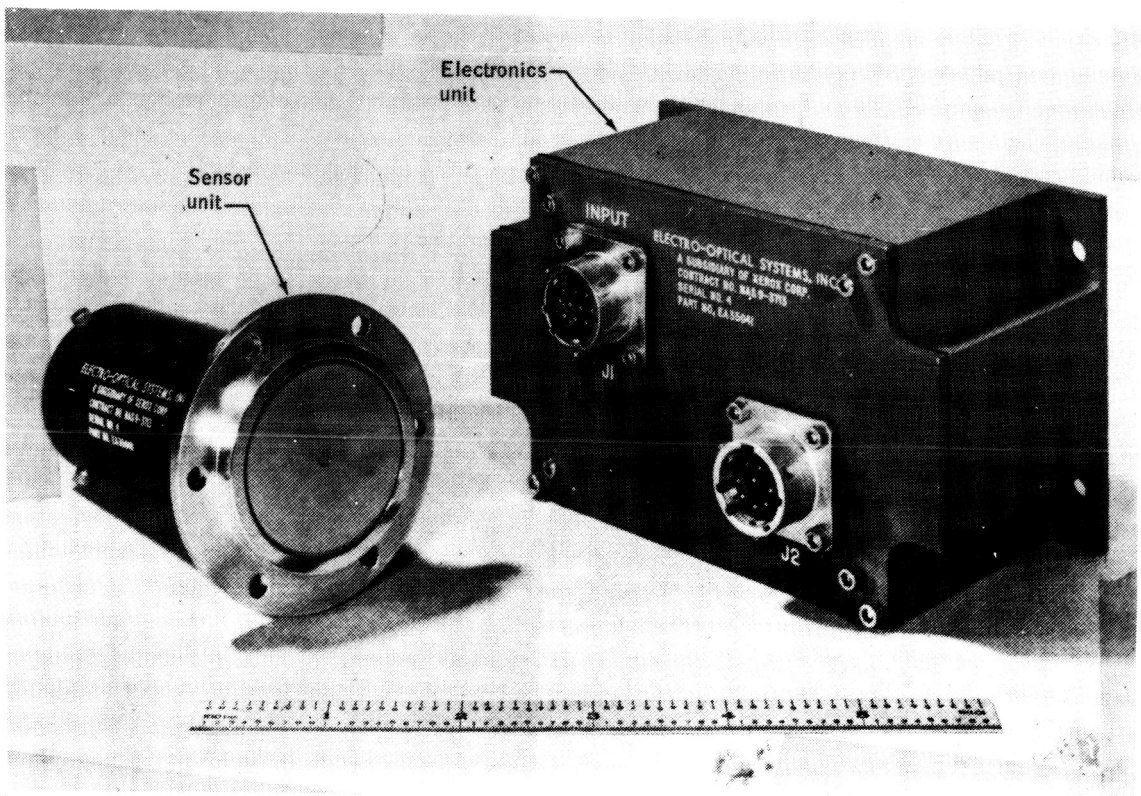

Figure 1. - The equipment components.

Figure 2. - The equipment location.

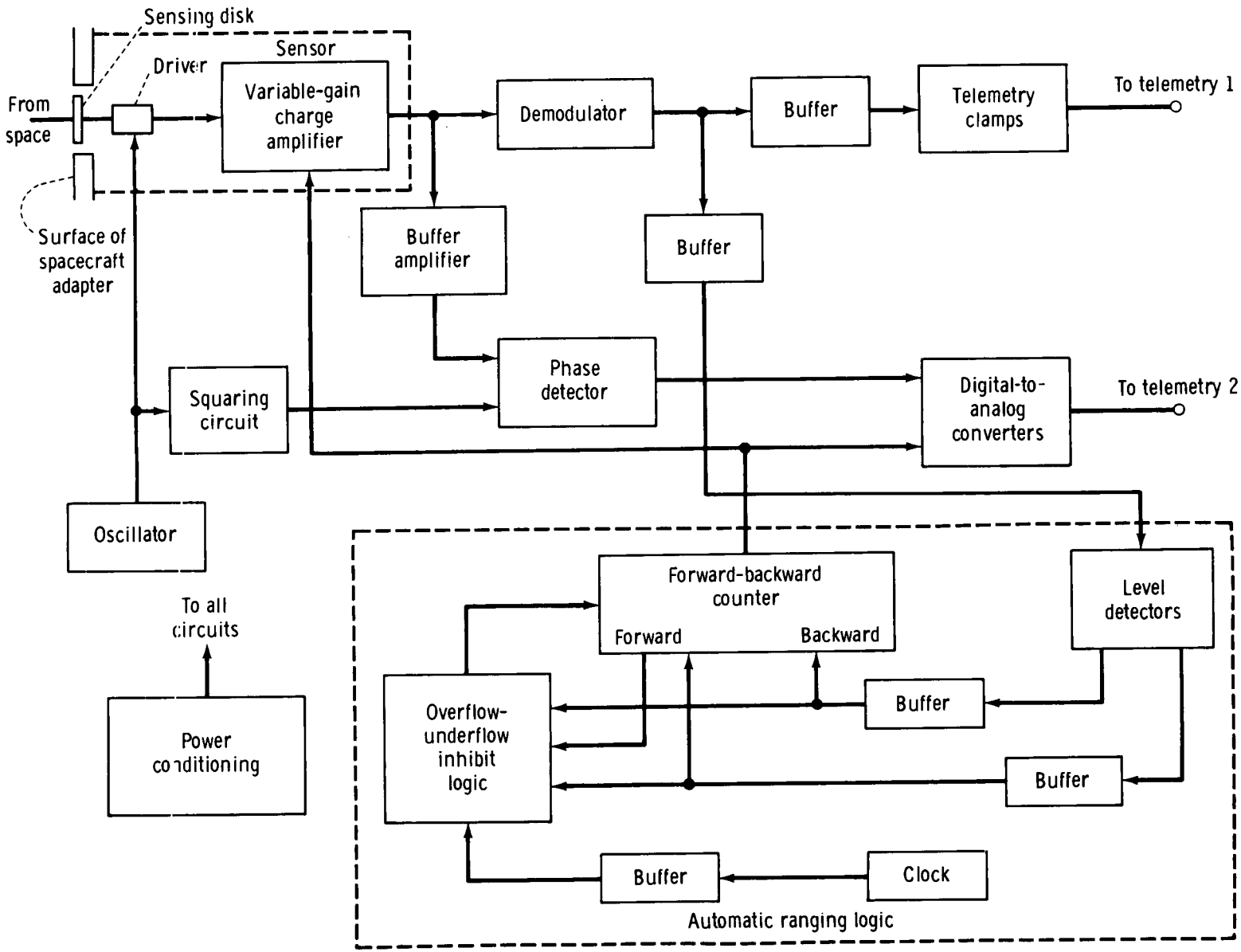

Figure 3. - The instrument block diagram.

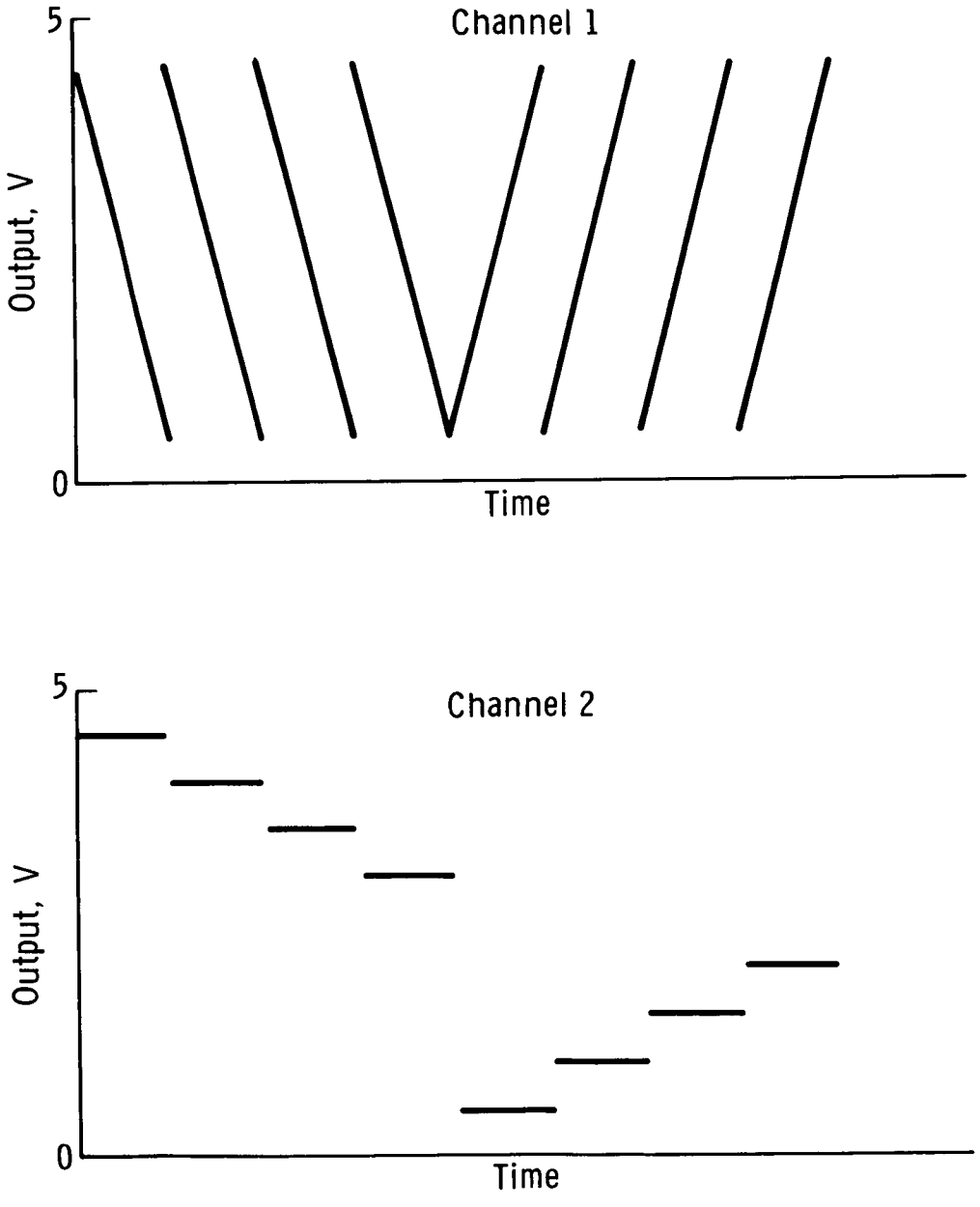

Figure 4. - The instrument outputs.

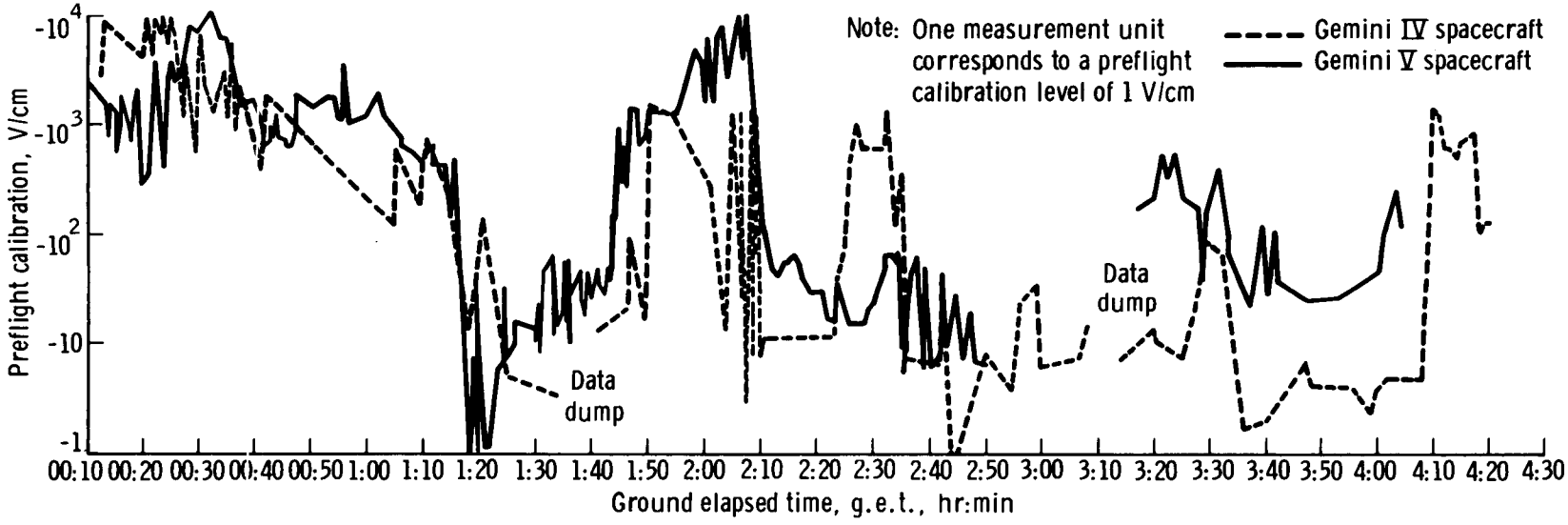

Figure 5. - Instrument measurements made during the first three revolutions.

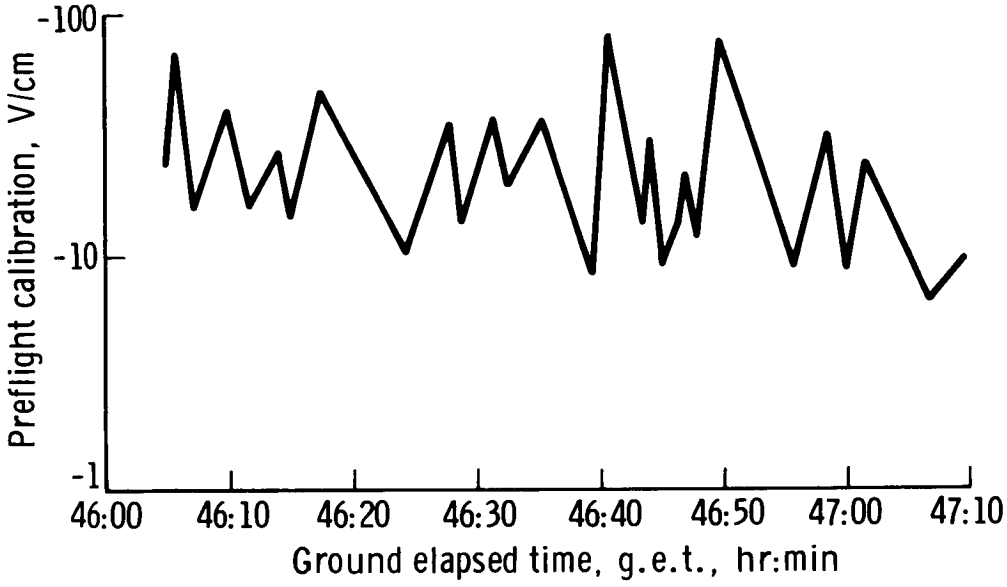

Figure 6.- Measurements made during revolution 30 of the Gemini IV mission.

EXPERIMENT M404

PROTON-ELECTRON SPECTROMETER

By James R. Marbach*

INTRODUCTION

Experiment M404 was one of a series of experiments performed during the Gemini IV mission to acquire a detailed description of the radiation environment. Data from these experiments were used as source terms for the calculation of radiation doses received by the crewmembers. The dose calculations not only necessitated an exact description of the radiation environment, but also necessitated a detailed shielding evaluation of the spacecraft and a knowledge of the modes of interaction between the spacecraft and nuclear particles. Comparison of theory with experimental data was accomplished by the use of dosimeters to monitor the integrated dose received by each crewmember. Experiment M405 was flown in support of Experiment M404 to establish the instantaneous direction of the magnetic field of the earth relative to the spectrometer. This information was needed for the reduction of data from Experiment M404 because the particle intensities were strongly directional with respect to the magnetic field.

Generally, the orbital altitude of the Gemini IV mission was far below the altitude at which the protons and electrons (trapped in the geomagnetic field of the earth) are encountered. However, there is an anomaly in the geomagnetic field over the South Atlantic, approximately between latitudes 15° S and 55° S and between longitudes 30° E and 60° W, where the field lines drop to lower altitudes. The revolutions of charged particles about a particular field line, governed by the magnetic moment of the particles, brought them to an altitude that was intersected by the Gemini IV orbits from revolution 4 to revolution 10; thereafter, intersection occurred every 16 revolutions.

The simultaneous measurement of the external radiation environment and the radiation dose received by the crewmen during a mission was useful to evaluate and perfect calculational techniques. By the use of these techniques, the dose to be received by the crewmen on any given mission can be estimated before that mission.

*NASA Manned Spacecraft Center, Houston, Texas.

EQUIPMENT

The spectrometer was designed, constructed, and calibrated by the experiment equipment contractor. A similar spectrometer was used on a polar-orbiting U. S. Air Force satellite. The specific function of the Experiments M404 and M405 instrumentation was to facilitate establishment of an accurate picture of the proton and electron intensities and energies. Another objective was establishment of the direction and magnitude of the magnetic field of the earth during selected portions of the Gemini IV and Gemini VII missions.

Gemini IV Mission

A pulse-height analyzer equipped with a plastic scintillator in an anticoincidence arrangement was used on the Gemini IV mission for the proton-electron measurement. Internal gain-shifting techniques made possible alternate measurements of the proton and electron environment every 13 seconds. The instrument monitored electrons of $0.45 < E < 6.0$ MeV and protons of $23.5 < E < 80$ MeV at fluxes between 0 and 3×10^5 particles/cm^2-sec. During the Gemini IV mission, a tri-axial flux-gate magnetometer was used in Experiment M405 to detect the direction and amplitude of the magnetic field of the earth. A cross section of the spectrometer is shown in figure 1. The main scintillator was used as a detector for both protons and electrons, and was shaped for an approximately uniform path length over a solid angle of approximately 1.2π steradians. The average thickness over the solid angle was approximately 5.0 g/cm^2.

Identical pilot B plastic (which was separated optically from the main scintillator by reflective paint) completely surrounded the main scintillator except for the aperture and the photomultiplier (PM) tube coupler. Its function was to establish anticoincidence to all particles that entered the main scintillator through any portion of the instrument other than the entrance orifice. A PM tube monitored the main scintillator through a lead-glass light pipe. The anticoincidence scintillator was monitored by the use of three parallel-connected PM tubes. To minimize anticoincidence rate and to guarantee a rugged mounting, the entire package (including the electronics) was set in an aluminum case. The 5.1 g/cm^2 shielding by the lead-glass light pipe coupled the main scintillator to the PM tube. The shielding, PM tube and electronics, and packaging reduced to a negligible quantity the number of particles that entered through that sector not controlled by the anticoincidence scintillator.

The spectrometer (which weighed approximately 12.5 pounds) and the magnetometer were placed on a mounting pedestal that was fixed to the blast-shield door on the Z-axis of the equipment adapter. The measurement was made by looking true aft through the thermal curtain to the outside. Calibrations were used to correct for the effects of the thermal curtain. The mounting location is shown in figures 2 and 3.

To measure the radiation environment in the anomaly, it was necessary to be able to distinguish between low fluxes of protons and high fluxes of (principally) fission electrons. Because electron measurements had been made already by the use of a proven

instrument, it was decided to modify this basic electron instrument to provide the capability to make proton measurements. The result was equipment that distinguished protons from electrons by the use of rather straightforward and proven pulse-height-analysis techniques with special gain shifting and discrimination. To monitor the flux and energy of electrons and protons, a combination of shielding and a knowledge of the approximate proton-electron flux ratios in the anomaly region were used in addition to gain shifting in the preamplifier of the main scintillator circuit. The ranges of particles to be measured were chosen to be $0.45 \leq E \leq 6.0$ MeV for electrons and $23.5 \leq E \leq 80$ MeV for protons. With the instrument in the proton-detection mode, negligible error caused by electron contamination was expected because fluxes of electrons of $E > 23.5$ MeV were known to be very small. Some contamination by low-energy protons in the electron measurement was expected, but all data on anomaly fluxes were indicative that the electron flux exceeded the proton flux by a large factor. Thus, the net contribution to the overall electron spectrum measured was expected to be negligible. Evidence that proton-anomaly spectra may have a large number of protons present at $E < 10$ MeV has been considered, and a spectrometer was designed for use on the Gimini VII mission. This instrument was expected to aid in the resolution of this question and to facilitate a check on the assumption made in this design. Also, the 0.001 g/cm^2 aluminized Mylar light shield that covered the entrance aperture helped minimize low-energy-proton contamination.

Gemini VII Mission

The spectrometer that was used on the Gemini VII mission involved the same pulse-height-analyzer technique that was used on the Gemini IV mission, except the anticoincidence scintillator was replaced with a thin dE/dx plastic wafer over the instrument entrance aperture. This modification facilitated measurement of protons of $5 < E < 18$ MeV instead of $25 < E$ 80 MeV. The electron range-and-flux-handling capabilities were the same as those that were used on the Gemini IV mission. Again, protons and electrons were measured alternately in time. The Gemini VII mission magnetometer was identical to the magnetometer that was used on the Gemini IV mission. The instruments as used on both spacecraft are shown in figure 1 and figures 4 to 6.

RESULTS

Gemini IV Mission

Both experiments were performed at the same time throughout the Gemini IV mission and were scheduled for turn-on during passes that would result in maximum coverage through the South Atlantic anomaly region between South America and Africa. This region was the only portion of the spacecraft trajectory that contained any significant intensities of protons and electrons. An intensity-time history for a typical pass through the anomaly is shown in figure 7. This particular revolution has been converted to true omnidirectional flux, and the peak count rate was approximately 10^4 electrons/cm^2-sec and 10 protons/cm^2-sec. Peak counting rates encountered

never exceeded approximately 6×10^4 electrons or 10^2 protons. Characteristic electron spectra observed through one anomaly pass are shown in figure 8. As is evident in the figure, the spectrum changed significantly through the anomaly. The proton spectrum for the same pass is shown in figure 9. In figure 9, the change in shape is much less obvious.

A plot of magnetometer data that were typical throughout most of the Gemini IV mission is shown in figure 10. The strong directional variation of the field lines with respect to the spacecraft during revolutions 7 and 22 was caused almost entirely by the tumbling motion of the spacecraft (which was free to drift in pitch, roll, and yaw throughout most of the mission). Revolution 51 was a pass during which the pilot held pitch, roll, and yaw as close to zero as possible. The total field strength that was measured during revolution 51 was compared with the theoretical values predicted for this region by the use of a computer technique (fig. 11). The difference was attributed to small errors in the measurement caused by stray magnetic fields from the spacecraft. To verify this assumption, the total field-intensity values, as predicted by use of the computer technique, were assumed to be correct, and the three axes were corrected appropriately so that the measured total field was in agreement with the predicted values. These corrected values are shown in figure 11.

A plot of the total field direction measured on revolution 7 with the correction included is shown in figure 12. The point at which the spacecraft Z-axis was (approximately) parallel with the magnetic field correlated with an observed dip in charged particle intensity (as monitored by the Experiment M404 spectrometer). Because the flux incident on the spectrometer was at a minimum whenever the Z-axis of the spacecraft was alined with the magnetic field, this dip would have been expected if the corrected data were true. Additional data are shown in figures 13 to 16.

To determine what intensities and spectra were encountered throughout the mission, the data shown in figure 7 were replotted in B and L coordinates. Then, this plot and figures 10 and 11 were used in the computer code (developed at the NASA Manned Spacecraft Center) to calculate what approximate dose should have been received by the crewmen for the entire mission. The B and L plots were based on only one revolution; thus, the plots contained only preliminary data with corresponding uncertainties in the dose estimates. The spectral data used were true to within a factor of approximately two.

Gemini VII Mission

Quick-look, strip-chart data were indicative that the spectrometer was operating as was expected for the electron measurement. However, proton data appeared to be somewhat erratic and were suspicious. Several days before the Gemini VII launch, the magnetometer Z-axis detector failed. Replacement of the sensor would have caused the launch date to be rescheduled; it was decided, based on the apparent reliability of the total intensity values (as determined on the Gemini IV mission), that the needed directional data could be obtained by the use of only two axes and the calculated total B values. Preliminary strip-chart data from the mission showed that the X- and Y-axes performed as was predicted.

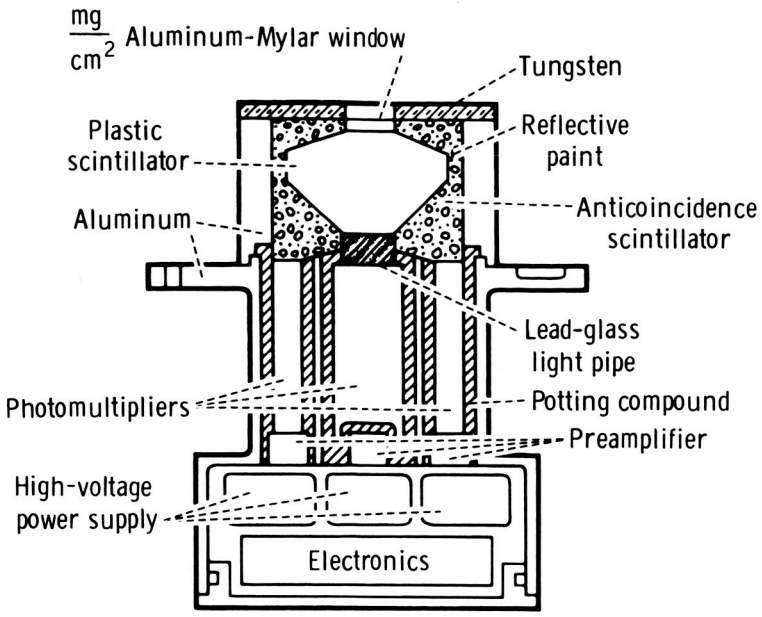

Figure 1. - Proton-electron spectrometer.

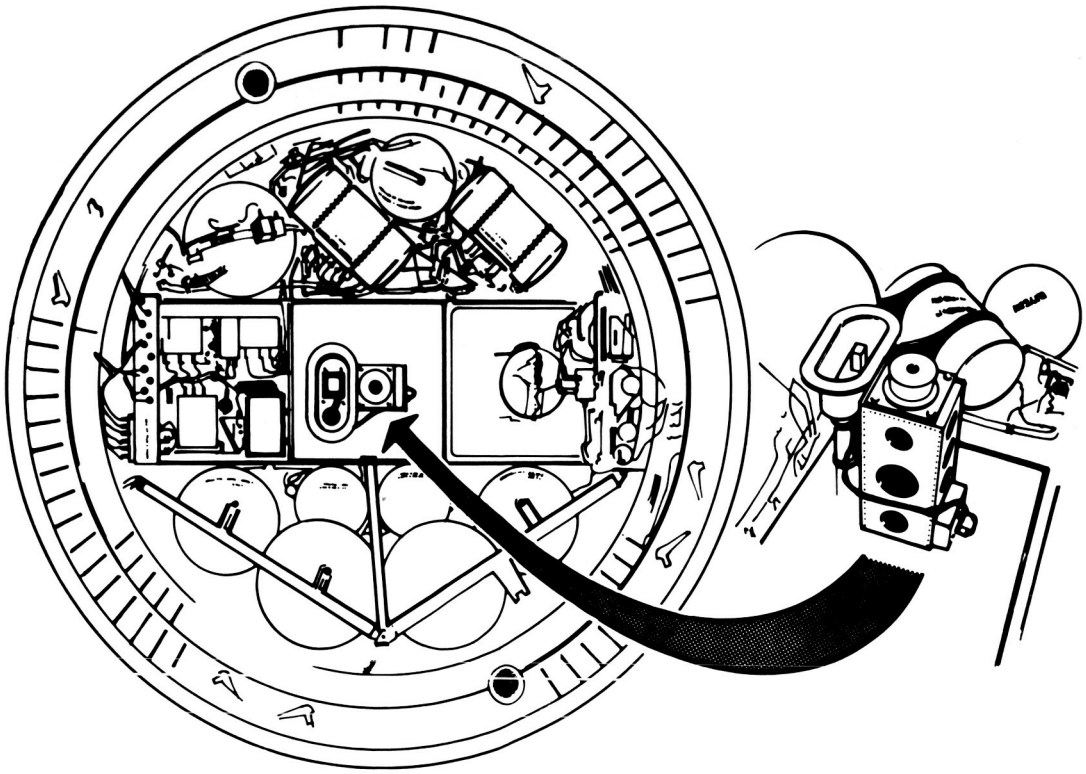

Figure 2. - Equipment location on the Gemini IV spacecraft adapter assembly.

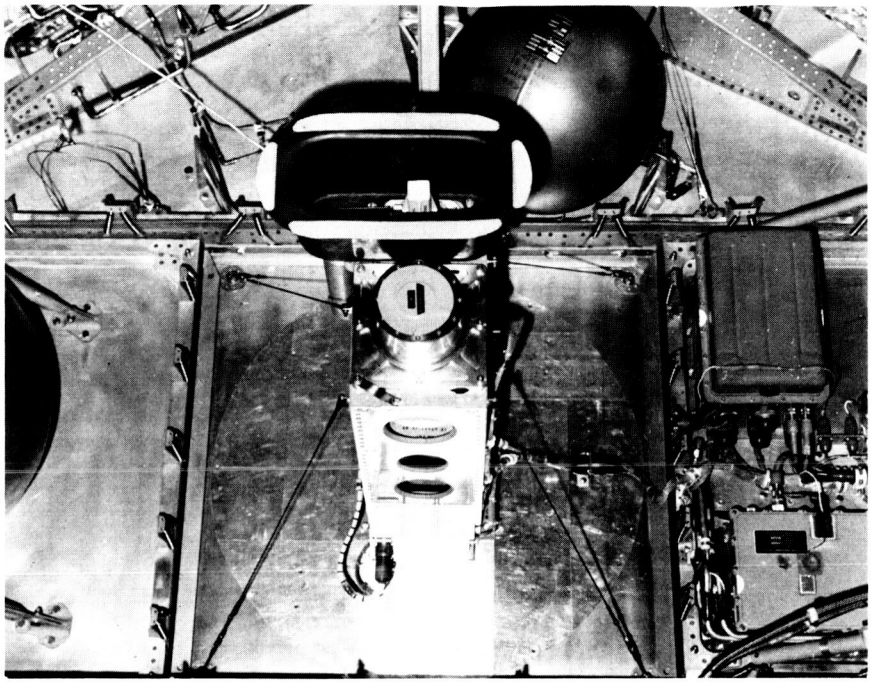

Figure 3. - Location of equipment on the Gemini VII spacecraft.

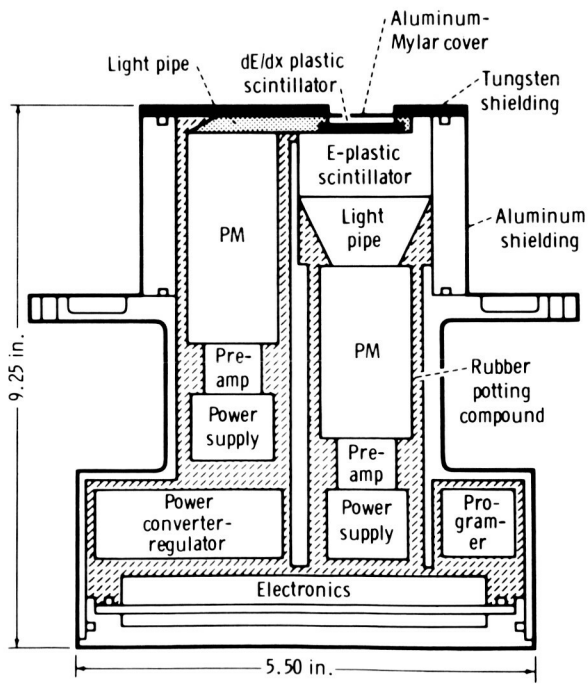

Figure 4. - Gemini VII proton-electron spectrometer.

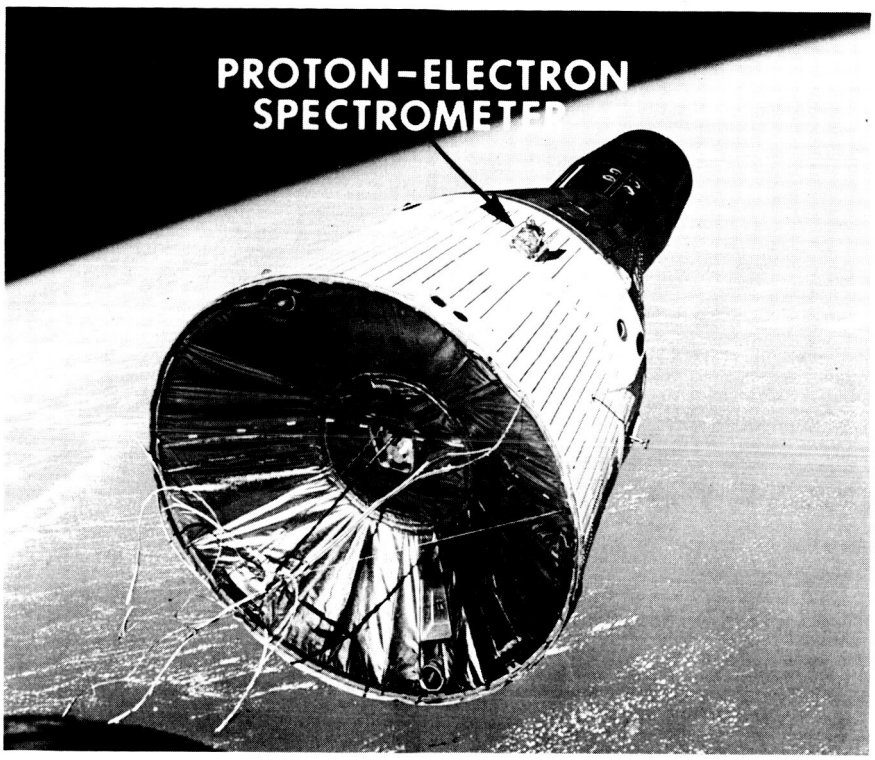

Figure 5. - Gemini VII spacecraft and a view of the equipment location.

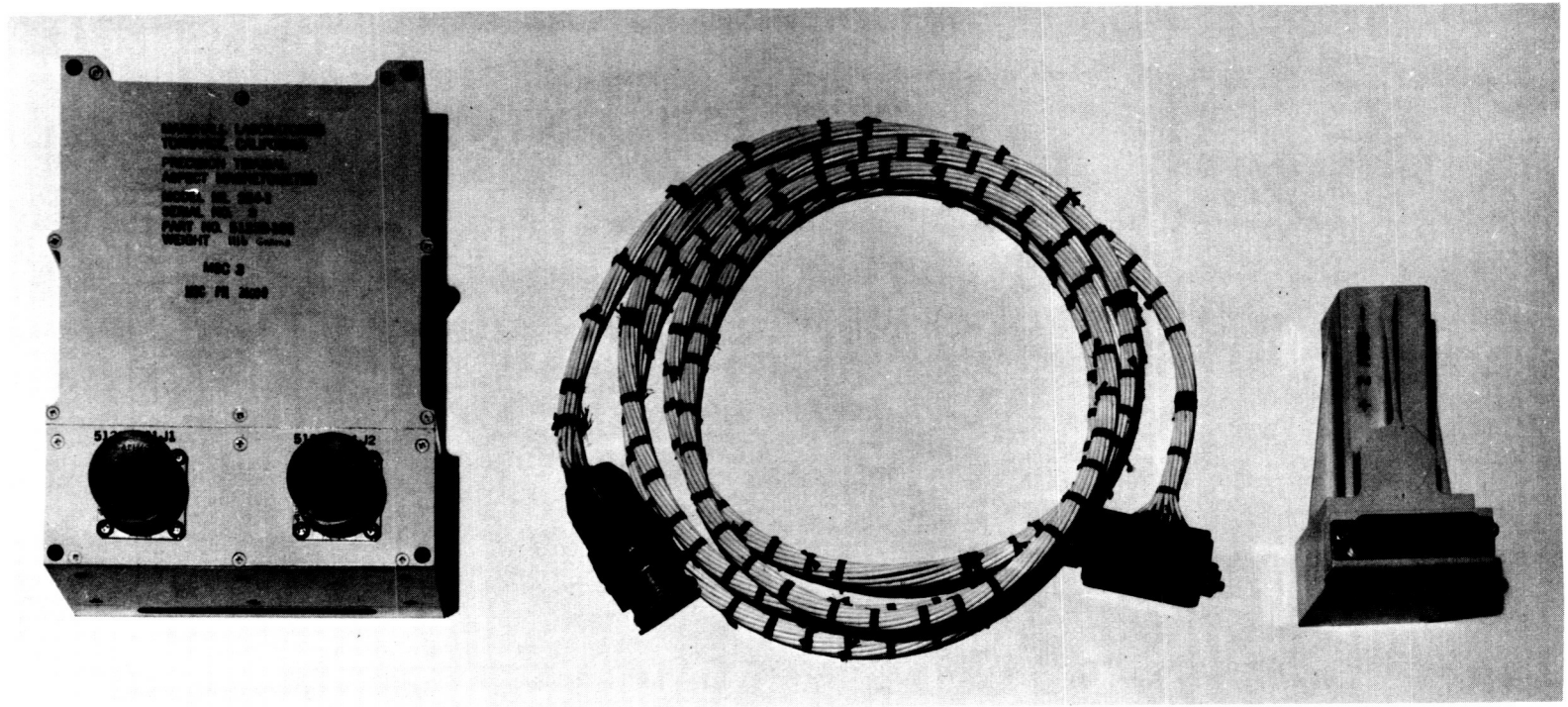

Figure 6. - Tri-axis flux-gate magnetometer.

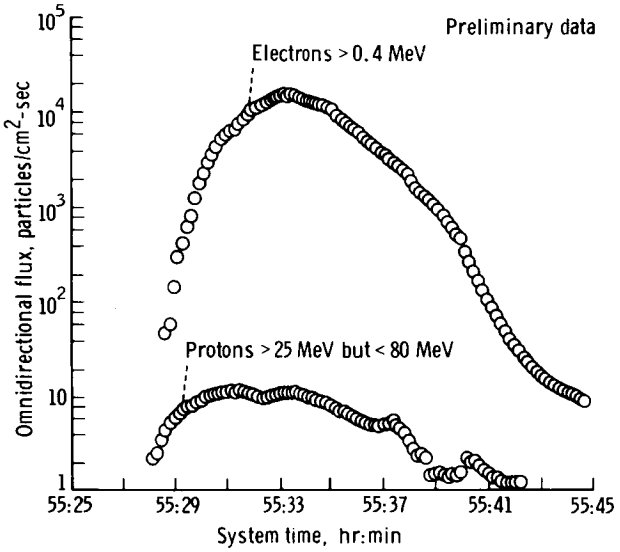

Figure 7. - Data collected on revolution 36 of the Gemini IV mission.

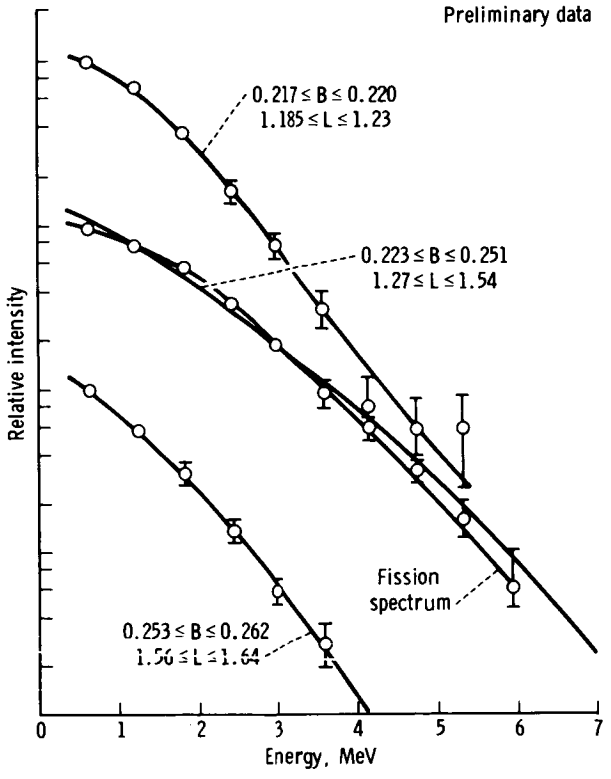

Figure 8. - Characteristic electron spectra noted on revolution 36 of the Gemini IV mission.

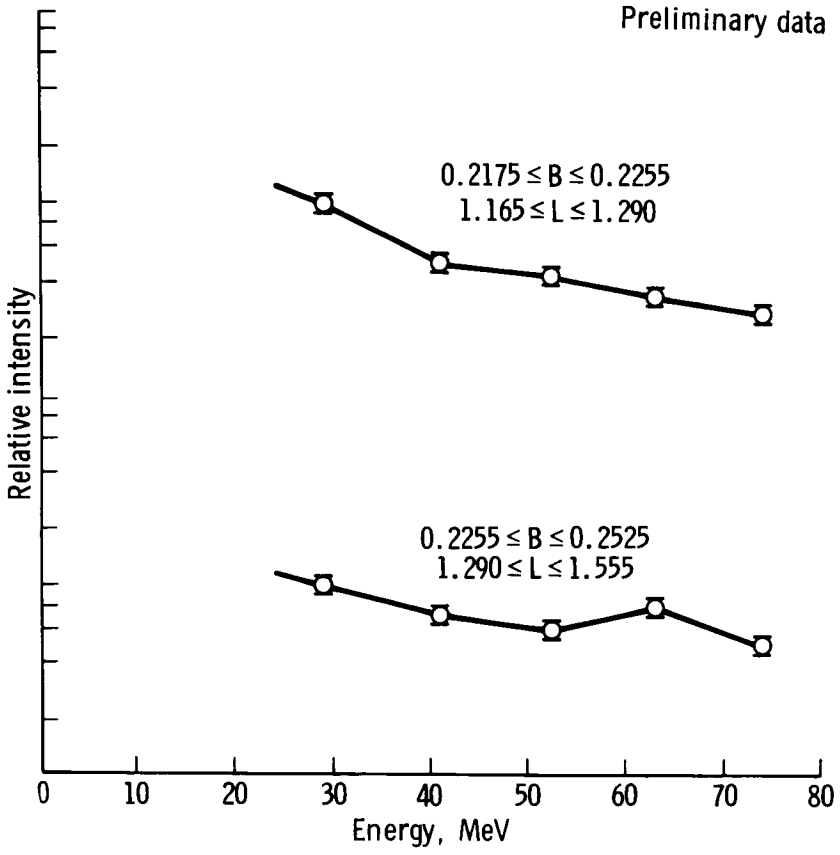

Figure 9. - Characteristic proton spectra for revolution 36 of the Gemini IV mission.

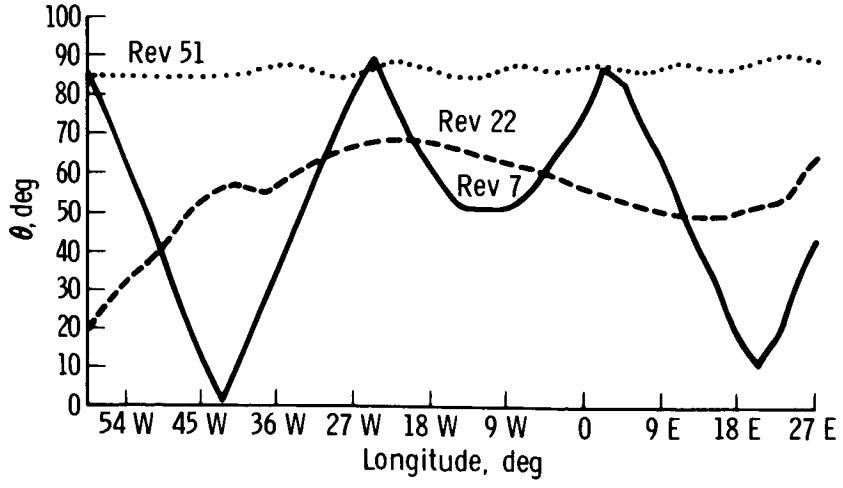

Figure 10. - Magnetic-field direction during the Gemini IV mission.

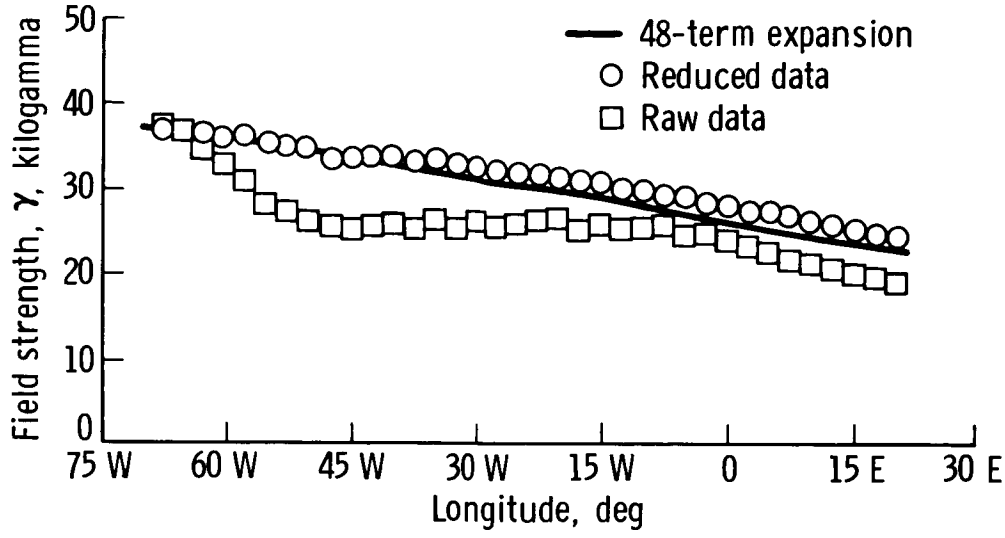

Figure 11. - Field strength measured during revolution 51 of the Gemini IV mission.

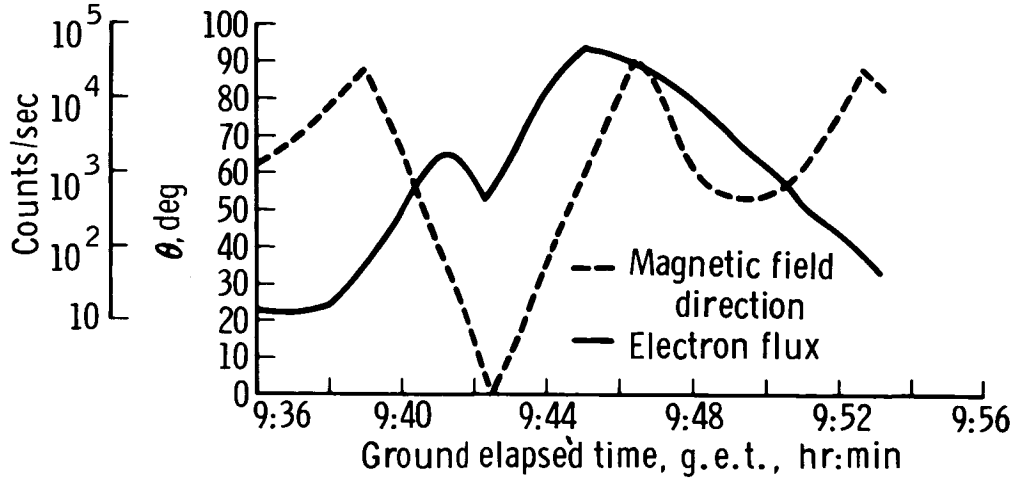

Figure 12. - Correlation of data from Experiments M404 and M405 for revolution 7 of the Gemini IV mission.

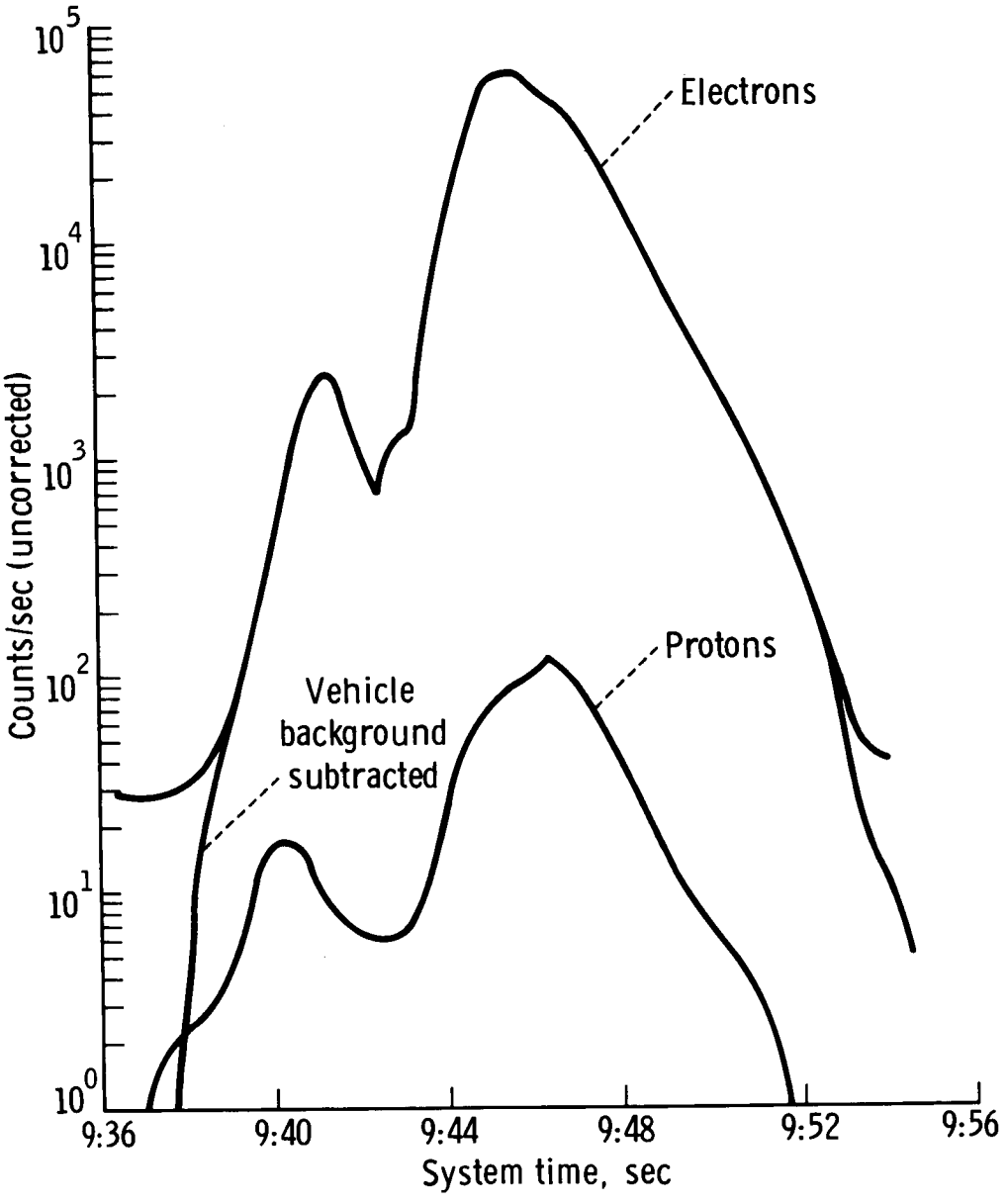

Figure 13. - Gemini IV proton-electron spectrometer readings for revolution 7.

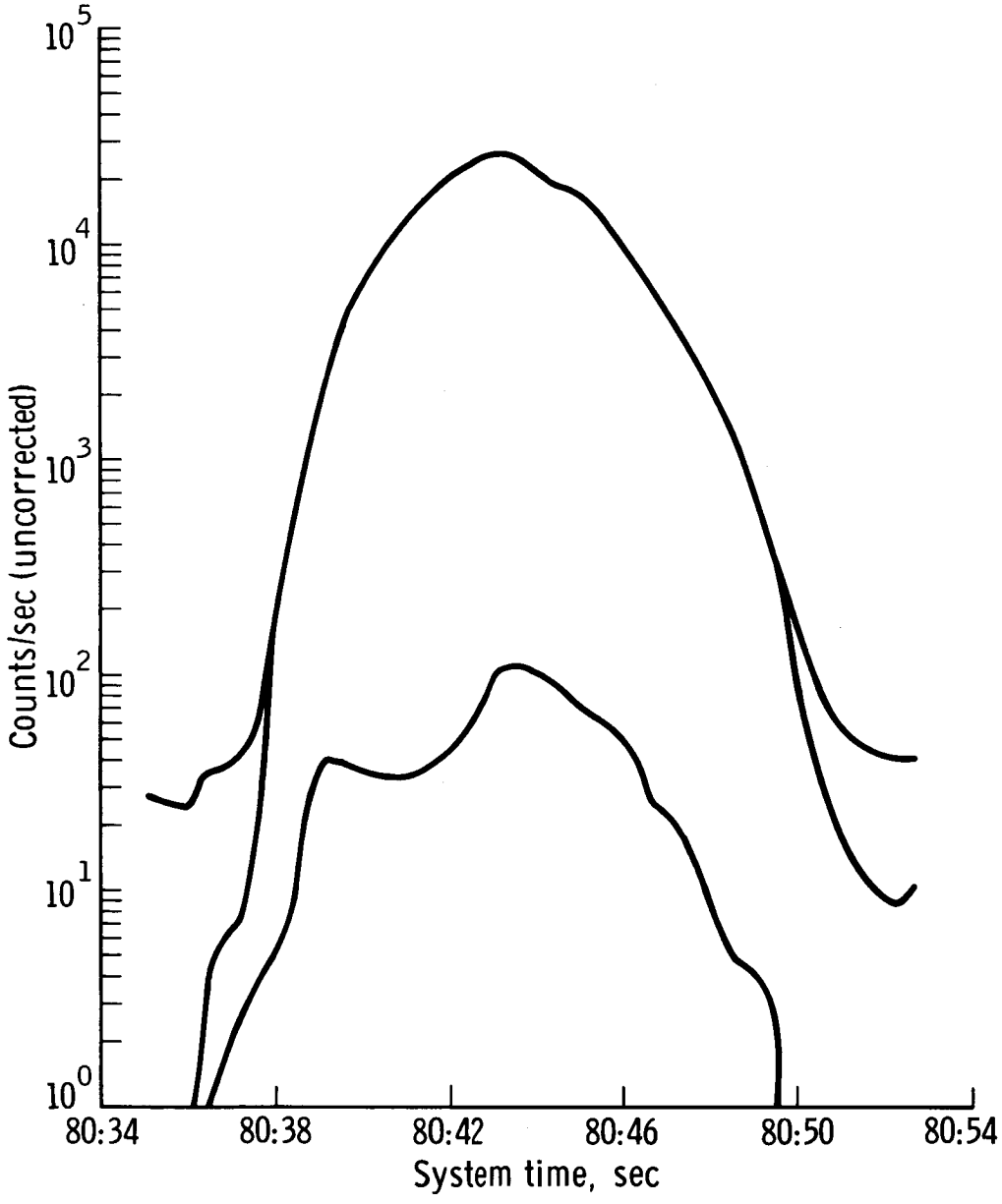

Figure 14. - Gemini IV proton-electron spectrometer readings for revolution 52.

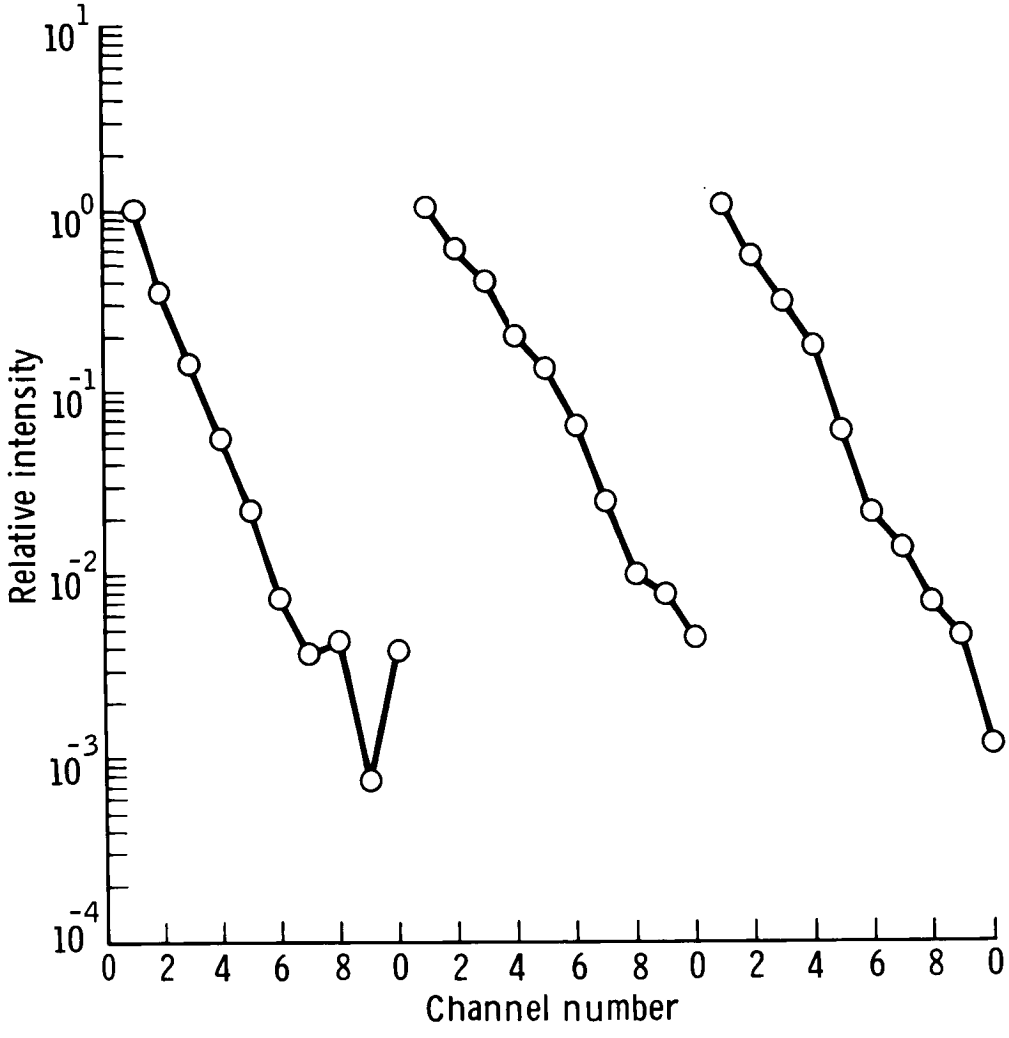

Figure 15. - Gemini IV electron spectra determined during revolution 7.

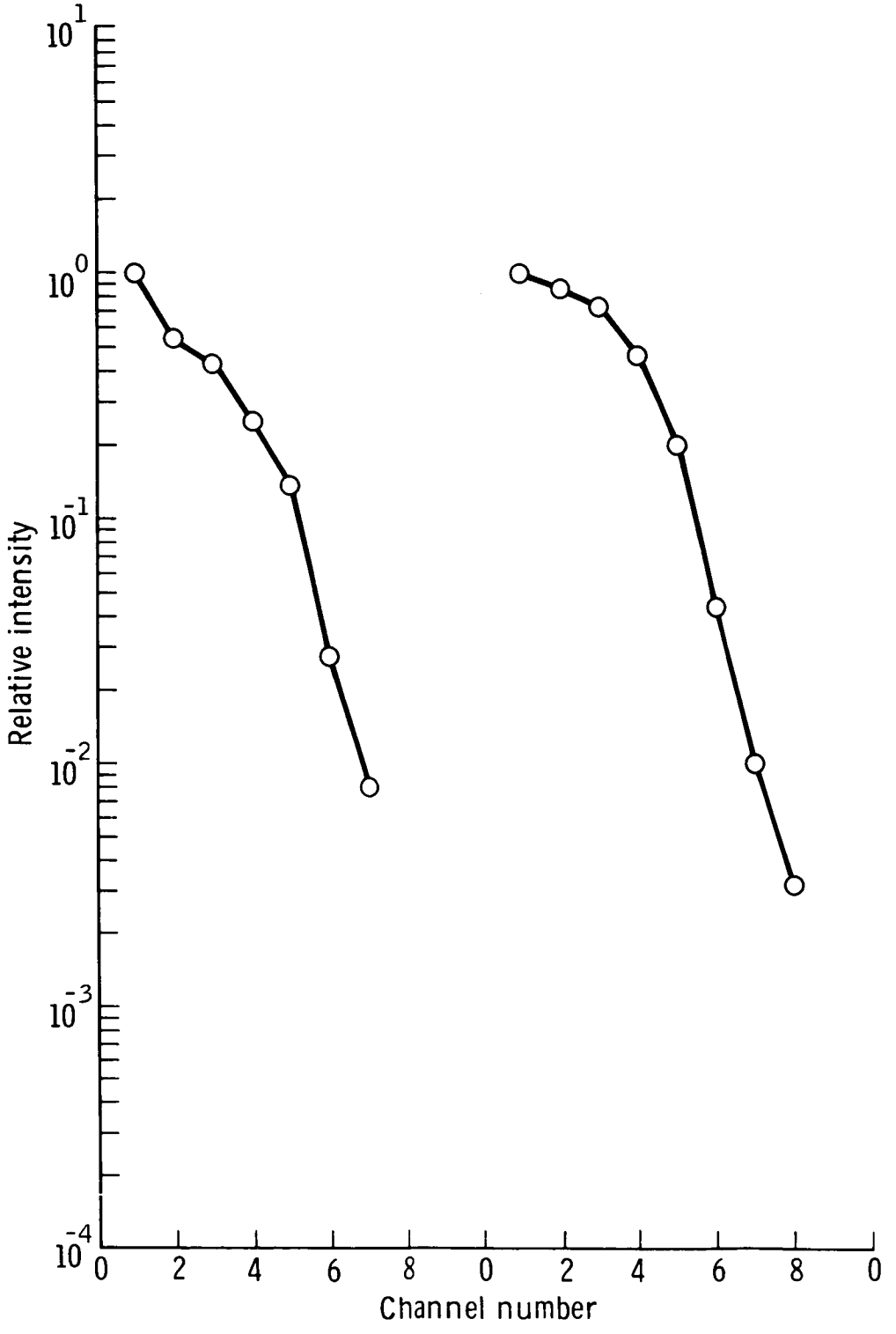

Figure 16. - Gemini IV proton spectra determined during revolution 7.

EXPERIMENT M408

BETA SPECTROMETER

By James Marbach*

OBJECTIVE

Experiment M408 was flown on the Gemini X and XII missions. The principal objective of the experiment was to measure the electron flux and energy distribution outside the spacecraft as it passed through the region of the South Atlantic anomaly (off the eastern coast of South America). This region was known to contain the only significant ionizing radiation encountered on typical Gemini flight paths. By comparison of dose estimates involving this environment with actual measured doses made on each flight, a knowledge of the reliability and accuracy of the mathematical technique of hazard prediction was acquired. These flux-energy spectra were needed to verify radiation-dose-computation techniques that were being developed.

EQUIPMENT

The function of the beta spectrometer was similar to the function of the proton-electron spectrometer that was used in Experiment M404; however, the instrument was of very different design. The beta spectrometer consisted of two containers, one which housed the detector/analyzer system and one which housed the data-processing system. The total weight was approximately 16 pounds, and power consumption was approximately 5.5 watts at 28 V dc. All data were processed in digital form and were relayed by the Gemini pulse code modulation (PCM) telemetry system. A photograph of the completed assembly is shown in figure 1.

Particles were detected by solid-state detectors in a dE/dx, total E arrangement, which provided seven channels of flux information that covered the energy bands of 0.41 to 0.67, 0.67 to 1.0, 1.0 to 1.22, 1.22 to 2.00, 2.00 to 2.88, 2.88 to 3.63, and 3.63 to 4.61 MeV. A cross section of the detector/analyzer system is shown in figure 2. The total E detector was a stack of four lithium-drifted silicon detectors that provided a total active region that was approximately 1 centimeter in depth. The outputs of all four detectors were connected in parallel to a common amplifier and pulse shaper. The dE/dx detector was a 60-micron surface barrier, and functioned solely as an anticoincidence device in conjunction with the total E detector to discriminate against protons. To minimize the probability of electrons being scattered

*NASA Manned Spacecraft Center, Houston, Texas.

out of the dE/dx detector and completely (or partially) missing the total E detector, the two detectors were mounted as close to each other as was practical. This necessitated that mass shielding be used for collimation. As shown in figure 2, lead spacers were arranged to provide a solid-angle aperture of approximately 0.25 steradian (half angle of approximately 15°). To eliminate analysis of particles entering the total E detector from a direction other than through the collimator, the rear and sides of the detector assembly were surrounded with plastic scintillator. This third detector was viewed by a photomultiplier (PM) tube, the output of which fed an anticoincidence circuit similar to that of the dE/dx detector. Additional aluminum was supportive and was a shield to minimize anticoincidence rate (and subsequent dead time) around the plastic and PM-tube assembly. The aluminized Mylar and aluminum housing surrounded the silicon detectors and served as an electromagnetic shield to minimize noise in the detector outputs. The effect of the combination of shielding and coincidence circuitry may be summarized as follows.

1. All particles that entered the instrument through any portion other than the entrance aperture either were stopped in shielding or were rejected by anticoincidence as they entered the plastic scintillator.

2. Protons of $E < 2$ MeV that entered the aperture were stopped completely in the front detector.

3. Protons of $0.2 < E < 20$ MeV would deposit more than 200 keV in the front detector; the threshold for coincidence rejection was adjusted to 200 keV, and these particles were not analyzed.

4. Protons of $E > 5.5$ MeV would deposit more than 4.6 MeV in the total E detector, and would be out of the range of the pulse-height analyzer (PHA); these protons were rejected on that basis.

5. Protons of $E > 70$ MeV would penetrate both silicon detectors and would enter the plastic coincidence scintillator for rejection.

6. Electrons of $E < 410$ keV and of $4.6 < E < 10$ MeV would deposit energies in the total E detector that were outside the range of the PHA.

7. Electrons of $E > 10$ MeV would penetrate to the scintillator for rejection.

8. Electrons of $0.41 \geq E \leq 4.6$ MeV would be analyzed.

A block diagram of the detector/analyzer system is shown in figure 3.

Pulses from either the dE/dx, the total E, or the scintillator detector were routed into essentially identical charge-sensitive amplifiers. The amplified and shaped pulses from the dE/dx and scintillator detectors were fed into level discriminators that were adjusted to an equivalent energy deposited of 200 and 100 keV, respectively. When an incoming pulse exceeded the threshold level, the discriminator triggered and remained latched on for approximately 0.7 microsecond. Then, the two discriminator outputs were routed through a complementary AND gate to a strobe-control circuit. The strobe pulse fed an AND gate in conjunction with the inhibit/enable logic-discriminator outputs. The function of the discriminator was to hold the analyzer

storage input closed to an analyzed pulse from the total E detector until the inhibit circuits had sufficient time to present an output (if they have one). The firing time of the strobe was adjusted to occur sufficiently down on the decay slope of the pulse to allow the latest and shortest, and also the earliest and shortest, inhibit pulses to be recognized.

A simplified block diagram of the PHA is shown in figure 4. The amplified and shaped signals from the total E detector were applied to eight voltage-to-current converters, each of which fed a tunnel-diode discriminator. Each discriminator was adjustable, to facilitate flexibility of the selected energy thresholds of approximately 50 percent of nominal levels. The first and eighth discriminators served to define the energy window of the analyzer. The discriminators were similar in operation to the inhibit logic discriminators. That is, the discriminators detected a level and then latched on for approximately 0.7 microsecond. The ninth circuit in the diagram is a dE/dt-to-I (current) converter, which operated the strobe.

To obtain differential rather than integral spectra, interconnecting logic circuitry was established between each discriminator output after strobe interrogation. As each discriminator fired, it inhibited the output of its next lower neighbor and left a pulse present on the highest energy line actuated. A pulse that had been interrogated and accepted by the strobe circuit then fed a one-shot multivibrator, which was connected to the data-processing package. Data pulses from the one-shot multivibrators at the output of each of the seven energy channels were routed directly to the digital data-processing system. Each channel was routed through a gate that was controlled by the time-base generator to control sampling time. When the gate was opened, pulses were fed into seven parallel 14-bit scaler accumulators. After the preset sampling had occurred, the gate was closed and the information in the accumulators was shifted in parallel into seven 14-bit shift registers. The registers were connected to seven parallel-sampled, bilevel PCM telemetry channels. Each time the telemetry (TM) channels were sampled, the next register bit was shifted for read-out. The sampling rate was 10 per second, so that 1.4 seconds were required to read out each seven-channel spectrum. Immediately after the accumulated data were transferred, the input gates were opened to begin another sample. In this way, data were accumulated and read out simultaneously.

A block diagram of the program-control circuitry is shown in figure 5. All sequences were slaved to a 10-per-second gate pulse that was obtained from the PCM telemetry system. If it is assumed initially that the index pulse was set and that the counters in the control circuitry are at zero, the sequencing can be traced as follows. A sync pulse entered the N/14 counter. The falling edge of this pulse triggered the N/14 counter one step and flipped the index signal off. The index signal was routed to an eighth bilevel TM channel that was sampled in parallel with the seven energy channels. The function of this channel was to define the first register bit sampled. Simultaneously, this first sync pulse sent a shift command to all registers. The second to 13th sync pulses advanced the N/14 counter and shifted the register; thus, they were left cleared. The N/14 counter, now filled, sent a pulse to a three-position sequencer. This sequencer consisted of six cascaded one-shot multivibrators. After a 75-microsecond delay, a pulse appeared at terminal 1 of the sequencer, reset the N/14 counter and the index flip-flop, and transferred data from the accumulators into the then depleted registers. After another 75-microsecond delay, a pulse appeared at

terminal 2 of the sequencer, which resets all accumulators. After a third 75-microsecond delay, a pulse appeared at terminal 3 of the sequencer and initiated the time base for control of the input gates to the accumulators. This completed the cycle and the next sequence could begin.

The time-base generator worked as follows. The pulse from terminal 3 of the sequencer opened in the input gates to the accumulators and simultaneously gated a 100-kilohertz crystal-controlled square-wave oscillator into a 17-bit scaler. After 2^{17} pulses, the time-base flip-flop was toggled, the input gates to the accumulators were closed, and the oscillator gate to the scaler was closed. The circuit waited until a pulse from the sequencer reinitiated the cycle. The accumulator gates were open in the scaler for 131 075 ± 15 counts, which corresponded to 1.31057 ± 0.00015 seconds. Stability was better than three parts per 13 000 over the temperature range of -65° to +170° F; this stability was ± 0.102 percent.

It should be noted that although the output registers required 1.4 seconds to be sampled, the accumulators were filled for 1.31 seconds. The difference was to allow for the time required to transfer the accumulator information into the output registers.

To ensure that the silicon semiconductor detectors were maintained at room temperature or below (the noise figure improved with decreasing temperature), an evaporative cooling device was incorporated into the detector/analyzer. Water, stored in the cylindrical reservoir on the top of the assembly in the left of figure 1, was fed to two identical evaporators mounted on the side of the detector subassembly. The evaporators consisted of ceramic disks, which facilitated water evaporation through to the vacuum maintained inside the instrument during orbit. The water was sealed inside the reservoir in a polyethylene bag, which left approximately half of the tank (which was sealed at atmospheric pressure) for air. During orbit, the 1-atmosphere pressure differential between the inside of the tank and the vacuum outside forced the water to the ceramic evaporators, where it slowly bled out and evaporated, and absorbed the heat of vaporization. The bleed rate was adjusted to approximately 5 grams per hour total, which maintained the detectors at room temperature or lower for 4 hours with the equipment mounting-structure temperature at 120° F.

PROCEDURE

The experimental equipment was located in the retrograde section of the spacecraft adapter. The detector/analyzer was mounted on the adapter ring structure and had an unobstructed view of the exterior environment through a hole in the spacecraft skin. The hole was covered with a half-hinged door for protection of the instrument during launch. The door was jettisoned automatically during separation of the spacecraft from the booster. Operation of the equipment during the flight was accomplished by means of a toggle switch on the control console of the pilot. The pilot turned on the instrument after orbital insertion, and left it on throughout the mission until just before retrofire.

To obtain information on the directionality of the electron radiation encountered, it was necessary that the instrument see as many different directions in space as

possible. Because the radiation was concentrated in the relatively small South Atlantic anomaly region at Gemini flight-path altitudes and was known to be trapped in the geomagnetic field, it was important that the instrument be made to look at several angles with respect to the magnetic field while in this region. To accomplish this part of the experiment, the crewmembers were requested to execute a slow roll maneuver while in the South Atlantic anomaly region. This maneuver rotated the instrument about the magnetic-field lines and swept the experimental sensors through the normal to the field twice for every 360° roll of the spacecraft. In addition to acquisition of directionality information, the maneuver also ensured that several data points were taken while the instrument was normal to the magnetic-field direction where the electron intensity was known to be greatest.

The principal investigator was stationed at the Kokee tracking site in Hawaii, where the dumped telemetry data were evaluated after each of the anomaly passes. The requirements for controlled spacecraft attitude then could have been augmented or reduced during the mission, depending on quick-look data that were obtained during other mission operations. The tri-axis magnetometer experiment (M405) facilitated instantaneous determination of the "magnetic attitude" of the beta spectrometer, so that the data received could be related to spacecraft attitude on a continuous basis.

RESULTS

Gemini X Mission

The unexpectedly great fuel usage that occurred during the first and second days of the Gemini X mission eliminated the possibility of controlled-altitude passes for the beta-spectrometer experiment. An evaluation of data from the first 2 days was indicative that very little, if any, usable data were obtained. On the third day, the spacecraft was flown in a random or tumbling mode through the anomaly, and one good traversal of the magnetic field resulted. Necessarily, all results and conclusions were based on this one set of data points. The location of these few data points within the anomaly was fortuitously good; however, the location was good only because data from previous scientific measurements were available for comparison.

A plot of relative counting rate, as measured by the spectrometer, compared with the angle that the spectrometer viewed with respect to the magnetic field direction is shown in figure 6. The indicated angle was derived directly from magnetometer data. Although the ordinate was not amply corrected for X-ray contributions or geometric factor, the data were indicative of a strongly peaked intensity distribution around the normal to the magnetic field. The full-width half-maximum points of $\pm 10^{\circ}$ around the normal generally are consistent with measurements made previously on scientific satellites.

A plot of the average electron spectrum as measured is shown in figure 7. As was just mentioned, the available data occurred at a convenient location (B = 0.22, L = 1.250, in B, L space) so as to be comparable with other measurements. The solid curve in figure 7 represents the predicted theoretical spectrum (ref. 1), which, for convenience of comparison, was normalized to the measured differential flux at

approximately 2.45 MeV. The Gemini X data points were obtained by the averaging of five spectra that were measured within $\pm 3.5^\circ$ of the normal to the magnetic field. Then, this average spectrum was corrected for X-rays by the use of count rates that were observed when the instrument was away from the normal to the field immediately before this time. The resultant spectrum was corrected for backscatter effects by the use of calibration data and on the assumption of an incident spectrum of the form

$$\Phi(E) - \Phi_o(10)\left(\frac{E_o - E}{1.34}\right)$$

where Φ = flux and E = energy.

The error bars are indicative because of statistics only. Actually, a somewhat harder spectrum in the energy band between 0.5 and 1.5 MeV would have been more realistic, but calculations were indicative that the overall effect of such an assumed spectrum would have been to raise the data point at 1.1 MeV more into line with that which was suggested by the other data points. The overall measured spectrum was consistent with the spectrum that was measured on the Gemini IV and Gemini VII missions, and was extremely consistent with the theoretical spectrum (ref. 1) except at low energies. The divergence at low energies has been suggested to be because of the presence of natural Van Allen belt electrons, which, at the time of the mission, were becoming a significant fraction of the fission electrons remaining from the high-altitude nuclear tests of 1962.

Summaries of the real-time data obtained during the mission were indicative that the equipment functioned exactly as was planned. The detector was provided with a specially designed cooler, and the detector temperature followed a satisfactory profile. Shortly after being turned on, the detector temperature sensor indicated temperatures of less than 10° C, and it cooled to approximately 3° C on the second revolution. Throughout the rest of the mission, temperatures remained between 2° and 3.5° C.

Gemini XII Mission

A preliminary analysis was performed on selected data that were obtained during the first 4 hours of instrument operation. A plot of count rate compared with energy as observed at the McIlwain coordinates (ref. 2) $L = 1.25$ and $B = 0.22$ is shown in figure 8. This particular spatial location was chosen for first analysis because considerable data from other measurements were available for comparison. The data that were plotted were not corrected for background and backscatter, but were representative of the general shape of the spectrum.

Above approximately 1.2 MeV, the spectrum closely resembled the decayed fission spectrum as was predicted by atmospheric-scattering theory (ref. 1). The departure from the predicted spectral shape below this energy was suggestive of a source of electrons separate from the Starfish explosion that was present at the time of the measurement. Similar measurements have involved this effect but not as significantly as these data indicate (refs. 3 and 4). It is possible that the Gemini XII

measurements were made at a time when the fission electrons had decayed sufficiently to make possible significant visualization of a superimposed spectrum of natural Van Allen electrons. Refinement of the data is necessary to establish the approximate shape of this superimposed spectrum, and detailed studies of geomagnetic activity and other possible involved phenomena must be performed to ascertain the true source of these electrons.

CONCLUSIONS

The beta spectrometer functioned as planned throughout the Gemini X mission. The cool temperatures that were recorded from the instrument during the mission were indicative that the evaporative cooler, coupled with apparently lower-than-expected spacecraft-adapter temperatures, maintained ideal operating conditions. The data facilitate a good analysis of the electron directional distribution. The omnidirectional flux that was calculated is apparently consistent with previous measurements. Representative electron spectra, measured during the Gemini XII mission, established the apparent decay of the artificially injected electrons (from the Starfish high-altitude nuclear test of July 1962) to such low levels that natural trapped electrons were becoming detectable.

REFERENCES

1. Walt, Martin: The Effects of Atmospheric Collisions on Geomagnetically Trapped Electrons. J. Geophys. Res., vol. 69, no. 19, Oct. 1964, pp. 3947-3958.

2. McIlwain, Carl E.: Coordinates for Mapping the Distribution of Magnetically Trapped Particles. J. Geophys. Res., vol. 66, no. 11, Nov. 1961, pp. 3681-3691.

3. Imhof, W. L.; and Smith, R. V.: Energy Spectrum of Electrons at Low Altitudes. J. Geophys. Res., vol. 70, no. 9, May 1965, pp. 2129-2134.

4. Regan, J. B.; et al.: Direct Measurement of Auroral Electrons of Low Energies. J. Geophys. Res., vol. 70, no. 9, May 1965, pp. 2119-2127.

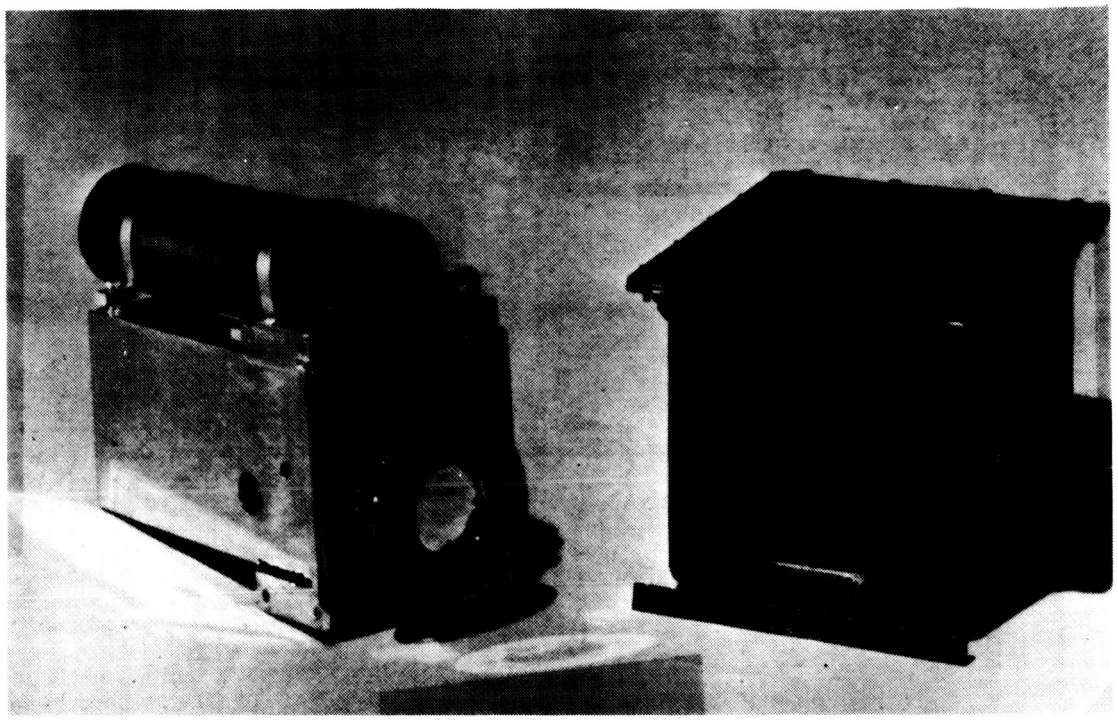

Figure 1.- The beta spectrometer.

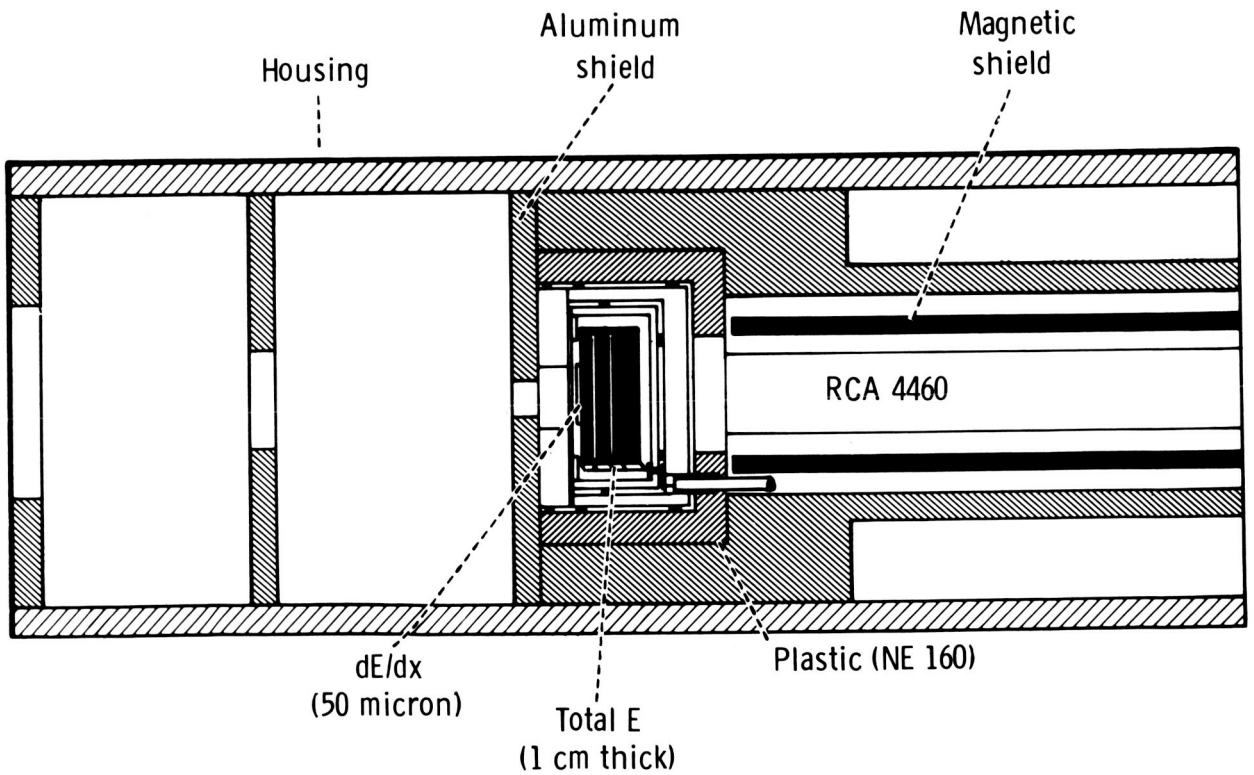

Figure 2.- A cross-section view of the electron detector.

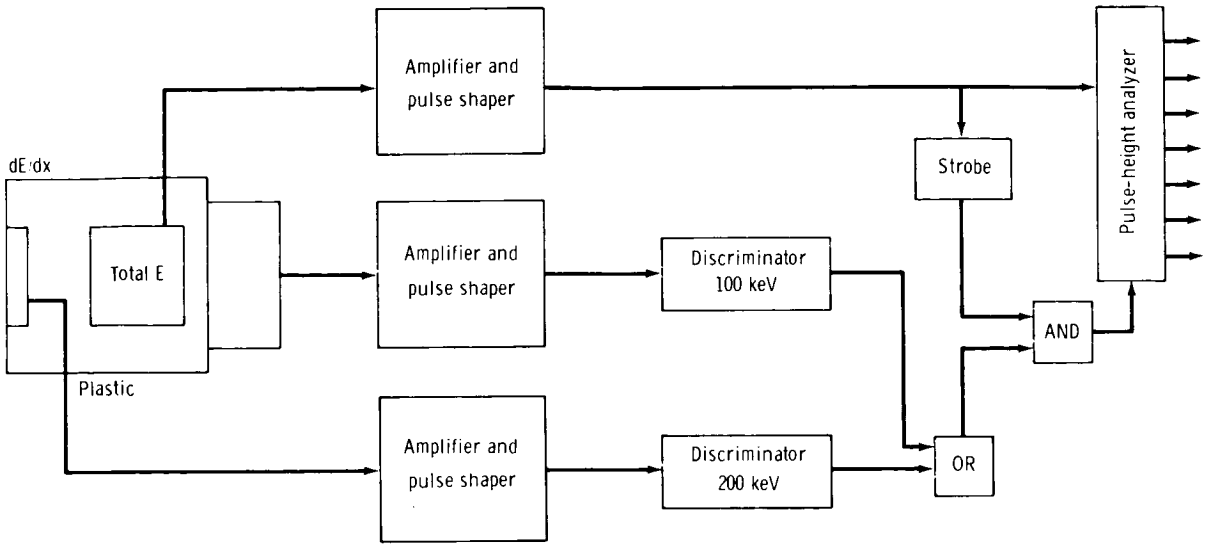

Figure 3. - The detector/analyzer block diagram.

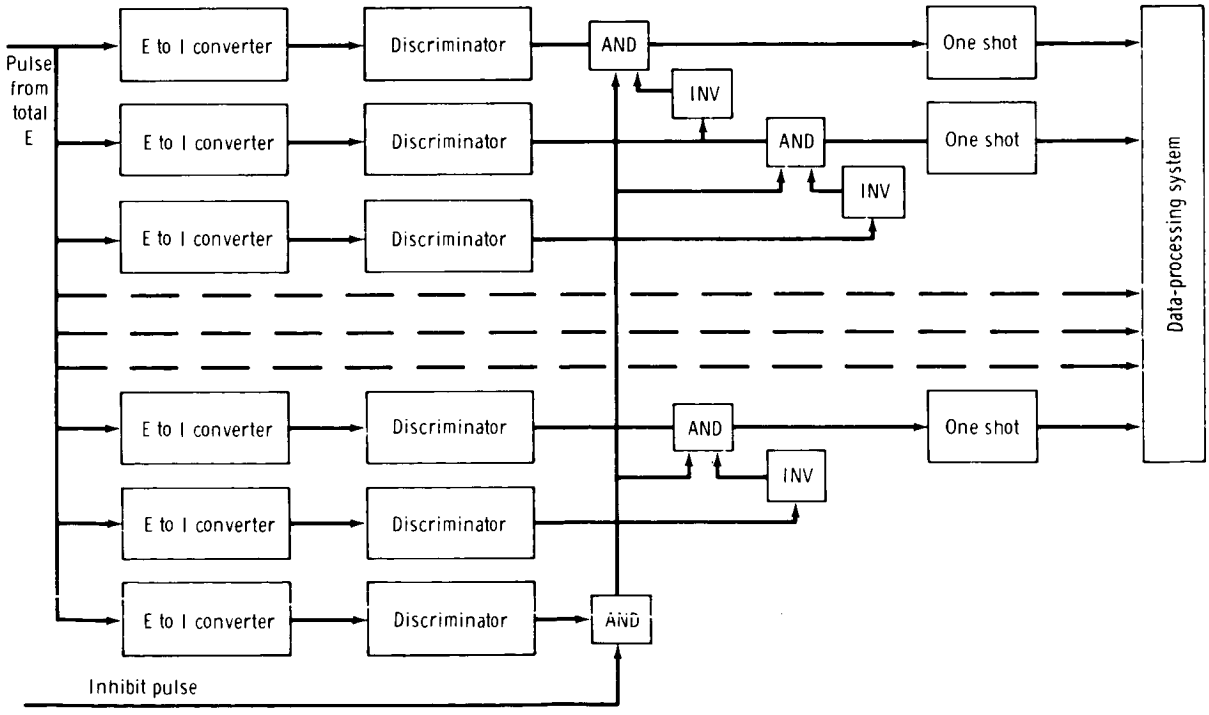

Figure 4. - The pulse-height analyzer.

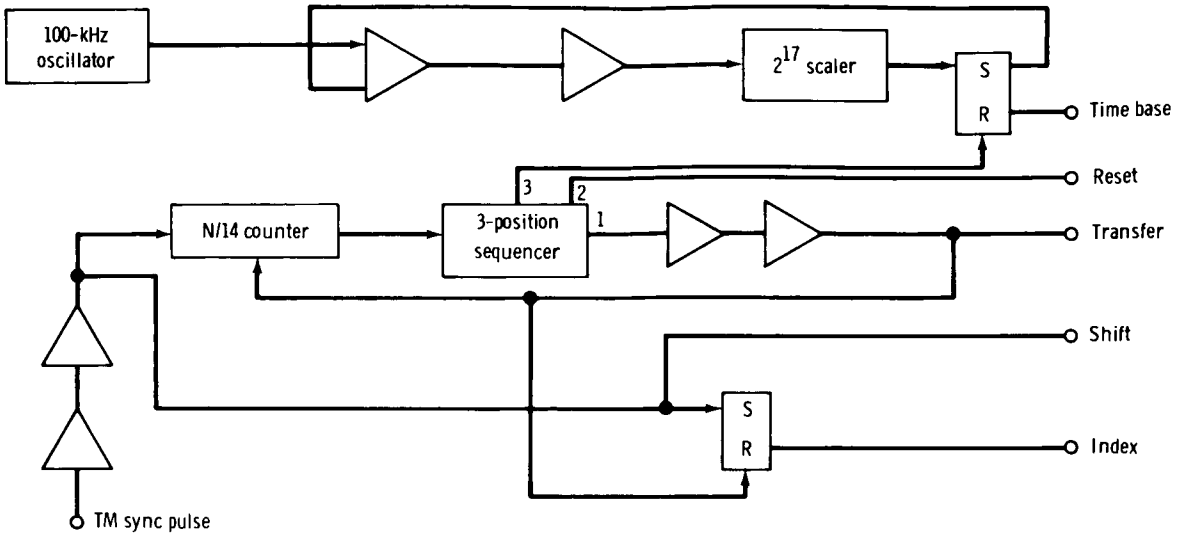

Figure 5. - The program-control circuitry.

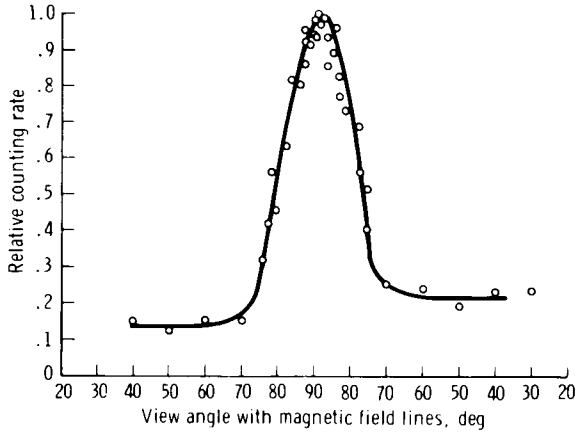

Figure 6. - The spectrometer-view-angle data.

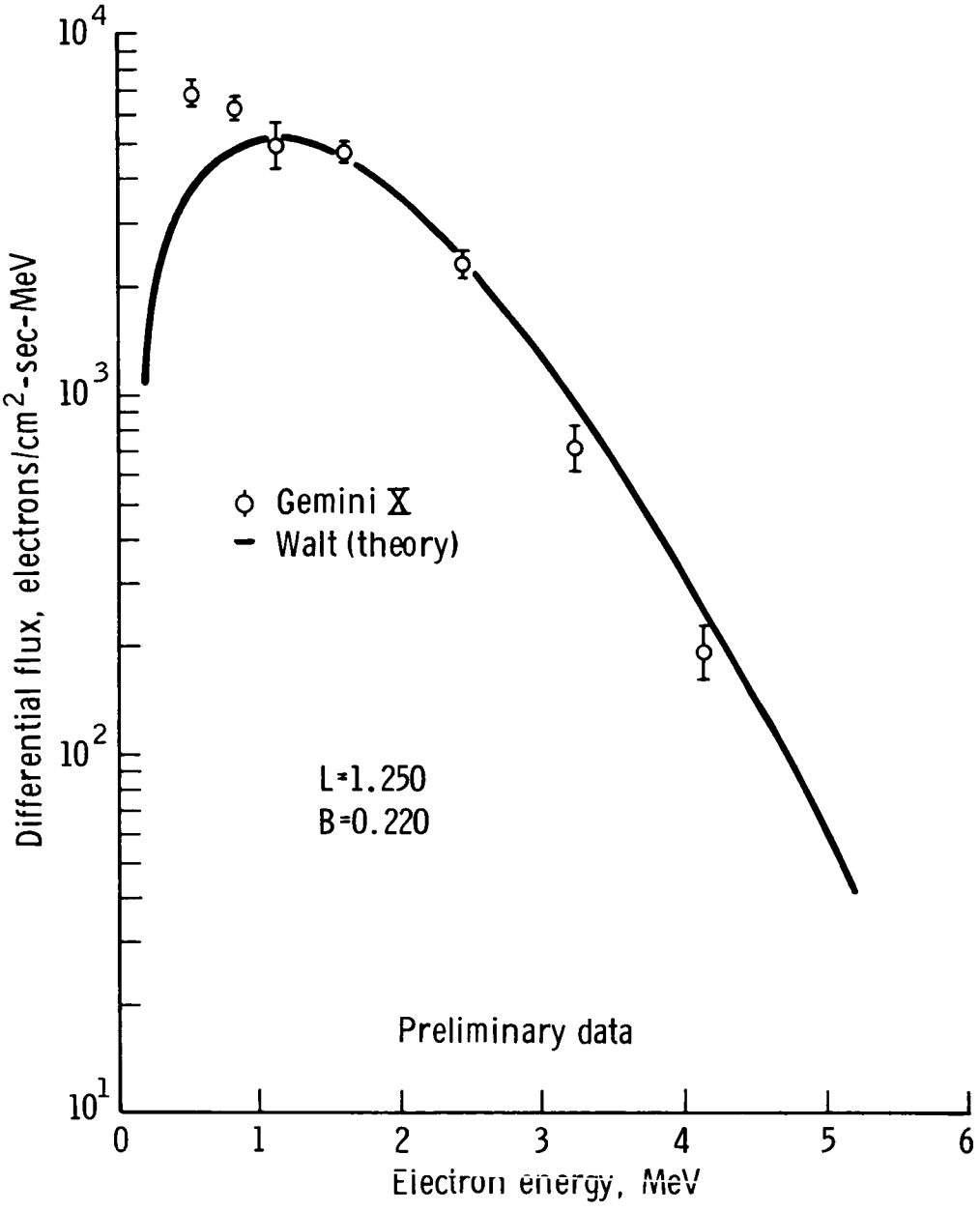

Figure 7. - The measured average electron spectrum.

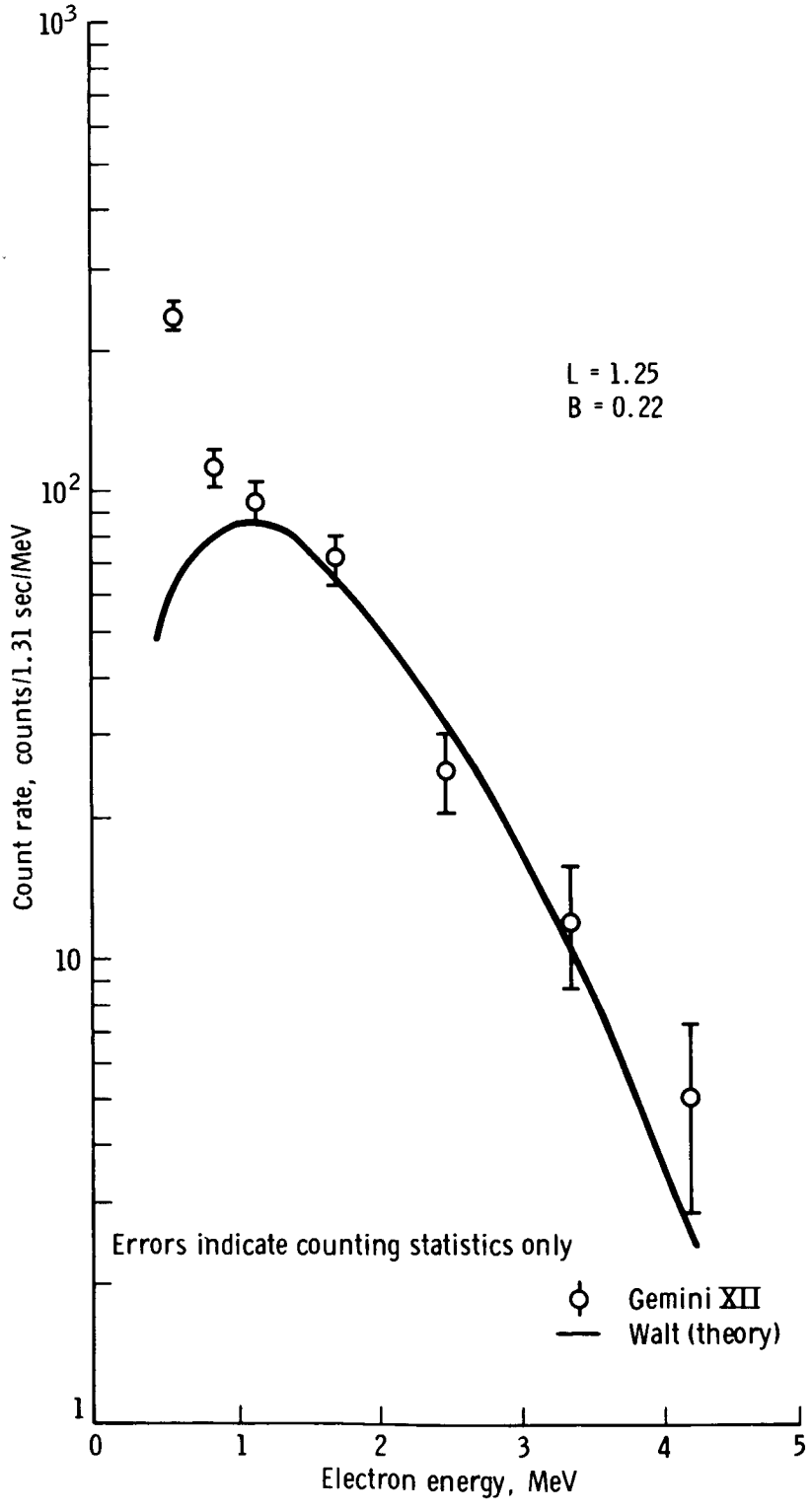

Figure 8. - The data that were collected at McIlwain coordinates.

EXPERIMENT M405

TRI-AXIS FLUX-GATE MAGNETOMETER

By William D. Womack*

INTRODUCTION

A tri-axis flux-gate magnetometer was used on four Gemini spacecraft for determination of the magnitude and direction of the local geomagnetic field with respect to the spacecraft. These data were useful in the interpretation of results from Experiments M404 and M408, and the data were essential in the interpretation of data from other Gemini missions on which directional spectrometers were employed. Knowledge of the direction of the local geomagnetic field was necessary because of the strong directionality of charged-particle fluxes in the anomaly region, wherein the particle pitch angles approximated 90°. The pitch angles were those angles between the particle direction and the magnetic-field line about which it was spiraling (fig. 1). The dependence of pitch angle upon local magnetic-field strength is shown by consideration of the first adiabatic invariant of trapped charged-particle motion; the magnetic moment of the particle may be considered as a constant of the motion. This consideration results in the relation $\sin^2\gamma/B$ = constant, where γ = particle pitch angle and B = magnetic field strength. Because γ is approximately 90° in the anomaly region, a measurement of the local magnetic-field strength includes consideration of the directionality of the particles.

OBJECTIVES

Experiment M405 was performed on the Gemini IV, VII, X, and XII missions. The object was to determine the direction and magnitude of the geomagnetic field of the earth in the South Atlantic anomaly region with respect to Experiment M408. The equipment for Experiment M408, which is described elsewhere in this document, consisted of a beta spectrometer with a half-angle of 15° that was attached to the Gemini X spacecraft. Experiment M408 was performed to determine the flux of charged particles external to the spacecraft. The South Atlantic anomaly region is between South America and Africa, bounded approximately by longitudes 30° E and 60° W and latitudes 15° S and 50° S. This region was the only portion of the spacecraft trajectory that contained any significant electron intensities. Knowledge of the magnetic-field magnitude and direction was most important for an evaluation of charged-particle measurements,

*NASA Manned Spacecraft Center, Houston, Texas.

especially where directional instrumentation was used. Because of the directionality of charged particles with magnetic-field lines, the measurement of those particles was impossible when a directional measurement instrument was used without determination of the direction of the magnetic-field line. Therefore, the objective of Experiment M405 of the Gemini XII mission was the determination of the magnitude and direction of the geomagnetic field of the earth in the South Atlantic anomaly region in support of Experiment M408. Experiment M408 also was flown on the Gemini XII mission.

EQUIPMENT

The experimental equipment consisted of the tri-axis magnetometer and an extendable boom. The tri-axis magnetometer was a flux-gate instrument that included an electronic package, a sensor unit, and an interconnecting cable (fig. 2). The electronic package contained a dc-to-dc converter and three electronic subassemblies that supplied the necessary sensor-drive voltages, detected and transformed the vector field alternating-current (ac) second-harmonic signals, and converted these signals to a 0- to 5-V dc analog signal. The sensor unit contained three orthogonal, monoaxial second-harmonic probes. The unit was capable of detection of a ±0. 6-gauss magnetic field with a 0- to 5-volt output. To minimize any stray magnetic fields produced by other instrumentation or by the metallic structure of the spacecraft, the sensor unit was extended from the spacecraft after orbital insertion (figs. 3 and 4).

The sensor unit contained three identical second-harmonic sensors that had a core material that was driven into saturation by a 15-kilohertz signal through a primary winding. A secondary winding obtained the second-harmonic frequency when an external field was applied; an auxiliary winding nulled the residual field. The three sensor probes were mounted orthogonally in one package. The three sensor probes were mounted orthogonally to measure the vector components H_x, H_y, and H_z of the magnetic field. By measurement of the vector components, the direction and total field were calculated from the following equations

$$H_t = \sqrt{H_x^2 + H_y^2 + H_z^2} \tag{1}$$

$$\theta_x = \cos^{-1}\left(\frac{H_x}{H_t}\right) \tag{2}$$

$$\theta_y = \cos^{-1}\left(\frac{H_y}{H_t}\right) \tag{3}$$

$$\theta_z = \cos^{-1}\left(\frac{H_z}{H_t}\right) \tag{4}$$

where H_t = total field

H_x, H_y, H_z = vector components of the field

$\theta_x, \theta_y, \theta_z$ = component angles measured from their respective axes

If the location of the sensor unit with respect to the spacecraft was known, the direction of the field with respect to the spacecraft could be calculated.

The interconnection was a 110-inch cable that established electrical continuity between the electronic and sensor units. The electronic unit and the sensor unit were located in the retroadapter section. The interior of the retroadapter section, with the electronic unit mounted to the retrobeam, is shown in figure 5. The skin of the adapter section, with the magnetometer boom door open and the boom extended, is shown in figure 6. This photograph was taken during experiment-hardware checkout at a contractor facility. The spring-loaded, telescopic boom extended the sensor unit approximately 42 inches from the spacecraft to ensure attenuation of any residual magnetic field produced by the electrical cables, instrumentation, or material within the region of the sensor assembly. The boom was fabricated from titanium tubes, was loaded with a beryllium-copper spring, and was actuated by means of pyrotechnics during sustainer-engine cut-off (SECO). The boom on a test fixture is shown in figure 7.

PROCEDURE

Reference is made to the discussion of Experiment M404 (elsewhere in this document) for the experimental procedure that was used on the Gemini VII mission. Because Experiment M405 was flown in direct support of Experiment M408 on the Gemini X mission, the experimental operation was determined by the requirements that were established in Experiment M408. All requirements imposed upon the spacecraft or crewmembers are described in the discussion of Experiment M408.

The tri-axis magnetometer was turned on during performance of the preinsertion checklist activities, and the unit remained on until the crewmen performed the preretrofire checklist activities. These were the only operational requirements for the experiment. The magnetometer and beta spectrometer were scheduled to be operated for at least 10 revolutions while the spacecraft passed over the South Atlantic anomaly region. Also, the equipment was to be operated for a period of at least 15 minutes while the spacecraft was not in this region.

On the Gemini XII mission, the equipment was turned on by the crewmen at 04:57:33 g. e. t. and was turned off at 14:44:20 g. e. t. The equipment was turned on again at 27:15:00, 51:06:00, and 75:05:00 g. e. t. The total experiment on time was

approximately 32 hours. The magnetometer and the beta spectrometer were scheduled to be operated for at least 10 revolutions while the spacecraft passed over the South Atlantic anomaly region. Also, the equipment was to be operated for a period of at least 15 minutes while the spacecraft was not within this region.

RESULTS

Gemini IV Mission

Data from revolutions 7, 22, and 51 were considered typical examples of data from the magnetometer operation through the South Atlantic anomaly region. The magnitude of the field for each revolution is shown in figure 8. The variations in magnitude were a result of the geocentric altitude changes of the spacecraft in each revolution. The magnitude of the field, based on the magnetometer data, compared favorably with the 48-term expansion of the Jensen-Cain coefficient.

The angle θ (fig. 9) set the direction of the magnetic-field vector with respect to the proton-electron spectrometer and the Z-axis of the spacecraft. It may be noted from revolution 7 data that the angle θ ranges from 90° to 0°. This is illustrative of the tumbling effect of the spacecraft during drifting flight. Data from revolution 22 were indicative of an attitude change in yaw or pitch, but without a tumbling effect as was noted during revolution 7. During the mission, the crewmen noted in their flight log that, while performing a blunt-end-forward maneuver through the anomaly region during revolution 22, the yaw attitude of the spacecraft was not held within ±5°. Data from revolution 51 were indicative of an exceptionally good small-end-forward maneuver of the spacecraft by the crewmen. The angle θ did not vary more than ±5° during the 20 minutes that were involved.

A comparison among the raw data taken from revolution 7 through the anomaly region, the 48-term expansion of the Jensen-Cain coefficient, and the data that were compiled after application of a correction factor for the stray magnetic field from the spacecraft is shown in figure 10. This was conclusive evidence that a magnetometer could be flown on a Gemini spacecraft for determination of the direction and magnitude of the magnetic field, and that these data could be used in the interpretation of data from directional spectrometers. Data from other revolutions were very similar to the three examples that have been given. The contractor attributed sharp decreases in the flux spectrum of protons and electrons to an increase in the angle of the spectrometer and the magnetic-field line.

Gemini VII Mission

The experiment results for the Gemini VII mission may be read as a part of the discussion of Experiment M404.

Gemini X Mission

The data were not conclusive, and are given only as an example of data that might be of interest. All computations that were made on the data to obtain the direction of the magnetic field were referenced to the beta spectrometer only. Other computations and analyses have to be performed before the direction of the magnetic field can be determined with respect to any other portion of the spacecraft or with respect to the earth.

An example of data obtained through an anomaly pass is presented in figure 11. For a typical pass, these data were illustrative of values of the total magnetic-field vector and the angle made with respect to the center line of the spectrometer detector. The total field vector (expressed in kilogammas) and the angle α (expressed in degrees) are shown from 51:20:00 g. e. t. to 51:30:00 g. e. t. The total field vector between 20 100 gammas and 23 800 gammas for this pass was consistent with the theoretical calculated total field. The wide variation in angle was explained by consideration of a tumbling motion of the spacecraft or its random attitude during this time. The data shown in the figure were collected during a sleep period.

The magnitude of the geomagnetic field that was measured during revolution 20 of the Gemini X spacecraft through the South Atlantic anomaly region is shown in figure 12. This magnitude was compared with the calculated theoretical magnetic-field magnitude by use of the McIlwain computer codes (ref. 1). The pattern formed by the data points of the measured field can be explained best by the random sample rate of the telemetry system and the accuracy of the flight hardware. If the measured field were interpolated to acquire a smooth curve, the measured field and the theoretical field would agree favorably. The trend in this figure seems to apply throughout all the data.

A comparison of the geomagnetic-field magnitudes that were measured at altitudes approximately 350 kilometers apart is shown in figure 8. These measurements were collected in the South Atlantic anomaly region. Data from 383 to 400 kilometers were collected during revolution 36, and data from 700 to 762 kilometers were collected during revolutions 6 and 7. The observed effect was an attenuation of field strength as altitude increased, as is common with magnetic-field sources.

Gemini XII Mission

Data that were obtained from the experiment hardware while passing through the South Atlantic anomaly region were played back by telemetry at the Hawaii tracking station for onsite evaluation in support of Experiment M408. The data resulted in proof that the equipment functioned as it was designed to function and provided information throughout the mission. All computations to obtain the direction of the magnetic field were referenced only to the beta spectrometer.

An example of data obtained through an anomaly pass is presented in figure 13. For a typical pass, these data are illustrative of relative values of the total beta spectrometer count rate and the angle made with respect to the center line of the spectrometer detector. The magnetic-field angle α is shown as a function of ground elapsed time. The data shown were measured during a sleep period.

A graphical view of the magnitude of the geomagnetic fields, measured during revolution 10 of the Gemini XII mission and compared with the theoretical calculated magnetic-field magnitude by the use of the McIlwain computer codes, is shown in figure 14. The pattern formed by the data points of the measured field could be explained by consideration of the random sample rate of the telemetry system and the accuracy of the flight hardware. If the measured field were interpolated to acquire a smooth curve, a valid comparison of the measured field and the theoretical field could be made. The trend illustrated by this figure seemed to apply throughout all data that were analyzed.

CONCLUSIONS

Conclusions derived from the data on the magnetometer experiment on the Gemini IV mission are not only important to the proton-electron spectrometer experiment, but also are of significance to any directional charged-particle experiments that may be conducted. Even though the Gemini spacecraft was not clean magnetically, the data could be reduced to a form that supplied directional information on the magnetic field in relation to the spacecraft. Stray fields were the result of spacecraft structure, not the result of current flows that were produced within the spacecraft electrical systems. As proposed, the experiment was a success and efforts were made on other missions to reduce spacecraft stray fields and to facilitate the acquisition of more accurate data.

REFERENCE

1. McIlwain, Carl E.: Coordinates for Mapping the Distribution of Magnetically Trapped Particles. J. Geophys. Res., vol. 66, no. 11, Nov. 1961, pp. 3681-3691.

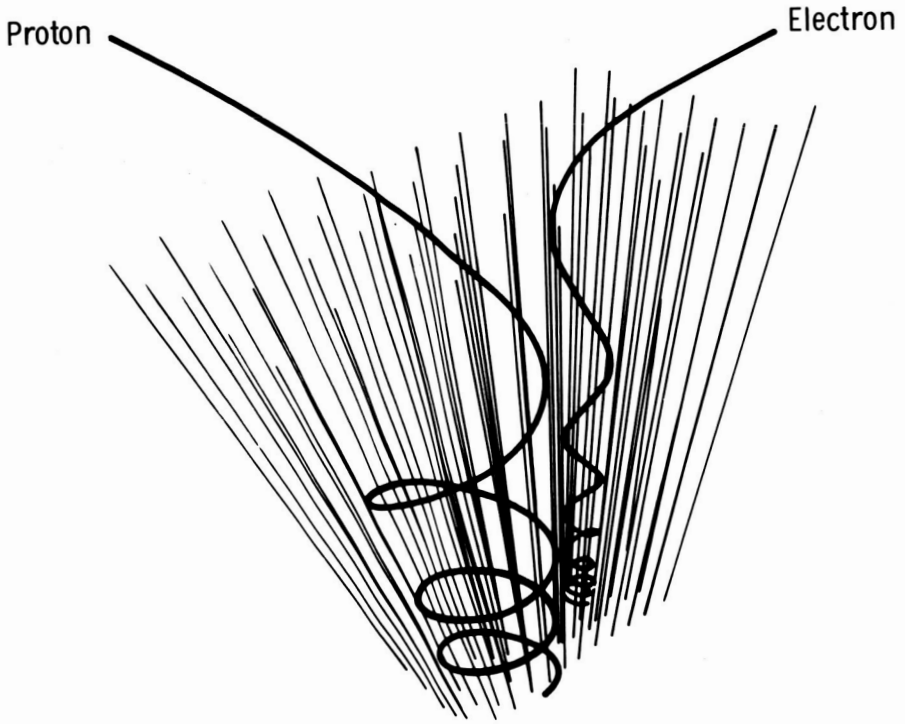

Figure 1. - The spiral of a proton and an electron in a magnetic field.

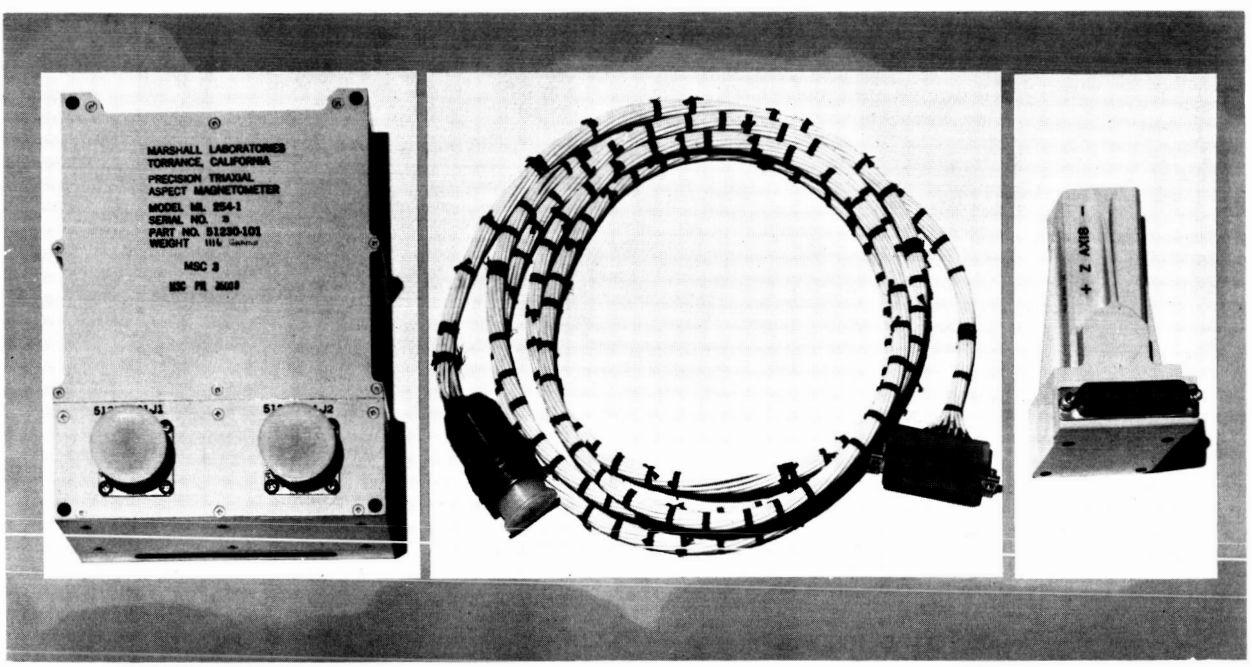

Figure 2. - The electronics and sensors.

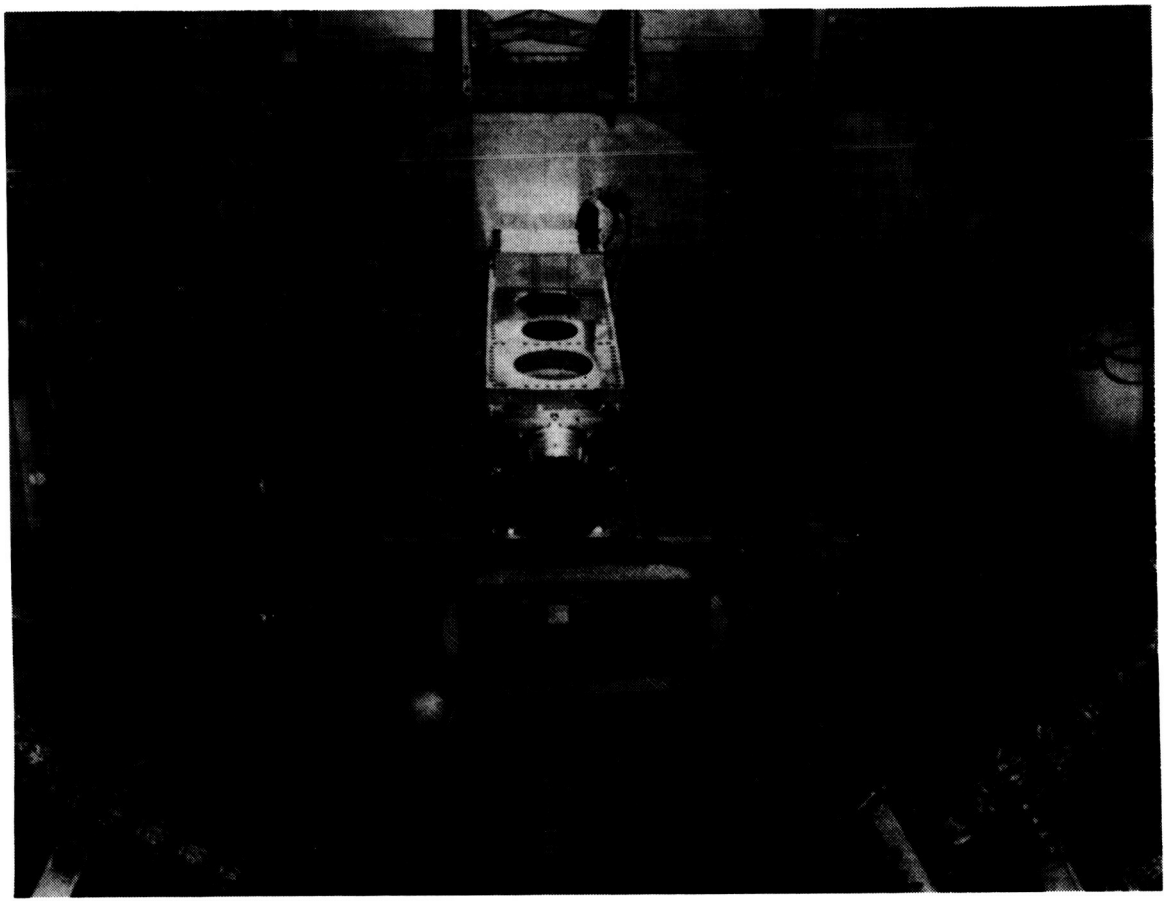

Figure 3. - The magnetometer location.

Figure 4. - The magnetometer boom extension.

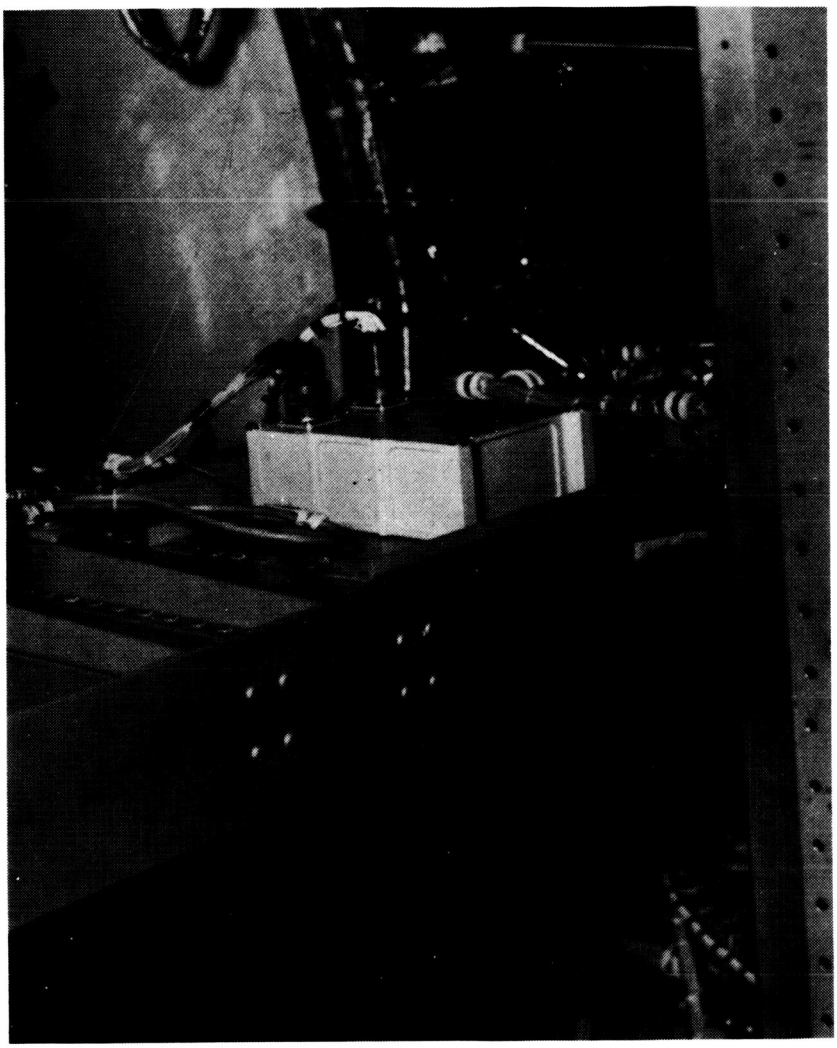

Figure 5. - The electronic unit attached to the Gemini adapter section.

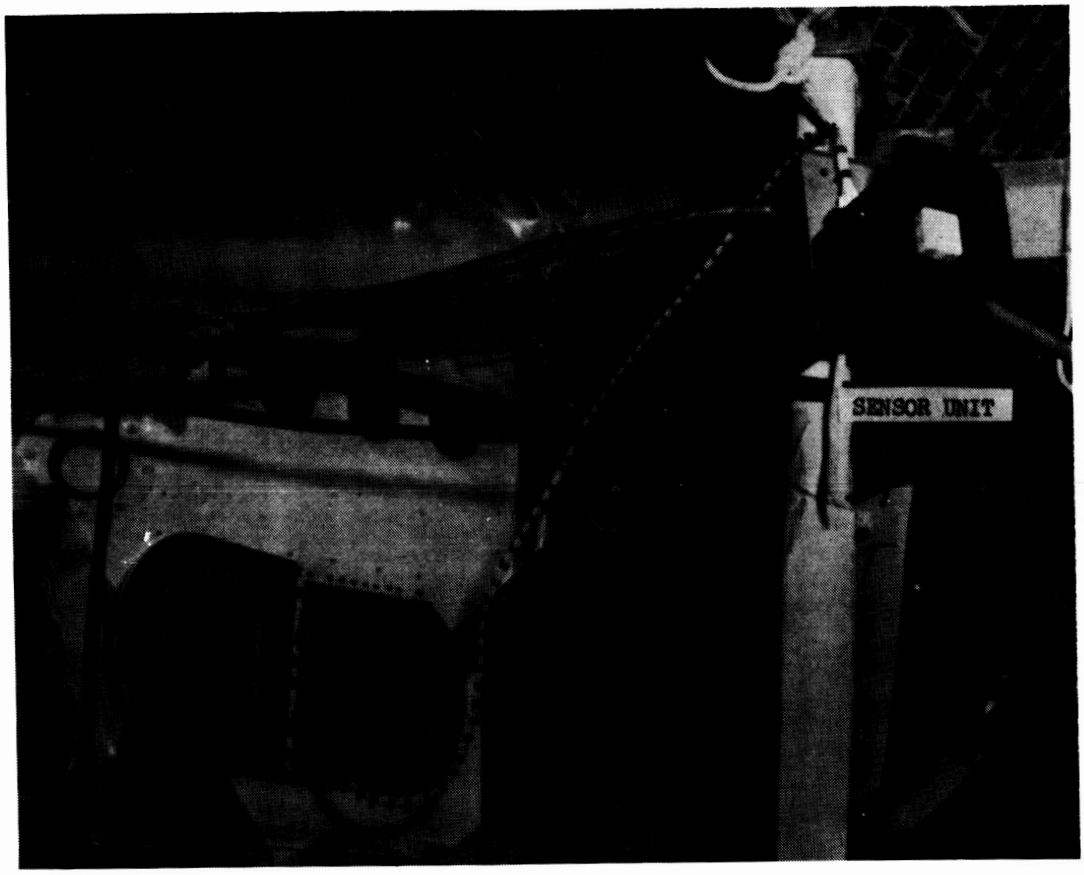

Figure 6. - The sensor unit.

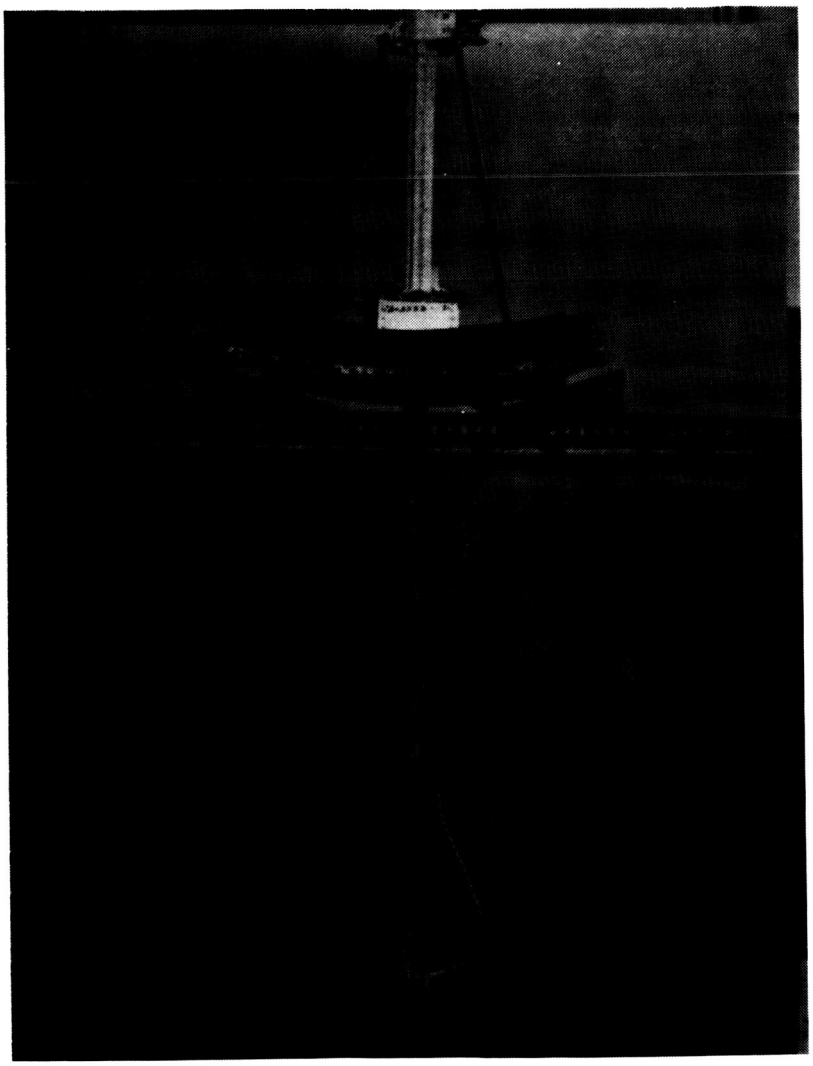

Figure 7. - The boom on a test fixture.

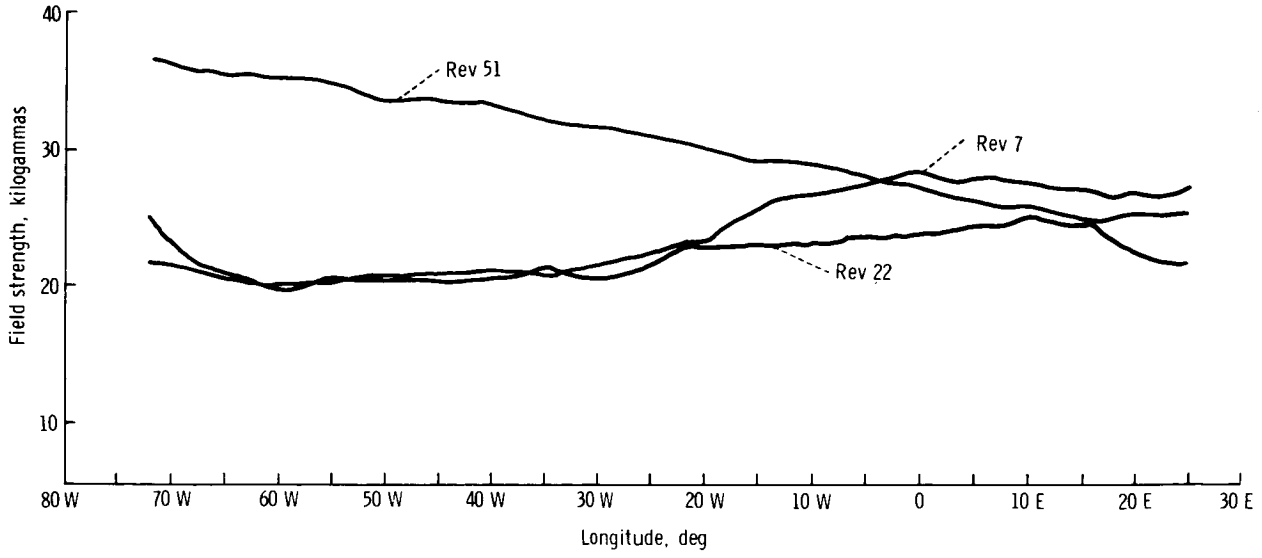

Figure 8. - Data regarding the magnitude of the anomaly field.

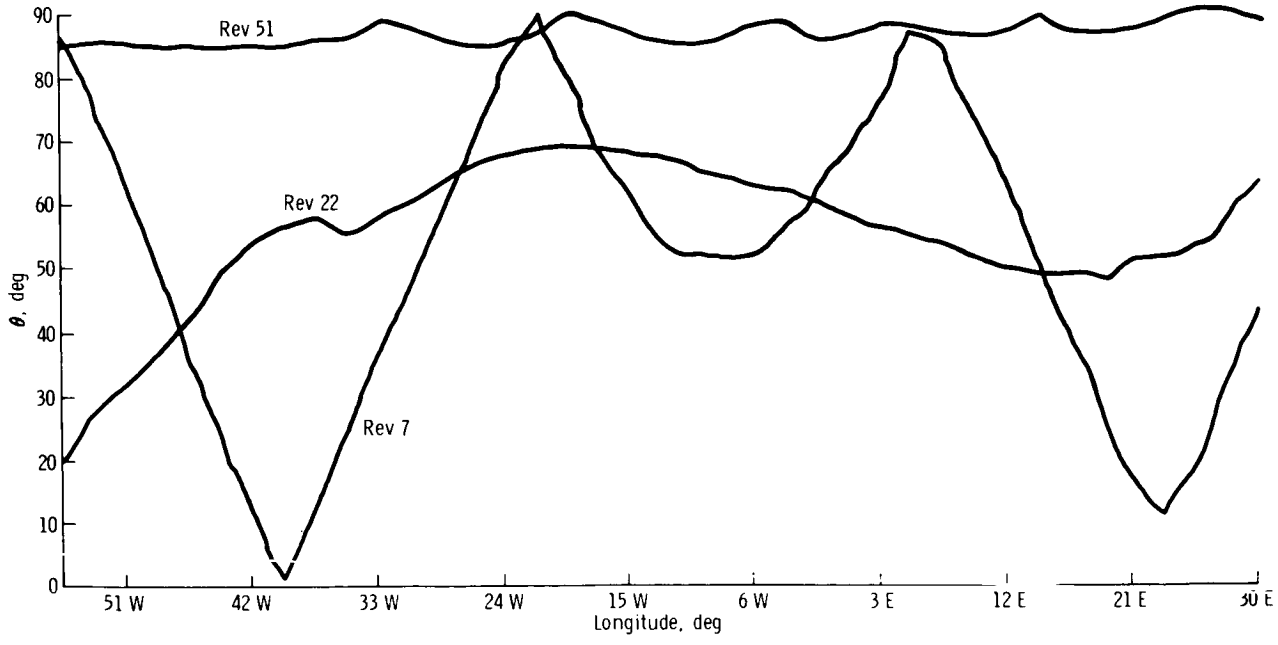

Figure 9. - Data regarding the magnetic-field direction.

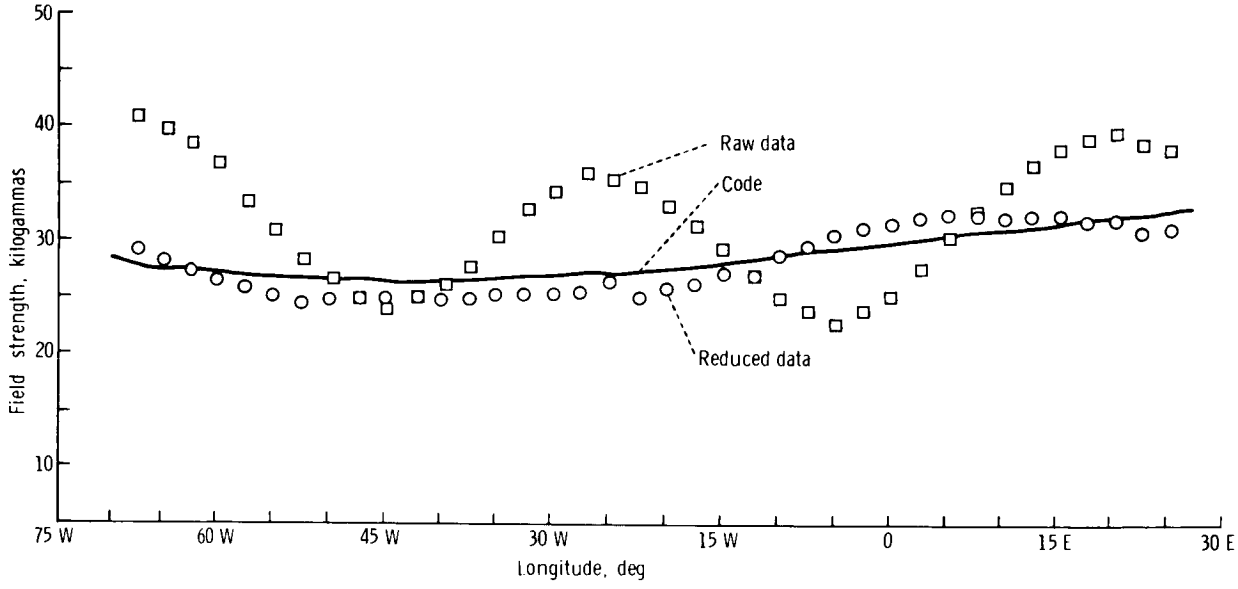

Figure 10. - The comparison among the raw data, the 48-term expansion of the Jensen-Cain coefficient, and the corrected data collected during revolution 7 on the Gemini IV mission.

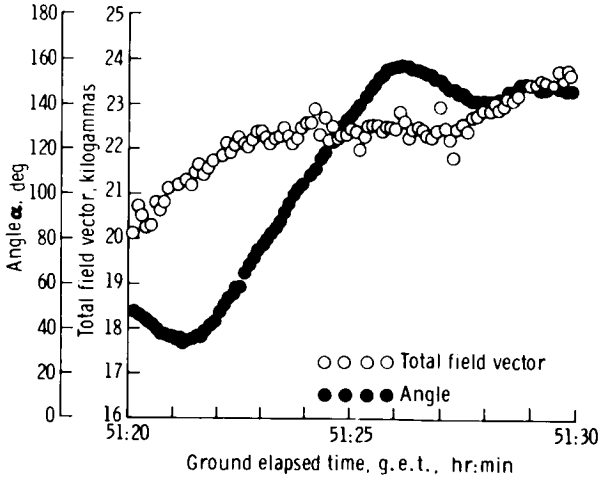

Figure 11. - Data on the magnetic field of the earth in the South Atlantic anomaly region.

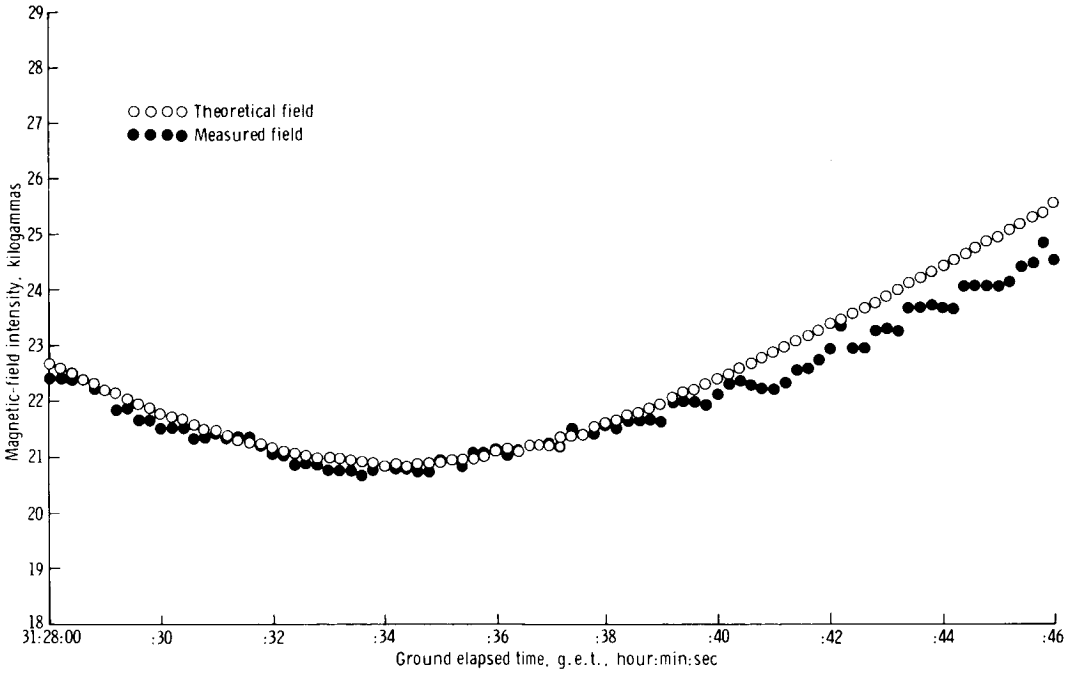

Figure 12. - The measured field compared with the theoretical field.

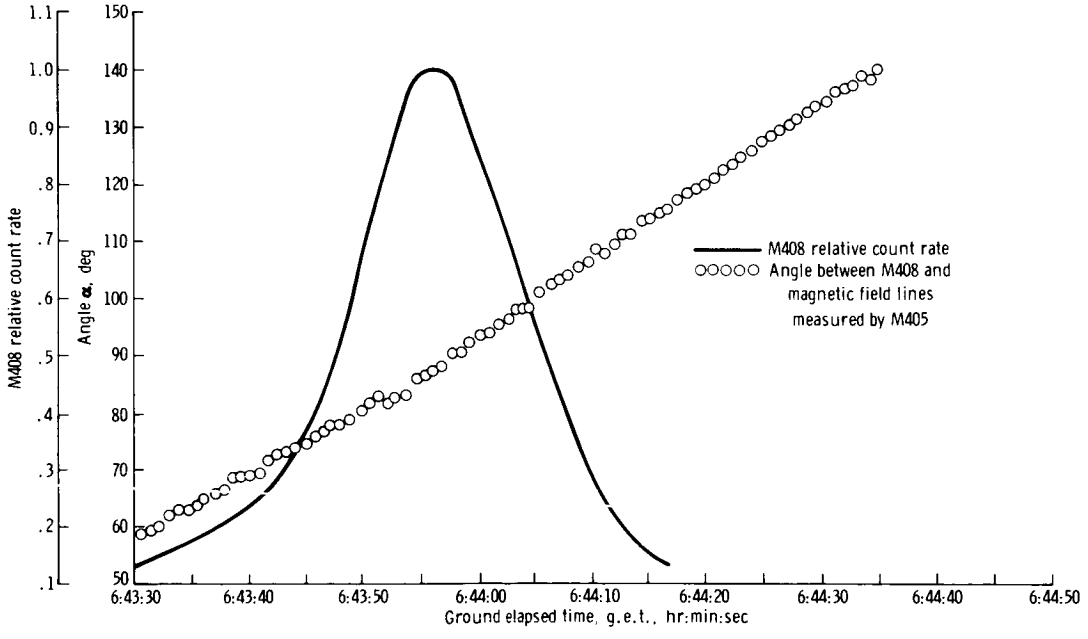

Figure 13. - Tri-axis-magnetometer response.

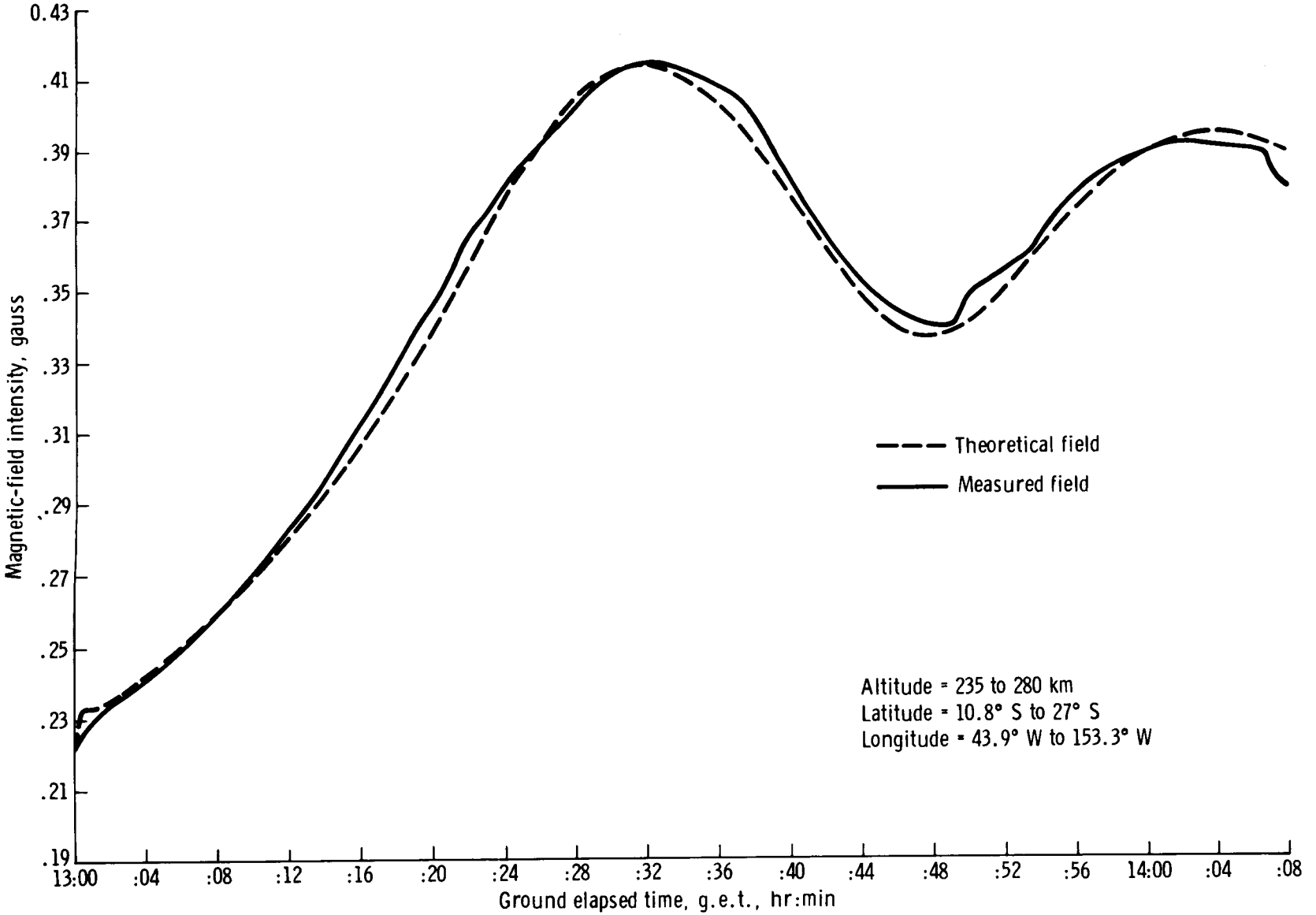

Figure 14. - The comparison of the measured and the theoretical magnetic-field magnitude.

EXPERIMENT M409

BREMSSTRAHLUNG SPECTROMETER

By Reed S. Lindsey, Jr.*

OBJECTIVES

The objectives of Experiment M409 were to gain information for computation of the flux-energy spectra of bremsstrahlung inside the Gemini spacecraft and to determine if energetic electrons are able to penetrate the vehicle walls. The spectra were compared with computer-predicted bremsstrahlung spectra by the use of data from the beta spectrometer (Experiment M408) flown on the Gemini X and XII missions. Gamma rays, produced in the Gemini spacecraft material by incident electrons, were not expected to attain biologically significant levels. On long-duration missions that may be flown in high-electron-flux environments, the problem will be more important. The calculations of bremsstrahlung radiation involved uncertainties because of the small amount of information available on cross-section interaction and because of the complex, heterogeneous composition of the spacecraft. The bremsstrahlung detector was designed for time-differentiated measurement of the electron-induced gamma rays over a large section of the vehicle.

EQUIPMENT

Gemini X Mission

The spectrometer (fig. 1) was of the standard phosphor-plastic design. It was a 10-channel spectrometer, the energy range capability of which was 0.1 to 4.0 MeV. The spectrometer occupied less than 148 cubic inches, weighed less than 7.5 pounds, and required 2 watts at 28 V dc. The instrument was located behind the command pilot seat, approximately at shoulder height. The telemetry complement consisted of eight bilevel 10-per-second telemetry channels sampled in parallel, two 1.25-per-second analog channels, and one 10-per-second telemetry channel which was pulse synchronized with the bilevel word. The bremsstrahlung spectrometer was designed to measure gamma-ray flux and energy spectra with ±5-percent accuracy. The data were time-correlated with exterior electron measurements. Determination of bremsstrahlung fluxes with this accuracy was a considerable improvement in technique.

*NASA Manned Spacecraft Center, Houston, Texas.

Calculation of the anticipated bremsstrahlung count rate was subject to large uncertainties because of the lack of information concerning spacecraft shielding and orientation in the directional electron field. For acquisition of a maximum count rate, the following assumptions were made.

1. The spacecraft was a uniform sphere of radius d.

2. The spacecraft was oriented so that approximately 100 percent of its area produced bremsstrahlung photons.

3. The efficiency of the number of bremsstrahlung photons produced in the spacecraft walls per electron per unit time was approximately 1 percent.

4. The expected flux of electrons was approximately $10^6/cm^2$-sec.

The bremsstrahlung production rate R, radiating into 4π steradians of solid angle, was equal to the electron flux F multiplied by the spacecraft surface area A multiplied by the efficiency E, as follows.

$$R = FAE = 10^6 \times 4\pi d^2 \times 10^{-2} = 4\pi d^2 \times 10^4 \text{ photons per second}$$

The solid angle subtended by a point on the spacecraft surface to the detector was described as follows, where the detector is a flat disk of area πD^2 that views a hemisphere.

$$\frac{a}{A} = \frac{\frac{\pi D^2}{4}}{4\pi d^2} = \frac{D^2}{16d^2}$$

The bremsstrahlung production rate into this solid angle was as follows.

$$\frac{D^2}{16d^2}\ 4\pi d^2 \times 10^4 \text{ photons per second} = 2.5\pi D^2 \times 10^3 \text{ photons per second}$$

For example, if the detector had a counting efficiency of 40 percent, the count rate C was

$$C \sim \pi D^2 \times 10^3 \text{ photons per second}$$

Therefore, a 1-inch detector diameter would produce a maximum count rate of approximately $C \sim 2 \times 10^4$ photons per second.

The bremsstrahlung system block diagram is shown in figure 2. The basic sensor was a CsI(T1) crystal surrounded by a plastic fluor of the thickness necessary to produce a usable pulse-height output for electrons and protons in the anticipated energy regions. Photomultiplier-tube anode signals consisted of two components, which are listed as follows.

1. A fast component caused by charged-particle interactions in the plastic fluor

2. A slow component that represented energy deposition in the CsI(T1) crystal

The fast component of the pulses was separated by a 10-nanosecond differentiator. If the fast component exceeded a threshold of approximately 100 keV, it produced an output that was used to inhibit the analysis of the slow component of the pulse, because such an output corresponds to a charged-particle event rather than to a bremsstrahlung interaction in the CsI(T1) crystal. To convert the tunnel-diode discriminators into a differential pulse-height analyzer, a strobe pulse was generated which served to interrogate the tunnel-diode discriminators at a time just after the peak of the signal pulse. Suitable coincidence logic within the tunnel-diode discriminators produced an output pulse from the highest tunnel-diode discriminator. The pulses from the various channels of this differential pulse-height analyzer were accumulated in binary counters from the 10-hertz telemetry clock pulse. To accommodate the very wide dynamic range of count rate that was anticipated, a data-compression system was used. The compression system contained 5 bits of number information and 3 bits of place information. Because the 5-bit number represented a binary number from 1 to 32, and the 3-bit place information represented a multiplier from 1 to 2^8, the largest number that could be transmitted was 2^{13}, or 8192; the smallest number was 2^0, or 1. By use of this output format, the error caused by compression always was positive and was less than 5.9 percent (so the average error was approximately 3 percent).

The data-processor circuit is shown in figure 3. The circuit was composed of 10 binary counters, a read matrix, a shift register, and a control logic. Each of the 10 channels was sampled every 1 second. The decoder connected a particular binary counter with the shift register through the read matrix. The decoder was driven by a 10-hertz telemetry clock pulse. As soon as the information from the counter was shifted, the decoder was free to accumulate again. This read time was approximately 30 microseconds. When the data had been transferred to the 13-bit shift register, a 50-kilohertz internal clock began to shift the contents of the register to the right. This process continued until a significant digit appeared at the 13th bit or until seven shifts occurred and stopped. The number of shifts was recorded in the place counter. The last 5 bits of information in the shift register, which represented the 5 most significant bits of data, were then read out with the 3 bits of place information. The total was 8 bits of information that represented the contents of one channel. When the next 10-hertz clock pulse transferred the next information from the binary counter to the shift register, the cycle began again. All 10 channels were read out in 1 second; the maximum dead time was 20 microseconds per channel.

The spectrometer shown in figure 4 was modified to measure electrons and bremsstrahlung, and consisted of two parts: the detector and the data processor. The detector and the data processor combined weighed approximately 8 pounds and required 6 watts. The detector unit was fastened to the command-pilot-side spacecraft hatch and was oriented to measure the flux and the energy of penetrating electrons. The data processor was located behind the seat of the command pilot. An 8-foot cable was electrical coupling between the two parts of the spectrometer. The detector unit (fig. 5) consisted of a 0.040-inch-thick, 0.40-inch-diameter Pilot-B plastic scintillator coupled to the top of a 0.50-inch-thick, 0.750-inch-diameter CsI(T1) scintillator that was viewed by a photomuliplier tube. The anode signal was fed through a shorted 10-nanosecond-delay line to a high-speed amplifier. The amplifier drove two high-speed discriminators that were adjusted for acceptable energy deposition in the plastic scintillator. Because bremsstrahlung in the energy region of interest did not interact appreciably with the thin plastic, whereas electrons did interact, an effective means of discrimination between the two types was available. The two discriminators operated effectively as a timing single-channel analyzer for electrons between 0.2 and 4.0 MeV. Signals below the lower level discriminator were assumed to be caused by bremsstrahlung. Those signals within the discriminator window were assumed to be caused by interesting electrons, and those signals above the upper level detector were assumed to be caused by heavier ionizing particles. Digital gating signals were derived from logic circuitry after the high-speed discriminators routed the linear signal to the proper analog-to-digital converter in the data processor.

Also, the detector unit included a phototype high-voltage power supply and low-voltage power supplies for the amplifiers, discriminators, and logic circuits. The unit was sealed in a dry-nitrogen atmosphere to facilitate proper operation of high-voltage components exposed to exterior vacuum conditions. The last dynode signal drove a linear amplifier, which in turn and through the interconnecting cable drove the data-processor amplifier.

The data processor (fig. 6) was a modification of the bremsstrahlung spectrometer flown on the Gemini X mission. It consisted of two linear amplifiers, two analog-to-digital converters, two sets of five scalers each, the necessary control logic, and power supplies. Digital control signals from the detector unit permitted operation of only one analog-to-digital converter at a time. The necessary dynamic energy range was covered by two linear amplifiers that had gains of approximately 1 and 4. The analog-to-digital converters were of the parallel tunnel-diode type. One extra channel was used to inhibit strobing of the analog-to-digital converters if the linear signal was too large, as in the case of cosmic rays or energetic protons which could penetrate the detector from any direction. Data from the analog-to-digital converters were recorded by 10 scalers and were shifted serially to the telemetry under the control of the telemetry synchronization pulse. The read-out rate was 10 channels per second. Because the telemetry word was 8 bits long (256 events), and the scalers were a maximum of 12 bits long, a data-compression technique was used. The 5 most significant digits of information from a scaler and 3 bits to locate their position in the 12-bit scaler were presented to the telemetry. Power supplies for the analog and digital circuitry and noise filters were located in the data processor.

PROCEDURE

The spectrometer, located behind the command pilot at approximately shoulder level, was controlled through the experiment circuit breaker by means of an on-off switch. The switch was turned on after orbital entry and was turned off just prior to entry; thus, data were collected during the entire flight. No other operational procedures were required during the mission. For example, the Gemini XII flight crewmembers turned the equipment on and off four times during the mission for a total on-time of approximately 32 hours. Approximately 5 hours of this time was within the geographic anomaly regions of interest.

RESULTS

Gemini X Mission

A few spectra were observed during postpass telemetry dumps at the Hawaii station. These spectra were indicative that the bremsstrahlung spectrometer functioned as was expected. The computer data processing consisted of reconstruction of spectra as a function of spacecraft time and path. The reconstruction involved decompression of transmitted numbers, addition of sensor efficiency, dead time, and calibration factors, and correlation of spacecraft attitude and position.

Relative count-time distributions for passages through the magnetic anomaly region on revolutions 20 and 32, respectively, are shown in figures 7 and 8. Bremsstrahlung relative count-rate time spectra for revolutions 6 and 34 (and electron relative flux-time spectra for the same points as taken from ref. 1) are shown in figures 9 and 10. Unfortunately, no data were available from Experiment M408 for these passes. The values were indicative that it should be possible to draw a strong correlation between electron and bremsstrahlung fluxes to facilitate a means of monitoring bremsstrahlung-calculation techniques. The rather strange behavior of the bremsstrahlung curve of figure 10 has not been explained. However, one interesting fact is that the bremsstrahlung energy-flux spectral shape changed during the depressed portion of the curve. Detector-efficiency corrections may result in a more regular shape. It will be possible to construct bremsstrahlung-flux-energy distributions for each traversal of the magnetic-anomaly region and to complete the bremsstrahlung dose at the location of the detector for comparison with dose calculations derived from theoretically produced bremsstrahlung spectra.

Gemini XII Mission

Preliminary analysis of the data that were obtained during the Gemini XII mission was indicative that electrons did penetrate the spacecraft wall, a condition which previously was doubted. Spacecraft interior-electron and bremsstrahlung integral-count-rate time spectra for Gemini revolution 6 are shown in figure 11. A strong correlation existed between the two general spectra, which was anticipated previously. An uncorrected electron-count-rate energy distribution is shown in figure 12. The

anomalous increased number in the highest energy spectrometer channel is an unexplained occurrence. An uncorrected bremsstrahlung-count-rate energy distribution is shown in figure 13 and was within a reasonable estimation of such distributions.

REFERENCE

1. Vette, James I.: Models of the Trapped Radiation Environment. Vol. I, Inner Zone Protons and Electrons. NASA SP-3024, 1966.

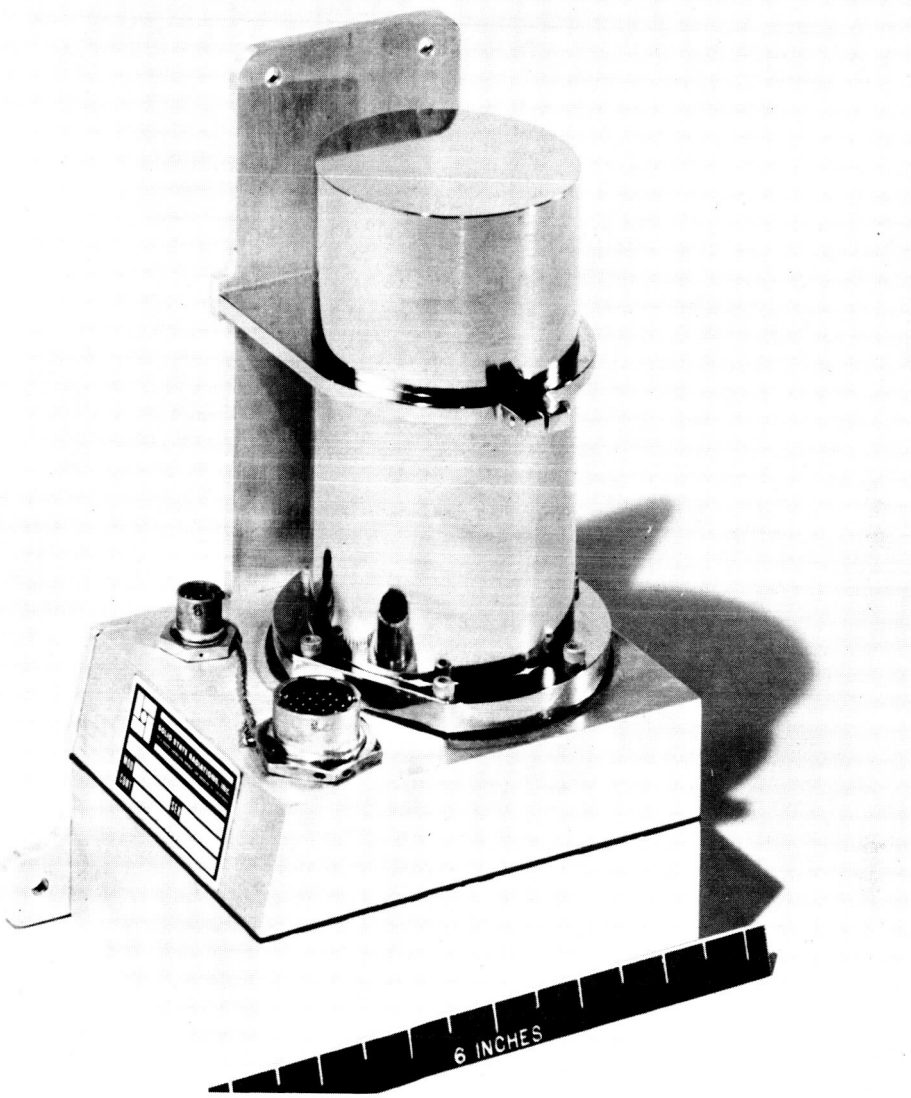

Figure 1. - The bremsstrahlung spectrometer that was used on the Gemini X mission.

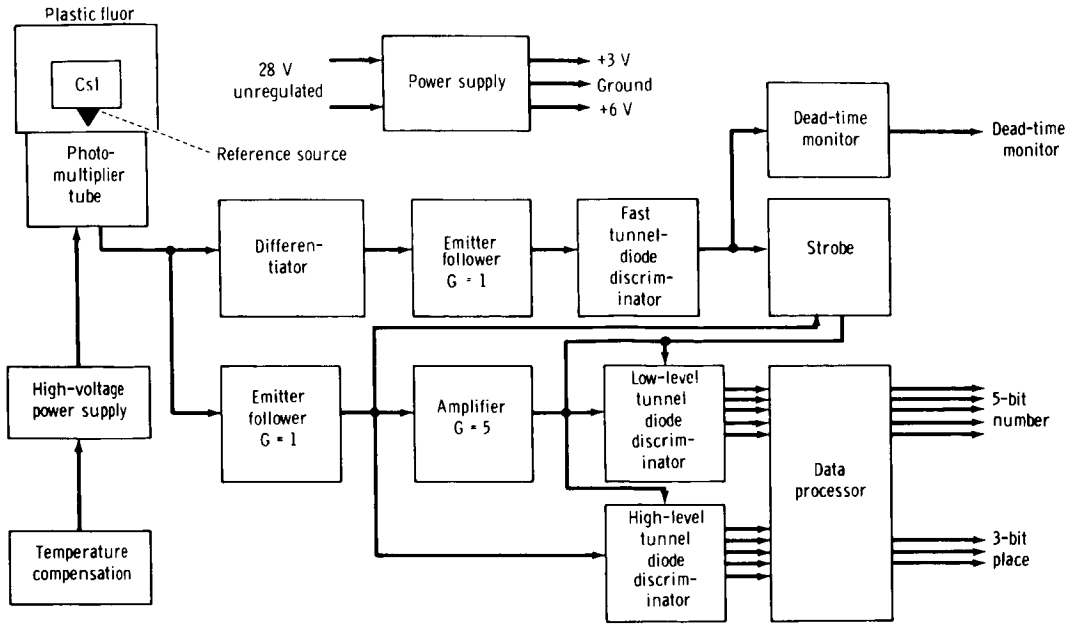

Figure 2. - A block diagram of the spectrometer.

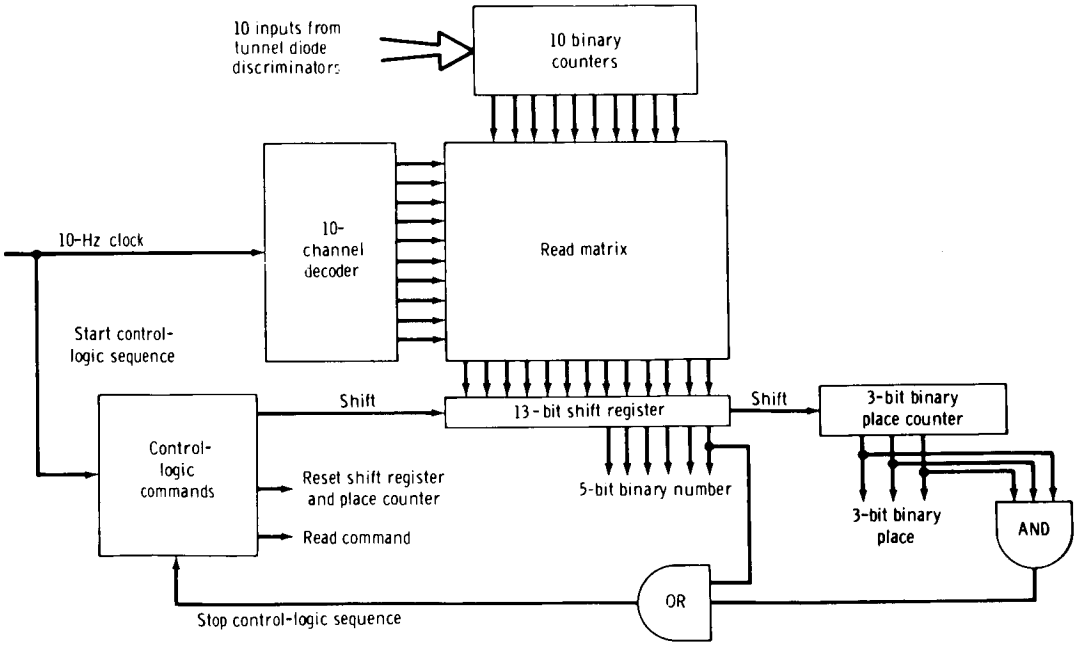

Figure 3. - The data-processor circuit.

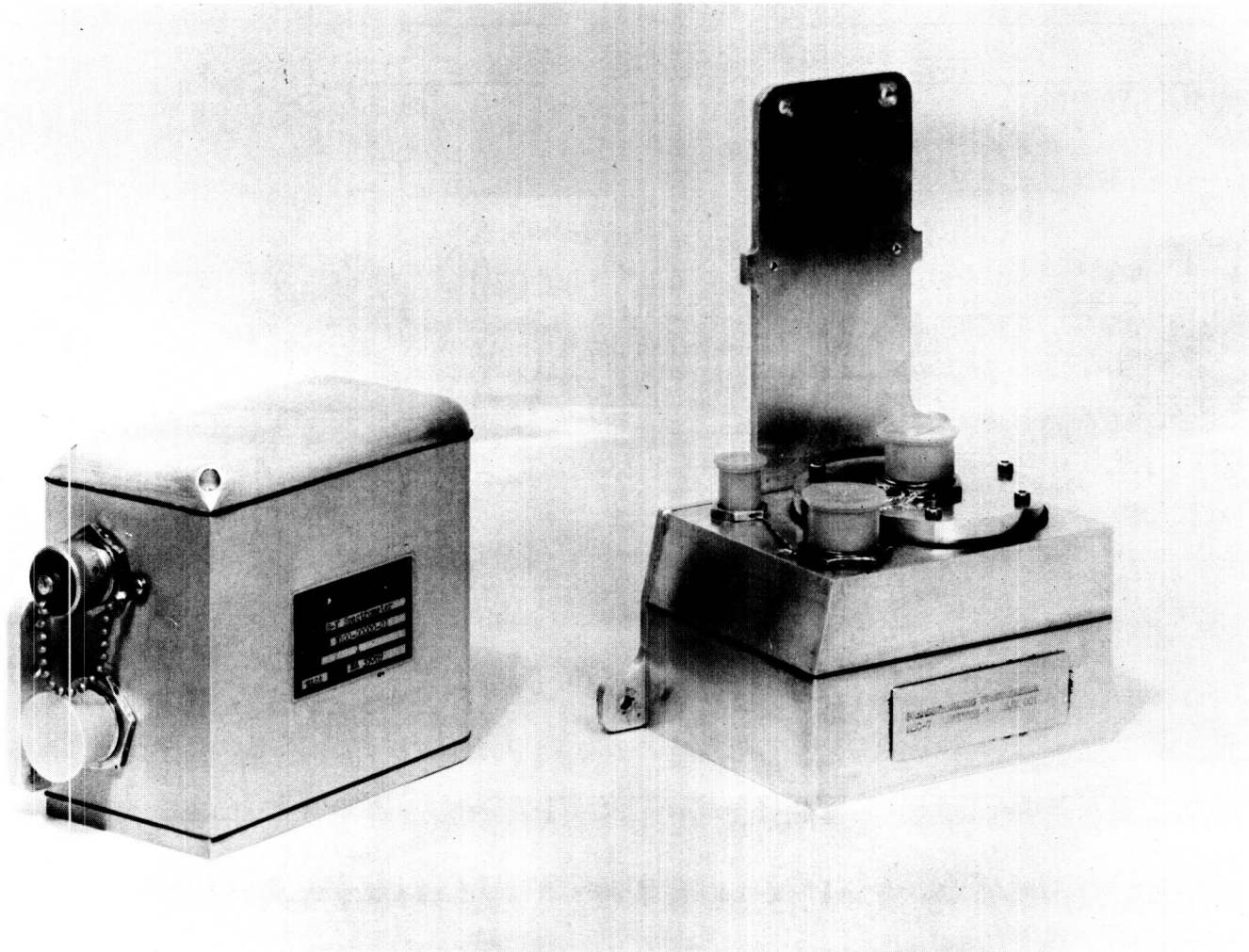

Figure 4. - The bremsstrahlung spectrometer that was used on the Gemini XII mission.

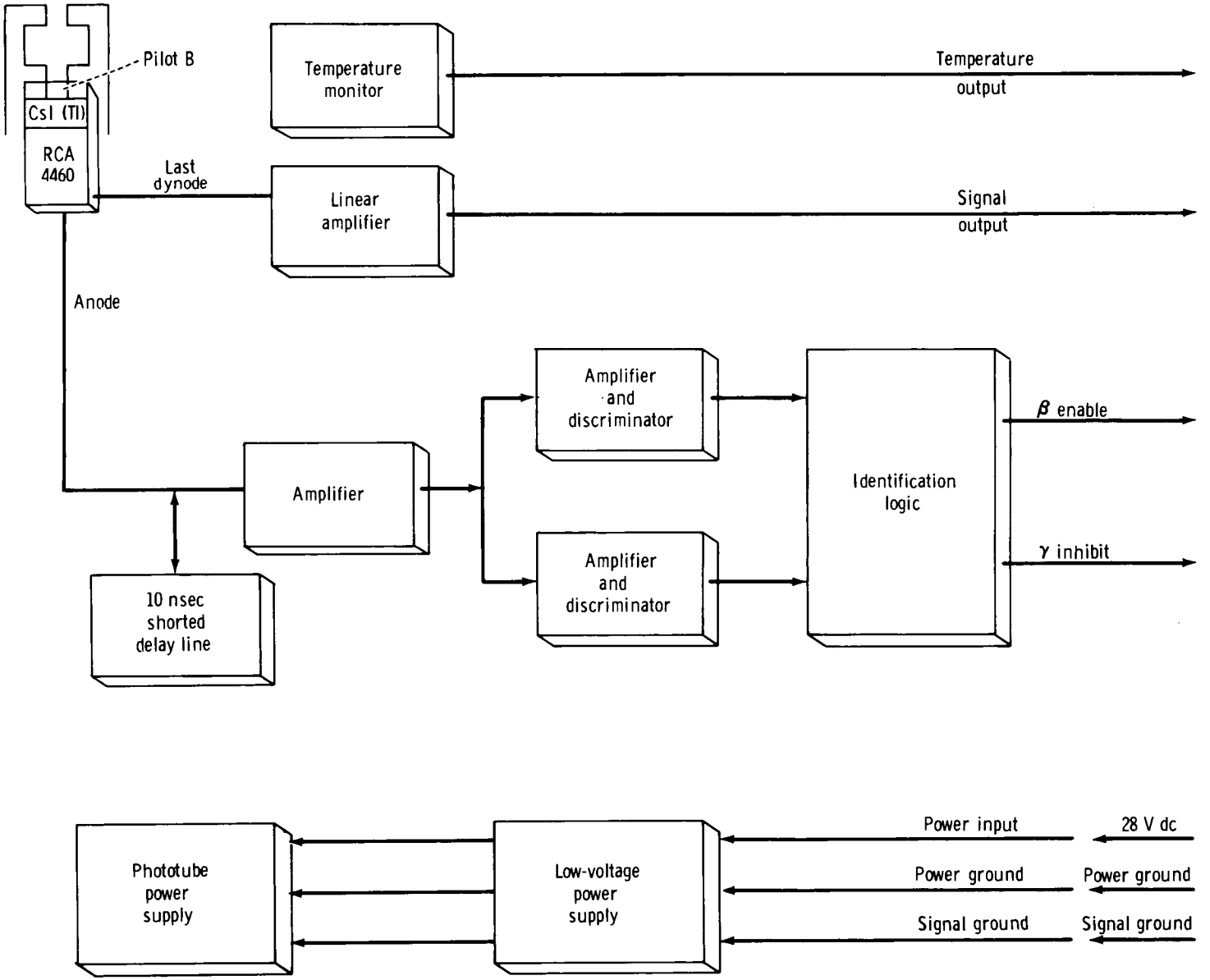

Figure 5.- The detector-unit schematic.

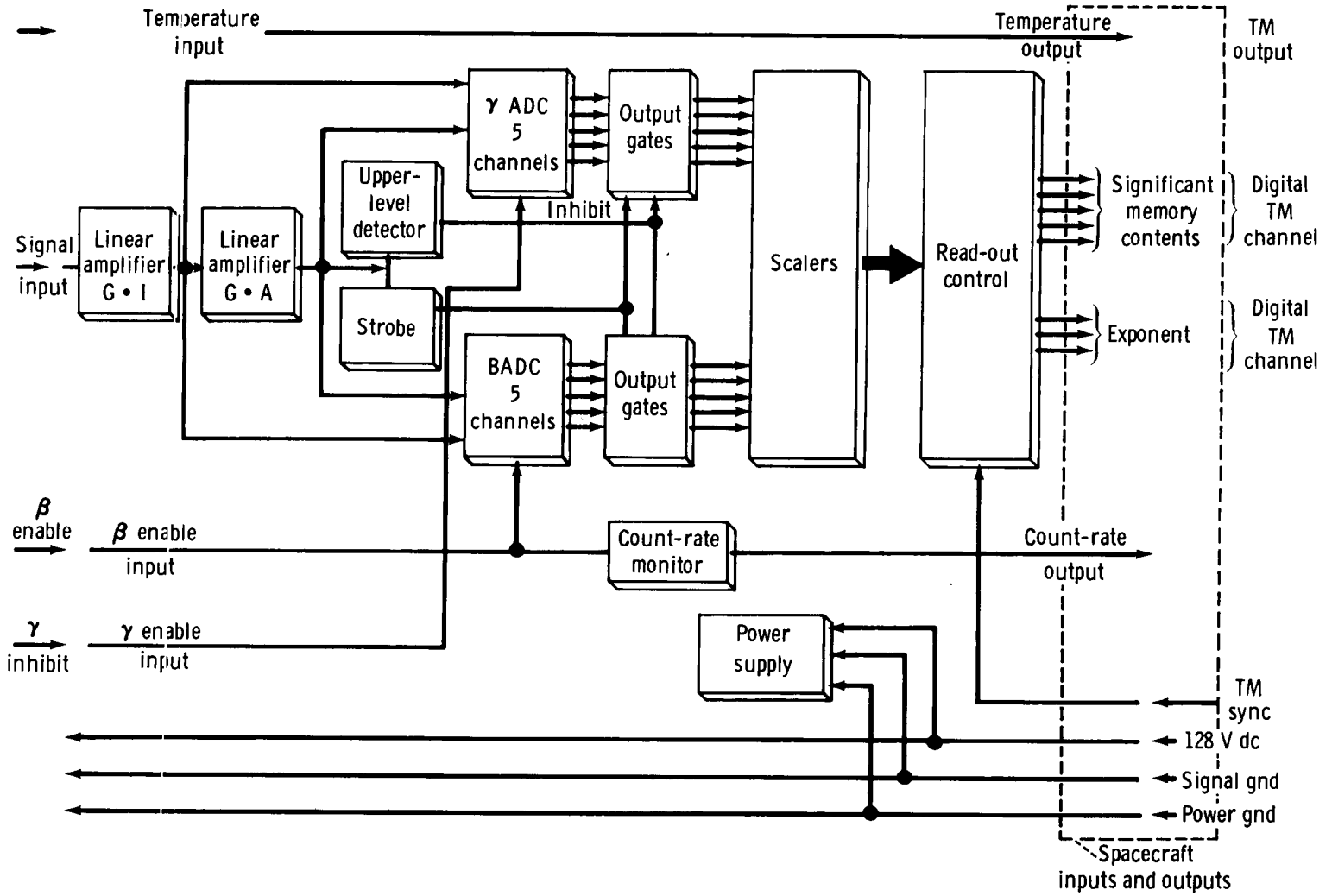

Figure 6. - The data-processor schematic.

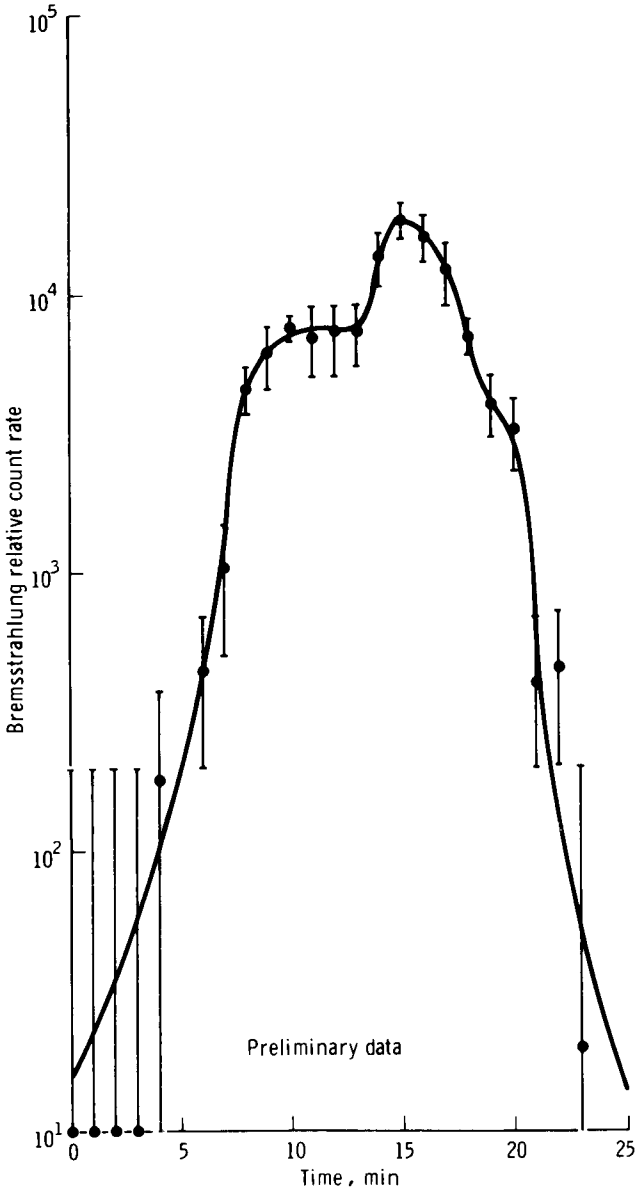

Figure 7.- The relative count-time distributions for revolution 20 on the Gemini X mission.

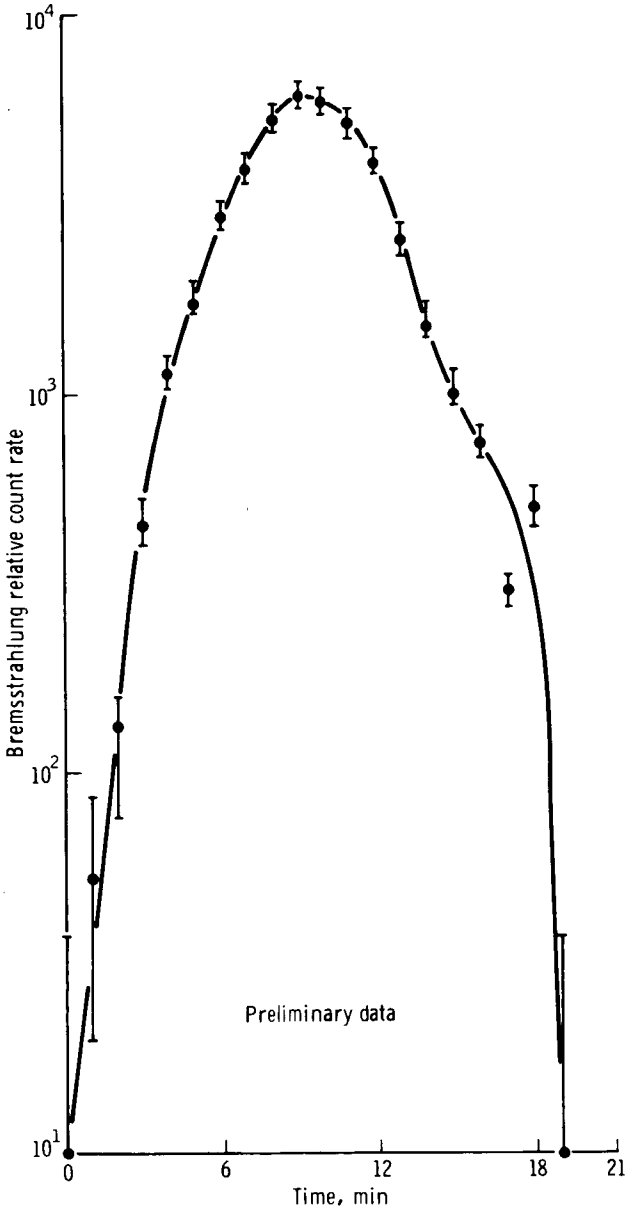

Figure 8. - The relative count-time distributions for revolution 32 on the Gemini X mission.

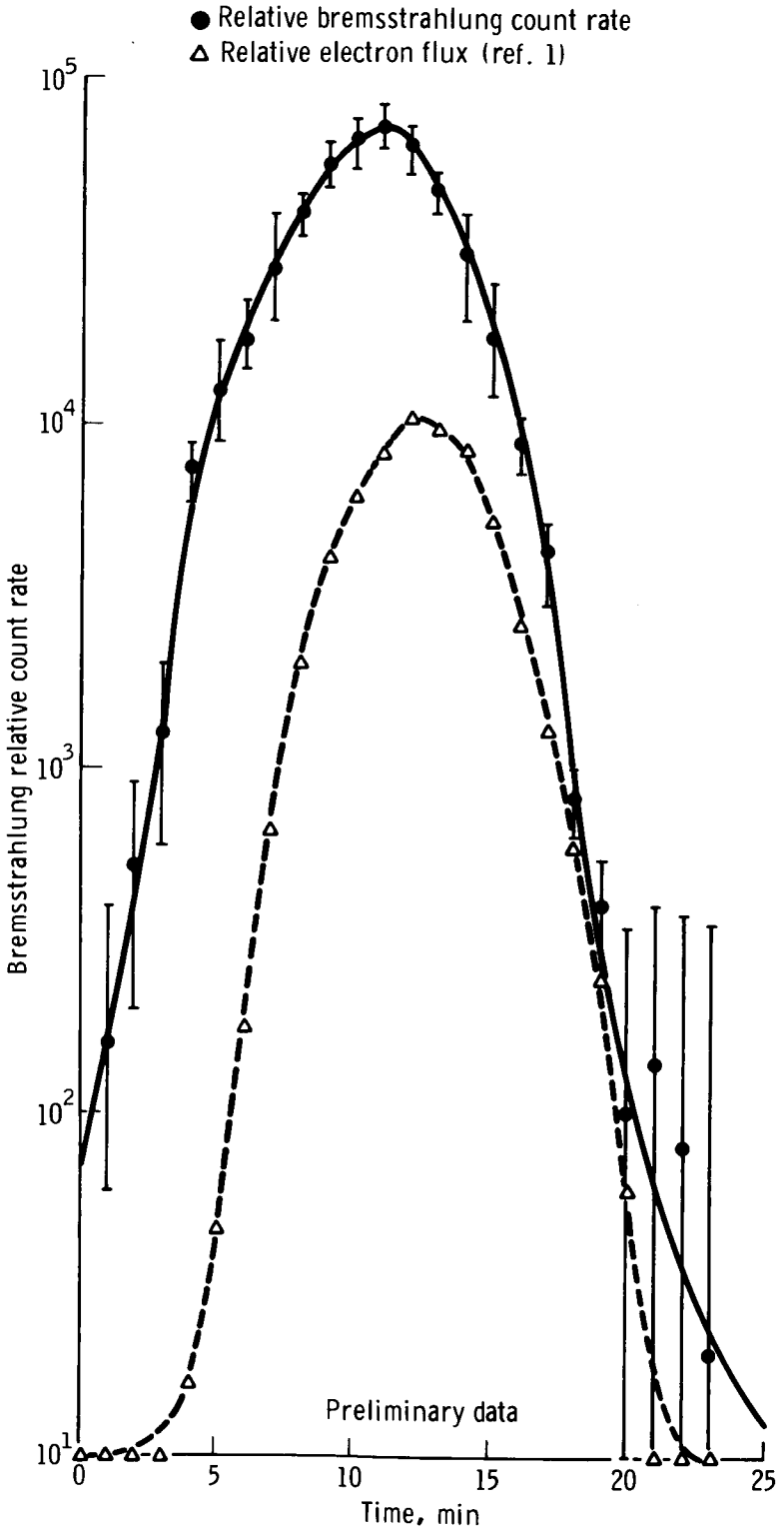

Figure 9.- The bremsstrahlung relative count-rate time spectra for revolution 6 on the Gemini X mission.

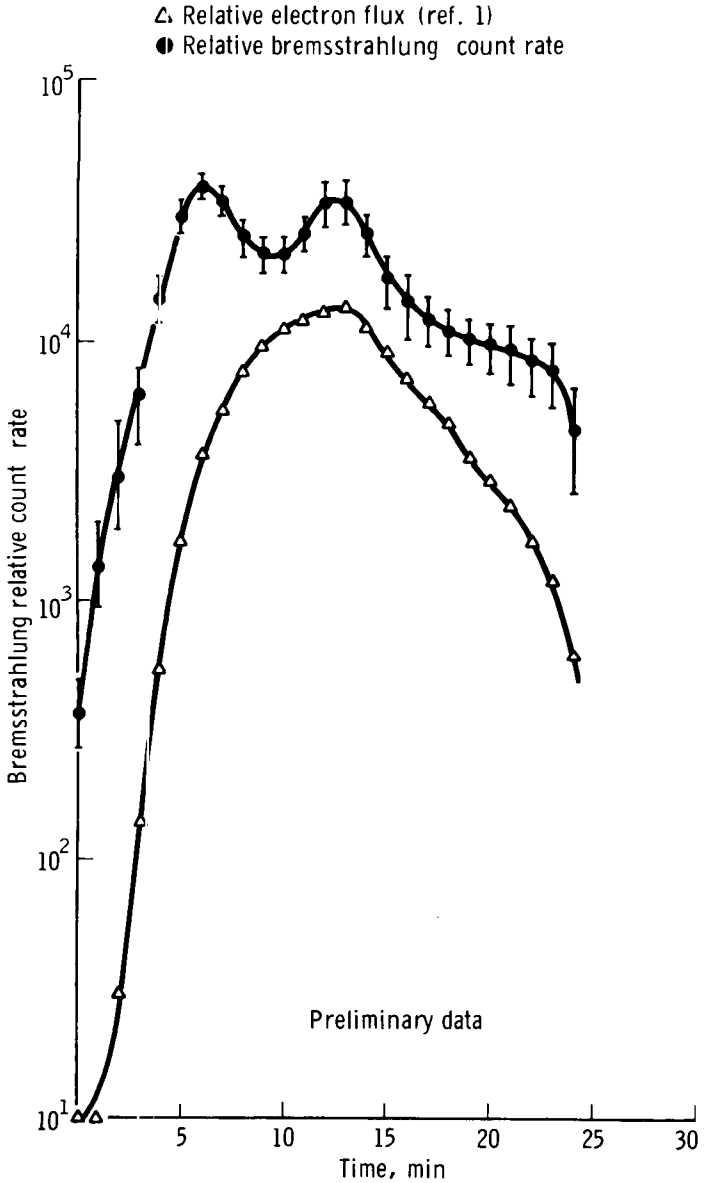

Figure 10. - The bremsstrahlung relative count-rate time spectra for revolution 34 on the Gemini X mission.

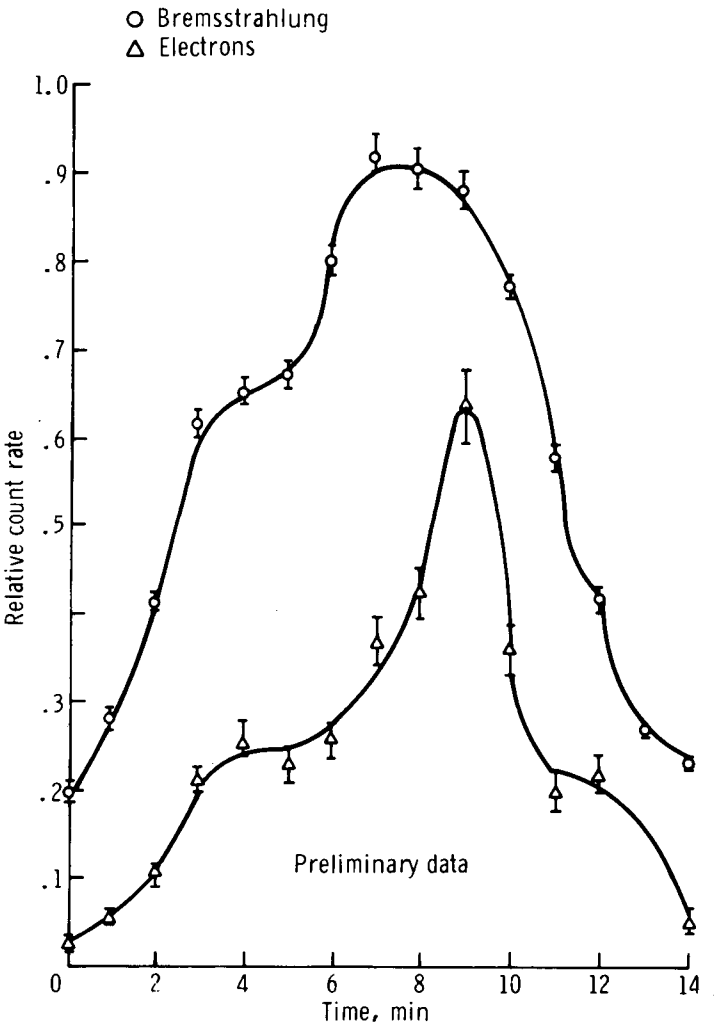

Figure 11. - The relative integral count-rate time spectra for revolution 6 on the Gemini XII mission.

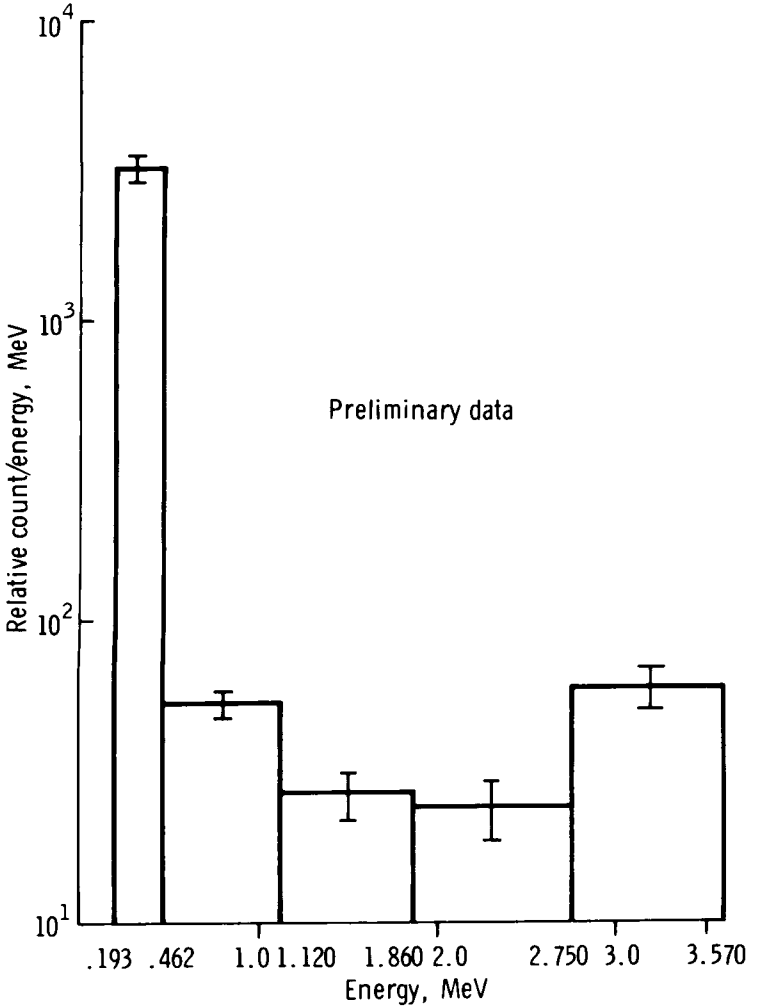

Figure 12. - The uncorrected electron relative count-energy distribution for revolution 6 on the Gemini XII mission.

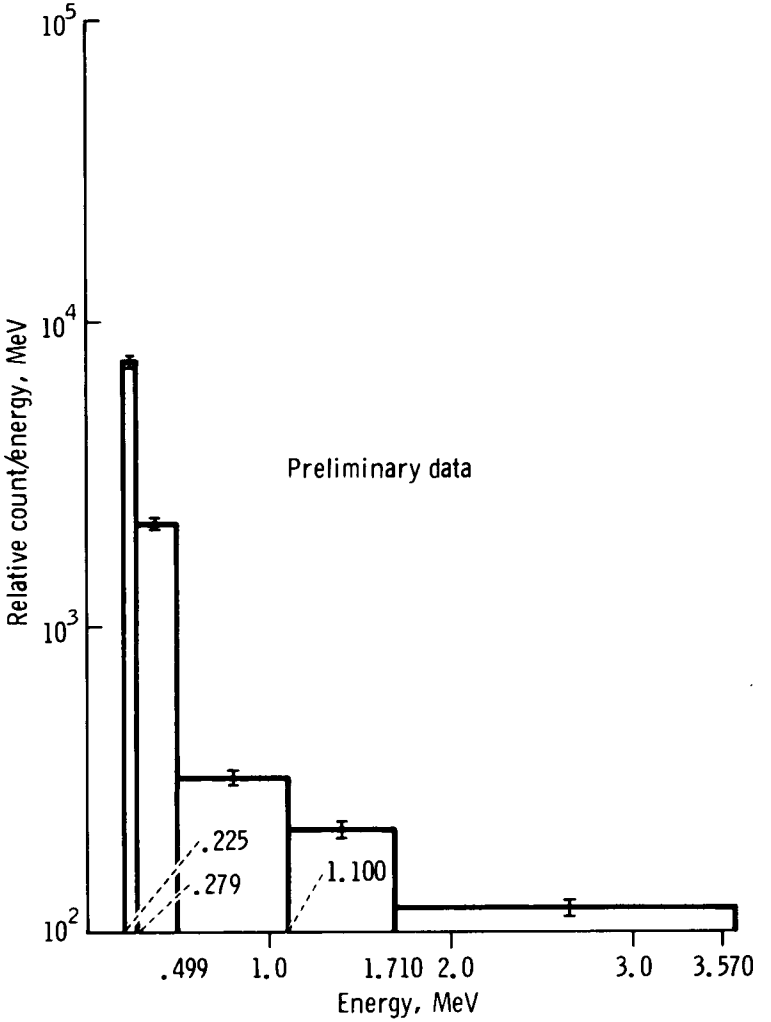

Figure 13. - The uncorrected bremsstrahlung relative count-energy distribution for revolution 6 on the Gemini XII mission.

EXPERIMENT S026

ION-WAKE MEASUREMENT

By David B. Medved* and Ballard E. Troy, Jr.**

OBJECTIVES

The objective of Experiment S026, which was flown on the Gemini X and XI missions, was the measurement of the ion-wake and electron-wake structure and other perturbations of the ambient medium produced by the Gemini spacecraft in orbit. The experiment was designed to include the following factors.

1. A map of the spacecraft ion-density wake as a function of position coordinates relative to the reference frame of the spacecraft

2. A contour map of the spacecraft electron-density wake as a function of the position coordinates just mentioned

3. Determination of electron temperature as a function of the position coordinates

4. Detailed information on ambient ion and electron densities and electron temperature as a function of altitudinal and diurnal variations from the Gemini Agena target vehicle (GATV)

5. Ionization transients caused by spacecraft thruster firings

BACKGROUND INFORMATION

During flight, the Gemini spacecraft moved through the ionospheric medium with a velocity that was high compared with the random thermal velocities of the ions, but that was small when compared with the random thermal motions of the electrons. The vehicle motion was supersonic with respect to the ions and was subsonic with respect to the electrons. Electrons approached the vehicle from all directions as if it were standing still, whereas the ions were swept up by the vehicular motion.

To an observer on the spacecraft, there is a ram ion flux to the vehicle along the direction of the vehicular velocity vector (fig. 1). The motion of the vehicle results in

*Electro-Optical Systems, Inc., Pasadena, California.
**NASA Goddard Space Flight Center, Greenbelt, Maryland.

a sweeping out of the ions and neutral particles in its path. If the constituents of the ionosphere were at rest completely, a shadow zone would extend an indefinite distance behind the spacecraft.

As a result of the random thermal motions, the shadow or hole region is filled by a sequence of interacting mechanisms, the region behind the orbiting vehicle actually being a plasma rather than an ion wake. Because the electrons approach the spacecraft from all directions, it would be expected that these would rapidly fill the shadow region. The electrostatic forces between the charged particles prevent the occurrence of substantial imbalances in the local space charge. A typical ion-wake profile, as predicted theoretically (refs. 1 and 2), is shown in figure 2. These profiles are based on the predictions of the quasi-neutral approximation.

EQUIPMENT

The electron detector (fig. 3) was located on the GATV target docking adapter (TDA) and operated continuously during the experiment. Operation of the inboard and outboard ion detectors depended upon the angular relationship of the GATV to the orbital velocity vector. The inboard ion detector collected useful data whenever the GATV moved TDA-forward, with the GATV axis parallel to the orbital path. The outboard detector was operative whenever the GATV yawed at a right angle to the orbital path. The placement of the equipment on the GATV is shown in figure 3, and a general ion-wake profile is shown in figure 4.

The sensors, shown in figures 5 and 6, were five-element retarding-potential analyzers with alternating-current modulation for low-threshold operation. They were designed to measure ion and electron densities over a range from 5×10^6 per cubic centimeter to 50 per cubic centimeter with space potential measurements in a range from 3 to 0 electron volts. Ion densities as low as 50 ions per cubic centimeter were considered detectable for this experiment. For contour mapping, position resolution to approximately 1-foot accuracy was obtained from a 16-millimeter general-purpose sequence camera. The sensor-electrometer systems each collected and modulated plasma current in a Faraday cup which contained four grids and a collector plate. The voltage bias placed on the front grid of the electron sensor limited the minimum-energy electron which could enter the sensor. This bias was swept from 8.8 to -3 volts relative to spacecraft potential. The second grid accelerated the properly charged particles which passed the first grid. On both sensors, the second grid prevented unwanted particles from entering the system. A third grid was driven by a 3840-hertz square wave, which modulated the plasma current by alternately blocking and accelerating the particles passing through the second grid. A fourth grid consisted of three screens connected to act as a capacitive shield between the modulation grid (grid three) and the final collector. The third screen in the final grid also served as a collector for secondary photo electrons produced in the sensor. The sensor output current was designed to swing from zero to the direct-current value of the input plasma current and back within 1 microsecond, with a 50-percent duty cycle at a frequency of 3840 hertz. This square-wave current was amplified by an alternating-current electrometer which was located behind the sensor. Electrometer signals were synchronously demodulated and averaged by an analog-signal processor on board the GATV. The resultant voltage, proportional

to the logarithmic average, was generated and buffered, then input to the analog-to-digital converter in the GATV telemetry system for transmission to the network tracking stations.

PROCEDURES

Gemini X Mission

Two modes were used during the Gemini X mission. These modes were designed to obtain a maximum amount of information on the wake structure with minimal fuel consumption. Mode A constituted a direct axial mapping of the wake, which was accomplished by linear separation of the spacecraft from the GATV. This type maneuver was accomplished during final departure of the spacecraft from the GATV. In this mode, ion data were obtained by the inboard ion sensor.

The primary data mode of the experiment was Mode B, illustrated in figure 7. The maneuvers were intended to map the spacecraft wake by use of inplane maneuvers. Mapping began with docked spacecraft-GATV configuration in a TDA-south orientation. The spacecraft was separated from the target vehicle and was maneuvered to a specific position. This position was on an axis along the orbital velocity vector of both the spacecraft and the GATV and passed through the outboard sensors; the spacecraft nose was approximately 1 to 3 feet from the target vehicle. The spacecraft then was translated downward; the axial separation was kept as constant as possible for a distance of approximately 15 feet. The spacecraft was stopped and then was involved in those aspects of the trajectory described in figure 7. The distances off-axis, which corresponded to the transverse motion of the spacecraft, purposely were chosen in excess of the anticipated wake dimensions so that all thruster firings required to change direction in the manner shown would occur in regions where plasma-wake data were not of critical interest.

Gemini XI Mission

The flight plan contained three modes for the ion-wake experiment. Mode A was a linear-departure maneuver. Mode B had three sequences which included two out-of-plane maneuvers (one at night and one in daylight), and one nighttime inplane mapping procedure. These four phases of Modes A and B were planned and executed between 02:10:00 and 03:50:00 g. e. t. Real-time telemetry and delayed-time telemetry received over the high-speed data lines were indicative that all sensors performed satisfactorily. Mode C of the experiment consisted of a 360° roll at the apogee of the first revolution of the highly elliptical 740- by 160-n. mi. orbit.

A 16-millimeter general-purpose sequence camera with a 180-millimeter lens was actuated for Modes A and B for collection of position and range information which was to be used for data correlation.

RESULTS

Gemini X Mission

The experiment was a success to only a limited extent because of fuel constraints encountered during the mission. The sensors were operative immediately after GATV shroud removal (6 minutes after Gemini Atlas-Agena target vehicle lift-off) until GATV power depletion several days after spacecraft landing. Local electron and ion concentrations and electron temperatures were measured during all phases of the mission. During the Gemini X mission, there were two distinct measurements of wake or bow-shock effects. These effects occurred during the docking and undocking maneuvers of the spacecraft. The bow shock effects were assumed to have resulted from reflection of positive ions from the Gemini spacecraft and their subsequent measurement by ion sensors of the target vehicle.

A large quantity of ambient data was obtained over the altitude band covered by the GATV from 160 to 750 n. mi. These data are of considerable interest to persons engaged in studies of the ionosphere and the effects of charges and the relaxation of charges on space vehicles during and after power propulsion in the ionosphere. Real-time telemetry data were obtained from all three sensors during passes over the Air Force Eastern Test Range. Real-time telemetry data from the Canary Islands were transmitted over the aeromedical lines during the crucial undocking maneuvers. This real-time information was essential, because the GATV delayed-time tape recorder was turned off inadvertently during part of the undocking.

Photographs obtained with the 16-millimeter general-purpose sequential camera during the undocking and separation maneuver were indicative that a considerable effort would be required in order to determine the effects of an apparent nonlinear separation which may have caused wake-structure oscillations. In the attempt to establish a frame-to-frame reduction of the relative position coordinates of the two vehicles, a problem existed because of poor GATV definition and total loss of the GATV image during most of the departure after the separation distance had become approximately 100 feet. Other data were obtained during docking and station keeping and during the GATV primary propulsion system posigrade and retrograde firings.

Gemini XI Mission

Data correlation and reduction, particularly correlation of the GATV telemetry data with the relative position coordinates of the two vehicles, required considerable effort. The radar system, which was to be used for backup range information did not function during the experiment. Also, the onboard voice tape recorder apparently was inoperative during periods when the crewmen were to record start-and-stop times of the 16-millimeter boresighted sequence camera. In addition, the auxiliary receptacle, which was to supply time markers, did not function. Some of the photographic data were of usable quality for correlation of experiment data with position information. Position correlation and time registration were attempted by use of thruster-firing durations and on-off times.

Real-time telemetry data, collected during the Gemini spacecraft and GATV tethered flight are shown in figure 8. Only approximate currents could be obtained from the telemetry data. During the tethered flight, the two vehicles were revolving about their center of mass while separated by a 100-foot tether. By observation of the oscillations in the sensor responses, a real-time estimate of the rotation period was formulated. This rotation rate was estimated to be approximately 7 minutes. The use of the aeromedical high-speed-data transmission lines made this possible during real time.

Telemetry data from Modes A and B are shown in figures 9 to 12. The outboard ion-sensor voltage, shown in the telemetry data in part (b) of each of these figures was compared with the mode procedural diagrams, shown in part (a) of the same figures. Data loss occurred during sequence 1 of Mode B and is indicated in figure 9(b). Dips in outboard ion-sensor output voltage were associated with thruster firings. The position-indication number of the thruster which was fired is shown in figure 12(b) near its associated ion-sensor output voltage dip. The following effects were observed in real time and from delayed-time telemetry during the mission.

1. The spacecraft wake shadow produced ion depletions at least an order of magnitude less than the ambient levels.

2. The bow shock for the enhanced ion-count phenomenon, reported during the Gemini X mission, was repeated during the terminal rendezvous-and-docking phases in the TDA-north configuration.

3. Reflection of ions from the pilot during extravehicular activity (EVA) was observed.

4. Strip-chart real-time data from Cape Kennedy and delayed-time telemetry from the U. S. S. Rose Knot Victor tracking ship were used to determine the rotation rate of the tethered spacecraft-GATV configuration.

5. A change in potential of the docked configuration under GATV primary propulsion system firings was observed. The same effect had been observed during the Gemini X mission.

6. The effects of thruster firings, apparent during the Gemini X mission, also were apparent on this mission. These effects appeared to be readily separable from the wake measurements. This was not possible with the Gemini X data.

CONCLUSIONS

Gemini X Mission

Quick-look analysis of the data from the GATV orbits was indicative that electron and ion temperatures were higher than was estimated. The high electron temperature accounted for the sensor saturation observed during the mission. This temperature measurement was 0. 3 electron volt at a 200-n. mi. altitude during daytime conditions. Spacecraft wake structure has been observed as far as 100 feet from the vehicle.

Thruster firings in the TDA-south configuration produced a decrease in the observed ion flux to the outboard ion sensor, produced an apparent increase in the ion flux to the inboard ion sensor, and produced an enhanced electron concentration to the outboard electron sensor. Visual inspection of strip-chart data was indicative that definitive wake-cone angles could be determined. It also was apparent for many cases that the electron distribution followed the ion-depletion effects; this was indicative that the wake was a plasma, not an ion wake.

REFERENCES

1. Gurevich, A. V.; Al'Pert, Ya. L.; and Pitaevskii, L. P.: Effects Produced by an Artifical Satellite Rapidly Moving in the Ionosphere or in an Interplanetary Medium. Soviet Physics Uspekhi (Eng. transl.), vol. 6, no. 13, 1963.

2. Gurevich, A. V.; Al'Pert, Ya. L.; and Pitaevskii, L. P.: Space Physics with Artificial Satellites. H. H. Nickle, trans., 1965.

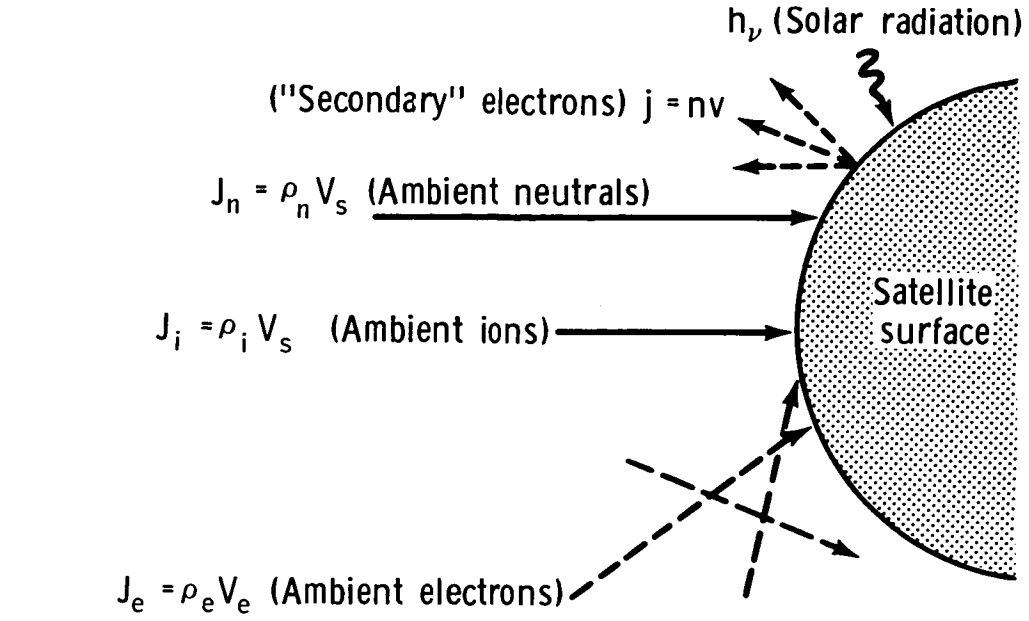

V_s = Satellite velocity
V_e = Ambient electron velocities
ρ_n = Neutral density of ambient
ρ_i = Ion density of ambient
ρ_e = Electron density of ambient
Assume $\rho_i = \rho_e$ and $V_e >> V_s$

Figure 1. - A model of particle fluxes incident on a satellite in the lower ionosphere.

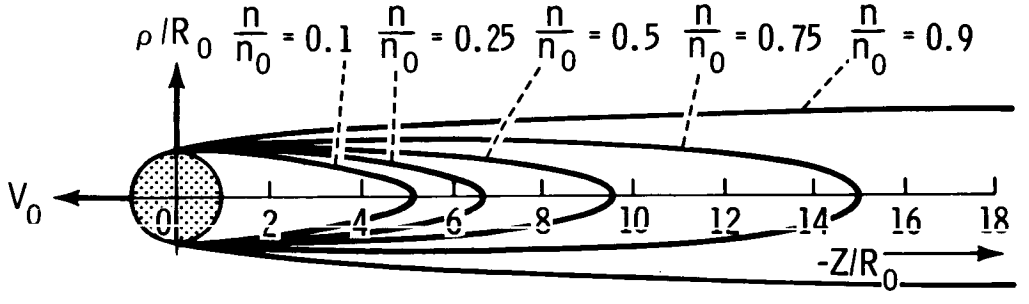

Figure 2. - Curves of constant particle density in the rarefaction region behind a body of circular cross section at a Mach number of 8.

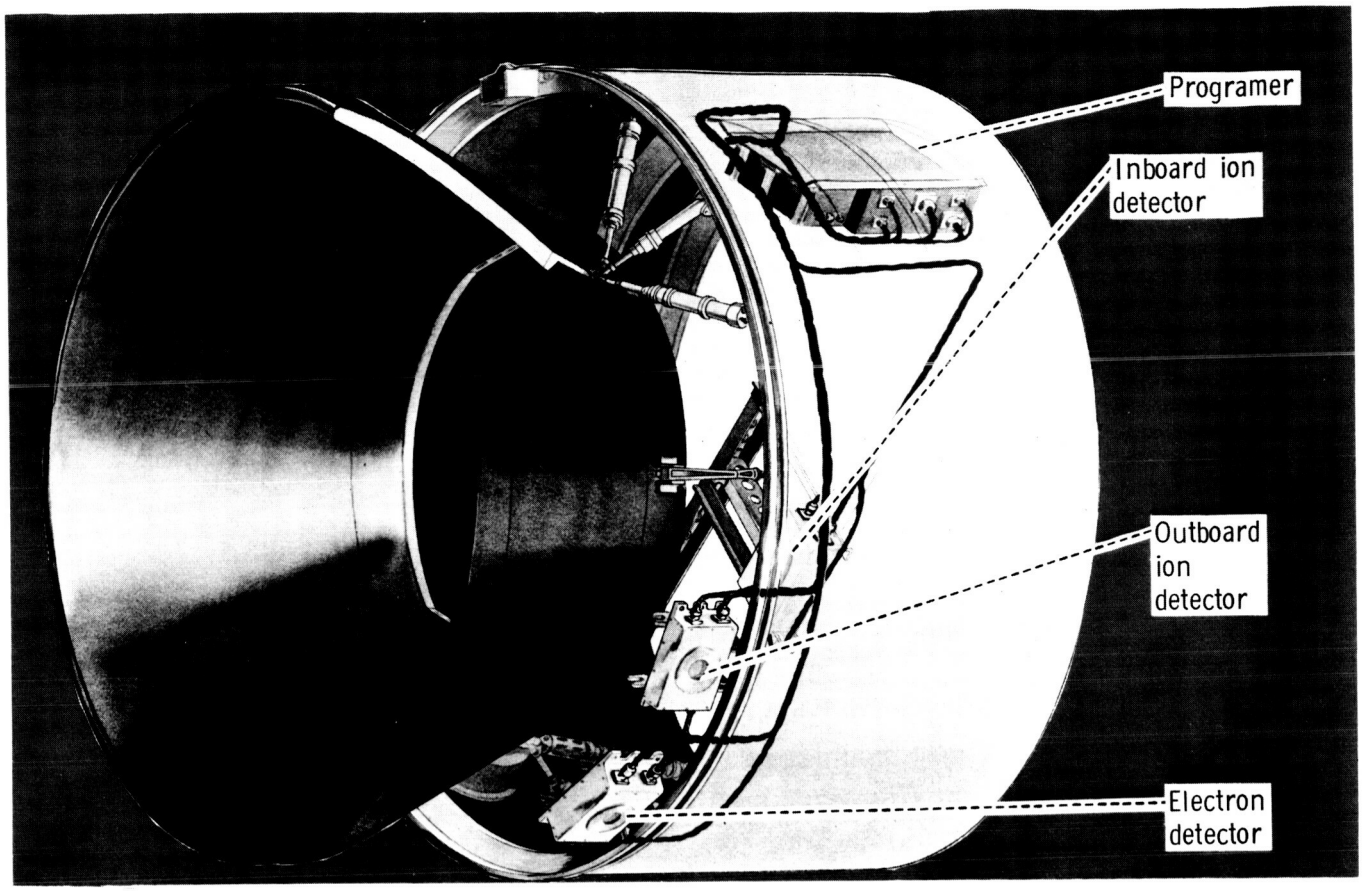

Figure 3. - The location of ion-wake-measurement equipment on the GATV.

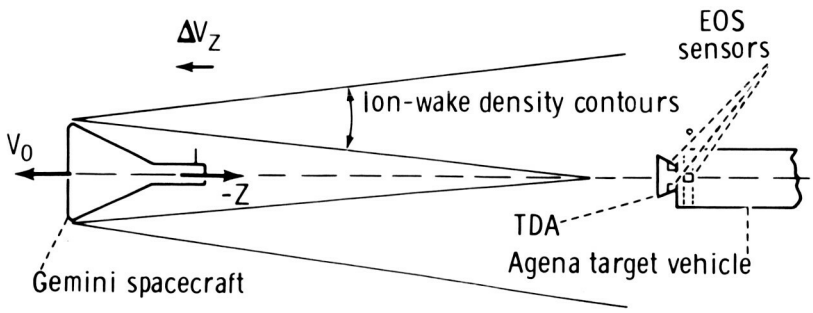

Figure 4. - The general ion-wake profile.

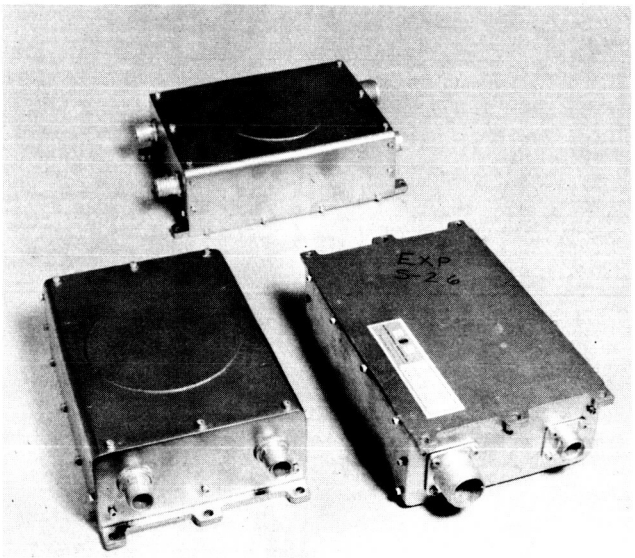

Figure 5. - An electron-sensor package.

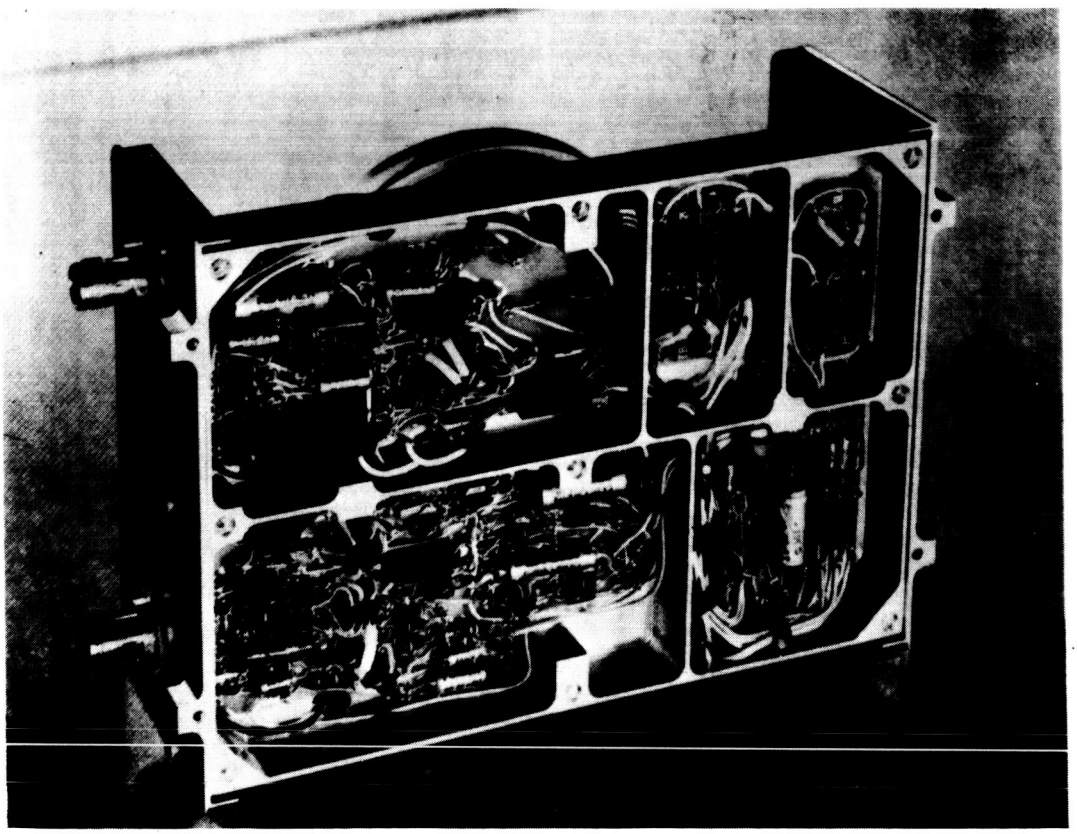

Figure 6. - The sensor circuitry.

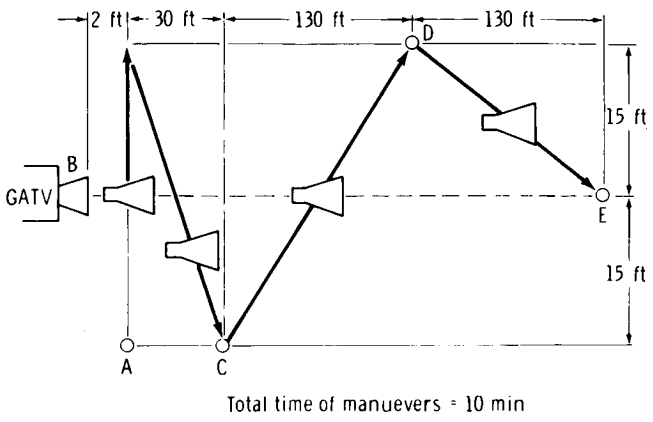

Figure 7. - Gemini X undocking manuever for ion-wake measurement.

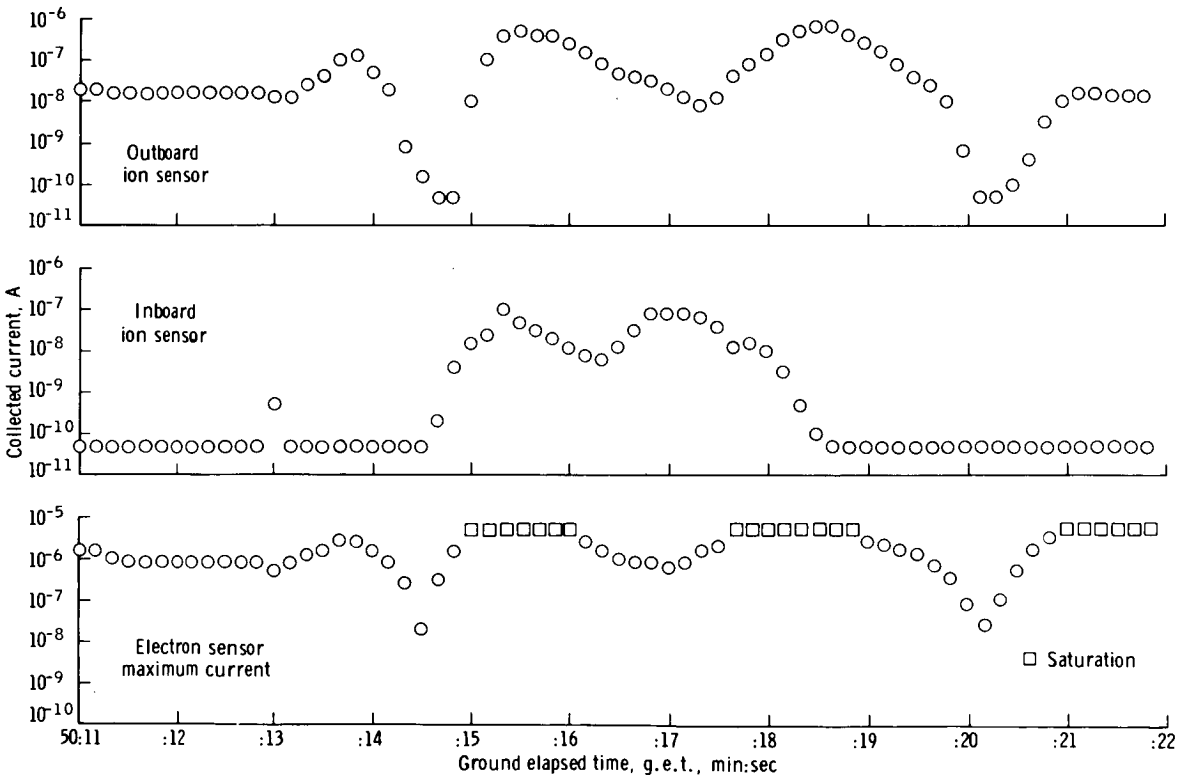

Figure 8. - Electron and ion-sensor current output during tethered flight at an altitude of 290 km.

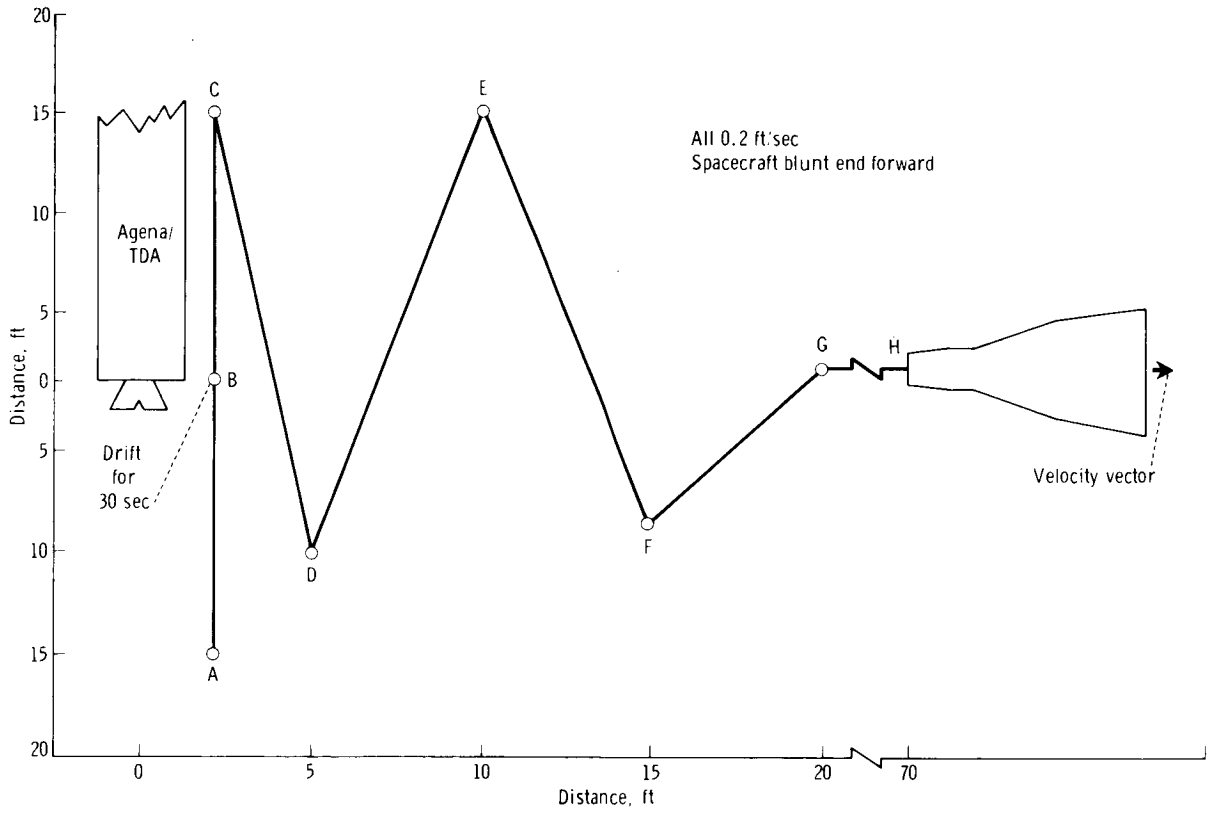

(a) Mode B/sequence 1; out of orbital plane, TDA pointing South from Agena.

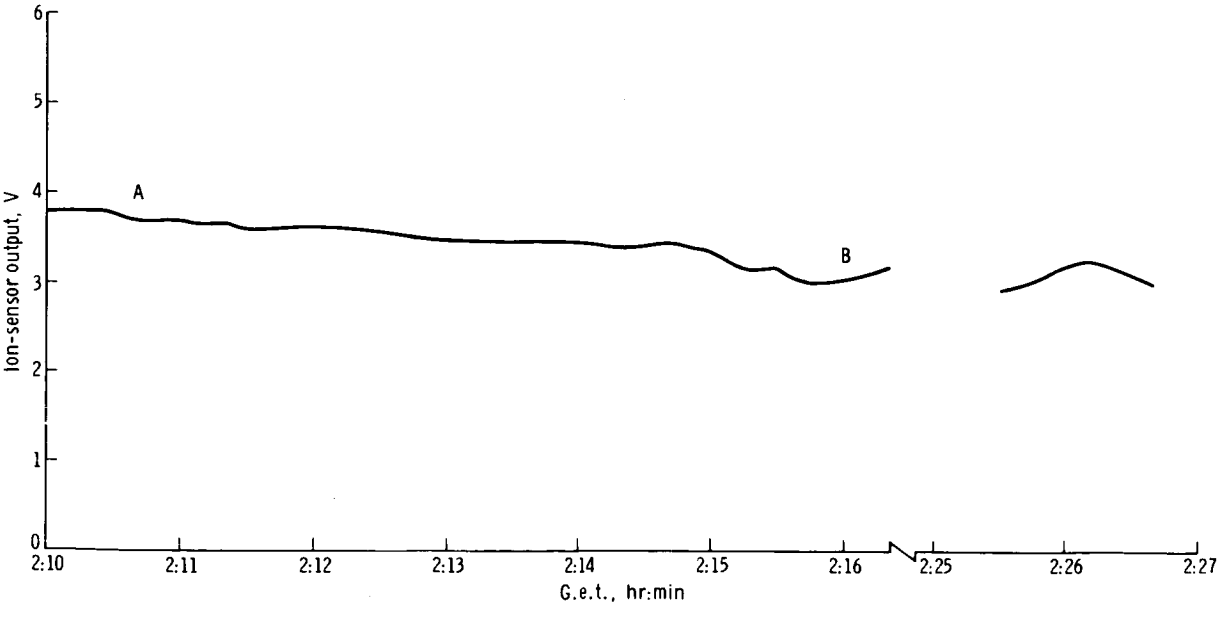

(b) Telemetry data.

Figure 9. - Ion-wake measurement during night out-of-orbital-plane manuever.

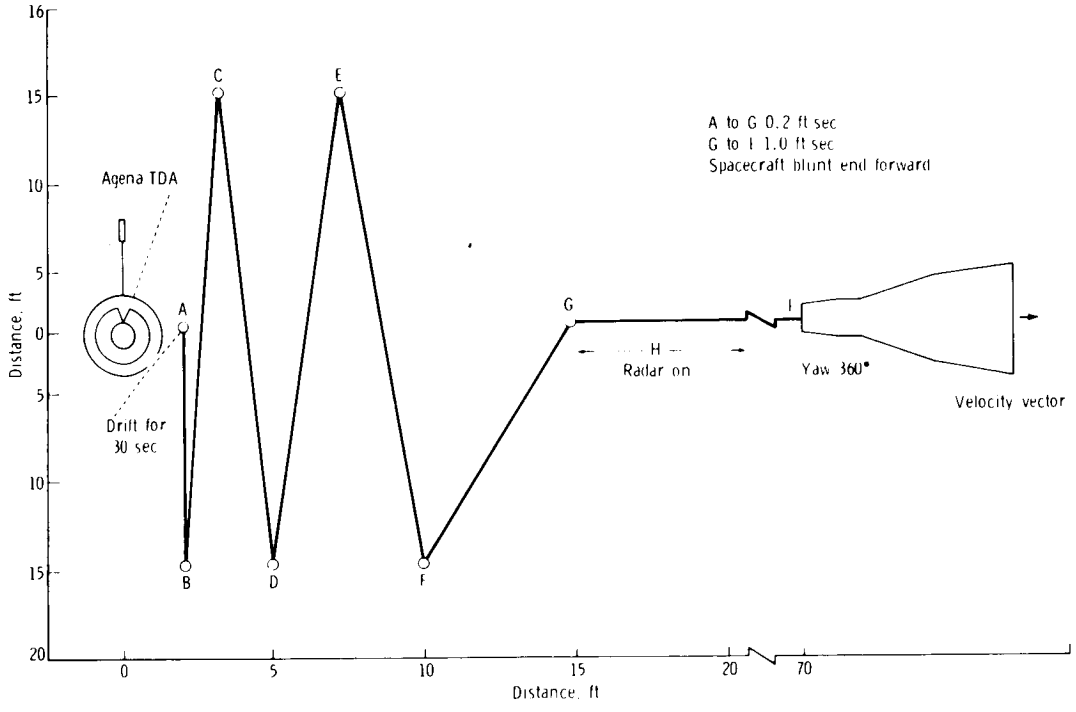

(a) Mode B/sequence 2; in orbital plane during darkness, TDA pointing south from Agena.

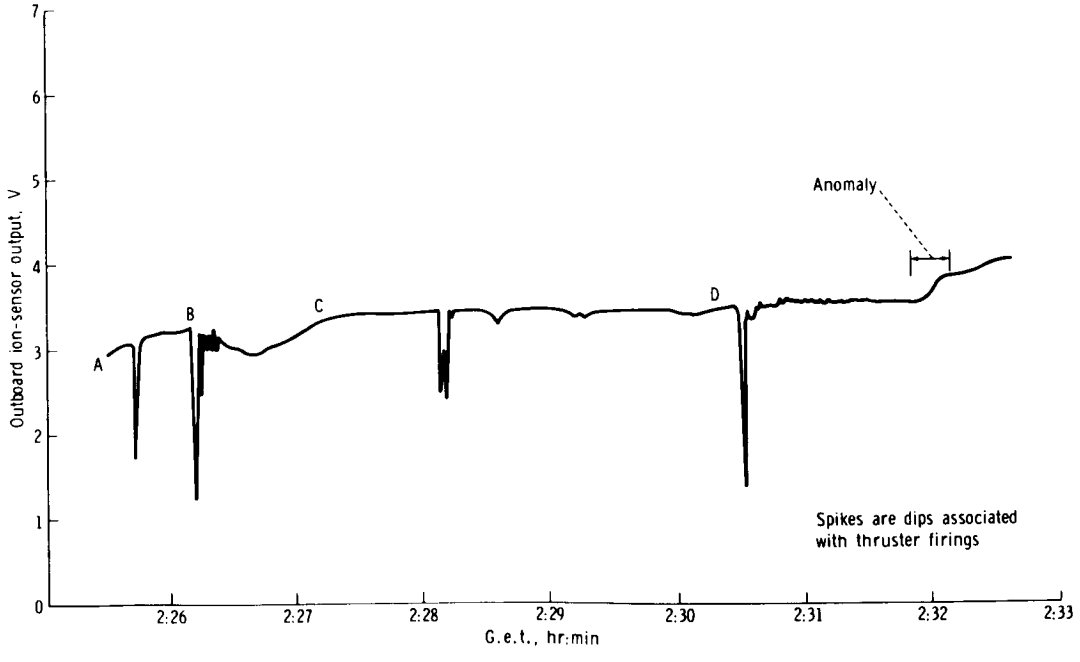

(b) Telemetry data.

Figure 10.- Ion-wake measurement during night in-orbital-plane maneuvers.

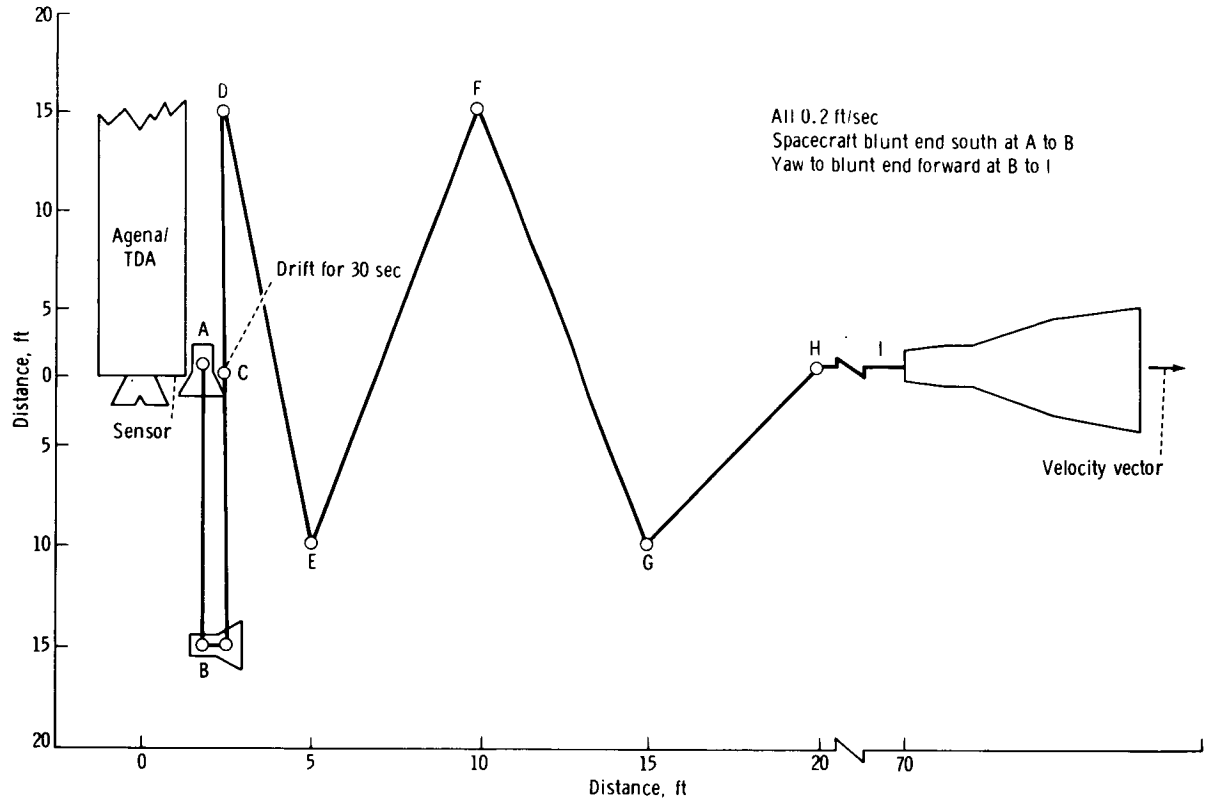

(a) Mode B/sequence 3; out of orbital plane, TDA pointing south from Agena.

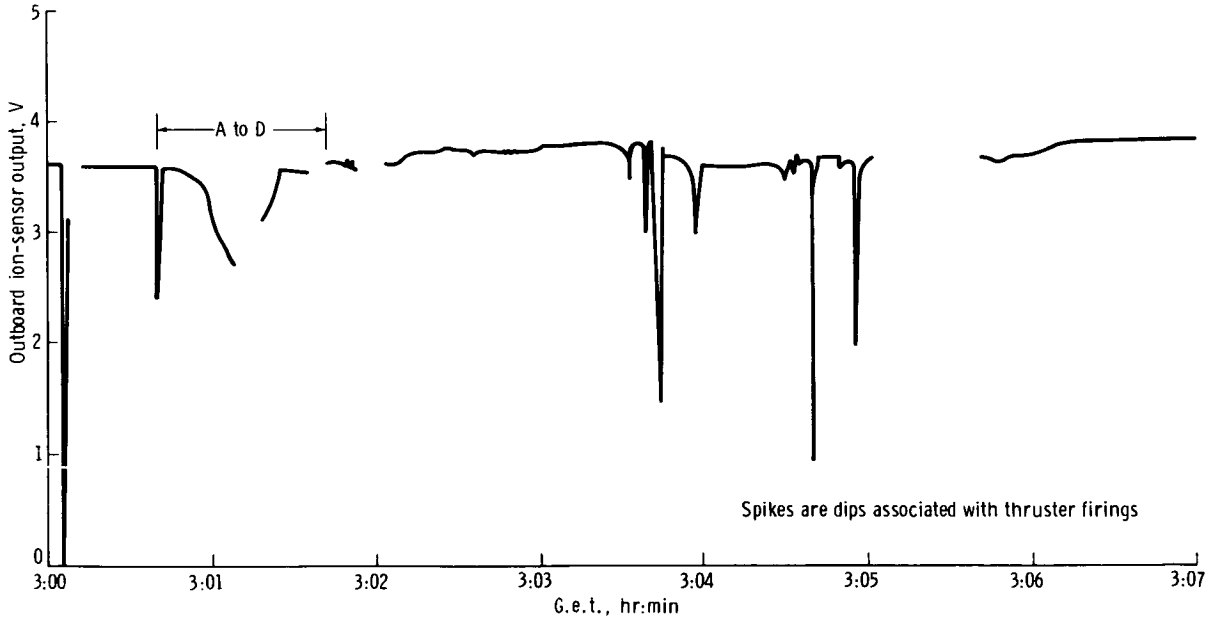

(b) Telemetry data.

Figure 11. - Ion-wake measurement during daylight out-of-orbital-plane maneuver.

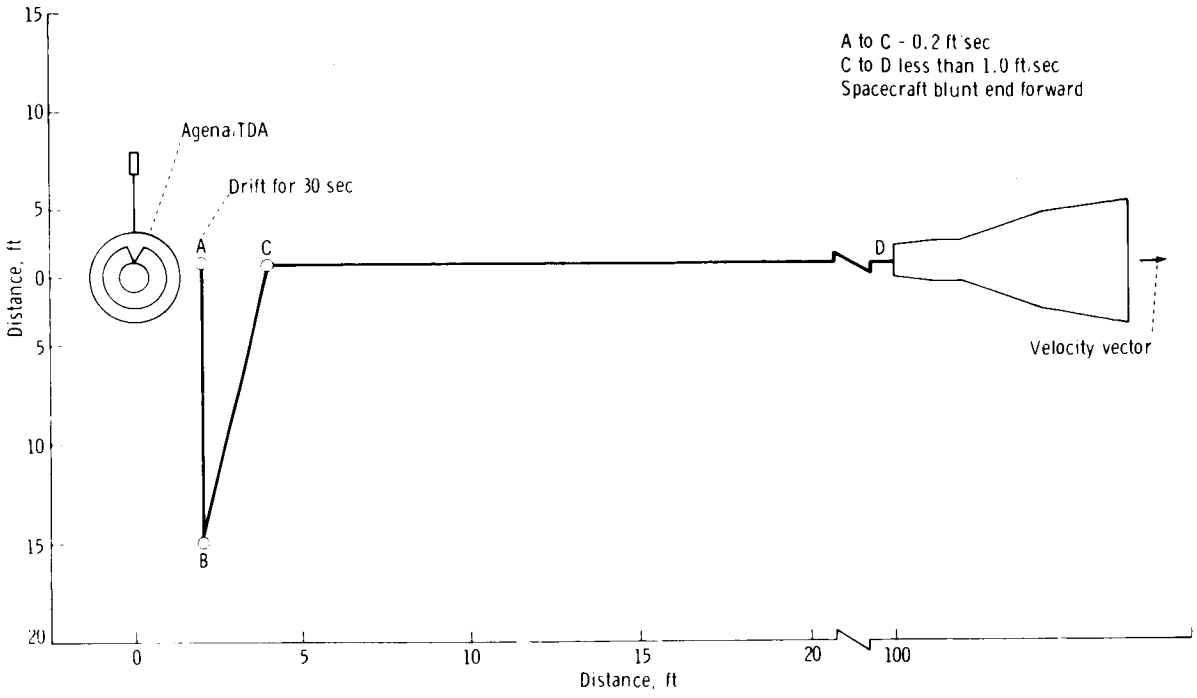

(a) Mode A; linear departure, TDA pointing south from Agena.

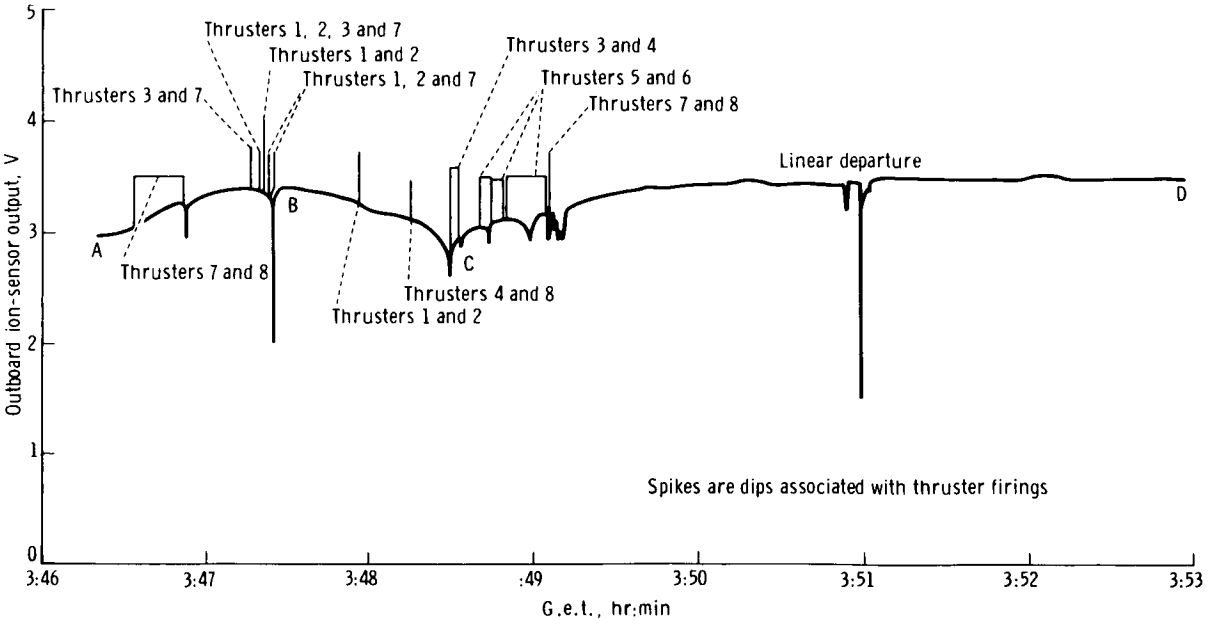

(b) Telemetry data.

Figure 12. - Ion-wake measurement during linear departure maneuver.

EXPERIMENT D010

ION-SENSING ATTITUDE CONTROL

By R. C. Sagalyn* and M. Smiddy*

OBJECTIVES

The principal objective of Experiment D010 was to investigate the feasibility of an attitude-control system that used environmental positive ions and an electrostatic detection system to measure spacecraft pitch and yaw. The secondary objective was to measure the spatial and temporal variations of ambient positively charged particles along the orbital path of the Gemini X and XII spacecraft.

THEORY

In the altitude range from 100 kilometers to 10 earth radii, positive ions and electrons, produced primarily by means of photoionization by the sun, exist in equal concentrations. The number density varies greatly in space and with time. For example, the charge density is a maximum, of the order of 10^6 particles/cm^3, in the vicinity of the F-ionosphere region (approximately 350 kilometers), and the charge density decreases to approximately 100 particles/cm^3 at approximately 10 earth radii. Also, there are great variations in the number densities on the dayside and nightside of the earth, in the vicinity of the geomagnetic equator, and in the lower ionosphere below approximately 1000 kilometers. Very rapid increases in ion and electron concentrations occur at sunrise because of photoionization and dissociation of the neutral-atmosphere constituents. More gradual decreases in density occur at local sunset when recombination and diffusion become important. This is illustrated in figure 1; the results are of positive ion measurements that were obtained by means of spherical electrostatic analyzers on a Discoverer satellite. The average energy of the charged particles varied from approximately 0. 01 eV at 100 kilometers to approximately 4. 0 eV at 10 earth radii. The kinetic temperature of the charged particles in the altitude range that was traversed by the Gemini spacecraft varied from approximately 250° K to approximately 3000° K. It has been demonstrated that charged particles in the upper

*U. S. Air Force Cambridge Research Laboratories, L. G. Hanscom Field, Bedford, Massachusetts.

atmosphere have an essentially Maxwellian velocity distribution. The average thermal velocity of the particles is given by the relation

$$v = \left(\frac{8kT}{\pi m}\right)^{1/2} \tag{1}$$

where k = Boltzmann constant

T = temperature, °K

m = mass, g

v = thermal velocity, cm/sec

By the use of representative values for the temperature and mass of the positive ions in equation (1), the positive-ion random thermal velocity is found to vary from 0.8 to 1 km/sec over the altitude range of the Gemini spacecraft orbit. The velocities of satellites orbiting in the upper ionosphere vary depending upon the nature of the orbit. Typical velocities vary from 7 to 11 km/sec. Therefore, the spacecraft velocity is approximately 10 times greater than the average thermal velocity of the positive ions. Relative to the spacecraft, positive ions possess negligible velocity. The situation is very different for electrons, because the average electron mass is approximately 10^4 times less than that of the positive ions. By the application of equation (1), the average electron velocity is found to be approximately 30 times greater than a spacecraft velocity. That positive ions may be considered stationary with respect to the spacecraft velocity is fundamental to the operation on the ion-sensing attitude control system.

EQUIPMENT

Gemini X Mission

The onboard equipment consisted of two independent systems that were used to measure pitch and yaw attitudes. Dimensionally and electrically, each system was identical except for placement of the sensor around the pitch and yaw axes. Each sensor configuration was mounted on a boom that was approximately 3 feet long. The boom was extended by crewmember command after spacecraft orbital insertion. The locations of the booms and sensors are shown in figure 2. The sensor locations and boom lengths used were selected to minimize vehicle shadowing and space charge effects.

The measurement of pitch is analyzed to illustrate the principle of operation of the sensor systems. Except for the alinement change, the analysis of the yaw

measurement is identical. By alinement of two sensors along the pitch axis, as shown in figure 3, the current to the collector of each sensor is given by the relation

$$i_1 = NevaA \cos (45 - \theta) \tag{2}$$

where i_1 is the current to sensor 1 and by the relation

$$i_2 = NevaA \cos (45 + \theta) \tag{3}$$

where i_2 = current to sensor 2

N = ambient positive ion density

e = electron charge

v = spacecraft velocity

a = experimentally determined grid transmission factor

A = aperture area of sensors 1 and 2 (identical)

θ = pitch-angle deviation from 0°

If equations (2) and (3) are solved for θ, then

$$\tan \theta = \frac{i_1 - i_2}{i_1 + i_2} \tag{4}$$

For $\theta \leq 20°$, $\tan \theta \approx \theta$ (in radians). Therefore, the output of the sensors may be displayed on a meter that is calibrated in degrees.

A block diagram for the pitch or yaw system is shown in figure 4. The output of each sensor was amplified by two electrometer amplifiers. To obtain the desired accuracy over the current range of 10^{-6} to 10^{-10} ampere, linear amplifiers that had range-switching capability were used. The outputs of the electrometers (V_1 and V_2) then were electronically added, subtracted, integrated, and compared. The final output $\tan \theta$, called the compared output, was indicated on a meter in the crewmember station and was transmitted by telemetry to the ground-based stations. For a complete evaluation of the experiment, the direct outputs of the electrometers, the range analog indication, and the calibrate monitor signal also were transmitted by spacecraft telemetry. These

outputs would not have been required in an operational attitude-control system. The experiment was designed for precise pitch and yaw angular measurements over the range of $\pm 20^{\circ}$; however, there was no basic limitation to the magnitude of the angle that could have been measured.

Sensor system characteristics for each of the two systems are given as follows.

Weight, including electronics and sensors, lb	7
Power at 28 V, W	3.5
Electronics response time, msec	<1
Dimensions, in.	11 by 6.5 by 6
Angular measurement range, deg	± 20

Gemini XII Mission

Two planar electrostatic analyzers, with a sensor configuration as indicated in figure 3, were used in this experiment. When the ratio of the satellite velocity to the random velocity of the ions was ≥ 2, and when grid and collector voltage was as indicated in figure 4, the current to the collector of a planar electrostatic analyzer was calculable by use of the relation

$$i = ANe|V|f(v)\alpha \tag{5}$$

where A = aperture area

N = charged particle density

e = particle charge

V = vehicular velocity

$f(v)$ = a function of the vehicle potential with respect to the undisturbed plasma

α = experimentally determined transmission factor for the grid electrodes

Under the experimental conditions that have been discussed, the ions were considered fixed and the magnitude of the velocity is given by

$$|V| = v_s \cos \theta \tag{6}$$

where v_s = spacecraft velocity

θ = angle between the direction of motion of the vehicle and the normal to the plane of the sensor

Then, equation (5) becomes

$$i = ANev_s(\cos\theta)f(v)\alpha \tag{7}$$

It was seen from equation (7) that the planar sensor current was highly dependent on its orientation with respect to the direction of motion. For example, for the yaw measurement, two identical sensors were alined at 45° with respect to the plane of zero yaw. An identical sensor system that was mounted symmetrically around the zero pitch plane was used for the measurement of pitch angles. These two independent systems were mounted on booms approximately 3 feet long, which were located in the aft section of the spacecraft. The booms were extended on command by a crewman at the appropriate time after orbital injection. The locations of the booms and sensors on the Gemini XII spacecraft are shown in figure 2. The location of the sensors and the boom lengths were set to minimize the influence of spacecraft wake, contamination, and space charge effects.

PROCEDURES

Gemini X Mission

Seven principal modes of operation were desired for the Gemini X mission; four operational modes were accomplished. These four modes are listed as follows.

1. Mode C, roll-attitude study: This procedure consisted of causing the spacecraft to roll through 720° at a rate of approximately 3° per second while the spacecraft pitch and yaw were held constant at zero.

2. Mode D, pitch-attitude study: This procedure consisted of the maintenance of a fixed yaw and roll attitude, then variation of the pitch angle through a specified angular range at a rate of approximately 0.1° per second. This particular rate was specified to ensure good comparison of the experiment results with data from the inertial guidance system. The rate of 0.1° per second was determined by the telemetry bandwidth that was available for the experiment.

3. Mode E, yaw-attitude study: This procedure consisted of maintenance of a fixed pitch and roll position, then variation of the yaw angle through a specified angular range at the rate of approximately 0.1° per second.

4. Mode G, random-data accumulation: The ion-sensor switch was left on in this mode while the spacecraft was in drifting flight.

The other three modes of operation were mode B (ambient-ion accumulation under controlled spacecraft conditions), mode F (the study of photoemission effects on the sensor), and mode H (the study of translation-thruster effects). These modes were not accomplished because of the real-time constraint that was placed on the use of spacecraft propellants.

Gemini XII Mission

Exclusive of mode A (equipment activation), six principal modes of operation were desired for the Gemini XII mission; four modes were accomplished. The six modes are as follows.

1. Mode B, roll-attitude study: This procedure consisted of rolling the spacecraft through 720° at a rate of approximately 3° per second while holding the spacecraft pitch and yaw constant at zero.

2. Mode C, pitch-attitude study: This procedure consisted of maintenance of a fixed yaw and roll attitude, then variation of the pitch angle through a specified angular range at a rate of approximately 0.1° per second. This particular rate was specified to ensure good comparison of the experiment results with data from the inertial guidance system. The rate of 0.1° per second was determined by the telemetry bandwidth available for the experiment.

3. Mode D, yaw-attitude study: This procedure consisted of maintenance of a fixed pitch and roll position, then variation of the yaw angle through a specified angular range of 0° to 360° at a rate of approximately 0.1° per second.

4. Mode E, photoemission effects and ambient-data accumulation: The equipment measured effects of the sun on the ion environment. The measurements were scheduled before, during, and after the sunrise phase of the vehicle orbit.

5. Mode F, random-data accumulation: The ion-sensor switch was left in this mode while the spacecraft was in drifting flight.

6. Mode G, translation-thruster effects: The spacecraft orbit attitude and maneuvering system (OAMS) thrusters were fired to facilitate observation of the degradative effects on the accuracy of the sensors.

CONCLUSIONS

Gemini X Mission

Discussions with the crewmembers at the experiment debriefing resulted in the acquisition of information on the operation of the experiment. These discussions resulted in the following conclusions.

1. In both mode D and mode E, the crewmen were able to compare the two flight-direction meters. One meter displayed the output of the inertial guidance system

and one meter displayed the experiment sensor output of pitch plus yaw. The results were indicative that the experiment sensors were consistent with the spacecraft flight director indicator.

2. The response of the experiment sensors to variations in pitch and yaw was extremely rapid.

3. When the spacecraft thrusters were firing, the experiment sensor indications went off-scale because of the charge variation on the vehicle or the contamination in the vicinity of the spacecraft. Readings returned to normal rapidly after thruster firing ceased.

4. The experiment operated for approximately 12 hours: 2 hours 15 minutes in mode A, 8 hours in mode G, approximately 1 hour in mode E, 35 minutes in mode D, and 15 minutes in mode C.

Both the postflight analysis of the transmitted data and the inflight comparison (made by the crewmen) of the ion-sensing system with the inertial guidance system proved that the absolute magnitude of the two systems was consistent with the measurement of pitch and yaw angles. The equipment response to variations in angular position was extremely rapid; the response was in the order of milliseconds.

An example of the simultaneous measurement of the ion-yaw-sensor output and the inertial yaw data that were collected during a controlled maneuver is shown in figure 5. The magnitudes of the angles at a given time were consistent within the experimental error of the systems. The inertial yaw measurement accuracy was approximately 2°. The ion-yaw accuracy for the Gemini spacecraft was $\pm 0.25^\circ$. The inertial data, given in figure 5, are illustrative of certain characteristics which introduced difficulties in the manual control of the spacecraft. When the yaw angle was varied, a lag of approximately 8 seconds in response time occurred. The steplike variations in yaw angle, giving jumps of the order of 1.5° in the inertial measurement, partly were because of the synchronous detectors that were used in the inertial guidance system; but also, this variation partly was because of the manner in which the data were digitized through the telemetry system. Therefore, the addition of an ion-yaw sensor alone would be a significant improvement in the attitude systems.

The inertial system required approximately 40 minutes to stabilize and warm up after power turn-on. This partly was because of the electronic circuits that were used and the adjustment of the gyroscopes on the unit. However, the crewmembers learned that the use of the ion-yaw angular measurements significantly decreased the time that was needed for platform alinement.

An example of the simultaneous measurement of pitch angles with the ion sensor and inertial systems is given in figure 6. It was noted that the absolute values of the angles were consistent within a fraction of a degree over the angular range of $\pm 20^\circ$. This figure is a good illustration of the response time of the two systems (between 66 hours 0 minutes and 66 hours 5 minutes). Although individual maxima and minima in pitch were consistent, the faster response of the ion sensor made it easier to detect angular changes. Operationally, this should be of particular importance in the conservation of thruster fuel and under conditions that necessitate very precise angular positioning.

Initially, the experiment was activated at 67:20:00 g.e.t. The experiment remained on for approximately 15 hours, of which 1 hour was in mode B, approximately 30 minutes in mode C, 30 minutes in mode D, 2 hours in mode E, 8 hours in mode F, and 1 hour in mode G.

The equipment operated properly throughout the activation period. Over the angular range for which the ion-attitude experiment was designed, both the pitch and yaw measurements on the Gemini XII spacecraft and the inertial guidance results were within the experimental error of both systems. The postflight analysis proved that the pitch-angle results were consistent within $\pm 0.5^\circ$. Comparison of yaw angles over the same angular range was indicative of an agreement within $\pm 1.5^\circ$. The inertial guidance system had ± 2 yaw accuracy.

An example of the simultaneous measurements of the ion-yaw-sensor output and the inertial yaw data during a controlled maneuver is shown in figure 7. The magnitudes of the angles at given times were consistent within the errors of the systems. The inertial yaw measurement accuracy for the Gemini spacecraft was approximately $\pm 2^\circ$, and the ion-yaw measurement accuracy was $\pm 0.25^\circ$. The inertial data illustrated characteristics which introduced difficulties in the manual control of the spacecraft. When the yaw angle was varied, a telemetry lag of approximately 8 seconds in the response time occurred; and the steplike variations caused jumps of 1.5°. The addition of an ion yaw sensor would be a significant improvement. Also, the fast response of the ion-attitude-sensing system will be of importance in conservation of thruster fuel when precise angular positioning is desired.

During controlled maneuvers on this mission, the ion-attitude sensors operated both in the forward and in the reverse direction. Therefore, ion-attitude measurements were obtained from 0° to 360°. It was anticipated that thruster (specifically numbers 14 and 16) firings might have affected the ion sensors adversely. These thrusters are fired either in the direction of the pitch or yaw sensors. Firings change the attitude of the vehicle; this was confirmed by the inertial results. The firings also changed the charge density for a period of 2 seconds. However, the density changes did not affect the angular measurement, and no deterioration of the ion sensors was observed.

An example of the variation of positive-ion density that was obtained during a complete spacecraft resolution is illustrated in figure 8. The large variations in charge density, from 10^3 to 10^6 particles/cm^3 on a given orbit, mainly were because of changes in photoionization on the nightside and dayside of the earth. Calculations of the charge densities from simultaneous outputs of the electrometers, by the use of either the inertial or the ion-attitude angles, were in agreement, a fact which was consistent with the experiment results on the Gemini X mission.

The dependence of ion angular measurements on latitude was determined from the postflight analysis of the experimental results. The geographic latitude range was approximately $\pm 30^\circ$. Any periodic variation in the difference between the inertial and ion-attitude ion measurements $\Delta\phi$ over this latitude range would have indicated variations in the mean ion-drift motions in the F-region along the spacecraft trajectory.

Only angular (pitch or yaw) measurements obtained over the range $\pm 20^\circ$ were selected for the analysis, and 5° intervals were used. The results are shown in figure 9; no significant dependence of $\Delta\phi$ on geographic latitude ($\pm 30^\circ$) was noted. The result implied a negligible influence of ion-drift motion on latitude over the geographic region that was investigated.

The results of Experiment D010 are proof that it is possible to measure pitch and yaw angles to within a fraction of a degree (based on results that were obtained during 45 hours of equipment operation). During this period, specific maneuvers were performed to determine the effects of photoemission currents, the effect of pitch and roll on yaw maneuver, the effect of yaw and roll on pitch maneuvers, and so forth. Also, the extent to which the crewmembers could control the motion of the spacecraft was demonstrated. The results proved that the firing of lateral thrusters directly into the sensors did not affect the operation for more than a fraction of a second. The response time of the ion-attitude-sensing system was much more rapid than was the response of the inertial guidance system (milliseconds compared with seconds).

Also, the results proved that the use of the ion-attitude-sensing system could considerably reduce the time required for special maneuvers, such as docking, photography, and entry. For example, during the Gemini XII mission the crewmen were able to reduce the time needed to aline the inertial platform from 40 minutes to approximately 5 minutes by the use of the ion pitch and yaw sensors as a reference. The yaw sensing part of the system is particularly valuable because no other instrument exists that can measure spacecraft yaw directly. One of the crewmen observed a transient in the ion-sensor indicator for a fraction of a second when certain thrusters were turned on. This could neither be detected in the real-time transmitted data nor in the tape-recorded playback. The latter data were played back at the rate of 1 bit per second. A transient could be caused by current surges or by ground loops in the electrical circuits (that resulted from varying spacecraft potential) or by transients in the power ground lines at the time of firing. Proper filtering could be introduced in future ion-attitude-sensing systems.

The results proved that the use of a horizon detector in conjunction with pitch and yaw sensors would facilitate complete description of the spacecraft position and attitude. Furthermore, with the addition of a servosystem, the unit could be used as a complete automatic attitude-control system that would be applicable from the lowest satellite altitudes up to at least 10 earth radii. Also, results established that the charge density along the trajectory of the satellite could be determined by transmission of output voltages from the individual electrometers. This could be very useful in the determination of phenomena that occur in manned or unmanned space flights. If a sweep voltage were periodically applied to the appropriate grids of the sensor, the spacecraft potential with respect to the undisturbed environment could be measured. Because spacecraft potential has been of interest in manned space flights, this type of measurement could be incorporated easily. The measurement of spacecraft potential is incorporated in unmanned satellite experiments in which the properties of thermal charged particles are studied. The experimental results also were proof that no significant systematic change existed in the ion-drift motion with latitude over the range of $\pm 30^\circ$. This demonstrated that for precise attitude determination, a mean ion-drift motion is not needed as a correction to the measurement.

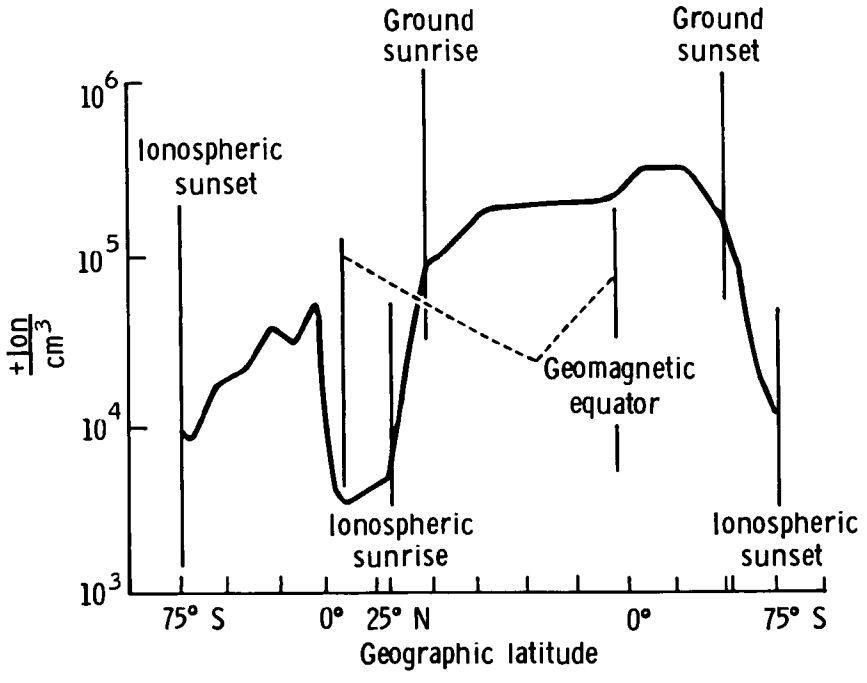

Figure 1.- The variation of positive ions in the F-region of the earth, measured during one revolution.

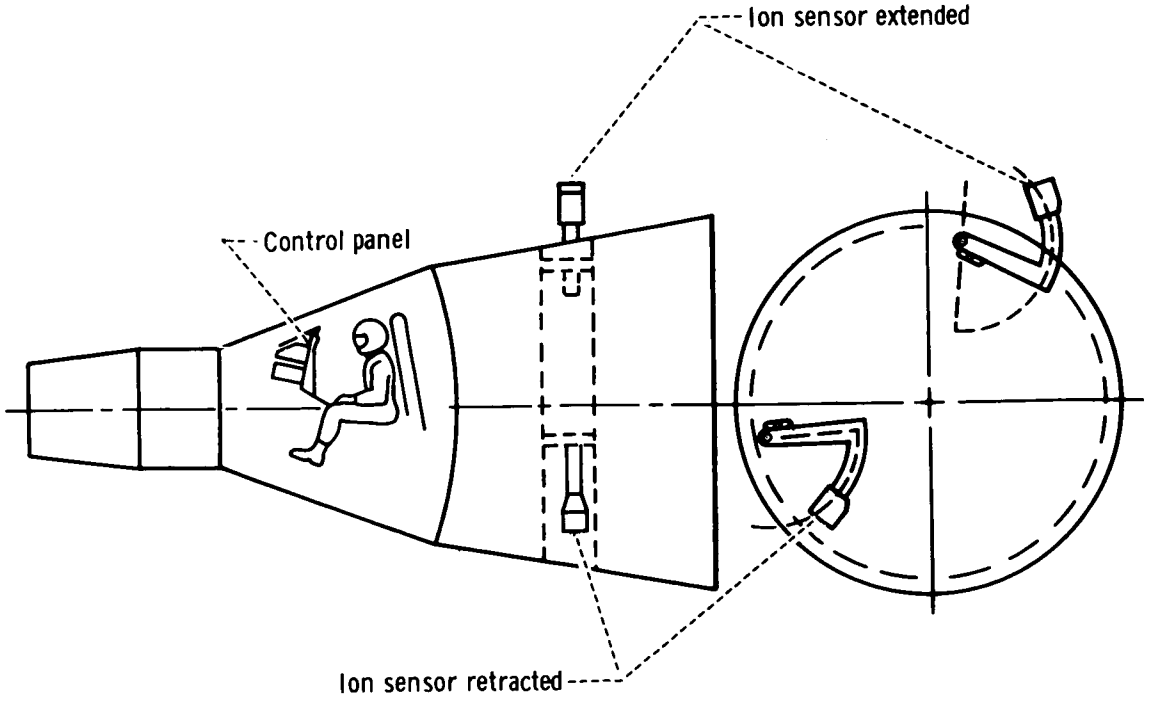

Figure 2.- The location of ion-sensing attitude-control equipment.

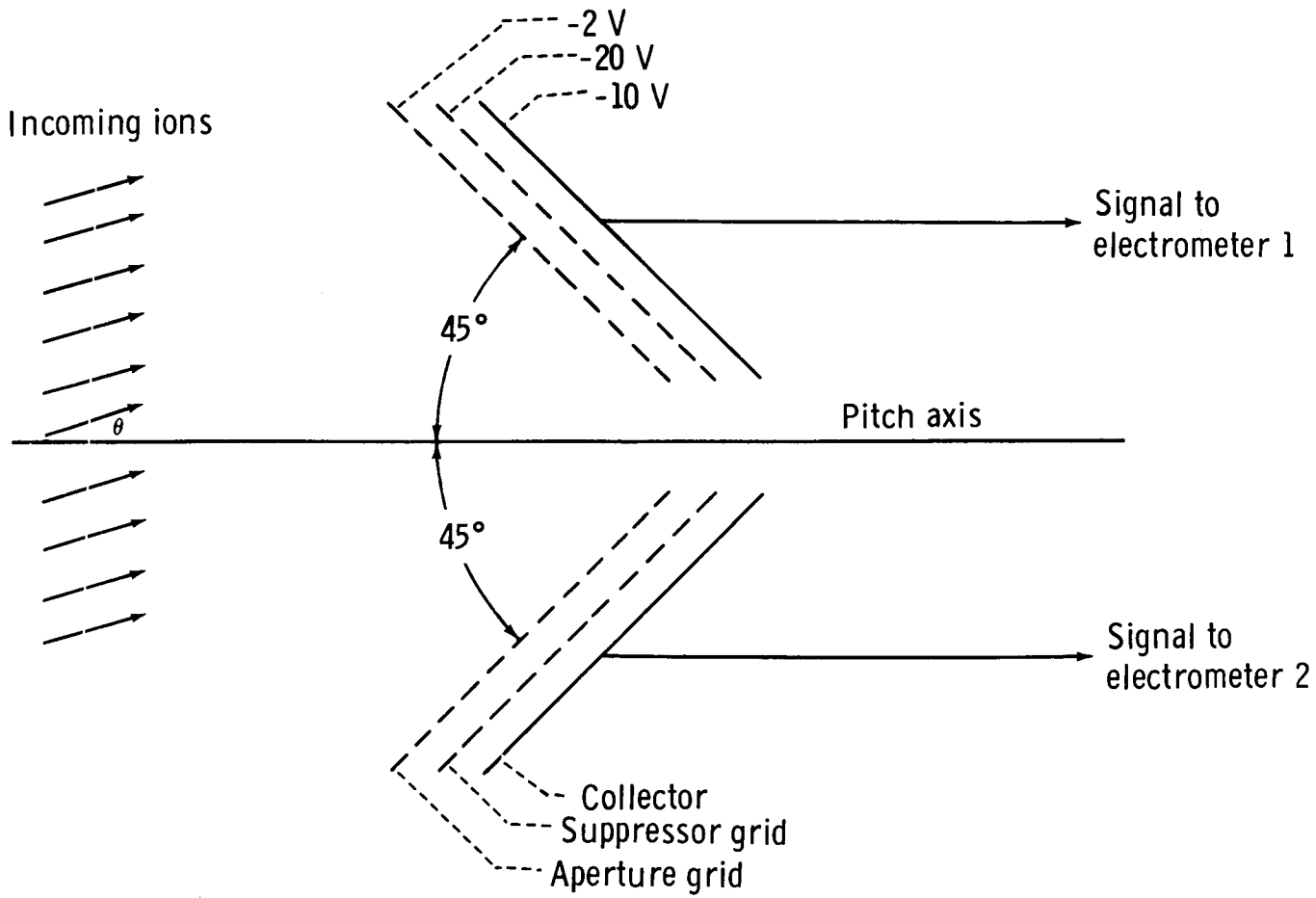

Figure 3. - The ion-sensing configuration.

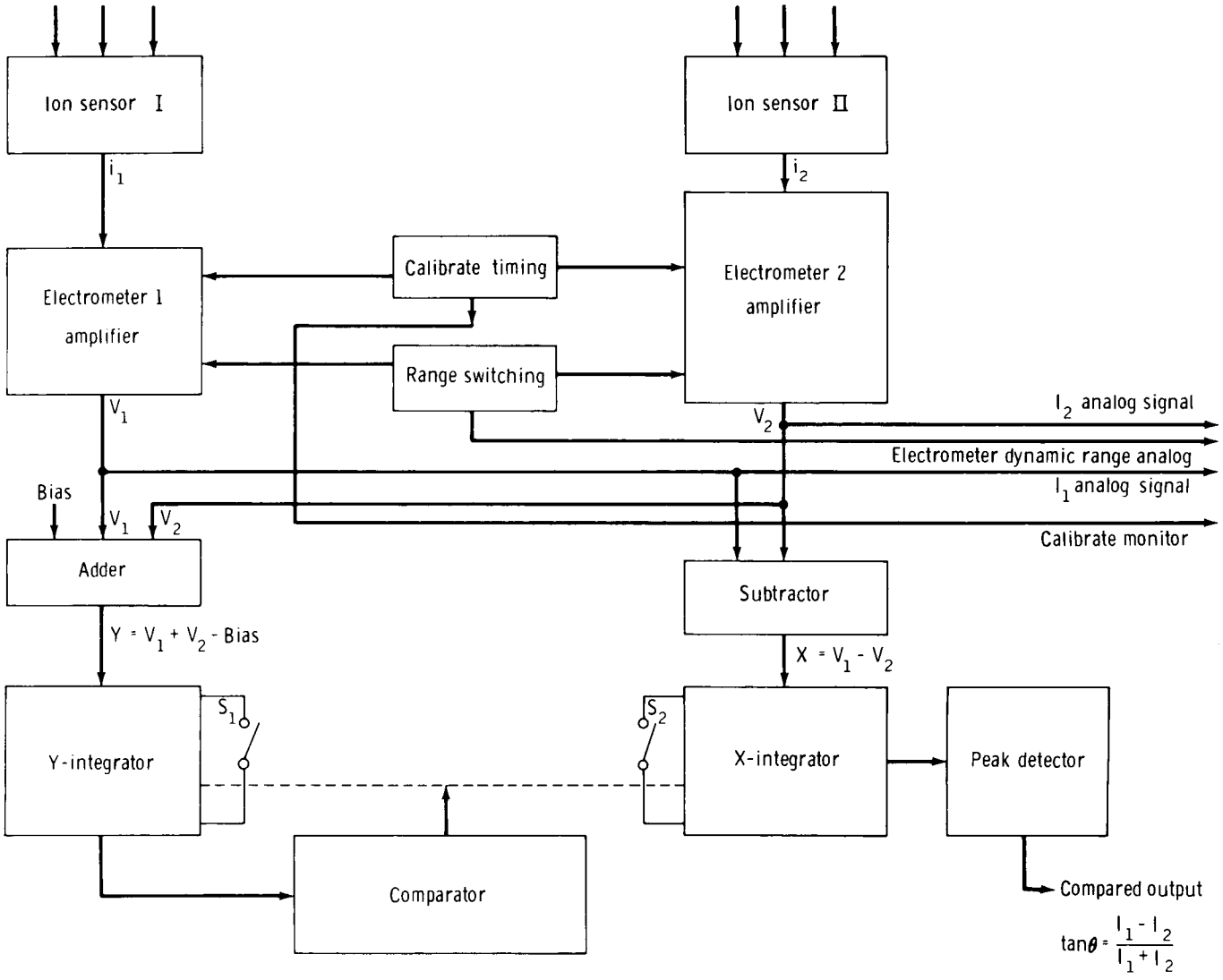

Note: $i_{1,2}$ = Ion-sensor current signals

$V_{1,2}$ = Ion-sensor voltage signals

Figure 4. - The ion-sensing attitude-control electronics system.

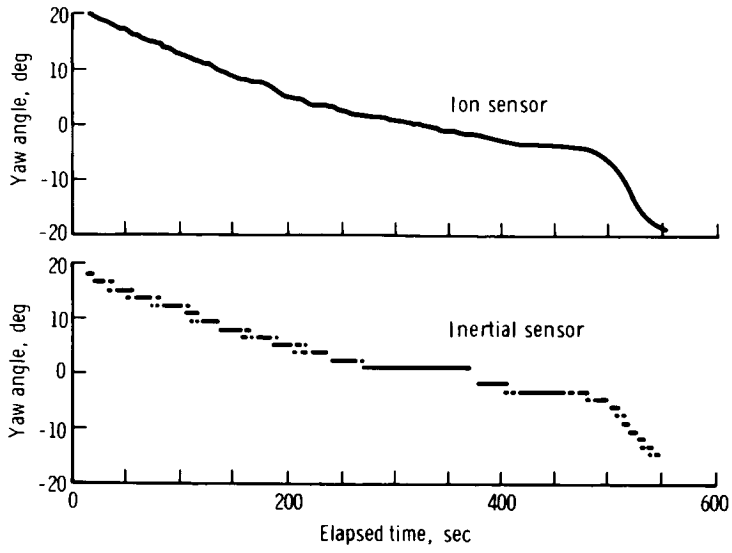

Figure 5. - A comparison of ion-attitude yaw-angle measurements with inertial-guidance-system data.

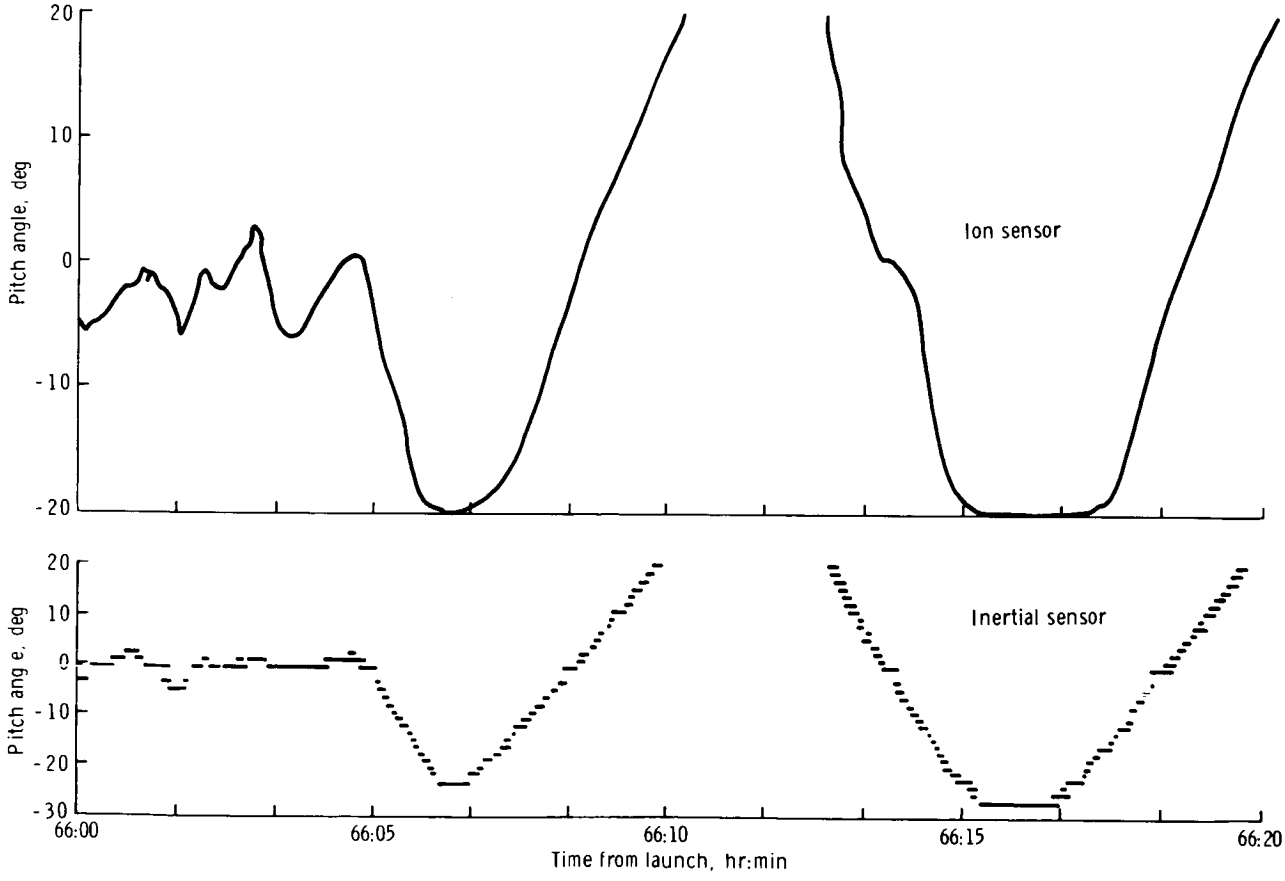

Figure 6. - A comparison of ion-attitude pitch-angle measurements with inertial-guidance-system data.

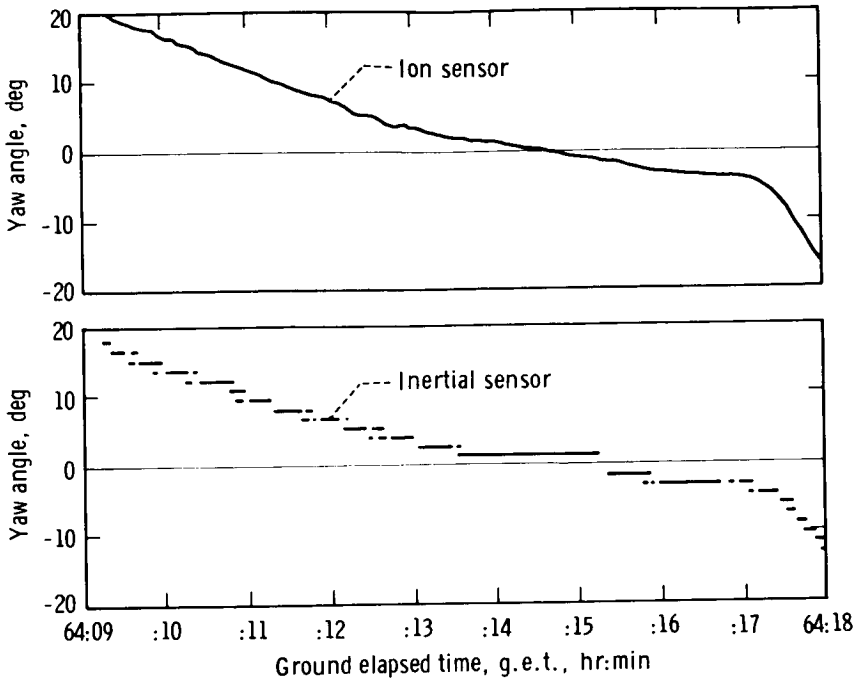

Figure 7. - A comparison of inertial-sensor data with ion-sensor data.

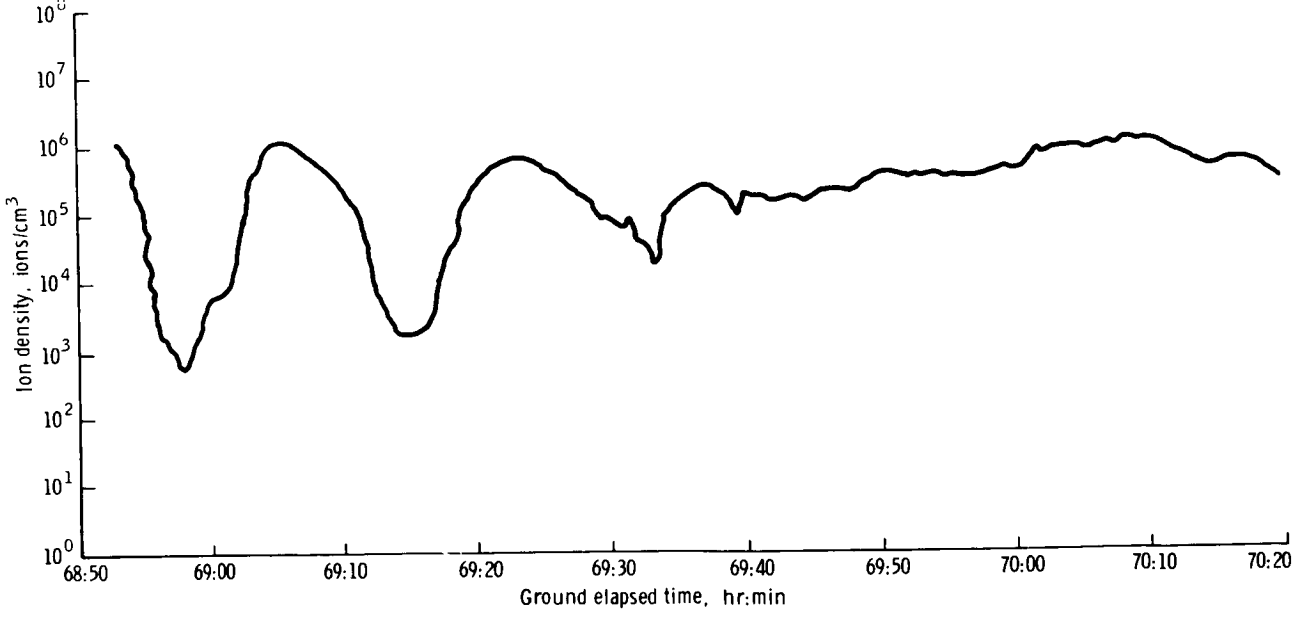

Figure 8. - Ion density plotted as a function of time for one revolution of the Gemini XII spacecraft.

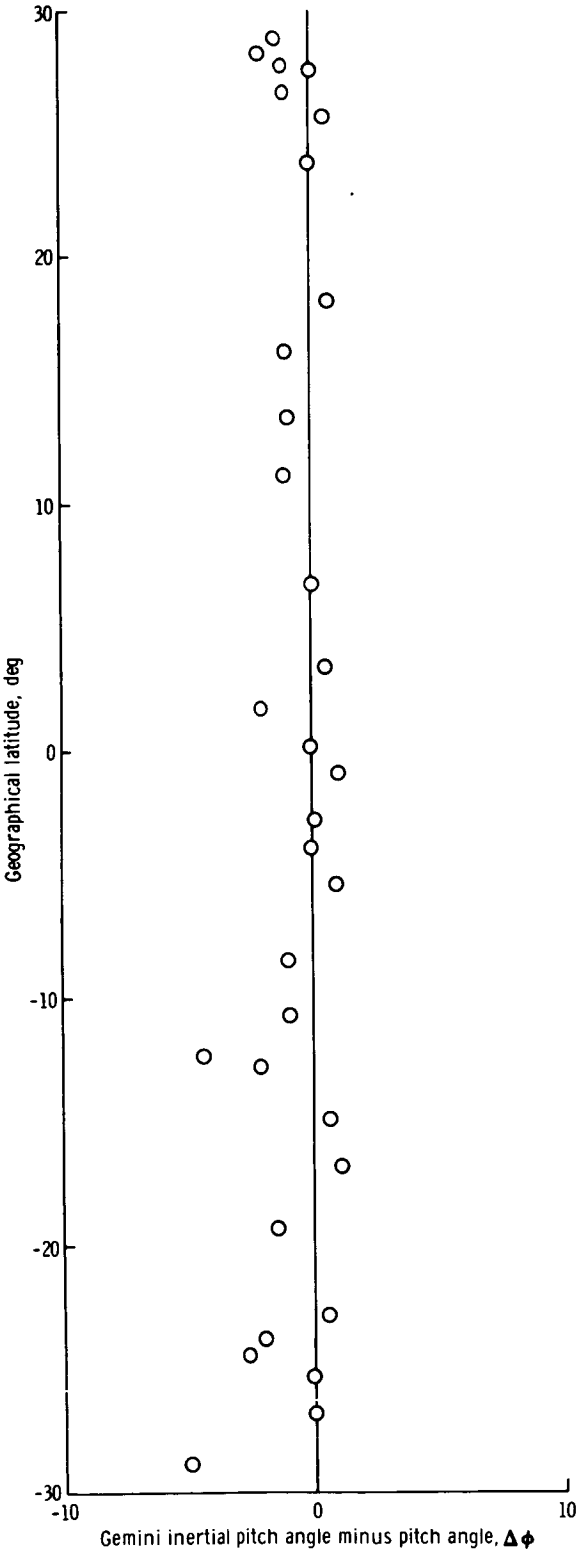

Figure 9. - The geographic latitude compared with $\Delta\phi$.

EXPERIMENT S009

NUCLEAR EMULSION

By F. W. O'Dell,* M. M. Shapiro,* R. Silberberg,* B. Stiller,* C. H. Tsao,* N. Durgaprasad,** C. E. Fichtel,** D. E. Guss,** and D. V. Reames**

INTRODUCTION

Experiment S009 represents the first exposure on a spacecraft of a nuclear-emulsion apparatus designed to collect 1000 high-quality tracks of heavy nuclei under a negligible thickness of matter (0.07 g/cm^2). Experiment S009, which was flown on the Gemini VIII (terminated early) and XI missions, was designed for the exploration of cosmic radiation incident upon the atmosphere of the earth by the use of a nuclear-emulsion stack under a negligible thickness of protective material. Cosmic rays consist of atomic nuclei that move at almost the speed of light; these nuclei are a means for investigating remote regions of the Milky Way where high-energy processes are occurring. In particular, there is considerable interest in the study of those components of the primary radiation that are nuclei heavier than hydrogen and helium. By comparing the abundance ratio of the group ($3 \leq Z \leq 5$) relative to another ($6 \leq Z \leq 9$), one can deduce the amount of interstellar material (mostly hydrogen) that cosmic rays have passed through. This quantity is 4 g/cm^2 (which is equivalent to 25 inches of liquid hydrogen). Furthermore, one can then deduce the primordial composition of cosmic rays, that is, the composition at the cosmic-ray source regions. In turn, this reflects the nuclear reactions that have taken place in cosmic ray sources (that is, the processes that resulted in fusing together lighter nuclei before their acceleration to cosmic-ray energies). Hence, cosmic-ray studies are pertinent to theories of nucleosynthesis and stellar evolution.

The cosmic-ray detector consisted of a stack of nuclear-research emulsions that were designed to register at least 400 heavy-nuclei tracks (the minimum acceptance number) for each 10 hours of useful exposure. The spacecraft had to be oriented in a heads-up attitude during the 10-hour period to eliminate atmospheric albedo particles.

*U. S. Naval Research Laboratory, Washington, D. C.
**NASA Goddard Space Flight Center, Greenbelt, Maryland.

EQUIPMENT

The equipment, shown in figure 1, consisted of a rectangular package 8.5 by 6 by 3 inches that weighed 13 pounds when loaded with approximately 1 liter of emulsion. An electrical connector on the bottom face of the package conducted power to and telemetry information from the package. The top face of the package had a 250-micron aluminum window for exposure of the emulsion to ambient radiation outside the spacecraft. The package was housed in a temperature-controlled well that was located directly behind the pilot-side hatch in the retrograde adapter section of the spacecraft. During launch, protection was provided by a hinged cover that was opened 190° at the time of launch vehicle-spacecraft separation. The package was equipped with a deployable handle for removal and placement inside the spacecraft after retrieval by the pilot.

Each of the two sections of the emulsion stack contained 92 sheets of 600-micron-thick nuclear emulsion that consists of silver bromide crystals embedded in gelatin. The plane of the emulsion sheets was in the plane of the picture (fig. 1). During the flight, when initiated by a switch, the lower section moved in steps of 25 microns per minute with respect to the upper section. The purpose of this movement was to obtain time resolution for particles that entered the detector through the collection face. By matching segments of the same track in the two sections, it was possible to determine the relative position that the sections had at the time the track was registered, and to determine thereby the time of particle entry.

The moving mechanism was below the emulsion stack and consisted of a 60-second timer, a gear-head motor, and a drive assembly. A high-resolution potentiometer, attached to the drive assembly, supplied a signal that was indicative of the amount of stack movement. Also, a bilevel-voltage signal, which indicated motor actuations, and a signal from a temperature sensor were read out. Telemetry information consisted of the following items.

1. A signal from the potentiometer that was indicative of the distance traveled by the lower stack

2. A bilevel-voltage signal that was indicative of motor actuation

3. The temperature of the experiment housing

PROCEDURES

The experiment package was installed in the spacecraft approximately 55 hours before launch. At 01: 42: 20 g. e. t., the experiment was activated by the pilot. Proper operation of the experiment was verified by telemetry at 04: 30: 00 g. e. t. The experiment operated satisfactorily until the package was recovered by the pilot during the first extravehicular activity at approximately 24: 05: 00 g. e. t. Then the package was stowed inside the cabin by the command pilot and it remained there for the remainder

of the mission. A spacecraft heads-up (within $\pm 15°$) attitude during the exposure period was a part of the flight plan, except during South Atlantic anomaly passes when a blunt-end-forward spacecraft configuration was specified.

RESULTS

The distribution of arrival times for the heavy primary nuclei are shown in figure 2. The peak on the right represents heavy nuclei that entered the detector during the last 2 days of the mission, when the package was inside the spacecraft cabin. The small peak to the left represents particles that were recorded early in the flight, before the stack movement was actuated. A time resolution of 5 minutes was achieved. Out of this sample of tracks, approximately 630 nuclei of charge 4 and greater had arrival times within the 22-hour period of useful exposure. Nuclei of charge 3 have not been included in this analysis because of the low detection efficiency for tracks at this ionization level in the relatively high background accumulated on the plates during the 3-day mission. To minimize the background effect of Van Allen particles accumulated on passages through the South Atlantic anomaly region, the attitude of the spacecraft was maintained so that the collection face of the detector was approximately normal to the direction of the magnetic field lines in the region. Thus, trapped particles produced tracks approximately at right angles to the tracks of the primary nuclei in the plates.

The methods that were used to determine nuclear charge are shown in figure 3. The lower stack contained emulsions of three different sensitivities, K. 5, K. 2, and G. 0. Charge estimates were based on delta-ray counting in K. 5 emulsions and on grain counting in the K. 2 and G. 0 emulsions. In the graph on the left in figure 3, the charge determined by delta-ray counting in K. 5 emulsion is plotted along the ordinate, and the charge from grain counting in G. 0 emulsion is plotted along the abscissa. In the upper right is a similar plot that contains delta-ray density in K. 5 compared with grain counting in K. 2. On the lower right is a plot of grain counts in K. 2 compared with G. 0. The final charge assigned to each particle was a weighted average of all the measurements made on the track.

The charge spectrum obtained by the use of 630 tracks is shown in figures 4 and 5. It is evident that good resolution between charges in the L ($3 \leq Z \leq 5$) and M ($6 \leq Z \leq 9$) groups is possible despite the fairly heavy background of electron and proton tracks. Also, peaks occur for higher charges. It is evident that the abundance of nitrogen is very low relative to carbon and oxygen; this fact is consistent with other results.

In table I, the results are summarized and are compared with averages of five sets of published results obtained on balloon flights (ref. 1) at a geomagnetic latitude of 41°. The Gemini XI orbits ranged between +28° and -28° geographic latitude. Measurements and extrapolated results obtained higher in the atmosphere on balloon flights of very high altitude are consistent with Experiment S009 data. There is an indication that secondary production of light nuclei in the atmosphere is not fully explained, because the L/M ratio of 0. 39 is much greater for the balloon flights at matter thicknesses greater than 6 g/cm^2.

A more detailed study of the relative abundances of elements is presented in figure 6. Here, the data are compared with those obtained at a lower energy (ref. 2) on the OGO-I satellite.

CONCLUSIONS

The results are as follows.

1. A definite odd-even effect, with low abundances for elements of atomic number 7, 9, and 11 — compared with abundances of the neighboring elements with even Z (for example, the ratio $N/C \approx 1/4$, $F/C < 0.03$, and $Na/C < 0.03$)

2. A ratio $O/C \approx 0.9$

3. Ne/C, Mg/C, and Si/C ratios between 0.2 and 0.3 (these ratios are somewhat higher than values deduced by extrapolation from observations at balloon altitudes, but only by approximately one standard deviation)

4. An abundance gap in the region $15 \leq Z \leq 19$ (the ratio of this ensemble relative to carbon is about 0.1)

5. A ratio $(20 \leq Z \leq 28)/C = 0.2$, with a large concentration at $Z = 26$

These results are indicative that successful exposures of nuclear-research emulsions were obtained on the Gemini XI mission.

REFERENCES

1. Judek, B.; and Van Heerden, I. J.: The Charge Spectrum and Interactions of Relativistic Heavy Nuclei in the Primary Cosmic Radiation. Can. J. Phys., vol. 44, 1966, p. 1121.

2. Comstock, G. M.; Fan, C. Y.; and Simpson, J. A.: Energy Spectra and Abundances of the Cosmic-Ray Nuclei Helium to Iron from the OGO-I Satellite Experiment. Astrophys. J., vol. 155, 1969, p. 609.

TABLE I. - CHARGE SPECTRUM AT TOP OF ATMOSPHERE

Charge, Z	Gemini XI data, percent	Average of published data from balloon flights, percent	
		Thickness <3 g/cm^2	Thickness ≥ 6 g/cm^2
L	13.4 ± 2	14.1	21.8
M	59.3 ± 4	62.7	55.4
H	27.3 ± 3	23.6	22.6
L/M	0.23 ± 0.03	0.22	0.39
L/S	0.155 ± 0.02	0.16	0.28

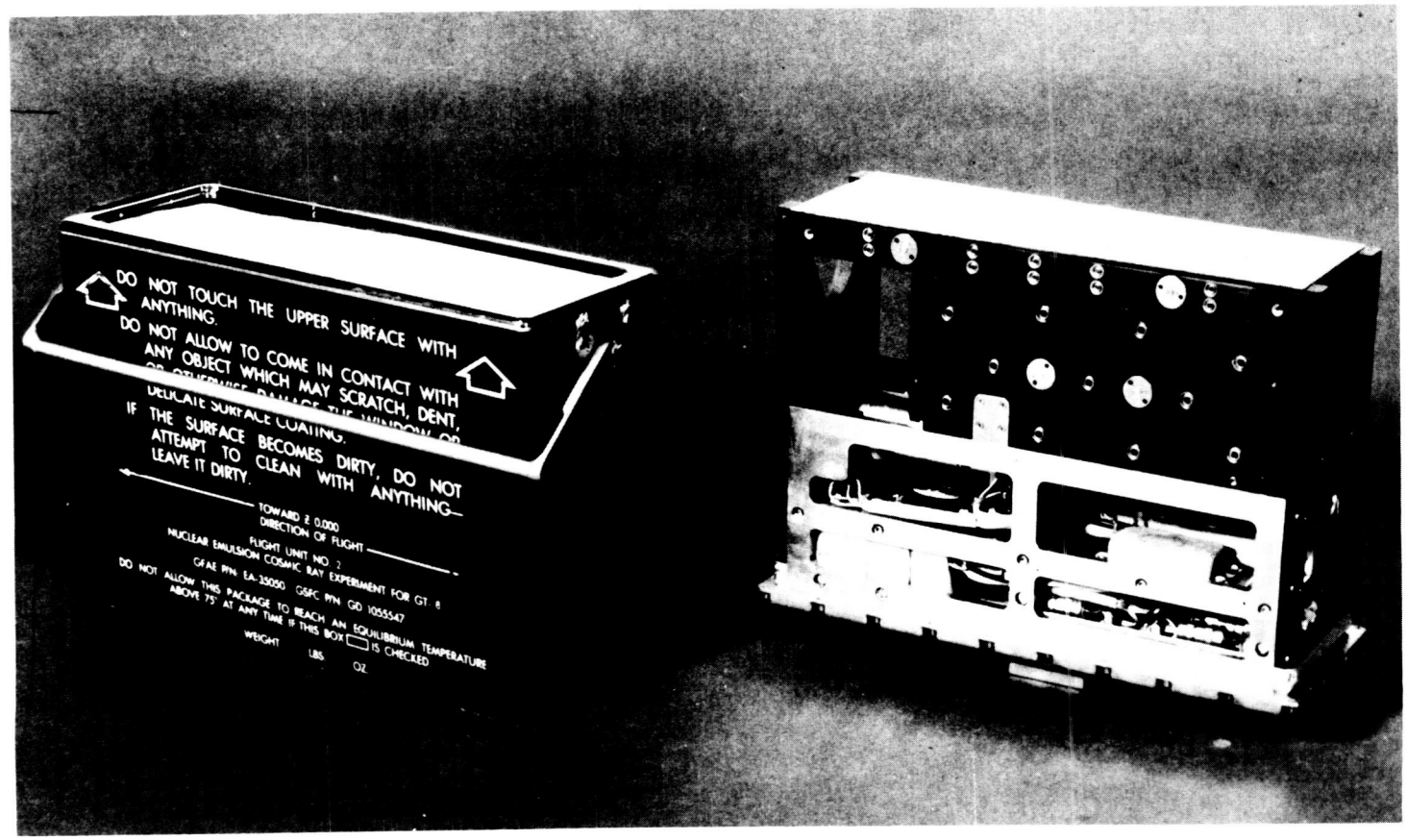

Figure 1. - Experimental hardware after recovery from Gemini XI.

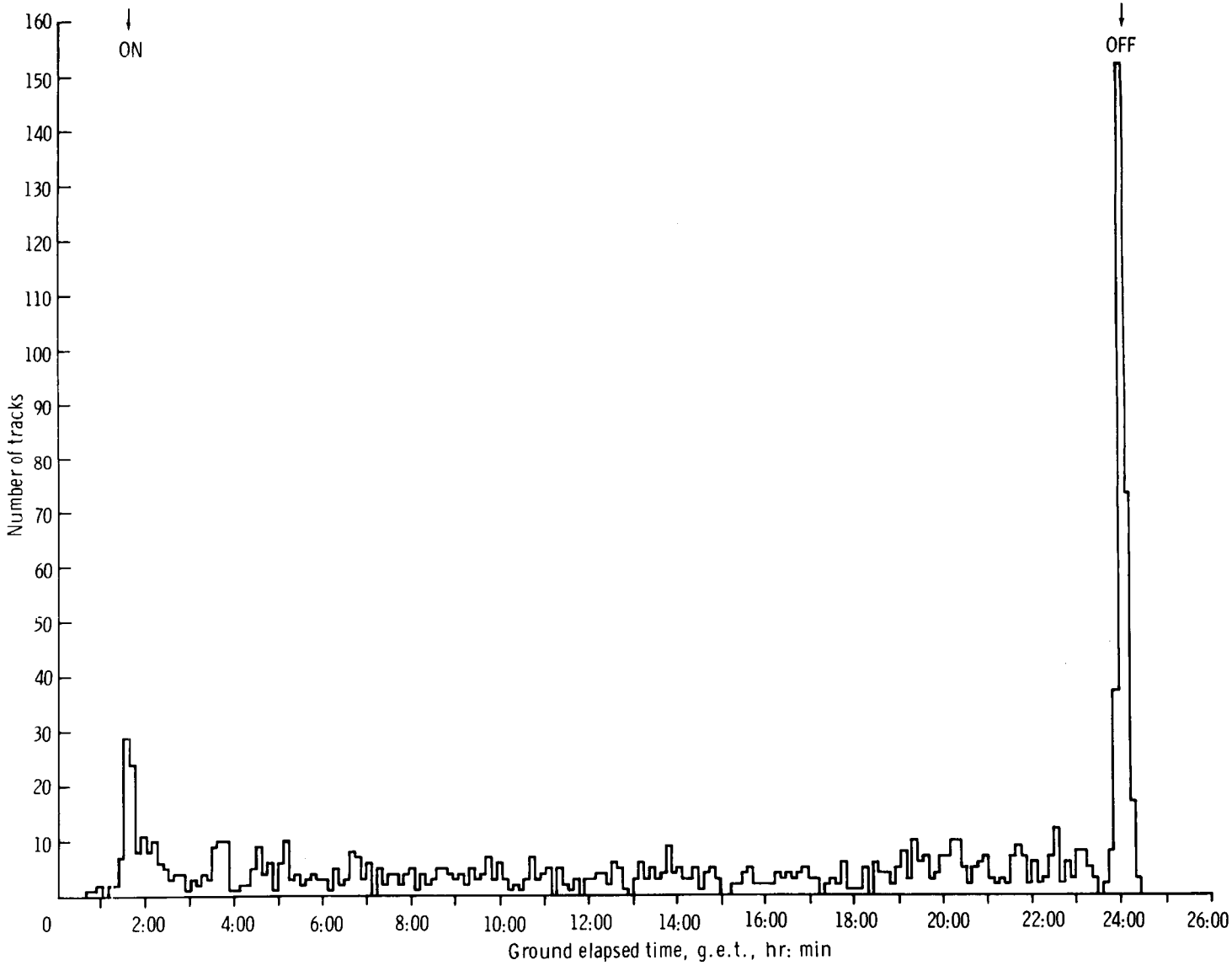

Figure 2. - Distribution of heavy primary nuclei arrival times.

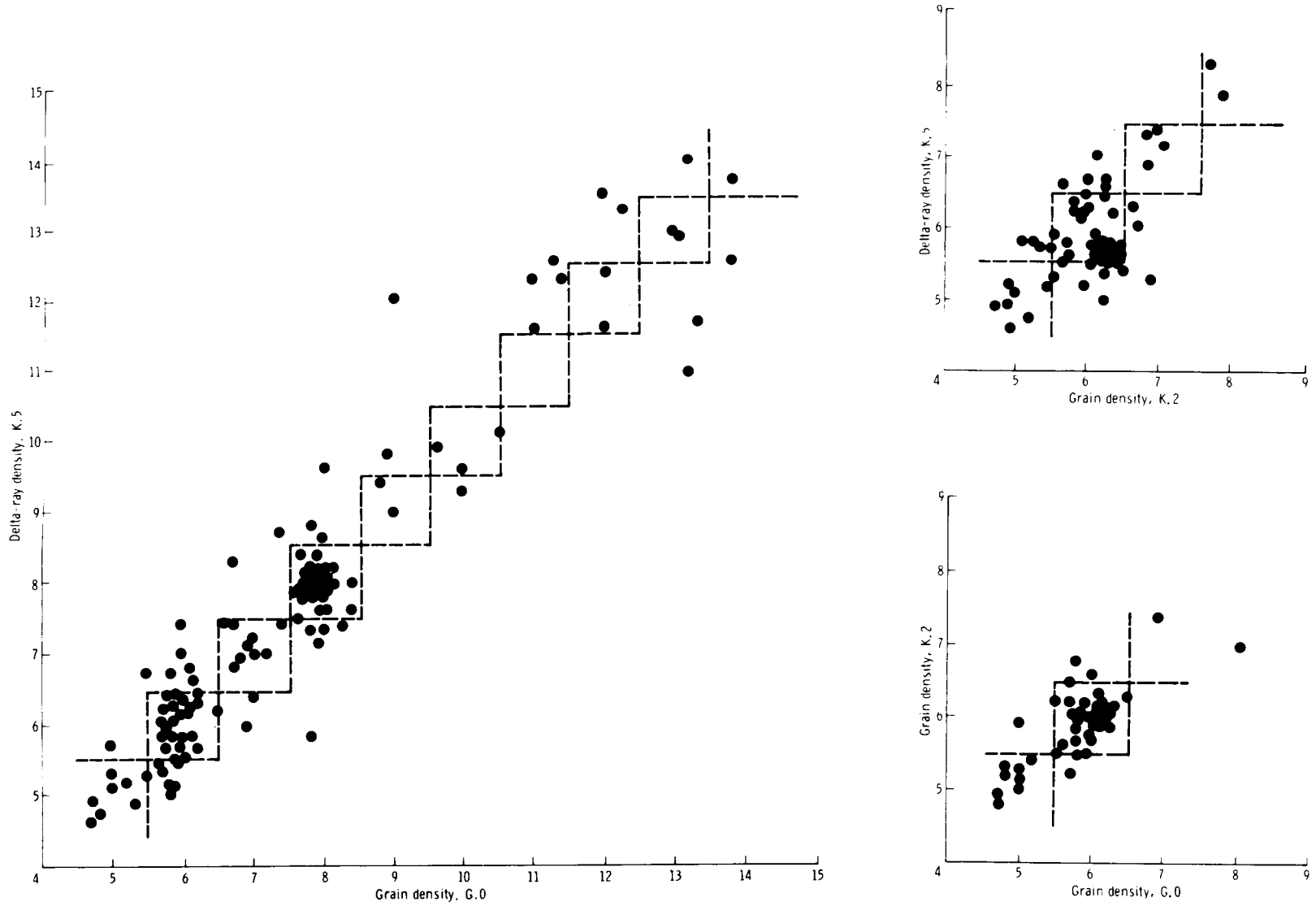

Figure 3. - Charge estimation from ionization measurements.

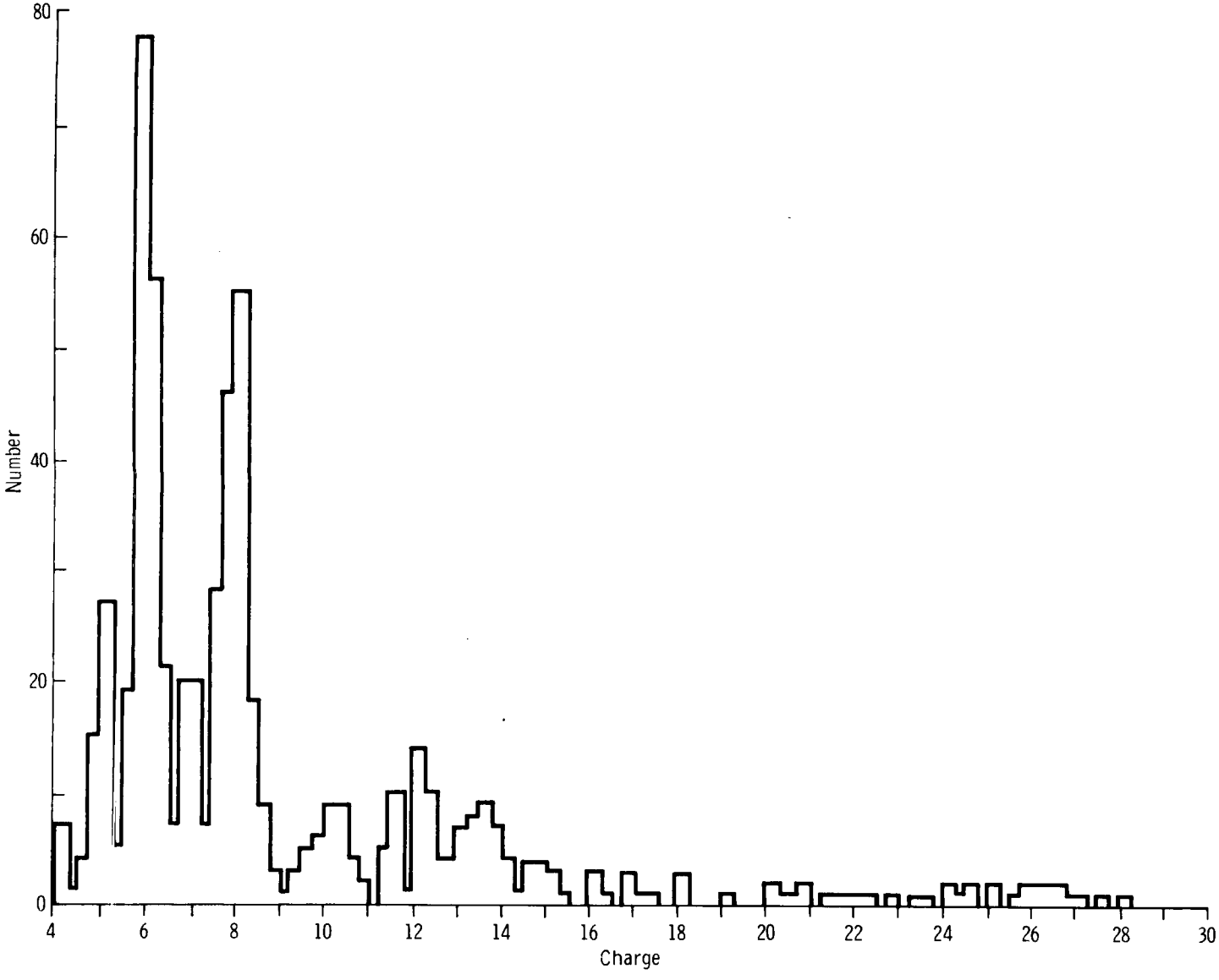

Figure 4. - Cosmic ray charge distribution.

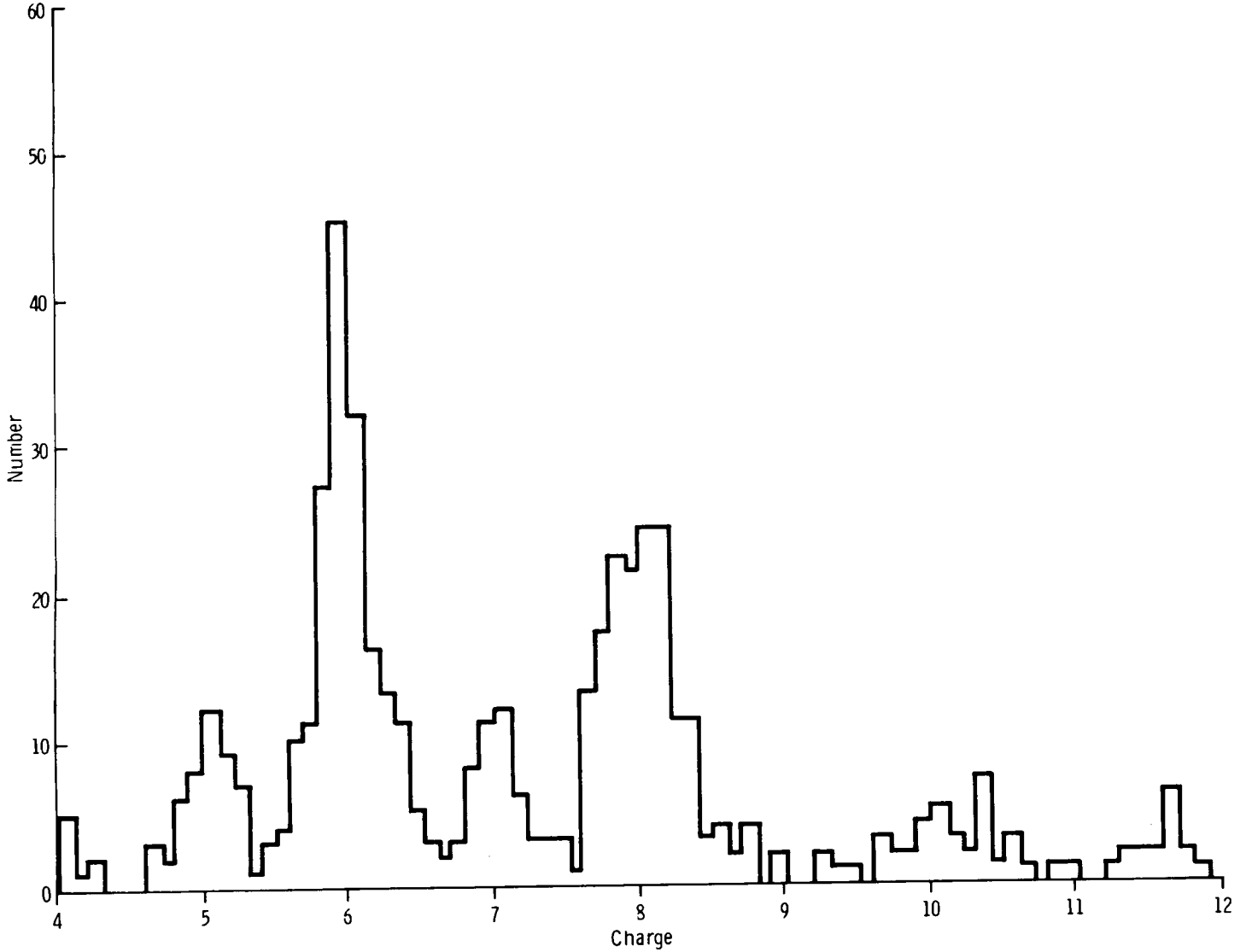

Figure 5. - Cosmic ray charge distribution expanded scale.

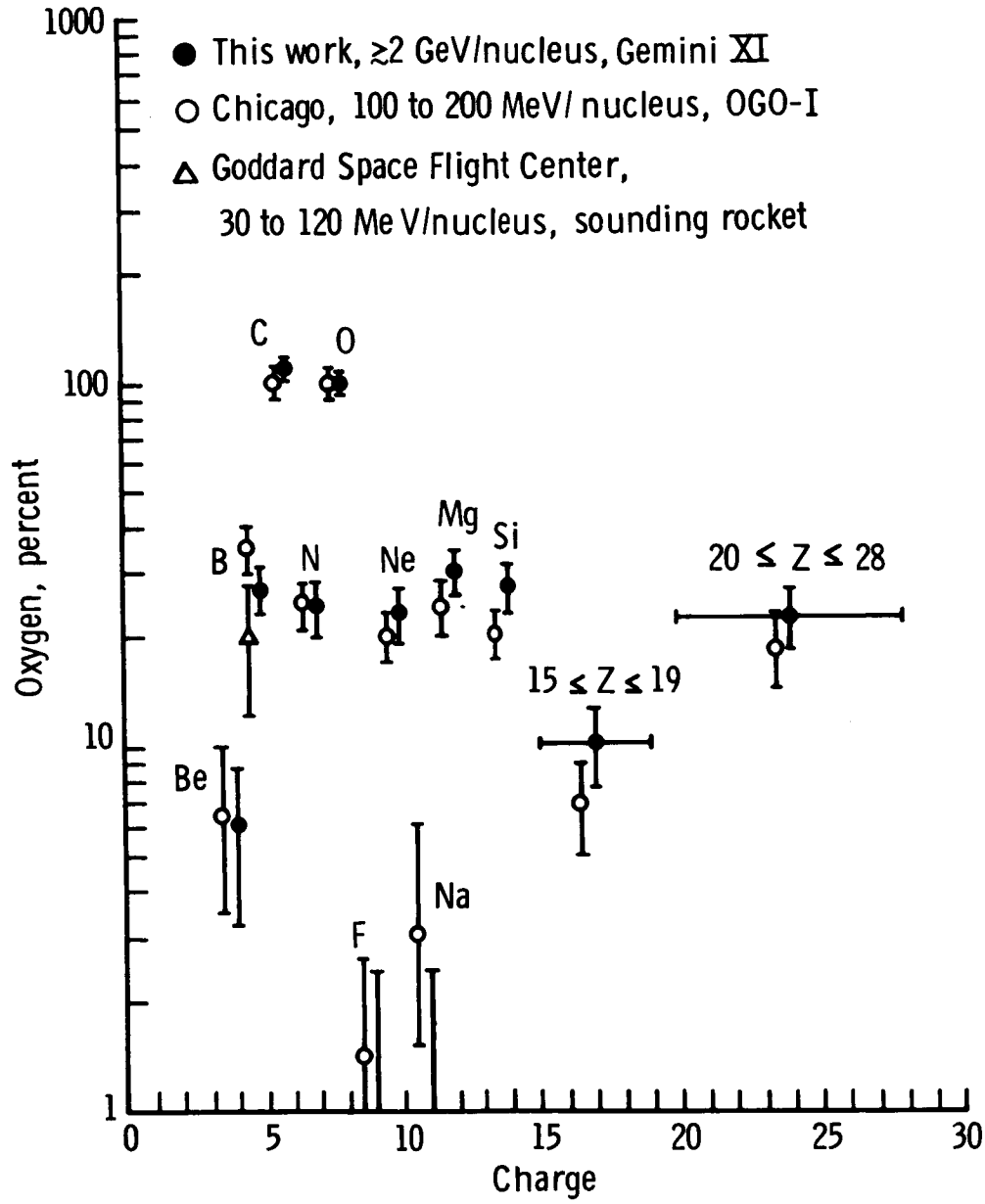

Figure 6. - Charge distribution normalized to oxygen.

EXPERIMENT D008

RADIATION IN THE SPACECRAFT

By M. F. Schneider,* J. F. Janni,* and G. E. Radke*

INTRODUCTION

The collection of adequate data concerning the radiation environment, its shielding interactions, and the dose-rate levels to be encountered are a prerequisite to successful completion of future manned space mission planning studies. Such data are necessary to ensure protection of the crewmen against ambient and occasionally harmful space radiation. This experiment was performed on the Gemini IV and VI missions to obtain a series of precision dosimetry and shielding measurements for use in space-planning studies in which an accurate prediction and interpretation of the radiobiological effects are of vital importance. The data that were collected resulted in quantitative and qualitative characterizations of the radiation levels associated with the Gemini IV and VI missions. Because these measurements were made under normal ambient solar conditions, the radiation environment that was encountered was composed mainly of the energetic protons and electrons present in the inner Van Allen belt; these particles were encountered each time the Gemini spacecraft passed over the South Atlantic anomaly region. In the anomaly region, the radiation belt dips close to the earth because of the anomalously low strength of the magnetic field of the earth. The instruments designed for this experiment were optimized for the radiation-level responses that were anticipated in the region of this geomagnetic anomaly. To facilitate measurement of the very low cosmic-radiation intensities to be encountered outside of the anomaly region, the dynamic range of the instrumentation was extended for the detection of all energy-deposition rates greater than 0.1 millirad per hour.

The experiment included a method for determination of the ionization power and the penetration power of various primary and secondary radiations that were present within the Gemini spacecraft. This was accomplished by measurement of the contributions to dose according to profile, particle type, time, and position (location) within the spacecraft.

The experiment was performed by use of two types of dosimeter systems. One system was active, whereas the other system consisted of passive radiation-detecting devices. Each system, and the measurements obtained from each, will be discussed separately.

*U.S. Air Force Weapons Laboratory, Kirtland Air Force Base, New Mexico.

ACTIVE DOSIMETRY

Instrument Theory and Design

The active instruments included tissue-equivalent ionization chambers, the response characteristics of which for all ionizing radiation match closely the response characteristics of soft muscle. This means that the tissue-equivalent ionization chambers have reaction cross sections for all measured radiations that are the same as standard muscle tissue as defined by the International Commission on Radiological Units (ICRU) (ref. 1). The tissue-equivalent chambers were operated in the Bragg-Gray mode (refs. 2 to 4), which was a basis for the energy-deposition dosimetry measurements that were performed. Briefly, the Bragg-Gray relationship is given by the following linear equation

$$E_m = S_m W J_{gas}$$

where E_m = energy absorption in the material, (eV/gram) sec^{-1}

S_m = relative mass-stopping power of the wall to the chamber filling gas

W = average energy dissipated in gas per ion formed in gas

J_{gas} = ion current, ion pairs per gram per second

This relationship is based on the assumption that the gas cavity will be traversed by the same flow of corpuscular radiation that exists in the material that is being considered. If the gas within the cavity is matched closely to the atomic composition of the walls, the cavity size will not disturb the flux of the secondary particles. Fano's theorem (ref. 5) is the basis for this conclusion: "In a medium of given composition exposed to a uniform flux of primary radiation, the flux of secondary radiation is also uniform and is independent of the density of the medium, as well as of density variations from point to point." Therefore, this cavity-ionization principle facilitates the determination of the energy absorbed in a solid medium (soft muscle) by the ionization measured in a small gas-filled cavity within that medium.

Two types of active dosimeters were used in the Gemini IV data-collection effort; one type was designed to be equipped with a fixed sensor, the other type involved a portable sensor. The mechanical design of each instrument is shown in figures 1 and 2. The Gemini VI instrumentation consisted of the same systems with the inclusion of a special 2.5-g/cm^2 depth-dose shield for the fixed dosimeter. This instrument, as modified for the shield, and the shield are shown in figure 3.

Instrument Calibration

Calibration of the active dosimeters consisted of a vigorous, many-phased program to determine the following instrument response characteristics.

1. The radiation input-to-output voltage-transfer functions
2. The radiation-response time at various radiation levels
3. Any temperature-time effects on the transfer or calibration curves

The initial calibration was performed approximately 90 days before launch by the use of cesium-137 and cobalt-60 gamma-radiation natural-emitting sources at the U. S. Air Force Weapons Laboratory (AFWL), Kirtland Air Force Base, New Mexico. Several 2-week time-drift-rate tests were performed on each active system after the initial calibration. Upon completion of the time-drift-rate test, the radiation response-time calibration to different levels of radiation (in the range from 0.5 millirad per hour to 100 rads per hour) was performed. Then, all instrumentation was temperature cycled from -40° to +160° F to check for any temperature-dependent characteristics in the instruments. Drift rates of less than 10 percent were observed in the outputs of the instruments. The effects of temperature on instrument outputs were negligible because of the relative constancy of the cabin temperature during the Gemini missions.

The instruments were recalibrated (by use of cesium-137 and cobalt-60 gamma radiation) before shipment to the facility of the spacecraft contractor for installation in the spacecraft. A specially designed portable 0.1-millicurie strontium-90 beta-particle source was used for performance of the functional calibration checks on the instruments during preinstallation acceptance and for the spacecraft-systems testing. This beta-particle source also was used to perform the final functional recalibration 7 days before launch at Cape Kennedy, Florida.

The active dosimeters were calibrated postflight at Kirtland Air Force Base by the use of National Bureau of Standards (NBS) calibrated gamma ranges for cesium and cobalt. This was done approximately 20 days after the termination of the Gemini IV mission and 10 days after the Gemini VI mission to ensure the greatest accuracy in the final data analysis. Flight-instrument prototypes were calibrated at Oak Ridge National Laboratory (ORNL), Oak Ridge, Tennessee, (by use of 40- and 60-MeV cyclotron-accelerated protons of various beam diameters and intensities) to obtain proton flux-to-dose and instrument-output-voltage-calibration curves and directional-sensitivity response curves. Similar calibration and response data were collected by the use of 3.0-, 2.0-, 1.0-, and 0.5-MeV electrons. All data have been corrected for the small omnidirectional-response differences between the two instruments.

EXPERIMENTAL METHOD

The fixed active dosimeter, designated type I, was mounted on the left-hand hatch of the Gemini IV spacecraft. The portable unit, designated type V, was mounted in a symmetrical location on the spacecraft right-hand hatch. These positions were reversed for the Gemini VI mission. The mounting location of the instrument is shown

in figure 4. All instruments were powered by regulated voltage from the spacecraft. The output signals from each instrument were recorded continuously throughout each flight. Each instrument was capable of recording instantaneous dose rates ranging between 0.1 millirad per hour and 100 rads per hour. This wide range facilitated instrument response to low-intensity cosmic-ray fluxes and to any unusual high-dose rates encountered in the South Atlantic anomaly region. Also, the instantaneous dose rates were integrated easily to give total dose for comparison with the passive-dosimetry components of the experiment.

The experiment on the Gemini VI mission differed from the experiment on the Gemini IV mission regarding the location of two of the passive dosimeters and in the addition of a removable 2.5 g/cm^2 brass shield on the tissue-equivalent ionization chamber on the command pilot hatch (fig. 3). The shield was designed to simulate the shielding provided to the gastrointestinal tract by the abdominal muscles. This shield was to be removed during one of the passes through the South Atlantic radiation anomaly; during this time, a radiation survey was to be performed by moving the portable dosimeter sensor next to it. The experiment performed on the Gemini VI mission was designed to collect additional depth-dose and shielding data.

The active portion of the experiment for the Gemini IV and VI missions was initiated at lift-off. The instrumentation automatically collected radiation data except for six selected passes through the central portion of the South Atlantic anomaly region, in which the portable type V radiation sensor was removed from the hatch and was positioned in the following locations by the pilot.

1. Against the chest, the sensor covered by a glove

2. Between the legs (groin)

3. In the left armpit

4. In front of the cabin window; next to the fixed active dosimeter on the Gemini VI mission

5. In front of the instrument panel, approximately midway between the floor and the ceiling

6. On the floor of the spacecraft, between the feet of the pilot

These six positions are illustrated in figures 5 to 10. The sensor was fixed in each of these locations for a period of 1.0 minute to ensure that full instrument response to the chosen radiation field would be attained.

As measured, the dose-rate levels were functions of position in the spacecraft and of depth in the crewmember (because portions of the body of the crewman were used as a shield). As a function of time, the dose-rate level beneath the hatch of the spacecraft was obtained from the fixed type I dosimeter. These data were used as a base line from which measurements made in the various survey positions by use of the portable unit could be compared.

RESULTS

The active-dosimeter measurements are discussed most conveniently in terms of two general fields of interest: the experimental determination of the dose levels obtained outside of the South Atlantic anomaly region and the measurement of the radiation characteristics during passage of the spacecraft through the South Atlantic anomaly. The active radiation sensors functioned perfectly, and 97 hours of data were collected during the mission. The five scheduled radiation-level surveys within the cabin were performed by the pilot during the anomaly passes of the spacecraft.

Cosmic-Radiation-Dose Measurements

Outside the South Atlantic anomaly region, the principal contribution to the radiation dose received by the astronauts was from cosmic radiation. The average, maximum, and minimum dose levels obtained during 19 revolutions of the Gemini IV spacecraft through regions outside the anomaly region are presented in table I. The average dose rate was obtained every 3.2 seconds for each revolution. The maximum and minimum dose levels were determined as the lowest or highest reading observed during a period of at least 1.0 minute for each revolution. The average dose rate for all revolutions that did not pass through the anomaly was 0.15 millirad per hour.

Because the revolutions that were selected for analysis cover the entire span of the Gemini IV mission, the average dose rate may be extended readily to obtain excellent approximations of the total integrated cosmic-ray dosage for the complete mission. Then, this may be projected to an estimate of cosmic-radiation levels for more extended missions at the Gemini operating altitudes and with similar shielding configurations. By use of this average yield, it was determined that the total integrated dosage caused by cosmic radiation during the 4-day mission was approximately 15.0 millirads.

Based on an assumed nominal period of 90 minutes for each revolution, the total accumulated tissue dose was approximately 0.23 millirad per revolution. The average daily cosmic-radiation levels that were received inside the cabin of the Gemini spacecraft were approximately 3.5 millirads per day. Such radiation levels are very low and constitute a permissible exposure dose for extended periods at Gemini operating altitudes.

During a portion of revolution 3 and during the period of crewmember egress, the right-hand hatch remained open, exposing the type V portable dosimeter to the external space-radiation environment over a 2π solid angle. The radiation levels measured by the type V instrument during this time never exceeded those obtained by the unexposed type I unit. Clearly, this was indicative of a total absence of softer (or trapped) corpuscular radiation in the regions of space where the crewman was extravehicular. The cosmic-radiation dose profile is shown in figure 11 as a function of orbital elapsed time and corresponding L-shell values. These dose profiles were indicative of an increase to approximately 0.5 millirad per hour at greater L values, and a rapid decrease to less than 0.1 millirad per hour for L values of approximately 1.0 earth radius. This effect was consistent with the predicted latitude-induced magnetic cutoff that was encountered by the spacecraft. Because the spacecraft traversed

only the lower geomagnetic latitudes, dosage was less than the polar (or free-space) values, which normally are as high as 14 millirads per day during periods of minimum solar activity.

Anomaly-Region Dose Levels

Dose-rate data obtained in the South Atlantic anomaly region increased rapidly to almost three orders of magnitude over the cosmic levels of radiation. For example, the anomaly dose rate during revolution 7 increased to more than 100 millirads per hour. The instantaneous anomaly dose levels that were encountered by the two active dosimeters for nine orbits of the Gemini IV spacecraft from the 7th revolution through the 54th revolution are shown in figures 12 to 20. The peak dose levels varied from 125 millirads per hour (revolution 7) to only 20 millirads per hour (revolution 51). The curve in figure 12 is indicative that an appreciable dose level was present in the spacecraft for 15 minutes during revolution 7 (a deeply penetrating anomaly orbit). For a grazing anomaly orbit (such as revolution 39), the transit time through the radiation belt was less than 7 minutes. For most passes, this transit time averaged approximately 12 minutes.

The dose-rate differences between the two dosimeters were indicative of the effects of the different shieldings that were interposed between the sensing elements and the measured radiation field. Generally, the type V (portable) dosimeter readings were slightly greater than were the type I (fixed) dose-rate-meter readings. Revolutions 7, 21, 22, 38, 39 and 54 were orbits in which the type V dosimeter readings were slightly greater than were the type I dosimeter readings during penetration of the anomaly. There was an interchanging of readings between the two dosimeters on revolutions 36 and 51 (which were similar orbits). For example, on revolutions 36 and 51, five distinct intersection points between the fixed-dosimeter and portable-dosimeter readings were noted. It is interesting to note that during revolution 51, attitude control was exercised so that only yawing motion was being executed by the spacecraft. These two curves clearly demonstrate appreciable directionality in the radiation that entered the spacecraft. Because the radiation sensors are 0.4 g/cm^2 thick and because the Gemini hatch is on the order of 0.87 g/cm^2 of shielding, these directionalities in the radiation field are a result of protons of $E > 30$ MeV and electrons with $E > 2$ MeV. Also, the radiation field indicated a lesser degree of directionality at a number of different places in the anomaly region. Spectrometer measurements that were performed in the anomaly region (ref. 6) also have shown the directional properties of the radiation field.

The Gemini IV pilot performed the series of radiation surveys at the locations shown in figures 5 to 10 during five orbits through the anomaly region. The results of the survey for revolutions 8 and 52 are shown in figures 21 and 22, respectively. It is apparent that considerable dose reduction resulted whenever the sensing element was buried beneath only a few grams per square centimeter of material. As the spacecraft approached the anomaly region, the portable dosimeter indicated slightly greater dose levels than did the fixed-base-line instrument. When the sensor was moved to the chest position and the sensing element was covered with a gloved hand, the dose level was reduced by 50 percent. Placement of the sensor at the groin and under the armpit resulted in an even greater dose-level attenuation. In these two regions, the dose was

reduced to approximately one-third of the fixed dosimeter levels. When the sensor head was placed in front of the window, the dose level was reduced to approximately one-third of the base-line reading. The panel and floor dose rates also were only one-third of the hatch dose values. The dose rates at the window, panel, and floor regions were somewhat higher on revolution 52 than they were on revolution 8. Shielding measurements for the two orbits at the chest, groin, and armpit locations — when the spacecraft was deeper in the anomaly region — were very close. The results of the two Gemini IV radiation surveys and the one Gemini VI radiation survey are shown in table II. The Gemini VI survey is in agreement with the two surveys performed on the Gemini IV mission. All survey readings were taken 30 seconds after the sensing element had been fixed in place at a particular location, to ensure that equilibrium response had been attained.

An integration of the dose rate for the fixed-base-line dosimeter (type I) was performed for all anomaly-region orbits during the Gemini IV mission. These data are shown in table III. The total integrated dose for the Gemini IV orbits was 69.9 millirads. The total extrapolated dose for other orbits near the fringe of the anomaly did not exceed 2.0 millirads. The type V portable-dosimeter dose rates were not integrated, because, during five passes through the anomaly region, surveys were being performed that would have lowered the dose readings appreciably.

An isodose mapping of the South Atlantic anomaly for a 280-kilometer altitude is shown in figure 23. The contours were mapped by use of the highest dose-rate reading from either instrument. The isodose contours have maximum values at longitude 37° W and latitude 32.5° S. Thus, revolutions 7 and 8 were shown to have penetrated more deeply into the belt than did other orbits. Revolutions 22, 23, 37, 38, 52, and 53 followed a pattern that resembled at least one of the revolutions shown in figure 23.

Comparison of Gemini IV Data with Computer-Code Information

One of the main objectives of Experiment D008 was to test the validity of the computer-code information by comparing the dose rate measured by the active instruments with the dose rate predicted by the existing computer codes. Predicted dose rates were computed by use of the actual Gemini IV trajectories. Radiation-flux maps of the radiation environment were used in conjunction with a 720-sector analysis of the Gemini spacecraft (supplied by the spacecraft contractor), which contained a description of the spacecraft shielding. A comparison of the measured dose rate with the measured electron and proton environment (ref. 6) in the anomaly region during revolutions 21 and 36 is shown in table IV. This measured dose rate was the average dose reading. In table IV, the measured dose is broken up into its proton and electron components. This was possible on these two orbits because the measured proton flux was constant for more than 5 minutes, whereas the electron flux increased several orders of magnitude (ref. 6). Because the dose increased in a corresponding fashion, it was possible to generate a proton dose-rate conversion from the external flux of approximately 3×10^{-4} (rad/hr)/proton/cm^2-sec and an electron dose-rate conversion factor from external flux of 1.2×10^{-3} (mrad/hr)/electron/cm^2-sec. To obtain calculated doses, the fluxes and spectra from reference 6 have been used as input data to the AFWL radiation-transport codes. The measured dose and calculated doses generally

have agreed well; the greatest separation between them being no greater than a factor of 2. This is well within the uncertainty error in the fluxes.

Initial theoretical predictions of the dose levels, performed with the AFWL computer code by use of the Vette grid, resulted in dose values that were in excess of the measured values for the Gemini IV anomaly orbits by a factor of approximately 3. Because these values are dependent on the flux map generated from the data gathered early in 1963 (when the electron population was much greater than it was at the time of the Gemini IV mission), the measured values would be expected to be much lower at the time of the Gemini IV mission.

PASSIVE DOSIMETRY

Instrument Theory and Design

The five passive-dosimetry packages (occasionally referred to as PDX units) located in the spacecraft cabin were designed to ascertain both total accumulated dose and the intensity of the radiation that caused it. These packages, each of which included several passive dosimeters, were located at points of maximum, intermediate, and minimum shielding locations (fig. 24). Package 1 was mounted near the type I active dosimeter to facilitate an empirical comparison between the dose measured by the passive unit and the integrated dose (that is, the dose obtained by integration of the dose rate over the total measurement time). Three other passive units were located at points of intermediate shielding, and a fourth unit was placed on the debris guard beneath the instrument panel (a region of heavy shielding).

Because the experiment might have been influenced adversely by the contribution to ambient radiation levels from radiation sources carried on board the spacecraft, the three onboard radiation sources were investigated for possible significant effects. The strongest of these sources was a 0.9-millicurie americium-241 source that was located in the carbon dioxide monitoring systems between and under the two seats. Although the shielding on the source was sufficient to stop all α-particle emission, the soft 60-keV λ-component that emanated from the americium was not attenuated enough to make its effect negligible to the experimental measurements. Three experimental dose-rate measurements were made; these extended from the surface of the source to 10 centimeters. In addition, a theoretical estimate was made of the total emission of the 60-keV λ-rays at distances greater than 10 centimeters. The evaluation of the dose rate delivered by the americium involved only air attenuation and did not involve shielding by the seats and equipment located between the source and the nearest PDX unit. Therefore, this dose rate (fig. 25) was an upper limit.

The dose rate at the surface of the luminous-dial watches worn by the crewmen was less than 0.1 millirad per hour. The dose rate varies inversely with the square of the source distance. Because no dosimeter in the cabin was closer than several inches to a wristwatch, the radiation from this source was negligible.

The third possibly significant radiation source was located in the adapter section, some distance behind the ablation shield. The source included those elements of the adapter section that contained thoriated magnesium, which is slightly radioactive.

Because the combination of shielding and distance for this source made its dose level extremely low, no attempt was made to measure the dose rate from this source alone.

The total contribution of all radiation sources in the spacecraft cabin was measured by five passive dosimeters that were placed on board the spacecraft at Cape Kennedy, Florida, for the 31-hour, simulated, wet mock-countdown period. Launch-vicinity radiation control was in effect at this time, and the measurements that were made on the passive units were a good indication of the cabin ambient-radiation level. These measurements were indicative of an ambient dose rate of less than 1 millirad per day, including the dose from radiation of sufficient energy to penetrate the spacecraft cabin.

These radiation measurements were indicative that almost all of the background radiation on board the capsule was from cosmic radiation. For this reason, no corrections were applied for onboard radiation sources, although ground-control background readings were subtracted from the data. The ground-level ambient dose was measured by the use of a calcium fluoride dosimeter for the 14-day period between preparation and evaluation. The dose for that period was 12.9 ± 1.2 millirads. The error estimate is a standard deviation. The five flight units and the ground-based control unit were assembled and were placed in a shielded aluminum container. They remained together there until 26 hours before launch, when the flight items were removed for installation in the spacecraft.

Extremely rigid controls regarding the location of all radiation sources in the launch vicinity were put into effect to avoid any undesired exposure of the dosimeters, some of which were capable of detection of radiation doses as low as 3 millirads. The ground-based control unit was separated from the flight units for 11 hours after splashdown and for 26 hours prelaunch. It was taken to the NASA Manned Spacecraft Center (MSC) immediately after launch, was reunited with the flight units after splashdown, and was returned immediately with the flight units to the AFWL for evaluation. All dosimeters had been checked previously for reproducibility, for absolute accuracy, and for dose fade.

Two types of photoluminescent glass dosimeters were selected for Experiment D008. One type, the glass-needle system, contained 12 very small, lightweight, radiation-sensitive glass needles. The glass needles were flown in the package on the left-hand hatch, their predose having been determined previously. The glass dosimeter readings were not significant statistically and could not be distinguished from those of the ground-based control needles. The second type of photoluminescent glass dosimeter, the Toshiba glass system, was very radiation sensitive and could detect doses as low as 25 millirads. Two Toshiba glass units were flown; one was shielded, the other was unshielded. The shielded system was enclosed by a Lucite shield that was 0.08 centimeter thick and by a lead shield that was 0.01 centimeter thick. This combination resulted in a total shielding thickness for the Toshiba glass units of 190 mg/cm^2. The U. S. Naval Radiation Defense Laboratory, San Francisco, California, supplied and evaluated these dosimeters for the experimenter. The shelf-shielding of each Toshiba glass dosimeter within the pack could not be neglected, because each unshielded unit was surrounded on three sides by emulsion packs and on the fourth side by the pocket ionization chamber. The low readings registered on the Toshiba glass were very likely the result of this shielding.

Several lithium fluoride dosimeters were flown, and each dosimeter included a small Teflon cylinder that had a minimum thickness of 0.22 g/cm^2 and that was filled with powdered lithium fluoride. Such a dosimeter was capable of measuring doses as low as 10 millirads. Approximately 6 percent of the powder contained the lithium isotope (^6Li) and would respond to ionizing radiation and to neutrons. Because the other isotope of lithium (^7Li) in this compound had a very low neutron cross section, the difference between the readings obtained on these two isotopes would be a measure of the neutron-radiation component within the spacecraft cabin.

Comparison of the Gemini IV mission data from each isotope was indicative that, within the limits of the experimental error, no neutron dose occurred. This result was reasonable because the only neutrons expected would come from secondary radiation produced by interaction of the high-energy protons with the spacecraft and its contents. Analysis of the activation foils also substantiated the lithium fluoride results. A set of activation foils also was included in Gemini IV passive-dosimetry packages for the purpose of the determination of the presence or absence of neutrons. The foils were chosen for detection of neutrons over a wide range of energies (including thermal energies). The foils were made of zirconium, sulfur, tantalum, gold, cobalt, and aluminum. None of these foils indicated a measurable number of neutrons during the Gemini IV mission.

A film-emulsion pack was supplied by the U. S. Naval School of Aviation Medicine, Pensacola, Florida. The particle tracks in the emulsion were more than 95 percent protons; there were only residual electron, α-particle, and heavy-particle tracks. Less than 2 millirads of dose was caused by particles other than protons in the emulsion. An exploded view of the passive-dosimetry packages flown is shown in figure 26. A summary of the Gemini IV passive-dosimetry results is presented in table V.

Temperature Dependence

Because many of the dosimeters flown were, to some extent, temperature dependent in their response and in dose fading, a temperature profile of the hatch region was obtained from data collected by use of the type I active ionization chamber. Temperatures at the other four locations, at which passive-dosimeter packs were located, were not expected to differ significantly. The temperature extremes were never more than 2° C on either side of the mean and usually were much less.

Gemini IV Mission Temperature Profiles on Left-Hand Hatch

Revolution	Mean temperature, °C
6	22.6
7	23.8
8	23.8
21	20.9
22	20.9
36	20.4
37	20.9

Revolution	Mean temperature, °C
38	20.4
45	20.9
50	26.2
51	25.6
52	25.0

Gemini VI Mission

Experiment D008 also was flown successfully on the Gemini VI mission. Twenty-five hours of continuous dose, depth dose, and shielding data were obtained. The cosmic-radiation levels for Gemini VI passes outside of the anomaly region are presented in table VI. The average cosmic-radiation dose for the Gemini VI mission was approximately 0.2 millirad per hour, which leads to a total-mission cosmic-ray dose of 4.8 millirads for the 25 hours. Multiplying this value by 4 to account for the 4 days of the Gemini IV mission, 19 millirads are obtained. This compares favorably with the 15-millirad cosmic-ray dose that was measured on the Gemini IV mission. Five Gemini VI passes through the South Atlantic anomaly recorded doses well above the cosmic-ray levels. These measurements are shown in figures 27 to 31 as a function of spacecraft orbital time. The peak dose rate for the unshielded active dosimeter was 73 millirads per hour recorded on revolution 6. The shielded active dosimeter also measured its highest mission dose rate on this revolution (42 millirads per hour). The unshielded dosimeter recorded approximately 56 millirads per hour less peak dose rate than the peak dose rate measured on the Gemini IV mission flown almost half a year earlier. The revolution 5 pass of the spacecraft through the anomaly was used by the pilot to perform the radiation surveys described previously. The radiation survey data were consistent with the same measurements conducted on the Gemini IV mission, as was shown in table II.

The integrated anomaly radiation doses on the Gemini VI mission are 19.0 millirads (table VII). If this value is multiplied by a factor of 4 to account for the additional 4 days of the Gemini IV mission, the result agrees to within 7 millirads of the Gemini IV anomaly integrated dose of 69 millirads. Also, the minimum possible proton dose and maximum possible electron dose for each revolution of the Gemini VI mission are shown in table VII. These values were derived under the assumption that the protons were not degraded appreciably by the 2.5 g/cm^2 shield. Although this is only an approximation, it provides upper-limit and lower-limit data that are valuable in estimating the relative electron and proton contributions to dose. The 2.5 g/cm^2 shield has the average effect of reducing the surface dose received in the anomaly by 34 percent. This shield had no measurable effect on the dose resulting from cosmic radiation.

The Gemini VI passive-dosimetry results are shown in table VIII, and these values are consistent with the Gemini IV passive-dosimetry results. Total dose agreement between the passive dosimeters and the active-dosimeter integrated dose is excellent for this mission.

CONCLUSIONS

Both active- and passive-dosimetry data collected in this experiment showed that no radiation hazard was associated with manned space operations within the Gemini spacecraft at altitudes as great as 310 kilometers in the South Atlantic anomaly region. This conclusion is warranted also by theoretical calculations. However, it has been shown (ref. 7) from unmanned satellite radiation measurements that the radiation doses behind 4.15 g/cm^2 of aluminum shielding reach as much as 10 rads per hour at L = 1.5 and B = 0.10 gauss (deeper in the inner Van Allen belt). Also, it is shown in reference 7 that behind an aluminum shield of 1.35 g/cm^2, the surface dose at the same B, L point above is 50 rads per hour. Extended operations in a Gemini spacecraft at these altitudes could be very hazardous.

Dose-rate contours for the anomaly have been generated in B, L space for the highest reading observed by either active dosimeter on the Gemini IV and VI missions (fig. 32). This dose map is very useful for comparison of dose measurements made behind equivalent shielding on other satellites flown in the radiation belts.

The consistency between the active and passive dosimeters was even better than had been anticipated. The differences between the integrated dose readings of the tissue-equivalent ionization chamber and the passive dosimeter in the same region of the left-hand hatch ranged from 30 percent (for the thermoluminescent devices) to only 12 percent (for the discharge ionization chamber). The differences in the dose readings that occurred between the passive and the active instruments resulted from shielding differences and the radiation-response differences between the thermoluminescent devices and the active dosimeters. For example, the tissue-equivalent ionization chambers respond to the proton radiation of the type encountered on the Gemini IV and VI missions (that is only 3 percent lower than standard tissue response of the ionization chambers). However, the calcium device responds to radiation of the type encountered at values from 18 to 32 percent less than the tissue-equivalent ionization chambers. Also, intricate differences in the shielding interposed between the various passive devices were somewhat greater than the shielding that surrounded the ionization cavities of the two active dosimeters. Thus, the number of electrons that reach these devices would be reduced.

Another valuable achievement was the development of flight-qualified space-dosimetry-instrumentation packages, the operational feasibility of which has facilitated adaptation of these devices to a variety of other types of satellites. In such uses, the devices have the capability for adequate and instantaneous warning in the event of an onset of radiation hazards caused by unexpected or unpredicted radiation environments.

REFERENCES

1. Anon.: Report of the International Commission on Radiological Units and Measurements (ICRU). National Bureau of Standards Handbook 78, 1959.

2. Bragg, W. H.: Consequences of the Corpuscular Hypothesis of Gamma and X-Rays and the Ranges of Beta Rays. Phil. Mag., series 6, vol. 20, 1910, pp. 385-416.

3. Gray, L. H.: The Absorption of Penetrating Radiation. Proc. Roy. Soc. (London), series A, vol. 122, 1929, pp. 647-688.

4. Gray, L. H.: The Ionization Method of Measuring Neutron Energy. Proc. Cambridge Phil. Soc., vol. 40, 1944, pp. 72-102.

5. Fano, U.: Note on the Bragg-Gray Cavity Principle for Measuring Energy Dissipation. Radiation Res., vol. I, 1954, pp. 237-240.

6. Reagan, J. B., et al.: Proton-Electron Spectrometer Experiments on Gemini-4 and Gemini-7. NAS 901587, 1966.

7. Thede, A. L.; and Radke, G. E.: A Correlation of Dosimetric Measurements With the Charged Particle Environment of the Inner Van Allen Belt. Presented to the 13th Meeting of the American Nuclear Society (San Diego, California), 1967.

TABLE I. - DOSE RATES OF COSMIC RADIATION FOR SPECIFIC REVOLUTIONS ON THE GEMINI IV MISSION OUTSIDE OF THE SOUTH ATLANTIC ANOMALY REGION

Revolution number	Average dose rate, mrad/hr	Maximum observed dose rate, mrad/hr	Minimum observed dose rate, mrad/hr
1	0.25	0.65	0.1
2	.25	.64	.1
3	.20	.30	.1
14	.15	.30	.1
15	.15	.30	.1
16	.18	.30	.1
17	.15	.30	.1
18	.22	.50	.1
29	.12	.45	.1
30	.18	.40	.1
31	.12	.50	.1
32	.12	.30	.1
44	.15	.30	.1
45	.12	.40	.1
46	.12	.30	.1
48	.15	.30	.1
59	.10	.15	.1
60	.10	.10	.1
61	.10	.10	.1

TABLE II. - ATTENUATION FACTORS FOR GEMINI IV AND VI SHIELDING EXPERIMENTS

Mission	L range	Shielding locations					
		Chest	Groin	Armpit	Window	Panel	Floor
Gemini VI (rev 5)	1.25 to 1.50	0.42	0.69	0.58	--	0.50	0.72
Gemini IV (rev 8)	1.25 to 1.45	.64	.74	.66	0.47	.62	.71
Gemini IV (rev 52)	1.25 to 1.55	.50	.70	.60	.20	.20	.45

TABLE III. - GEMINI IV DOSES FOR SELECTED SOUTH ATLANTIC ANOMALY REVOLUTIONS

Revolution number	Integrated dose per anomaly revolution, mrad
6	[a]3.0
7	10.4
8	10.6
9	[a]3.5
21	2.9
22	7.1
23	[a]6.0
24	[a]3.0
36	3.5
37	6.0
38	3.4
39	2.5
51	1.7
52	2.3
53	[a]2.0
54	2.0
Total	69.9

[a]These data were not measured, but were extrapolated from plots of revolutions of similar type.

TABLE IV.- ELECTRON AND PROTON DOSE RATES FOR REVOLUTIONS 21 AND 36 OF THE GEMINI IV MISSION

Revolution number	Orbital time, hr: min	Measured electron dose rate, mrad/hr	Calculated electron dose rate, mrad/hr	Calculated proton dose rate, mrad/hr	Measured proton dose rate, mrad/hr
21	31: 50	2.0	3.0	12.7	13.9
21	31: 51	6.5	7.1	12.7	13.9
21	31: 52	13.0	14.8	12.7	13.9
21	31: 53	24.9	25.0	12.7	13.9
21	31: 54	32.0	23.8	12.7	13.9
21	31: 55	22.5	12.5	12.7	12.9
21	31: 56	8.7	7.5	12.7	13.9
36	55: 29	Negligible	.05	4.1	6.2
36	55: 30	6.8	.39	4.7	6.2
36	55: 31	12.4	1.3	5.9	6.2
36	55: 32	19.2	14.1	5.2	6.2
36	55: 33	25.3	21.7	5.9	6.2
36	55: 34	25.8	21.7	6.1	6.2
36	55: 35	18.2	16.1	4.4	6.2

TABLE V. - SUMMARY OF THE PASSIVE DOSIMETRY RESULTS ON BOARD THE GEMINI IV SPACECRAFT[a]

[Location: Figure 24]

Dosimeters	Location				
	1 (left hatch)	2 (abort panel)	3 (right switch panel)	4 (left-side panel)	5 (debris guard)
^{6}LiF	50 ± 10	--	44 ± 19	--	53 ± 18
^{7}LiF	--	52.5 ± 19	43 ± 12	50 ± 14	59 ± 14
CaF_2					
Unshielded, 0.091 g/cm^2	--	49.4 ± 6.1	--	57.9 ± 6.5	49.4 ± 4.7
Unshielded, 0.091 g/cm^2	54.7 ± 7.0	47.1 ± 4.1	55.3 ± 5.4	55.7 ± 5.1	48.5 ± 6.1
Shielded, 0.871 g/cm^2	53.6 ± 5.7	48.9 ± 3.8	49.0 ± 3.8	55.9 ± 5.9	--
Pocket ionization chamber	73 ± 5.1	45 ± 2.3	46 ± 3.2	54 ± 3.8	47 ± 3.3
Toshiba glass[b]					
Unshielded	52 ± 23	27 ± 15	42 ± 20	--	37 ± 18
Shielded	37 ± 18	17 ± 12	37 ± 18	--	12 ± 10
Emulsion[c]	68	--	--	--	35

[a]With the exception of the emulsion, all readings in this table are in milliroentgens equivalent exposure.

[b]The Toshiba glass was calibrated by the use of ^{60}Co; all other calibrations were made by the use of ^{137}Cs.

[c]The emulsion readings are in millirads; the error is less than 5 percent.

TABLE VI. - COSMIC-RADIATION DOSE RATE FOR SPECIFIC REVOLUTIONS OF GEMINI VI OUTSIDE THE SOUTH ATLANTIC ANOMALY

Revolution number	Average dose rate, mrad/hr	Maximum dose rate, mrad/hr
3	0.20	0.7
4	.20	.7
10	.25	1.0
12	.15	.6
12	.20	1.0

TABLE VII. - MINIMUM POSSIBLE PROTON DOSE RATES, UNSHIELDED, AND SHIELDED INTEGRATED DOSES, DEMONSTRATING MINIMUM PROTON AND MAXIMUM ELECTRON DOSES FOR SELECTED GEMINI VI REVOLUTIONS

Revolution number	Minimum peak proton dose rate, mrad/hr (E_p > 50 MeV) (a)	Unshielded dose, mrad	Shielded dose, mrad	Minimum proton dose, mrad (E_p > 50 MeV) (a)	Maximum possible electron dose, mrad
5	10	1.78	1.24	1.24	0.54
6	39	6.80	4.83	4.83	1.97
7	38	5.84	3.03	3.03	2.74
8	29	3.22	2.40	2.40	.82
9	12	1.40	1.10	1.10	.30
Total		19.0	12.6	12.6	6.4

[a]50 MeV is a measure of proton energy external to the spacecraft.

TABLE VIII. - SUMMARY OF THE PASSIVE DOSIMETRY RESULTS ON BOARD THE GEMINI VI SPACECRAFT[a]

Dosimeters	Location				
	6 (right hatch)	7 (abort panel)	8 (right-side panel)	9 (left-side panel)	10 (debris panel)
CaF_2					
Unshielded	19.9 ± 2.0	14.2 ± 1.8	20.7 ± 2.3	21.9 ± 2.4	13.0 ± 1.5
Unshielded	20.2 ± 2.1	13.7 ± 1.7	20.3 ± 1.9	18.8 ± 2.0	13.7 ± 1.8
Unshielded	20.1 ± 2.2	14.3 ± 1.9	18.2 ± 2.0	21.0 ± 2.1	14.9 ± 1.8
Shielded	--	14.1 ± 1.8	19.0 ± 1.8	20.8 ± 2.1	13.7 ± 1.7
Pocket ionization chamber	18.5 ± 1.3	10.5 ± 1.0	18.5 ± 1.4	22.5 ± 1.6	14.5 ± 1.4

[a]All readings are in milliroentgens equivalent exposure.

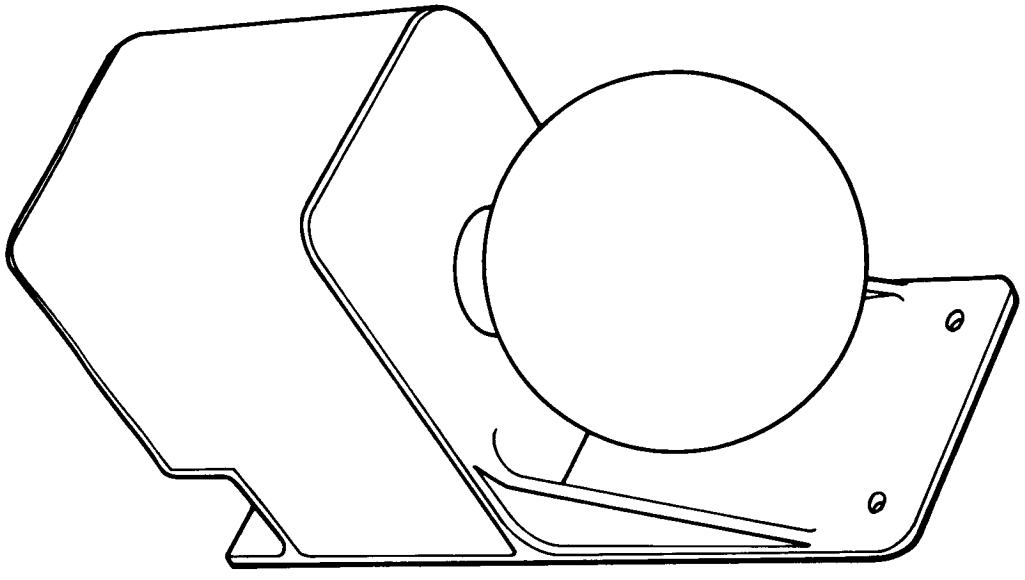

Figure 1. - Type I active ionization chamber.

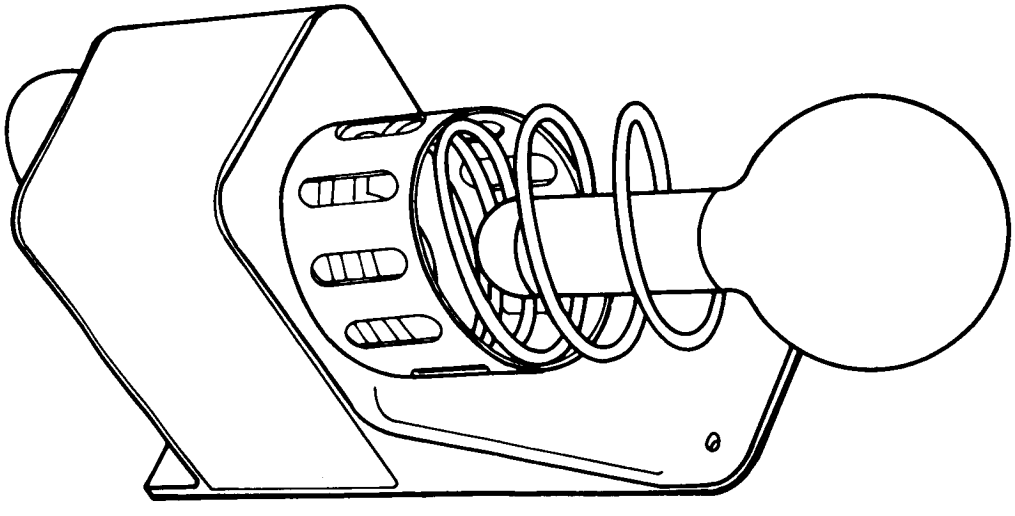

Figure 2. - Type V portable ionization chamber.

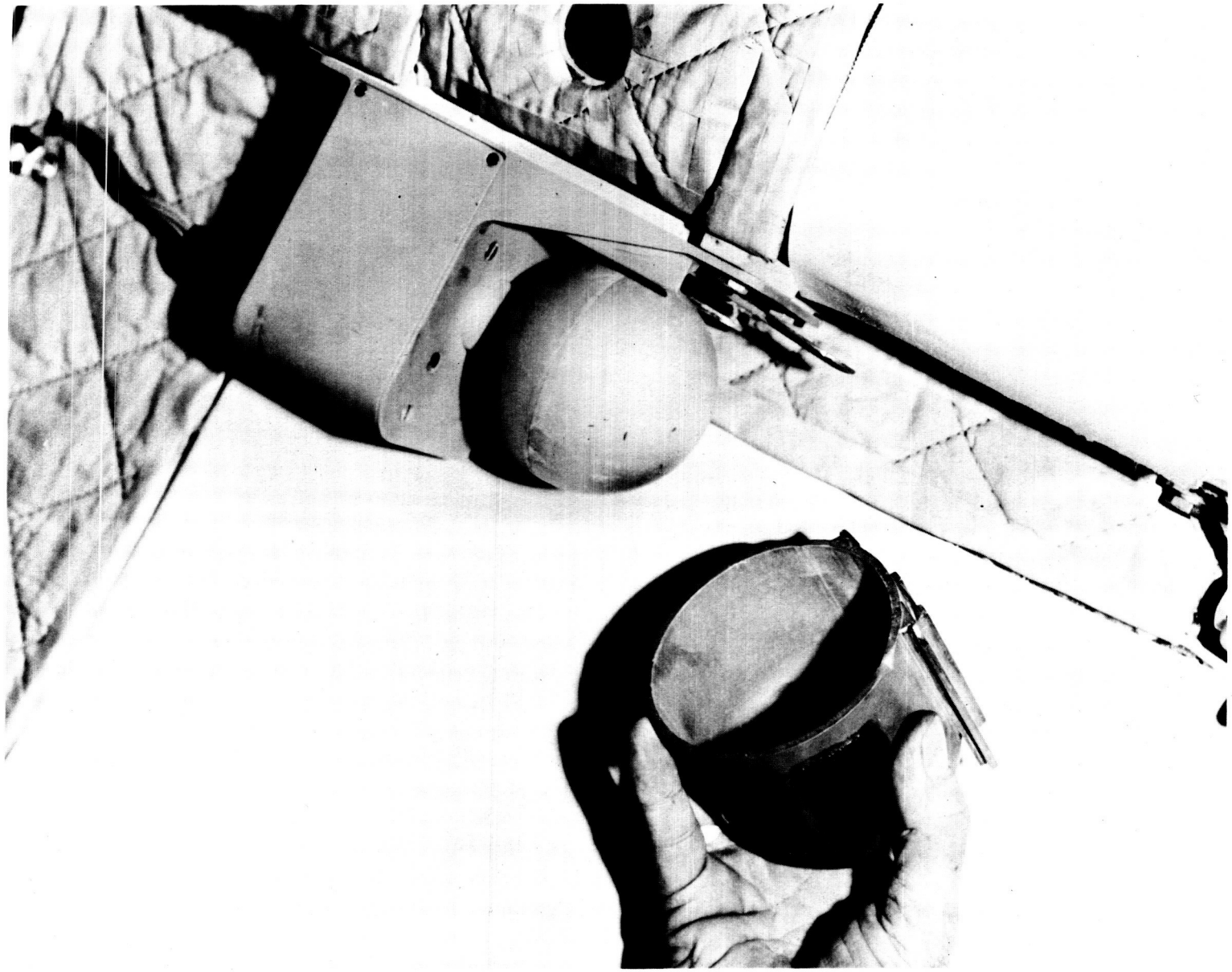

Figure 3. - The Gemini VI fixed active dosimeter and 2.5-g/cm^2 depth-dose shield.

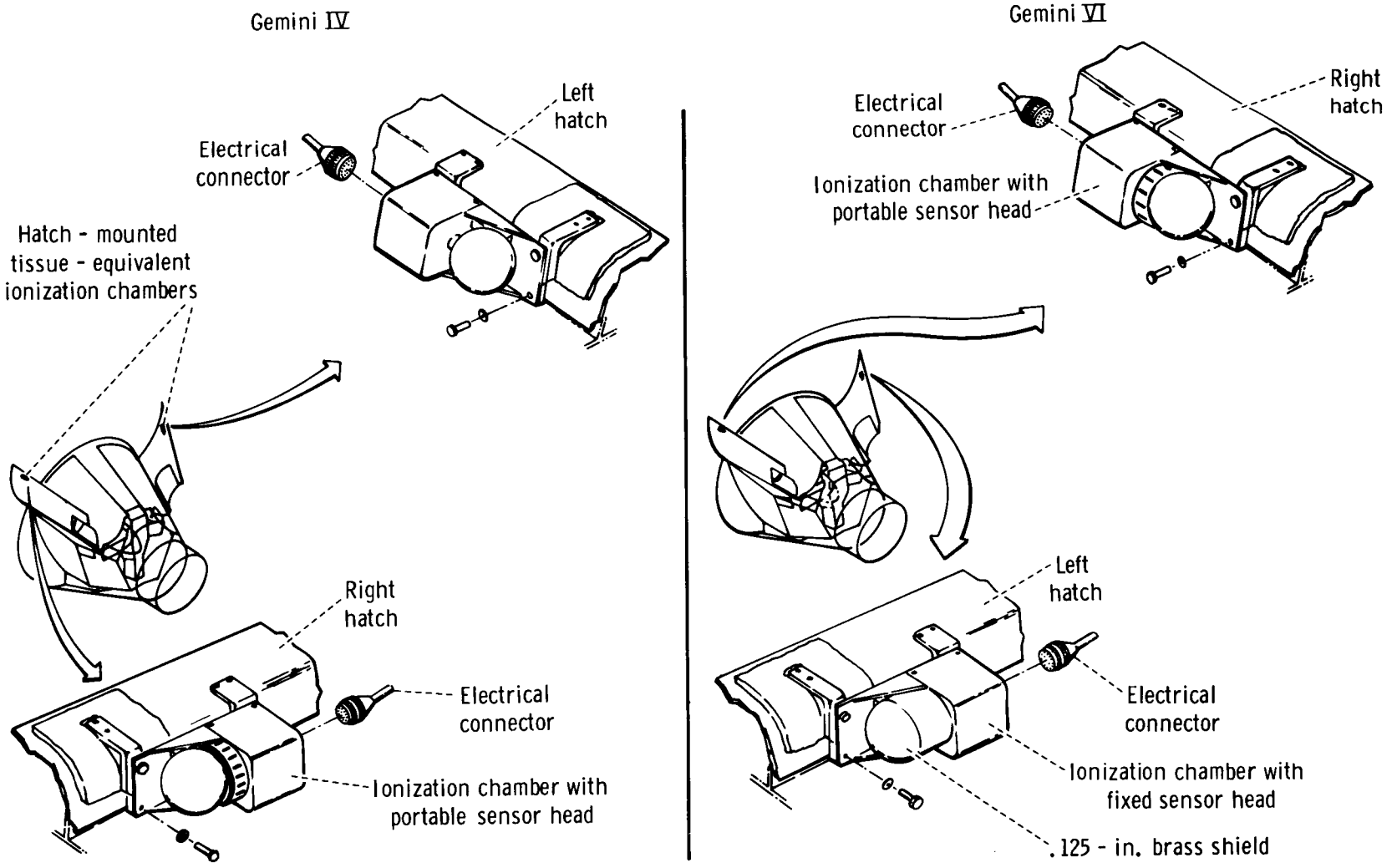

Figure 4. - The Gemini IV and VI spacecraft mounting locations for the portable and fixed ionization chambers.

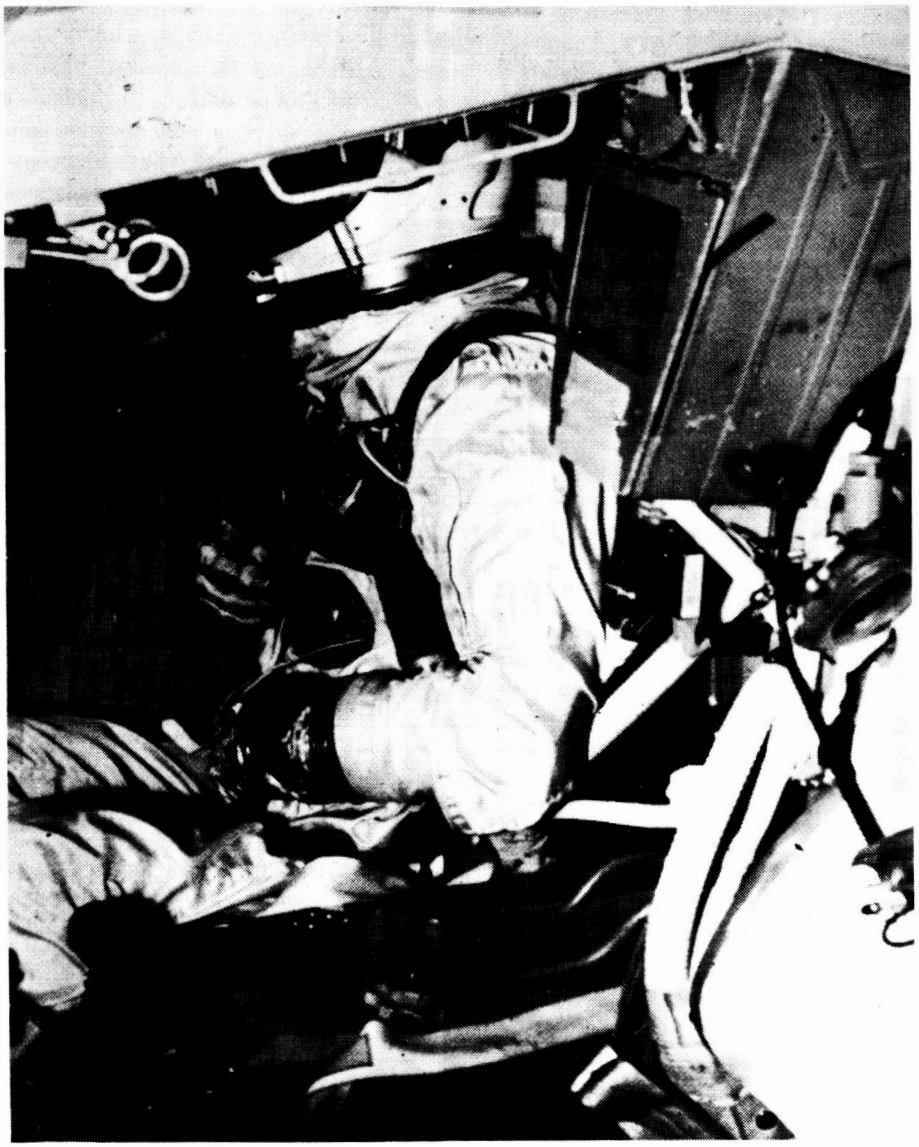

Figure 5. - The portable ionization chamber held against the chest and covered by a glove.

Figure 6. - The portable ionization chamber held in the groin.

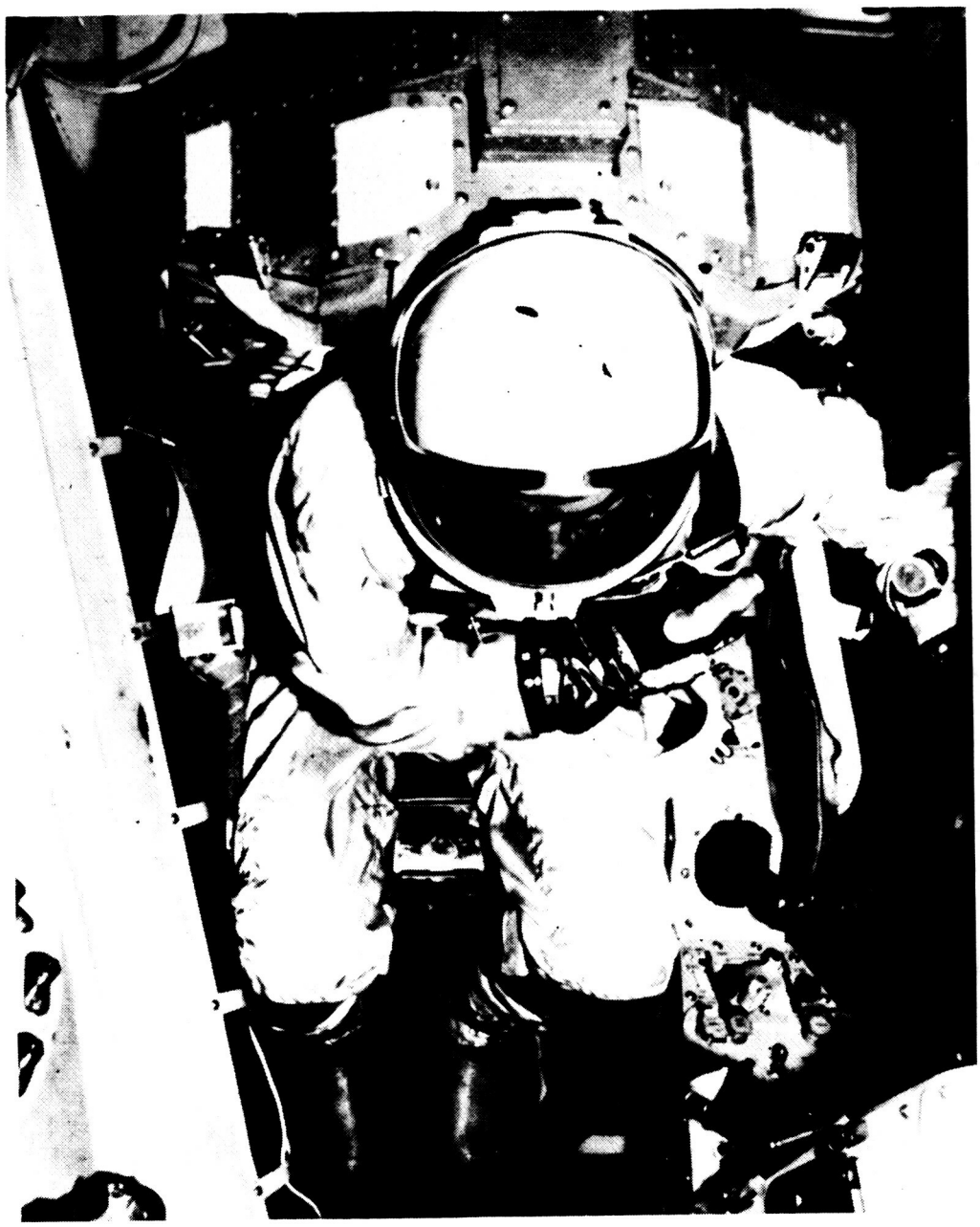

Figure 7. - The portable ionization chamber held under the left armpit.

Figure 8. - The portable ionization chamber held in front of the cabin window.

Figure 9. - The portable ionization chamber centered in front of the instrument panel.

Figure 10. - The portable ionization chamber placed on the floor between the feet of the crewman.

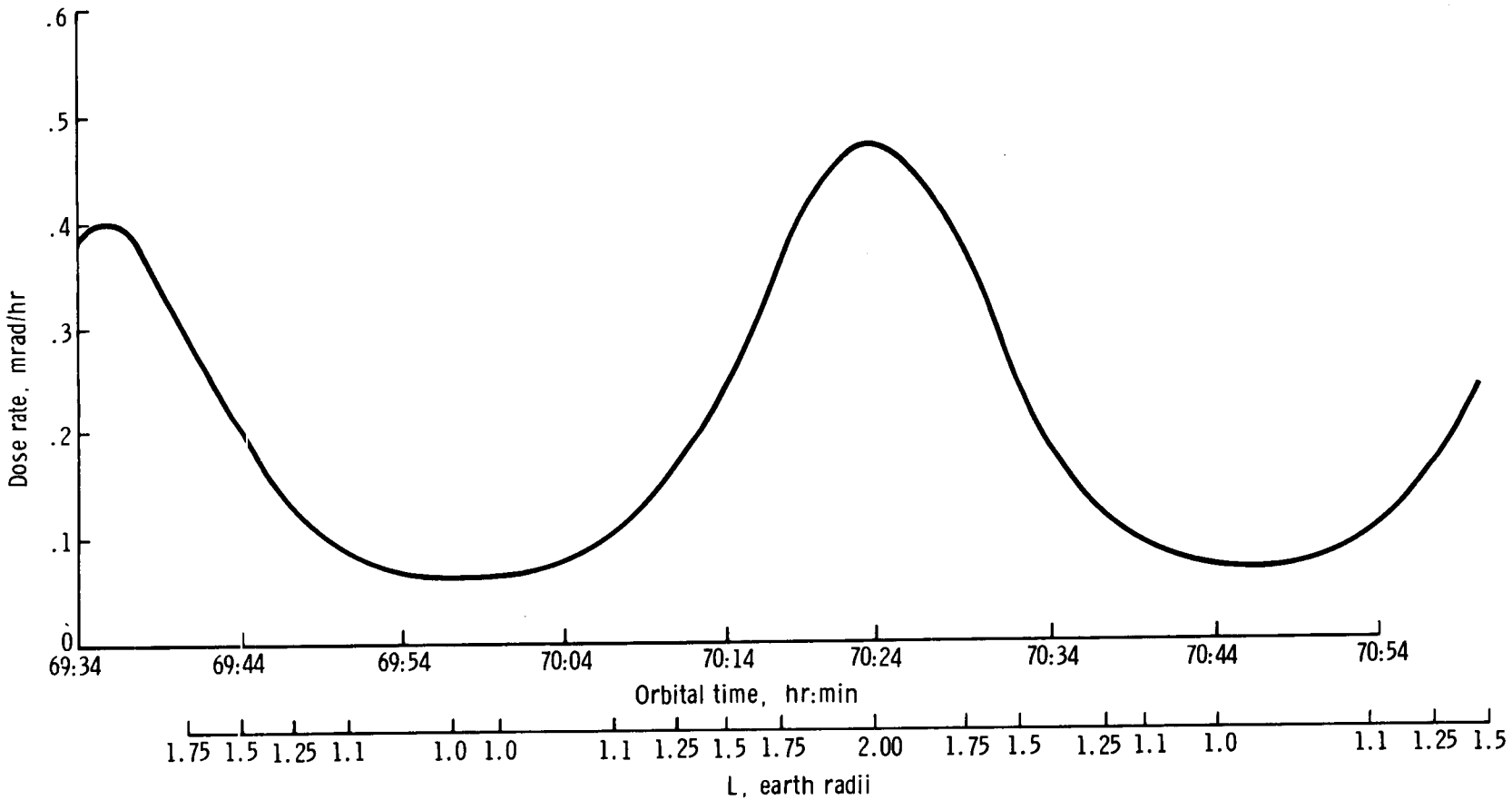

Figure 11. - Cosmic-radiation dose levels plotted as a function of orbital time and L values for revolution 45.

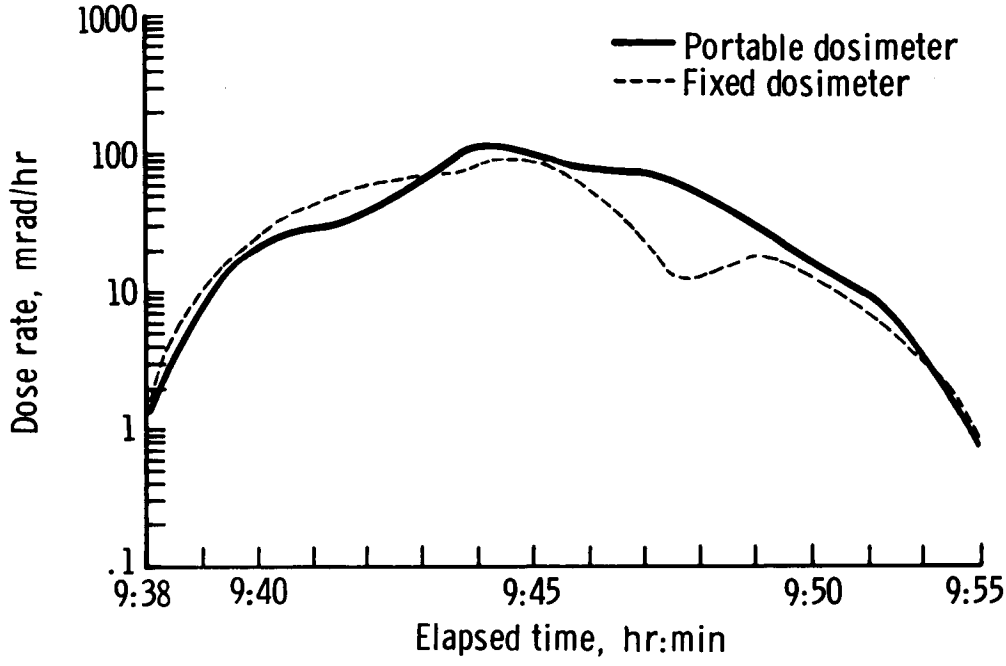

Figure 12. - Instantaneous dose rate measured during revolution 7.

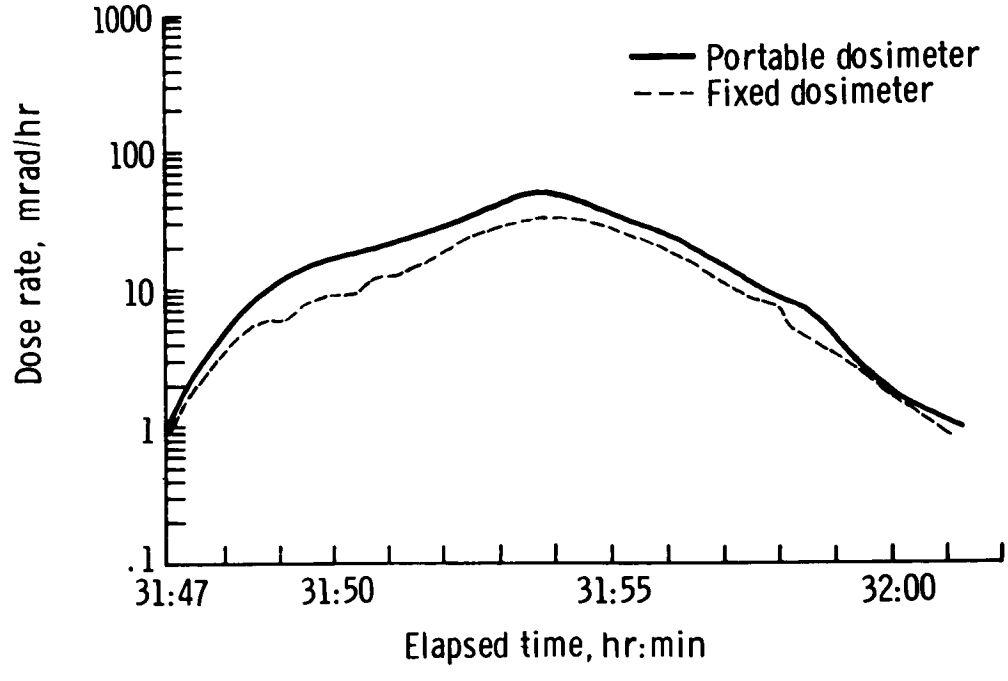

Figure 13. - Instantaneous dose rate measured during revolution 21.

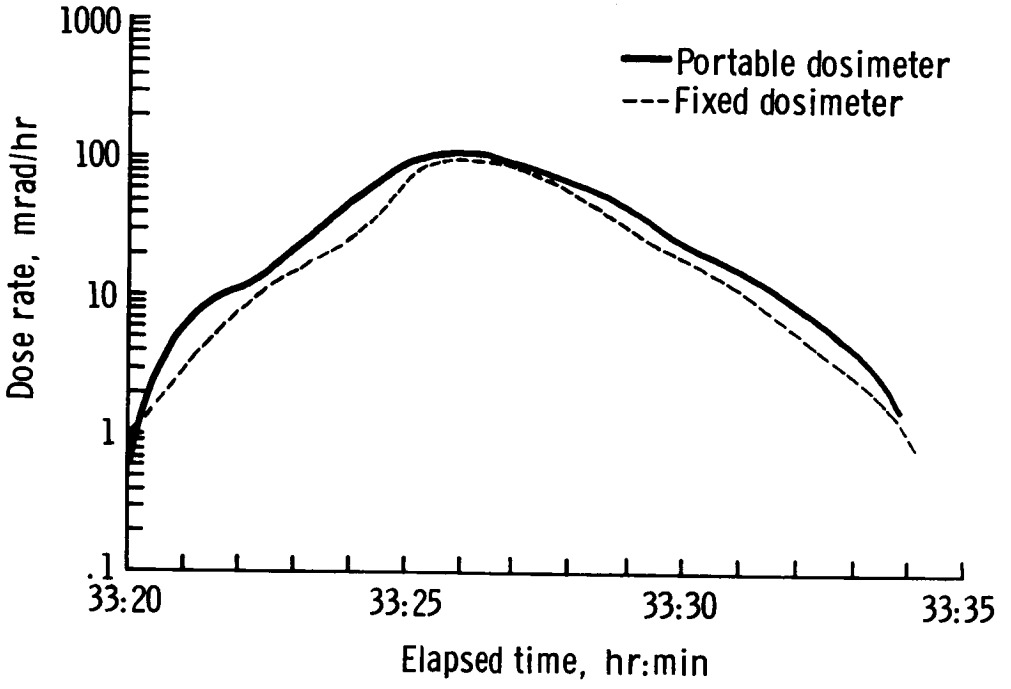

Figure 14. - Instantaneous dose rate measured during revolution 22.

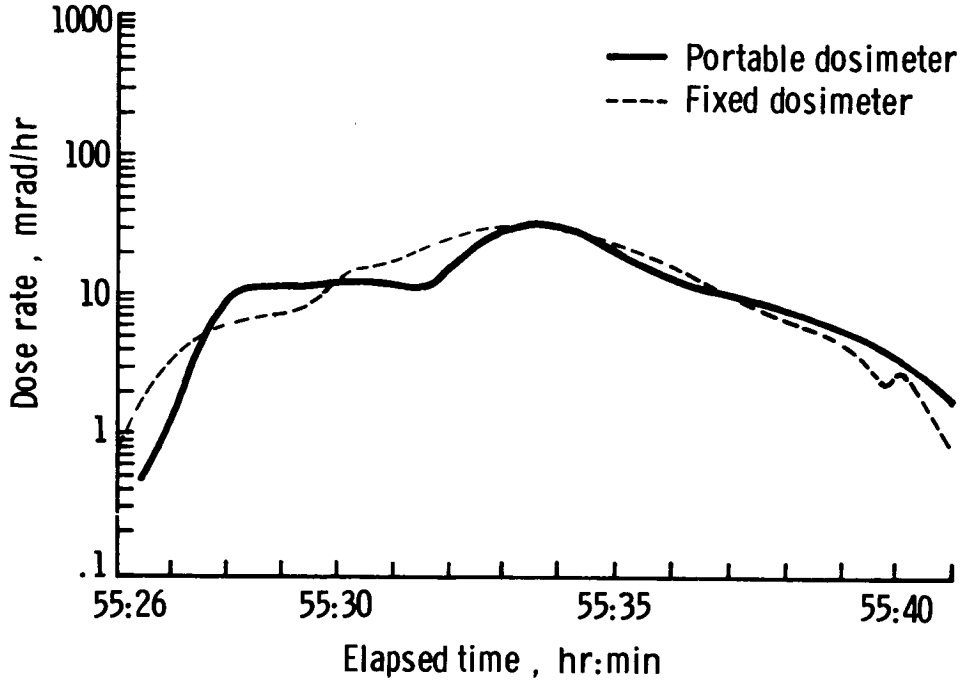

Figure 15. - Instantaneous dose rate measured during revolution 36.

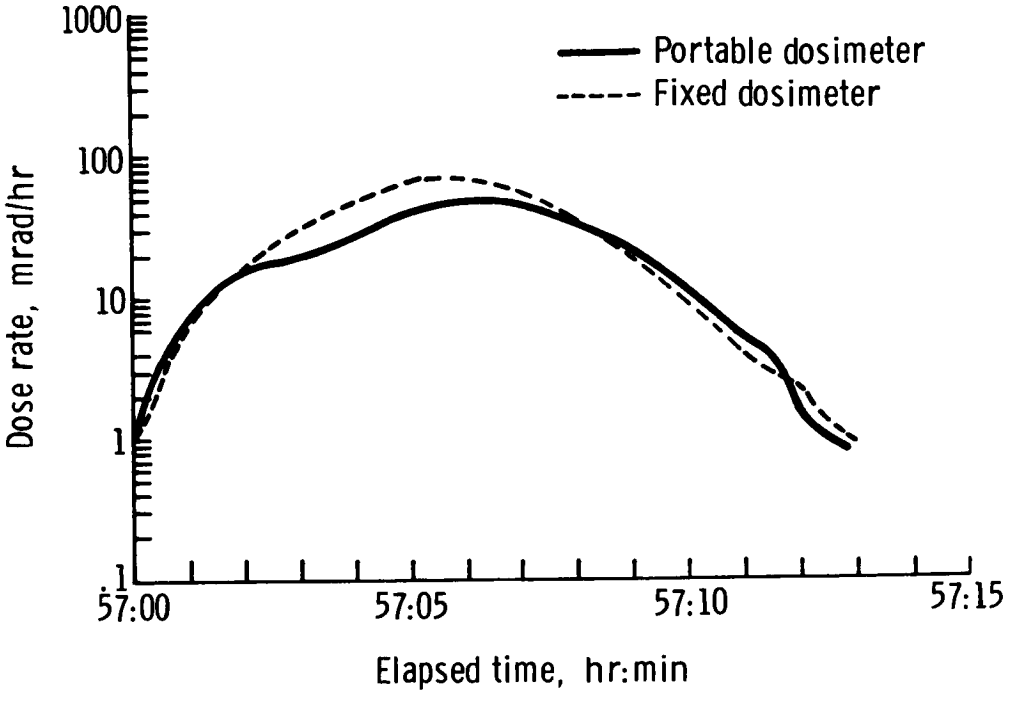

Figure 16. - Instantaneous dose rate measured during revolution 37.

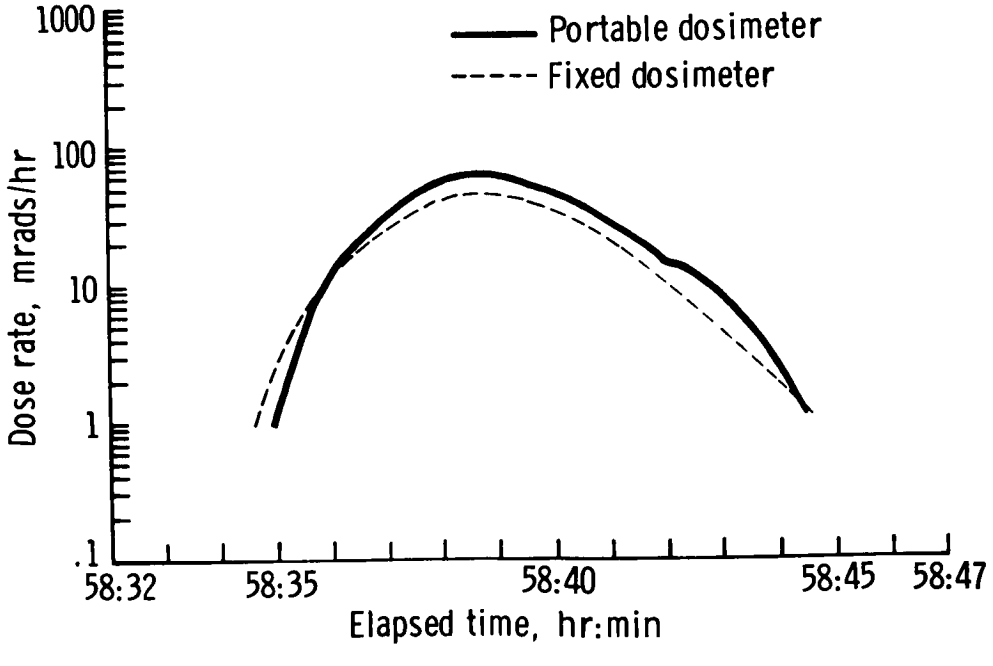

Figure 17. - Instantaneous dose rate measured during revolution 38.

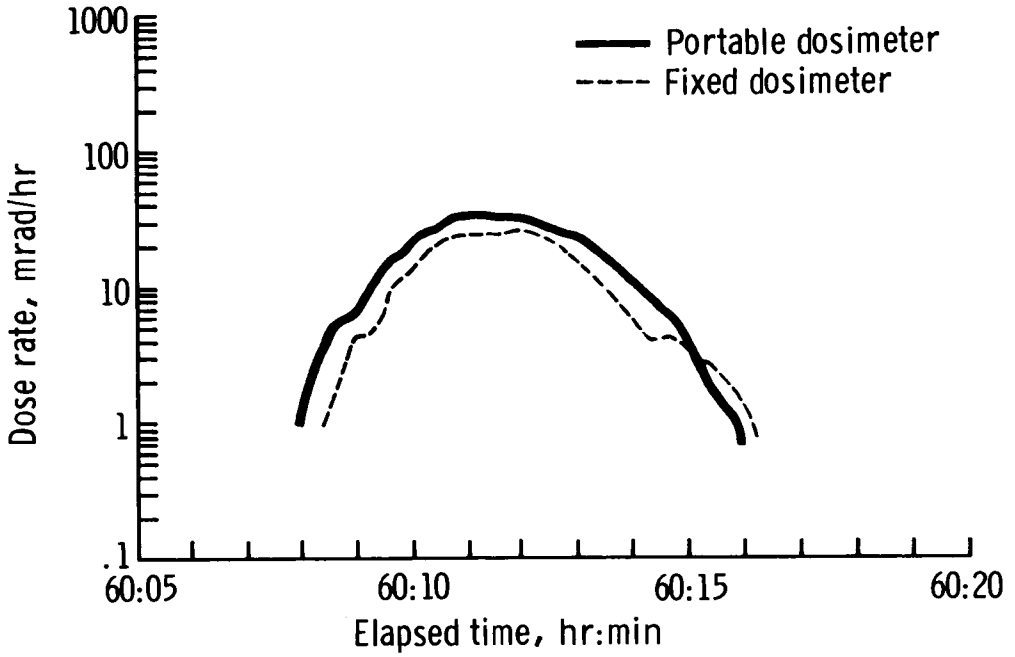

Figure 18.- Instantaneous dose rate measured during revolution 39.

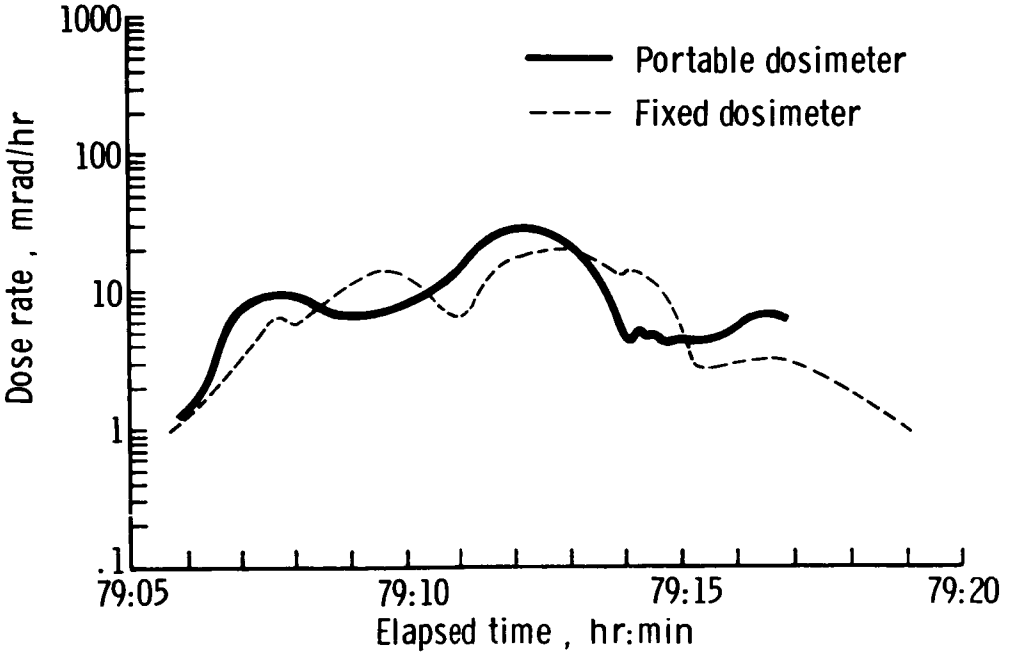

Figure 19.- Instantaneous dose rate measured during revolution 51.

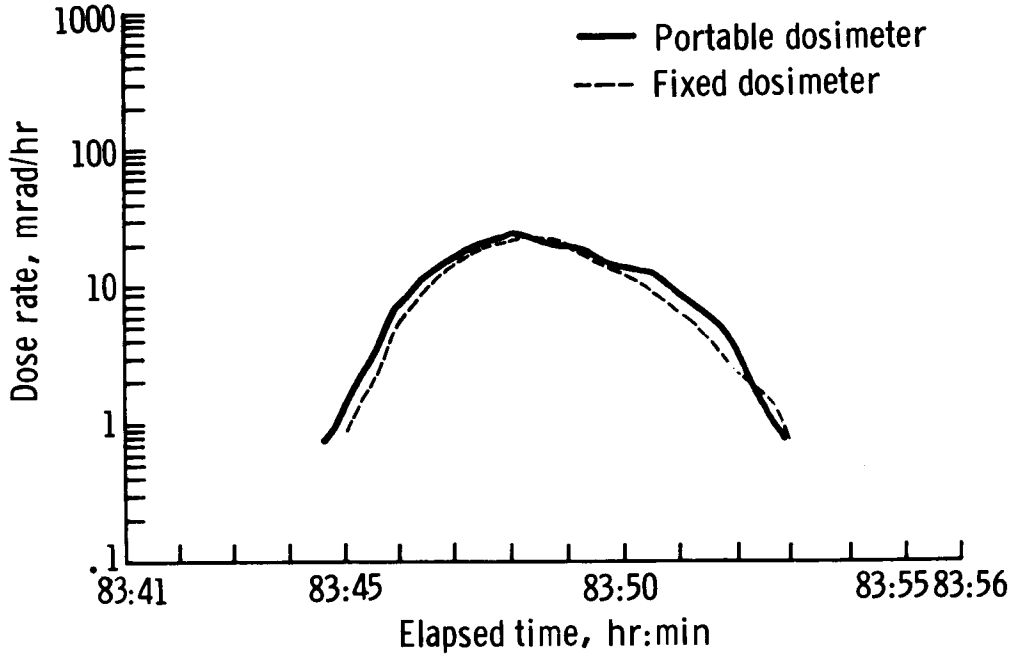

Figure 20. - Instantaneous dose rate measured during revolution 54.

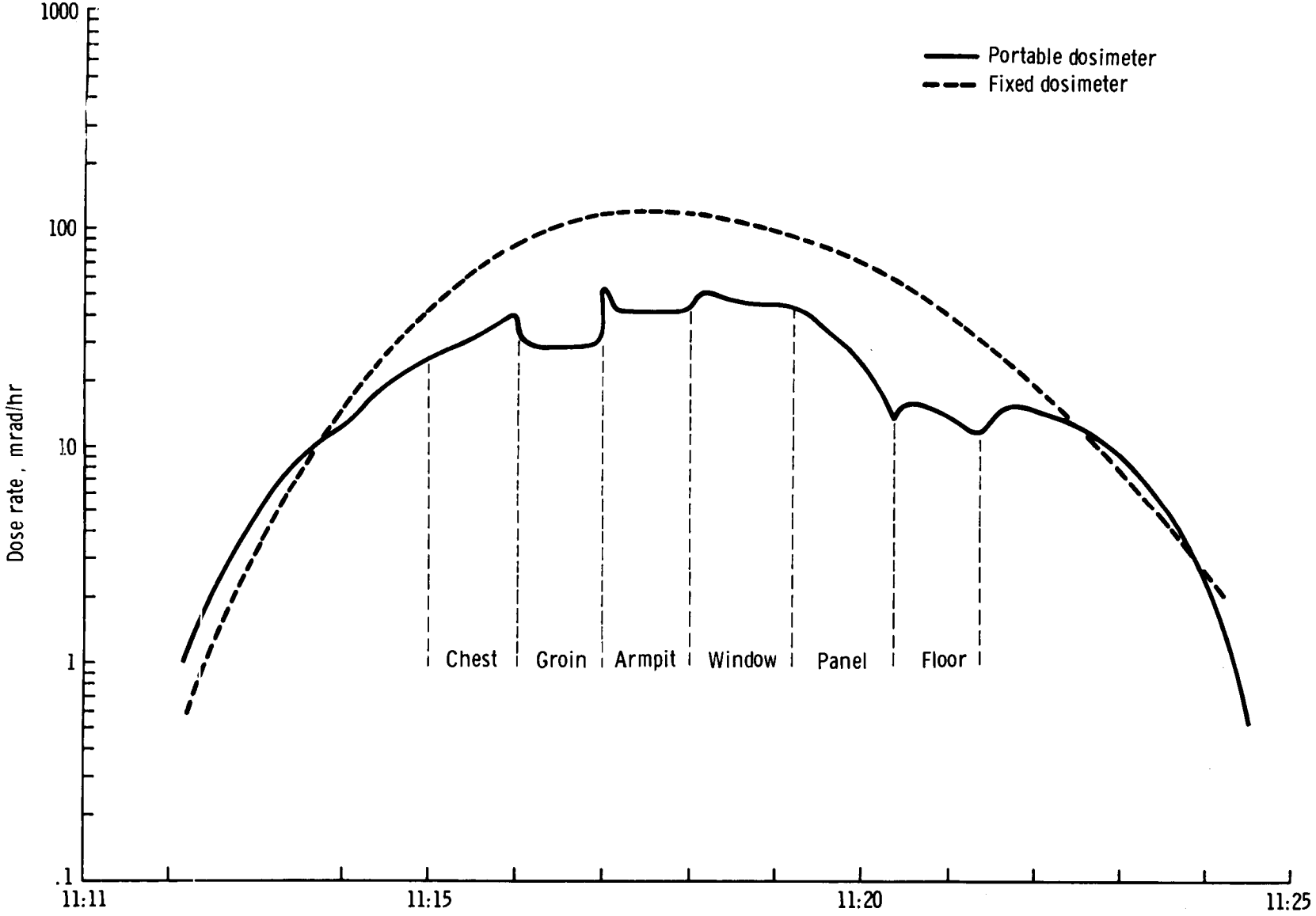

Figure 21. - Results of the radiation survey made during revolution 8.

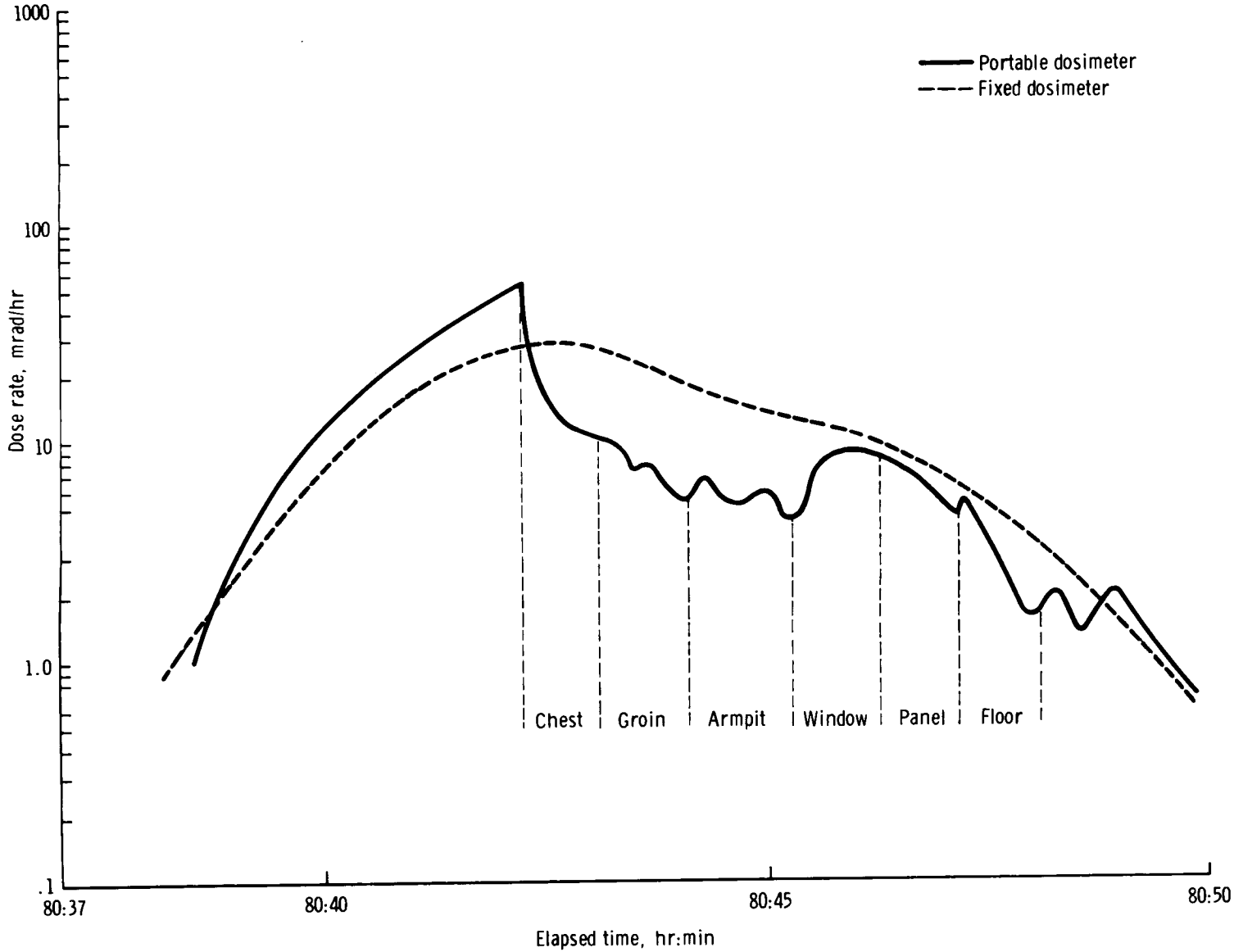

Figure 22. - Results of the radiation survey made during revolution 52.

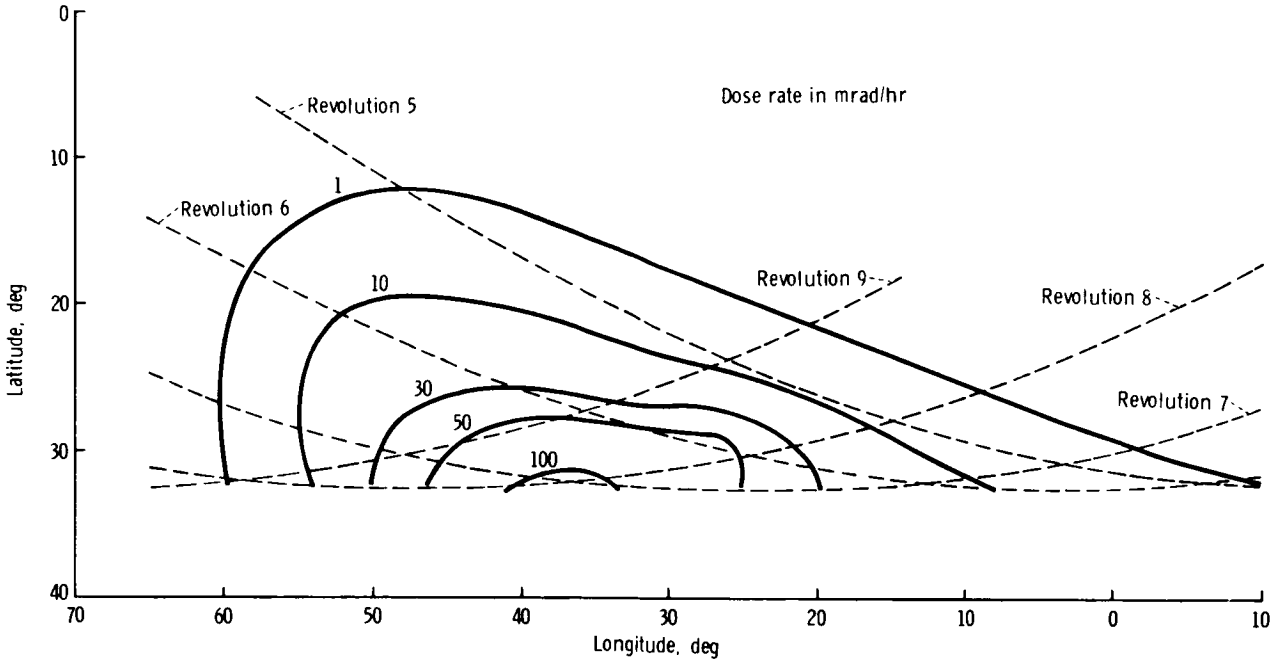

Figure 23. - Isodose contours at 280 kilometers.

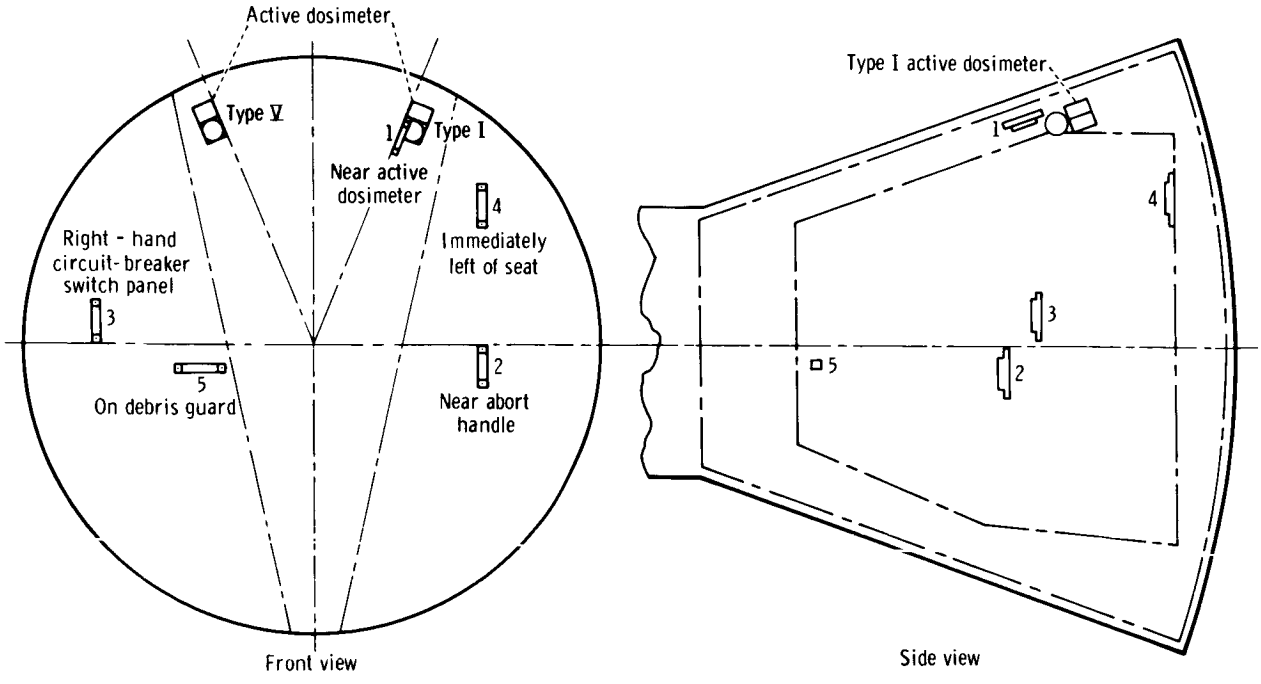

Figure 24. - Passive-dosimeter locations.

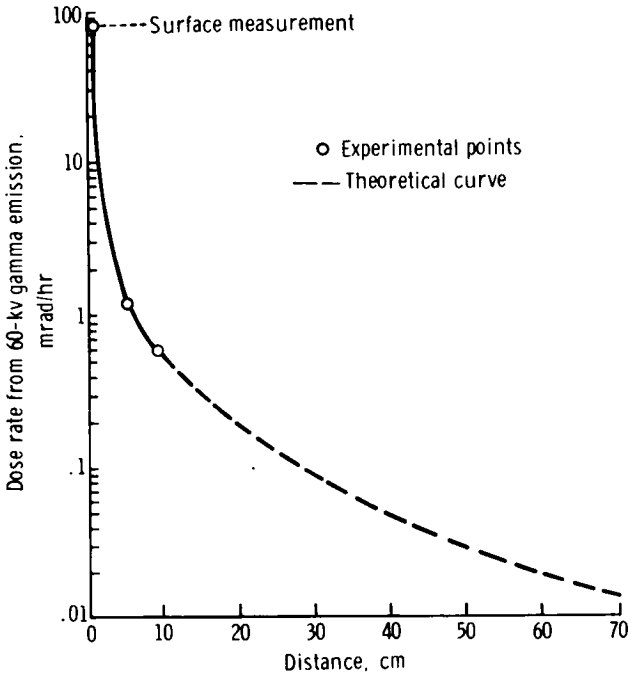

Figure 25. - Distance from the 0.9-millicurie americium source.

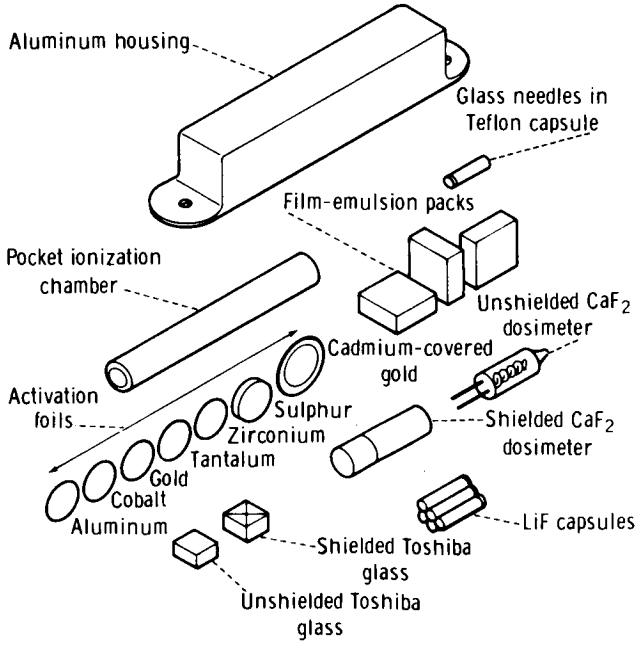

Figure 26. - An exploded view of the passive dosimeter.

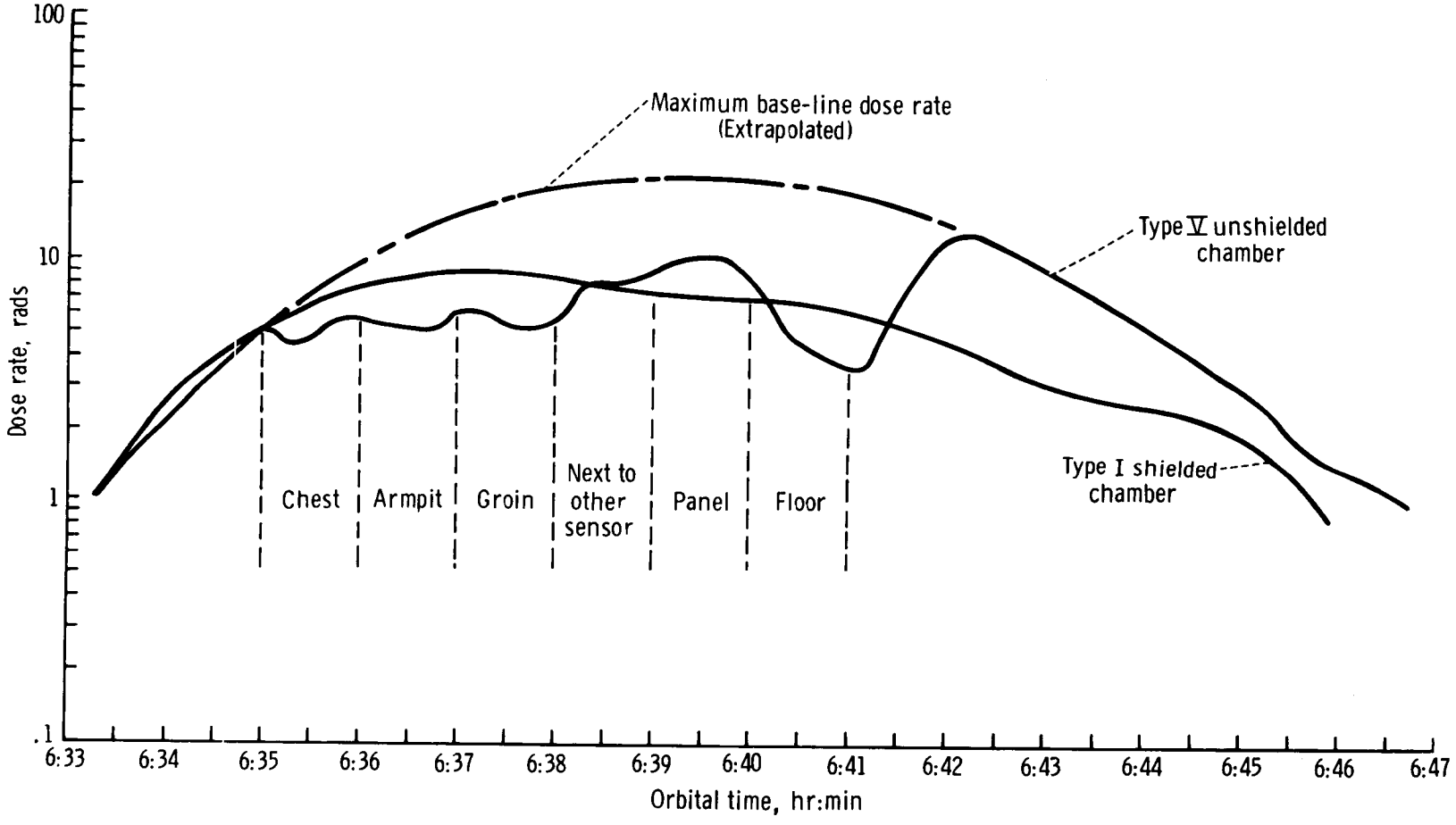

Figure 27. - Gemini VI dose rate and radiation survey; cabin interior, revolution 5.

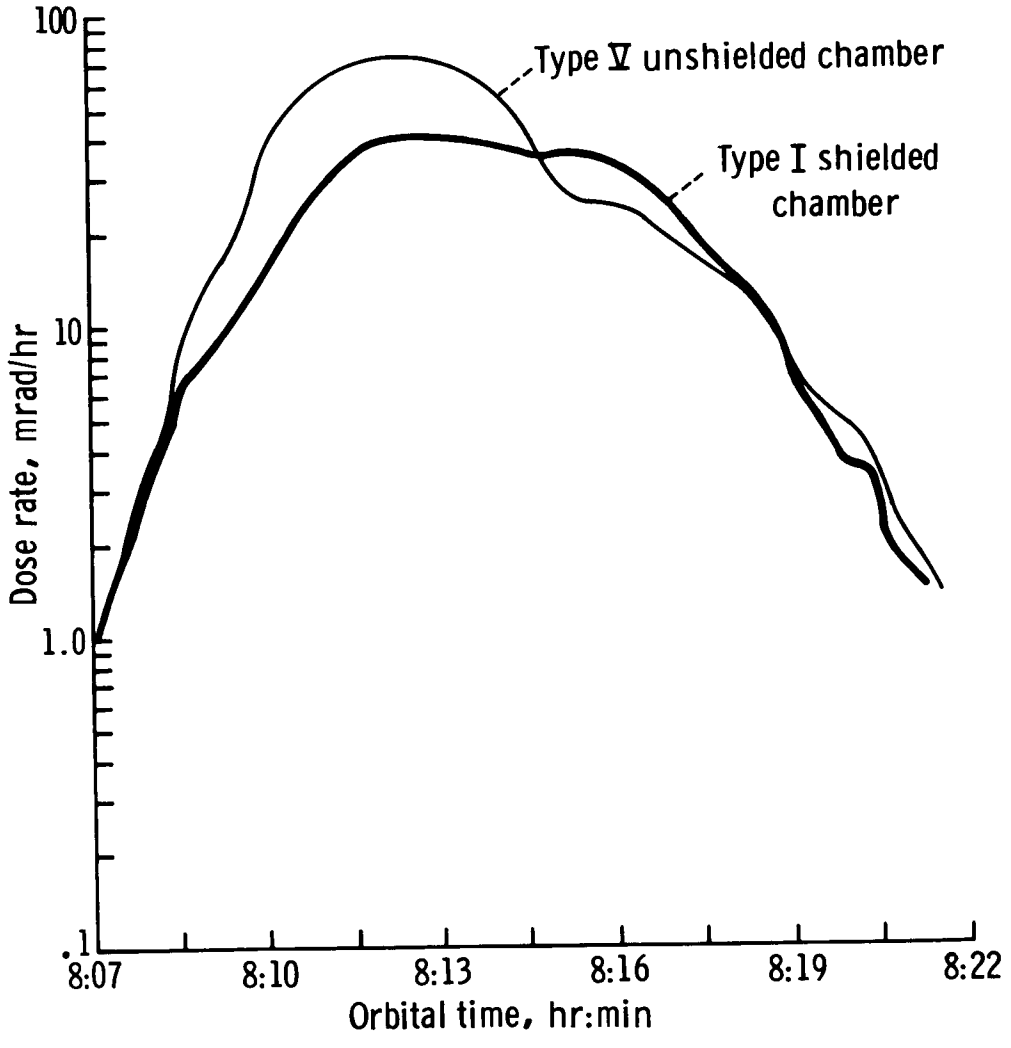

Figure 28. - Gemini VI trapped-particle dose rate; cabin interior, revolution 6.

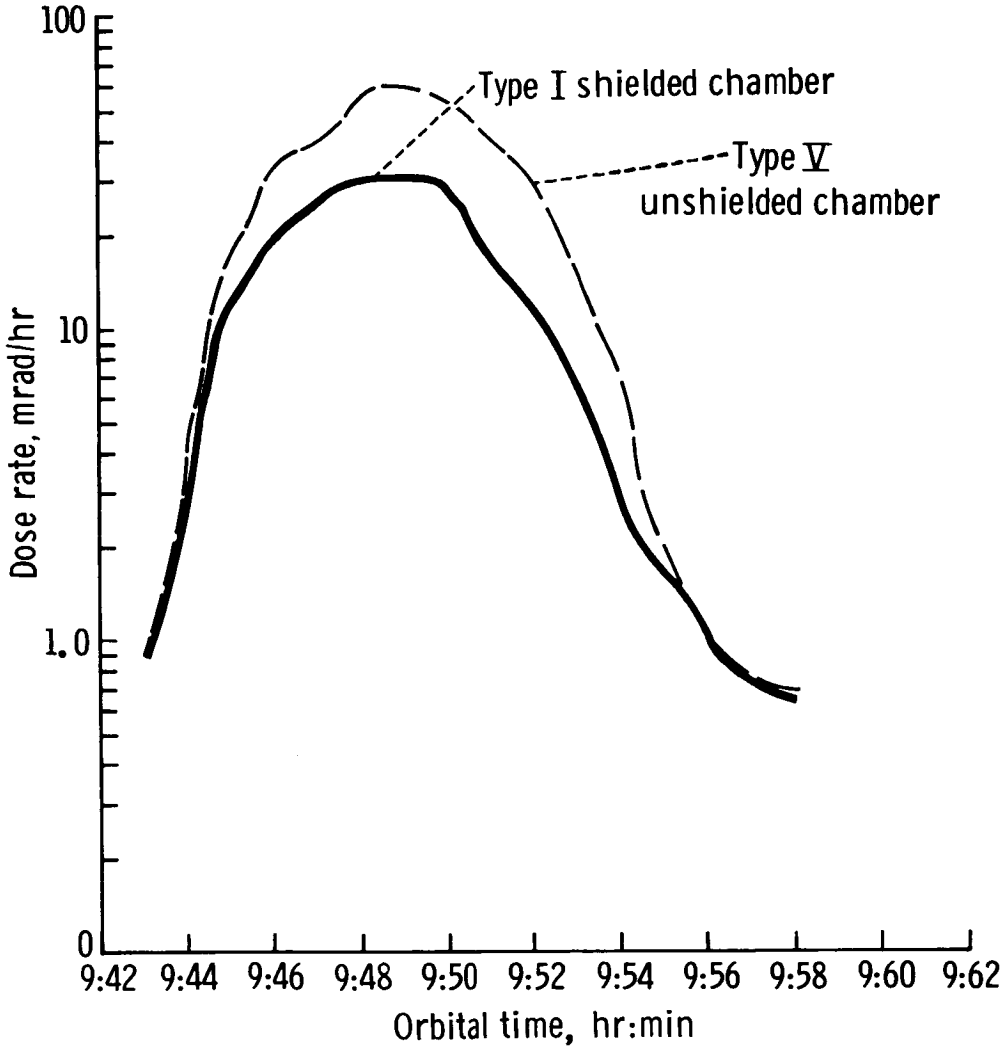

Figure 29. - Gemini VI trapped-particle dose rate; cabin interior, revolution 7.

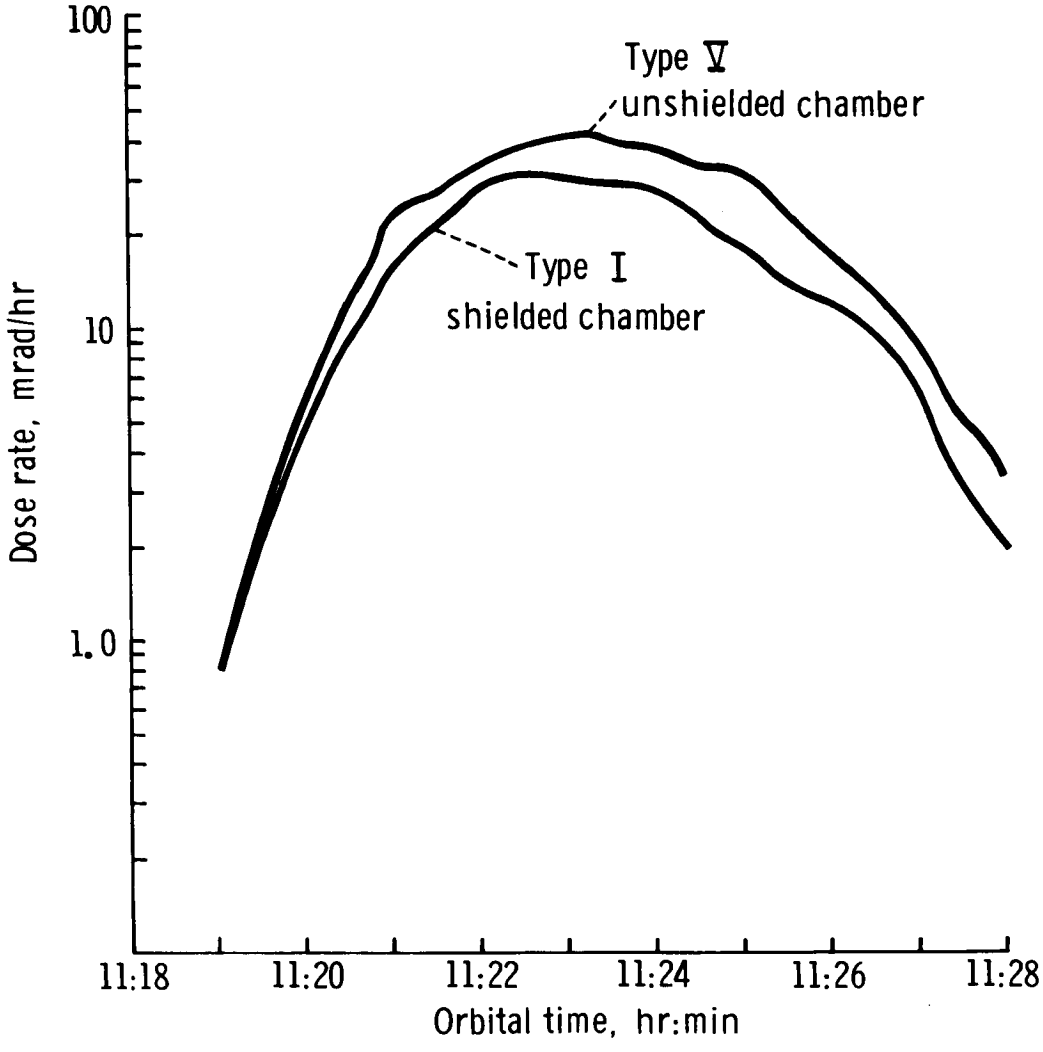

Figure 30. - Gemini VI trapped-particle dose rate; cabin interior, revolution 8.

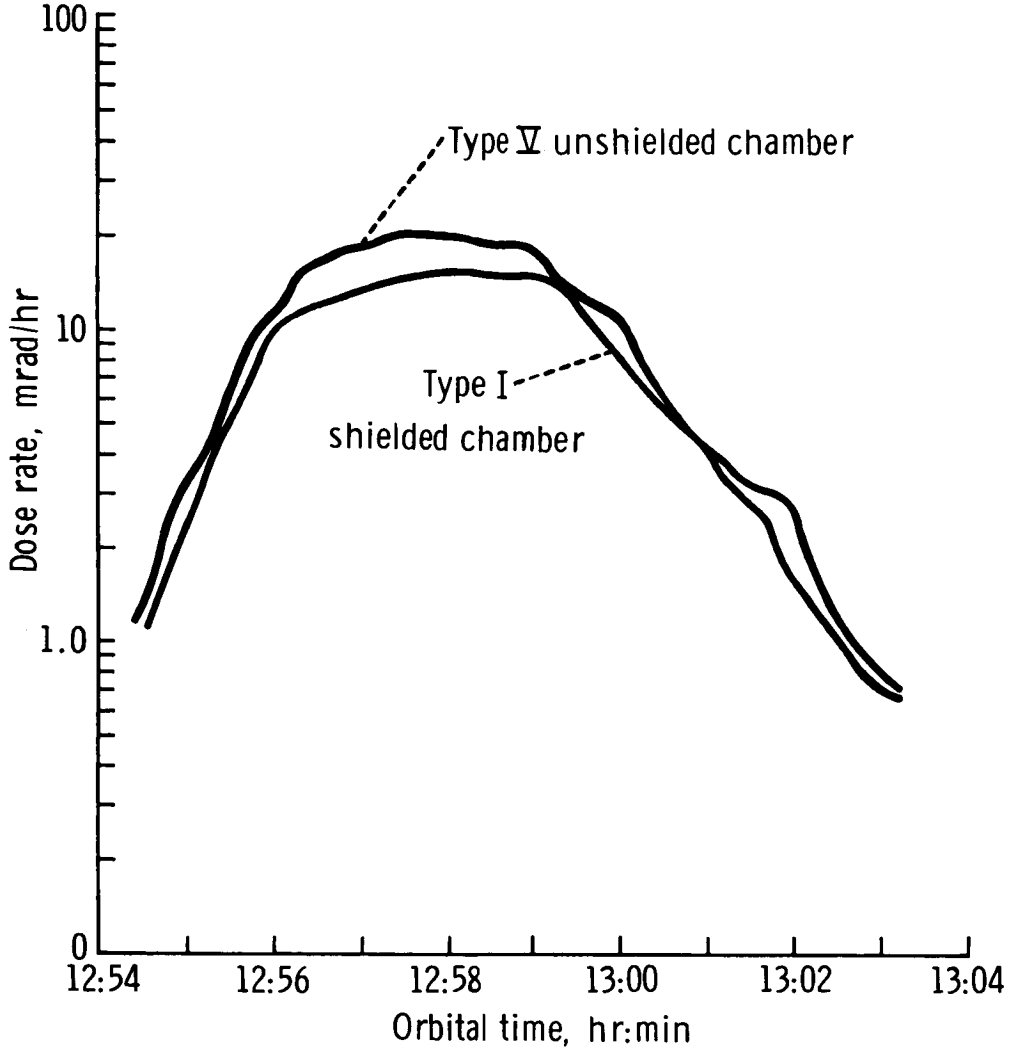

Figure 31. - Gemini VI trapped-particle dose rate; cabin interior, revolution 9.

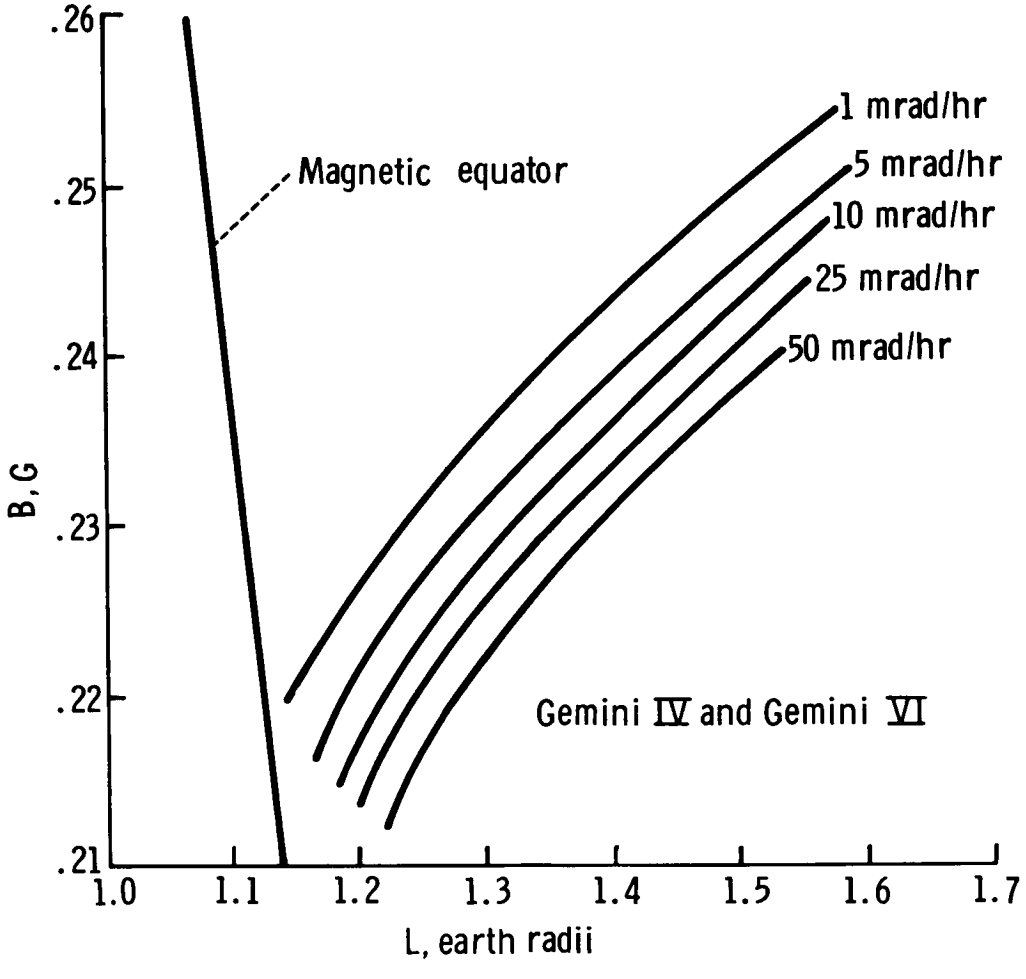

Figure 32. - Isodose rate contours obtained from Gemini IV and VI, plotted in the B, L magnetic-coordinate system.

EXPERIMENTS D004 AND D007

CELESTIAL RADIOMETRY AND SPACE-OBJECT RADIOMETRY

By J. Lovett*

INTRODUCTION

Two interferometer spectrometers and a multichannel spectroradiometer were used as sensing instruments in Experiments D004 and D007, which were performed during the Gemini V and VII missions. The selection of the instruments and of the particular detectors in the instruments was based upon the spectral bands to be investigated in each flight (fig. 1) and upon the nature of the intended measurements. The instrument characteristics (for example, field of view and resolution) were a compromise among optimization for a particular type of measurement, a need for a broad selection of spectral information, and performance and other pertinent characteristics of the spacecraft.

FLIGHT EQUIPMENT

Because the equipment was contained in several units, it will be reviewed by component, and then integrally as an experimental system on board the Gemini spacecraft.

Radiometer

One of the three measuring instruments that were used in the experiments was a multichannel, direct-current spectroradiometer. As shown in a functional diagram of this radiometer (fig. 2), the impinging energy was focused by the collecting optics, mechanically chopped and filtered to obtain the specific bands of interest, and then received by the three detectors. Then, the detector signals were amplified and demodulated. The resultant signals were a function of energy intensity in a given spectral band. The radiometer (fig. 3) parameters for each flight are presented in table I. As a result of a review of the data collection on the Gemini V mission, a decision was made to modify the Gemini VII radiometer to incorporate a more sensitive ultraviolet (uv) photomultiplier tube. An ASCOP 541F-05M tube was installed in place of the

*U. S. Air Force Cambridge Research Laboratories, L. G. Hanscom Field, Bedford, Massachusetts.

IP 28 tube that was flown on the Gemini V mission, and the bolometer detector was eliminated to make room for the larger photomultiplier tube. Thirteen signals were provided from the radiometer on the Gemini V mission; 11 signals were provided on the Gemini VII mission. The signals included detector temperatures, gain, filter-wheel position, and analog signal output from the detectors.

Interferometer Spectrometer

The second sensing instrument was a dual-channel interferometer spectrometer (fig. 4). The interferometer section was patterned after the Michelson interferometer (fig. 5).

The beam splitter split the optical path and directed part of the beam to the movable mirror M_1 and the other part to a fixed mirror M_2. As a result of the optical path changeability, the waves that returned from the mirrors could be in phase (additive) or out of phase to some extent and could have a canceling effect. The total effect was to produce cyclic reinforcement or interference with the wave amplitude at the detector at any given frequency. The frequency of this alternate cancellation and reinforcement at the detector was a function of the particular spectral energy wavelength λ, the optical retardation B of the mirror, and the time required to move the mirror (scan time) T. Thus,

$$F\lambda = \frac{B}{\lambda T}$$

The detector produced an alternating-current signal, which was the sum of the alternating-current signals that corresponded to all the wavelengths from the source. The amplitudes of the signals varied directly with the source brightness at each wavelength. The output of the interferometer was a complex waveform called an interferogram, which was the Fourier transform of the incident-radiation frequencies (fig. 6(a)). This transform was reduced to a plot of wavelength compared with intensity by the use of the inverse transform of the interferogram (fig. 6(b)). An interferogram made with the interferometer spectrometer used in Experiments D004 and D007 is shown in figure 6(c), and a measurement of the California coast during the Gemini V mission is shown in figure 6(d).

The interferometer spectrometer (referred to nontechnically as the "uncooled" or "IR" spectrometer) contained a lead sulfide detector and a bolometer detector. Thus, information correlative to that of the spectroradiometer was collated. The parameters of the interferometer spectrometer are listed in table II. Data output from the instrument included signals from the two detectors, gain settings, detector temperatures, and automatic calibration-source data. Lead sulfide signal data were processed on a data channel-sharing basis with the detector output from the cryogenic spectrometer.

Cryogenic Interferometer Spectrometer

The cryogenic interferometer spectrometer was similar in operation to the IR spectrometer, although dissimilar in appearance (fig. 7). The principal difference was that the highly sensitive detector had to be cooled cryogenically to make measurements in the region of interest (8 to 12 microns). Cooling was accomplished by the immersion of a well containing the detector, the optics, and some of the electronics in liquid neon. The cryogenic subsystem was an open-cycle, subcritical, cryogenic, cooling system, that maintained the instrument well at -397° F for approximately 14 hours. An X-ray view of the cryogenic tank and instrument well is given in figure 8, and the parameters for the cryogenic instrument are listed in table III.

Electronics Unit

The electronics unit used in conjunction with the three sensing devices contained the circuits necessary for the experiments. The circuitry included an electronic commutator, filter motor logic, variable-control oscillators, a mixer amplifier, a clock-pulse generator, and other secondary electronic circuitry.

Recorder Transport and Electronics

The tape recorder used in Experiments D004 and D007 was separated into two modules: the tape transport and the recorder electronics. This separation was made so that the recorder would fit into the available space on the entry vehicle. The recorder capability was 56 minutes of tape for three channels of data. The recorder was not capable of dump, and data were stored and were retrieved with the spacecraft.

Frequency-Modulation Transmitter and Antenna

In parallel with the recorder, the transmitter transmitted three channels of real-time frequency-modulated (FM) data to selected ground-based stations located around the earth. The transmitter, which operated through an antenna extended from the pilot side of the spacecraft, transmitted 2 watts on an assigned ultrahigh frequency.

Control Panel

Most of the switches associated with the experiment were located on the main console of the pilot (fig. 9). Additional functions were performed by a meter and by sequencing switches.

Experiment System

The experiment system, which consisted of the components previously mentioned, was mounted in the Gemini V and VII spacecraft (fig. 10). The radiometer and spectrometers were mounted on swingout arms in the Gemini retroadapter section. After

the spacecraft was in orbit, doors in the adapter were opened pyrotechnically, and the three sensing units swung through the openings into boresight alinement with the spacecraft optical sight. After the sensing units were erected, the spacecraft was pointed at the desired region for measurement. In figure 11, the Gemini VII spacecraft is shown with the instruments extended. The Gemini V experiment equipment was similar in appearance. Data from the radiometer were telemetered through the spacecraft pulse code modulation (PCM) system. Data from the spectrometers were telemetered through the transmitter or routed to the recorder; or both methods were used when desired.

MISSION PLAN

The desired objectives for the measurements taken on Experiments D004 and D007 included the following.

Objective	Range, microns
Earth backgrounds	0.2 to 12
Sky backgrounds	.2 to 12
Sky-to-horizon spectral calibrations	8 to 12
Rocket exhaust plumes	.2 to 3
Natural space phenomena (stars, moon, sun)	.2 to 12
Manmade objects in space	.2 to 12
Weather phenomena (clouds, storms, lightning)	.2 to 10
Equatorial nadir-to-horizon spectral calibrations	8 to 10

Because the lifetime of the cryogenic neon in the cooled spectrometer was limited to 14 hours (5 hours of which were spent on the launch pad), the measurements that necessitated the use of the cooled spectrometer were planned for the first few revolutions. The rocket-plume measurements were planned for those revolutions on which the spacecraft was closest to the firing site, yet for as early or late in the day as was feasible to minimize background radiation. Because calibration of the detectors might be affected, sun measurement was planned to be the final measurement. The remainder of the measurements, those which required real-time updating, were interspersed throughout the flight.

RESULTS

Gemini V Mission

Approximately 3 hours 10 minutes of data were collected during the Gemini V mission. Twenty-one separate measurements, on 30 subjects, were made. The PCM and FM transmitted data resulted in 125 000 feet of magnetic tape. Data processing required a great amount of time. The interferometer data had to be run through a wave analyzer or a high-speed computer. The wave analyzer integrated 35 interferograms and gave the results, in the form of Fourier coefficients, in approximately 30 minutes. The computer required approximately 2 hours to perform the transform on one interferogram. More than 10 000 interferograms were made during the Gemini V mission. The PCM data were reduced in terms of filter settings and gain; then, calibration coefficients were applied. Both PCM and FM data were correlated with crewman comments and photography, where applicable. The following is a list of the measurements made during the Gemini V mission.

Revolution	Location	Measurement
1	Carnarvon, Australia	Operational readiness check of cryogenic spectrometer
2	Africa-Australia	Rendezvous evaluation pod (REP) measurements during darkness
14	Australia	Night water and night land measurements
16	Africa	Mountains and land with vegetation
16	Malagasy	Night water and night land measurements
16	Australia	Star measurement, Vega
16	Australia	Equipment alinement check
17	Australia	Moon irradiance measurement
31	Africa	Cloud-blanket sweep, nadir to horizon
31/32	Florida	Land with vegetation
45	Australia	Night void-sky measurement
47	Australia	Zodiacal light

Revolution	Location	Measurement
47	Australia	Star measurement, Deneb
47	California	Minuteman missile launch
51	Hawaii	Island measurement
61	New Mexico	Rocket-sled firing
62	California	Minuteman missile launch
74	Africa	Water, land, mountains, desert
88	Africa	Desert
89	Africa	Mountains
103	Australia	Horizon-to-nadir scan

The equipment was erected and verified operationally over Carnarvon, Australia, during the first revolution. During the second revolution, the REP was ejected, and measurements were made of its separation from the spacecraft during the spacecraft darkness period. The primary instrument for this measurement was the cryogenic spectrometer. The cover on the spectrometer was jettisoned when the REP was approximately 2500 feet from Gemini V, and measurements were made during the remainder of the darkness period. After 15 minutes of operation, the filter wheel on the radiometer stopped and remained on filter settings of 4000 angstroms, 2.2 microns, and 4.3 microns for the remainder of the flight. Because the interferometers still functioned satisfactorily, the restriction in radiometer data was not of major concern. The main loss of data was in the uv region, not covered by the spectrometers, where only the 4000-angstrom information was available. In playing the onboard recorder after its retrieval, it was discovered that no REP measurement data were recorded on the tape. This limited the information from the cryogenic spectrometer to the FM data received during the pass over Carnarvon. A review of the interferograms made at Carnarvon was indicative that the signal was significantly greater than the noise level. Attempts are being made to separate the background signal and spacecraft radiance from the signal of the REP. This task is made more difficult by the lack of data from the onboard recorder. Because of the date of the Gemini V launch, the moon measurements had to be made on a partially illuminated moon. Radiometer data from this measurement are presented in figures 12(a) and 12(b).

Quick-look information on the 4000-angstrom radiometer data on Vega and Deneb was excellent. The values on that spectral band were slightly higher than those predicted theoretically. For example, the value for Vega was 1.2×10^{-11} W/cm^2/μ at 4000 angstroms. An example of the IR-spectrometer data is shown in figure 13. The return at 1.88 microns on the California land background also is shown in figure 13.

Gemini VII Mission

The experiment results from the Gemini V mission did have some effect on the experiment on the Gemini VII mission. Because there were only 4 months between the two missions, there was little time for data-evaluation inputs to use for design-modification purposes. One modification, as has been mentioned, was made to the radiometer. Another modification, a switch guard on the recorder switch, was added to the instrument panel. Otherwise, the experiment system was identical for the spacecraft on both missions. The measurements made on the Gemini VII mission were affected by the data gathered on the Gemini V mission. Certain measurements were repeated when information in addition to the Gemini V data was desired. New measurements were added, based on the capability demonstrated by the crewmen and equipment on the Gemini V mission. Data gathered on the Gemini VII mission totaled 3 hours 11 minutes, which was almost the same as the amount gathered on the Gemini V mission. There were 36 separate measurements made of 42 designated subjects. The following is a list of the measurements made during the Gemini VII mission.

Revolution	Location	Measurement
1	Africa-Malagasy	Launch-vehicle measurement and cooled-spectrometer alinement check
1	Malagasy	Launch-vehicle background measurement
1	Malagasy-Australia	Launch-vehicle measurement
2	Ascension	Void-space measurement
2	Ascension	Star measurement (Rigel) with cryogenic spectrometer
2	Ascension	Launch-vehicle measurement
2	South Atlantic	Star measurement (Sirius) with cryogenic spectrometer
2	Malagasy	Night-sky/earth-horizon calibration sweep with cooled spectrometer
6	Malagasy	Cryogenic-lifetime check
6	Hawaii	Cryogenic-lifetime check
7	Hawaii	Cryogenic-lifetime check
8	Ascension	Cryogenic-lifetime check

Revolution	Location	Measurement
15	Malagasy	Radiometer and IR-spectrometer alinement check on nearly full moon
30	Malagasy	Star measurements (Betelgeuse and Rigel) without cryogenic instrument
31	Florida	Polaris launch
32	Ascension	Milky way
32	North America	Earth background; coastal, mountains, desert, land with vegetation
45	North America	Earth background; water, mountains, plains, coastal regions correlated with IR color-film photographs
49	Malagasy	Night airglow
49	Malagasy	Large fire on earth at night
59	Malagasy	Full-moon measurement
59	Australia	Night land, water, cloud reflectance with full moon
59	Australia	Lightning at night
74	Africa	Cloud-blanket sweep with camera correlation
75	Africa	Lightning at night
76	Ascension	Horizon-to-nadir scan
88	Africa	Desert
89	Malagasy	Celestial measurement (Venus)
104	Australia	Night land and night water
117/118	Florida	Gemini VI abort
148	New Mexico	Rocket-sled firing
149	Pacific Ocean	Night measurement of Minuteman entry

Revolution	Location	Measurement
161/162	Florida	Gemini VI (climb to orbit)
166	Hawaii	Gemini VI (stationkeeping)
169	South America	Gemini VI (separation burn)
193	Texas	Sun measurement

Nineteen minutes after Gemini VII lift-off, the sensors were erected and the equipment was turned on. At sunset, an 8-foot-per-second separation burn was made away from the launch vehicle, and measurements on the launch vehicle were begun. Cryogenic-spectrometer measurements were made for the remainder of the night cycle as the spacecraft separated from the launch vehicle. Periodically, launch-vehicle background measurements were made; and once, the launch vehicle was measured against a moon background. During the second revolution, cryogenic-spectrometer measurements were performed on void space, on the launch vehicle, and on the stars Rigel and Sirius. At the conclusion of the measurement on Sirius, a slow pitch-down maneuver was made to the horizon. The purpose of this measurement was to do a night sky-to-horizon calibration sweep in the 8- to 12-micron region. The radiometer produced uv-correlation data during this measurement.

Alinement of the radiometer and IR spectrometer was performed December 5, 1965, on a nearly full moon. Simultaneous photographic coverage of the measurement objective was obtained by a camera boresighted along the instrument axis (fig. 14). The equipment alinement was checked by the use of a meter in the center console. The crewmen boresighted the spacecraft on the moon, and then made minor excursions in pitch and yaw to locate the aiming point for optimum signal return (fig. 15). This maneuver accounted for the dips in the curves seen on figures 16 and 17. The values of moon irradiance from 2000 to 3060 angstroms and from 1 to 3 microns, as measured on December 5 by the radiometer, are shown in figures 18 and 19. The data correlated effectively with the other instruments and with the measurements made on December 8 at the full moon. As an illustration, a plot of the lead sulfide channel readings taken December 5 on the radiometer was compared with the lead sulfide channel readings made on December 8 on the IR spectrometer (fig. 20). The values taken on December 8 were slightly higher than those taken on December 5, as was expected. In figure 21, the flight measurements from Gemini V are shown on a predicted 25-day-moon curve; the measurements for Gemini VII are shown against a full-moon curve.

Throughout the measurements, a high level of photograph and voice correlation was maintained. A cloud bank measured during the cloud-blanket sweep over Africa is shown in figure 22. A photograph, made with IR film, of the Gulf Coast during a land-water measurement is shown in figure 23. Also, photographic coverage was accomplished during Polaris launch, airglow measurement, Gemini VI retrograde maneuver, rocket-sled run, and horizon-to-nadir calibration.

During the Gemini VII mission, all sensing equipment functioned perfectly. The experiment recorder operated intermittently during the first two revolutions and operated satisfactorily thereafter. The recorder difficulty caused no serious loss of data, however, because vital parts of the measurements were scheduled over experiment ground-based receiving stations. The transmitter worked properly throughout the mission. Crewmember performance during the flight was outstanding. In addition to performance of all scheduled measurements, several targets of opportunity (for example, a ground fire and lightning) were measured as a result of crewmember initiative. In addition to the acquisition of a large amount of significant radiometric data, adjunctive information was obtained. First, the alinement check after the Gemini VII spacecraft was maneuvered into orbit was indicative that ground alinement between the optical sight and the equipment in the adapter was valid within 0.5°. Concern had been expressed that alinement under unit-gravity conditions and shifting at the heat-shield interface with the adapter during launch might cause some problems. Second, the cryogenic lifetime for the cooled spectrometer (nominally 14 to 15 hours under quiescent unit-gravity conditions) essentially was unchanged by subjection to the launch environment and then to zero-gravity conditions. The system was a subcritical, open-cycle, liquid-neon system in a fixed-wall Dewar flask; it operated for 8 hours 50 minutes in space after 5 hours of ground-based operation prior to lift-off. Globularization of the neon because of weightlessness caused no perturbations in the operating characteristics of the cryogenic system. Finally, in pictures of the Gemini VII spacecraft, frost or snow can be seen in a roughly oval pattern aft of the cryogenic spectrometer. This frost was still on the spacecraft approximately 10 days after the cryogen had been depleted, which is interesting with respect to the sublimation characteristics of a hard vacuum.

Voice annotations, photographic coverage, and debriefing comments contributed significantly to the meaning and correlation of the data. Crewmember contributions in the choice of targets, mode of equipment operation, and ability to track selectively with the spacecraft have been unique in establishment of the flexibility necessary to accomplish such a diverse group of radiometric measurements.

TABLE I. - RADIOMETER INSTRUMENT PARAMETERS

(a) Gemini V detectors

Characteristics	Photomultiplier tube (IP 28)	Lead sulfide	Bolometer
Spectral band, μ	0.2 to 0.6	1.0 to 3.0	4 to 15
Nominal filter width, μ	.03	.1	.3
Filters used, μ	.22 .24 .26 .28 .30 .35 .40 .50 .60	1.053 1.242 1.380 1.555 1.870 2.200 2.820	4.30 4.45 6.00 8.0 9.6 15.0
Dynamic range	10^5 in four discrete steps	10^3 log compressed	10^3 log compressed

TABLE I. - RADIOMETER INSTRUMENT PARAMETERS - Concluded

(b) Gemini VII detectors

Characteristics	Photomultiplier tube (ASCOP 541 F-05M)	Lead sulfide
Spectral band, μ	0.2 to 0.35	1.0 to 3.0
Nominal filter width, μ	.03	.1
Filters used, μ	.2200 .2400 .2500 .2600 .2800 .2811 .2862 .3000 .3060	1.053 1.242 1.380 1.555 1.870 1.9000 2.200 2.725 2.775 2.825
Dynamic range	10^5 in four discrete steps	10^3 log compressed

(c) Gemini V and VII radiometer description

Weight, lb	17.5
Power input, W	14
Field of view, deg	2
Optics, in. Cassegrain	4

TABLE II. - PARAMETERS OF THE INFRARED SPECTROMETER

Characteristics	Detectors	
	Lead sulfide	Bolometer
Spectral band, μ	1 to 3	3 to 15
Dynamic range	10^3 automatic gain changing	10^3 automatic gain changing
Spectrometer description		
Weight, lb	18.5	
Power input, W	8	
Field of view, deg	2	
Optics, in. Cassegrain	4	

TABLE III. - PARAMETERS OF THE CRYOGENIC INTERFEROMETER SPECTROMETER

Weight, with neon, lb	33.5
Power input, W	6
Field of view, deg	2
Optics, in. Cassegrain	4
Detector	Mercury-doped germanium
Spectral band, μ	8 to 12
Dynamic range	10^3 automatic gain changing
Coolant	Liquid neon

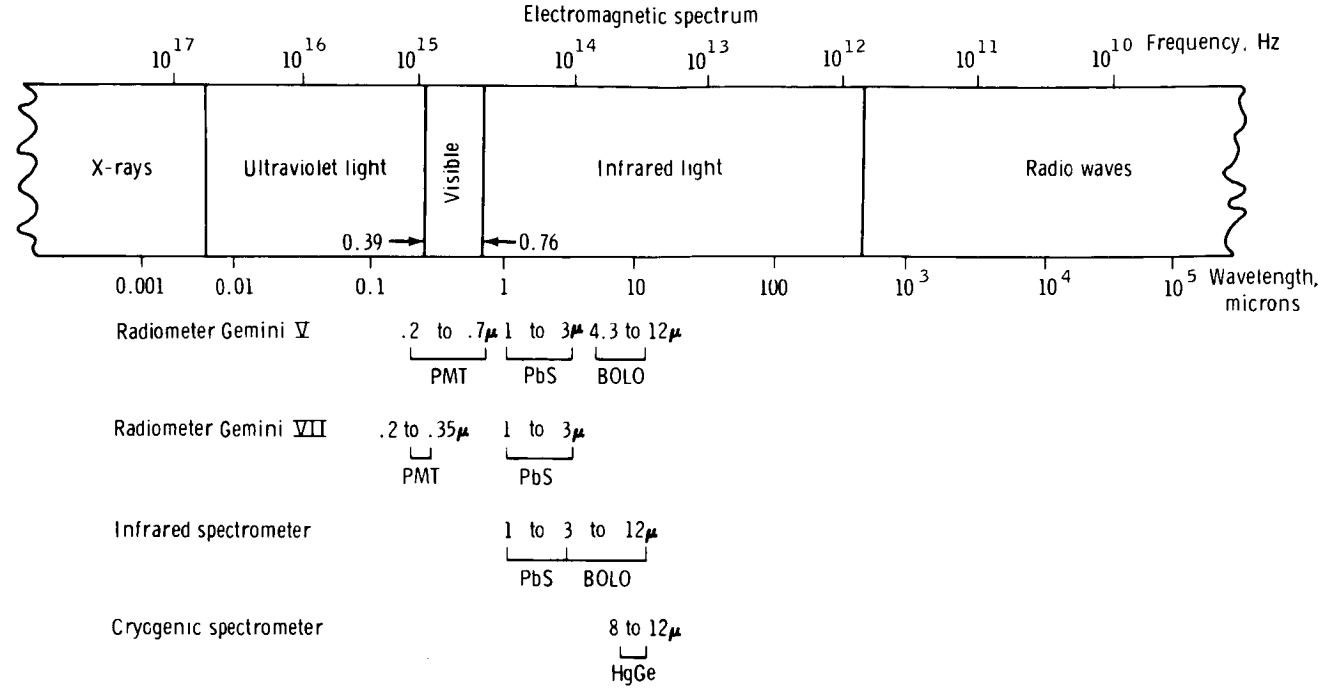

Figure 1.- The spectral bands that were investigated.

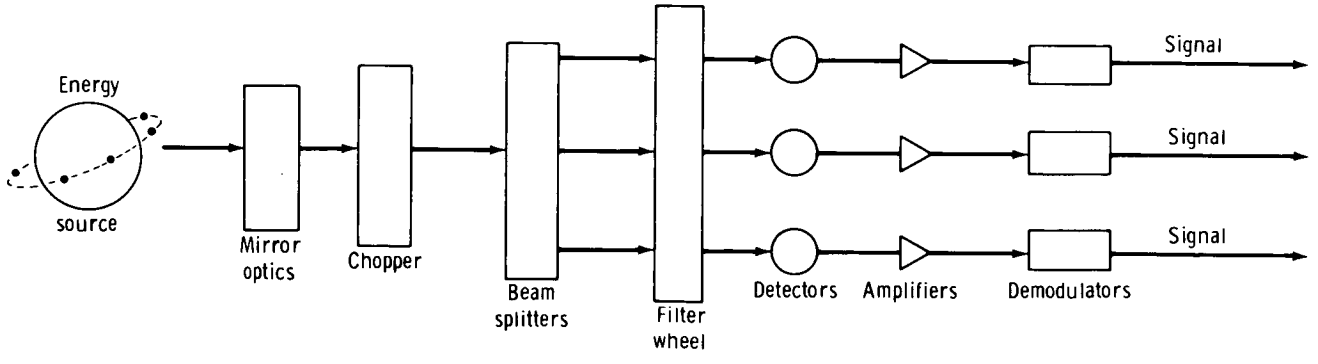

Figure 2.- A functional diagram of the radiometer.

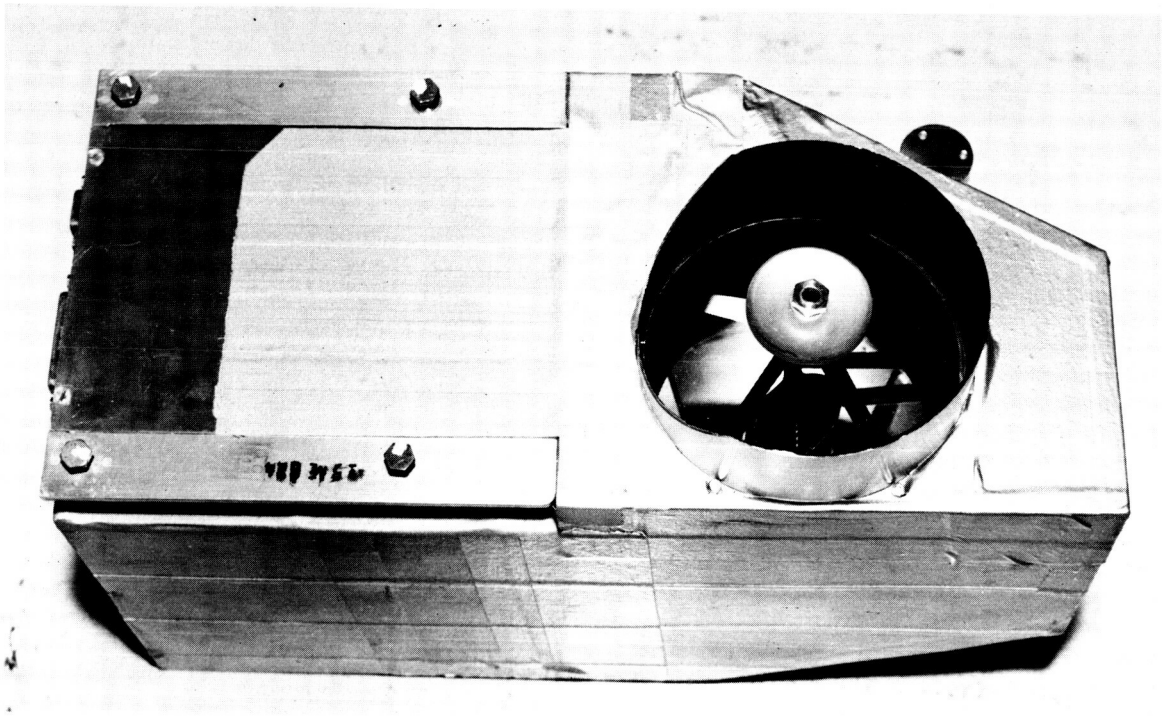

Figure 3. - The trichannel spectroradiometer.

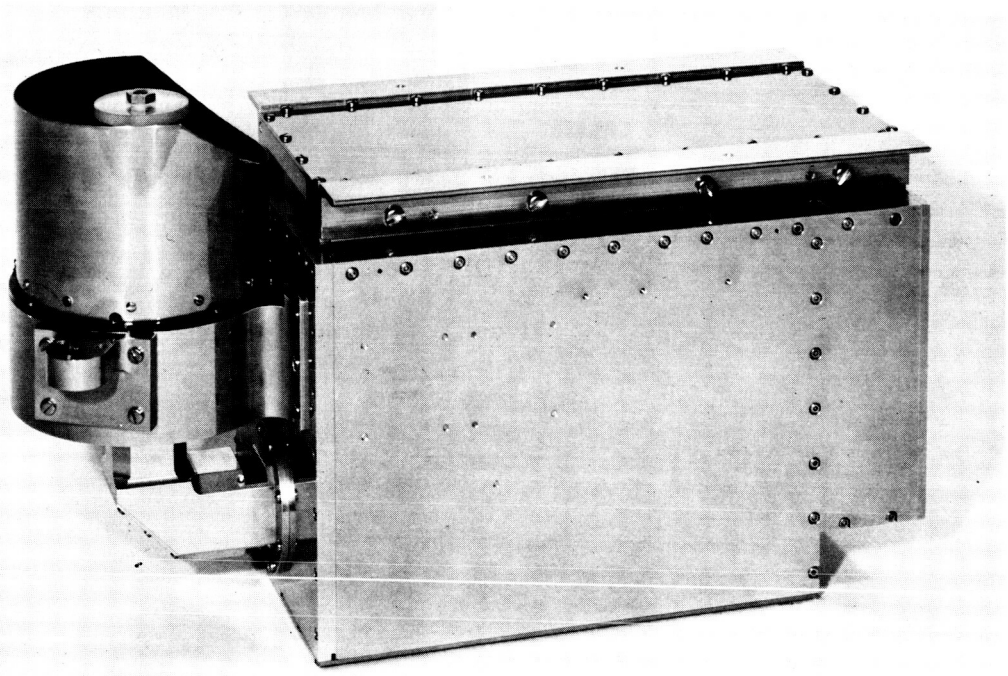

Figure 4. - The dual-channel interferometer spectrometer.

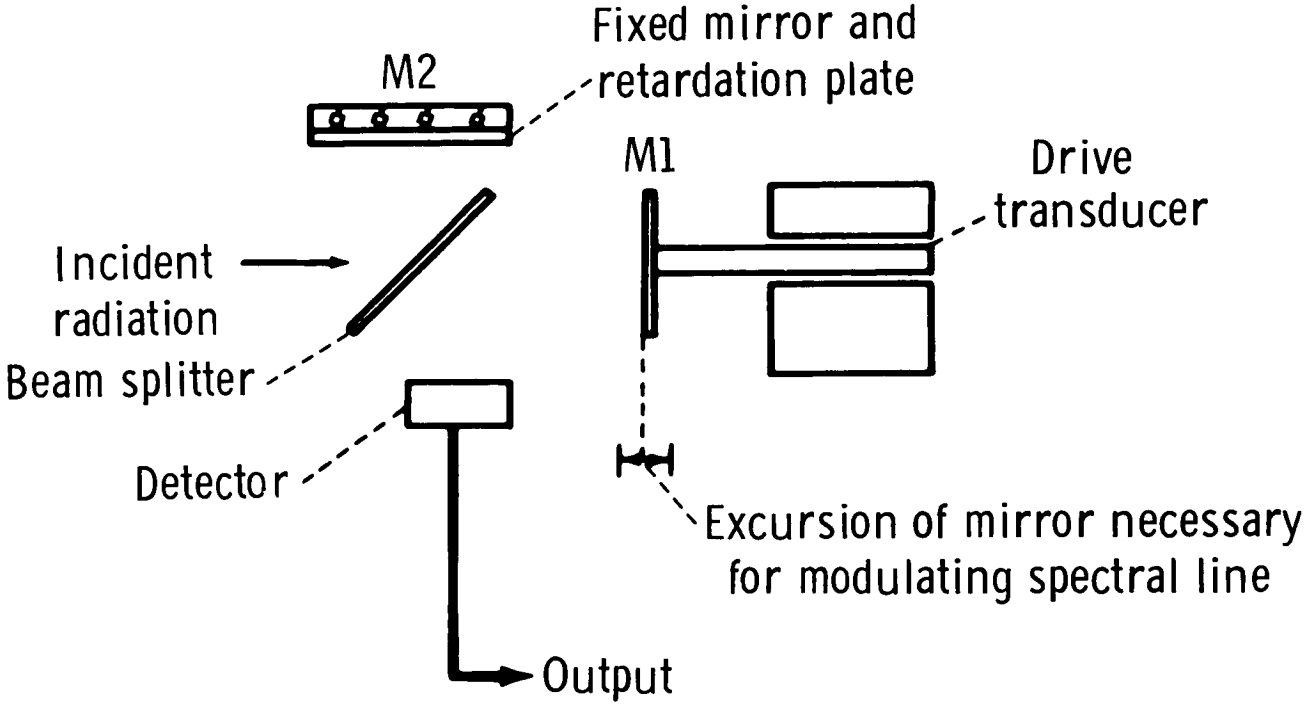

Figure 5.- A schematic of a Michelson interferometer.

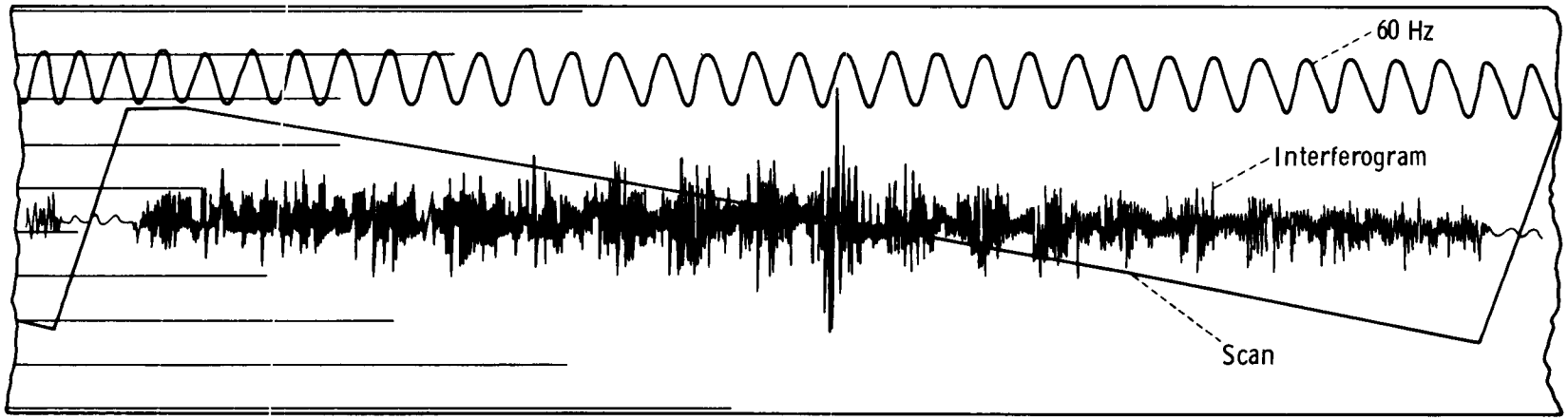

(a) Interferogram.

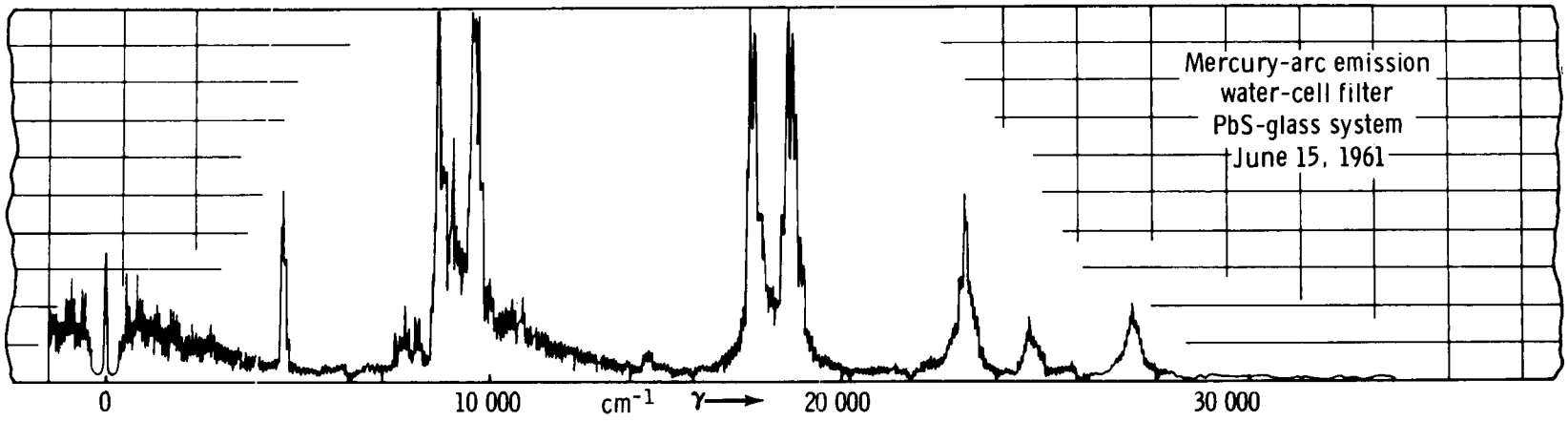

(b) Interferogram reduced to a spectrum.

Figure 6. - Interferometer measurements.

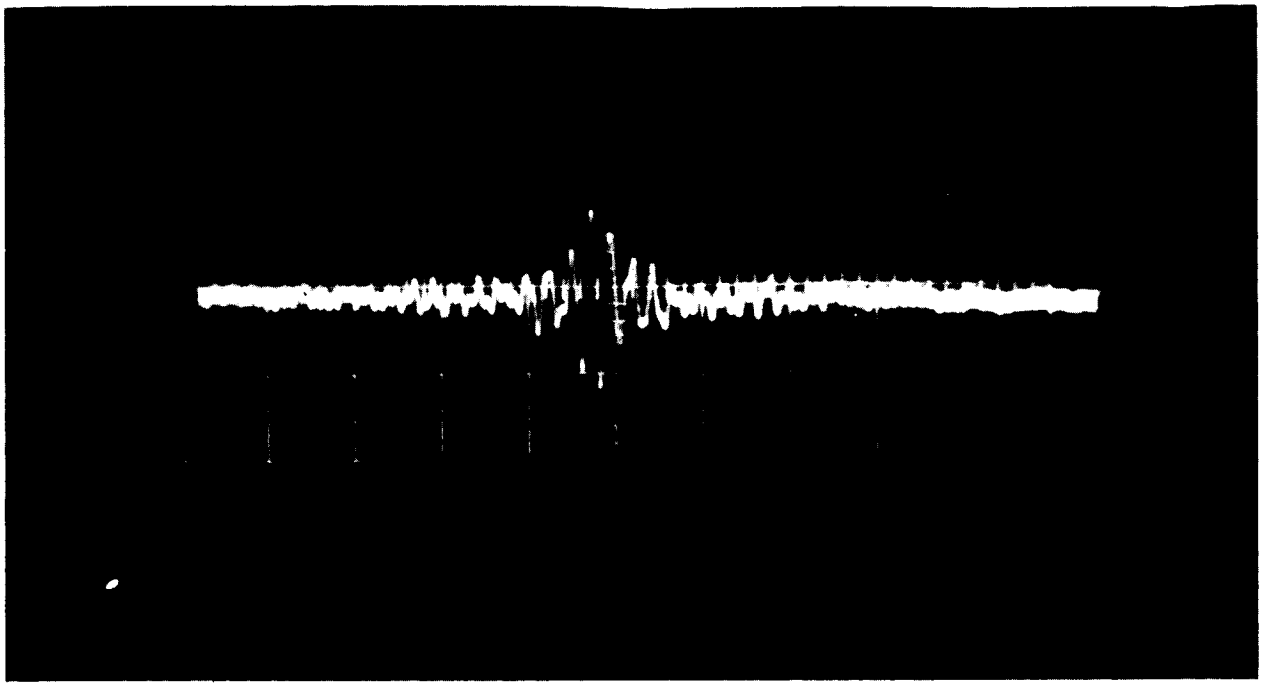

(c) Spectrometer interferogram (2100° C calibration source).

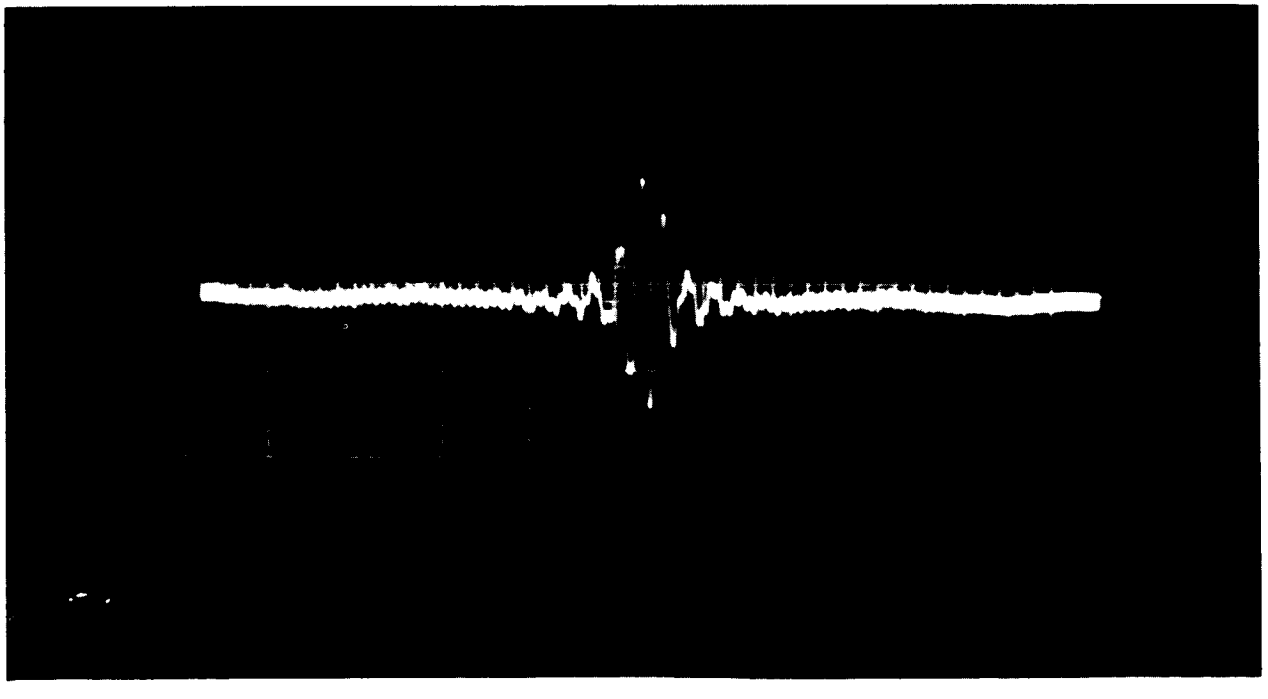

(d) Infrared spectrometer interferogram made during the California coastal-land overflight on the Gemini V mission.

Figure 6. - Concluded.

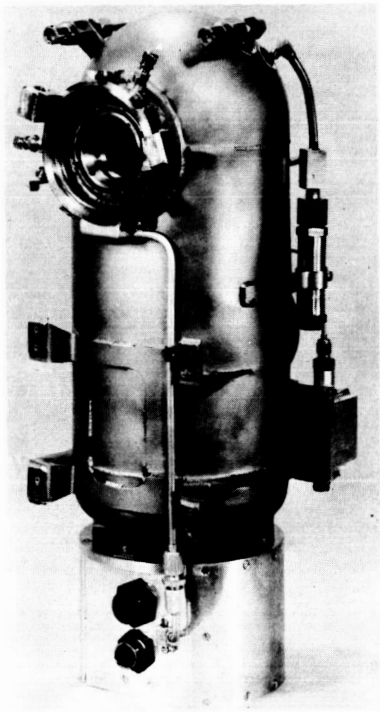

Figure 7.- The cryogenic interferometer spectrometer.

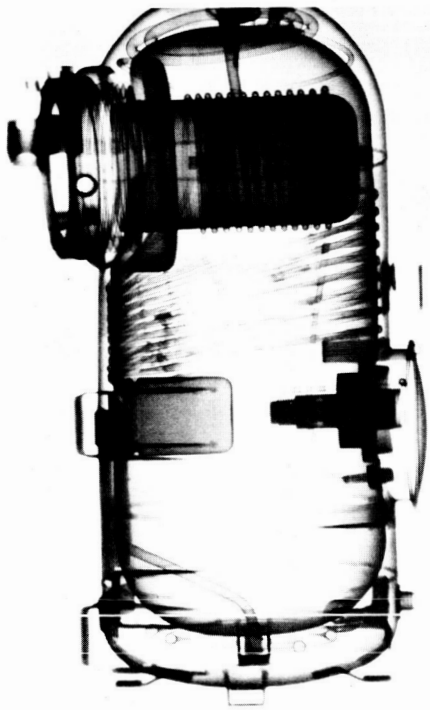

Figure 8.- Roentgenographic view of the cryogenic interferometer spectrometer.

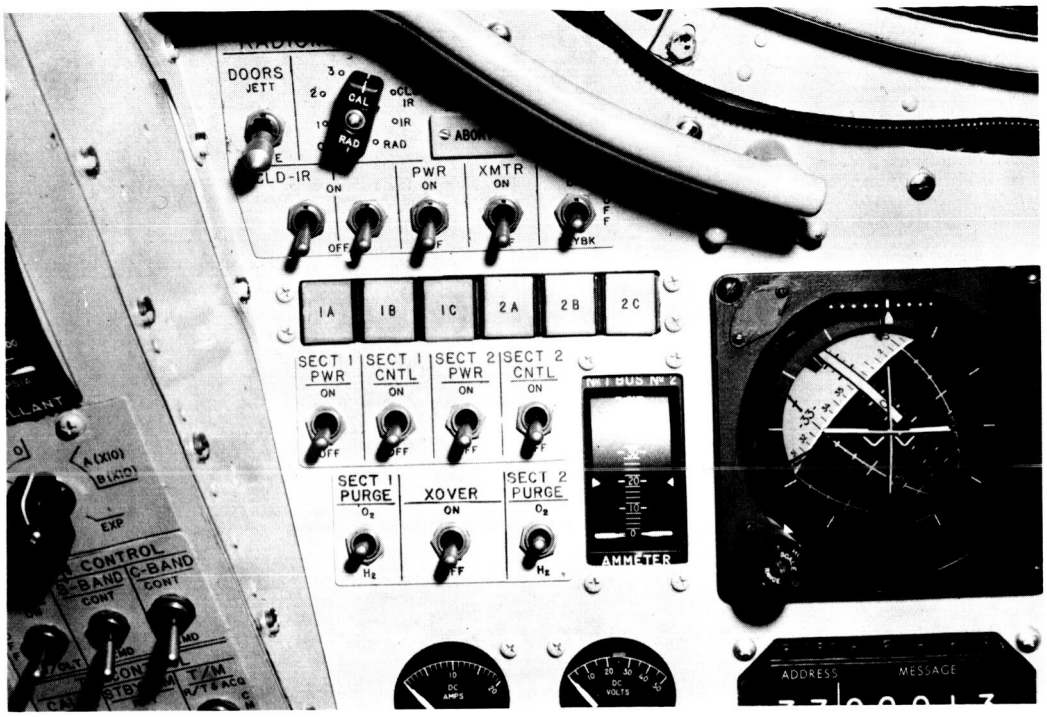

Figure 9. - The instrument panel for Experiments D004 and D007.

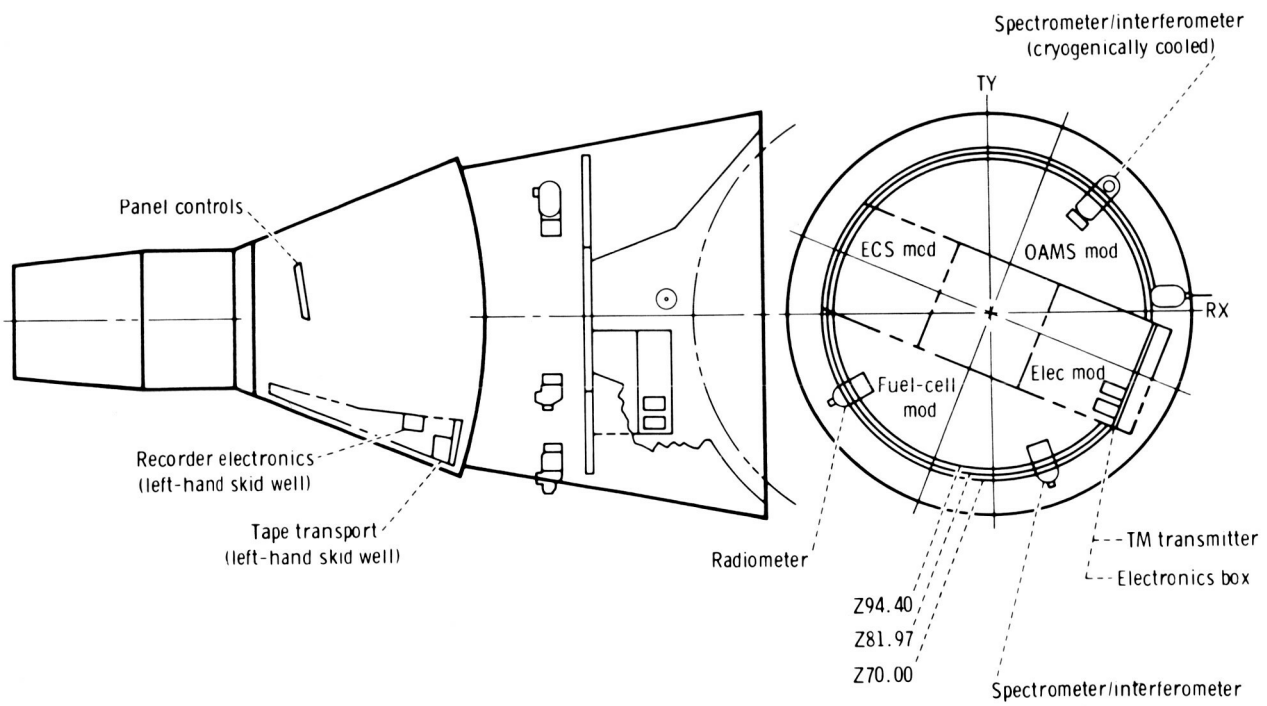

Figure 10. - The location of Experiments D004 and D007 in the spacecraft.

Figure 11.- The cryogenic spectrometer and radiometer erected on the Gemini VII spacecraft.

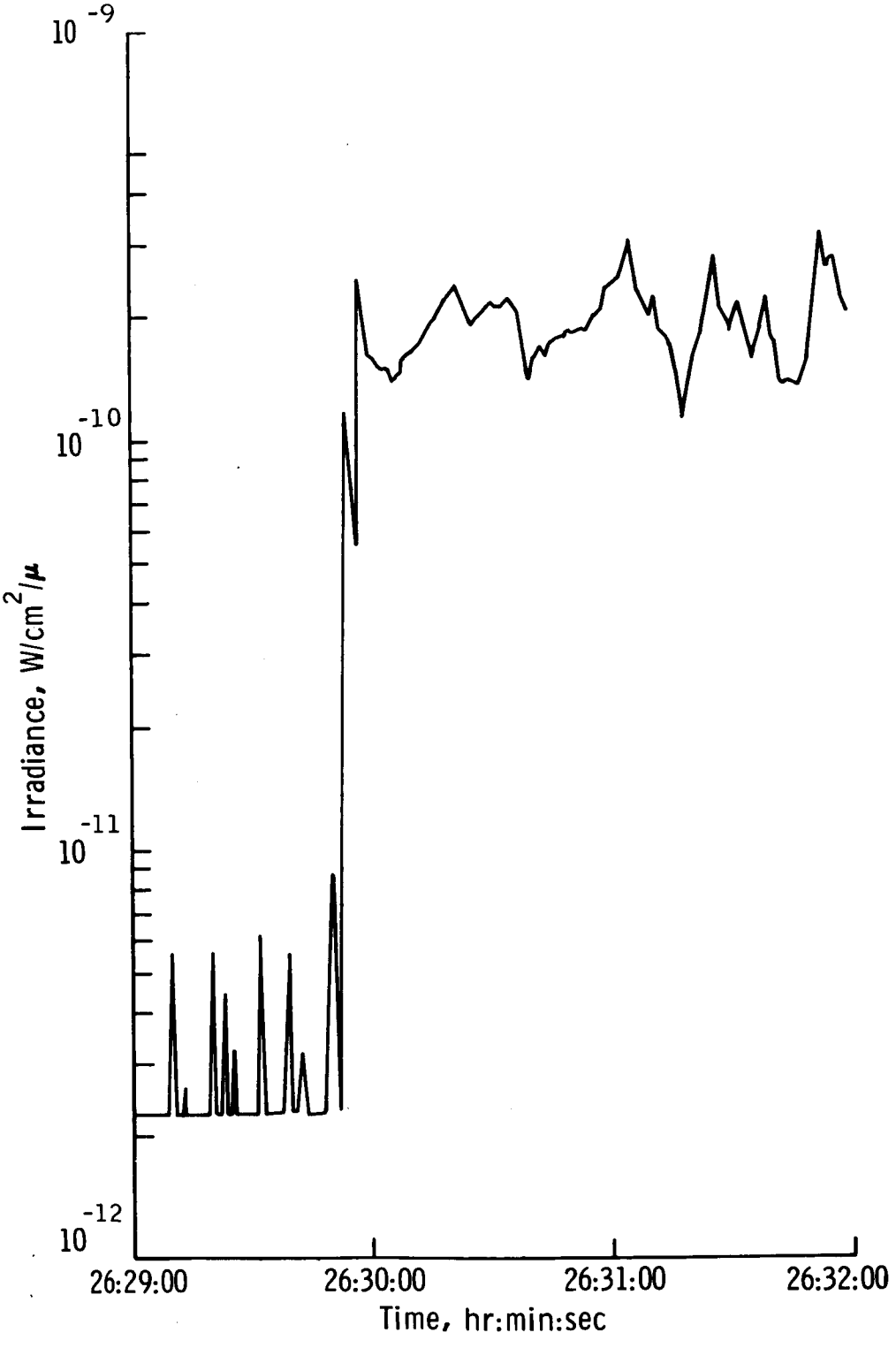

(a) Measurements made during revolution 17 of the Gemini V mission.

Figure 12. - Radiometer data from moon measurements.

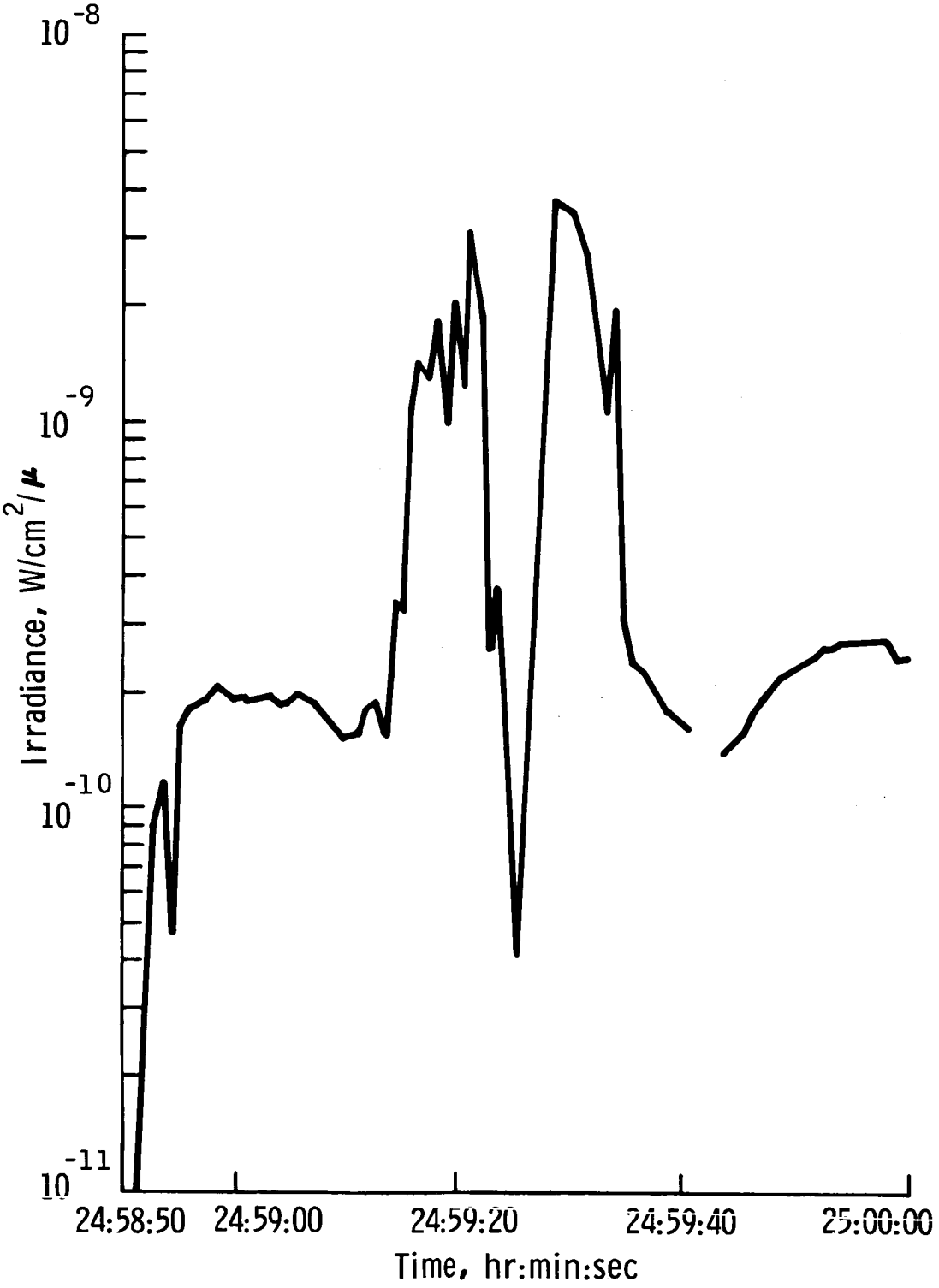

(b) Measurements made during alinement check, revolution 16, of the Gemini V mission.

Figure 12. - Concluded.

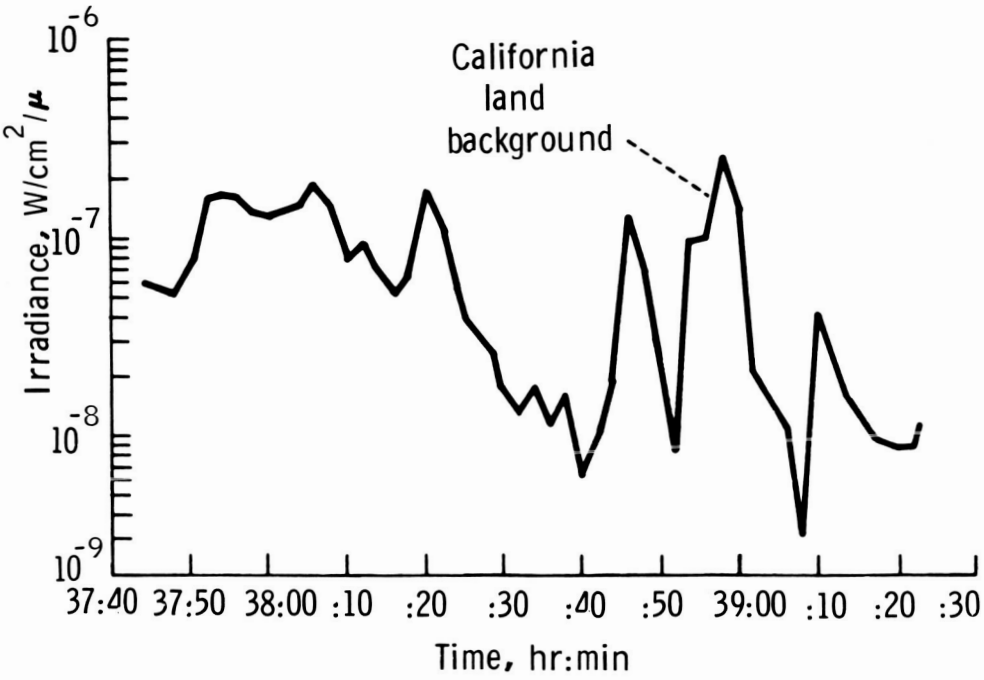

Figure 13. - Interferometer-spectrometer data (1.88 microns).

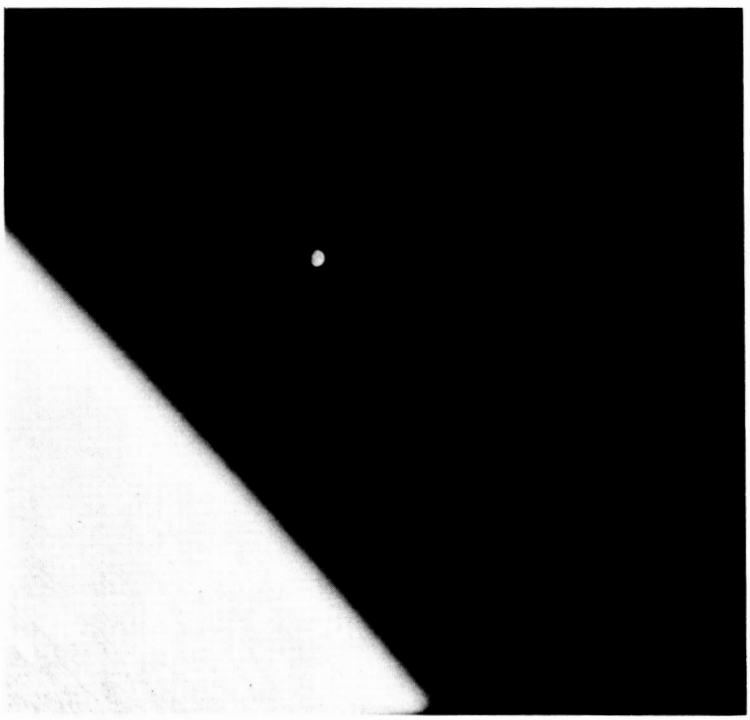

Figure 14. - A photograph of the almost-full moon, taken during alinement of the radiometer and the IR spectrometer.

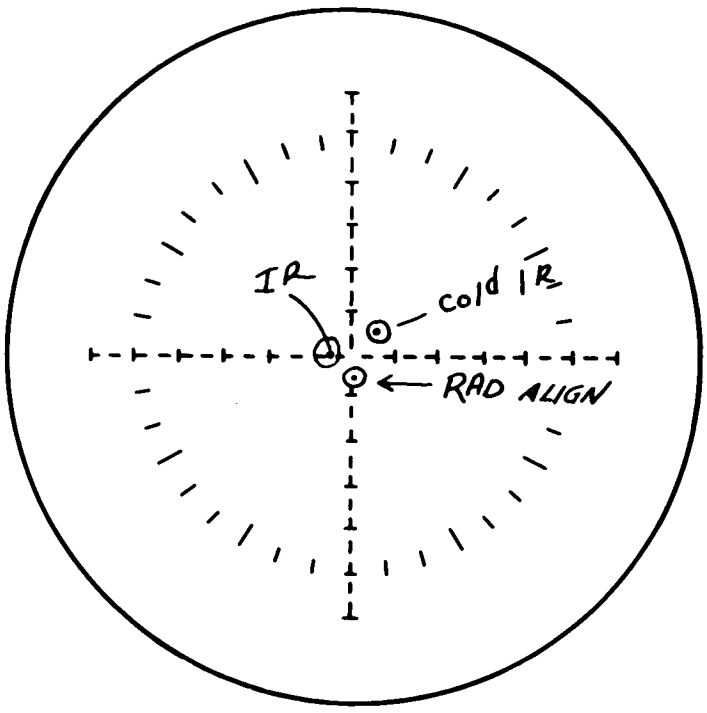

Figure 15. - The alinement pattern as noted in the flight log book.

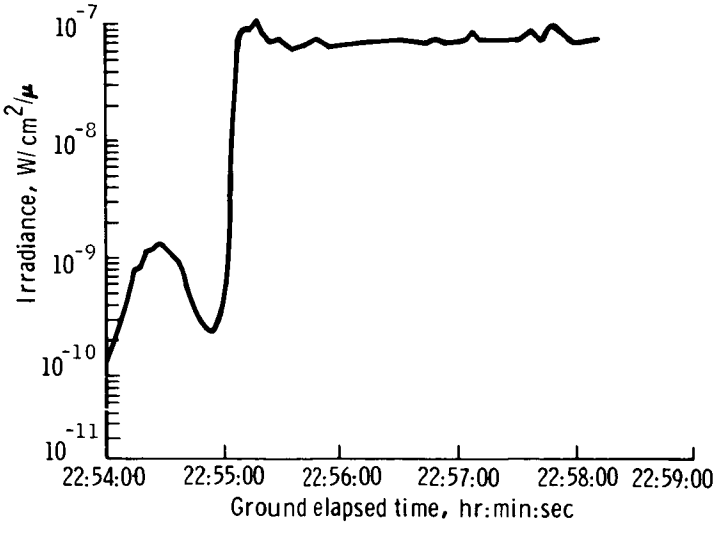

Figure 16. - Moon irradiance during alinement optimization (3000 angstroms).

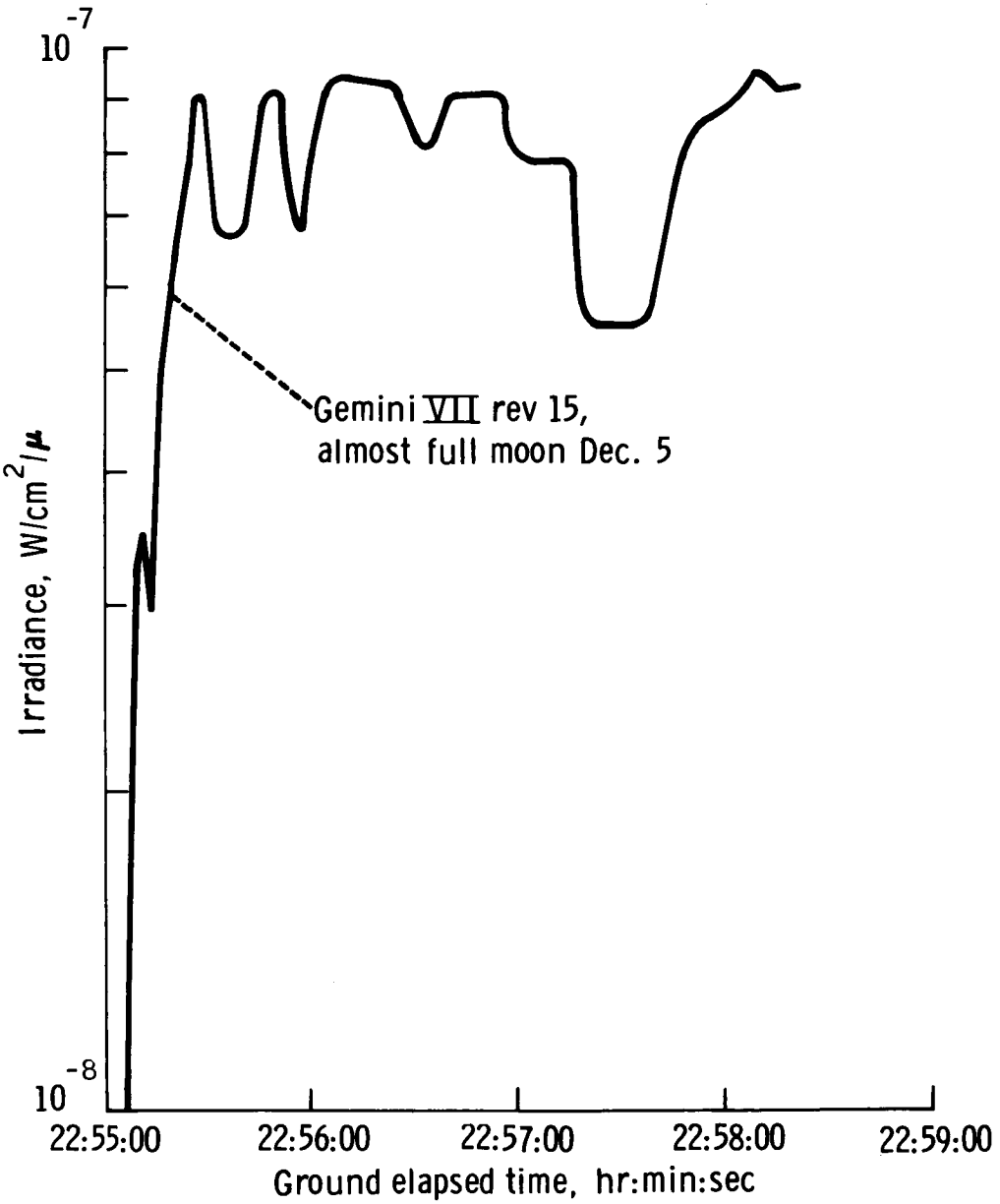

Figure 17.- Moon irradiance during alinement optimization (1.555 microns).

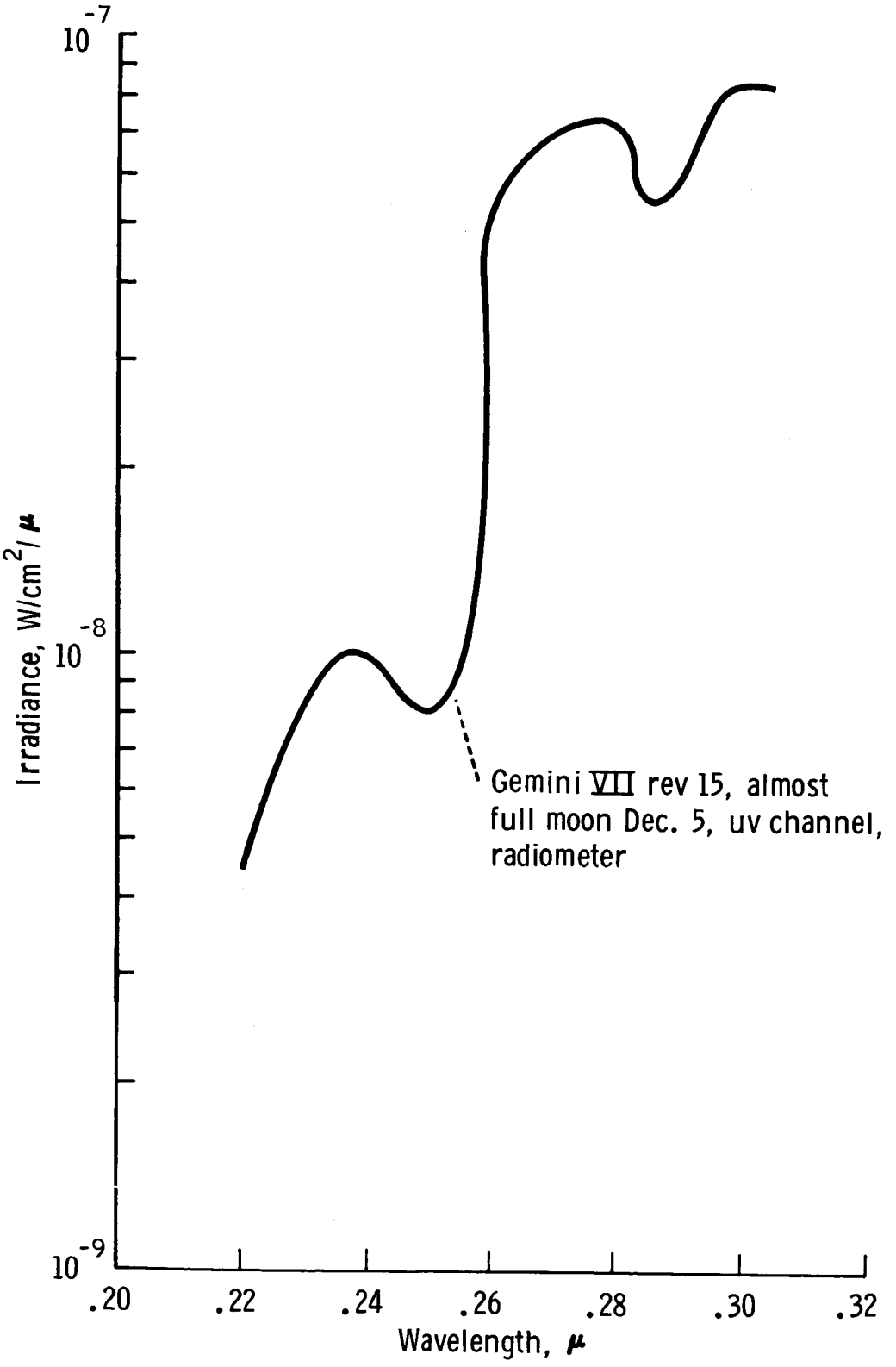

Figure 18.- Values of moon irradiance from 2000 to 3060 angstroms.

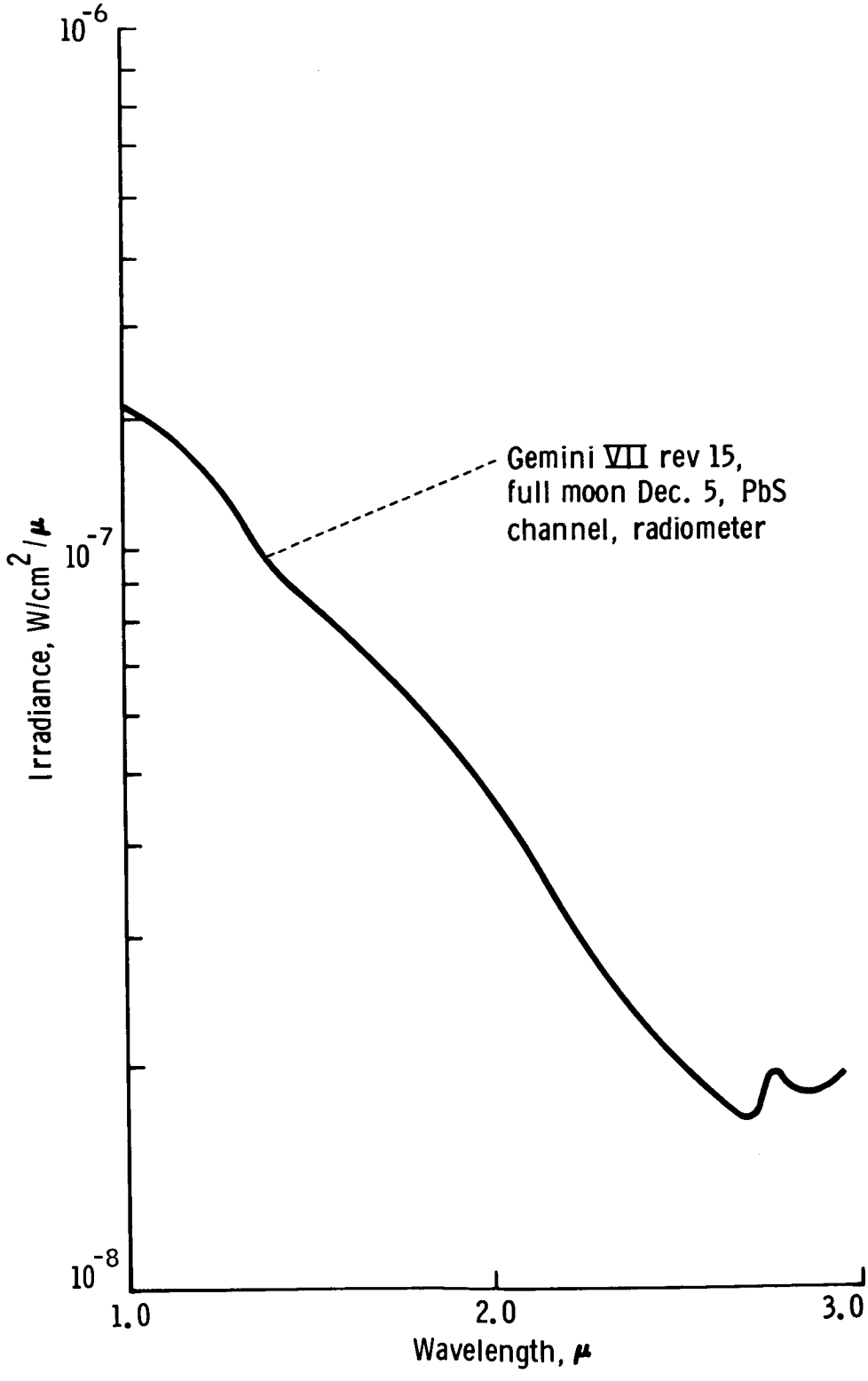

Figure 19. - Values of moon irradiance from 1 to 3 microns.

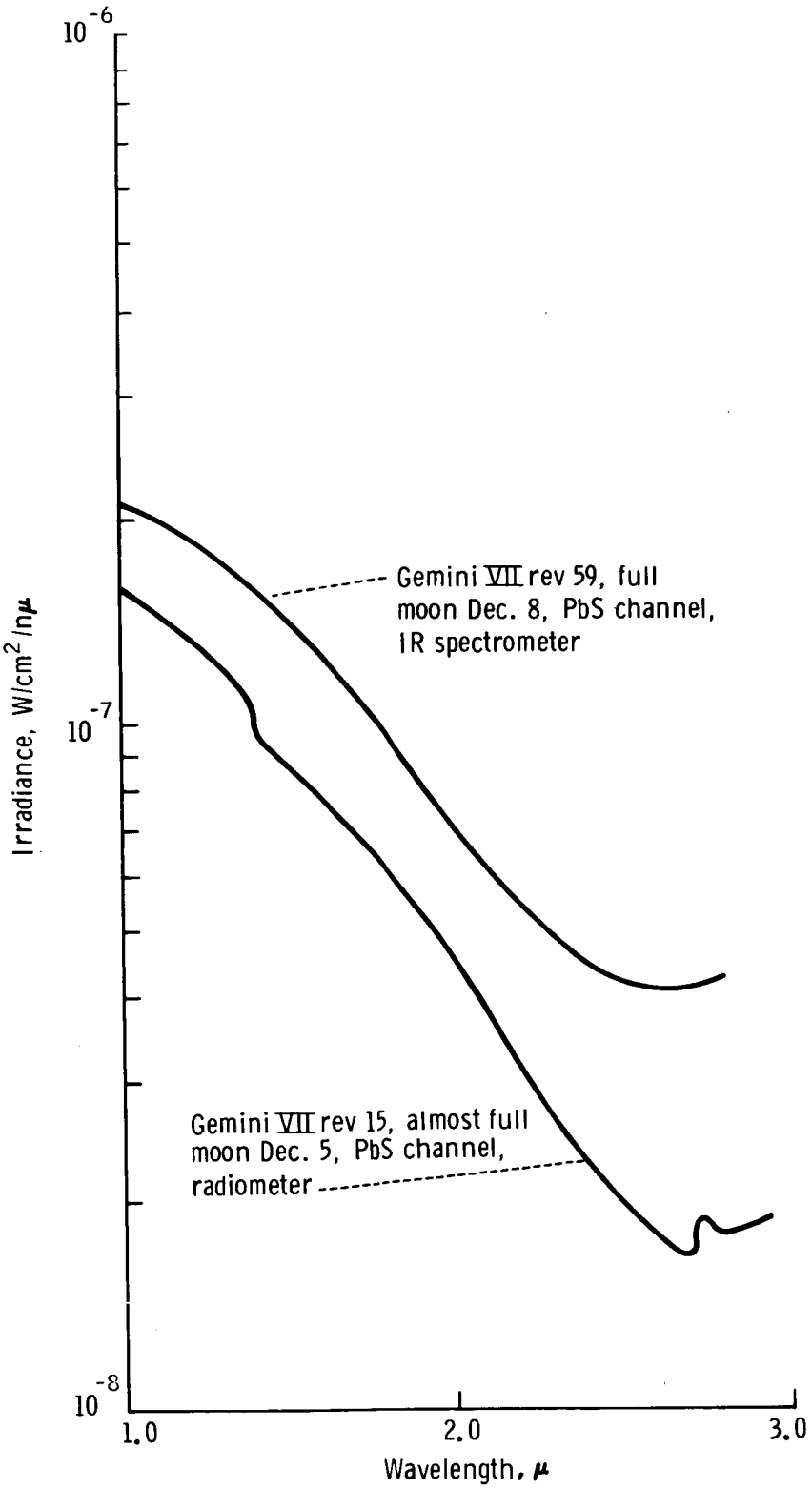

Figure 20. - Composition of lead sulfide channel readings on December 5 and 8, 1965.

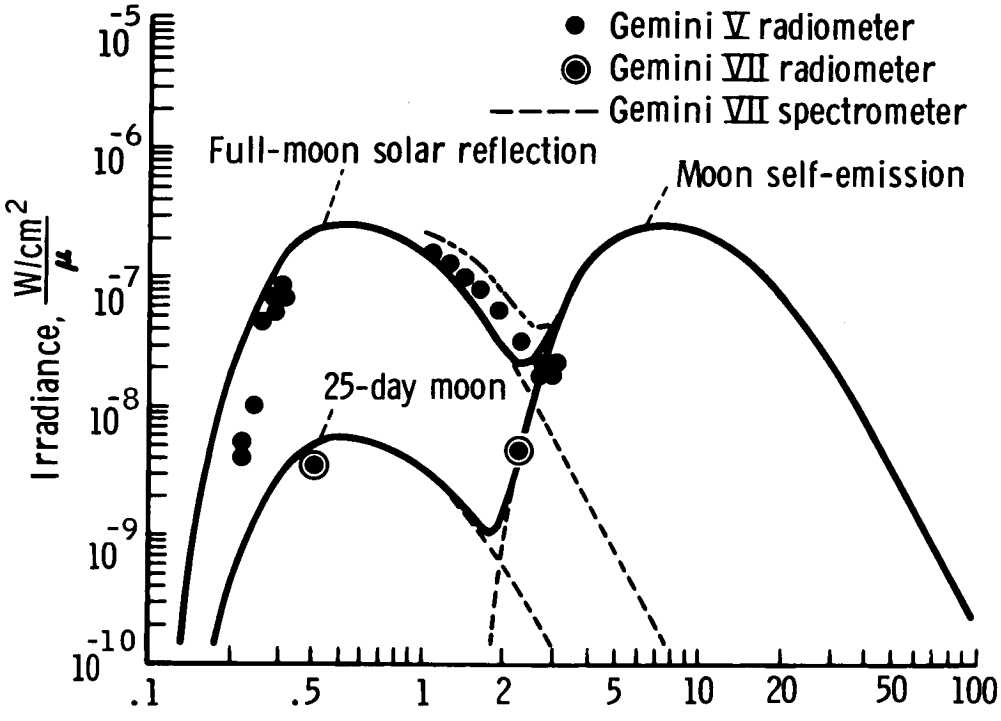

Figure 21. - Lunar-irradiance measurements made during the Gemini V and VII missions.

EXPERIMENT S010

AGENA MICROMETEORITE COLLECTION

By Curtis L. Hemenway*

INTRODUCTION

A study was made of the micrometeoroid content of the upper atmosphere and the near-earth space environment. Highly polished collection surfaces attached to the target docking adapter (TDA) were exposed to micrometeorite impact and debris collection during the Gemini VIII, IX, and X missions. Also, the device was attached to the Gemini Agena target vehicle (GATV) during the Gemini XII mission. The effects of space-environment exposure on viable micro-organisms were recorded. Experiment S010 was designed to obtain new data and to confirm flux values that had been obtained by short exposure to micrometeorite bombardment of sounding rockets, satellite microphones, and other equipment. The values obtained were compared with those values obtained by the large area-time product exposure of the micrometeoroid-detection plates. Surfaces from which data were collected were exposed for approximately 4 months.

EQUIPMENT

The basic hardware package was interfaced with the target vehicle by the use of a mounting plate by which the hardware could be detached from the vehicle (figs. 1 and 2). The package size was 5.50 by 6.25 by 1 inches, and the package weight was approximately 4 pounds when loaded for flight (fig. 3). The exterior surfaces were highly polished stainless-steel plates; six small circular depressions were cut in one of the plates. These depressions were used for seeding and space exposure of micro-organisms. The micro-organisms that were used on the outside of the package were the T_1-bacteriophage, Penicillium roqueforti spores, and Bacillus stearothermophilus spores. Cratering samples were installed on the outside surface of the aluminum structure. During launch and during the orbital insertion of the target vehicle, these external surfaces were protected from the direct impact of airborne particles by a fairing that diverted the airflow over the mounting. The box contained other collection and detection samples that were designed for exposure during the planned extravehicular activity (EVA) on the Gemini VIII mission.

*The Dudley Observatory, Albany, New York.

METHODS

Data collection was attempted by the following procedures.

1. Exposure of polished-metal and plastic surfaces to the particle flux and the subsequent study of the resultant impact craters

2. Exposure of highly polished sections of meteorite material to the particle flux to obtain direct measurements of meteor erosion rates

3. Exposure of polished optical-glass surfaces to the particle flux for determination of the deterioration of optical-surface properties

4. Exposure of thin films to the particle flux and observation of thin-film penetration

5. Exposure of extremely clean surfaces to the particle environment in an attempt to collect ultrasmall particles

6. Exposure of biological specimens to the space environment (fig. 4)

RESULTS

Gemini IX Mission

The hardware was taken to Kennedy Space Center (KSC) and mounted on the TDA approximately 24 hours before lift-off. The protective plastic cover was removed 6 hours before lift-off, just before removal of the access tower. After launch, the Atlas vehicle malfunctioned and the target vehicle did not achieve orbit. Thus, the experiment hardware was lost. Another unit was prepared, taken to KSC, and mounted on the augmented target docking adapter (ATDA) for the Gemini IX mission (fig. 5). Mounting, launch procedure, and the time sequence were identical to those procedures that were intended originally for use on the mission. After completion of the rendezvous maneuver, it was determined that EVA to the ATDA would not be possible because the ATDA shroud failed to jettison.

Gemini X Mission

The exterior collection unit was taken to KSC and installed in the same manner and sequence as the unit for the Gemini IX mission. Also, a unit similar to the one mounted on the exterior of the vehicle was installed inside the spacecraft. It was hoped that the extravehicular crewmember could deploy this unit on the Gemini VIII Agena target vehicle and recover the unit previously attached to this vehicle. Orbital insertion and the rendezvous maneuver were successful. Upon completion of the double rendezvous, the extravehicular crewmember retrieved the experimental hardware from the TDA of the Agena vehicle and handed it to the command pilot at approximately 49: 05 g. e. t. The hardware package was closed. Only the four outer test panels had

been exposed to the space environment. The proposed placement of the unit carried inside the spacecraft was abandoned because of the possibility of its entanglement with the umbilical. This unit was jettisoned into space by the extravehicular crewmember.

Gemini XII Mission

The experiment package for the Gemini XII mission was attached to the GATV, was inserted into orbit, and subsequently was docked to the Gemini XII spacecraft. At approximately 43:11 g.e.t., while the spacecraft was docked with the GATV, the EVA crewmember removed the protective fairing from the experiment package and exposed both its exterior and its interior collection surfaces to the space environment. The hardware was left on the GATV for possible recovery during a later Gemini mission.

CONCLUSIONS

Gemini IX Mission

Inflight photographs were indicative that the outer surfaces of the experiment package (mounted on the ATDA) were in good condition. However, no definitive conclusions could be made because the hardware could not be retrieved for study.

Gemini X Mission

Particulate material collected, holes and craters in the specially prepared surfaces, and viable micro-organisms that remained on the exposed collection plates (fig. 6) were retrieved from the experiment package. The collection surfaces incurred erosions during exposure. Two macroscopic craters were found by partial scanning of the surface of one plate (figs. 7 and 8). The macroscopic crater shown in figure 8 (light micrograph) is also shown in figure 9 (scanning electron micrograph). The greater definition and depth of focus of the electron microscope resulted in a three-dimensional image that could not be achieved by light microscopy. At the time of the initial analysis of these data, the electron microscope had just been installed. Other data on impact sites are expected from further scanning of the collection surfaces by use of the electron microscope. Also, other data are expected to result from an analysis of the debris retrieved from the exposed collection surfaces.

Gemini XII Mission

The GATV, to which the experiment package was attached, was inserted into orbit and was docked with the Gemini XII spacecraft. The EVA crewmember exposed the exterior and interior collection surfaces of the experiment package. Subsequently, an attempt was made by NASA personnel to put the GATV into a higher, longer-life orbit. The attempt failed because of primary system malfunctions. The calculated GATV lifetime was 84 days, insufficient for experiment-hardware retrieval during

subsequent missions. The Gemini XII pilot is shown retrieving the micrometeorite-collection package in figure 10.

DISCUSSION

No substantive data regarding space-environment micrometeorite content were derived from the Gemini IX or XII missions. However, some substantive data were obtained from the experiment package that was retrieved from the Gemini X mission. The micrometeorite-flux values obtained were in general agreement with values obtained from previous experiments by the use of other experimental equipment. The micro-organisms that were retrieved from the Gemini X experiment package (that had been exposed to the space environment for approximately 4 months) did not survive. However, the same kinds of specimens inside the package had good survival rates. Upon initial analysis, it appeared that the closed-cover shielding was a contributing factor in the protection and survival of the micro-organisms.

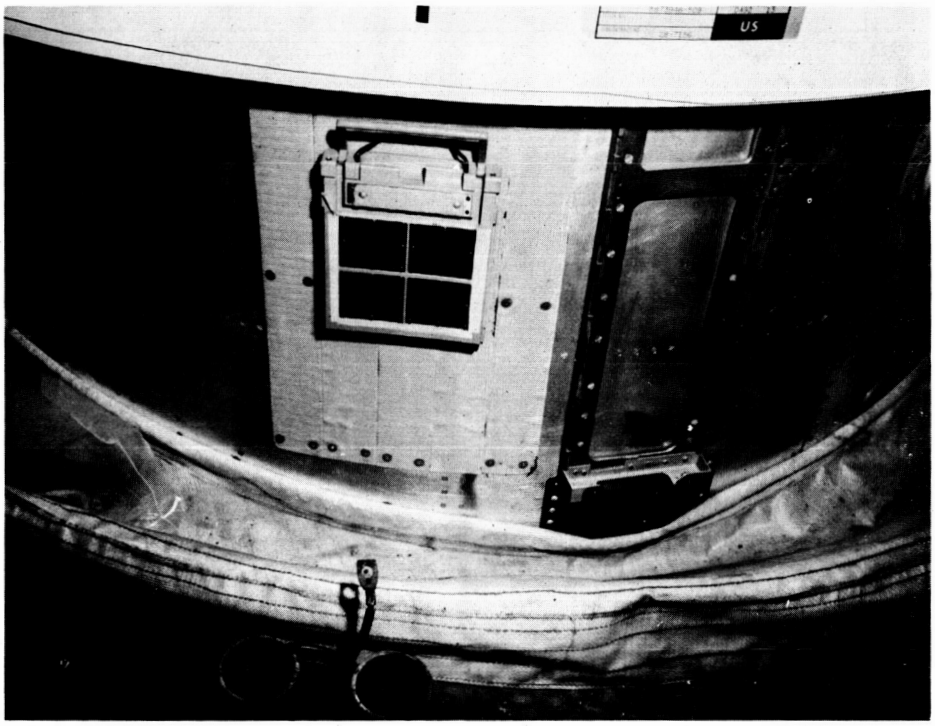

Figure 1. - The location of the micrometeorite collector.

Figure 2. - The micrometeorite-collection device installed and in the launch configuration.

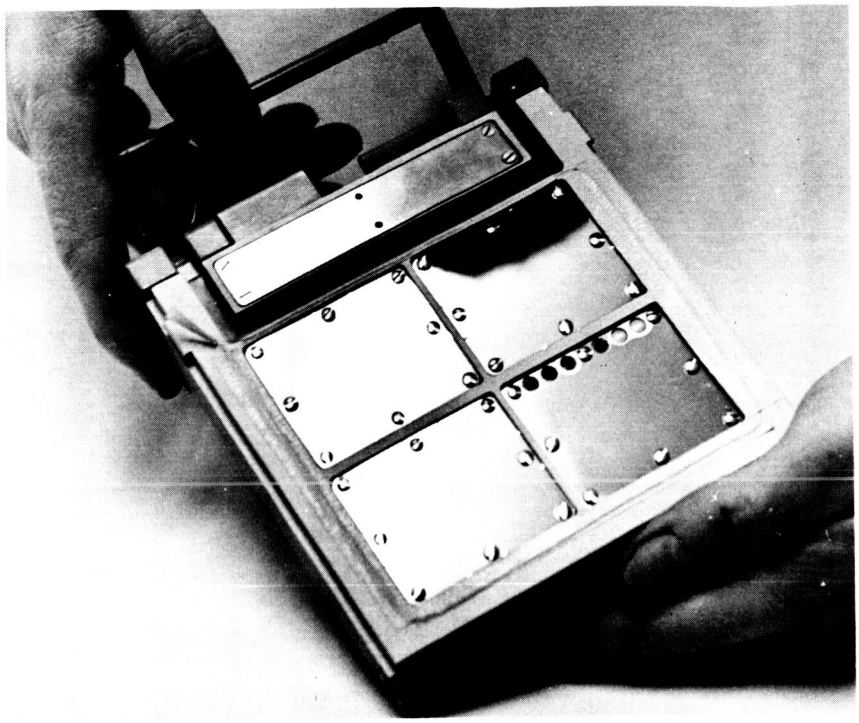

Figure 3. - The micrometeorite collector.

1. Shielded screening
2. Chromium-coated glass
3. Biological exposure with filters
4. Glass
5. Polished glass
6. Gold foil 2μ thick; two layers plus thick plastic film below
7. Stereoscan samples, copper and stainless steel
8. Stainless steel

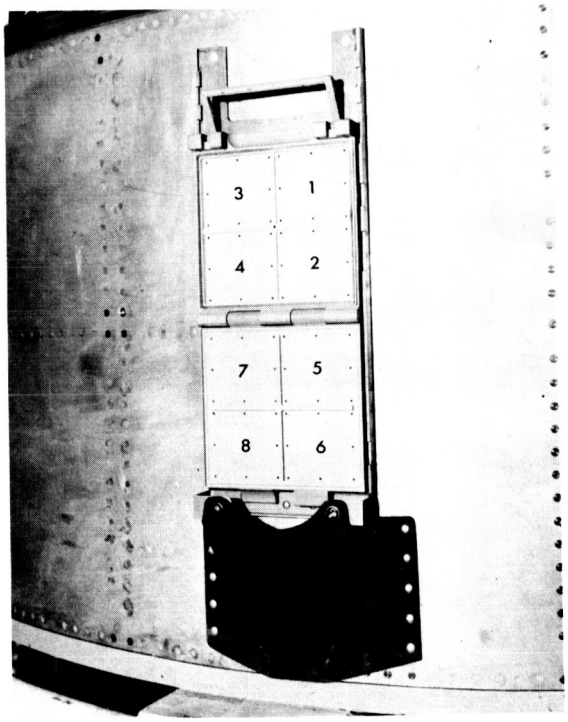

Figure 4. - The specimen-loading locations.

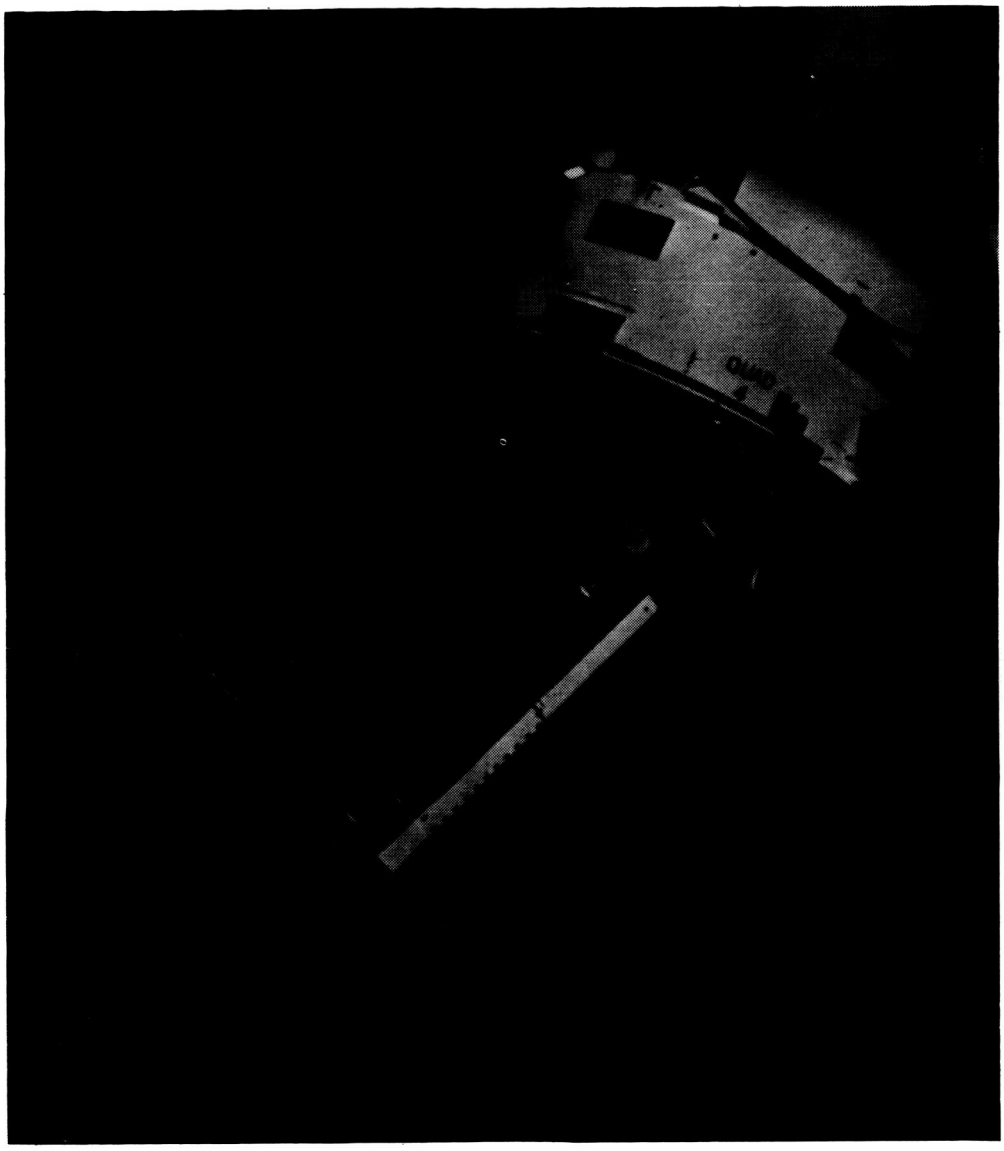

Figure 5. - The collector on the ATDA.

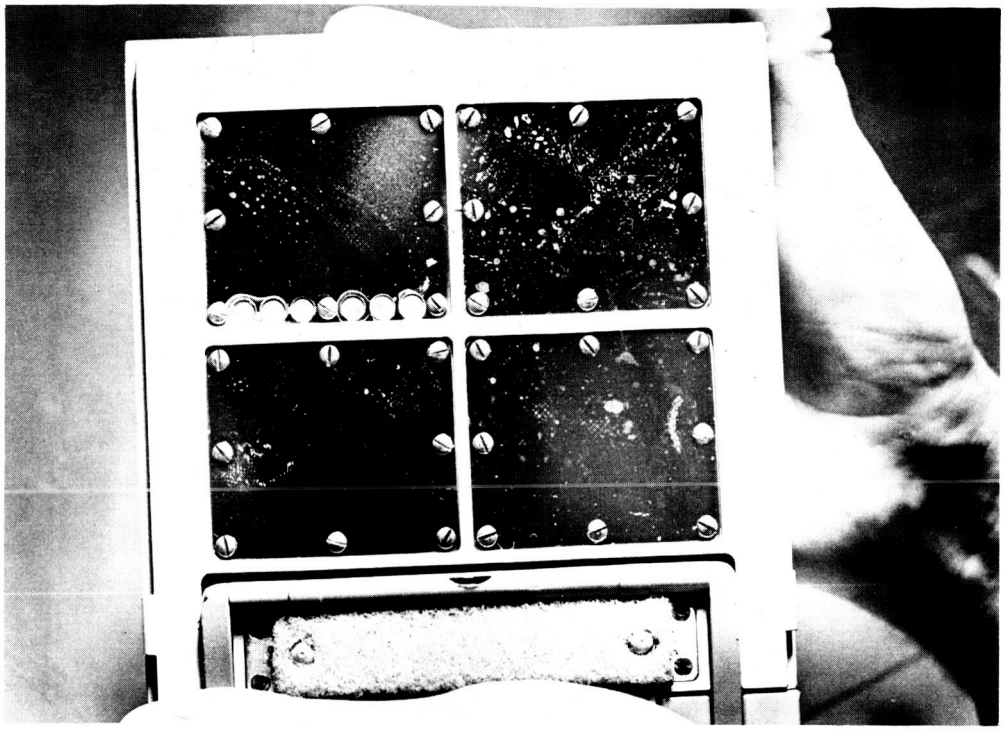

Figure 6. - The collection unit after a 4-month exposure.

Figure 7. - A macroscopic crater in a stainless-steel plate (light micrograph, ×500).

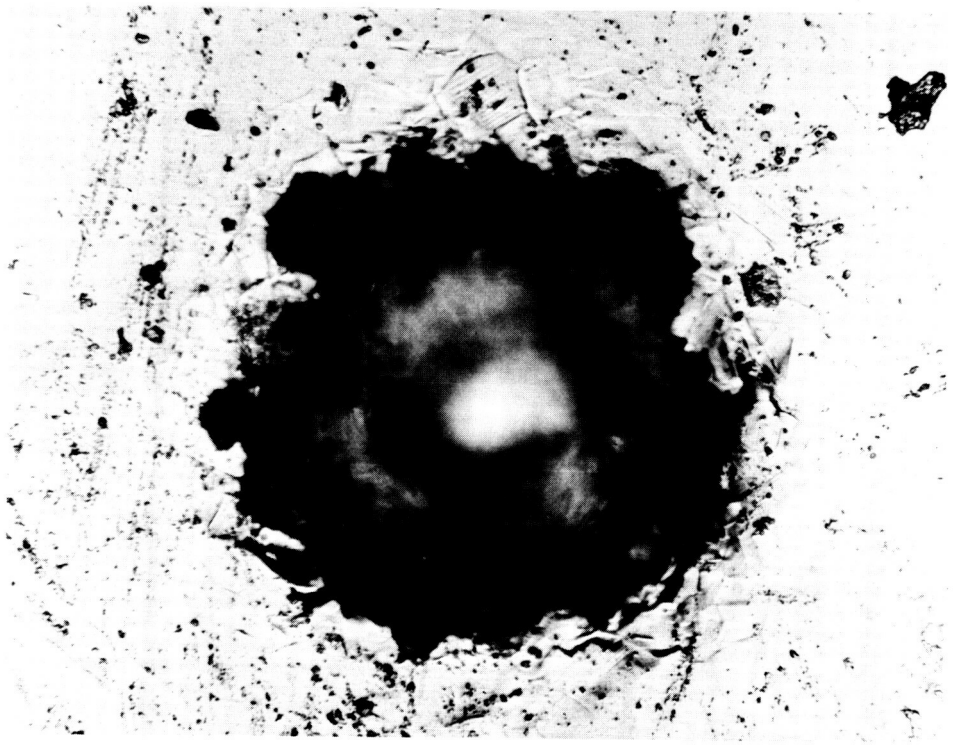

Figure 8. - A second macroscopic crater in a stainless-steel plate (light micrograph, ×500).

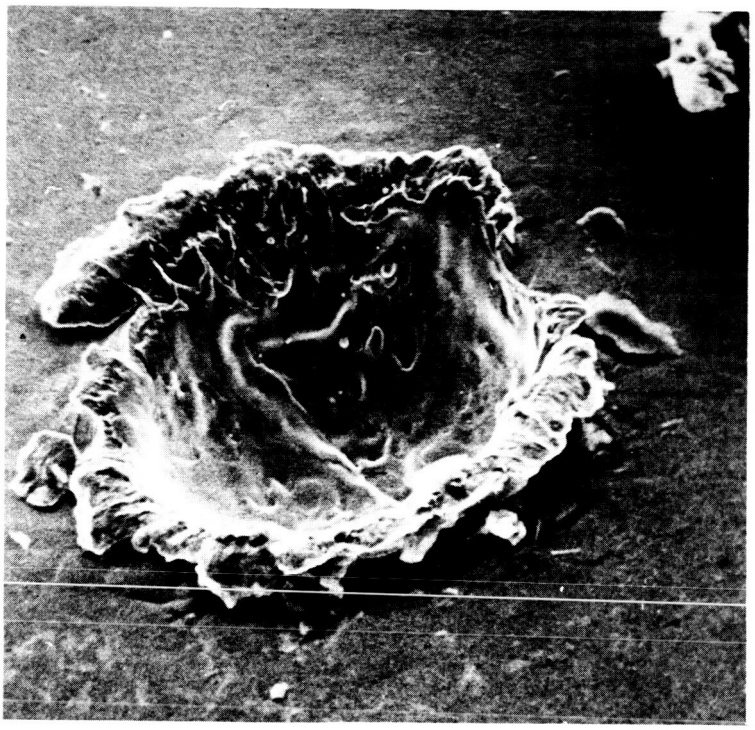

Figure 9. - The second macroscopic crater in a stainless-steel plate (scanning electron micrograph, ×500).

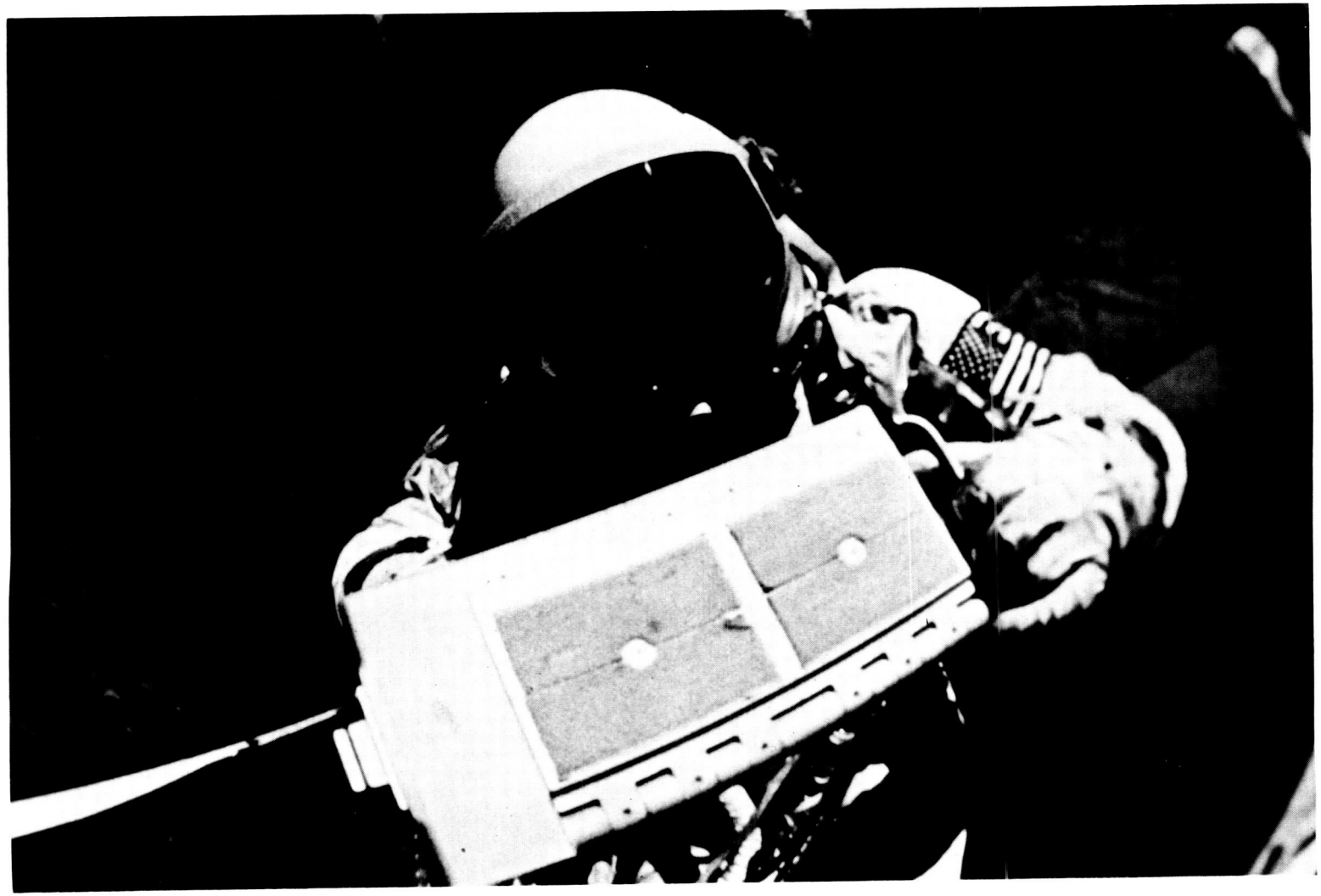

Figure 10. - The Gemini XII pilot retrieving the micrometeorite-collection package.

EXPERIMENT S012

MICROMETEORITE COLLECTION

By C. L. Hemenway,* D. S. Hallgren,* R. E. Coon,*
L. A. Bourdillon,** J. Hotchin,** and P. Lorenz**

OBJECTIVES

Experiment S012, flown on the Gemini IX, X, and XII missions, was designed to facilitate determination of the micrometeorite activity in a near-earth environment and to study the effect of the environment on micro-organisms. The objectives were to be accomplished by exposure of polished metal and plastic surfaces to the environment outside the Gemini spacecraft. The information to be acquired included data regarding the particulate material collected, holes and craters in the specially prepared surfaces, the penetration characteristics of micrometeorites on thin films, and the survival fractions of viable micro-organisms remaining on the exposure plates. Also, a search was to be conducted for viable micro-organisms in the particle flux in the vicinity of the spacecraft. The micro-organisms used were ubiquitous agents that are harmless to man. These organisms were resistant to adverse conditions, as has been proven in laboratory tests; hence, they were selected for use in this experiment. All material specimens were to be returned to earth by stowage in the Gemini entry assembly for postflight examination and analysis. Also, through a guest-experimenter program, scientists from various institutions were invited to provide samples within the context of the topics mentioned. Guest experimenters for Gemini X were Robert Skrivanek (U.S. Air Force Cambridge Research Laboratory), Hugo Fetchig (Max Planck Institute), Neil Farlow (NASA Ames Research Center), Uri Shafrir (University of Tel Aviv), John Kerridge (Birkbeck College), H. Ferandez-Moran (University of Chicago), Paige Burbank (NASA Manned Spacecraft Center), Michael Carr (U.S. Geological Survey), Otto Berg (NASA Goddard Space Flight Center), Francis Wright (Smithsonian Observatory), and Paul Hodge (University of Washington).

EQUIPMENT

The micrometeorite collector is shown in figure 1. The unit was 5.5 by 11 by 1.25 inches and weighed approximately 6.5 pounds when loaded for flight. Not visible in the figure are the dual internal battery package, the cover drive motor and gear

*The Dudley Observatory and The State University of New York, Albany, New York.

**The New York State Department of Health, Albany, New York.

train, the cover limit switches, and the squib-actuated unlatching and locking devices. The unit, with cover open, is shown in figure 2. This figure is illustrative of the 12 sample slides contained in one compartment of the device. The dual-cover arrangement was used to facilitate the inclusion of sterile samples in one section and of live micro-organisms in the other section. The sample slides in the second compartment are shown in figure 2. A diagram of sample locations and a brief description of the nature and source of the sample are shown in table I.

EXPERIMENTAL PROCEDURE

Preflight Phase

Gemini IX mission. - The final loading procedures were begun approximately 10 days before launch. The hardware was cleaned thoroughly. The compartment to be sterilized was loaded in a dust-free hood, and the cover was closed. Then, the unit was placed in a clean stainless-steel box, the covers of the unit were opened partially, and ethylene oxide was introduced for sterilization purposes. After sterilization, the covers were closed and secured. The unit was removed to a dust-free hood, and the nonsterile compartment was opened manually for loading the sample slides. After completion of loading and final mechanical adjustments, the unit was wrapped in plastic, placed in a special container, and hand-carried to the Kennedy Space Center (KSC) 3 days before the scheduled launch. Two units were loaded in this way and were designated as the flight unit and the backup unit.

After prelaunch tests, designed for verification of operational readiness, the flight unit was installed on the spacecraft retroadapter 17 hours before launch. As part of the final countdown, three sterile swabs were used to sample the microbiological environment of three selected regions inside the spacecraft. After the Atlas failure and the decision to delay the mission, the unit was removed from the spacecraft, and the internal batteries were charged. Then, both the flight and the backup units were stored in the Biomedical Sciences and Flight Experiments Laboratory, KSC, at 50° F until installation on the spacecraft retroadapter on May 31, 1966. The unit remained on board the spacecraft during the 2-day hold necessitated by the computer malfunction.

Gemini X mission. - Preflight procedures were the same on the Gemini X mission as they were on the Gemini IX mission. No launch problems affected the experimental procedure, however.

Gemini XII mission. - Slides were loaded at the Dudley Observatory, Albany, New York, in a small clean room under a dust hood equipped with filters. The air to which the samples were exposed during loading was filtered doubly. Two collector units were loaded for each flight, one for flight and the other for a backup unit. The sterile compartment was loaded first, and all slides within that compartment were loaded before sterilization. The collector was inserted in a stainless-steel box with a small Millipore-filter-covered port (10 millimicrons porosity) equipped with an electrical connection. The collector was sterilized for 4 hours with ethylene oxide at 54° C, approximately 1000 torr, and 40 percent relative humidity. After sterilization, the compartment was closed electrically and was sealed with a temporary door clamp. Then, the collector was removed from the steel box and was returned for loading in

the nonsterile compartment. The two units were taken to KSC 3 days before launch, and they were stored in a sealed, clean air-conditioned locker compartment. The flight unit was mounted on the spacecraft behind the pilot hatch approximately 16 hours before launch. Then, the outside of the collector was given a final cleaning by swabbing it with a nylon cleaning cloth dampened with ethyl alcohol.

Inflight Phase

Gemini IX mission. - After the successful launch of the Gemini-Titan II at 08:39:33 e.s.t. on June 3, 1966, the unit was opened by the pilot at 09:29 g.e.t. and was closed at 17:10 g.e.t. It was opened again at 35:48 g.e.t. and the unit was closed and locked at 44:54 g.e.t. The total exposure time was 16 hours 47 minutes. The crewmembers were unable to hear the cover drive motor during any of the opening or closing sequences. It is not certain whether the locking mechanism was heard. However, postflight examination indicated that the unit did open and close as planned. The experiment hardware was recovered by the pilot and stowed within the spacecraft cabin.

Gemini X mission. - The cover door of the micrometeorite collection device remained in the closed position until immediately before the first sleep period, a period of drifting flight. This activation time was chosen to prevent exposure of the sample surfaces to particles caused by thruster firing, fuel-cell purging, or dumping of liquids overboard. The collector door was left open for an 8-hour period.

Gemini XII mission. - The cover door of the micrometeorite collection unit remained in the closed position during flight until the first sleep period, as was done on the Gemini X mission. The collector door was opened for one period of 6 hours 24 minutes. The exposure was made while the spacecraft was coupled to the Agena vehicle and oriented so that the collector surfaces faced outward, away from the earth and tilted forward approximately 15° in the direction of vehicle travel. Orientation was maintained during exposure by the use of cold-gas vernier thrusters on the Agena vehicle. The opening and closing of the collector was verified by the inclusion of photographic film in the unit. The film was so blackened by exposure to sunlight that development was not necessary. Also, the biological exposure experiments were verification that the opening and closing functions had been successful. Both compartments of the collector were under vacuum when returned after flight exposure.

Postflight Phase

Gemini IX mission. - The experiment hardware was removed after the spacecraft was brought on board the recovery vessel. The unit was placed in a special case and was flown to Patrick Air Force Base, where a Dudley Observatory representative received it and returned it to the observatory on June 7, 1966. During the recovery procedure, three swabs were taken from the same regions of the spacecraft cabin, as were the preflight swabs. These were included in the recovery case and were taken to the observatory. After arrival at Dudley Observatory, the outside of the unit was sterilized by ultraviolet light prior to opening. The unit was opened in a dust-free hood, and the samples were removed for analysis. Two methods were used to assure that the collector did open in space. One method was a piece of photographic paper

located in a section of the collector. The paper appeared to be almost black, even without processing. The second assurance of opening was that portions of the various micro-organisms were killed.

Gemini X mission. - The hardware was retrieved during the egress part of extravehicular activity (EVA), at 49:50 g.e.t. and then was stowed in the spacecraft. The crewmen reported at 64:15 g.e.t. that the hardware could not be found in the spacecraft. They believed that the experiment hardware floated through the open hatch during EVA. A subsequent check of the crew compartment, after spacecraft retrieval, verified that the collection device had been lost.

Gemini XII mission. - Immediately after recovery of the spacecraft, the flight unit was flown to Dudley Observatory. The contents of the nonsterile compartments were unloaded first in a clean room. The collectors were sent to the Virus Research Laboratory of the New York State Department of Health and were placed in a sealed box. Sterilization of the collector unit and tools was accomplished by the use of an ultraviolet germicidal lamp for 15 minutes. The collector was then left overnight in the box with air recirculating through a Cambridge absolute filter. The following day, the sterile samples were removed. The collector box was shut and was returned to the Dudley Observatory clean room, where micrometeorite samples in the sterile compartment were removed.

RESULTS

Two of the eight samples from the Gemini IX mission were examined in detail. These samples consisted of thin nitrocellulose films supported by 200-mesh copper screen. One sample was preshadowed with palladium to "tag" any possible contaminants; the other sample was preshadowed with aluminum. On the palladium-shadowed sample, an area of approximately 5 mm^2 was scanned with an electron microscope at sufficient magnification to detect all structures larger than 0.1 micron. Also, a total of 6 mm^2 of control sample was scanned. For the aluminum-shadowed samples, approximately 2 mm^2 of exposed area and an equivalent control area was scanned. The control samples were located in recesses in the bottom of the sample slides. The samples were scanned to detect and record any particulate matter on the surface of the film and to observe any damage to the film caused by high-velocity particles. Generally, the particulate material that was collected had an irregular shape. A few "fluffy" particles have been observed, and these were similar to those found on samples exposed on sounding rockets.

The most common effects observed in the thin films are penetration holes. Several types of holes have been noted. The most common type is a single hole, often with flapped edges. The ragged holes produced by the fast-moving particles are shown in figures 3 and 4. A relatively large area that has been deformed by a large particle or group of particles is shown in figure 5. A cluster of holes, all confined to a small area, is shown in figure 6. This cluster may have been a single conglomerate particle that was broken by the interaction of the particle with a "gaseous atmosphere" in the vicinity of the spacecraft. A single large penetration and a few small associated holes

are shown in figure 7. Similar hole structures were observed during the control flight or the noctilucent-cloud-sampling experiment in 1962.

Two hundred holes or groups of holes of the types shown have been found on the palladium-shadowed films. All of these have been found to be grossly different from any holes or imperfections on the control surfaces. The aluminum-shadowed samples appear to have fewer hole structures than does the palladium-shadowed material. This apparent difference may be caused by the smaller number of aluminum-shadowed samples studied. A unique hole structure is shown in figure 8. Twenty-five of these structures have been observed on the palladium-shadowed samples. In general, these structures appear to have a rounded outline, an elliptical intermediate region, and an elongated hole in the center. Generally, the entire structure rises above the surface a distance equal to approximately one-fifth of the diameter of the structure. These structures may be the result of higher velocity impacts than the holes previously discussed.

The biological experiments have produced some useful and interesting results. The sterile surfaces that were intended to collect organisms have been sampled and cultured, but they have shown no indication that any viable organisms were collected. Swab samples, taken before and after the flight, were a control for this experiment. In three of the five survival tests of known organisms, definite fractions of the organisms survived. The results are tabulated as follows.

Organisms	Surviving fraction
T_1-bacteriophage in broth concentrate	2×10^{-6}
T_1-bacteriophage in B-4 lysate	0
Penicillium sp.	3×10^{-5}
Tobacco mosaic virus	2×10^{-3}
Bacillus stearothermophilus	0

The sample preparation of thin nitrocellulose films for the experiment was performed in a manner similar to that used on previous rocket sampling experiments (refs. 1 and 2). Preflight and postflight metal shadowing was used to reduce the contamination noise level. Inflight controls were included by the use of slides of half-thickness and letting the controls slide face-down in the individual slide compartment. The flight-control and the flight-exposed films were made for each sample location at the same time. A relatively large number of holes was found in the Gemini IX unit. However, very few holes were noted in the Gemini XII unit. Only one hole was observed in the first 23 mm^2 of the Gemini XII thin-film data. It is apparent that the fluxes inferred from the Gemini IX and XII missions are in disagreement by

approximately a factor of 100 in the size range from 0.1 to 1 micron. The types of holes found in the Gemini IX unit, but not found in the Gemini XII unit, are discussed as follows.

An electron micrograph of a typical isolated flapped hole found in a palladium-shadowed nitrocellulose film is shown in figure 9(a). The nitrocellulose film was deformed in the vicinity of the hole. Another flapped hole without any film deformation in the nitrocellulose film adjacent to the hole is shown in figure 9(b). A group of clustered flapped holes is shown in figure 10. In the figure, the nitrocellulose films are deformed significantly adjacent to many of the holes. Similar film deformations have been observed in surfaces exposed during rocket-borne sampling experiments. The cluster is believed to be the result of an impact of a slightly broken, fragile, extremely irregular particle. It is possible that the particle consisted of several relatively large, solid particles, held together lightly by a material that appears to evaporate easily and to react with the nitrocellulose film. The slight separation of the holes may be caused by an interaction with a weak atmosphere in the vicinity of the spacecraft before particle impact. Another multiple-hole structure, with a different film deformation in the vicinity of the individual holes, is shown in figure 11. Here, the film deformations contain large numbers of low-density particles of 100 to 500 angstroms diameter and consequently are close to the resolution limit of the photoanalysis processes. In the center of the film, a rounded particle is noted, which could be a portion of the impacting particle structure.

In addition to the flapped-hole structures, significant numbers of structures not observed previously in rocket-borne collection experiments have been found. Two examples of the large structures are shown in figures 12(a) and 12(b). Apparently, the structures consist of elongated holes, surrounded by elliptical, deformed regions, that are, in turn, surrounded by regions of circularly symmetrical film deformation. The structures are believed to be the result of an ultrahigh velocity impact on the film, the size of the impacting particle being approximately the width of the elongated hole. The region of near-circular symmetry that surrounds the hole may represent energy dissipation in the impact. The second shadows observed around these structures are indicative that the surface of the film has been elevated slightly above the normal plane of the film.

Typical data from the Gemini IX mission and all data from the Gemini XII mission are shown in table II. The masses of the impacting particles have been estimated from the widths of the individual holes. Multiple-hole structures have been counted as single impact sites. The data given are conservative in that only the hole structures clearly distinguishable from those in the inflight controls were counted. Ten to 20 times as many holes were discounted as were assumed to be real penetration holes. Most of the discounted holes could be identified clearly as holes commonly found in thin nitrocellulose films. Flux values from the preliminary results of Experiments S012 and S010 are shown in figure 13. A rough correction for earth shielding has been made by multiplication of the raw fluxes by 2. These values are compared with several other flux measurements: The satellite and rocket microphone data as have been published for curve A (ref. 3); the Pegasus data (ref. 4); the nonshower balloon-top collections (ref. 5); the Venus flytrap and noctilucent-cloud control collection of 1962 (ref. 6); the zodiacal-light estimates and others (refs. 7 and 8); and the flux implied by a large crater observed in the Project Mercury periscope lens during the flight of Eros (ref. 9).

Also, some previously unpublished data from the Dudley Observatory are included from a rocket sampling with the Pandora collector in four discrete altitude ranges 2 days after the peak of the Leonid shower of 1965.

Preliminary results of Experiments S010 and S012 may be summarized as follows.

1. The cumulative influx rate in the size ranges from 10^{-15} to 10^{-14} gram was approximately 2 particles/m^2/sec, as determined from Experiments S010 and S012 on the Gemini XII mission.

2. The cumulative influx rate in the same mass range, as determined by the data from Experiment S012 on the Gemini IX mission was almost 200 particles/m^2/sec.

3. The large-particle cumulative influx rate was approximately 3×10^{-5} particle/m^2/sec, with a mass of the order of 10^{-7} gram.

Sterile Collection Attempts

No living organisms could be found on the Gemini XII sterile collection surfaces after recovery and handling; extreme precautions were used against contamination within a sterile chamber. The experiments flown on the Gemini IX and XII missions failed to result in any evidence of live entities having been collected in space during the exposure periods. Tests for the presence of live organisms in an aqueous solution from the sterile surfaces included several different broth media for aerobic and anaerobic bacteria, fertile chicken egg inoculation, and monkey-kidney and Hela-cell tissue-culture inoculation. All of these tests were negative.

Survival of Terrestrial Micro-Organisms in Space

The results of the Gemini XII exposure of Penicillium roqueforti spores and Escherichia coli bacteriophage T_1 are shown in table III. In this experiment, there was no survival of the Penicillium sp., but a small fraction of the T_1 coliphage survived. The space exposure caused only approximately 50-percent reduction in titer, compared with laboratory controls when solar radiation was shielded by approximately 0.4 millimeter of aluminum.

The biological samples on board the spacecraft were exposed to cosmic radiation and the solar electromagnetic radiation. The fact that a 0.4-millimeter thick aluminum shield used in the Gemini Program experiments could almost completely protect the Penicillium sp., and protection to the extent of at least 3000-fold higher survival of the T_1-coliphage is indicative that the nonpenetrating radiation, probably solar ultraviolet and soft X-rays, was responsible for the death of micro-organisms directly exposed to space. Previous sounding rocket experiments that involved very thin-film metal filters (ref. 10) resulted in the same conclusion, that solar ultraviolet radiation and soft X-rays probably were responsible for the inactivation.

A measure of the lethal effect of the solar radiation from the results of the two Gemini missions are shown in table IV, expressed as surviving fractions relative to the shielded flight controls. Variations in stability of the sample batches, prepared some months apart, are controlled as are differences caused by inactivation during transportation and storage of the flight units. The coliphage samples are indicative of a remarkable similarity of survival. Because radiation flux essentially was constant during exposure periods, the extreme resistance of a fraction of the population of organisms is likely because of differences in the susceptibility of individuals in the population. Presumably, this susceptibility was caused by shielding of a small proportion of organisms, at the base of the air-dried layer of organisms, by the aggregated individuals.

REFERENCES

1. Hemenway, C. L.; and Soberman, R. K.: Studies of Micrometeorites Obtained from a Recoverable Sounding Rocket. Astron. J., vol. 67, no. 5, June 1962, pp. 256-266.

2. Hemenway, C. L.; Soberman, R. K.; and Witt, G.: Sampling of Noctilucent Cloud Particles. Tellus, vol. 16, no. 1, June 1964, pp. 84-88.

3. McCracken, C.; and Dubin, M.: Dust Bombardment on the Lunar Surface. NASA TN D-2100, 1963.

4. Stuhlinger, E.: Meteorite Measurements in the Pegasus Project. Astronautik, vol. 3, July-Aug. 1966, pp. 100-104.

5. Hemenway, C. L.; Hallgren, D. S.; and Coon, R. E.: High Altitude Balloon-Top Collection of Cosmic Dust. COSPAR, International Space Science Symposium, Vienna, 1966.

6. Soberman, R. K.; and Hemenway, C. L.: Meteoric Dust in the Upper Atmosphere. J. Geophys. Res., vol. 70, no. 19, Oct. 1965, pp. 4943-4949.

7. Ingham, M.: Observations of the Zodiacal Light from a High Station IV. The Nature and Distribution of Interplanetary Dust. M. N. Royal Astron. Soc., vol. 122, no. 2, 1961, pp. 157-175.

8. Elsasser, H.: Die Raumliche Vertielung der Zodiakalichtmaterie Z. Astrophys., vol. 32, 1964, p. 274.

9. Hemenway, C. L.; Linscott, I.; Secretan, L.; and Dubin, M.: Preliminary Studies of Possible Cosmic Dust Impacts on Project Mercury Vehicle Periscope Lenses. Annals of the N. Y. Academy of Sciences, vol. 119, Nov. 1964, pp. 106-115.

10. Hotchin, J.; Lorenz, P.; and Hemenway, C. L.: The Survival of Micro-organisms in Space. Nature, vol. 206, May 1965, pp. 442-445.

TABLE I. - EXPERIMENT S012 LOADING FOR THE GEMINI XII MISSION

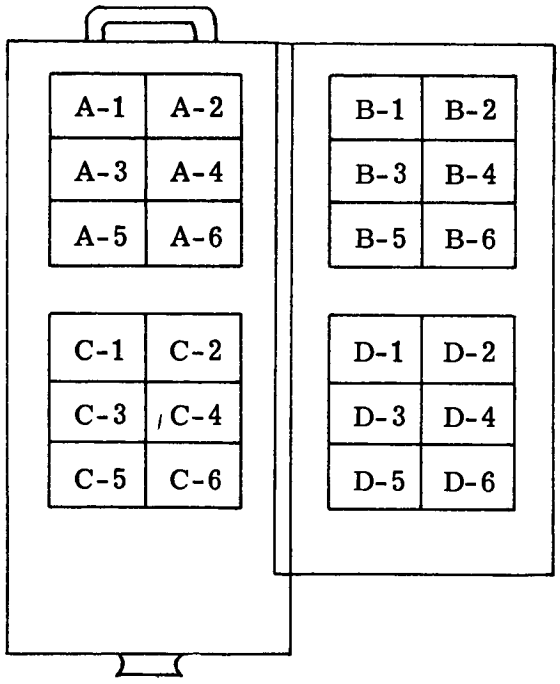

Location	Sponsor	Specimen type
A-1	Dudley Observatory	Nitrocellulose film over glass
A-2	U. S. Air Force Cambridge Research Laboratory	Nitrocellulose film
A-3	Dudley Observatory	Biological exposure
A-4	Dudley Observatory	Biological exposure
A-5	Dudley Observatory	Stereoscan sample, gold and indium-coated glass
A-6	Dudley Observatory	Nitrocellulose film over glass
B-1	U. S. Air Force Cambridge Research Laboratory	Layers of nitrocellulose film
B-2	Dudley Observatory	Stereoscan sample, copper

TABLE I. - EXPERIMENT S012 LOADING FOR THE GEMINI XII MISSION - Concluded

Location	Sponsor	Specimen type
B-3	U.S. Geological Survey	Nitrocellulose on gold mesh
B-4	University of Tel Aviv	Penetration through film
B-5	Dudley Observatory	Layers of silicon oxide film
B-6	Max Planck Institute	Layers of nitrocellulose film
C-1	Dudley Observatory	Nitrocellulose film over glass
C-2	Max Planck Institute	Stereoscan plates
C-3	Dudley Observatory	Sterile collection plates
C-4	Dudley Observatory	Sterile collection plates
C-5	NASA Ames Research Laboratory	Gold-coated plastic
C-6	University of Washington	Polished copper
D-1	Dudley Observatory	Stereoscan samples, stainless steel
D-2	NASA Manned Spacecraft Center	Aluminum on stainless steel
D-3	Birkbeck College	Aluminum on stainless steel
D-4	Smithsonian Observatory	Gold on plastic
D-5	NASA Goddard Space Flight Center	Chromium on glass
D-6	NASA Ames Research Laboratory	Metal-coated plastic

TABLE II. - EXPERIMENT S012 DATA SUMMARY

Exposed	Control
Gemini IX mission Aluminum-shadowed nitrocellulose (location B-2)	
2735 frames[a] 28 holes	825 frames[a] No holes
Gemini IX mission Aluminum-shadowed nitrocellulose (location A-1)	
528 frames[a] 13 holes	95 frames[a] No holes
Gemini XII mission Aluminum-shadowed nitrocellulose (location A-1)	
2858 frames[a] 1 hole	1394 frames[a] No holes

[a]A frame has an area of approximately $8100\mu^2$.

TABLE III. - SURVIVAL OF PENICILLIUM ROQUEFORTI MOLD AND T_1 PHAGE AFTER 6 HOURS EXPOSURE TO SPACE AND SOLAR RADIATION DURING THE GEMINI XII MISSION

Organism	Lab control	Flight shielded	Flight exposed
Penicillium roqueforti	5.5×10^5	2.0×10^5 (0.4)	0 (<0.000002)
T_1 phage	7.7×10^4	3.1×10^4 (0.5)	9.1 (0.0001)

TABLE IV. - SURVIVAL OF PENICILLIUM ROQUEFORTI SPORES AND T_1 PHAGE ON THE GEMINI SPACECRAFT IN ORBIT

Organism	Survival fraction[a] relative to shielded flight control	
	Gemini VIII mission (17 hr)	Gemini XII mission (6 hr)
Penicillium roqueforti	0.00004	<0.000005
T_1 phage	0.0003	0.0005

[a] $\text{Survival fraction} = \frac{n_{\text{exposed}}}{n_{\text{shielded}}}$.

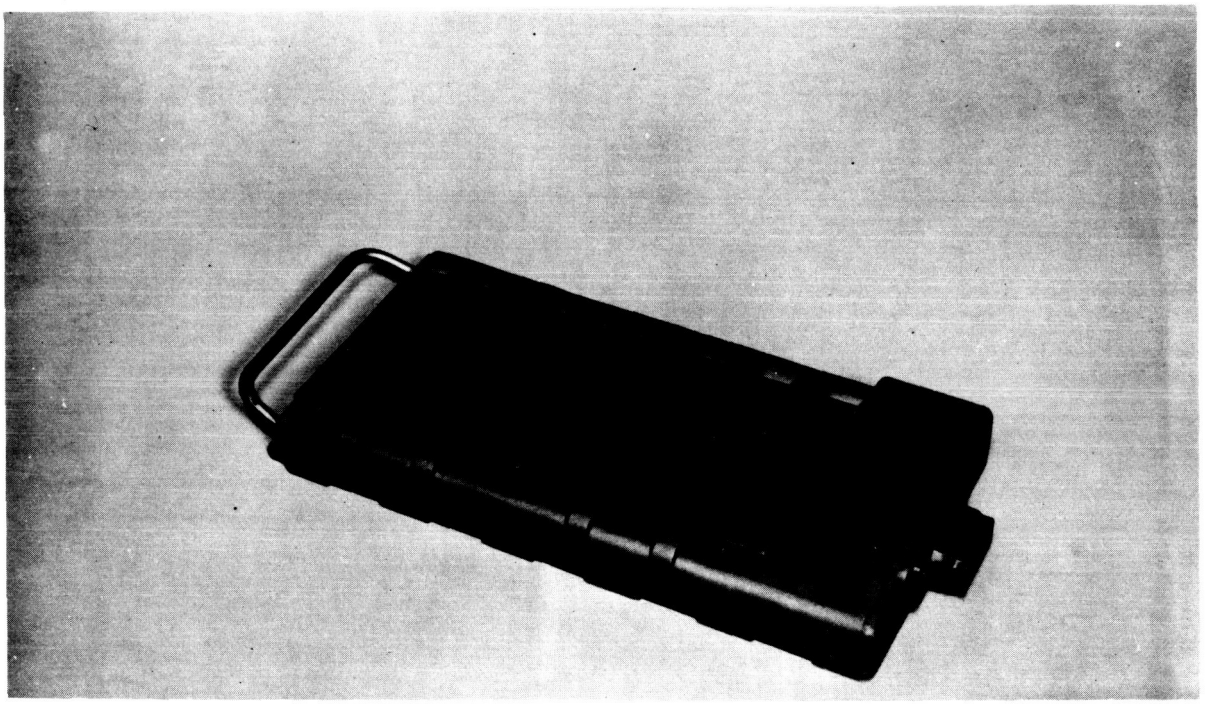

Figure 1.- The micrometeorite collector.

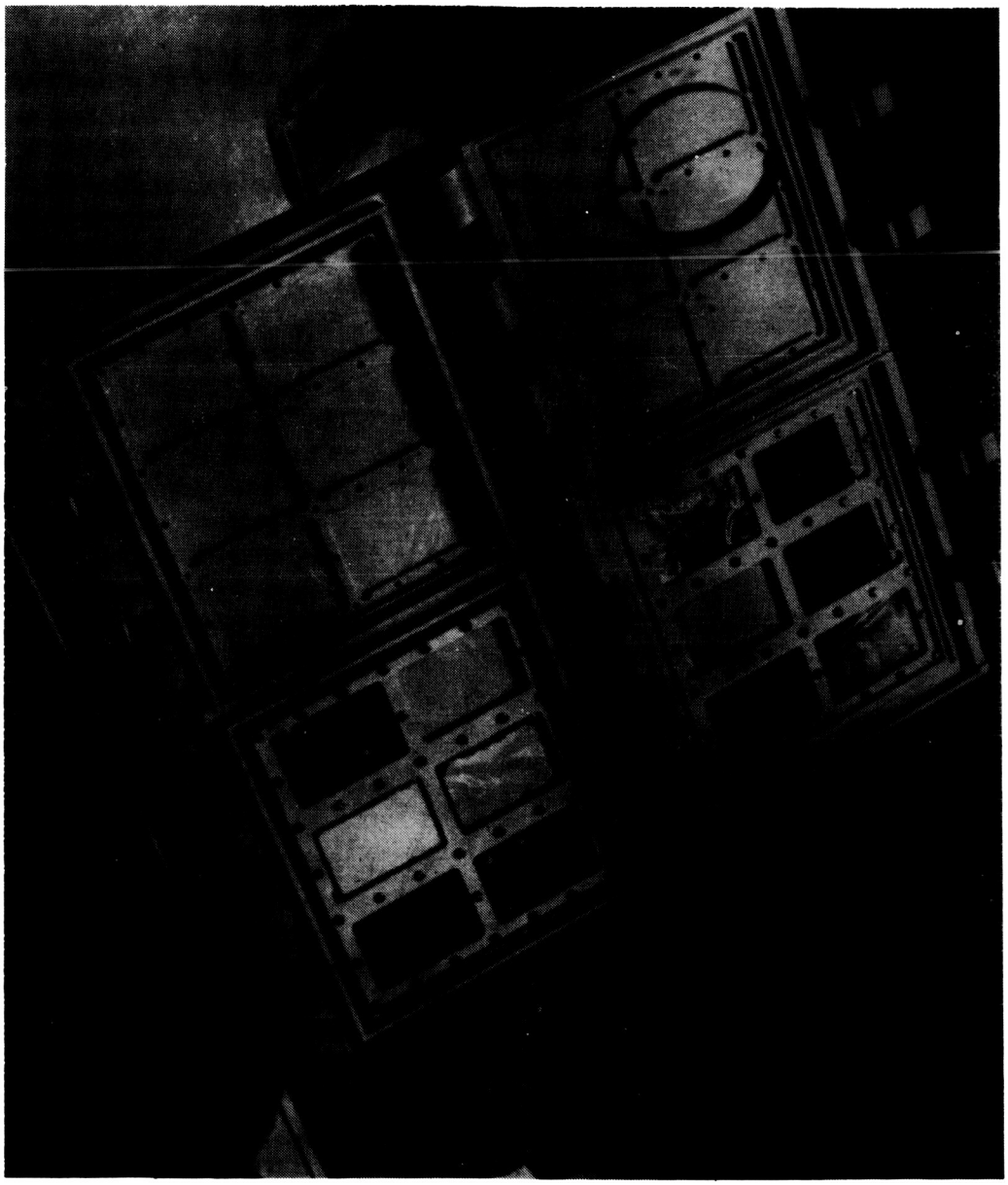

Figure 2. - The collector with one cover open.

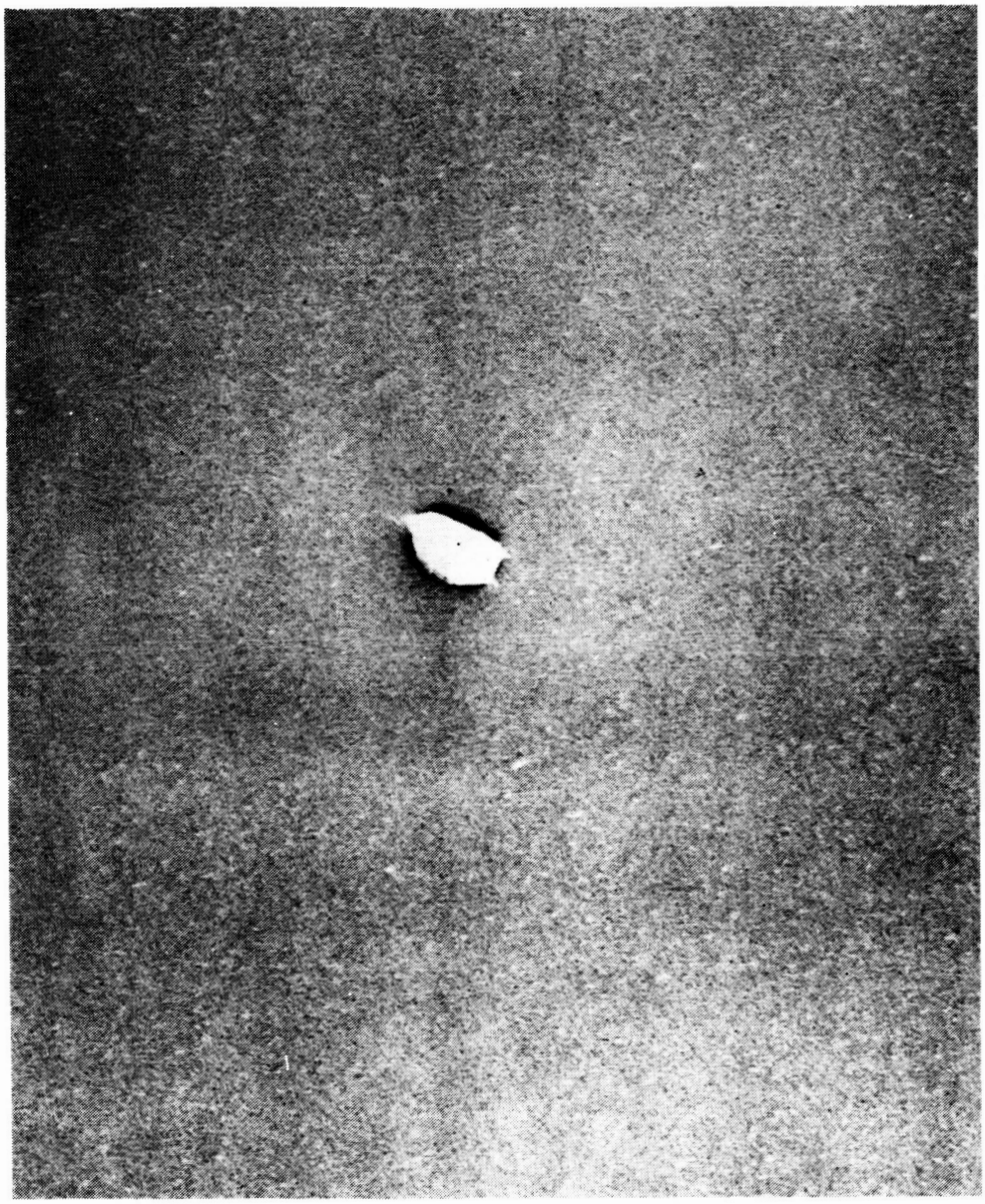

Figure 3. - A ragged hole produced by a fast-moving particle (× 40 000).

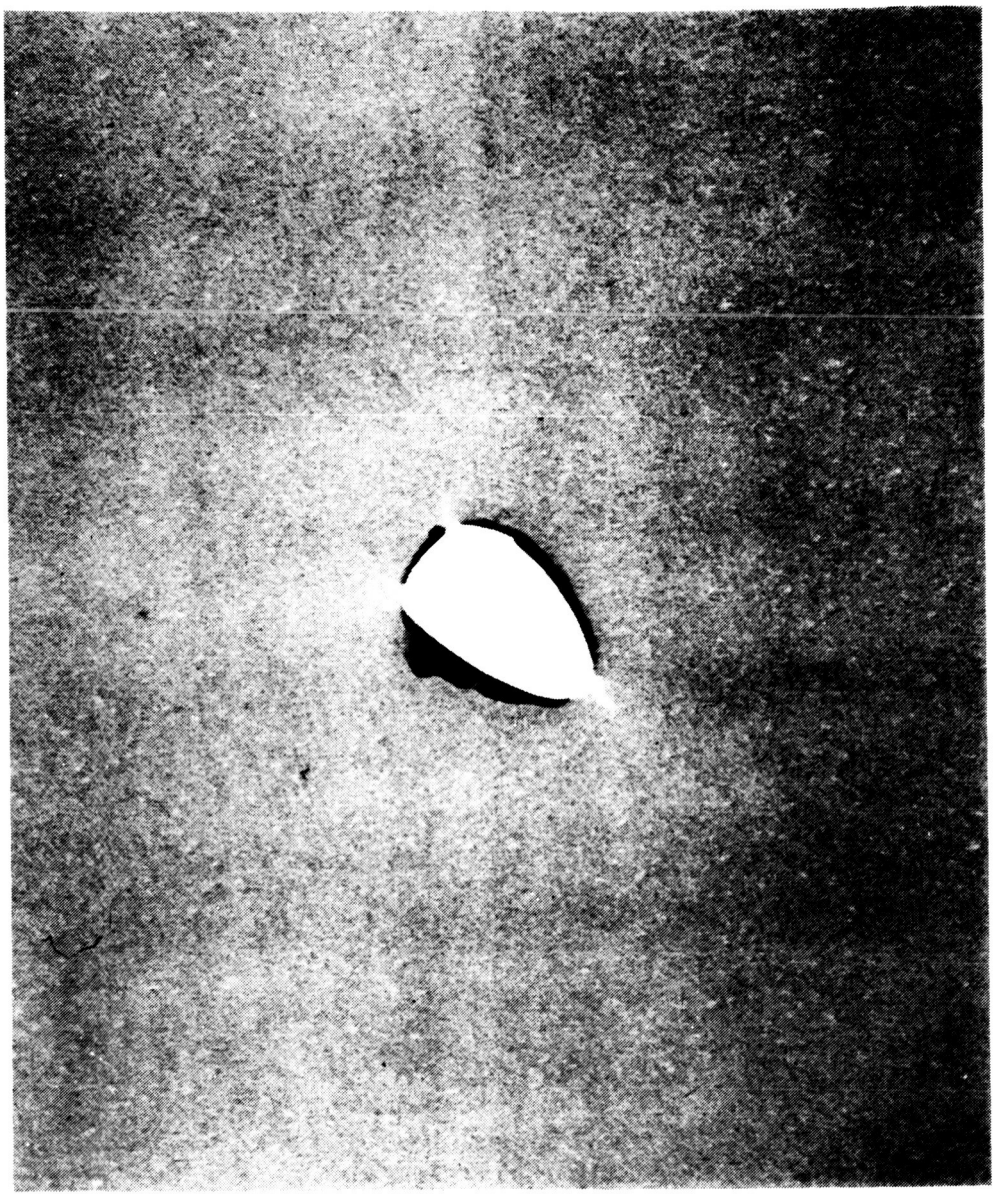

Figure 4. - Another ragged hole produced by a fast-moving particle (× 40 000).

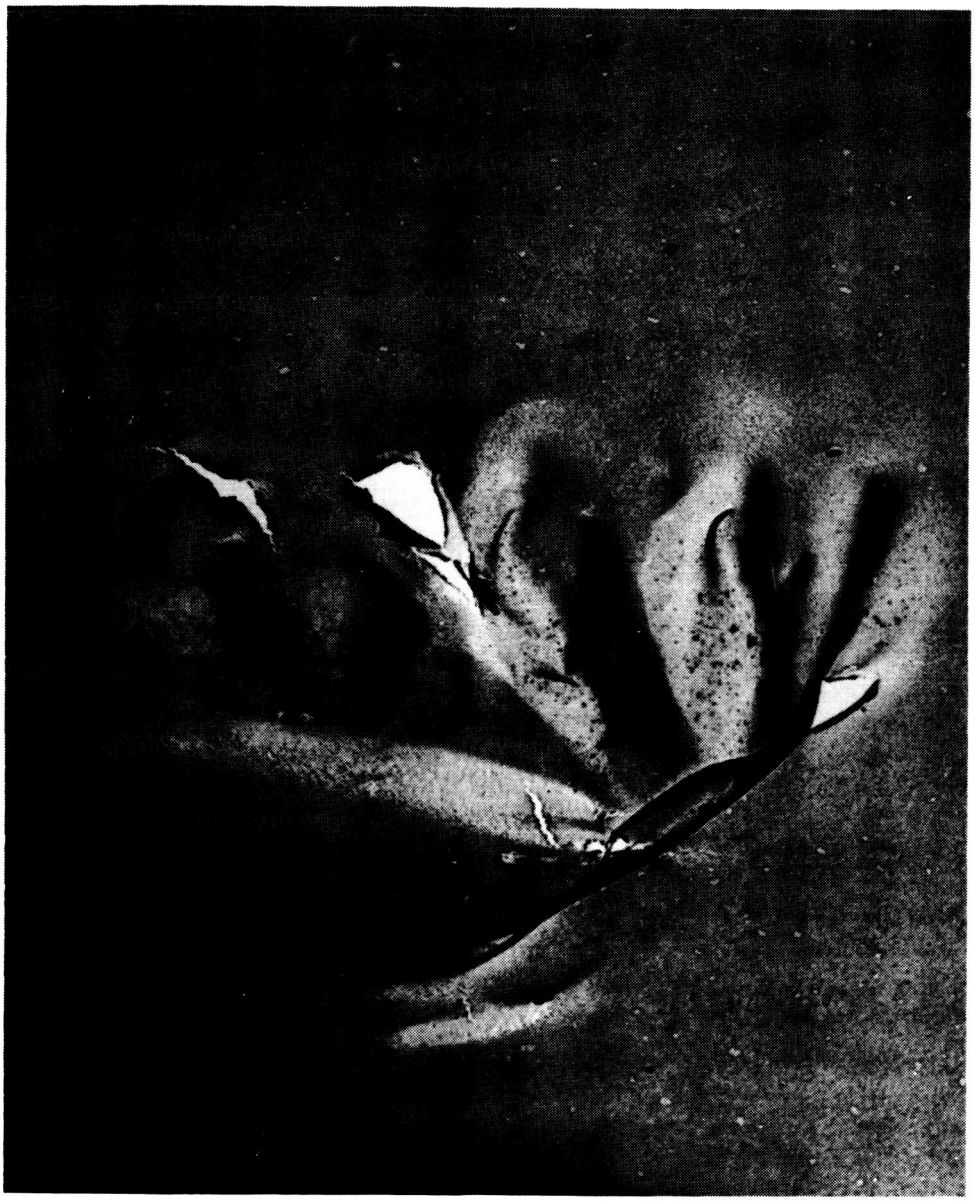

Figure 5. - A relatively large region that has been deformed by a large particle or group of particles (× 20 000).

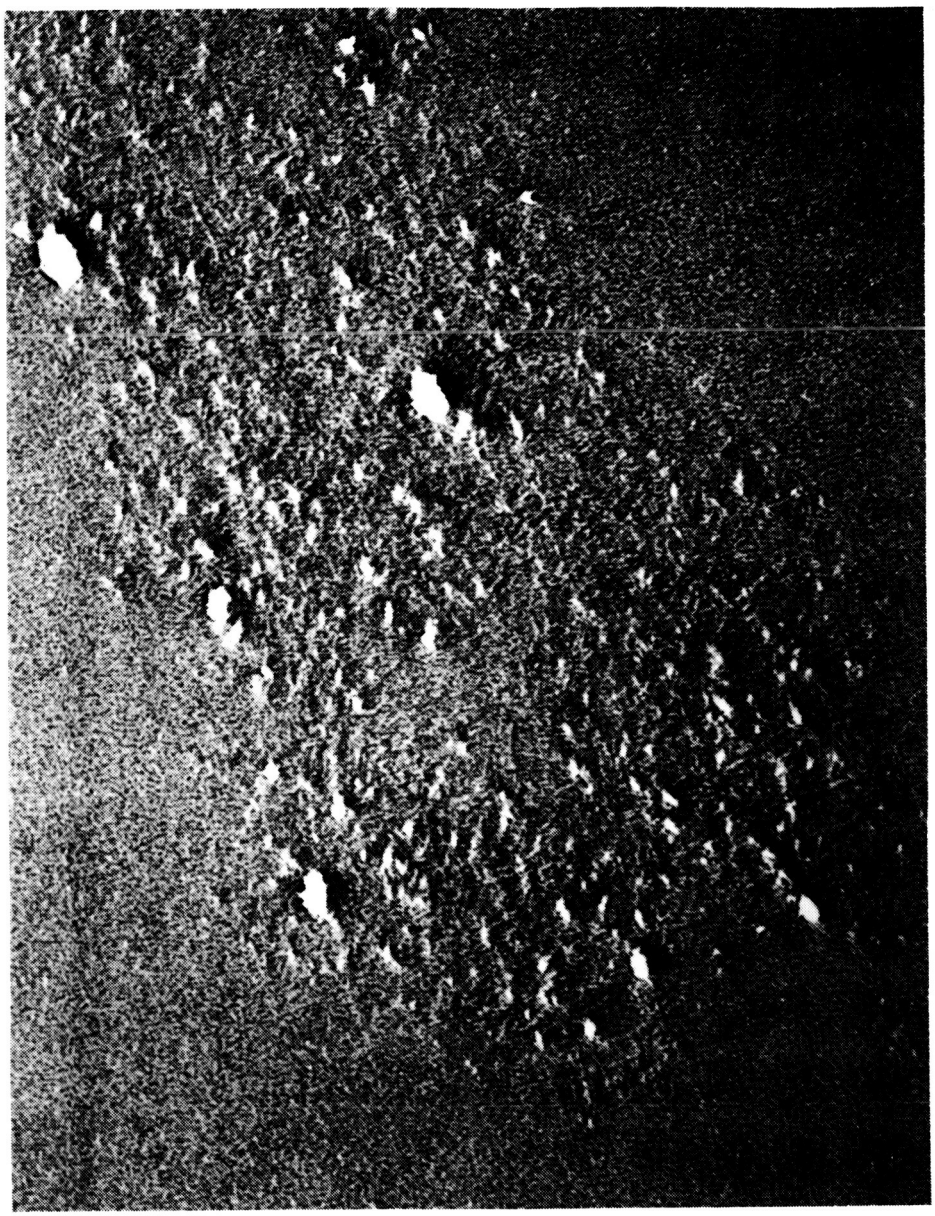

Figure 6. - A cluster of holes confined to a small region (× 40 000).

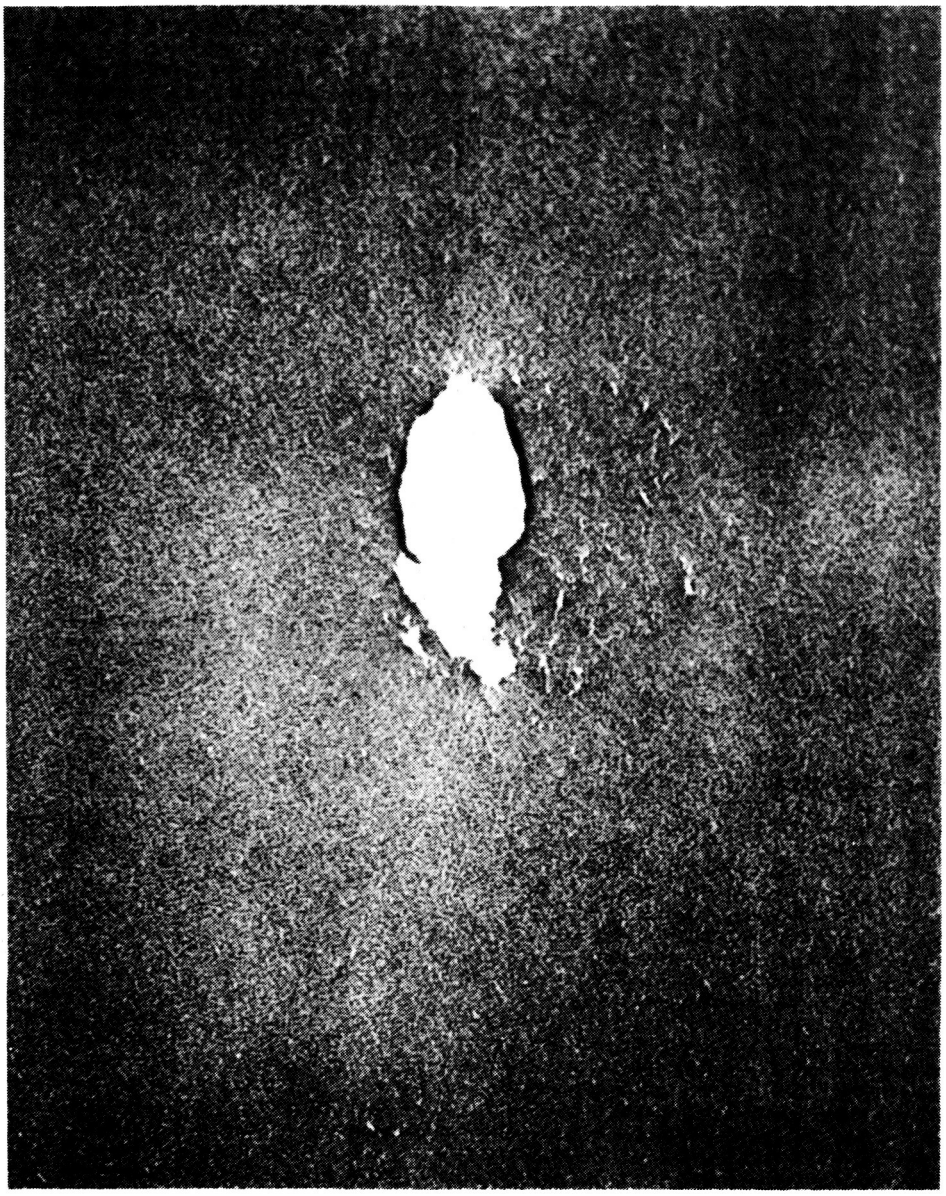

Figure 7. - A single, large penetration plus a few small associated holes (× 40 000).

Figure 8. - A unique hole structure, perhaps the result of a high-velocity impact (× 40 000).

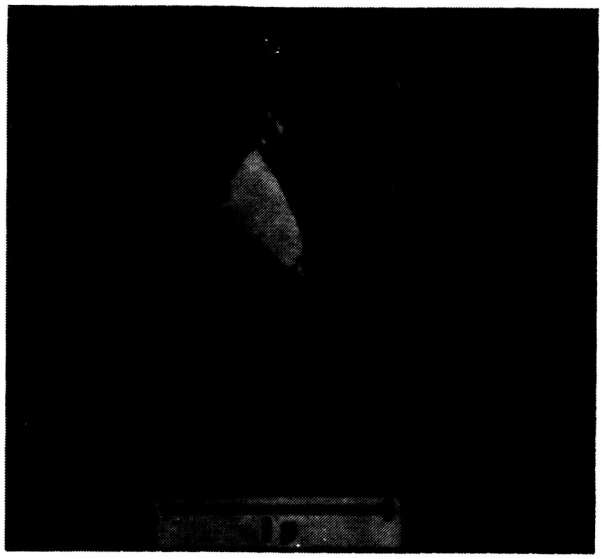

(a) Deformation visible.

(b) No deformation.

Figure 9. - Thin-film penetration holes.

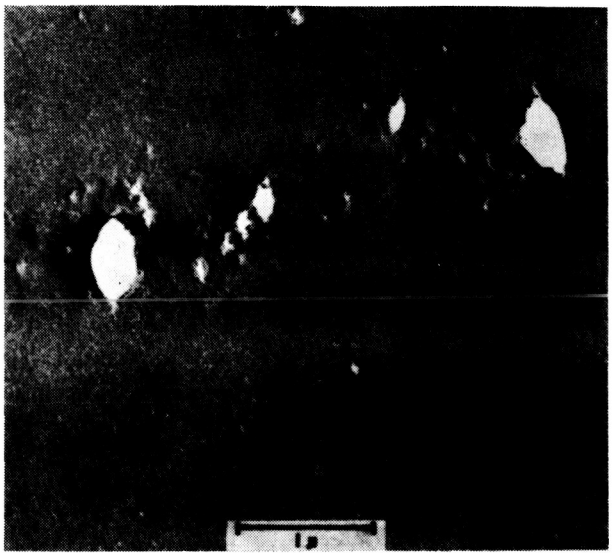

Figure 10. - A group of thin-film penetration holes with adjacent deformations.

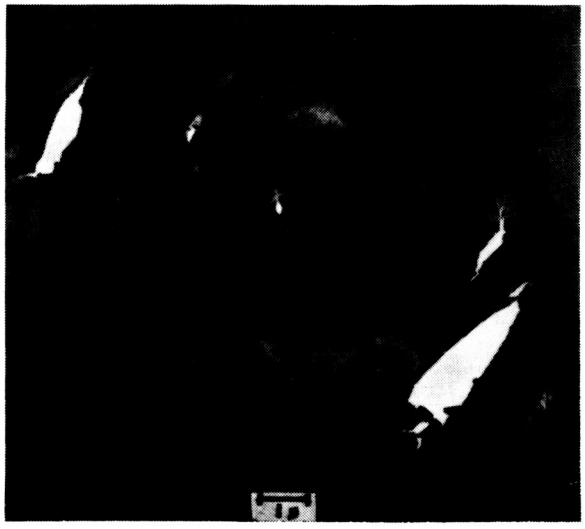

Figure 11. - A multiple-hole structure with deformation from low density (100 to 500 Å).

(a) First view.

(b) Second view.

Figure 12. - An elongated hole surrounded by an elliptical, deformed region.

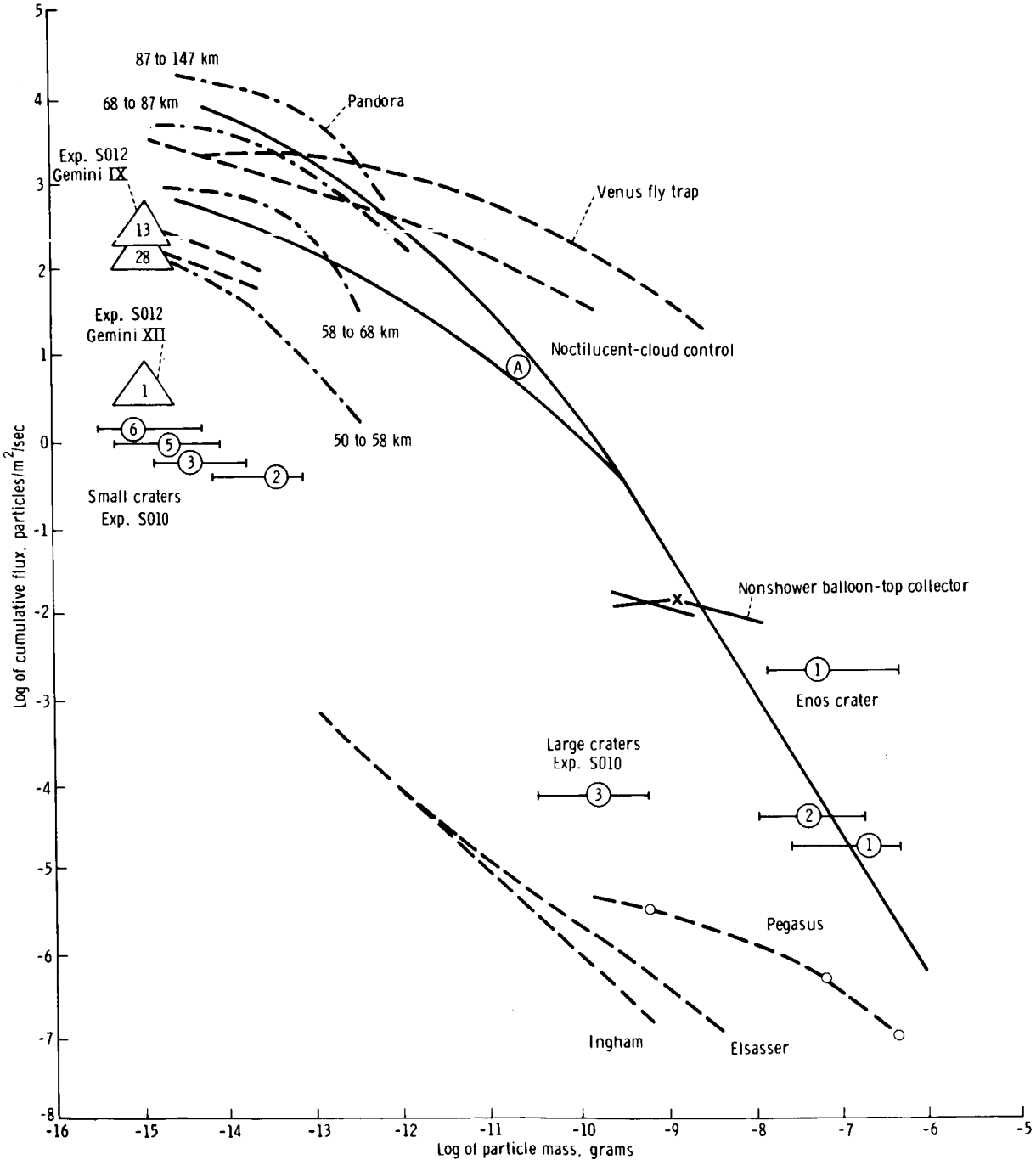

Figure 13. - Flux values from Experiments S010 and S012.

EXPERIMENT S005

SYNOPTIC TERRAIN PHOTOGRAPHY

By Paul D. Lowman, Jr.,* and Herbert A. Tiedemann*

OBJECTIVE

The objective of Experiment S005 — performed on the Gemini IV, V, VI, VII, X, XI, and XII missions — was to obtain high-quality color photographs of specific regions of terrain for geologic, geographic, and oceanographic study.

EQUIPMENT

Gemini IV, V, VI, and VII Missions

The camera, film, and filter (Hasselblad 500C, Planar 80-millimeter lens, Ektachrome S0-217, and haze filter) were the same as used on the Gemini IV, V, VI, and VII missions. On the Gemini VII mission, a Zeiss Sonnar 250-millimeter camera with telescopic lens and Ektachrome infrared, type 8443 film were used. Camera preparation and loading and preliminary identification of the pictures were performed by the Photographic Technology Laboratory staff of the NASA Manned Spacecraft Center (MSC).

Gemini X Mission

Two cameras were used on the Gemini X mission: the 70-millimeter Maurer space camera, with Xenotar f/2.8 lens (80-millimeter focal length), and the 70-millimeter Hasselblad superwide angle (SWA) camera, with Zeiss Biogon f/45 lens (38-millimeter focal length). Haze filters were used. Eastman Ektachrome MS (S0-217) film with a 55- by 55-millimeter format was used in both cameras. The medium-speed color-reversal film was on a 2.5-mil polyester base.

*NASA Goddard Space Flight Center, Greenbelt, Maryland.

Gemini XI Mission

Two cameras suitable for terrain photography were used on the Gemini XI mission, and both cameras were similar to those used on the Gemini X mission. Many of the pictures were taken with the 70-millimeter extravehicular activity (EVA) camera that had a 38-millimeter focal length lens and a 90° prism assembly. A 70-millimeter general-purpose camera, which had an 80-millimeter f/2.8 lens, was used also. Standard film magazines were used, and both cameras contained medium-speed color-reversal film (2.5-mil polyester base). A haze filter was used on both cameras.

Gemini XII Mission

Two cameras, the Hasselblad SWA 70-millimeter camera and the Maurer 70-millimeter space camera, were used on the Gemini XII mission. The Hasselblad camera was equipped with a Zeiss Biogon lens of 38-millimeter focal length and a Hasselblad haze 63 filter (essentially an ultraviolet filter with cut-off at 3400 angstroms). The film was Ektachrome MS, S0-368. The recommended setting for this film over general terrain was 1/250 second at f/11 and 1/250 second at f/16 for desert regions.

PROCEDURES

The procedure for Experiment S005 was to take pictures through the spacecraft window when the selected region, or any other cloudfree land region, was overflown. Specific points that were emphasized are listed as follows.

1. Vertical photographs were very desirable. The camera was to be pointed straight down or as nearly vertical as possible.

2. Strip photographs (mode 1) were to be taken at 5-second intervals; individual or small numbers of photographs (mode 2) were to be taken as necessary to cover the region.

3. The spacecraft window was to be in the shade to prevent light scattering.

4. Pictures were to be taken within approximately 3 hours of local noon, except for sun glitter pictures, which might have required low sun angles.

5. The crewmen were to record the time, region, mode, magazine, and the frame numbers on the onboard voice recorder and/or in the logbook.

The crewmen followed this procedure as closely as possible. Also, the pilot took a number of photographs during standup EVA which were of excellent quality.

RESULTS

Because of the extensive discussion that is required, the results of Experiment S005 are discussed according to individual mission.

Gemini IV Mission

The five magazines of 70-millimeter Ektachrome film that were exposed during the Gemini IV mission resulted in approximately 100 pictures that are usable for terrain studies. Most pictures were of excellent quality with respect to exposure, resolution, and orientation. Priority was given to photography of East Africa, the Arabian peninsula, Mexico, and the southwestern United States; pictures of all these regions were obtained. Spacecraft fuel and power restrictions prevented the crewmen from always orienting the spacecraft vertically, as preferred for photography. However, a continuous series of pictures with nearly vertical orientation was taken. This series covered the flight path on the 32nd revolution from the Pacific coast of Mexico to central Texas. A detailed description of all the terrain photographs is beyond the scope of this report; instead, representative pictures are presented and discussed briefly.

The first of the photographic series taken over Mexico and the United States during the 32nd revolution is of an area approximately 75 miles square in Baja California (fig. 1). Bahia de Todos Santos, on the Pacific coast of Mexico, is visible at the lower left. A large amount of geologic detail is visible in the picture. The contact between Quaternary alluvium (light-colored material at upper and center right) and bedrock is apparent. A number of different igneous rock types were distinguished on the basis of color, although they could not be identified on the basis of only this picture. Possibly the most prominent geologic feature shown is the long linear valley at lower left, parallel to the edge of the spacecraft window. This valley, which was identified immediately as a fault (even on a preliminary examination of the picture), follows the Agua Blanca fault zone, one of the major tectonic features of Baja California. A number of linear valleys, either parallel to the Agua Blanca fault zone or intersecting it, are apparent; presumably they represent subsidiary faults. The potential value of hyperaltitude photography for regional tectonic studies is illustrated by the fact that this fault, so obvious from space, was not discovered until 1956 (ref. 1); and then, interestingly enough, discovery was made from aerial reconnaissance. The most recent authoritative publication on the geology of Baja California (ref. 2) contains no information regarding the existence of the fault, nor does it contain more than one rock type. Oddly enough, no evidence is shown in figure 1 of what was mapped (ref. 2) as a probable major fault (the San Pedro Martir fault) bounding the east side of the Sierra de Juarez. It is likely that figure 1 itself will be of value in the study of the tectonic structure of Baja California, because it is possible to delineate other faults outside the region mapped and reported in reference 1.

The third photograph taken in the 32nd revolution is shown in figure 2. The mouth of the Colorado River entering the Gulf of California is shown; the distance is approximately 70 miles across at the bottom of the picture. Considerable geologic detail is shown, such as the various rock types near the eastern shore of the gulf and

the fault just east of the Colorado River (the southward-trending linear feature outlined in white). Sand dunes in the desert (right) are visible also. Of particular interest is the amount of detail in the Gulf of California. The sinuous patterns off the river mouth resemble those near the Ganges River that were photographed on the Mercury-Atlas 9 flight and were identified as turbidity currents (ref. 3). However, the staff of the U.S. Naval Oceanographic Office has demonstrated that this pattern is actually the bottom topography of the Gulf of California, which is only a few feet deep at this point. Although these investigations state that figure 2 is unsuitable for actual depth mapping, the photograph reveals that the synoptic view of sediment distribution, photographed from this altitude, is of great interest to oceanographers.

Fifth in the 32nd revolution series, figure 3 is a view of part of the Gulf of California (left), the Pinacate volcanic field (center), and part of Yuma County, Arizona (upper right). The photograph is of geologic value in several respects. In addition to the submarine topography in the Gulf of California (previously mentioned), many major structural and lithologic features are obvious. The most prominent of these features is, of course, the Pinacate volcanic field. The Pinacate field has been known for hundreds of years; however, it was not delineated on the latest (1960) geologic map of Mexico, which had a scale approximately equal to that of the Gemini IV mission photograph. Figure 3 could be used to revise the alluvium-bedrock contacts on the geologic map. However, of greater interest is the fact that many bedrock lithologic units can be differentiated, and with the aid of available geologic maps, these units can be identified. For example, in Yuma County the contacts between Mesozoic granite (light) and Mesozoic schists and gneisses can be traced and, in many places, can be extrapolated across the Mexican border. The apparent similarity and continuity of granites in the various northwest-trending ranges tend to support the inference (ref. 4) that the entire region is underlaid by one or more batholiths. Based on a preliminary study, it appeared that most of the geologic detail shown in the 1:375,000 geologic map of Yuma County can be seen on the part of the county shown in figure 3 (with an original scale of approximately 1:2,000,000). Furthermore, some new information may be derived from the Gemini pictures. For example, just north of the Pinacate volcanic field, the bedrock appears to be cut by a series of north-trending fractures, outlined by drainage, which are not shown on the Yuma County map.

Portions of southern New Mexico, and Chihuahua and Sonora in Mexico are shown in figure 4, which was taken a few minutes later than figure 3 in the 32nd revolution. Two potential geologic applications of space photography are proven by figure 4. The first application, a refinement of existing geologic maps, is typified by the Sierra Carizarilla (the cluster of dark circular hills near the center of the photograph). The mountains are identified easily as volcanoes (for comparison, see fig. 3) belonging to a single field. Probably, they are relatively young, judging from their fresh-appearing topography. However, on the geologic map of Mexico (1960), only a few isolated outcrops of volcanic rock are shown, and they are dated as pre-Quaternary (more than one million years old). Another potential use of space photography is suggested by the fact that figure 4 covers a region in which two major tectonic provinces merge. The linear mountains (at the left) are the continuation of the Sierra Madre Oriental, characterized by folds similar to those in the Appalachians. However, the mountains at the lower right are chiefly block-faulted mountains, typical of the Basin and Range Province, and are placed in the Basin and Range class (ref. 4). It may be seen that these two types of mountain structure merge without significant change of direction, a relation that only could be realized by extensive field mapping in two countries.

During the 25th revolution, figure 5 was taken looking northwest over the Tibesti Mountains in the Republic of Chad, North Africa. This photograph was chosen to illustrate the geologic applications of space photography in remote regions. Despite the unfavorable angle, considerable topographic and geologic detail is visible. The most conspicuous feature is the crater of the volcano Emi Koussi, the highest point in the Sahara. However, of equal geologic significance, is the concentric lineation pattern in the foreground. This pattern is believed to represent a regional set of fractures, emphasized in places by sand deposition. Although these fractures were shown partially on the latest U.S. Army Map Service (AMS) map of the region, their existence has not been mentioned in any of the relevant geologic publications and apparently was not known to geologists. Another structure, also shown on the AMS map but unknown geologically, is the circular feature in the center of the picture (about eight crater diameters to the right of the Emi Koussi crater). This structure appears to resemble many of the "fossil" impact craters that Canadian geologists have discovered by study of aerial photographs of the Canadian shield. Although there is no a priori reason for the postulation of an impact origin for the Tibesti structure, especially because of its nearness to a volcanic region, its discovery demonstrated the potential value of space photography in the search for ancient impact structures.

Gemini V Mission

A photograph of the Zagros Mountains in Iran (an area approximately 90 miles on a side), approximately 50 miles east of the city of Shiraz, is shown in figure 6. The two large lakes, partly surrounded by salt flats, are the Daryacheh-ye Tashk (to the north) and the Daryacheh-ye Bakhtegan. The northwest-trending ranges are predominantly Mesozoic and Tertiary sedimentary rocks folded into a series of anticlines and snyclines. The dark hills at bottom center are composed of volcanic rock. This picture appears potentially to be useful for refinement of existing maps of the region. The figure contains considerably more geologic and topographic detail than the Geological Map of Iran (ref. 5), the scale of which (1:2,500,000) was close to that of the Gemini photograph. The picture would be useful in mapping Quaternary alluvium and evaporite deposits and in delineating major faults.

An area of great geologic interest in southeastern Iran is shown in figures 7 and 8. The mountain ranges are Cenozoic sedimentary rocks folded into anticlines and synclines of remarkable complexity. Of particular interest is the fault scarp at the left in the figure. This feature reflects a recent, and probably still active, fault of the "scissors" type in which movement has opposite directions at opposite ends. Toward the bottom of the picture, the right-hand fault block has moved upward; toward the top of the figure, the left-hand side has moved upward. The virtually negligible amount of dissection of the scarp manifests the recent nature of the fault. The linear features to the left of the fault are probably truncated strata not sand dunes, because they may be seen to continue under the alluvium.

The mouth of the Yangtze River and the East China Sea, looking toward the east, are shown in figure 9. This picture is typical of many taken during the Gemini V mission which are illustrative of submarine topography and turbidity currents. Such photographs are believed to be of great potential value for hydrologic and oceanographic

studies (ref. 6) because they are a simultaneous view of large regions of ocean, with the added advantage of color.

One of the most northerly pictures of the United States obtained on any of the Mercury or Gemini flights was taken over New Mexico (fig. 10). A wide variety of rock types and structures is shown in the figure. The white patch at top center (marred by a flaw) is the gypsum sand of the White Sands National Monument. West of the monument are the San Andres Mountains, bordered on the south by the Tertiary volcanics of the Organ Mountains. West of the Rio Grande, at the top left, a series of northerly trending faults in the vicinity of Magdalena Peak are visible. At least two units can be distinguished in the Quaternary basalt flows west of the Rio Grande at the left, although the most recent geologic map of New Mexico (ref. 7) contains only one map unit. The availability of a recent geologic map of this region makes this photograph of particular value for comparison purposes. Preliminary study is indicative that many of the major lithologic units and structures (especially faults) shown on the 1:500,000 scale geologic map are visible on the photograph, the original scale of which was approximately 1:2,000,000. Many features of Quaternary alluvium are shown in the photograph but are not shown on the map. This facilitates rapid determination of the extent of the pediments surrounding the mountains, features which are not shown clearly on either topographic or geologic maps.

Because of daylight restrictions, photographing southern Africa was not possible during flights prior to the Gemini V mission. However, a large number of excellent pictures of this region were obtained during this mission. One of these, taken over southwest Africa, is shown in figure 11. It includes a significant part of the Namib Desert (which extends for several hundred miles along the coast of southern Africa) and part of the Precambrian shield. This picture is illustrative of the potential value of hyperaltitude photography for study of regional sand-dune distribution and structural geology. The conspicuous fracture pattern at the right is covered more completely by an adjoining photograph. An interesting circular feature is shown at the top right, vaguely suggestive of the Richat structure that was photographed on the Gemini IV mission.

Gemini VI and VII Missions

Experiment S005 was successful on the Gemini VI and VII missions, especially with respect to the changes that were made in mission objectives after the experiment was planned. Approximately 60 pictures were obtained that were useful for study. The regions that were covered included the southern Sahara Desert, south-central Africa, northwestern Australia, and several islands in the Indian Ocean.

Gemini VI mission. - A portion of central Mali, including the Niger River and the vicinity of Tombouctou, is shown in figure 12; this figure was one of a continuous series taken during the 15th revolution. The Aouker Basin and part of the southwestern Sahara Desert are visible in the background. The picture is an excellent view of what probably are stabilized sand dunes (foreground), such as sand dunes that are no longer active and have been eroded partially (ref. 8). These dunes probably represent a former extension of the arid conditions that now characterize the northern Sahara. This photograph,

and others in the series, should prove valuable in the study of the relationship of the stabilized dunes to active dunes and to bedrock structure.

The Air ou Azbine, a plateau in Niger, is shown in figure 13. The dark and roughly circular masses are Cenozoic lava flows on sandstone and schists (ref. 9). The crater at the lower left apparently was of volcanic origin because of its nearness to lava flows; however, this region has been thought to be capped by sandstone (ref. 9). The picture is an excellent view of the general geological structure of the entire uplift. One of several extremely clear pictures of this region (fig. 14) was taken over Somalia in the vicinity of the Ras Hafun (the cape at left). The region is underlain by Cenozoic marine and continental sedimentary rock (ref. 10), and appears to be somewhat recently emerged. An excellent opportunity to study development of consequent drainage exists because much of the region is in a youthful stage of geomorphic development.

Several lakes in the portion of the Rift Valley south of Addis Ababa, Ethiopia, are shown in figure 15. Considerable structural detail, such as the presumably fracture-controlled drainage on the east side of the Rift Valley, is visible. In addition, several regions of volcanic rock can be distinguished. This photograph may be helpful in testing the suggestion (ref. 11) that volcanism in the Rift Valley is independent of structure. This region is of great geologic interest, and was a prime subject of study during the Upper Mantle Project (ref. 12).

Gemini VII mission. - The scope of the experiment was expanded considerably for the Gemini VII mission, because of the much greater mission length and the greater film capacity available. Government agencies and universities had requested photographs of several specific regions, and these requests were incorporated into the mission plan. Approximately 250 pictures that are usable for geologic, geographic, and oceanographic purposes were obtained. These pictures cover parts of the United States, Africa, Mexico, South America, Asia, Australia, and various ocean regions. However, two major difficulties were encountered. First, the cloud cover was exceptionally heavy over many of the regions selected. Second, a deposit remained on the spacecraft windows, apparently from second-stage ignition; this deposit seriously degraded several of the pictures.

One of a series of photographs taken over the southern part of the Arabian peninsula is shown in figure 16. The series had partial stereoscopic coverage. The region shown, also photographed during the Gemini IV mission, is the Hadramaut Plateau; the Hadramaut Wadi is at lower right. The plateau is underlain by gently dipping marine shales, deeply dissected in a dendritic pattern. Several interesting examples of incipient stream piracy are visible, in which streams cutting headward intersect other streams. Of course, all are now dry.

The view in figure 17 was taken over Chad, looking to the southeast over the Tibesti Mountains. This photograph was specifically requested for the purpose of investigation of geologic features discovered on Gemini IV photographs (ref. 6). One of these features is the circular structure at far left center. Although probably an igneous intrusion, such as a laccolith, its similarity to the Richat structures is suggestive that an impact origin be considered. Another structural feature is the series of concentric lineaments at the far left. These features probably are joints emphasized by wind and stream erosion; they may be tensional fractures associated with the epeirogenic uplift of the Tibesti massif. In addition to these structures, considerable detail

can be seen in the sedimentary, igneous, and metamorphic rocks of the western Tibestis. The large circular features are calderas, and are surrounded by extensive rhyolite or ignimbrite deposits (ref. 13).

Because figure 18 was taken with the 250-millimeter lens, it is of considerable interest in evaluation of the usefulness of long-focal-length lenses. The region covered is the Tifernine Dunes (ref. 9) in south-central Algeria. Despite the longer focal length, the region included in the picture is approximately 90 miles from side to side because of the camera tilt. The picture is a synoptic view of the dune field and its relation to surrounding topography, which should prove valuable in studies of dune formation.

A portion of the Erg Chech in west-central Algeria, is shown in figure 19, (view toward the southeast). The dark ridges at the lower left are the Kahal Tabelbala and Ougarta, folded Paleozoic sandstones, limestones, and schists (ref. 14), separated by the Erg er Raoui, a dune field. The variety of dunes in the lower right is of considerable interest. At least two major directions of dune chains at large angles to each other are visible, which is suggestive of a possible transition from transverse to longitudinal dunes. The value of such photographs in the study of sand-dune formation and evolution is obvious.

One of several photographs taken with color infrared film, used for the first time in scientific terrain photography on the Gemini VII mission, is shown in figure 20. Despite the window obscuration (caused by the deposit mentioned previously) and the artifacts at the right, the picture is clear evidence of the potential value of this type of film for hyperaltitude photography. The region shown in figure 20 includes the Gulf Coast of Alabama, Mississippi, and Louisiana; Mobile Bay is at the lower right, Lake Pontchartrain and New Orleans are at the far left, and the arc at the left center is the Chandeleur Island chain. The picture is of interest for several reasons. First, the infrared sensitivity facilitated considerable haze penetration, as had been expected from the behavior of black-and-white infrared film flown on rockets (ref. 3). This is shown by the fact that highways can be distinguished at slant ranges of approximately 200 miles (at upper left: Interstate 55 and Route 190). Other cultural features include highways, the bridge for Interstate 59 across the east end of Lake Pontchartrain (however, the causeway is not visible), and the Mississippi River-Gulf of Mexico outlet canal (the white line crossing the delta parallel to the left border). Many color differences can be seen in the Gulf of Mexico and the adjacent inland waters. Apparently there is considerable correspondence between water color and depth. For example, the dark tonal boundary just above the spacecraft nose (lower left) may outline the 60-fathom contour (as shown on Coast and Geodetic Chart 1115). Also, the tone contours just east of the Mississippi Delta at the lower left roughly correspond to the depth of water between the delta and Breton Island. However, it is probable that the water temperature and the overlying air influence the color response of this film; more detailed analysis is needed. Considerable color detail is visible in land regions. Probably, differences are caused by vegetation rather than by soil or geologic units, because the expected color response (for example, red replacing green) is present on the color prints. From this and adjacent pictures, it is obvious that much more color discrimination is possible with color infrared film than with conventional color film. This is of great importance for the application of hyperaltitude photography to range

management, forestry, and agriculture, because terrain photography on other Gemini missions has proved that the color response of conventional color film in green wavelengths is poor, probably because of atmospheric scattering.

Gemini X Mission

Approximately 75 useful pictures were taken, most of which were of good quality although cloud cover was extensive over several regions. Apparently, window obscuration affected some pictures. Regions covered included northwestern South America, northwestern and north-central Africa, the Formosa Straits, and several islands in the Indian and Pacific Oceans. As the spacecraft approached the coast of Africa, the photographs in figures 21 and 22 were taken. The view in figures 21 and 22 is to the northeast over the Spanish Sahara and Morocco. Although they are obliques, these photographs were of considerable value. They were useful for precisely locating other, more nearly vertical photographs taken of the same region, a task that has been difficult in some cases. They are potentially useful geologically because of the extremely large region involved. The broad plateau at the left in figure 22 is the Hamada du Dra which overlies the Tindouf Basin, a large synclinal structure. The prominent curvature to the south is of interest in relation to continental drift, in that it is demonstrative that not all pre-Mesozoic structures are truncated by the continental margins, as might be implied by some maps such as those in reference 15.

A view over Niger, looking to the southwest, is shown in figure 23. The Air Mountains, photographed on other Gemini missions (ref. 6), are visible on the horizon. Visible in the foreground are poorly understood arcuate or linear features, which evidently consist of fractures and dune chains. These were first photographed on the Gemini IV mission (east of the Tibesti Mountains). It is hoped that synoptic photography of this type will be informative regarding the origin of these fractures. The Gulf Coast of Texas and Mexico from Baffin Bay almost to Laguna del Barril are shown in figure 24, which was taken over the Rio Grande Delta. Despite the window obscuration, considerable terrain detail is visible. Of particular interest are the features of Laguna Madre, the prominent coastal lagoon at center, and Padre Island and the barrier island bounding it. Numerous units, which presumably reflect sedimentation, can be distinguished in the lagoon. The effects of manmade structures, such as the Intracoastal Waterway, on normal sedimentation can be seen in the photograph. This region has been the subject of extensive study (ref. 16) in connection with sedimentation.

A nearly vertical view of the coast of China in Fukien Province is shown in figure 25. It is of interest because of the considerable detail in the bottom topography in coastal regions. Although not of a primary region for the experiment, the picture is suggestive of the oceanographic value of such photography. This value was first indicated in the photographs made on the Gemini IV mission. The southern end of Formosa is shown in figure 26. In addition to the detail visible in land sectors, most of which is indicative of vegetation and cultivation, considerable structure is apparent in the glitter pattern at the southern tip of the island. Possible elements in this structure include internal waves, slicks, near-surface ocean currents, and currents of fresh water from the numerous rivers. Several atolls in the Maldive Islands are shown in figure 27; the view is to the southwest over the Indian Ocean. This picture, although not taken at the optimum angle, is indicative of the value of orbital photography in correcting map positions of widely separated ocean islands.

Gemini XI Mission

Approximately 145 photographs of good to excellent quality were obtained; these photographs included all the desired sectors plus several additional regions. The command pilot window was obscured, as on previous flights, but the pilot window was relatively clear. Consequently, the pilot took most of the terrain photographs, alternating between the 70-millimeter EVA still camera and the 70-millimeter general-purpose camera. This technique, which had not been planned as part of this experiment, not only resulted in stereoscopic coverage, but also resulted in an excellent comparison of the capabilities of the two camera lenses. In general, pictures from both cameras were of good quality, but those from the EVA camera were the clearest.

The majority of the terrain photographs were taken during the two high-apogee revolutions. During this period, most land regions (except Indonesia and Ceylon) were free from cloud cover. Picture quality is good to excellent for most of the photographs. Reds and blues are somewhat exaggerated in several photographs taken with the EVA camera. The pictures taken through the command pilot window were degraded seriously by deposits on the window. The pictures were of great value for research purposes, and, because of the wide coverage obtained, were useful for the location of regions photographed on earlier flights. Representative photographs are presented in figures 28 to 32.

Gemini XII Mission

Continuous strip photography was to include the regions that are listed as follows.

1. Southern India: For geologic study of the Precambrian region and Indian Upper Mantle Project

2. Lower Baja California: For geologic study of the structure of the Gulf of California and for improvement of geologic maps of the peninsula

3. West Pakistan: Requested by the U.S. Geological Survey for geologic mapping photography of Gulf of Cambay to the south; also desired for use in oceanographic research by the Bureau of Commercial Fisheries

4. African Rift Valley: For geologic study of the structure of the Rift Valley, a prime sector of interest in the Upper Mantle Project

5. Northwest South America: For geologic study of the structure of the Andes Mountains

6. Southern Mexico, Yucatan Peninsula, Yucatan Straits: For geologic study of the Neovolcanic Plateau, believed to be the continental expression of the Clarion fracture zone, and for oceanographic research

Individual photographs or small groups of photographs of the following regions were desired for oceanographic research by the U.S. Navy Oceanographic Office and the Bureau of Commercial Fisheries.

1. Mississippi Delta and adjacent waters
2. Ganges Delta and adjacent waters
3. Amazon Delta and adjacent waters
4. Bay of Bengal
5. Arabian Sea

The objectives of the photographs for oceanographic research included photography of the muddy water flowing from major rivers into the ocean and of slicks (relatively smooth patches of water visible as dark regions in glitter patterns).

Approximately 130 photographs usable for the purposes of this experiment were obtained during the Gemini XII mission. Almost all of the photographs were made with the Hasselblad camera. The photographs are listed, with the reference to the preflight objectives, in table I. The photographs of greatest potential value for photogeological interpretation appear to be those of southwestern Asia, the northern Red Sea, the Gulf of Mexico, and the Gulf Coastal Plain. In many of the photographs of other sectors, enhancement and rectification will be necessary to overcome the effects of poor lighting, tilt, and haze. Cloud cover, as on previous flights, was intense, even over normally clear targets such as the Sahara.

Part of the Zagros-Makran Mountains of southern Iran and western Pakistan is shown in figures 33 to 35. A geologic sketch was drawn on the photograph in figure 34 to delineate geologic features of interest. The large anticlines in the foreground, west of the Strait of Hormuz, are most prominent. This region is the source of a substantial part of the oil production of the world. A feature of considerable geologic importance, clearly shown in figures 33 to 35, is the abrupt change in structural trends and lithology on the north side of the Strait of Hormuz. Generally, this discontinuity is shown on small-scale geologic maps simply as a bend in the regional structure. Study of these photographs, in conjunction with the available geologic maps of the locale (refs. 17 and 18), is suggestive that there has been a general southward movement of the Makran Range between the Strait of Hormuz and the Kirthar Range north of Karachi. The apparent displacement of the Pliocene and Miocene rocks, with the continuity of structure along the north side of the Gulf of Oman, is similar to the outcrop pattern shown by major overthrust faults (such as the Pine Mountain overthrust of the southern Appalachian Mountains). Also, it is similar to the pattern of the Salt Range in northern Pakistan (ref. 19) for which an overthrust origin is suspected.

The Makran Range may represent a remarkable example of overthrust faulting by gravitational gliding; that is, the movement of sheets of rock down slight slopes under their own weight after initiation of movement by uplift and lateral compression. Conditions favorable for gravitational gliding include thick sedimentary sections and the existence of a stratum that can serve as a lubricating layer (ref. 20). The stratigraphic

section (ref. 17) at Bandar Abbas, just north of the Strait of Hormuz, consists of over 24 000 feet of post-Cambrian rocks, and overlies the Cambrian Hormuz salt layer. The Hormuz salt layer could serve as a lubricating stratum because of the plasticity of salt.

An oblique view (figs. 36 and 37) to the north over northeast Mexico, taken by canting the camera, is another exception to the general rule that vertical photographs are more valuable than oblique ones. In normal practice, the camera is aimed directly at the horizon and the principal line is normal to the horizon. The locale shown in figure 35 includes the major deflection of the Sierra Madre Oriental Range south of Monterrey, Mexico, and also the sharp front of the range to the southeast. The origin of this deflection is not known, but it has been suggested that the folds of the Sierra Madre Oriental Range have been shifted to the west by a major left-lateral wrench fault, for which the name Saltillo-Torreon fracture zone has been proposed (ref. 20). In a study of the Sierra de la Gavia, northwest of Monterrey, Krutak (ref. 21) applied the strain ellipsoid theory of deformation to the structure and concluded that the Saltillo-Torreon fracture zone is a shear which resulted from southwesterly directed compression. The Saltillo-Torreon fracture zone is not evident east of the mountain front in figures 36 and 37. However, because of the foreshortening caused by the camera angle, subtle stream alinements might be missed easily. The foreshortening can be interpreted by application of strain-ellipsoid mechanics to the structure. If the Saltillo-Torreon fracture exists and is a shear caused by southwesterly compression, a complementary shear direction at a large angle to the fracture should be evident. As shown on the sketch, this direction should pass directly under the spacecraft from the vicinity of the bend in the Sierra Madre, and might take the form of stream alinements, rows of igneous intrusives, or alined breaks in ridge lines in the Sierra Madre itself. Furthermore, the foreshortening in the northwesterly direction should accentuate any such trends. An examination of the photograph reveals no definite evidence of the predicted complementary shear direction. Although more orbital photographs of this region should be studied before a conclusion is established, it is apparent that the structure south of Monterrey is not a complementary shear structure of the Saltillo-Torreon fracture.

Almost the entire Gulf Coastal Plain of Texas, from San Antonio northeast into Louisiana, is shown in figure 38. Interpretation of this photograph is much more difficult than interpretation of photographs of desert regions, chiefly because of the dense vegetation and intensive cultivation. The prominent curved boundary just west of San Antonio is probably the contact between the Cretaceous Comanche and the Navarro series (ref. 22). A dark band just east and southeast of San Antonio apparently corresponds to the Tertiary Midway group. Further distinction among Tertiary units to the east cannot be made reliably. It is somewhat surprising to find that the central mineral district (Llano Uplift) cannot be delineated on this photograph, although the Paleozoic-Cretaceous contact northwest of it can be delineated. To the north, the general outcrop pattern of gulfward-dipping sediments, which is paralelled by many normal faults, is visible clearly. In this region, the effects of bedrock geology are obscured by the combined effects of natural vegetation, farming, topography, and soil types. To the east, in the Gulf of Mexico, sedimentation patterns are visible; this fact can be used in the study of recent sedimentation in this locale.

The branching of the Rift Valley into the Gulf of Suez and Gulf of Aqaba is shown in figure 39. The fracture pattern expressed in the topography of the opposing shores and the Sinai Peninsula should indicate whether the nature of the faulting that produced the rift is predominately transverse or normal. The photograph in figure 40, the northern Bahama Islands, was taken during the standup EVA. Because the view was not obscured by the spacecraft window, the photograph has excellent color rendition and clarity, and the amount of visible submarine topographic detail is of particular interest. Such photographs have potential value for the revision of hydrographic charts after new channels have been cut by major storms. Comparison of this photograph and similar photographs taken in the same sequence with maps of about the same scale (ref. 23) is suggestive that the bottom is observable to depths greater than 20 meters. In the photograph, the boundaries of the Northwest Providence Channel appear to follow closely the 100-fathom contour. Because the bottom drops off rapidly, precise position measurements must be made before the actual depths that are visible can be determined.

The mouths of the Irrawaddy River, Burma, and the Gulf of Martaban are shown in figure 41. The striking color boundary between the Gulf of Martaban and the Andaman Sea apparently corresponds to the 50-meter contour. The color of the Gulf of Martaban probably is affected by muddy water coming from the various major rivers. The nature of the two dark patches in the center of the photograph is unknown, and it may represent deep water. The dark land regions at the mouths of the Irrawaddy River correspond to mangrove swamps typical of deltas in this region (ref. 24).

The photograph shown in figure 42 will probably be of little specific geologic value because of the camera angle. However, the photograph is of a region approximately 250 000 square miles in the western United States and a portion of northern Chihuahua, Mexico. Topographic features are identifiable for a remarkable distance. All the major ranges in the photograph are identifiable easily. In particular, the Wind River Mountains and the Bighorn Mountains in northwest Wyoming are visible in the center far horizon.

CONCLUSIONS

Several tentative conclusions can be derived from the results of the Synoptic Terrain Photography experiment, with particular reference to the results from the Gemini XII mission. The photographs are additional confirmation of the feasibility and value of orbital photographs for geology, geography, and oceanography. The photographs have proven to be of value in the study of the tectonic problems of the Makran Range and the Sierra Madre Oriental province. Although vertical or near-vertical photography is superior to oblique photography, photographs from the Gemini XII mission have proven that low oblique photographs, and even high oblique photographs, may be of value for certain situations. The oblique views of the Makran Range were useful substitutes for vertical photographs. Equivalent aerial coverage by vertical photographs would have necessitated a camera altitude of several hundred miles. The oblique views of the Sierra Madre Oriental have been used in the search for structures that are approximately normal to the horizon and are enhanced by the foreshortening because of the photograph.

The value of short-focal-length wide-angle lenses (38 millimeter) has been demonstrated for orbital photography of the surface of the earth from altitudes of approximately 100 nautical miles. Although the normal-focal-length lens (80 millimeter) apparently is still the best combination of field of view and resolution, the short-focal-length wide-angle lens (38 millimeter) can be used successfully under favorable conditions of altitude and visibility.

Interpretation of orbital photographs of heavily vegetated regions, such as the Texas Coastal Plain, entails a comprehensive knowledge of a wide range of factors because of the combined effects of bedrock geology, soil, natural vegetation, cultivated regions, and topography. Interpretation of orbital photographs is similar to interpretation of conventional aerial photographs.

REFERENCES

1. Allen, C. R.; Silver, L. T.; and Stehli, F. G.: Agua Blanca Fault — A Major Transverse Structure of Northern Baja California, Mexico. Geol. Soc. Am. Bull., vol. 71, 1960, pp. 457-482.

2. Beal, C. H.: Reconnaissance of the Geology and Oil Possibilities of Baja California, Mexico. Geol. Soc. Am., Memoir 31, 1948.

3. Lowman, P. D., Jr.: A Review of Photography of the Earth from Sounding Rockets and Satellites. NASA TN D-1868, 1964.

4. Eardley, A. J.: Structural Geology of North America. Second Edition, Harpers, New York, 1962.

5. National Iranian Oil Company: Geological Map of Iran (1:2 500 000). 1957.

6. Lowman, P. D., Jr.: Experiment S-5, Synoptic Terrain Photography. Gemini Midprogram Conference, Including Experiment Results. NASA SP-121, 1966, pp. 347-351.

7. Dane, C. H.; and Bachman, G. O.: Geologic Map of New Mexico. U.S. Geological Survey, 1965.

8. Smith, H. T. U.: Eolian Geomorphology, Wind Direction, and Climatic Change in North Africa. AFCRL-63-443. Geophysics Research Directorate, Air Force Cambridge Research Laboratories, Bedford, Mass., 1963.

9. Raisz, E.: Landform Map of North Africa, prepared for Quartermaster General, U.S. Army, 1952.

10. Pepper, J. F.; and Everhart, G. M.: The Indian Ocean: The Geology of Its Bordering Lands and the Configuration of Its Floor. Miscellaneous Geologic Investigations, U.S. Geological Survey, Map I-380, 1963.

11. Bucher, W. H.: The Deformation of the Earth's Crust. Princeton University Press, Princeton, New Jersey, 1933 (Reprint authorized, Hafner Publishing Company, New York).

12. Beloussov, V. V.: The Study of the Great African Rifts: Draft Program. International Upper Mantle Project, Programs and International Recommendations, 1960-1963, issued by Secretariat of the Upper Mantle Committee, Los Angeles, California, 1963.

13. Grove, A. T.: Geomorphology of the Western Tibesti Region with Special Reference to Western Tibesti. Geographical Journal, vol. CXXVI, 1960, pp. 18-27.

14. Morrison, A.; and Chown, M. C.: Photography of the Western Sahara Desert from the Mercury MA-4 Spacecraft. NASA CR-126, 1964.

15. Holmes, A.: Principles of Physical Geology. Second edition, The Ronald Press, London, 1965.

16. Shepard, F. P.; Phleger, F. B.; and van Andel, T. H.: Recent Sediments, Northwest Gulf of Mexico. Am. Assoc. Petroleum Geologists, Tulsa, Oklahoma, 1960.

17. Geological Maps and Sections of South-West Persia. Prepared by the geological staff of the British Petroleum Company, Limited, for the Proceedings of the 20th International Geological Congress, Mexico City, Mexico, 1956.

18. Iran 1:250 000 Series (geological maps). Compiled by Survey Branch, British Petroleum Company, Limited: Bandar Abbas (sheets G-40 C and D), Strait of Hormuz (sheets G-40 I and J and part of G-40 P), 1963.

19. Geological Map of Pakistan, 1:2 000 000. Geological Survey of Pakistan and U.S. Geological Survey, 1964.

20. Murray, G. E.: Geology of the Atlantic and Gulf Coastal Province of North America. Harper and Brothers, New York, 1961.

21. Krutak, P. R.: Structural Geology of the Sierra de la Gavia, Coahuila, Mexico. Bull. Geol. Soc. Am., vol. 78, 1967, pp. 59-76.

22. Geological Highway Map of Texas. Compiled by P. F. Oetking, Dallas Geological Society, Dallas, Texas, 1959.

23. National Geographic Atlas of the World. National Geographic Society, Washington, D.C., 1963.

24. The Time Atlas of the World, Mid-Century Edition. Vol. I, Houghton Mifflin Company, Boston, Mass., 1958.

Figure 1. - Baja California (revolution 32, Gemini IV).

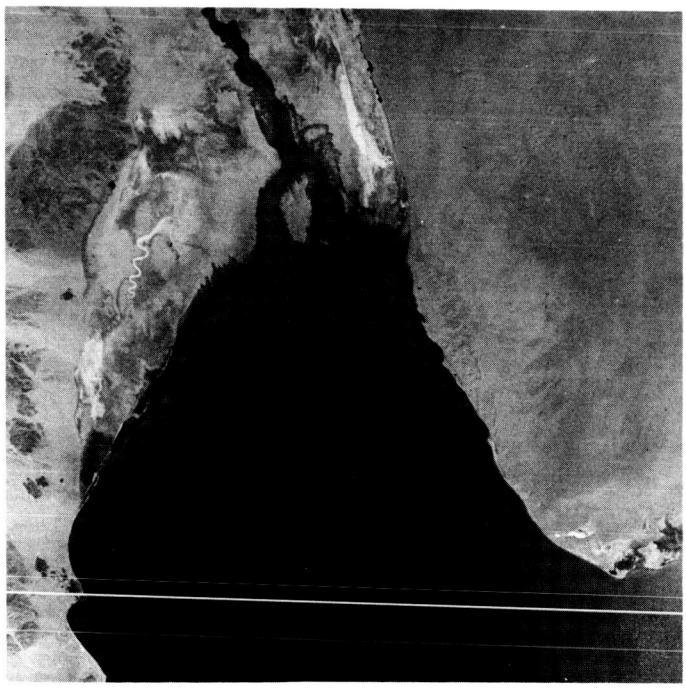

Figure 2. - The Colorado River mouth at the Gulf of California (revolution 32, Gemini IV).

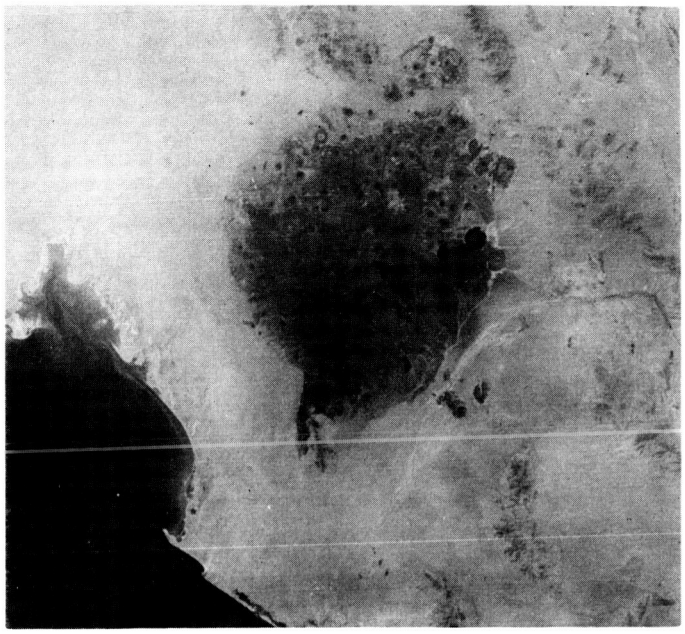

Figure 3. - The Gulf of California, the Pinacate volcanic field, and part of Yuma County, Arizona (revolution 32, Gemini IV).

Figure 4. - Southern New Mexico and Chihuahua and Sonora, Mexico (revolution 32, Gemini IV).

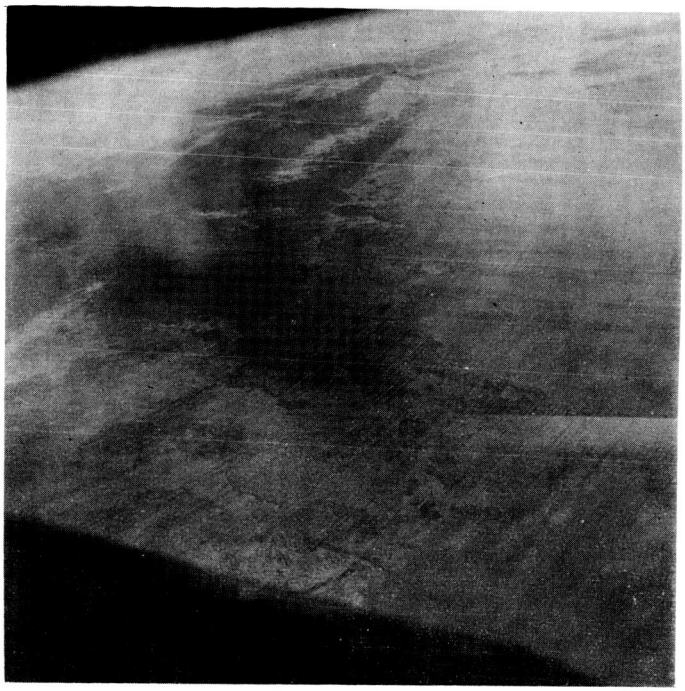

Figure 5. - The Tibesti Mountains, Republic of Chad, North Africa (revolution 32, Gemini IV).

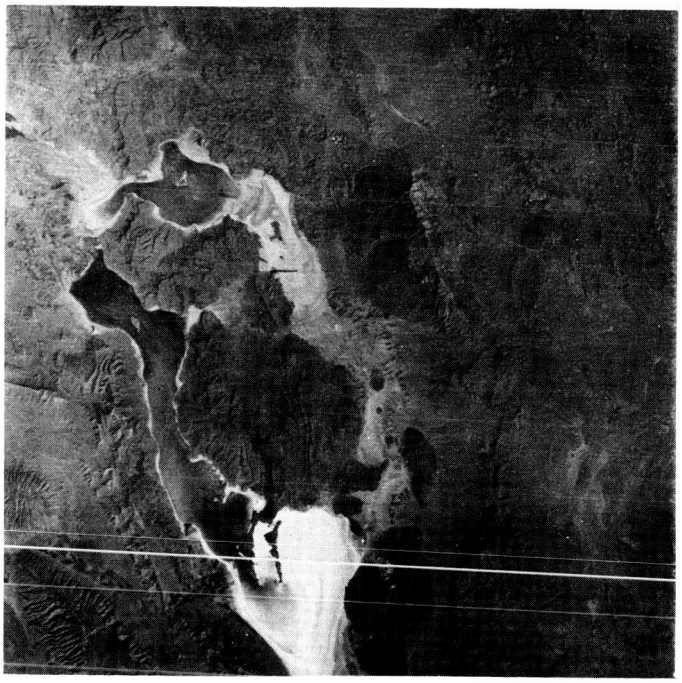

Figure 6. - South-central Iran; note the Zagros Mountains.

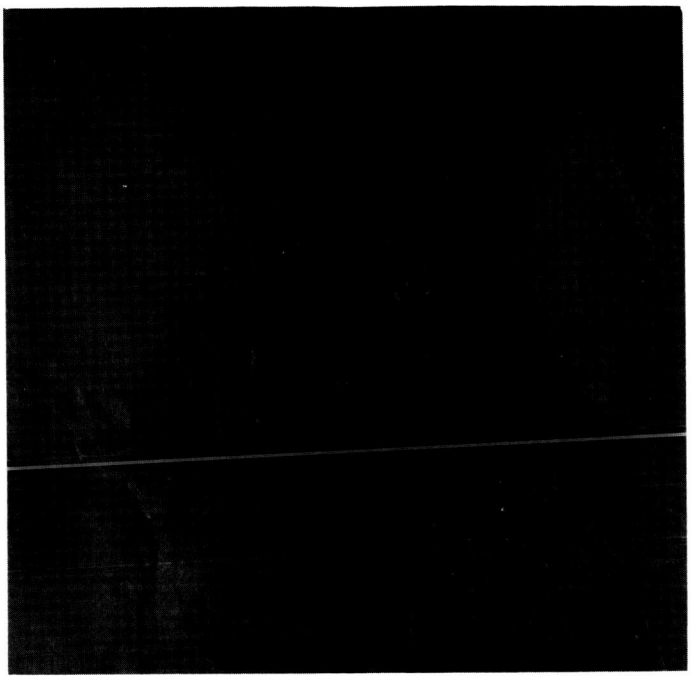

Figure 7. - Southeastern Iran; note the folded mountains cut by a scissor fault (left).

Figure 8. - Southeastern Iran; note the region of folded mountains that overlap the sector shown in figure 7.

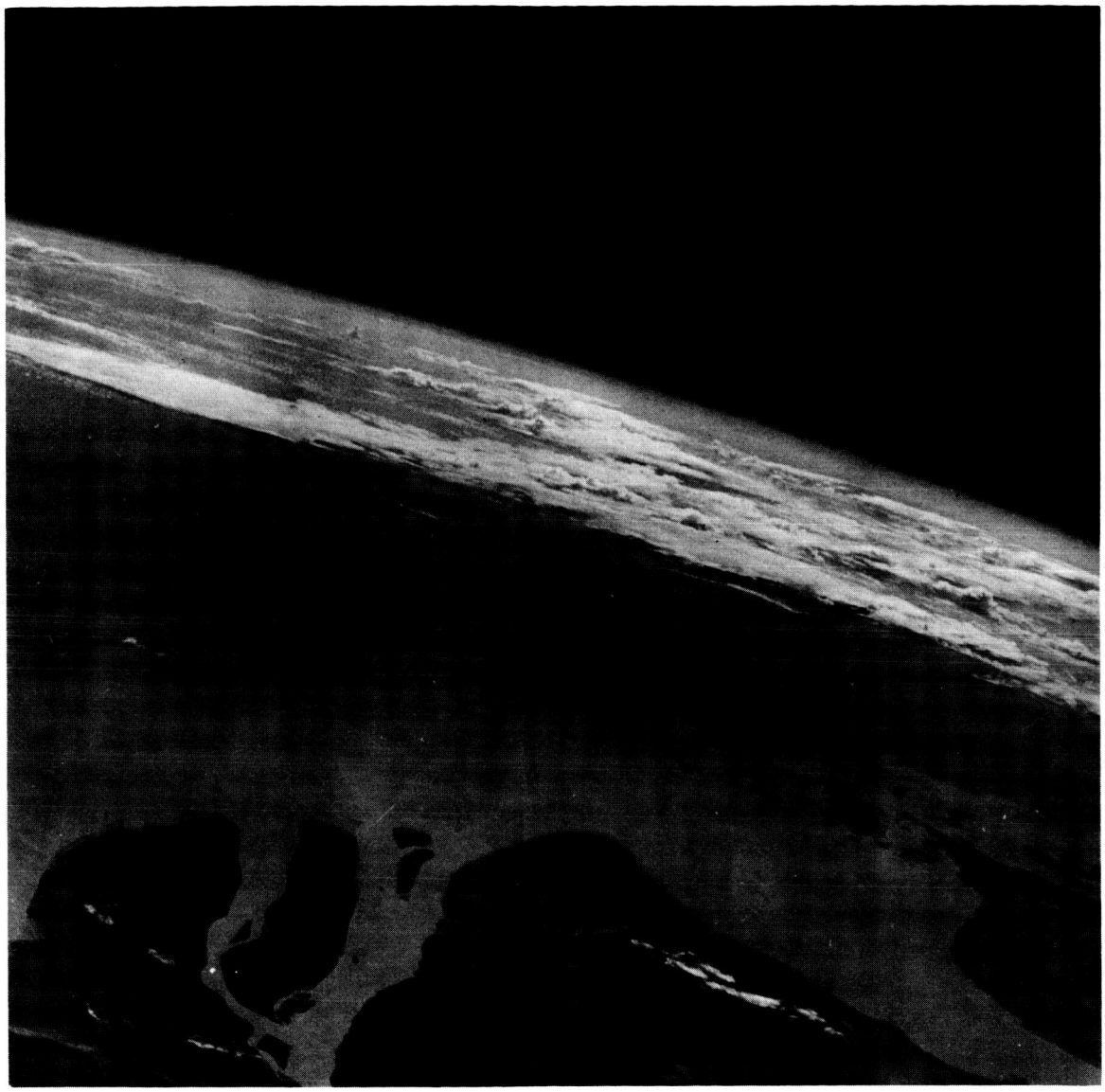

Figure 9. - The mouth of the Yangtze River; note the bottom topography or turbidity currents.

Figure 10. - South-central New Mexico; note the Rio Grande valley, the San Andres and Organ Mountains, and the White Sands National Monument (top).

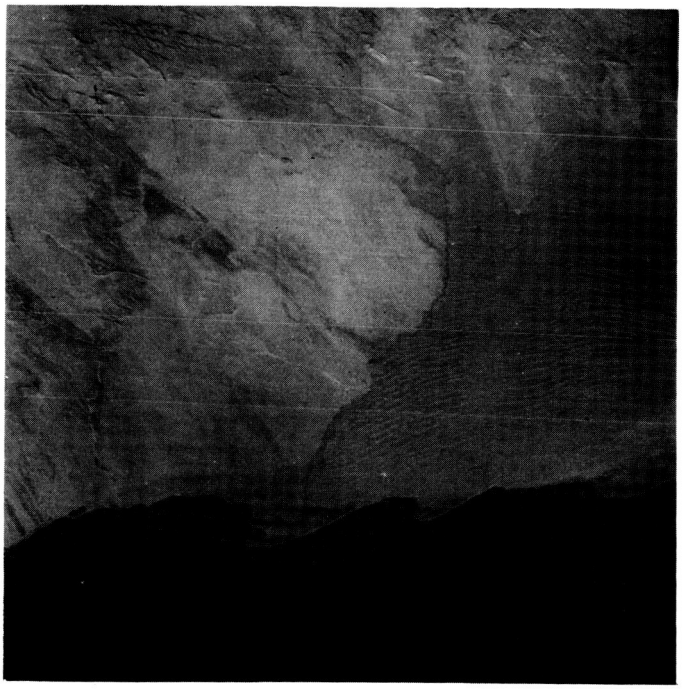

Figure 11. - Southwestern Africa; note the Namib Desert and the structure in the Precambrian rocks.

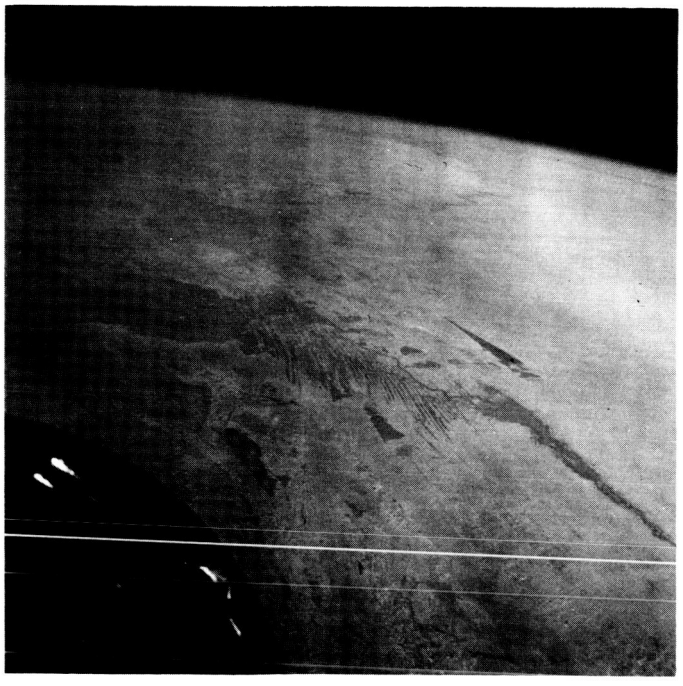

Figure 12. - The Niger River and the vicinity of Tombouctou, Mali; northwesterly view.

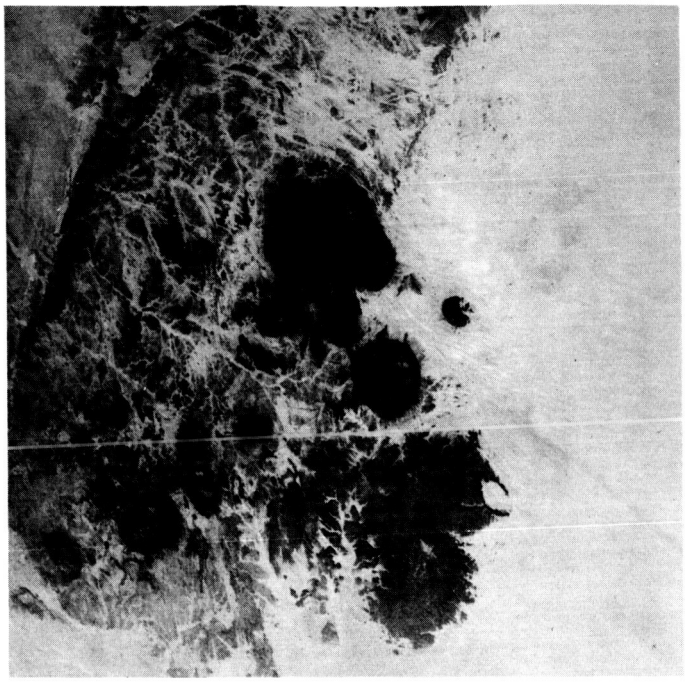

Figure 13.- The Air ou Azbine, a volcanic plateau in Niger.

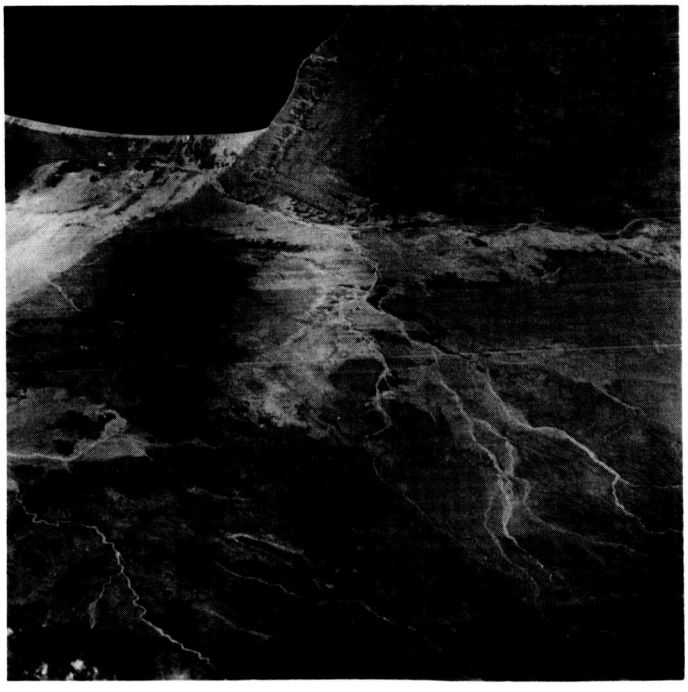

Figure 14.- The Indian Ocean coast of Somalia; Ras Hafun is at the left.

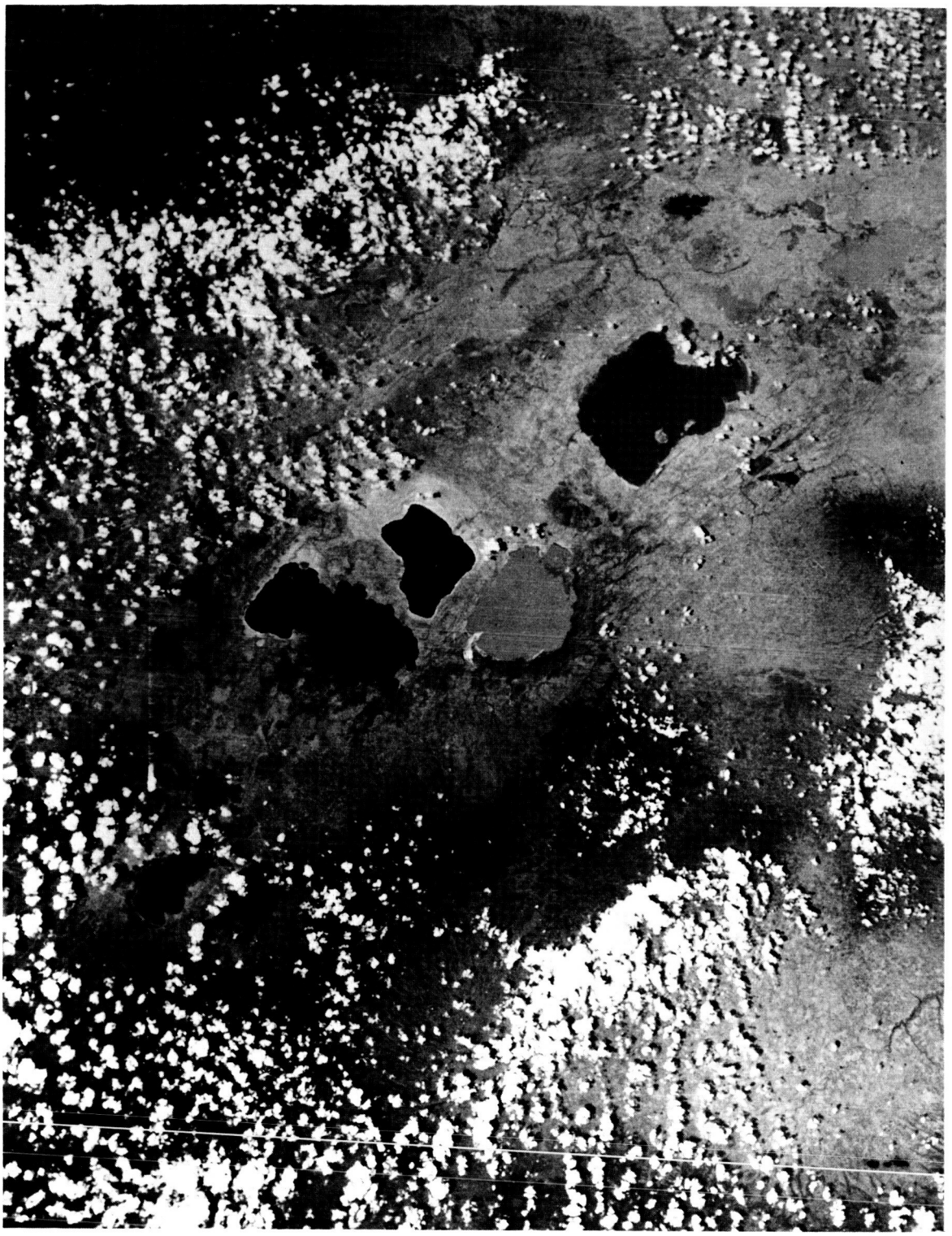

Figure 15. - Lakes in the Rift Valley, Ethiopia, south of Addis Ababa.

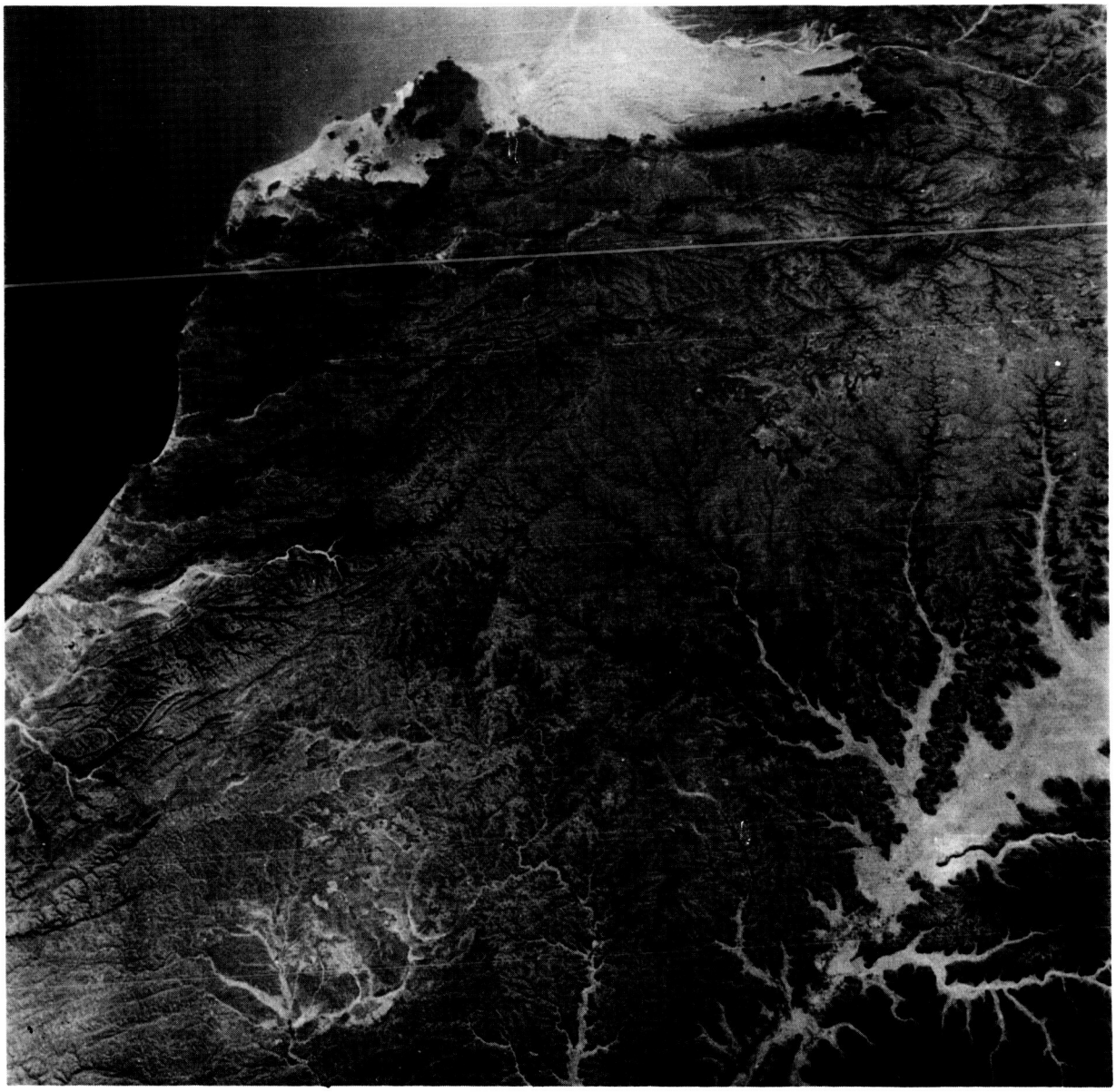

Figure 16. - An almost vertical view of the Hadramaut Plateau on the south coast of the Arabian Peninsula.

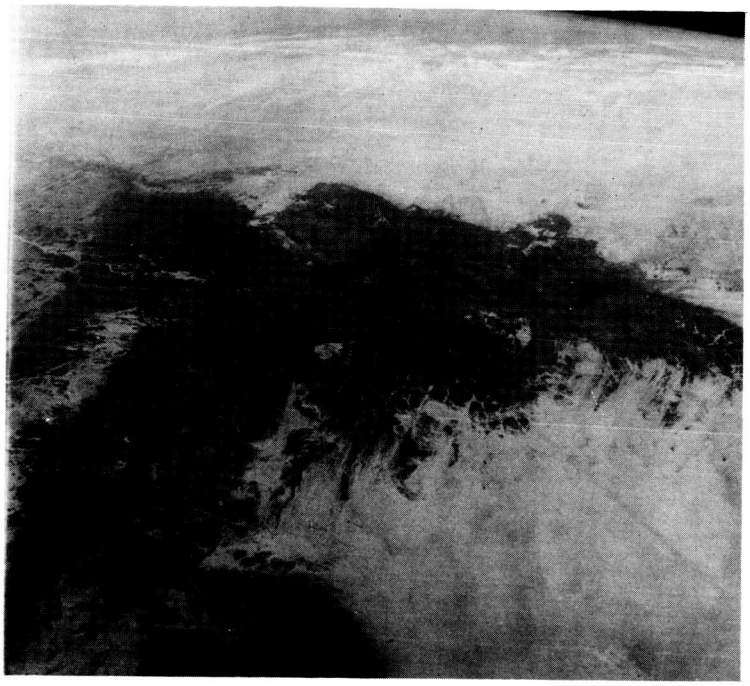

Figure 17. - The Tibesti Mountains, Republic of Chad; a southeasterly view.

Figure 18. - The Tifernine dune field, Algeria; a southeasterly view.

Figure 19. - Part of the Erg Chech, Algeria, and the Erg er Raoui; a southeasterly view.

Figure 20. - A color photograph taken with infrared film over the Gulf of Mexico; a northwesterly view over Mobile Bay and the New Orleans coast.

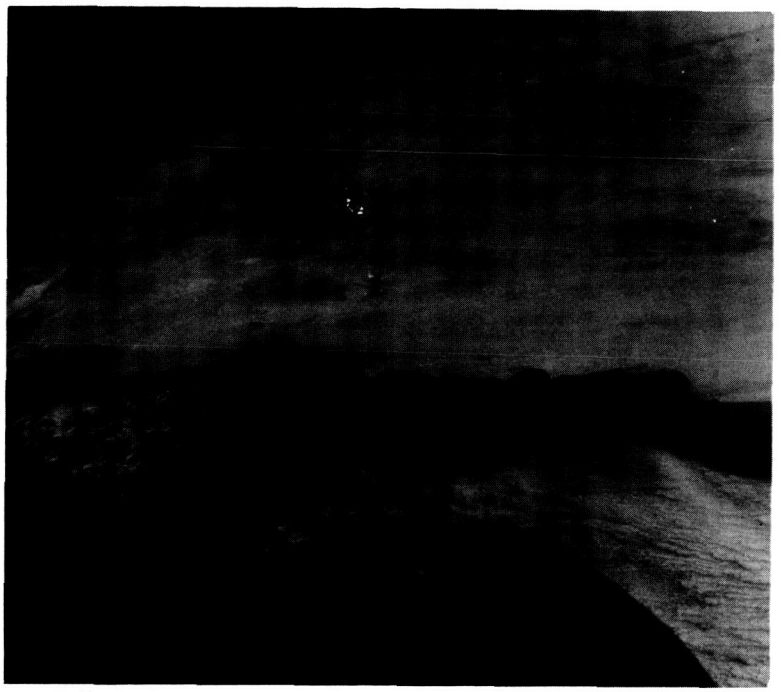

Figure 21. - The Spanish Sahara and Morocco; a northeasterly view.

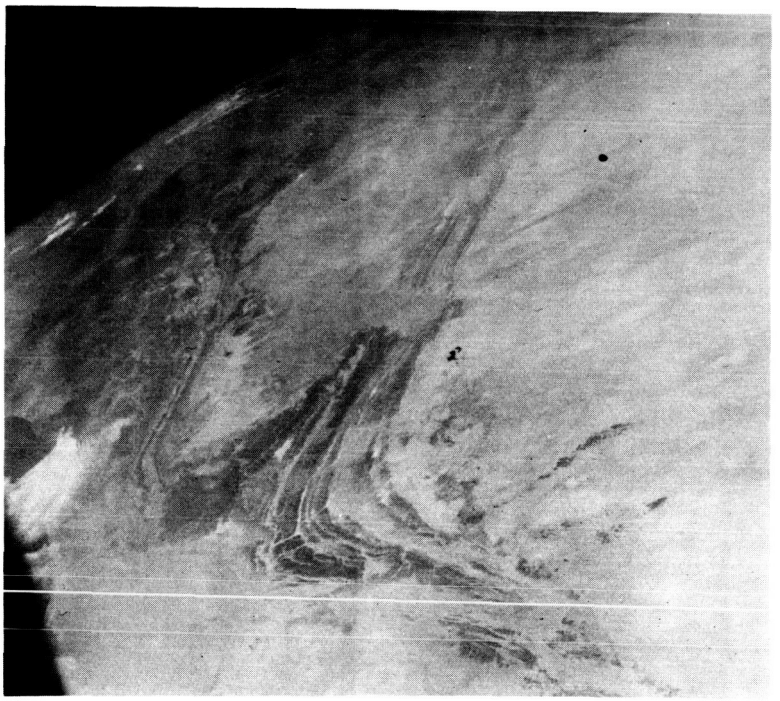

Figure 22. - The Sahara; Hamada du Dra is toward the top.

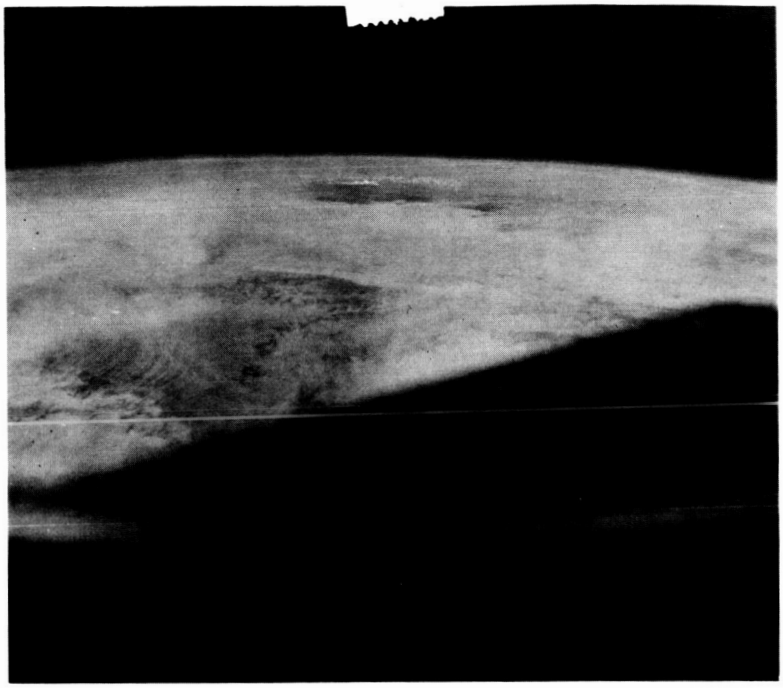

Figure 23. - A southeasterly view over the Niger River.

Figure 24. - The Rio Grande Delta.

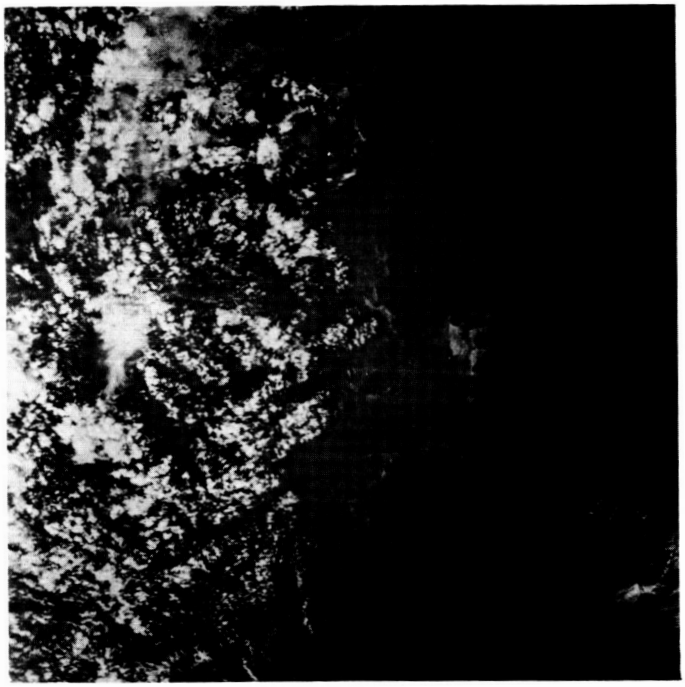

Figure 25. - The China coast.

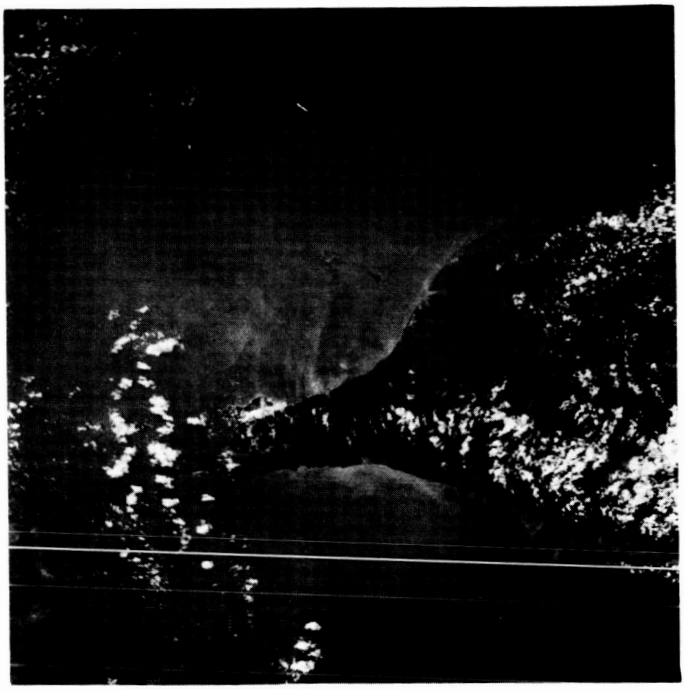

Figure 26. - Southern Formosa.

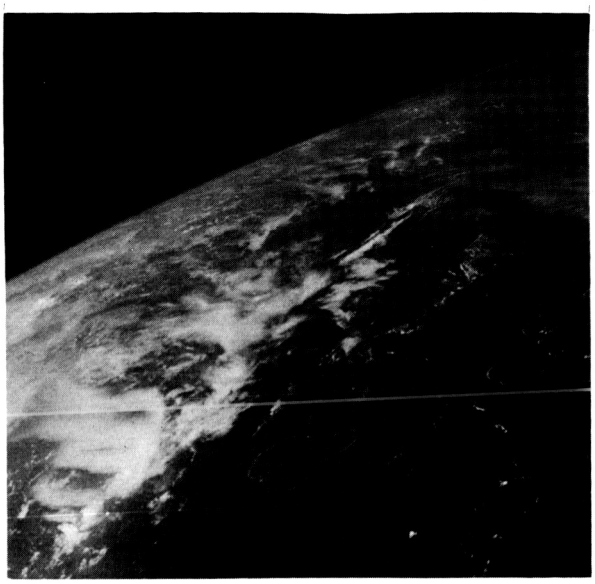

Figure 27. - Atolls in the Maldive Islands.

Figure 28. - Egypt, Jordan, Saudi Arabia, Lebanon, Syria, Iraq, Turkey, and Israel; water regions include the Red Sea, Dead Sea, Sea of Galilee, Mediterranean Sea, Suez Canal, and Euphrates River; a northerly view at 220-n. mi. altitude.

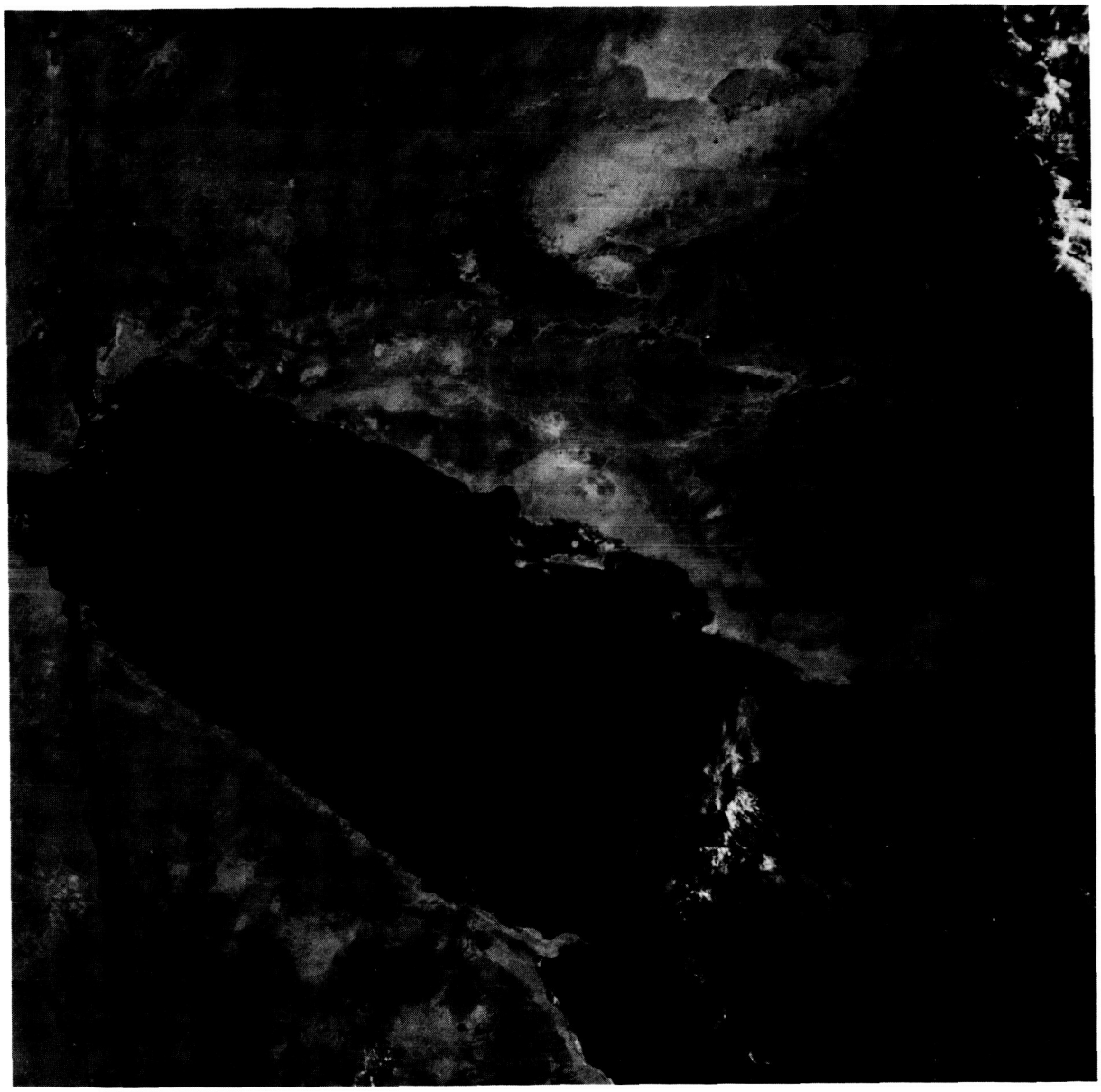

Figure 29. - Egypt and Saudi Arabia region; coverage includes Jordan, Israel, the Sinai, the Red Sea, the Dead Sea, and Al Hijaz; the photograph was taken at 220-n. mi. altitude, and north is toward the top.

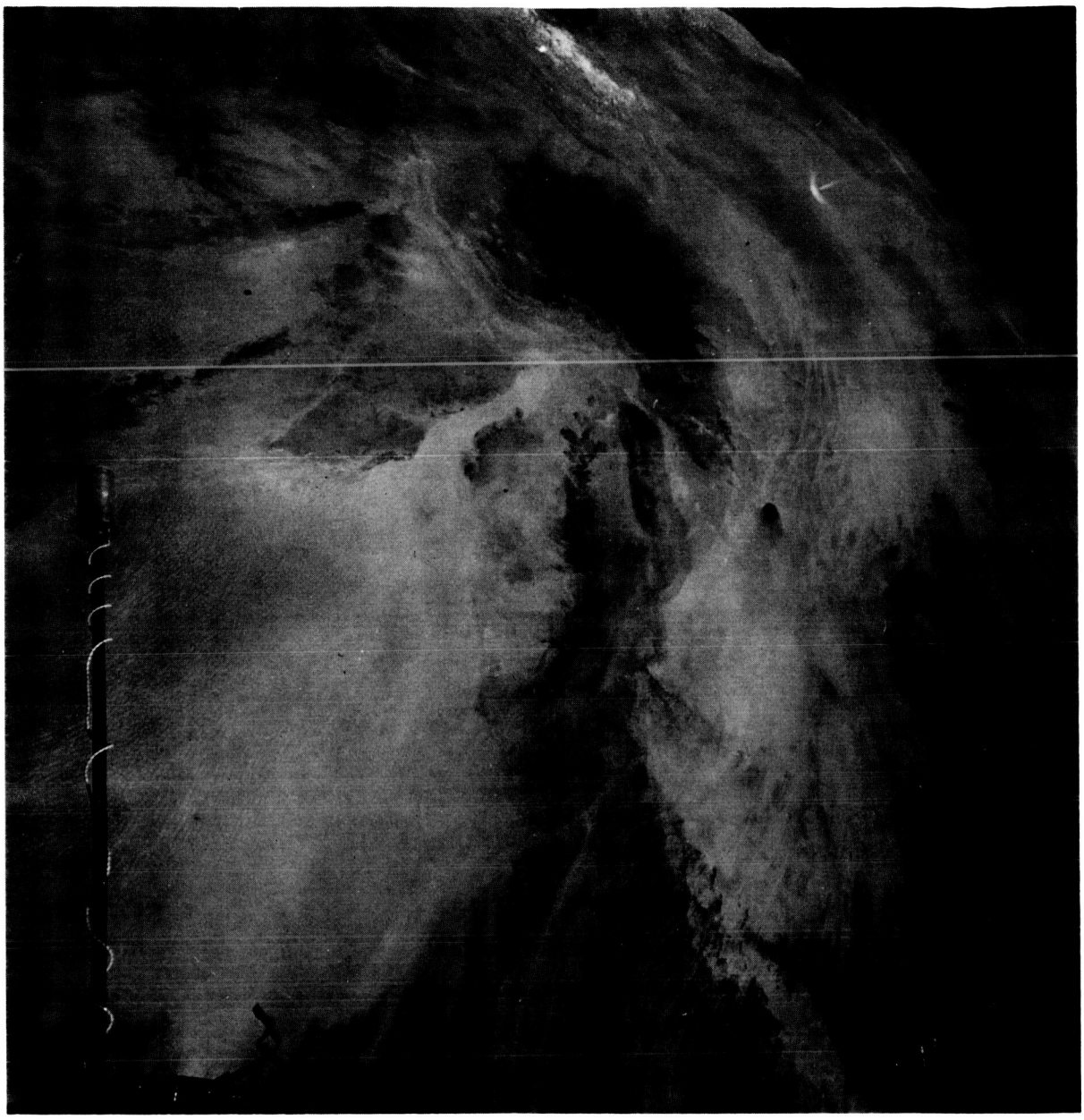

Figure 30. - Libya, Chad, Sudan, Egypt, and Niger; the Tibesti Mountains, Al Haruj, Al Swad, the Mediterranean Sea, and the Great Libyan Land Sea are in the background; the photograph was taken from an altitude of 240 n. mi., looking northeastward.

Figure 31. - Egypt, Libya, Sudan, the Red Sea, the Tibesti Mountains, Gulf El Kebir, and the Great Libyan Land Sea; photographed from an altitude of 260 n. mi., looking east-northeast.

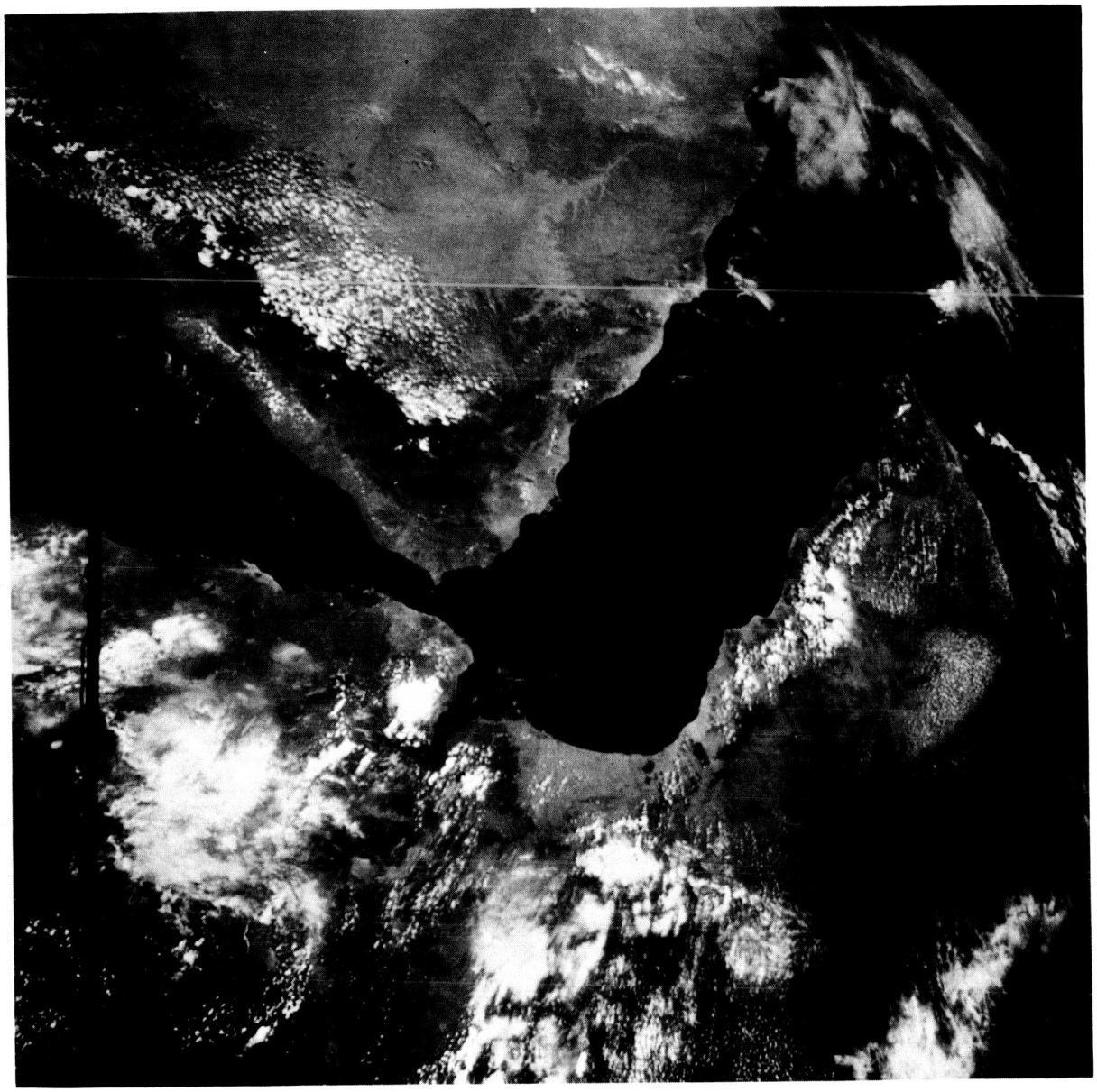

Figure 32. - Ethiopia, Somali, French Somaliland, Saudi Arabia, Yemen, and South Arabia; the Red Sea and The Gulf of Aden are below the spacecraft; the photograph was taken at an altitude of 350 n. mi., and southeast is toward the top of the figure.

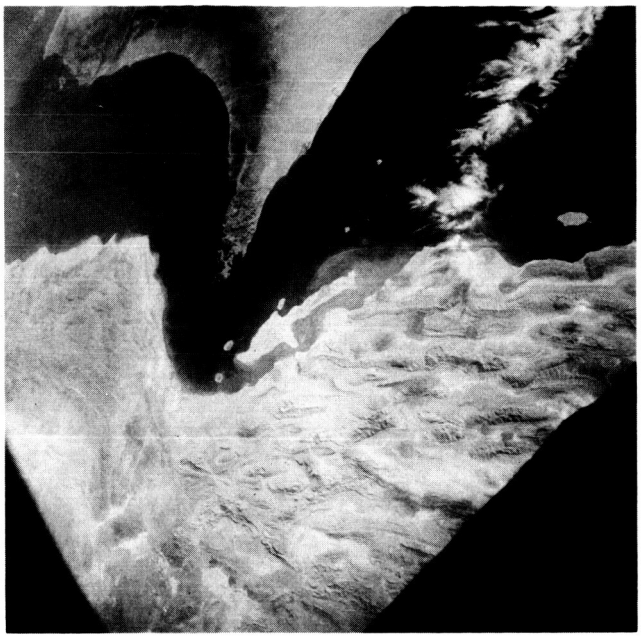

Figure 33. - The Strait of Hormuz and the Persian Gulf (bottom center) and the Arabian Peninsula (right); the view is easterly, over southeast Iran and western Pakistan.

Figure 34. - A photograph of southeastern Iran and western Pakistan, taken on a different revolution than was figure 33.

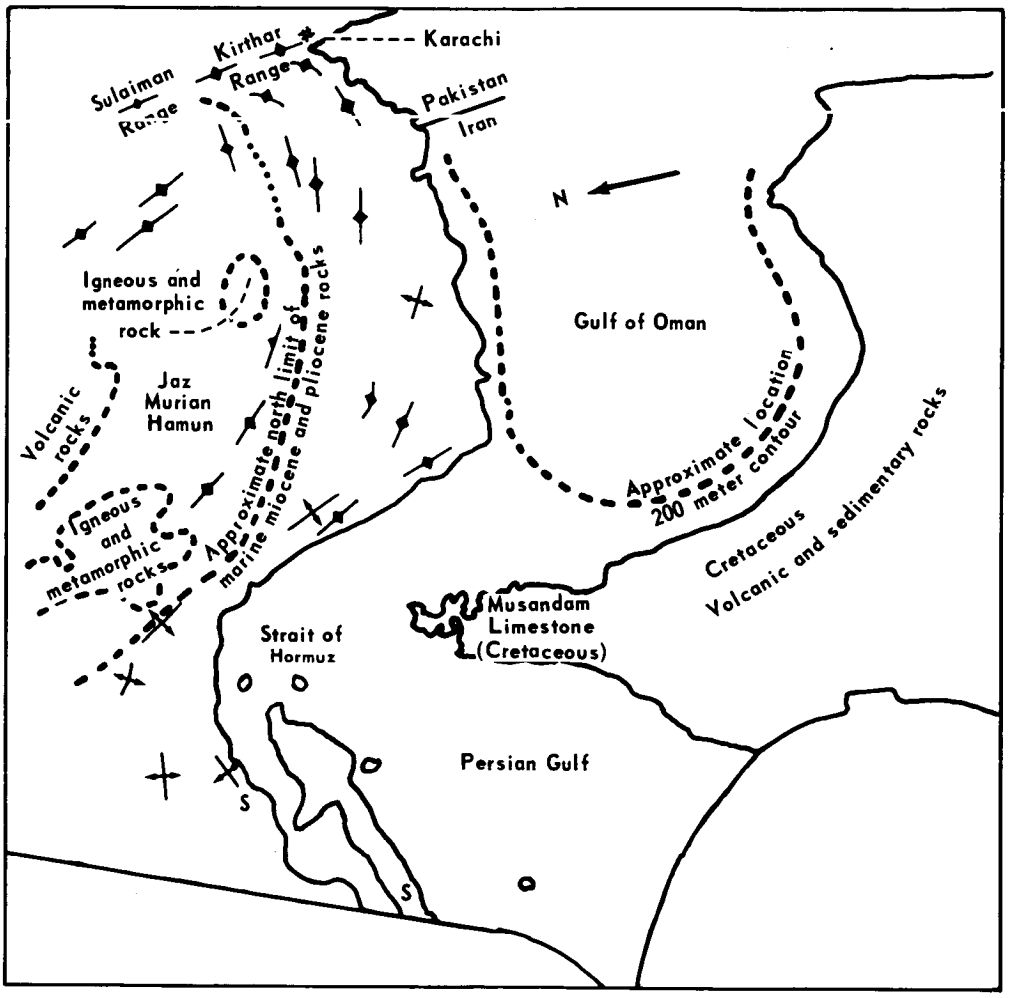

Figure 35. - A geologic sketch that corresponds to figure 34.

Figure 36. - A photograph of northeastern Mexico and southern Texas, taken northward during standup EVA.

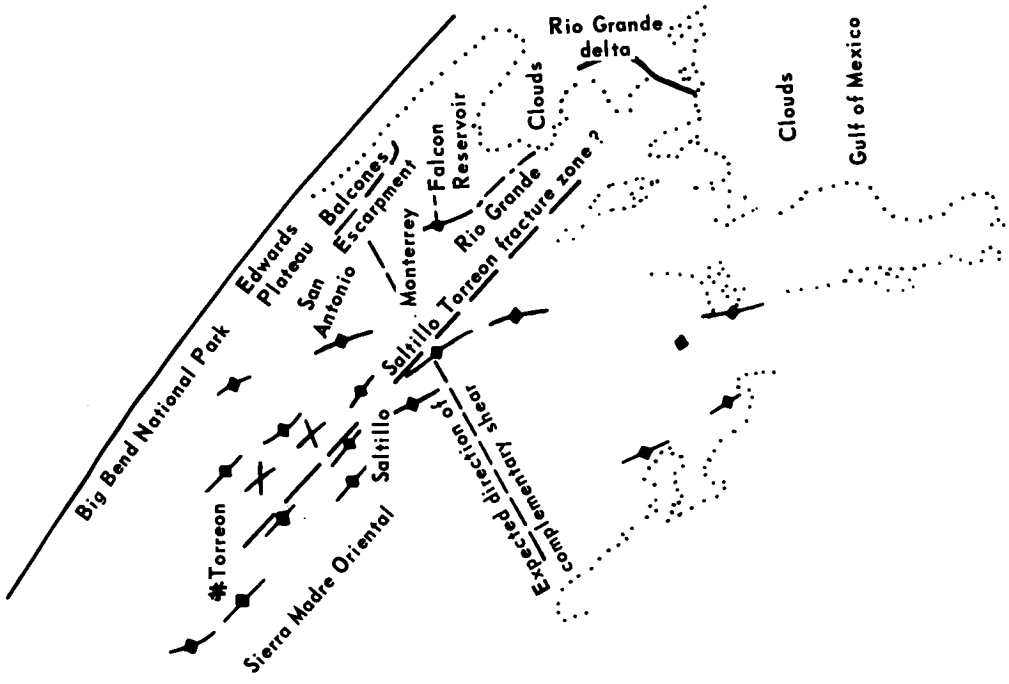

Figure 37. - A geologic sketch that corresponds to figure 36.

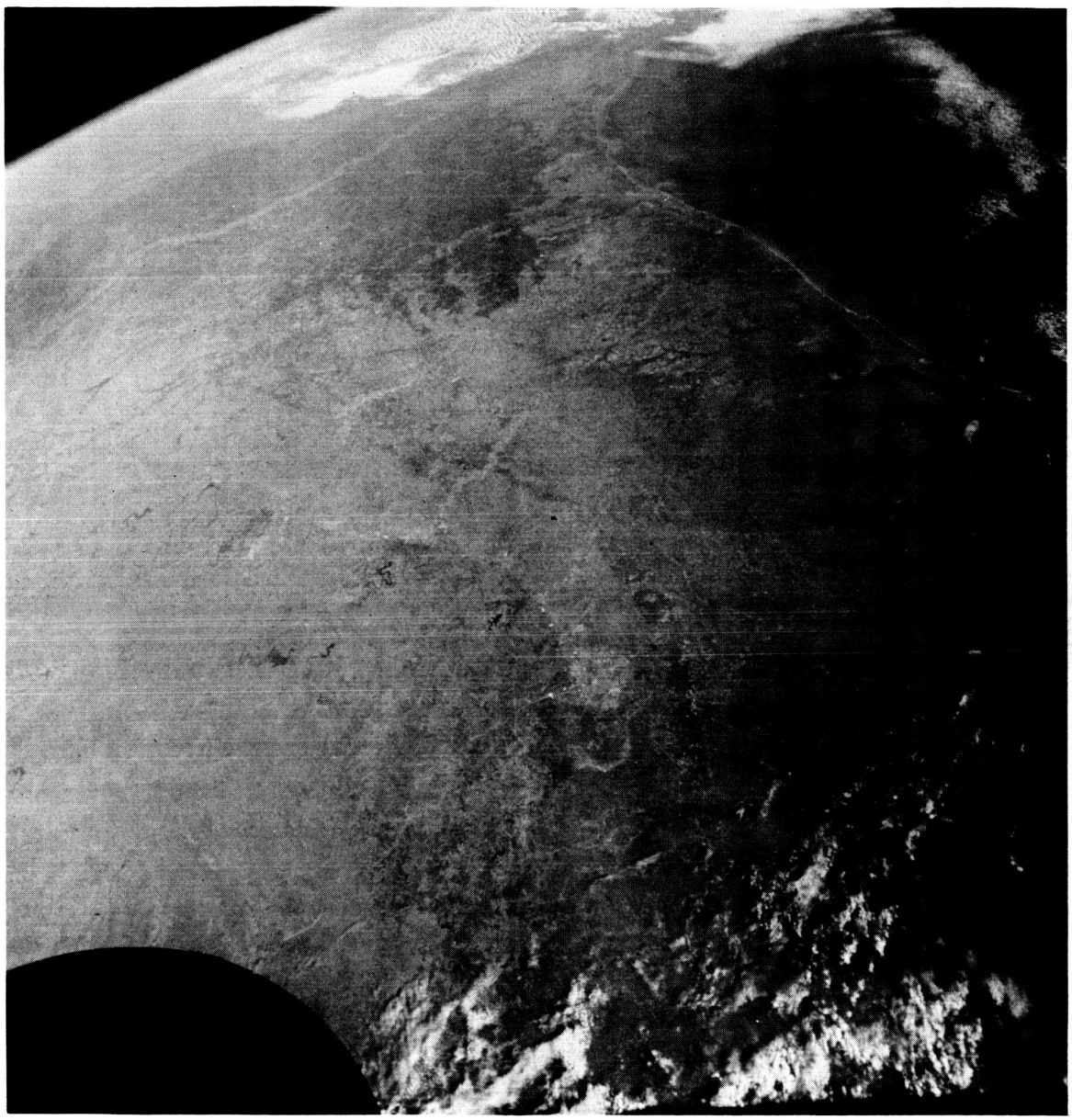

Figure 38.- An easterly view over the Texas Gulf Coast; the Gulf of Mexico is at the upper right; San Antonio (east of the Balcones Escarpment) is at the bottom center; the boundary across the center is the Edwards Plateau; and the dark region is pine forest in east Texas.

Figure 39. - A northeasterly view over southern Egypt, the Sinai Peninsula, and the Red Sea (lower right); a pipeline fire, which started a few minutes before the photograph was taken, is at the extreme upper right.

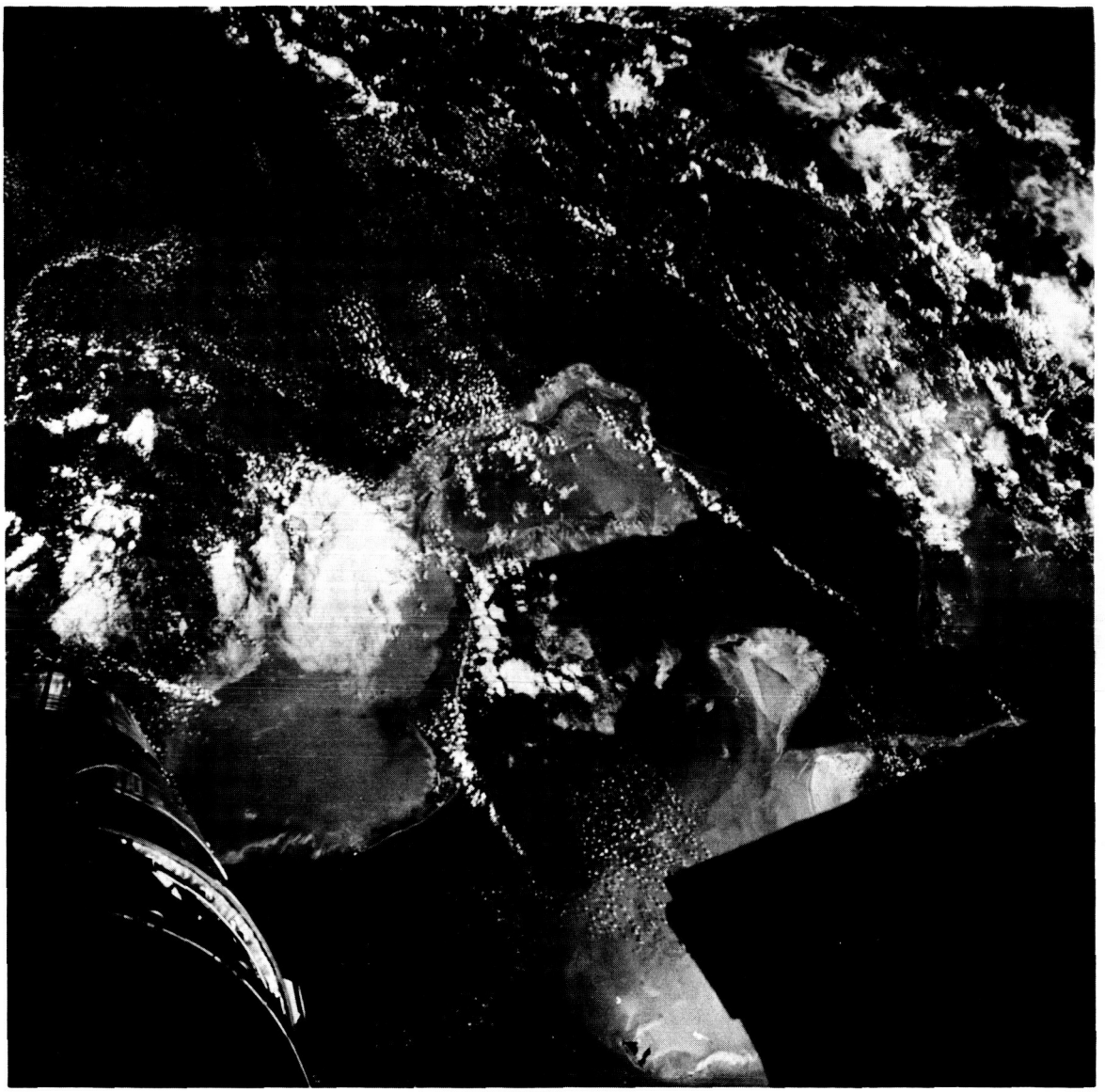

Figure 40. - A photograph of the Bahama Islands, taken during standup EVA: the Little Bahama Bank is at the left, and the Great Bahama Bank is below the open hatch, Nassau and Eleuthera are at the upper right (partly cloud covered); the water in the light regions is 10 to 20 feet deep, and in the dark regions the water depth is as much as several thousand feet.

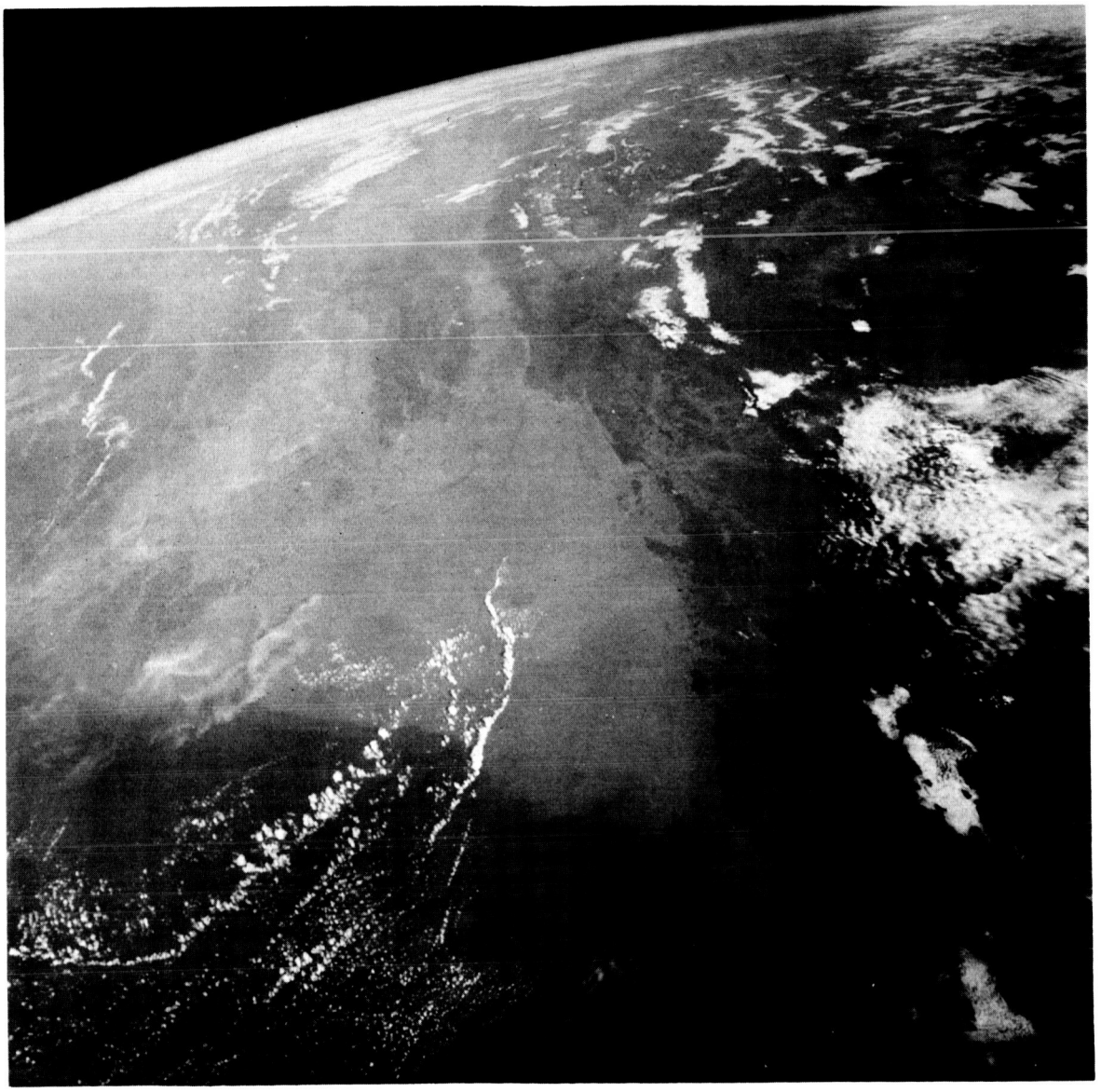

Figure 41. - A northerly view over the Gulf of Martaban (light-colored water) and the mouths of the Irrawaddy River (left), Burma.

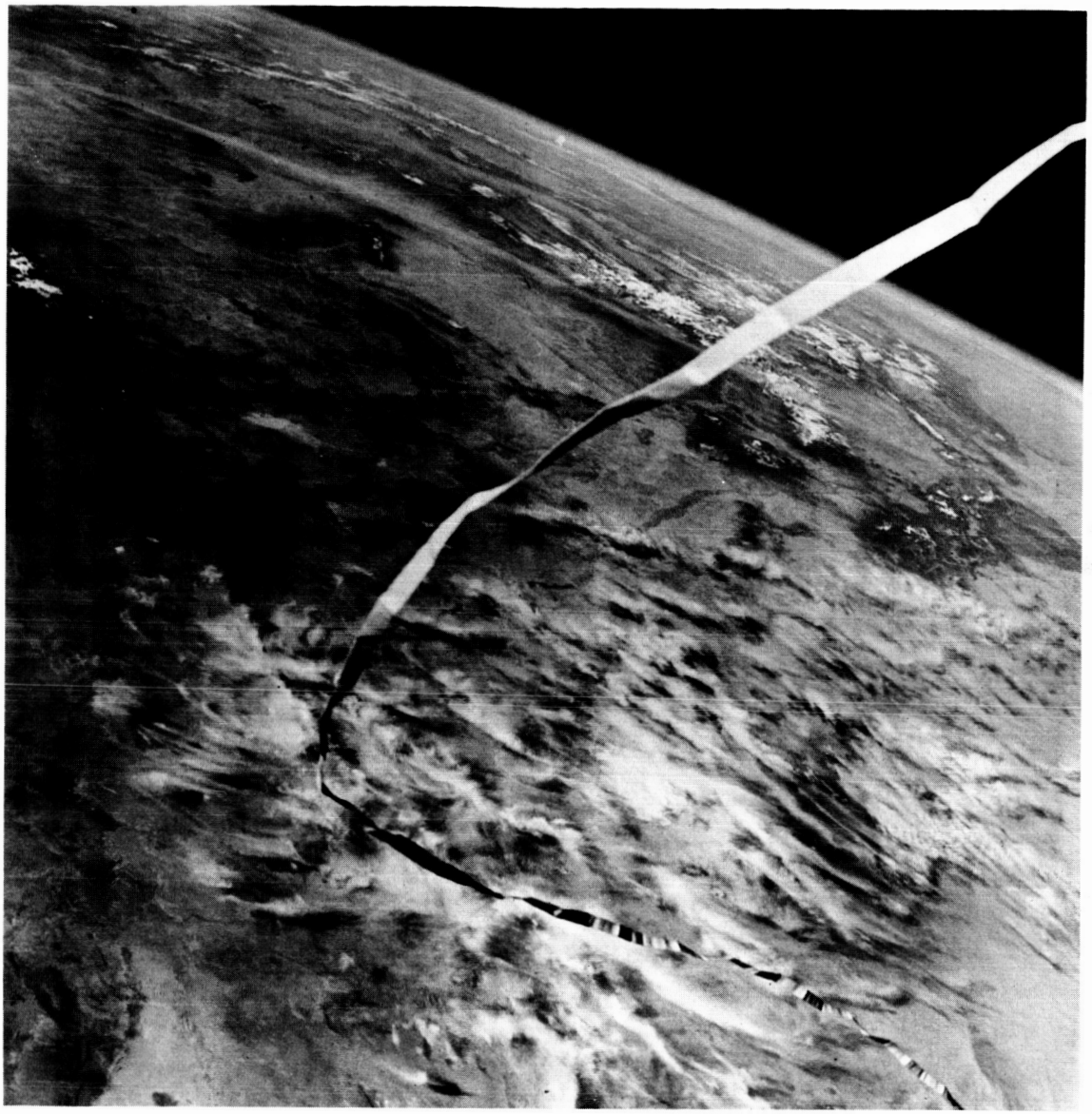

Figure 42. - A northerly view of northern Chihuahua (directly below at bottom) and White Sands, New Mexico (right of the bend in the tether); the dark boundary at the far right is the eastern boundary of the Rocky Mountains (Colorado), and the Colorado Plateau is at the far left.

EXPERIMENT S006

SYNOPTIC WEATHER PHOTOGRAPHY

By Kenneth M. Nagler* and Stanley D. Soules**

OBJECTIVE

Experiment S006 was essentially a data-gathering effort; the general purpose was to provide a set of pictures that would cover a broad range of meteorological phenomena. The more specific purpose was to obtain views of a number of cloud systems that would be of particular interest to various investigators. On both manned and unmanned Mercury missions and on the Gemini III mission, a number of good pictures of cloud systems were obtained. Also, specific experiments were performed by the crewmembers on the Mercury missions. Those experiments involved some of the spectral-reflectance characteristics of clouds, land, and water regions of the earth surface as viewed from outside the atmosphere. The results from earlier manned space flights have contributed to man's knowledge of meteorology. However, there is great variety in the weather systems on earth, and photographs on the scale obtainable from the Gemini Program can help man to understand these systems. In particular, detailed color photography is useful to those studying meteorological satellite pictures. These pictures have yielded meteorological coverage of most of the world, and this contributes to the routine surveillance of the weather. Some pictures are understood imperfectly because the smaller features cannot be resolved. Therefore, for a number of selected meteorologically interesting cloud systems, it was desirable to get many more detailed color views taken from manned spacecraft. Such pictures can be used to verify and amplify information obtained from weather satellites. Also, some pictures are significant by themselves, whether or not they can be associated with simultaneous meteorological-satellite coverage.

Another need that can be satisfied through use of manned satellites is the depiction of cloud systems at fairly short time intervals. For example, pictures can be obtained on successive revolutions of a Gemini spacecraft. These pictures are indicative of the changes in and the movements of clouds at approximately 90-minute intervals at certain points beneath the track of the spacecraft. A series of such views can be of assistance in the explanation of various meteorological phenomena.

*U.S. Weather Bureau, Environmental Science Services Administration, Washington, D.C.

**Meteorological Satellite Laboratory, Environmental Science Services Administration, Washington, D.C.

EQUIPMENT

Gemini IV, VI, and VII Missions

The S006 experiment on these missions involved the same Model 500C Hasselblad camera that was used in Experiment S005, as well as the same 70-millimeter Ektachrome MS film. A total of five film magazines, each with sufficient film for 55 exposures, was carried on the spacecraft for use on Experiments S005 and S006 and for general photography. To reduce the intensity of the blue light scattering back from the atmosphere, a haze filter was fitted to the standard 80-millimeter f/2.8 lens.

Gemini X Mission

A Maurer 70-millimeter space camera was used with Kodak Ektachrome MS (SO-217) film. The camera had an f/2.8 lens with an 80-millimeter focal length. An ultraviolet haze filter was used. Five film magazines were on board for all experiments.

Gemini XI Mission

The equipment for this experiment consisted of 70-millimeter Kodak Ektachrome MS film on a 215-mil polyester base, the Hasselblad camera, and the Maurer general-purpose camera. A superwide angle (SWA) lens with a 38-millimeter focal length was used on the Hasselblad camera; an 80-millimeter focal-length lens was used on the Maurer camera. Five rolls of film were exposed for Experiments S005 and S006 and for documentary photography.

Gemini XII Mission

Most views were obtained with the SWA 70-millimeter camera by use of a 38-millimeter f/4.5 lens. Some pictures of interest were taken with the 70-millimeter general-purpose camera by the use of an 80-millimeter f/2.8 lens. A haze filter was used on both cameras.

EXPERIMENTAL PROCEDURE

Before the Gemini missions, several meteorologists (primarily from the National Environmental Weather Satellite Center of the Environmental Science Services Administration) were queried regarding the types of cloud system they were interested in and what particular geographical regions were of interest. The experiment goals were discussed in detail with the crewmembers. A number of specific cloud types or conditions were suggested as possibilities for photography. These types included cellular patterns, vortexes in the lee of subtropical islands, thunderstorms, sunglint, shadows of cirrus clouds on lower cloud layers, intertropical convergence regions, and tropical storms.

The mission plan was arranged so that the crewmen could devote part of their time to cloud photography over the preselected locales. On the day preceding launch, the crewmen were briefed on several interesting features likely to be seen on their mission. This information was revised later, and, on some flights, this information was updated and relayed to the crewmen shortly before they entered the spacecraft. During the mission, features of interest were selected from weather analyses and from Tiros weather satellite pictures. Whenever feasible operationally, this information was communicated to the crewmen from the NASA Manned Spacecraft Center (MSC) at Houston, Texas, in time for them to locate and to photograph the clouds in question; this activity was not permitted to interfere with their other duties. When fuel was available for changing the attitude of the spacecraft for this purpose, the crewmembers were able to search for the desired phenomena. Otherwise, they could take pictures only of scenes that happened to come into view. On the Gemini XI mission, specific emphasis was placed on conditions available on revolutions 26 and 27, when the Gemini vehicle was to be at an apogee of approximately 740 nautical miles.

RESULTS

Because of the large quantity of information involved, the experimental results are presented according to mission. Examples of the photographs and explanations of their meteorological content are given.

Gemini IV Mission

The crewmen took approximately 200 70-millimeter color pictures. Of these, approximately half were of cloud formations or contained information of other meteorologic interest. A selection from these views is shown in this report to illustrate the types of pictures obtained.

A view of southern Florida is shown in figure 1. Cumulus cloudiness over the land regions, typical for the daytime, is shown. The absence of cumulus clouds over most of the adjacent ocean and over Lake Okeechobee is apparent. Acklins Island and Crooked Island in the Bahamas are shown (fig. 2) nearly enclosing a shallow lagoon. To the left of the picture, the reflection of the sun from the sea surface is interrupted by the tiny dark shadows of clouds, which cannot be seen against the brightly reflecting waters. Long-period swells are discernible near the edges of the sunglint region. A widespread area of cloudiness typical of disturbed tropical conditions is shown in figure 3. This view was taken near latitude 16° N, longitude 178° E. Several vortexes in the lee of some of the Canary Islands are shown in figure 4. Often, pictures from Tiros had shown vortexes in the lee of mountainous subtropical islands, but the fine cumulus lines that delineated the eddy motion found in this view were too small to be detected on routine pictures from meteorological satellites.

A view of convective cellular clouds over the eastern North Pacific is shown in figure 5. Such cellular patterns had been observed in weather-satellite pictures over many parts of the earth. These patterns result from weakly organized convection currents in the absence of any significant vertical wind shear. Of particular interest in

this picture are the vortexes which appear along the boundaries of the cells; such vortexes had not been apparent in Tiros views.

A view from over central Texas is shown in figure 6. The photograph was taken as a part of Experiment S005. It is of the region to the north and west of San Angelo, Texas. As described in reference 1, two large dark sectors, not caused by differences in land usage, but caused by a heavy rainfall on the previous day, are shown in the figure. In lighter regions, little or no rain had fallen during the same period.

With the many different types of weather systems of interest and with the day-to-day and seasonal changes in weather, meteorological features remain that are of interest for future missions. It was planned to photograph additional features on other Gemini missions.

Gemini V Mission

The crewmembers used all the film and, with very few exceptions, obtained photographs of excellent quality. More than half the pictures involved clouds. A selection of views of special meteorological interest is presented in this report.

Views of tropical storms are always of interest. A small tropical storm near the Marshall Islands is shown in figure 7. The spiral cloud bands and the surrounding clouds associated with this immature disturbance are shown in great detail. Tropical storm Doreen in the eastern North Pacific is shown in figure 8; it was a large storm, almost of typhoon intensity. In addition to taking pictures of this storm, the Gemini V crewmen twice provided timely information on its location; this information was used by the Weather Bureau in the preparation of advisories on Doreen.

Views of a portion of Florida, taken on successive passes of the spacecraft, are shown in figures 9 to 11. In figure 9 (approximately 10:30 a.m. local time), it can be noted that cumulus clouds had formed over most of the landmasses, but with a few exceptions (such as the one over Merritt Island), the clouds did not have much vertical development. By approximately noon local time (fig. 10), a line of towering cumulus clouds had formed 20 to 30 miles inland from the east coast. By approximately 1:30 p.m. local time (fig. 11), some of these towering cumulus clouds had reached the thunderstorm stage, and their cirrus anvil tops had spread westward over central Florida. The view of Florida was completed by the photograph shown in figure 12. This view overlaps the view shown in figure 11 and shows a large thunderstorm southwest of Miami. On the following day, approximately 24 hours after figures 11 and 12 were taken, the cloud pattern over Florida was as shown in figure 13. Again, the line of greater vertical development occurred, but the strong thunderstorm development was confined to the western part of the Florida Keys. The cloud streets are well formed and are alined with the easterly winds blowing straight across Florida. These and other views of Florida were studied relative to the location and timing of thunderstorm formation in the vicinity of Cape Kennedy and Merritt Island, Florida.

Some features other than clouds are of interest to meteorologists and scientists in related fields. A view of interest to oceanographers is shown in figure 14. The detail in the shallow-water bottom configuration in the Bahama vicinity, as seen in this

and other views, was studied. Vortexes induced by the flow of air past islands or coastal prominences have been photographed on several missions. A coastal-prominence type vortex is shown in figure 15.

Gemini VI and VII Missions

A large number of additional views of interest were obtained on the Gemini VI and VII missions (December 1965). On all of the missions, views were taken that were illustrative of cloud fields that resulted from organized convection under a variety of meteorological conditions. These included the cumulus cloud streets, long lines of cumulus clouds parallel to the windflow, as illustrated in figure 16 (Gemini VII). Also, some other scenes showed a broad pattern of branching cumulus streets.

Sometimes, on meteorological satellite views, the determination as to whether the clouds present are high (cirrus) or lower (altostratus or stratus) clouds is difficult. Often, the suggestion is presented that dark regions on such pictures may be shadows of cirrus clouds on lower cloud decks. Sometimes, by their orientation, the long dark lines are indicative of the direction of the winds at the cirrus level because cirrus clouds in the strong wind core of the upper troposphere (jet stream) frequently occur in long bands parallel to the winds. On the Gemini VI and VII missions, several examples of such cirrus shadows on lower clouds were obtained (one of which is shown in fig. 17).

Pictures of features other than clouds are sometimes of interest in meteorology and related fields. For example, smoke from forest fires or from industrial sources may be indicative of the low-level wind direction and may yield quantitative information on the stability of the lower atmosphere. Sand dunes of various types are of interest to investigators interested in the relationship between winds and deposition patterns. One of many dune scenes is shown in figure 18. Similarly, the configuration of bottom sand in some shallow water regions can be related to motions in the ocean.

Gemini X Mission

More than 200 high-quality pictures of cloud patterns were obtained. Several of the frames had sufficient overlap for stereoscopic viewing. Cloud layers could be resolved readily by this method, and important information was acquired on the relative altitudes of the cloud tops. Cumulus cloud lines are prominent features in the convective cloud patterns (fig. 19) of northern South America. The Essequibo River system in Guiana, which has relatively cool waters, has suppressed the development of clouds above it. The flow of the sediment-laden waters can be traced into the Atlantic. Over the oceans, convective clouds can form open polygonal cells. In figure 20, these cells are 3 to 6 miles in diameter. Cells of this size are undetected by weather-satellite television pictures because the cloud walls are too thin and because the cell diameter is very small. The cell configuration is indicative of the structure of the atmosphere in its lower level.

Frequently, large cloudy regions 300 to 400 miles in diameter appear in weather-satellite photographs of the equatorial convergence zone. These cloud masses sometimes grow into tropical storms. A cloudy region such as this was photographed over

the Indian Ocean by the crewmen, and a detailed view (fig. 21) showed a great amount of convective activity in the cloud mass. The cirrus plumes from the thunderstorm tops are carried downwind from the northeast, and low-level cumulus cloud lines are oriented from southeast to northwest. One of a series of photographs taken over Sumatra and Malaya is shown in figure 22. Equatorial cloud conditions at various altitudes in the atmosphere are shown in the figure.

Another series of photographs depicted the cloud cover over the Gulf of Mexico and the Caribbean. Part of tropical storm Celia, which was southeast of Florida, appeared in several frames, which facilitated stereoscopic viewing. Cirrus cloud bands over northern Africa and cloud eddies off the northwest coast of Africa, the Canary Islands, and Guadalupe Island were among other subjects that were photographed. A sunglitter pattern, formed by sunlight reflected from the ocean surface, was photographed several times. An analysis of the brightness of the pattern may result in information concerning the surface roughness. Considerable cirrus cloudiness, which formed long bands, was noted near Sumatra and southwest of India.

Gemini XI Mission

Approximately 180 good-quality color photographs were taken of cloud formations. Most of the pictures were taken on September 14, 1966, during revolutions 26 and 27 over Africa, Arabia, the Indian Ocean, and Australia. Pictures were taken with both cameras during these revolutions. Between revolutions 26 and 27, photographs were taken over the Indian Ocean from the Environmental Science Services Administration meteorological satellite (ESSA I). The Gemini XI pictures of this region facilitate comparison of the aerial coverage and detail obtainable from cameras that have different lenses and from concurrent operational weather satellites. Cloud movements and changes that occurred in the interval between photographs can be evaluated.

A typical photograph taken with the Maurer camera (80-millimeter focal-length lens) is shown in figure 23. The photograph is of the southern part of India and the surrounding Indian Ocean, and it was taken from an altitude of approximately 410 nautical miles. Patterns of cumulus clouds formed by midday over the land and the absence of many clouds along the coastline were indicative that a sea breeze was blowing from the cool ocean water. Cloud diameters as small as 0.25 mile are recognizable in this photograph. A striking picture of southern India and Ceylon, taken with the Hasselblad camera and the wide-angle, 38-millimeter focal-length lens, is shown in figure 24. Although the field of view is larger, the magnification is approximately one-half that of figure 23. The additional regions in figure 24 give a better indication of the larger scale cloud patterns; the gain in areal coverage compensates for the factor-of-2 loss in resolution. The larger field of view in figure 24 contains a feature that is not readily apparent in figure 23. A zone, almost free of clouds, extends along the west coast of India; the zone varies from 30 to 50 miles in width and is continuous around the southern tip of India into the Bay of Bengal, where a line of convective clouds had formed several hundred miles offshore. This clear region is not understood entirely, but two reasons for its existence are suggested. The lack of clouds may be the result of drier air subsiding offshore; this has the tendency to suppress cloud development. Where the low-level winds are moving the air toward the land, the sea breeze may cause the air to descend in the clear region. Also, there may be cool-water upwelling along the coast. Surface winds are northwesterly along the west coast

of India and are southwesterly along the east coast of India. The northwest winds would transport the surface water southeastward. However, the coriolis force would tend to deflect the water toward the southwest (away from the land). This deflection would permit the upwelling of cooler water along the coastline, and the water temperature may be low enough to suppress the development of cumulus clouds. A surface temperature change of approximately 1° might accomplish this. To the east of India, where southwest winds prevail, the coriolis force would act to transport the surface water in an easterly direction. Again, this produces a favorable condition for upwelling near the coastal region. Observations of sea-water temperatures from ships were scarce, but the few reports available were indicative that the coastal waters were 1° to 2° cooler than sea-water temperatures farther west in the Arabian Sea.

A montage of weather-satellite pictures made by ESSA I is shown in figure 25. These photographs were taken approximately 45 minutes after the photographs in figures 23 and 24 were taken. The cloud-free zone is evident in figure 25. An examination of ESSA pictures taken of India on other days revealed several similar phenomena. Many of the smaller cumulus clouds, which are seen easily in the Gemini pictures, cannot be resolved in figure 25. Because it is an oblique view, the resolution in the region of northern Ceylon (fig. 25) is only approximately 5 miles. The crewmen took another series of photographs while crossing the Indian Ocean during revolution 27. The photograph shown in figure 26 was made at a considerable distance south of India with the Maurer camera and the 80-millimeter lens. The cloudiness in the foreground is typical for a convergence zone in tropical regions. Very long streamers of cirrus clouds extend across the upper part of the picture. Easterly winds at high altitudes have carried these clouds of ice particles from the tops of thunderstorms near Malaysia.

Ceylon is obscured partly by these clouds, but the large thunderstorms near the northern end of the island are clearly visible. The great change in these thunderstorms can be seen by reference to figures 24 and 25. In 96 minutes, these clouds changed from the towering cumulus stage to well-formed thunderstorm clouds with anvils spreading westward approximately 100 nautical miles. The wind velocity at the cirrus cloud level probably exceeded 67 knots and accounted for this rapid cloud movement.

Other photographs made during the Gemini XI mission included views of extensive cloudiness associated with tropical storm Grace in the western Pacific Ocean, a vortex in stratocumulus clouds south of Cape Rhir off northwest Africa, a variety of organized patterns of convective clouds, and extensive regions of cumulonimbus activity in the Tropics. The photographs that were obtained from this mission have proved that the Hasselblad camera with a 38-millimeter wide-angle lens can photograph large-scale cloud patterns. Although there is a decrease in magnification, cloud types still are identified easily. Pictures made with the 38- and 80-millimeter focal-length lenses have been compared with televised pictures from weather satellites. From photographs made with these two lenses, meteorologists will be able to better interpret the cloud patterns seen in satellite pictures which contain less detail and lack color. Changes that occur in the same cloud patterns over short periods of time (successive vehicle revolutions) also can be analyzed in detail.

Gemini XII Mission

Approximately 200 photographs were taken during the Gemini XII mission; the photographs show cloud patterns and are of excellent quality. Several categories of photographed cloud systems are of particular interest for study.

Observations made from the ground and from aircraft have been indicative that often there is a band of cirrus clouds on the equatorial side of the core of the upper westerly winds. These "jet stream" cirrus clouds also appear frequently on weather-satellite pictures, and they are used to approximate the location and orientation of upper-wind maxima. Recently, these cloud bands have been observed to extend for thousands of miles, sometimes from near the equator to middle latitudes. The crew-members obtained several excellent views of this phenomenon in response to real-time requests. A narrow cirrus band of this type above the Red Sea is shown in figure 27. A photograph taken on the previous revolution showed the band location to be about the same, except for certain changes in the cirrus elements that comprised the band. Other views of jet stream cirrus clouds were obtained over western North Africa, over western Mexico, and (above lower frontal cloudiness) across the south-eastern United States (fig. 28). The wind maximum at the cirrus level at that altitude (approximately 30 000 feet) was approximately 100 knots.

Vortexes that occurred in stratocumulus clouds in the lee of mountainous islands have been the subject of several studies. Several such vortexes in the lee of Guadalupe Island, off the west coast of Mexico, are shown in figure 29.

Also shown in figure 29 are cellular patterns that are the result of organized convection in regions of little wind shear. In this photograph, both the "open" and "closed" types occur in proximity, the former with ascending motion around the edges of the cell and descending motion in the center, and the latter with a circulation in the opposite direction.

Sunglint patterns, which often appear on weather-satellite pictures, are related to sea conditions; hence, they are related to windspeed. The crewmen obtained a number of sunglint photographs; a very large region of reflected sunlight is shown in figure 30. Wind velocities in the vicinity were less than 10 knots and were less than 5 knots in some parts of the region. Ships in the vicinity reported sea waves of 3 feet or less in height.

Several interesting pictures of atmospheric contaminants were obtained. For example, fires on the Louisiana coast (on Marsh and Pecan Islands) created smoke plumes that were visible approximately 100 miles out over the Gulf of Mexico (fig. 31). The western plume, from Pecan Island, is an example of weak atmospheric diffusion. The line of brighter clouds where the plume enters the cumulus cloud region may be related to condensation nuclei in the smoke. A striking view of a dust-storm is shown in figure 32. Clouds of dust from southern Iran were carried by northerly winds a distance of almost 100 miles over the Gulf of Oman.

Other features of interest that were photographed during the Gemini XII mission included clouds near island weather stations (which can be related to a concurrent atmospheric sounding), cloud streets, and clouds associated with a typical frontal

low-pressure system in the North Pacific and another system in the North Atlantic. Views of the same cloud systems on successive revolutions, notably over the southern United States, are of interest. These views were studied relative to change and cloud movement.

Daily coverage of most of the world by the ESSA III meteorological satellite provided photographic data for comparison with the photography from this experiment. The Gemini XII photographs and those taken on previous missions are being used extensively in the study and interpretation of the meteorological satellite views.

REFERENCES

1. Hope, J. R.: Path of Heavy Rainfall Photographed from Space. Bull. Meteorol. Soc., vol. 47, no. 5, May 1966, pp. 372-373.

2. Nagler, K. M.; and Soules, S. D.: Cloud Photography from the Gemini 4 Spaceflight. Bull. Am. Meteorol. Soc., vol. 46, no. 9, Sept. 1965, pp. 522-527.

3. Nagler, K. M.; and Soules, S. D.: Experiment S-6, Synoptic Weather Photography During Gemini IV. Manned Space Flight Experiments Symposium, Gemini Missions III and IV, Washington, D.C., Oct. 18-19, 1965, pp. 24-30.

4. Nagler, K. M.; and Soules, S. D.: Experiment S-6, Synoptic Weather Photography. Manned Spacecraft Center Gemini Midprogram Conference Including Experiment Results, NASA SP-121, 1966.

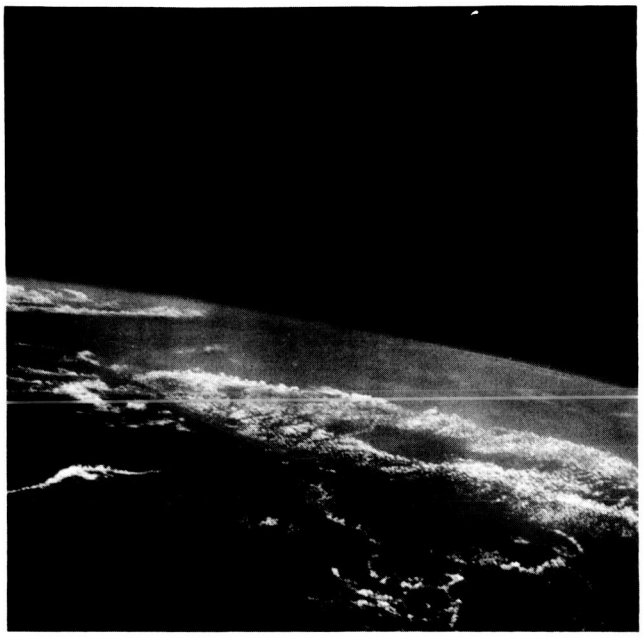

Figure 1.- A southwestward view across southern Florida; Grand Bahama Island is in the left foreground, and Cuba is in the left background.

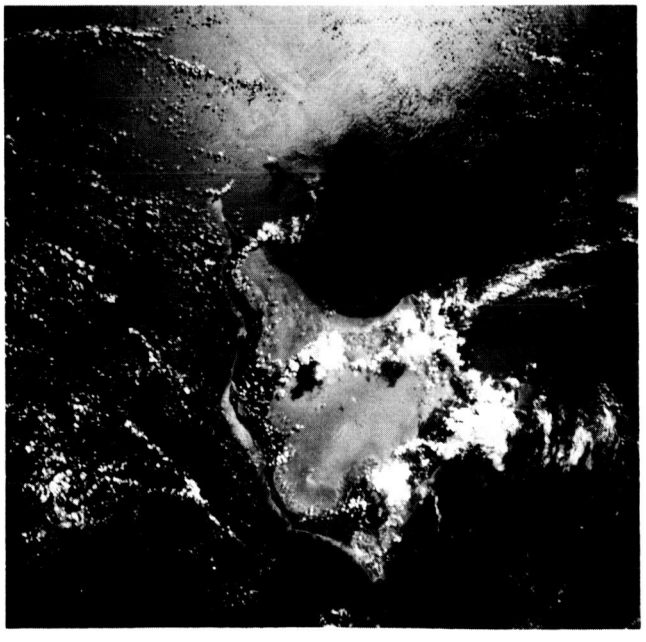

Figure 2.- Acklins Island and Crooked Island (Bahamas); the sun is reflected from the sea surface.

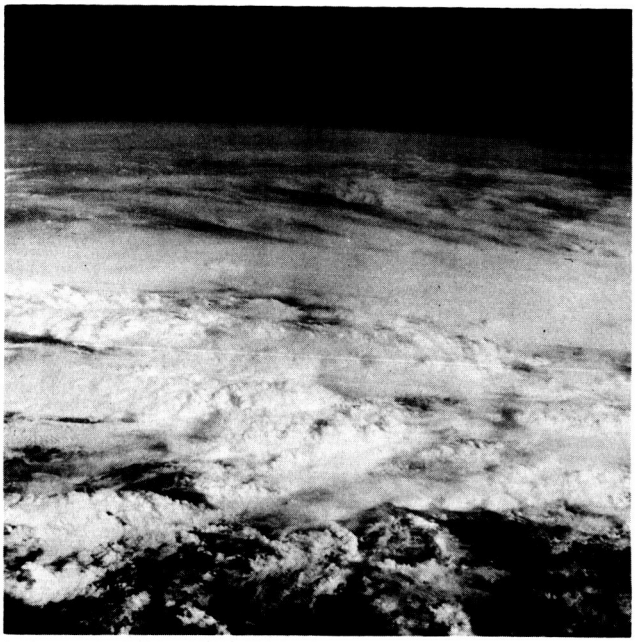

Figure 3.- A disturbed region over the tropical North Pacific Ocean.

Figure 4.- Curved cloud lines that locate eddies in the atmosphere near the Canary Islands.

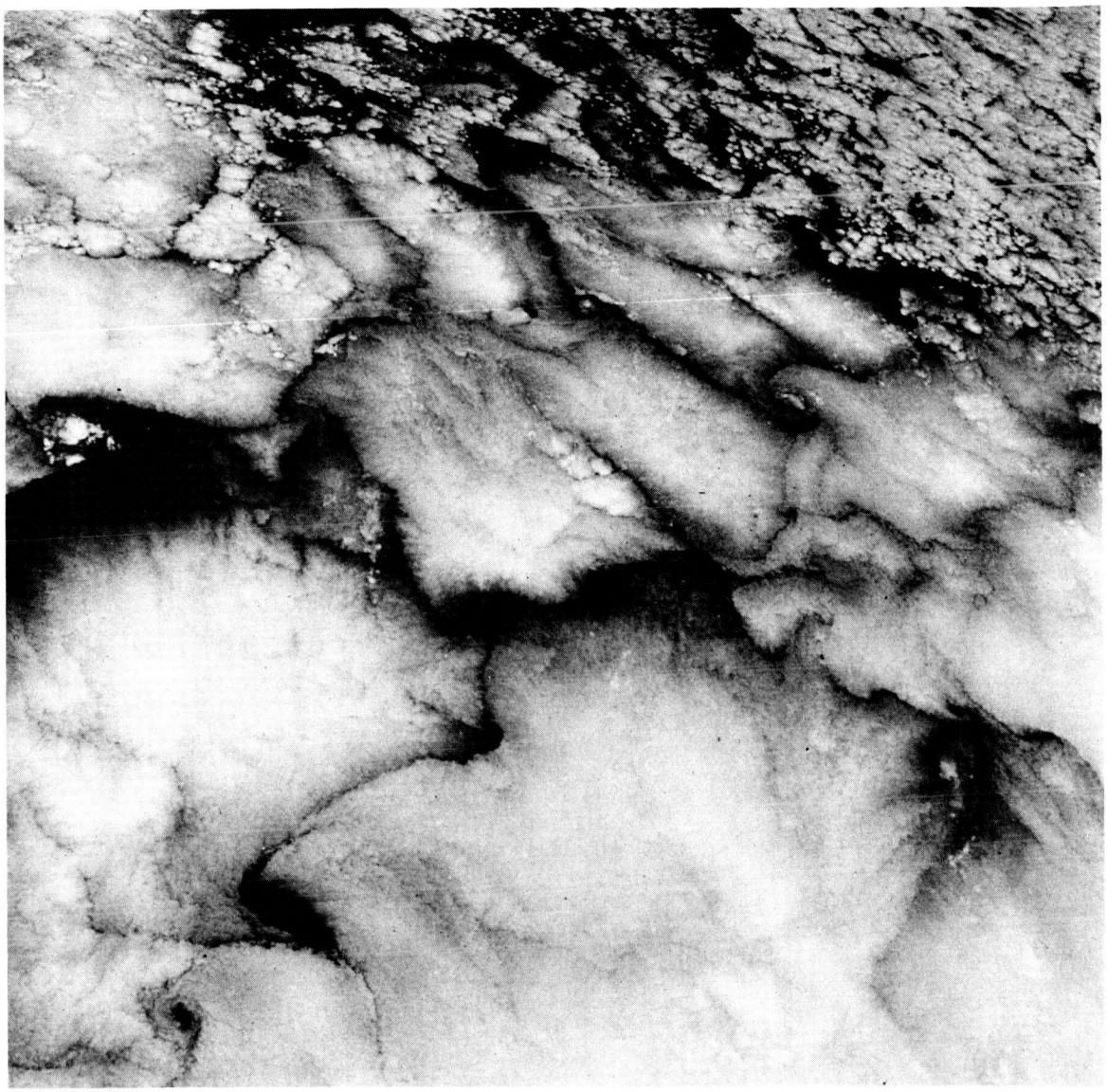

Figure 5.- Cellular cloud patterns over the eastern North Pacific Ocean; photographed during the Gemini IV mission.

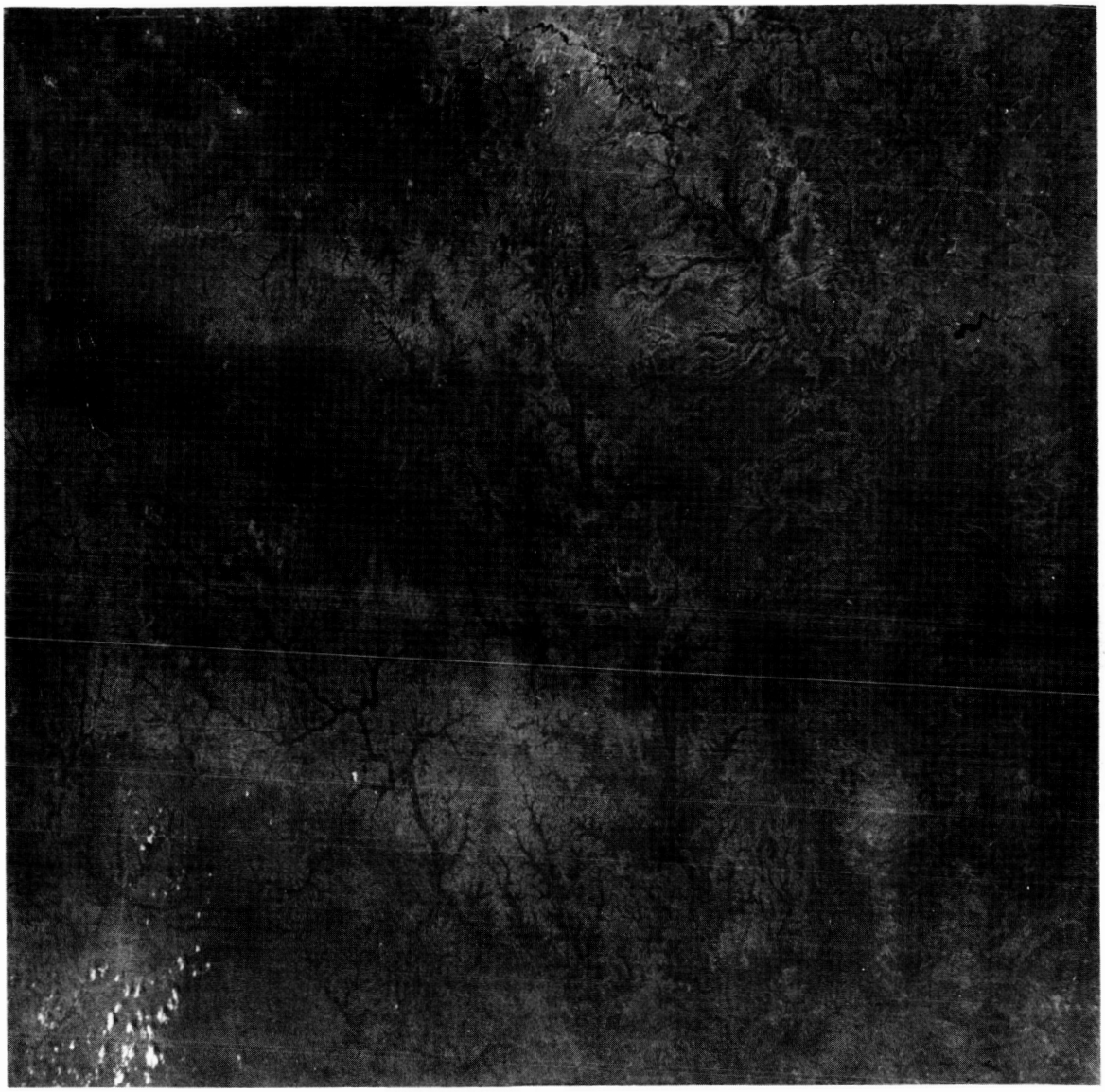

Figure 6. - Terrain shading in central Texas, caused by heavy rainfall the previous day; the highway prominent in the upper left corner connects Odessa and Midland, and the stream in the center of the picture is the North Concho River near San Angelo.

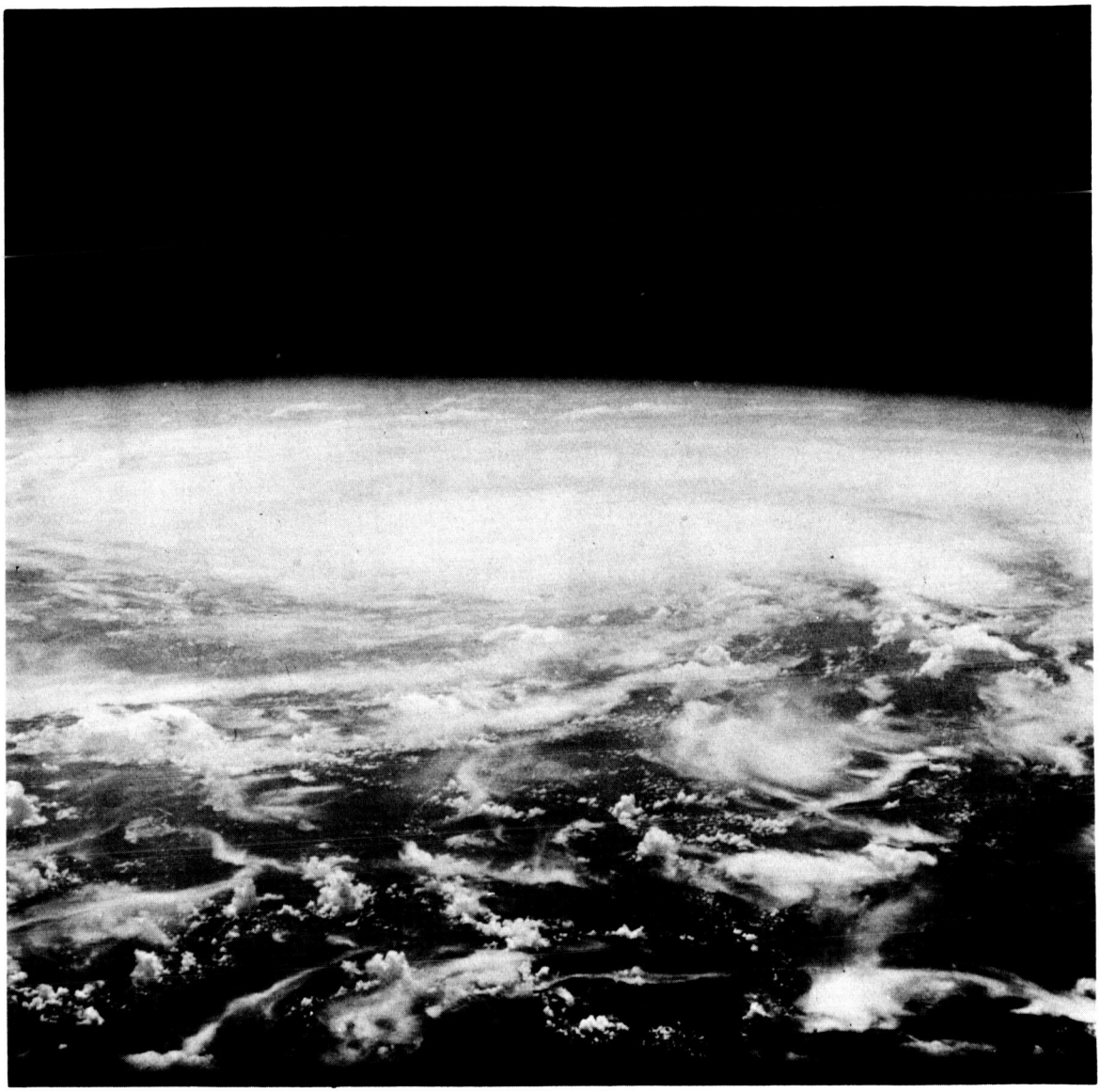

Figure 7. - A small tropical storm near the Marshall Islands; photographed at 01:25 G.m.t., August 27, 1965, during the Gemini V mission.

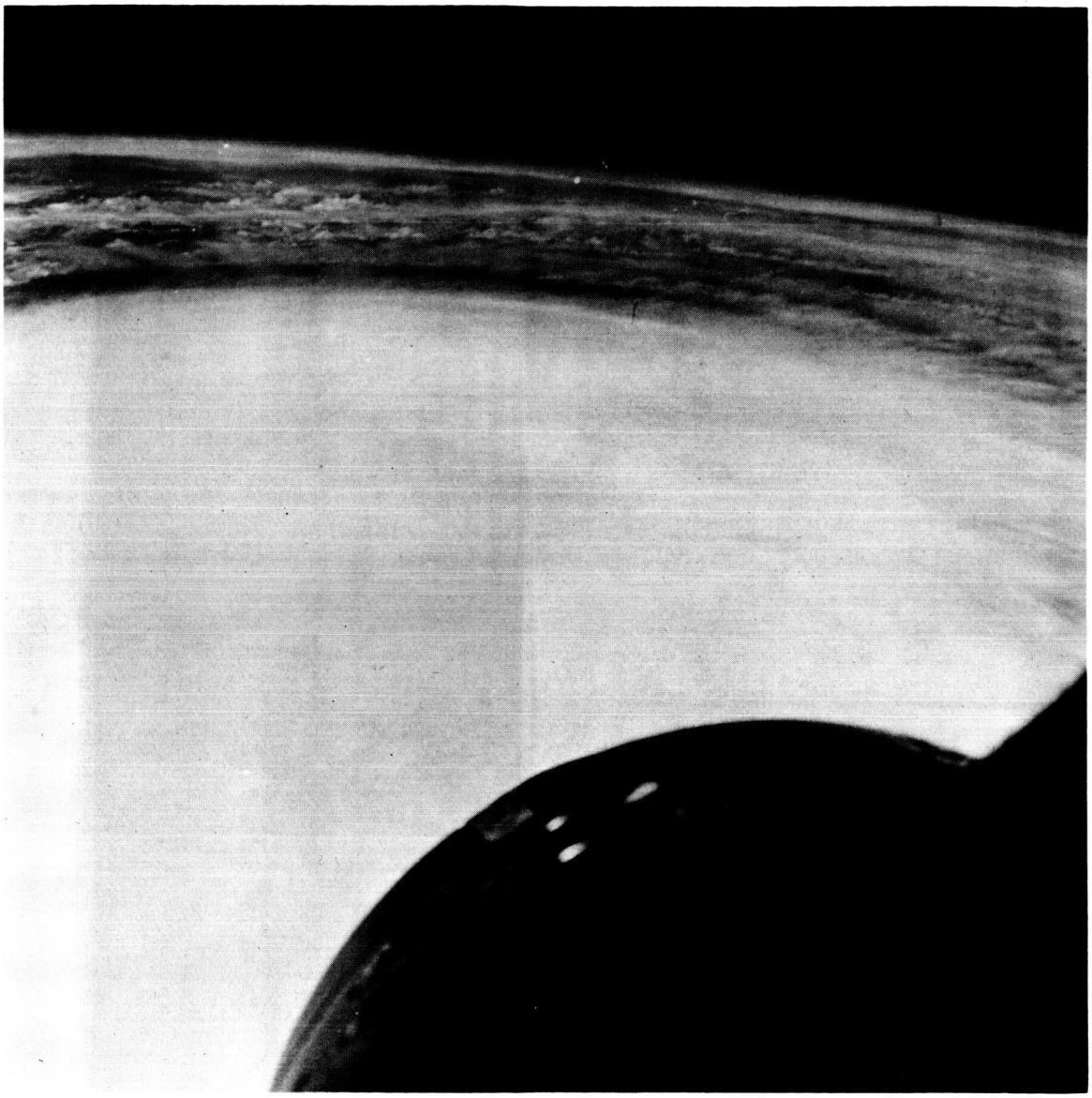

Figure 8. - Tropical storm Doreen over the eastern North Pacific Ocean, at 21:33 G.m.t., August 23, 1965, during the Gemini V mission.

Figure 9.- A view of Florida, photographed at 15:31 G.m.t., August 22, 1965; the first of three views of this region photographed on successive passes of the Gemini V spacecraft.

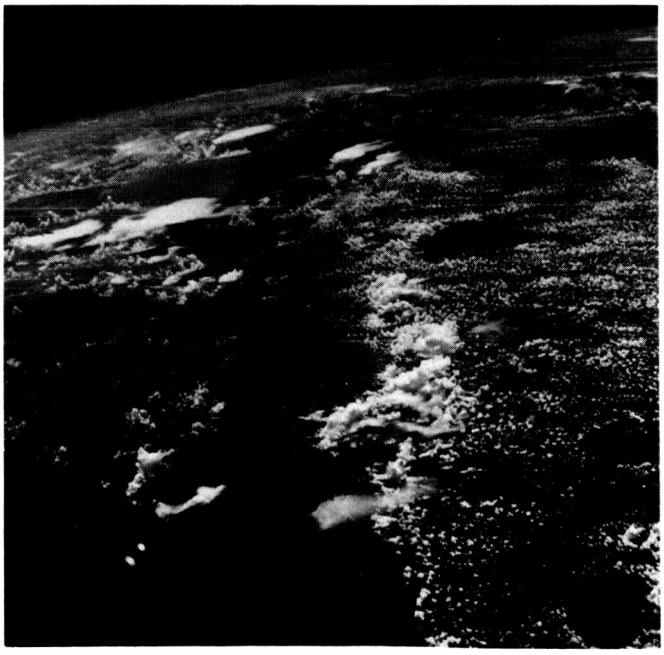

Figure 10.- A view of Florida, photographed at 17:07 G.m.t.; the second of the Gemini V series of three views.

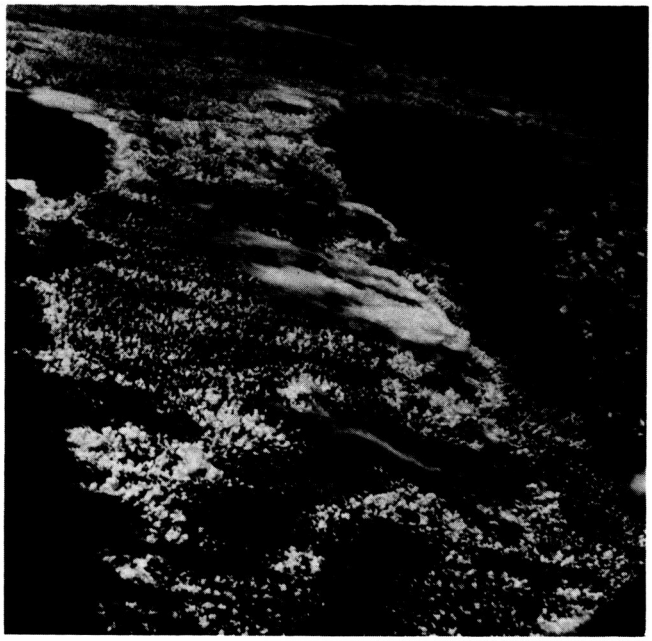

Figure 11.- A view of Florida, photographed at 18:38 G.m.t.; the third of the Gemini V series of three views.

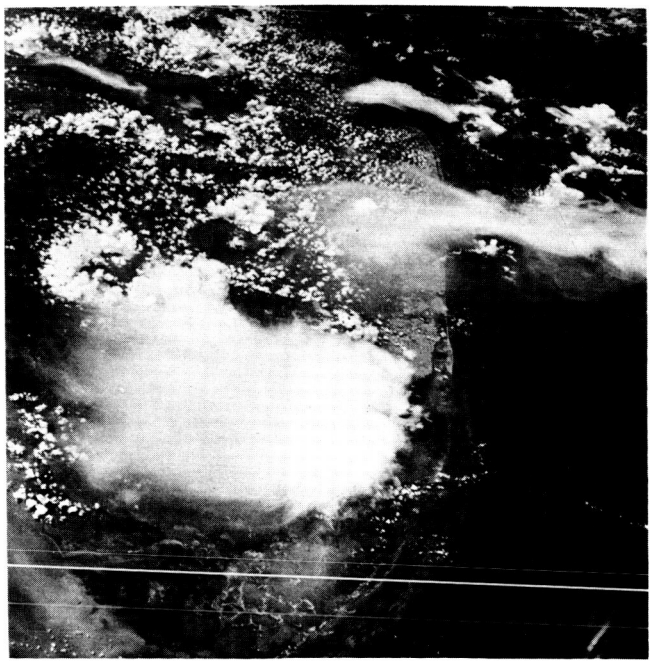

Figure 12.- A view of a large thunderstorm over southern Florida, photographed at 18:38 G.m.t., August 22, 1965, during the Gemini V mission.

Figure 13.- A view of Florida, photographed at 18:26 G.m.t., August 23, 1965, 24 hours after figures 11 and 12 were taken.

Figure 14.- Great Exuma and nearby islands in the Bahamas, showing the interesting bottom configuration in the shallow water, taken at 18:39 G.m.t., August 22, 1965, during the Gemini V mission.

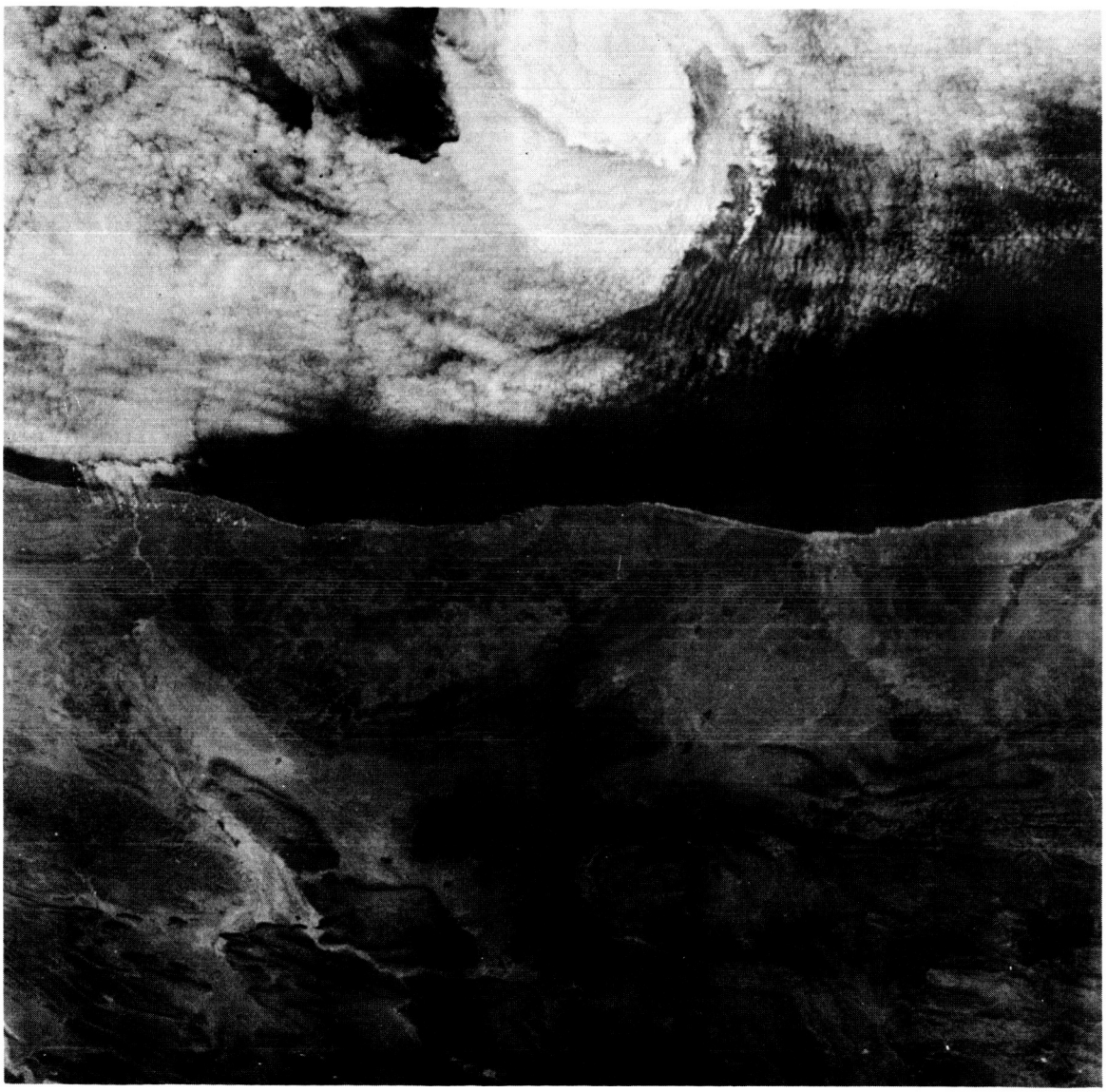

Figure 15. - A vortex in stratocumulus clouds off Morocco, induced by strong northeasterly winds flowing past Cape Rhir just north of this scene; photographed by the Gemini V crewmen at 10:25 G.m.t., August 26, 1965.

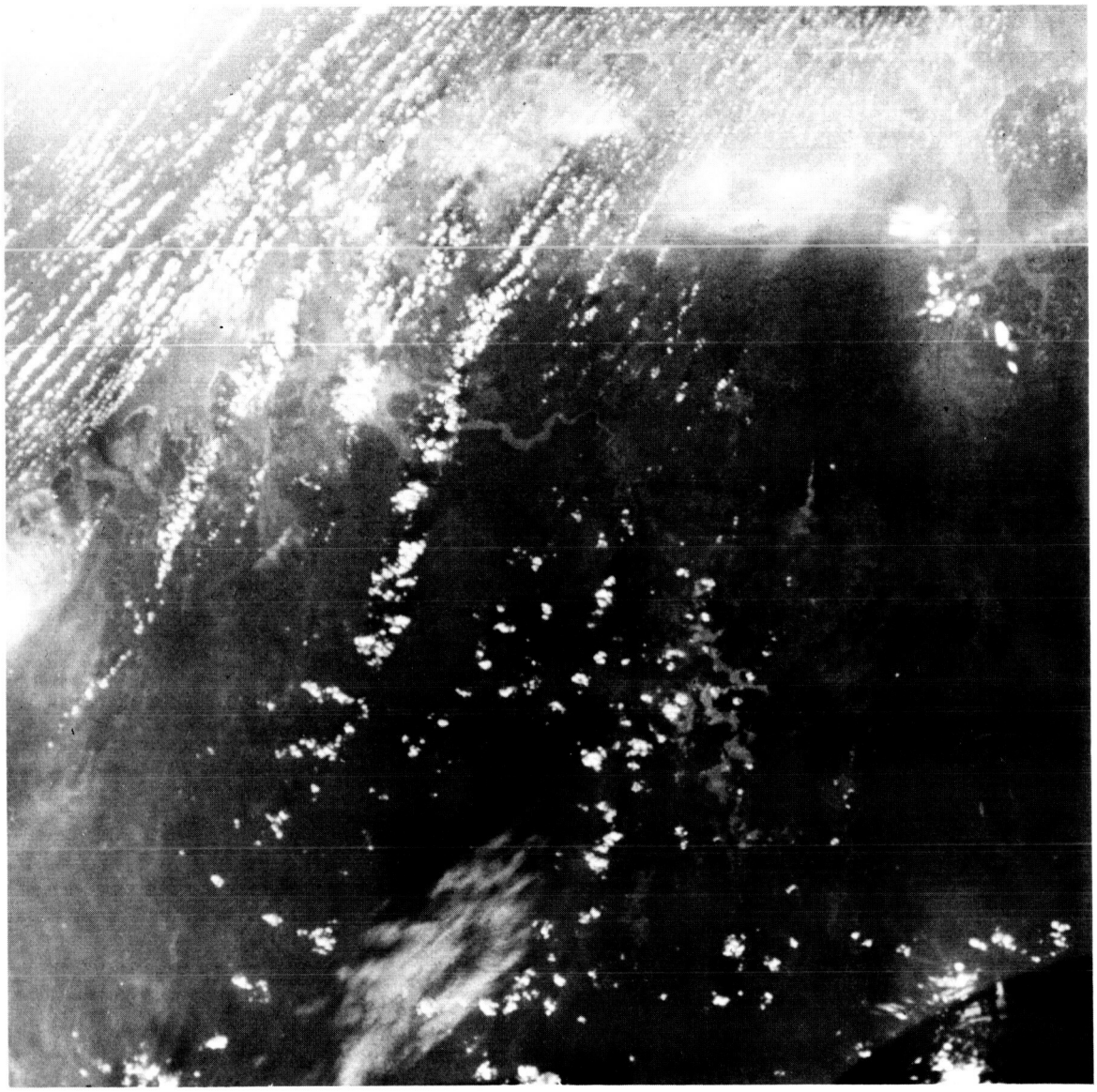

Figure 16. - Typical cumulus cloud streets in the South Atlantic Ocean near the mouth of the Para River, Brazil; photographed by the Gemini VII crewmen at 19:53 G. m. t., December 12, 1965.

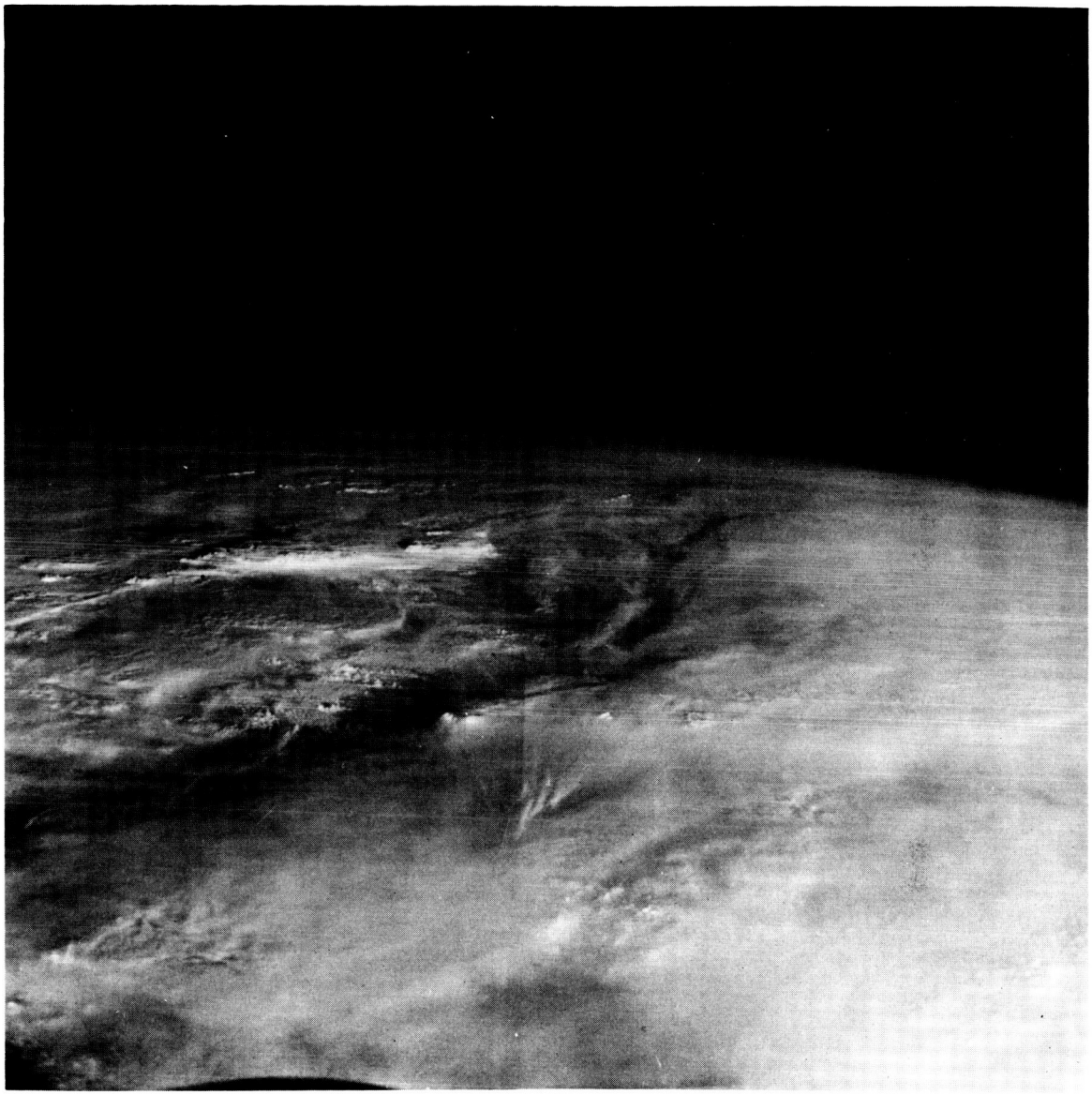

Figure 17. - Cirrus shadows on lower cloud layers over the North Atlantic Ocean; photographed by Gemini VI crewmembers at 10: 38 G. m. t., December 16, 1965.

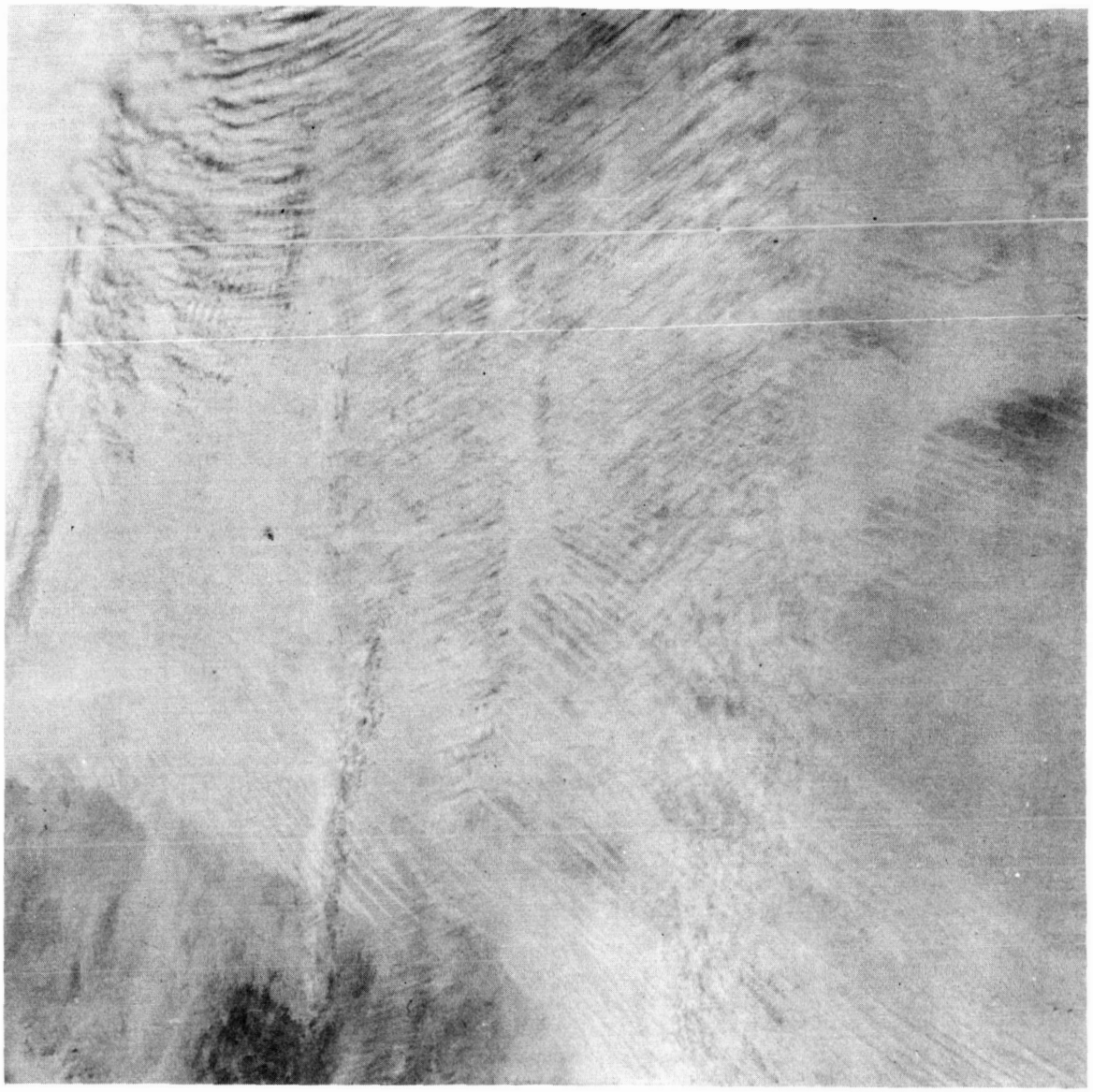

Figure 18. - Seif dunes in the northwestern Sudan, with a banded cloud structure above (one of several views of dune formations taken on the Gemini missions); photographed by the Gemini VII crewmembers at 12: 02 G. m. t., December 11, 1965.

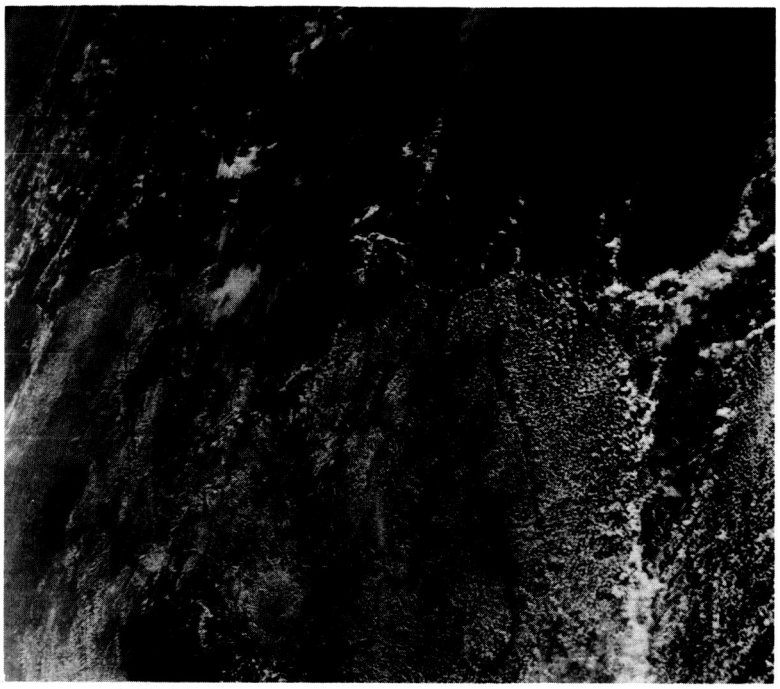

Figure 19.- Convective cloud patterns over northern South America.

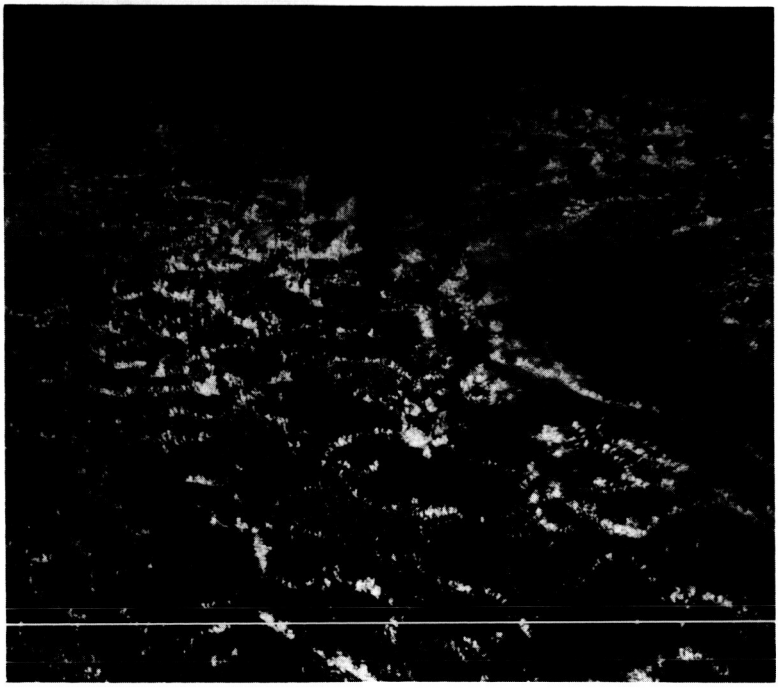

Figure 20.- Open polygonal cloud cells, 3 to 6 miles in diameter, formed over the oceans.

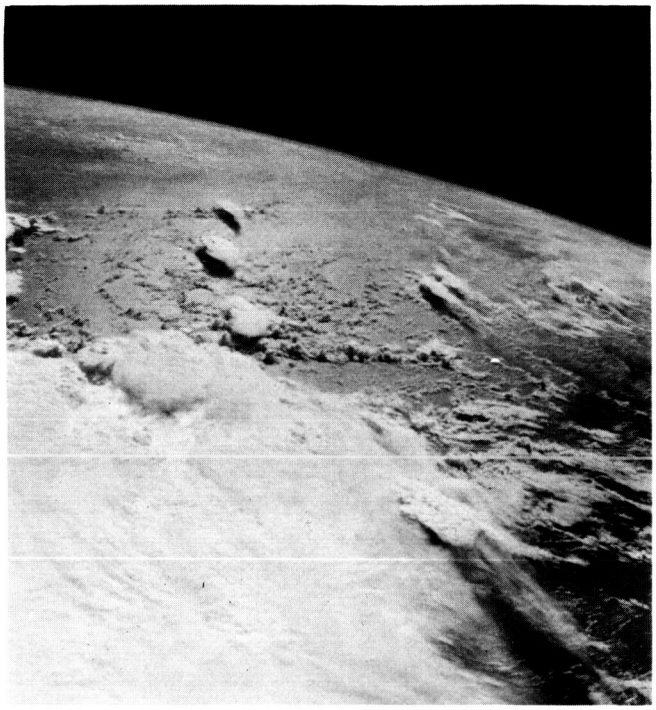

Figure 21.- Convective activity in a cloud mass over the Indian Ocean.

Figure 22.- The equatorial cloud condition over Sumatra and Malaya.

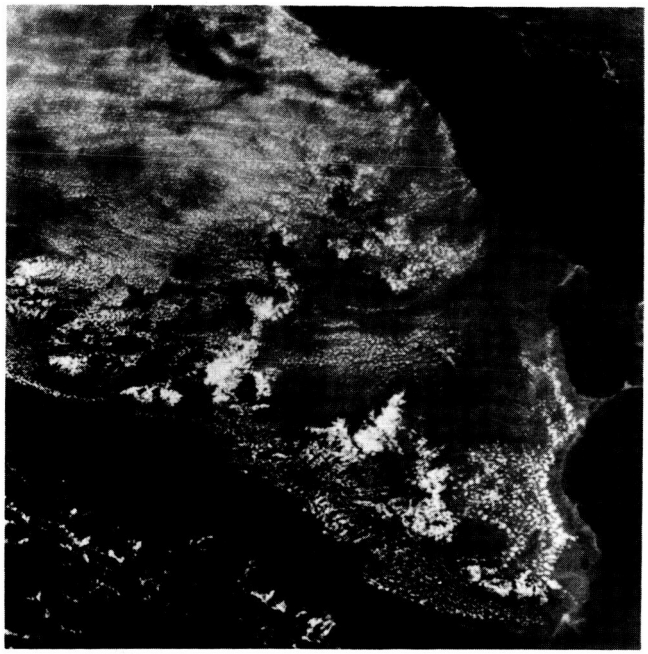

Figure 23.- Southern India, photographed on revolution 26 of the Gemini XI mission; the Maurer camera and 80-mm focal-length lens were used.

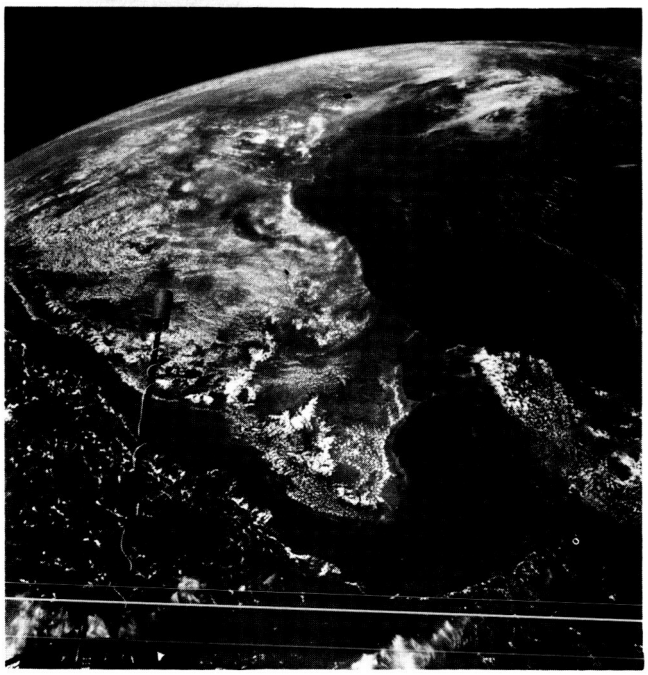

Figure 24.- Southern India and Ceylon, photographed on revolution 26 of the Gemini XI mission; the Hasselblad camera and the 38-mm wide-angle lens were used.

Figure 25.- A montage of pictures, televised from ESSA I, of southern India and Ceylon (photographed at 08:14 G.m.t., September 14, 1966); the coastline and the latitude-longitude grid are shown as white dots and lines.

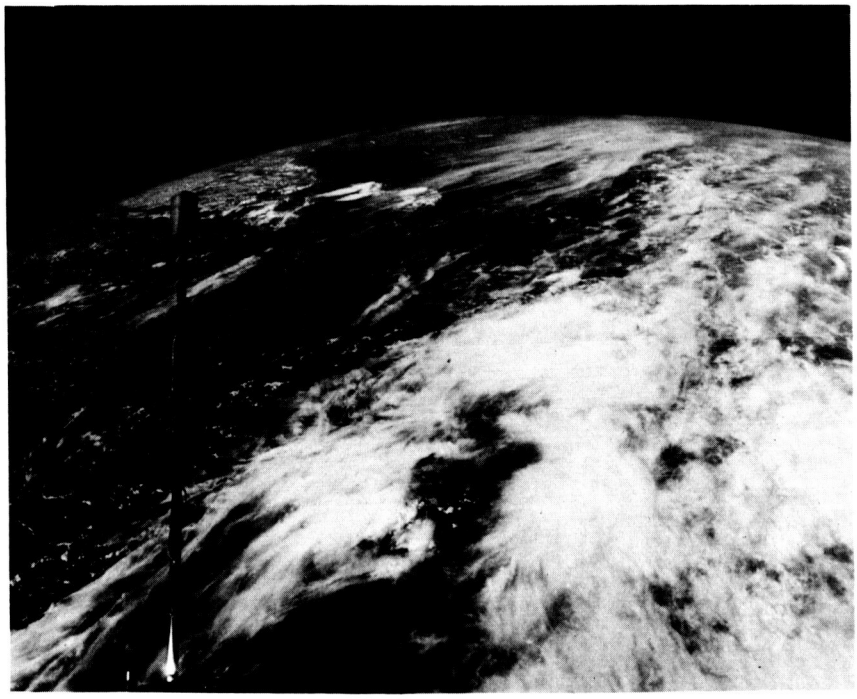

Figure 26.- Southern India and Ceylon, at the upper left, photographed on revolution 27 of the Gemini XI mission with the 80-mm lens and the Maurer camera.

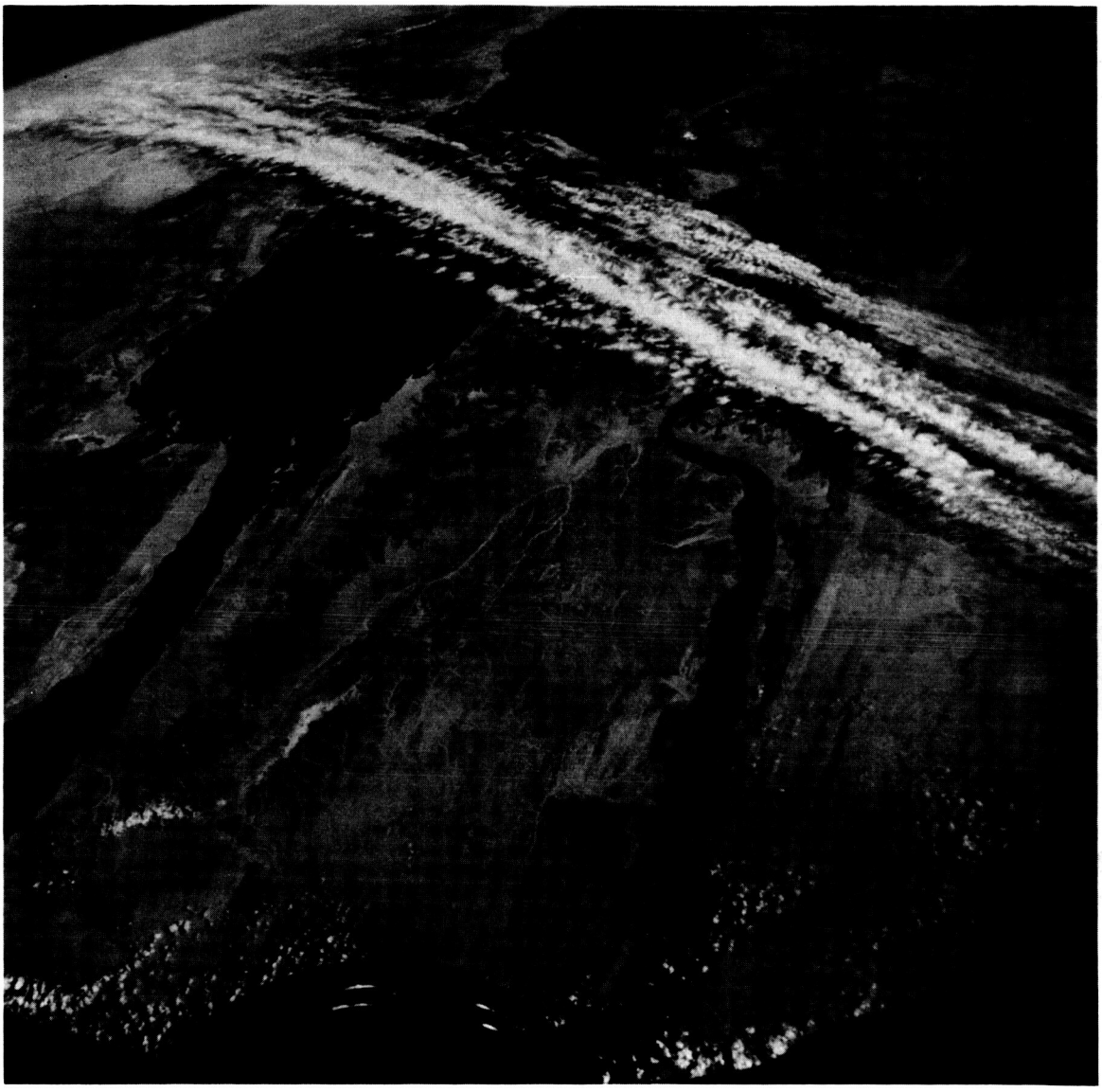

Figure 27. - A band of cirrus clouds showing strong upper winds above the Red Sea region (spacecraft was pointing down with the southeast toward the top of the page); the photograph was taken at 61:18 g.e.t., November 14, 1966, on the Gemini XII mission.

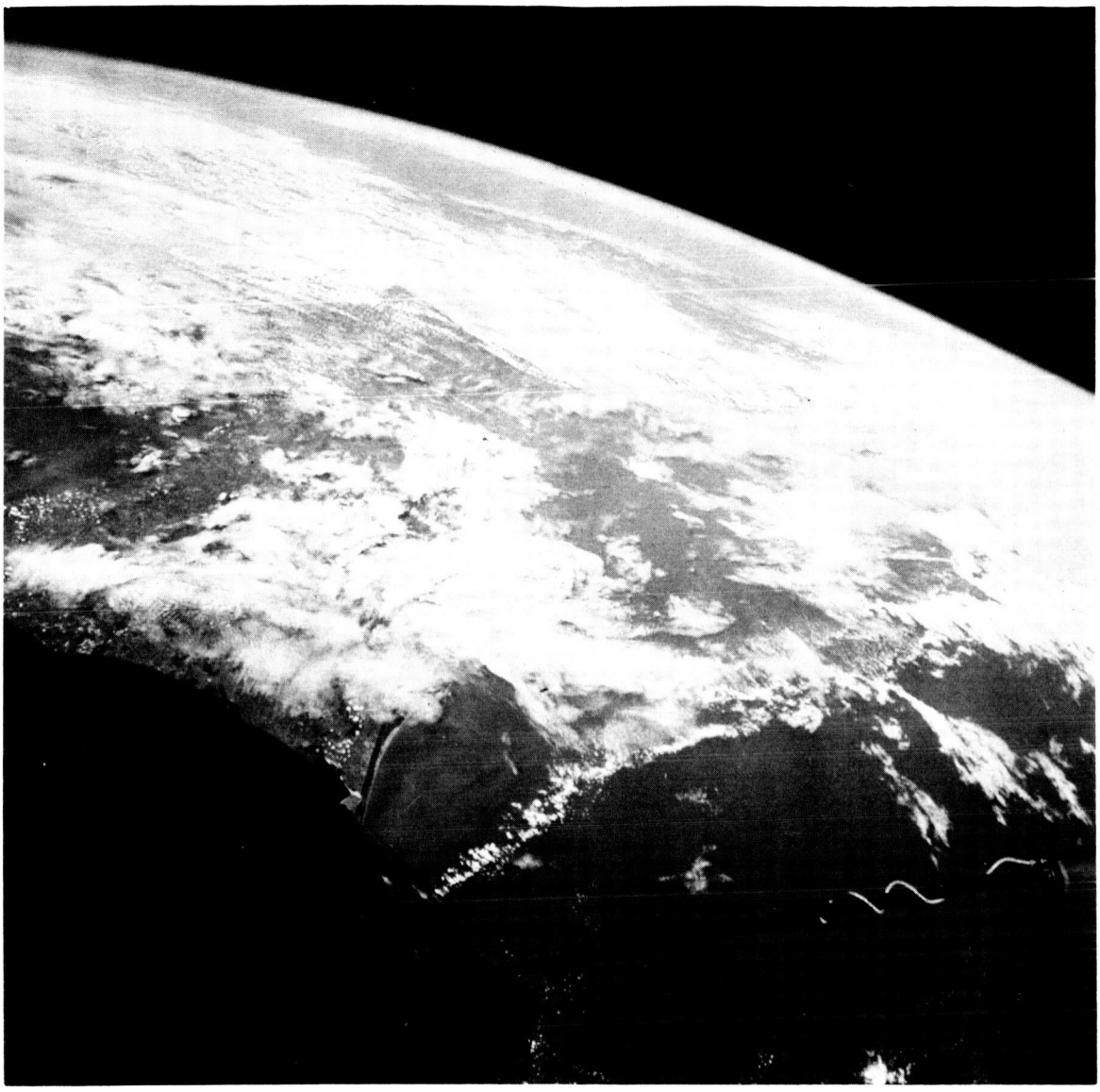

Figure 28. - A narrow band of cirrus clouds is shown above lower frontal clouds over the southeastern United States and the adjacent portion of the Atlantic Ocean (spacecraft was pointing down toward the north with Florida in the foreground); the photograph was taken at 19:15 g. e. t., November 12, 1966, on the Gemini XII mission.

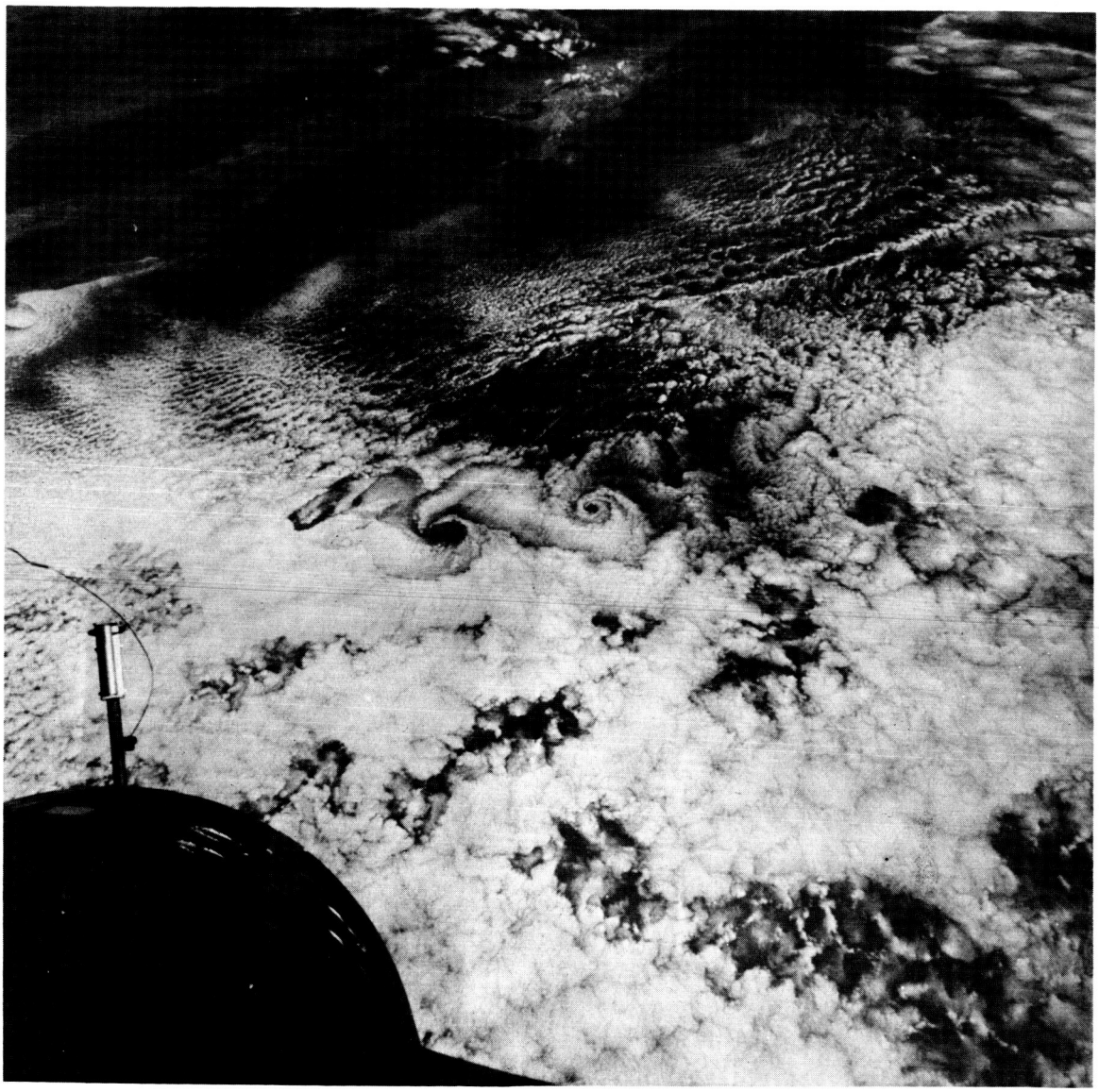

Figure 29. - Vortexes and cellular cloud patterns in stratocumulus clouds near Guadalupe Island (spacecraft was pointing toward Baja California, toward the east); the photograph was taken at 46:13 g. e. t., November 13, 1966, on the Gemini XII mission.

Figure 30. - Sunglint from the ocean surrounding the southern part of Florida (right) and the nearby Bahama Islands (foreground) (spacecraft was pointing south with Cuba in the background); the photograph was taken at 22: 32 g. e. t., November 11, 1966, on the Gemini XII mission.

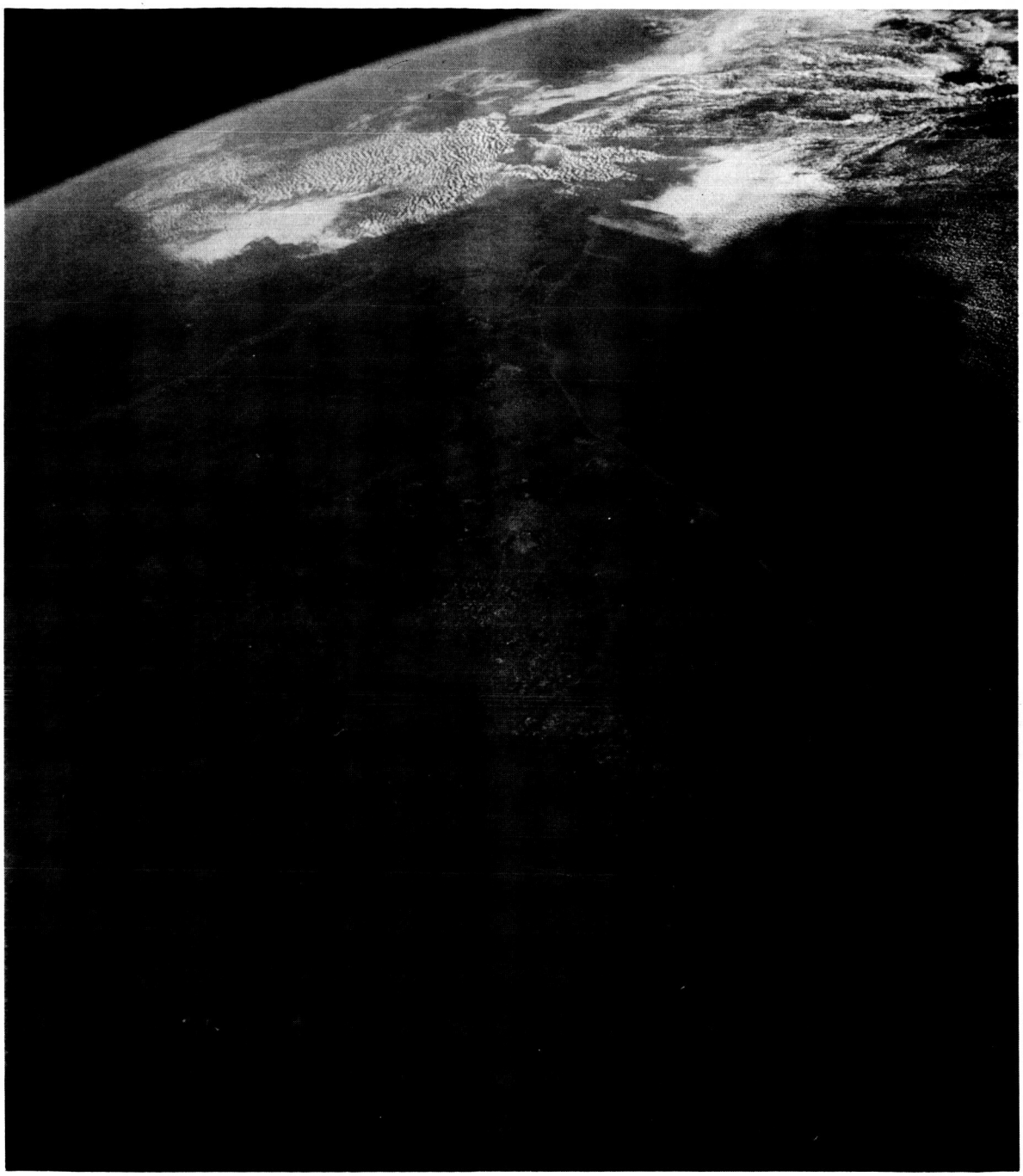

Figure 31. - A view of the Texas-Louisiana area looking east; plumes of smoke extend from the Louisiana coast far out over the Gulf of Mexico; the westernmost plume is very narrow and seems to have caused increased cumulus cloud development where it intersects the cloud region.

Figure 32. - A view looking east of the Gulf of Oman, windblown dust from Iran (left) extends approximately 100 miles offshore.

EXPERIMENT S007

CLOUD-TOP SPECTROMETRY

By F. Saiedy,* D. Q. Wark,** and W. A. Morgan**

INTRODUCTION

Meteorologists and weather forecasters have collected cloud pictures by the use of Tiros weather satellites that revealed the geographic distribution of cloudiness and facilitated qualitative judgment of cloud types (cloud types are classified according to altitudes). Meteorologists are interested in cloud altitudes because altitudes are indicative of the dynamic and thermodynamic state of the atmosphere upon which weather forecasts are based. In 1961, it was suggested (ref. 1) that the absorption by the 2.0-micron carbon dioxide band in sunlight reflected from a cloud be used for the determination of cloud altitude. The same year, it was noted (ref. 2) that the carbon dioxide band is on the wing of the water band (1.87 microns). The accuracy of such a determination would be compromised by variations in the amount of atmospheric water vapor. The use of the oxygen A band (7600 angstroms) measurements was recommended because such determinations would not be affected by water vapor. Experiment S007 was scheduled for the Gemini V and VIII missions. However, early termination of the Gemini VIII mission prevented execution of the experiment on that mission.

METHOD

The method that was used in Experiment S007 involved a comparison of cloud radiance at a specified wavelength inside the band with the radiance of the cloud in an atmospheric window outside the band. This ratio was indicative of the absorption or transmission of oxygen in the atmosphere above the cloud top. Because oxygen is mixed uniformly in air, oxygen transmission is a function of the pressure altitude of the cloud and the atmospheric path traversed by light from the sun to the cloud top and,

*The University of Maryland, College Park, Maryland.
**Environmental Science Service Administration, Washington, D.C.

after reflection, from the cloud top to the measuring instrument (fig. 1). A mathematical representation of the process is given in the following equation.

$$\tau = f[\, p, (\sec z + \sec \alpha)\,]$$

where τ = oxygen transmission, percent

p = pressure altitude, millibars

z = zenith angle of the sun, degrees

α = viewing angle, degrees

The instrument that was used on the Gemini V mission was designed to test the feasibility of measurement of cloud altitude by this method. The wavelength chosen inside the band was 7631 angstroms for low clouds and was 7607 angstroms for high clouds.

INSTRUMENT AND FILM CALIBRATION

A cross section of the spectrograph is shown in figure 2. The instrument was a small hand-held spectrograph that consisted of a 3.2- by 3.2-centimeter replica grating that had 1200 lines per millimeter blazed for 7500 angstroms in the first-order spectrum. A filter (cut-off at 6700 angstroms) was used to eliminate higher order spectra. The entrance slit was 6.0 millimeters long and 0.1 millimeter wide; these dimensions corresponded to a resolution of 5 angstroms.

The spectrum from 7500 to 7800 angstroms, which included the oxygen band, was recorded on high-speed infrared film that was carried in a camera that was equipped with a focal-plane shutter. Also, the instrument was used to photograph the cloud on the upper part of the film frame by the use of another lens. The complete spectrograph is shown in figure 3. The capability of the spectrograph is shown in figure 4, which represents a densitometer trace of a photographed spectrum. The oxygen doublets are 5 angstroms apart and barely are resolved. The density variation of the flight film was calibrated carefully in terms of variation in relative intensity by the use of a special method (ref. 3).

OBSERVATIONS FROM THE GEMINI V MISSION

One of the primary objectives of Experiment S007 was the observation of a cloud from the spacecraft coincident with observation of the same cloud from aircraft. Consequently, a plan for the reporting of cloud height by the crewmembers of civilian and military aircraft was initiated. The geographic regions were restricted by operational requirements to the southern United States, the eastern Pacific Ocean, the western Atlantic Ocean, and the Guam-Philippines region. An around-the-clock weather watch was established by a special meteorological staff on the day before the Gemini V launch.

The geographic regions that both coincided with projected spacecraft orbits and coincided with promising cloud covers were selected, and the information was conveyed to the Gemini mission control staff. When the selected regions were introduced into the Gemini V mission plan, civilian and military aircraft were notified of the place and time of observation. The U. S. Weather Bureau Research Flight Facility plane stationed in Miami, Florida, was placed on an alert status for use in cloud observation in the Florida vicinity.

Over the prescribed regions, the crewman pointed the spacecraft down, aimed the spectrograph through the viewfinder at the selected clouds, and operated the instrument. Then the crewman recorded the time of observation (to the nearest second), the spacecraft pitch and yaw angles, and a description of the cloud. The selective capability of the crewmember was dependent upon his background in meteorology. Knowledge of cloud types, derived from aviation training, resulted in the efficiency of this experiment compared with the same experiment performed on board an unmanned satellite. The cooperation of the various organizations in the measurement of cloud height from aircraft was good; but because of the vast area surveyed, only a few of the aircraft observations were in near coincidence. The only coincident observation obtained was over Florida where the U. S. Weather Bureau Research Flight Facility plane was vectored to the region of the observation that was being made by the Gemini V crewman.

During the Gemini V mission, 26 spectrographic observations were obtained on various cloud types; some observations were made for a low cloud over the west coast of Baja California, some observations were made for a fairly high cloud in a tropical storm in the eastern Pacific Ocean, and some observations were made on tropical storm Doreen. The instrument was operated correctly by the Gemini V crewman, and all pictures were aimed and exposed correctly.

RESULTS

An example of the types of spectrum and photograph involved in this experiment is shown in figure 5. The figure represents a cloud in the intertropical convergence zone. Densitometer traces of the spectra of three types of clouds (high, medium, and low) are shown in figure 6. It was apparent qualitatively that radiation transmission in the oxygen band for a high cloud was much greater than that for a low cloud. The results proved the feasibility of the cloud-altitude measurements from a spacecraft by this method.

Some of the experiment observations are summarized in table I. To obtain the pressure altitude, the oxygen transmission measured from the Gemini V spacecraft is compared with the calculated oxygen transmission from another experiment (ref. 4). The values of pressure altitude that were calculated and are presented in table I did not include the correction necessitated by the multiscattering of radiation inside the clouds before the radiation was reflected to the spacecraft. Multiscattering inside the clouds causes altitude measurements that are lower than actual. This problem has been discussed elsewhere (ref. 3). The magnitude of necessary correction mainly depends on the thickness of the cloud. Calculations done on this problem showed that the thickness of the cloud can be determined with an accuracy that is adequate for correction of the cloud-top altitudes from measurements of the cloud brightness. The

dependence of the cloud brightness on cloud thickness, zenith angle of the sun, and viewing angle is shown in figure 7. An observation of a white card in sunlight was obtained during the Gemini V mission. The angle between the card and the rays of the sun was not recorded; thus, an absolute inflight calibration of the spectrograph was not possible. Regarding the relative brightness, an estimate of the cloud thickness (table II) could not be made. To some extent, these results supported the calculation of the relationship between brightness and thickness.

DISCUSSION

Aircraft coverage should be more complete, and two or three aircraft should be available for vectoring into the selected cloud cover. The observation of the white card that is used to calibrate the spectrograph while in orbit must be planned carefully for cloud brightness measurement. With the results of such measurements, the possibility for measurement of cloud thickness can be tested. Cloud thickness is a valuable parameter by itself, in addition to its importance for cloud-top measurements. The staff of the National Environmental Satellite Center, working on the basis of the experience gained from the Gemini V mission, has proven the feasibility of and has determined the system design requirements for a complex second-generation weather-satellite instrument.

REFERENCES

1. Hanel, R. A.: Determination of Cloud Altitude From a Satellite. J. Geophys. Res., vol. 66, Apr. 1961, p. 1300.

2. Yamamoto, G. A.; and Wark, D. Q.: Discussion of the Letter by R. A. Hanel, Determination of Cloud Altitude From a Satellite. J. Geophys. Res., vol. 66, Oct. 1961, p. 3596.

3. Saiedy, F.; Hilleary, D. T.; and Morgan, W. A.: Cloud-Top Altitude Measurements From Satellites. Applied Optics, vol. 4, Apr. 1965, pp. 495-500.

4. Wark, D. Q.; and Mercer, D. M.: Absorption in the Atmosphere by the Oxygen "A" Band. Applied Optics, vol. 4, July 1965, pp. 839-845.

TABLE I. - RESULTS FROM OBSERVATIONS OF CLOUD HEIGHT

Date in August 1965	Ground elapsed time, (g. e. t.), hr: min: sec	Cloud identification and location	Oxygen transmission, percent		Calculated mean pressure altitude, mb	Actual pressure altitude, mb
			At 7631 Å	At 7607 Å		
23	21: 33: 05	Tropical storm, eastern Pacific Ocean	--	0. 48	290	--
24	21: 20: 08	Tropical storm Doreen, eastern Pacific Ocean	--	0. 51	320	350 to 220
25	19: 44: 02	I. T. C., eastern Pacific Ocean	--	0. 39	440	--
25	16: 37: 00	Cumulonimbus, Florida	--	0. 45	370	323
27	17: 43: 00	Stratus, Baja California	0. 32	--	980	960

TABLE II. - APPROXIMATE RESULTS ON CLOUD THICKNESS

Cloud identification	Solar zenith angle, deg	Relative brightness, percent	Estimated thickness, m
Tropical storm	29	$\simeq 0.85$	>3000
Tropical storm Doreen	13	$\simeq 0.85$	>3000
Cumulonimbus	22	0.66	1000
I. T. C.	16	0.43	500
Stratus	34	0.47	600

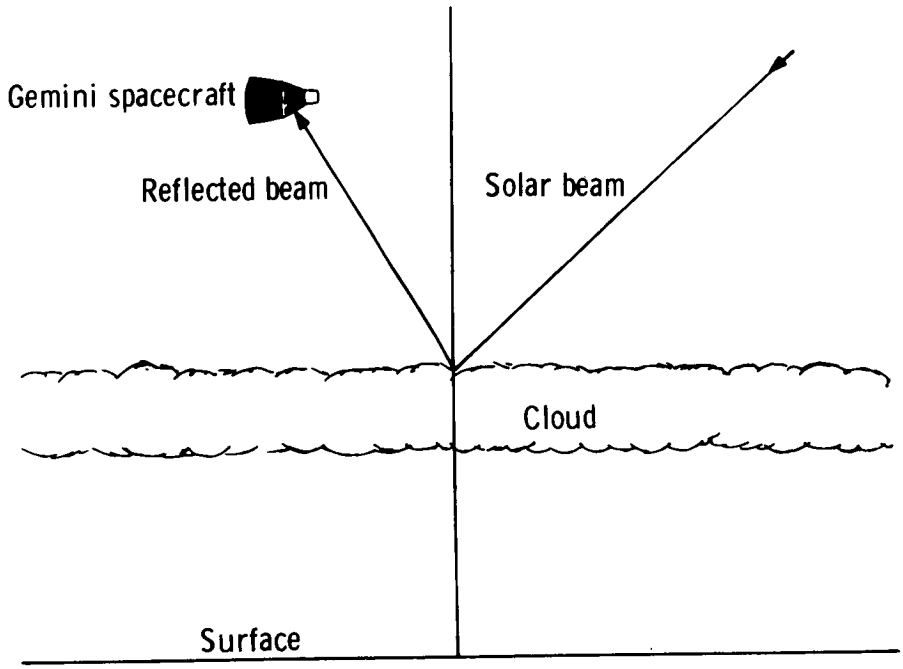

Figure 1. - A representation of the path of the beam.

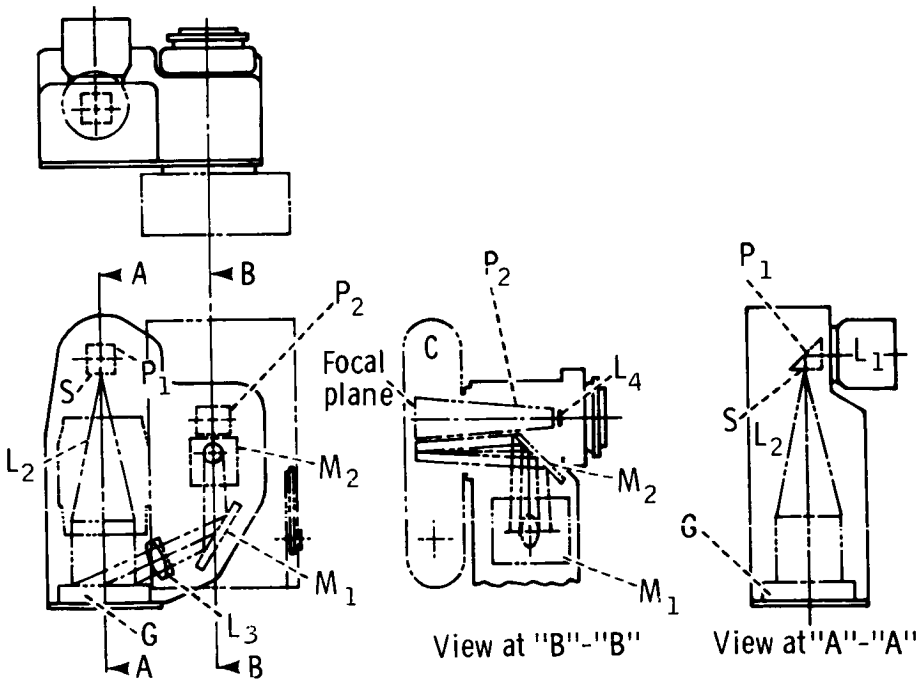

Figure 2. - An optical layout of the spectrograph.

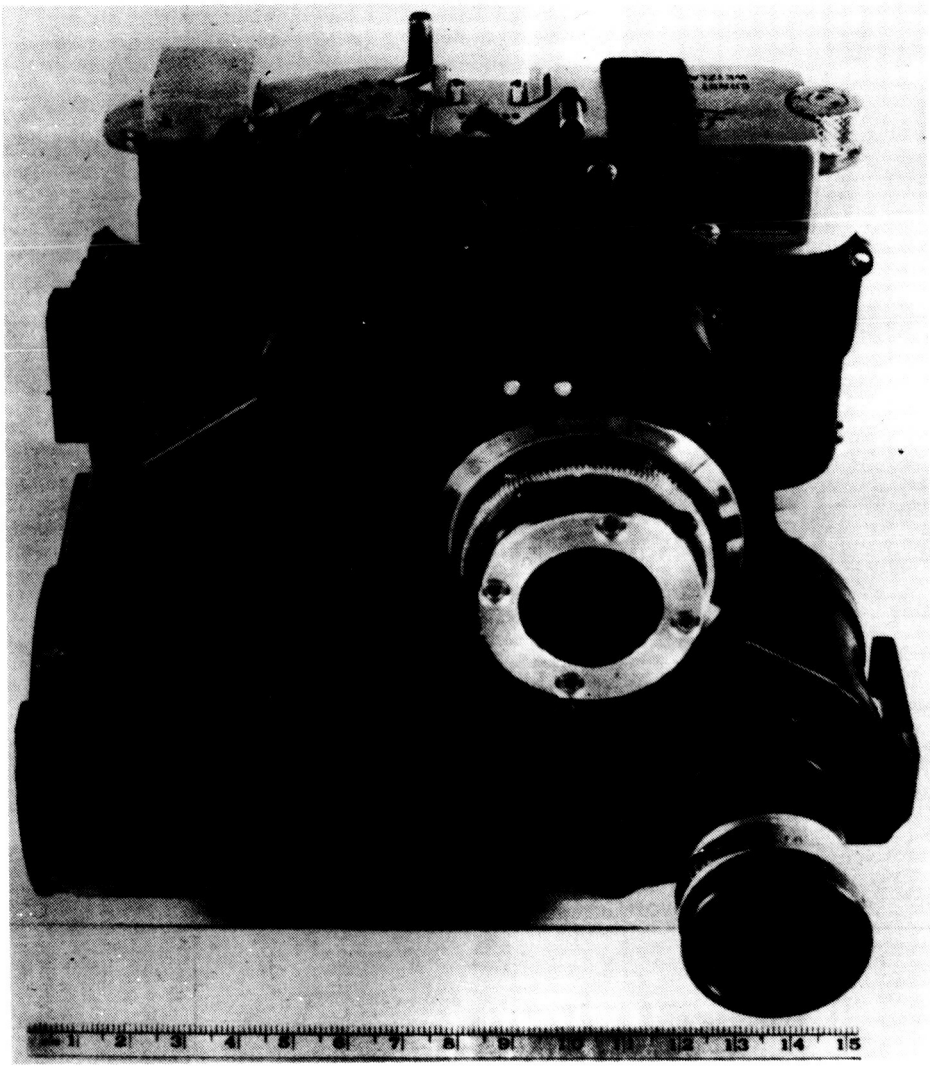

Figure 3. - A spectrograph with two objective lenses.

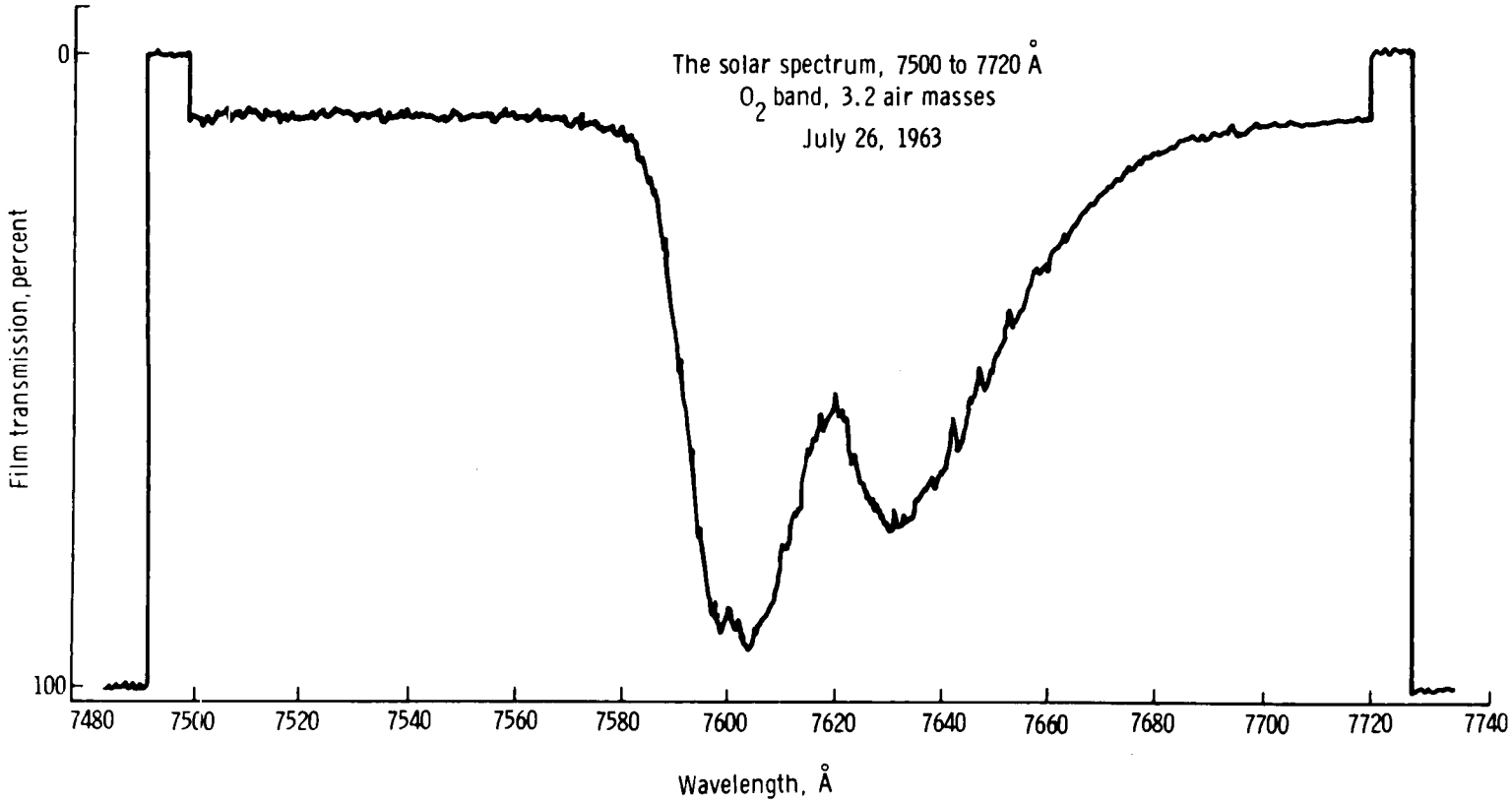

Figure 4. - A microdensitometer trace of the spectrum.

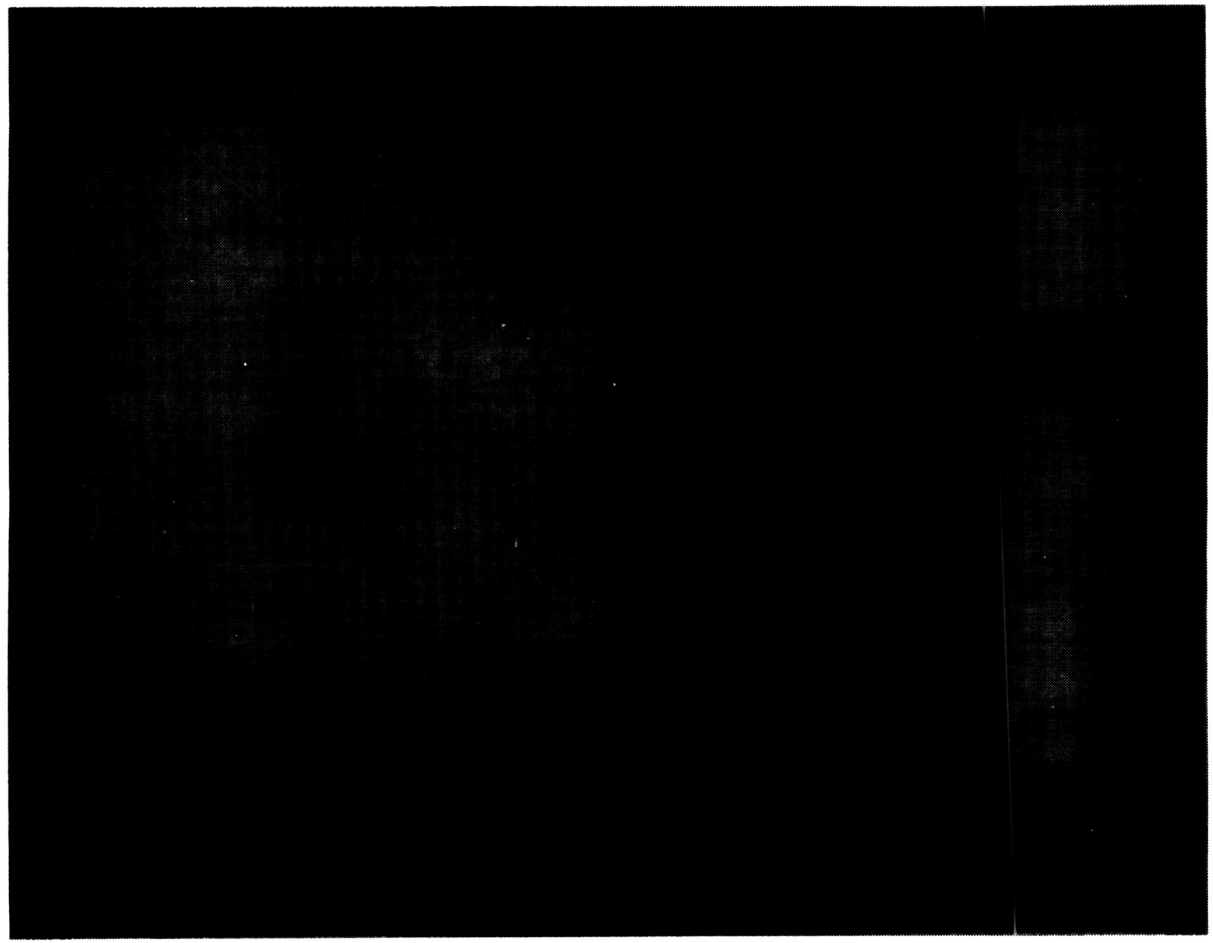

Figure 5. - A photograph (left) and a spectrogram (right).

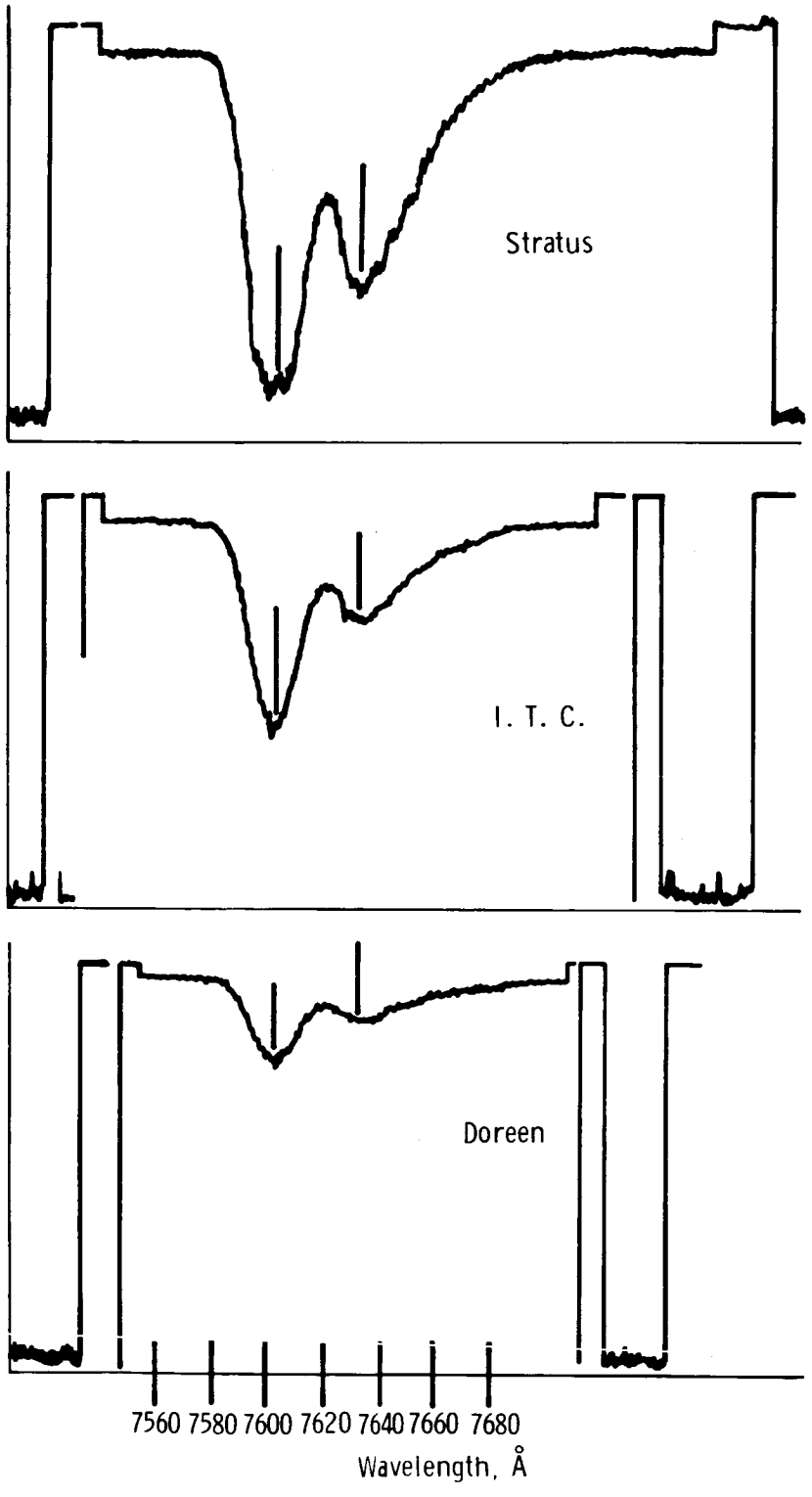

Figure 6. - Microdensitometer traces of three spectra obtained on the Gemini V mission; the dashed vertical lines are at 7607 and 7631 angstroms.

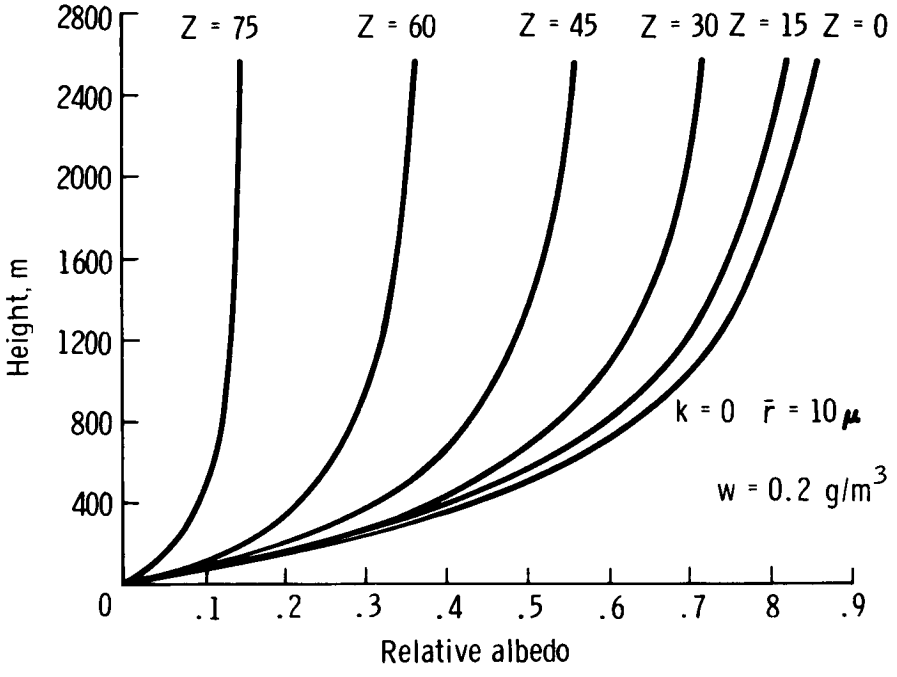

Figure 7. - The variation of the relative brightness of the cloud-to-cloud thickness and the solar zenith angle.

EXPERIMENT S051
DAYTIME SODIUM CLOUD

By Jacques-Emile Blamont*

OBJECTIVE

The objective of Experiment S051, which was performed on the Gemini XII mission, was to measure the daytime wind velocity of the high atmosphere of the earth as a function of altitude (30 to 80 nautical miles). The measurements were to be obtained from the deformations of a rocket-made vertical sodium cloud. Rockets were to be launched in front of the spacecraft, and the rockets were to eject sodium vapor continuously from an altitude of approximately 35 to 100 nautical miles during ascent and descent. The vapor should have been visible from the spacecraft as a faint yellow-white cloud above the horizon.

EQUIPMENT

Sodium clouds were to be photographed sequentially by the use of the 70-millimeter general-purpose camera that was used on other experiments. At least 20 frames from the Experiment S011 film pack were required in order to ensure adequate photographic coverage. An interference filter, the wavelength response of which was dependent upon incidence angle, was mounted on the camera. This filter passed sodium-yellow light to a camera cone angle of 10°. For larger entrance angles, the wavelength response was displaced in the spectrum toward green. It was essential that the camera be aimed precisely (within a tolerance of 1°) in the direction of the cloud.

PROCEDURES

Sodium was released from a Centaur rocket that was launched from Hammaguir, Algeria. This launch facility was under the responsibility of the (Centre National de la Recherche Scientifique) CNRS-French Space Agency. The Centaur was a two-stage solid-propellant rocket that ejected sodium continuously during flight from an altitude of 70 kilometers to an apogee of 180 kilometers and down to the ground. Two rockets were launched in the southeast direction from Hammaguir; there was a delay of approximately 1.5 hours between launches. Firing conditions were such that the rockets

*Centre National de la Recherche Scientifique, Paris, France.

descended from apogee when the Gemini XII spacecraft was at a distance of 1000 kilometers. Based on an assumed nominal spacecraft altitude of 161 nautical miles, the position of the cloud relative to the horizon could be determined.

From airglow pictures (Experiment S011), it was apparent that the horizon line did not correspond to the real geometrical limit of the solid earth, but corresponded to the sunlit atmosphere up to an altitude of 30 kilometers. This distance was used as the horizon line, and the horizon angle was considered to be 16.50° below the spacecraft horizontal plane. The evolution of the sodium-cloud sightings, as predicted by observation by the crewmembers, is shown in figure 1. When the cloud was below the horizon, it was not visible because of poor contrast against the sunlit background. The background might have been 250 times more intense than the cloud. Therefore, this experiment could have succeeded only if the cloud had been above the horizon.

From a study of figure 1, it is apparent that wind measurement can be obtained from slant distances between 1000 and 800 kilometers in the altitudes of interest. This was the basic objective of the experiment. When the distance between the spacecraft and the cloud was less than 800 kilometers, the lowest part of the cloud began to sink below the horizon. The possibility of acquisition of useful pictures of the cloud on top of the background of the earth was another objective of Experiment S051. This necessitated acquisition of a series of exposures during the time the spacecraft went from a cloud-distance of 800 kilometers to a cloud-distance of 500 kilometers. The average wind velocity measured was of the order of magnitude of 50 to 100 meters per second. To measure this wind velocity, the motion of the cloud had to be a few times larger than the film resolution. This corresponded to a difference of approximately 30 seconds between successive exposures at a distance of 100 kilometers. Two cloud pictures taken approximately 60 kilometers apart would have resulted in tridimensional cloud shapes by stereogrammetric recombination. From a second identical pair of pictures taken some time later, the tridimensional configuration of the cloud could have been obtained again. A comparison of the condition of the cloud at different times would have facilitated determination of the wind velocity in the atmosphere at all relevant altitudes, with the assumption that only horizontal winds existed. A series of successive photographic pairs was necessary to reduce wind-velocity errors to an acceptable level.

RESULTS

The Centaur was launched from the French site at 62:41:48 g.e.t. Visual acquisition was not established by the crewmen; however, the spacecraft was pointed in the direction of the anticipated location of the sodium cloud, and 13 exposures were taken. Another sodium rocket was launched from the site near Hammaguir, Algeria, at 64:16:49 g.e.t. The crewmen again did not visualize the sodium cloud. Thirteen additional photographs were taken of the geographic regions specified during premission planning. The launch crewmen in Algeria confirmed the successful launch, activation, and observation of sodium clouds from the ground during both of the spacecraft passes. Evaluation of the film was indicative that all 26 photographs were overexposed during the photographic sequences. The overexposures were caused by a camera shutter locked in the open position. Therefore, useful photographic data were not obtained for analysis.

The locked-open shutter was in the red-lens assembly. The probable cause for this open-shutter condition was (1) the use of forces that exceeded design limits when the red-lens assembly was mounted on the camera body and (2) the misalinement of the shutter-actuating coupling caused by partial camera-shutter cock. The coupling misalinement could have caused dowel-pin deformation, with the resultant chain of misalinements and possible shutter override, which would have prevented the return movement of the shutter-closure mechanism.

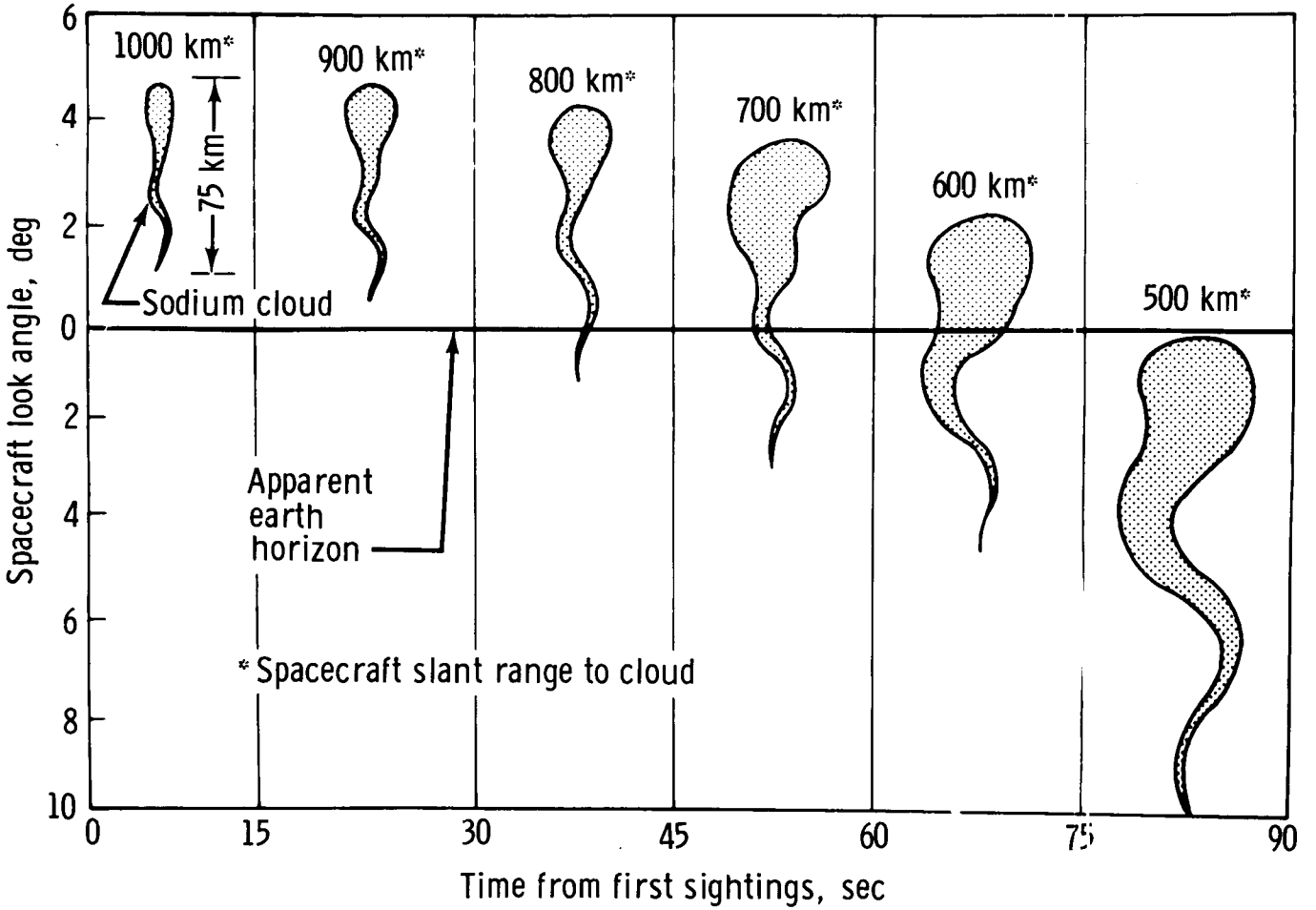

Figure 1. - Predicted visual characteristics of the sodium cloud.

EXPERIMENT D015

NIGHT IMAGE INTENSIFICATION

By Thomas J. Shopple,* George F. Eck,* and Albert R. Prince*

INTRODUCTION

The results of Experiment D015 were indicative that the capability of the crewmembers to discriminate objects on the ground in darkness can be increased through use of night image-intensification equipment. The performance of the experimental equipment established a base line for the evaluation and design of image-intensification equipment for use in future manned space flight. The experiment was flown on the Gemini VIII and XI missions; early termination of the Gemini VIII mission prevented experiment completion. The objective of Experiment D015 was a performance test of a night image-intensification system for use as a visual aid by the crewmen.

EQUIPMENT

The equipment package consisted of five basic units (fig. 1); these components are listed as follows.

1. Image-intensification camera
2. Camera control unit
3. Viewing monitor
4. Recording monitor and photographic recorder
5. Monitor electronics and equipment control unit

The camera viewed a scene; then, the image was focused on a sensor that converted the optical image into an electronic video signal that was conducted by cable to the monitors. The camera line of sight was parallel to the longitudinal axis of the spacecraft and to the line of sight of each crewmember when he looked through the spacecraft windows. The viewing monitor and recording monitor received the video signal from the camera, and reproduced and displayed the scene that was viewed on cathode-ray tube read-outs. The recording-monitor display was photographed by a photographic camera

*U. S. Naval Air Development Center, Johnsville, Warminster, Pennsylvania.

that was actuated by means of a manual pushbutton switch located on the viewing monitor. Then, a permanent photographic record was obtained for postflight analysis. The locations of the equipment in the spacecraft are shown in figure 2. A description of each unit is given as follows.

Image-Intensification Cameras

The optical sensor of the camera viewed a scene and converted the optical image into an electrical video signal that was conducted by cable to the monitors. The camera system contained an objective lens; a light-control and protective-shutter assembly; an image-intensifier assembly; an image-orthicon tube; a deflection, focus, and alinement-coil assembly; an amplifier and regulator assembly; automatic beam-control circuitry; and a video processor and regulator assembly.

The light-control and protective-shutter assembly regulated the amount of light that struck the photocathode of the image intensifier. This was accomplished by movement of a tape (of variable density) that provided a constant average brightness to the photocathode as the light level changed. Also, this assembly placed a shutter into the light path when light levels exceeded 10^4 foot-candles to protect the image-intensifier tube.

The image-intensifier assembly was a 40-millimeter electrostatic tube with an S-20 photocathode and a P-20 phosphor. The intensifier was operated with a nominal 20-kilovolt differential between the photocathode and the phosphor. Voltage was supplied by an oscillator and voltage-multiplier assembly that transformed 20 V dc to 20 000 V dc. The phosphor of the intensifier was operated at -600 volts, and the intensifier photocathode was operated at approximately -20 000 volts.

The image-orthicon tube was designed to withstand abnormal environmental conditions. This tube (General Electric type Z7852), which was magnetically focused and deflected, had a fiber-optic faceplate and a thin-film magnesium oxide target.

The deflection-coil assembly consisted of a vertical- and horizontal-deflection, alinement, and focus coils, and wiring that provided power and signal continuity from the front to the rear of the camera head. The amplifier and regulator assembly included a high-voltage power supply, the image-orthicon grid-voltage regulators, a focus-current regulator, and the preamplifier subassembly.

The purpose of the automatic beam-control circuit was to increase the light-level dynamic range of the camera by automatic adjustment of the beam current to the proper level for maintenance of an optimum target current to beam current ratio. The beam current was adjusted continuously to maximize the signal-to-noise ratio and to increase the dynamic operating range of the camera.

The video-processor circuits provided constant-amplitude, balanced, noncomposite video both to the viewing monitor and to the recording monitor and also furnished control signals to the automatic light-control assembly. The regulator circuits provided constant current to the vertical- and horizontal-alinement coils and regulated direct current voltages for the automatic beam-control circuits.

The camera-control unit controlled the operation of the television camera by supplying power, timing and gating signals, horizontal- and vertical-sweep drives, and blanking and automatic light-control signals. Also, this unit supplied power, synchronization, and drive signals for both monitors.

The power-supply assembly was a high-efficiency, variable-pulsewidth, regulated converter that had constant input power and converted a 26 ± 4 V dc input into the various direct current levels that were required for operation of the system.

The synchronization-generator assembly supplied all the synchronization pulses that were necessary for system operation. The assembly was composed of a crystal-controlled oscillator, countdown stages, logic gates, multivibrators, flip-flops, level translators, and output amplifiers.

A fail-safe circuit was located on the vertical-deflection assembly and supplied target blanking and bias voltages to the image-orthicon tube. The fail-safe circuit cut off the image-orthicon target to prevent damage to the tube in the event of loss of either horizontal or vertical drive.

The program assembly supplied control signals for the automatic light-control unit. Signal-conditioning circuits, that were located on the programer, processed the image-orthicon target blanking, video output level, and camera shutter-command signals before those signals were processed by the spacecraft telemetry system.

Viewing Monitor

The viewing monitor received the video signal and reproduced a display of the scene that was viewed by the camera. This unit contained a cathode-ray tube and yoke assembly, a video amplifier, a horizontal-deflection circuit, a sweep-failure-protection circuit, a 12-kilovolt high-voltage power supply, and a multiplier and regulator assembly. The square viewing screen (3.5 by 3.5 inches) had a maximum screen brightness of 20 foot-lamberts. The unit contained a monitor-brightness control and a manually operated pushbutton switch for control of the photographic-camera recorder.

Vertical deflection for the viewing monitor was supplied by a vertical-deflection assembly that was located in the monitor-electronics and equipment-control unit. When the viewing monitor was observed at a distance of 12.9 inches, the magnification power of the presentation was 1:1 if the spacecraft was at an altitude of 160 nautical miles above the viewing region.

Recording Monitor and Photographic Recorder

The recording monitor received the video signal, reproduced and displayed the image that was received by the camera, and recorded the monitor display by the use of the photographic recorder. The unit contained a video amplifier, vertical- and horizontal-deflection amplifiers, a photographic drive logic assembly, data lamps, lamp-driver assembly, high-voltage converter and multipliers, and a photographic-recorder assembly. The photographic-recorder optics included mirrors for folding the optical path to the recorder lens. The film magazine contained 180 feet of thin-base film. The operational rate of the photographic recorder was 3 frames per second.

Monitor Electronics and Equipment Control

The monitor electronics and equipment-control unit contained a synchronization-drive assembly, sawtooth-generator assembly, vertical-deflection assembly, horizontal-deflection timing assembly, and a low-voltage power converter. The unit supplied operating power, vertical-deflection current, operating power and deflection-sawtooth generation for the recording monitor and the photographic recorder, and horizontal-deflection timing pulses to the viewing monitor.

PROCEDURES

Both crewmembers participated in Experiment D015. The crewmen operated the experiment equipment, maintained the proper spacecraft attitude, maneuvered the spacecraft when necessary to keep a scene in view, and recorded their observations vocally.

The experiment was actuated at approximately the end of revolution 34 and was performed during the nightside passes on revolutions 35 and 36. The experiment mission plan for this time period is shown in table I. The equipment was installed in the spacecraft so that the line of sight of the camera was parallel to the longitudinal axis of the spacecraft. During each observation, the spacecraft was oriented so that its longitudinal axis was approximately normal to the surface of the earth. The intensification camera viewed an earth scene that was displayed on the viewing monitor of the pilot and that was transmitted to the recording monitor. The command pilot viewed the same scene through the left-hand window of the spacecraft. Three operational modes were planned for observation by the crewmembers. These modes are described as follows.

Scan Mode

Proper function of the scan mode necessitated alinement of the longitudinal axis of the spacecraft normal to the surface of the earth as the spacecraft overflew the region that was to be observed. A photographic record was made of the features of interest; this was recorded as long as the feature remained within the field of view.

Track Mode

Correct operation of the track mode necessitated orientation of the spacecraft to an attitude from which acquisition of a specific feature (not necessarily on the ground track) was facilitated. After acquisition, a feature was tracked and recorded photographically until it was 20° past the nadir.

Search and Track Mode

During the use of the search and track mode, the spacecraft had to be oriented to facilitate the search for a specific feature on the ground track over which the spacecraft

would pass. After acquisition, the feature was tracked until it was 20° past the nadir; during that time a photographic record was made.

An oral report was made by both crewmembers. The command pilot viewed the scene directly through the left-hand window while the pilot observed the viewing monitor. Because there was a resolution loss in the photographic recording system compared with the viewing monitor, the photographs did not contain all the information that was observed by the pilot (on the viewing monitor). Verbal description was necessary to determine what the pilot inferred from the view that was observed. The evaluation of the results of the experiment was based on a comparison of the three records that were obtained for each observation.

RESULTS

Forty-two film sequences of the experiment were recorded; 9 minutes 8 seconds of available film time were used. Of the 42 film sequences taken, 13 sequences were of medium to heavy cloud formations, and 14 sequences were of open ocean regions. Some of the sequences were taken during daylight as the spacecraft passed over South America; however, most of the sequences were taken at night during a new-moon phase. The ambient earth-scene illumination was approximately 1×10^{-4} foot-candle during that lunar phase.

The daylight sequences, which were taken over South America, contained no useful information. These sequences were taken to ensure sufficient scene illumination for determination of the limiting resolution of the system and for evaluation of the maximum capability of the system. At the postflight debriefing, the crewmen reported that during the daylight sequences they were able to identify visually features (on the monitor) that they recognized as dry lakebeds. Unfortunately, the photographs were of regions that did not include these features; thus, system-performance correlation was not possible.

The content of the sequences filmed during the night observation part of this experiment is summarized in table II. Representative photographs of these observations are shown in figures 3 to 10. Because of the lack of suitable sites overflown during revolutions 35 and 36, the film sequences are predominantly of lights and clouds. The characteristic shape of Calcutta, India, is shown in figure 3(a); a map of the Calcutta region is shown in figure 3(b). Several coastlines were photographed and the results are shown in figures 4 and 5. Photographs of three different sections of coastline revealed a contrast between the images of land and ocean. These images ranged in quality from good to poor. Because the terrain of the region that was photographed was fairly regular, the contrast was sufficient only for delineation of the coastline. The most significant photograph that was obtained was of the Istmo dos Tigres (Angola) on the western coast of Africa. This photograph, shown in figure 6(a), was clearly identifiable when compared with the 1:1,000,000 scale map of the region (fig. 6(b)). The shape of this peninsula is that of a long, narrow strip, of approximately 7:1 length-to-width ratio, that extends from the mainland and is terminated by a large rounded region that has a length-to-width ratio of approximately 3:1.

Deviation from the experiment plan was necessary during the mission because heavy cloud cover was encountered over many parts of the ground track. A suitable presentation was obtained only when the spacecraft was pitched down a nominal 70° or more from the horizontal. As a result, the regions listed in the mission plan were observed, but no attempt was made to perform the tracking tasks for sites that were located at points off the ground track. Most observations and recordings were made in the scanning mode, and only those features that appeared prominent were tracked. Generally, tracking was accomplished by pitching the spacecraft downward. During night periods, the pilot was able to observe earth scenes, such as coastlines and peninsulas, on the television monitor. The same scenes were not visible to the command pilot. However, the window through which these observations were made by the command pilot was dirty. The pilot stated that the quality of the monitor presentation was superior to that of the film sequences of the same coastlines and peninsulas. This degradation had been observed during laboratory tests and was expected. The crewmembers were able to see the flashing light of the Gemini Agena target vehicle on the television monitor when they were not able to see it with an unaided eye.

The equipment functioned properly, except for the anomalies that are listed as follows.

1. During experiment activation, the field of view appeared tilted approximately 45° on the viewing monitor. Photographs from the recording monitor contained a similar misalinement, an indication that the anomaly originated in the intensification camera or mirror. The camera was mounted 20° off the Y-axis of the spacecraft. Provisions were made in the spacecraft for an upright display on the viewing monitor. The pilot corrected the display orientation by removal of the viewing monitor from its bracket, rotation of the monitor until the scene was corrected, and then stabilization of the unit. An analysis was performed to determine if a change had occurred that would have caused this tilt during the mission. Results of the analysis were indicative that no change in the equipment had occurred. Records of the inspection of the installation and alinement procedures were indicative that the camera was installed and alined properly before the mission. Because the camera was installed in the retrograde adapter section, which was jettisoned before entry, no postflight analysis could be performed on the flight hardware. The cause of the rotation was not established from the data that were available.

2. The field of view of the camera did not appear to be alined properly with the optical sight on the window of the command pilot. After installation, the camera was alined optically at the facility of the spacecraft contractor to within 0.5° of the spacecraft center line. The camera was removed from the spacecraft for shipment to the Kennedy Space Center (KSC). Tolerances on the camera mounting base and the spacecraft mounting fixture were sufficient to retain the desired alinement accuracy during camera removal and replacement. A comparison of test results by the contractor and by KSC personnel was indicative that the camera was reinstalled properly at KSC. The effect may have been related to the tilted field of view.

3. A bright region near the center of the viewing and recording displays persisted throughout the experiment. Adjustment of the beam control reduced the region, but the condition could not be eliminated entirely. A selected frame from the 3 frames per second, 1/30-second exposure, 16-millimeter film is illustrative of this condition (fig. 7). The bright region probably was caused by an ion spot developing in either the image-intensifier assembly or in the image-orthicon tube in the camera.

4. Several photographic sequences taken during Experiment S030 with the Experiment D015 equipment were not on the flight film. A failure analysis, conducted after the flight on the recording monitor and photographic recorder, resulted in proof that a failure had occurred in the cathode-ray tube during Experiment S030. After the cathode-ray tube failure, photographic data could not be recorded, and many of the Experiment S030 data were lost.

5. Stowage and handling of the viewing monitor within the cabin was performed without difficulty. However, stowage of the viewing monitor in the footwell was a cause of crewmember discomfort during the mission.

CONCLUSIONS

Geographic features on the surface of the earth were observed in starlight illumination of an intensity as low as 5×10^{-5} foot-candle. Airglow was very prominent under a new-moon condition and resulted in an apparent reduction in scene contrast, a washed-out presentation, and a reduced resolution. Airglow probably was the cause of the reduction in picture quality when the spacecraft was pitched down at angles less than a nominal 70° below the horizontal. Objects that were observed on the viewing monitor were tracked by the crewmembers; the monitor was used as a reference. Images of clouds were clearly visible in the photographs that were taken at night. This may have resulted from the high reflectivity of these features. The feasibility of mapping cloud patterns over large areas at night was indicated by the photographs of this sequence and by the comments of crewmembers. Light regions on the surface of the earth (such as cities) appeared as extremely bright spots on the monitors. Many of the light regions that were viewed over Africa were reported by the crewmembers as being fires (figs. 8 and 9). Lights under cloud cover were also readily distinguishable from the background. Earth horizon, airglow, and star fields are shown in figure 10.

Images of stars frequently were observed on the monitor by the crewmen. During revolution 41 (65:27:21 g. e. t.), the Gemini Agena target vehicle was sighted on the viewing monitor while it was in total darkness and approximately 15 miles from the spacecraft. The acquisition light was distinguished easily in the starfield background. The successful operation of the experiment equipment was indicative that delicate electronic components such as image-orthicon tubes can be designed, packaged, and installed to withstand the severe launch environment of space vehicles.

TABLE I. - FLIGHT PLAN FOR EXPERIMENT D015

Task	Area to be observed[a]	Mode of operation	Film recording time, sec
Revolution 35			
1	West coast of South America	Search and track[b]	30
2	South America	Scan[c]	30
3	Sea features Africa	Scan	60 120
4	East coast of Africa	Search and track	30
5	India	Scan	60
6	Calcutta	Track[d]	30
Revolution 36			
7	San Felix Island	Track	30
8	South America	Scan	50
9	Sea features	Search and track	60
10	St. Helena Island	Track	30
11	Africa Saudi Arabia coast	Scan	120 60
12	Gulf of Kutch	Track	30
Total			740

[a]Features of interest: coastlines, islands, peninsulas, rivers, lakes, deserts, snowcapped mountains, cities, clouds, and ships.

[b]The search and track mode required that the spacecraft be oriented to a specific feature ahead of the spacecraft ground track. Upon acquisition, tracking was performed until 20° past the nadir. Photographic features were recorded until 20° past the nadir.

[c]The scan mode required that the spacecraft longitudinal axis be alined normal to the surface of the earth as the spacecraft passed over the ground track area to be observed. Photographic features of interest were recorded as long as they remained in view.

[d]The track mode required that the spacecraft be oriented to an attitude which would facilitate acquisition of a specific feature as the spacecraft approached the feature. Upon acquisition, the feature was tracked until 20° past the nadir. Photographic features were recorded from time of acquisition until 20° past nadir.

TABLE II. - FILM SEQUENCES MADE DURING NIGHT OBSERVATIONS

Contents	Remarks
Lights of towns and cities	Cities identifiable by lights
Cloud formations	Good quality
Lightning flashes	Good quality
Horizon and stars	Good quality
Airglow	Good quality (excellent when compared with night photographs)
Coastlines	Good to poor contrast
Peninsula	Most significant geographic feature

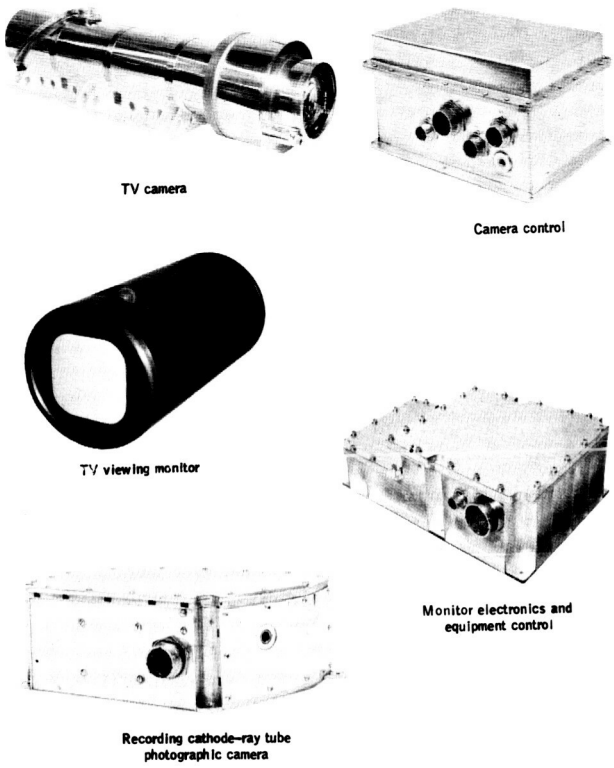

Figure 1. - Experiment D015 equipment.

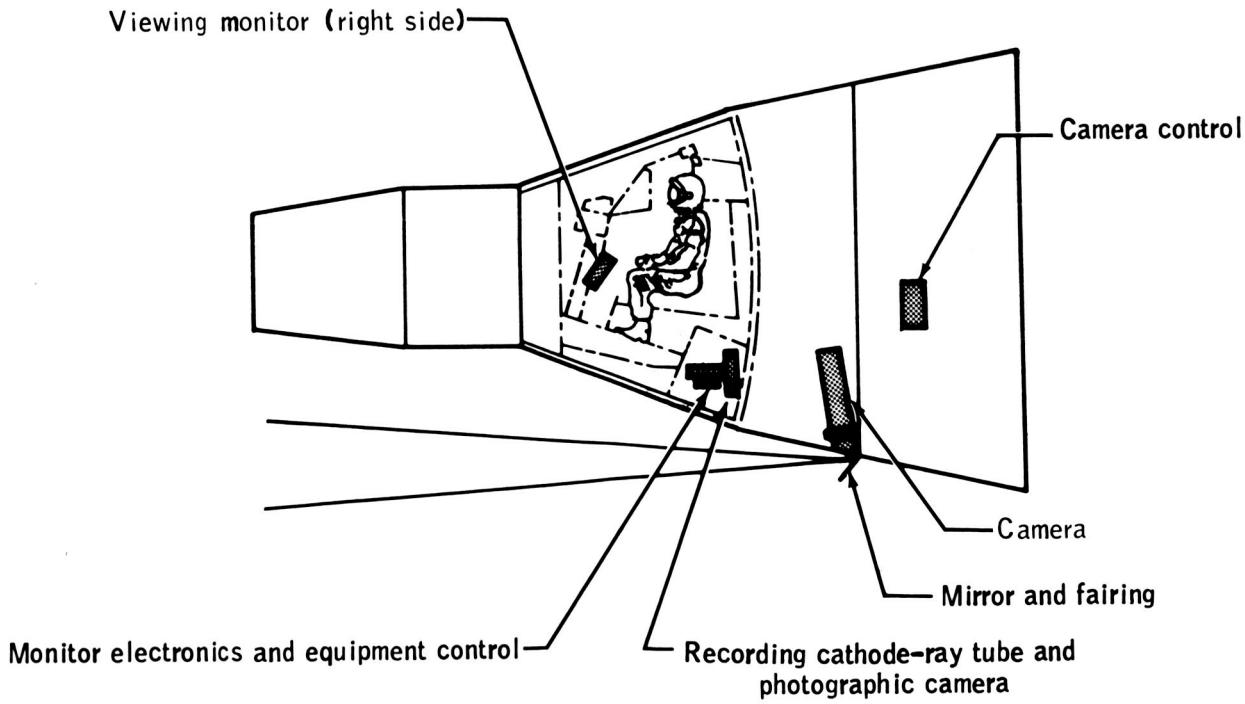

Figure 2. - Equipment location in the spacecraft.

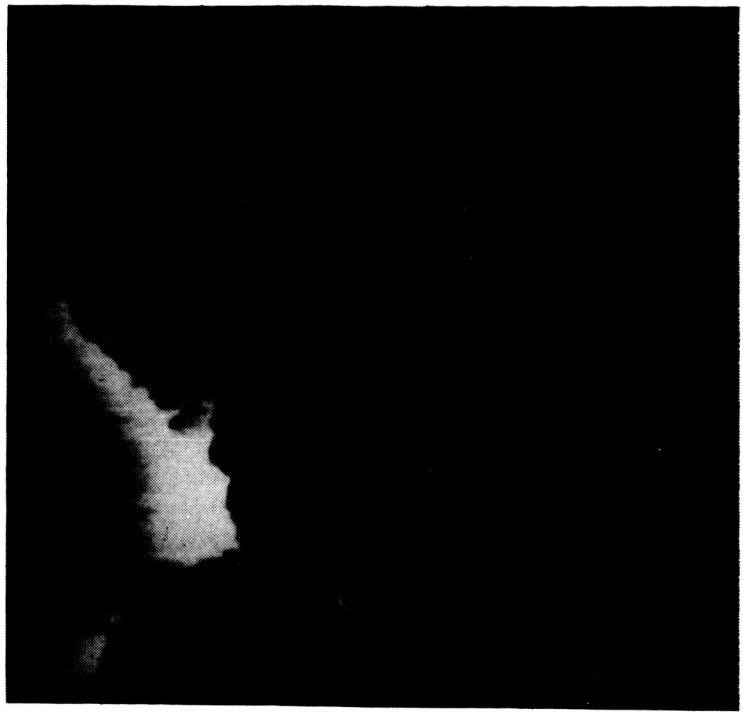

(a) Photograph.

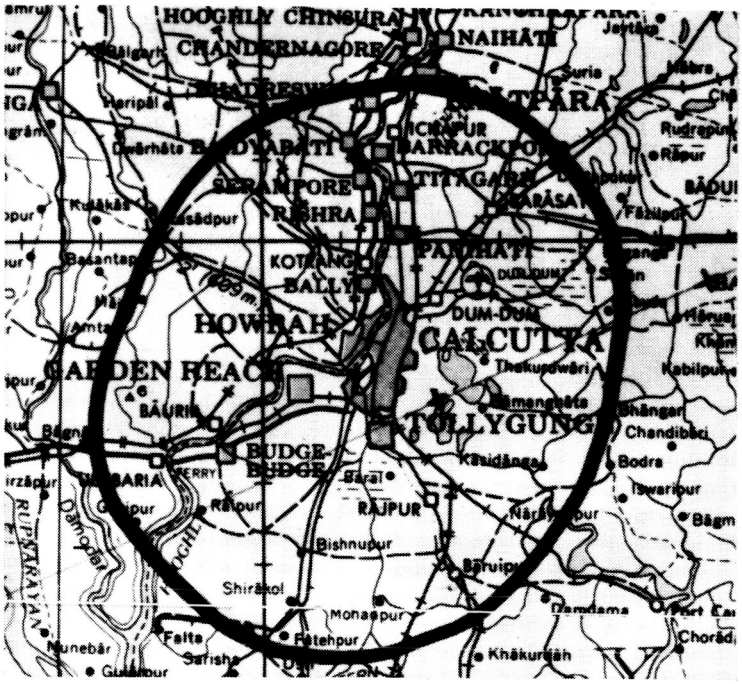

(b) Map.

Figure 3.- A comparison of the record for Calcutta, India, with a map of the same region.

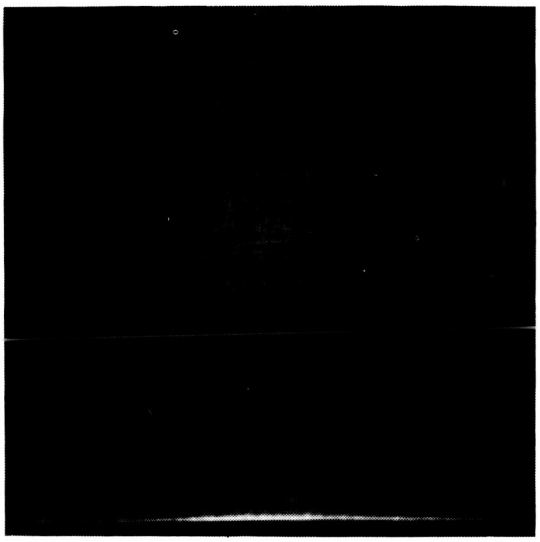

Figure 4. - Coastlines of Western Africa and Saudi Arabia.

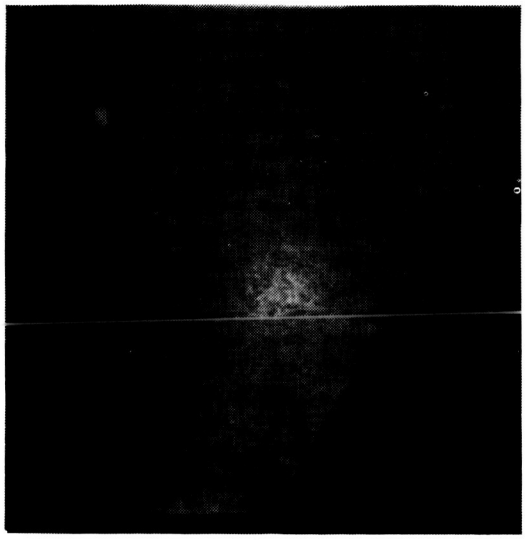

Figure 5. - The coastline of the Somalia Republic.

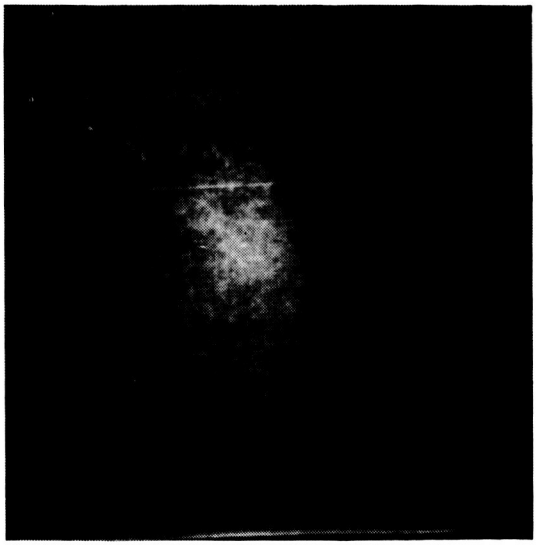

(a) Photograph.

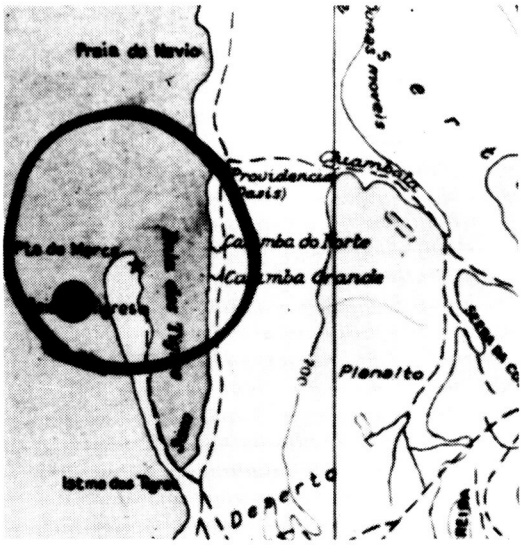

(b) Map.

Figure 6. - A comparison of the record for Istmo dos Tigres with a map of the same region.

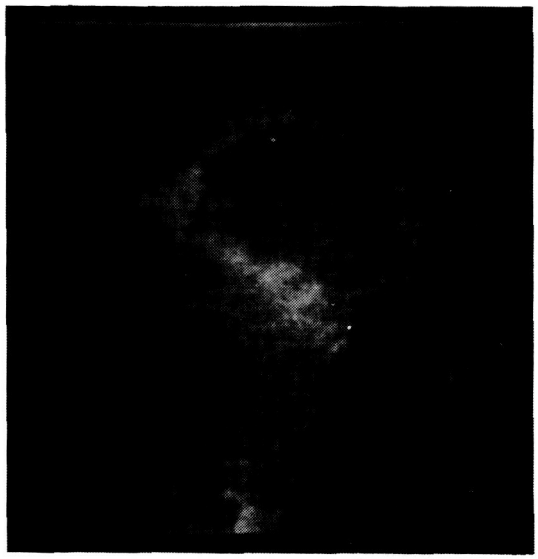

Figure 7.- A frame selected from the 3 frames per second, 1/30-second, 16-mm film.

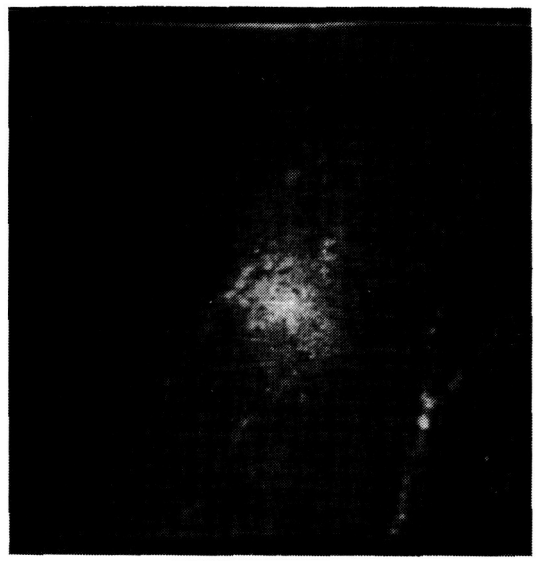

Figure 8.- Light regions viewed over Africa.

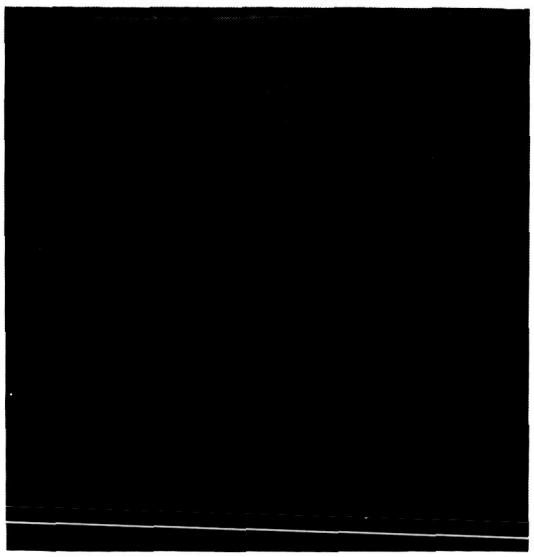

Figure 9.- Lights of villages and cities in Africa.

Figure 10.- Earth horizon, airglow, and star fields.

EXPERIMENT S030

DIM-SKY PHOTOGRAPHY/ORTHICON

By Lawrence Dunkleman,* Robert D. Mercer,**
Edward P. Ney,† and Curtis L. Hemenway‡

INTRODUCTION

The Gemini VI, VII, and XI missions included Experiment S030, which was an attempt to photograph a variety of dim-light astronomical phenomena. The Gemini VI and VII mission photographs were taken on an opportunity basis. Eastman 2475 film was selected for the morphological photography of the comet Ikeya-Seki. This work had been intended for performance on the Gemini VI mission, which was scheduled originally for October 25, 1965, only 5 days after perihelion passage of the comet. The investigation was planned for several reasons, including the following.

1. The possibility and desirability of recording certain phenomena on film had been suggested after Project Mercury and Gemini Program crewmen made unaided-eye observations of phenomena that should have been photographed.

2. Unusual or interesting phenomena or objects, such as the newly discovered comet Ikeya-Seki, could be photographed.

3. Additional information (for example, on airglow) was needed for use in the interpretation of the results from the first of the unmanned polar-orbiting geophysical-observatory series of satellites.

4. Information on nocturnal cloud cover was needed for use in satellite design.

5. Information was needed regarding the luminance of the day sky.

6. Studies of the earth atmosphere by the use of twilight-limb photography were needed.

Another consideration, particularly in relation to the Gemini VII mission, was that a 14-day mission might involve sufficient time to exploit a number of observational

*NASA Goddard Space Flight Center, Greenbelt, Maryland.
**U. S. Air Force, NASA Manned Spacecraft Center, Houston, Texas.
†University of Minnesota, Minneapolis, Minnesota.
‡Dudley Observatory, Albany, New York.

possibilities. Consideration of mission requirements, operational procedures, and the scheduled experiments and the attendant fuel and time usages understandably would preclude the performance of many of the dim-light photography tasks.

On the Gemini XI mission, the image-orthicon system of Experiment D015 was used to obtain photographic data on faint and diffuse astronomical phenomena for Experiment S030. The crewmen performed the entire observation program. However, pictures were taken of the gegenschein only immediately after sunset, and the scan of the horizon was incomplete because the recording camera did not function during the airglow sequence.

PROCEDURES

Gemini VI and VII Missions

The following are specific phenomena that were included for possible study and photography during the Gemini VI and VII missions.

1. A twilight scene
2. A nocturnal cloud cover
3. A sunlit airglow
4. A day-sky background
5. A night airglow, edge-on view
6. An aurora
7. Meteors
8. Lightning
9. Lighting, artificial
10. A galactic survey
11. Zodiacal light and the gegenschein
12. Comets

Experiment S030 was performed with the use of the following cameras.

1. A Hasselblad (70-millimeter) camera equipped with an 80-millimeter f/2.8 lens and a 250-millimeter f/5.6 telephoto lens

2. A Maurer movie-sequence 16-millimeter camera

For dim-light photography, faster lenses would have been desirable. Nevertheless, in some cases, these relatively slow lenses were considered reasonable for survey use when they were used with the highest-speed film available.

Maximum utilization of the photographic equipment allocated to the missions was permitted in an onboard checklist and related written instructions as time and fuel became available. A reproduction of the detailed information written for the crewmembers is available from the authors.

Several other factors that were considered when this investigation was begun are discussed as follows. The ease with which an observation or an experiment could be synthesized on board the spacecraft was studied. One provision of the study was that basic equipment would be available to the crewmembers. Basic equipment in Experiment S030 included a flexible-capability camera, an interchangeable lens, a variety of black and white and color film, and optical filters. The experiment was based on either phenomena that were observed by the crewmembers or on information regarding these phenomena that was transmitted to them from the ground. Transmitted information came either (1) as a result of observations made from the ground, from a rocket, from a satellite, or (2) in response to a spontaneous need for information from the spacecraft. Related experiments might be affected by the additional information that could be gained from photographic data. Stellar spectroscopy and airglow photography were examples of related experiments that were selected for performance on other Gemini missions. The optical environment of a manned satellite could be studied further (1) by acquisition of photographic data, (2) by crewmen given the opportunity to bring back objective information to support and to add to their visual observations; and (3) by providing information needed to aid in the planning of design, procedure, and scheduling of other experiments.

Formal briefings and training of the crewmembers were kept at a minimum for several reasons. The study was given low priority in a busy schedule of events because the study was approved and was inserted in the mission plan late in mission planning. The investigators and the crewmen did not wish to add a disorganizing influence late in mission planning; therefore, the investigators chose to omit a formal briefing.

The deletion of formal briefings and training of the crewmembers was made possible in several ways. Except for three narrow-bandpass filters, only onboard equipment with which the crewmen were familiar was used for this study. Even the use of lens filters was not new to the crewmembers, because a minus blue-haze filter was on board the spacecraft for use in terrestrial photography. The crewmembers had been briefed on dim-light phenomena on several occasions during their basic training in astronomy and atmospheric physics. The crewmembers had reinforced their knowledge by discussions and debriefing sessions with crewmembers of other missions. A crewmember had observed some of these phenomena directly during the Mercury-Atlas 8 mission.

Gemini XI Mission

The astronomical phenomena that were to be photographed were the Milky Way, a profile view of the airglow layer, the zodiacal light, the gegenschein, and the stable Lagrangian libration points. The noise threshold sensitivity of Experiment D015 was

estimated to be 10^{-7} foot-lamberts of object brightness. The brightness of the astronomical objects that were to be photographed are shown in the following list.

Airglow layer, ft-L	1×10^{-4}
Brightest Milky Way, ft-L	3×10^{-5}
Zodiacal light, ft-L	1×10^{-5}
Gegenschein, ft-L	1×10^{-6}
Lagrangian libration points, ft-L	1×10^{-7}

The airglow layer should have been photographed by the use of the Experiment D015 equipment, whereas the Lagrangian libration points (if they actually exist) have a noise level that approximates the noise level of the system. The low brightness of the gegenschein necessitated evaluation techniques other than observation of photographs. Photographic negatives were examined with a microdensitometer to extract the maximum amount of astronomical information and to derive absolute values of the surface brightness of the objects in question.

The equipment consisted of the Experiment D015 apparatus that produced 16-millimeter photographs of a television display of an image-orthicon output. Photographs were taken with a 1/30-second exposure time.

The procedures for Experiment S030 were different from the procedures for Experiment D015 only in the objects that were observed and recorded photographically. The Gemini XI mission plan included 12 operational sequences for Experiment S030. The sequences were performed during the night phase of revolution 41 at 65: 35 g. e. t. The sequence of events that required crewmember participation is given as follows.

Sequence 1: Activate Experiment D015 equipment before sunset.

Sequence 2: After sunset, acquire the gegenschein region according to instructions from ground-based stations, then drift in the general star region for 10 seconds; observe the television monitor screen and activate the photo-record button as required.

Sequence 3: Acquire the earth horizon and make a 360° sweep of the earth airglow and record observations photographically.

Sequence 4: Reacquire the gegenschein and repeat sequence 2.

Sequence 5: Acquire the dark region 15° east of Canopus; drift through this region for 30 seconds and record observations photographically.

Sequence 6: Position the spacecraft to acquire the Magellenic clouds (15° south of Canopus); drift within this region for 15 seconds and record observations photographically.

Sequence 7: Repeat sequence 4.

Sequence 8: Acquire and occult the moon with the spacecraft nose for 15 seconds; observe and record observations.

Sequence 9: Repeat sequence 4.

Sequence 10: Acquire the eastern horizon before sunrise; observe and record zodiacal regions.

Sequence 11: Acquire, observe, and record photographically the Lagrangian libration regions for a 30-second period in accordance with instructions from ground-based stations.

Sequence 12: Acquire and observe other astronomical phenomena as recommended in instructions from the Mission Control Center.

RESULTS

Gemini VI and VII Missions

A more detailed description of the phenomena (listed elsewhere in this report) that were possibly suitable for photographic observation has been prepared by the authors (ref. 1). The checklist that was placed on board the spacecraft is shown in figure 1. The exposures were based on an American Standards Association value of several thousands for the Eastman 2475 film by the use of data that have been reported elsewhere (ref. 2). Photographs that were taken on the Gemini VI and VII missions (February 6, 1966) and that were identified included the following.

1. Black and white and color photographs of the twilight scene

2. A series of photographs that show the nocturnal cloud cover illuminated by the combination of lunar, airglow, zodiacal, and stellar light

3. Lightning

4. Airglow, edge-on view

5. Thrusters

6. The Gemini VII spacecraft photographed from the Gemini VI spacecraft

7. The probable third stage of a Minuteman rocket and the possible Minuteman entry vehicle

Many tasks were not performed because of fuel-related and weather-related schedule problems. Also, the approved experiments were of higher priority.

Reproductions of three photographs are shown in figures 2, 3, and 4. A photograph of the Gemini VII spacecraft was taken from the Gemini VI spacecraft during the

rendezvous exercise and is shown in figure 2. Most of the illumination for the photograph came from the Gemini VI docking light, because the moon was in the last quarter and only provided light equivalent to 10 percent of full moonlight. A photograph (140-n. mi. slant angle) of a Minuteman missile entering the atmosphere of the earth is shown in figure 3. The glow from the third-stage rocket (and possibly the Minuteman entry vehicle) can be seen in the photograph. One of a series of photographs that show the nocturnal cloud cover is given in figure 4. The exposure was 8 seconds at an f/2.8 lens setting; the photograph was taken when the moon was almost full. The night airglow may be seen in the original photographs as a rather faint but distinctly visible layer. A comparison of figure 4 may be made to similar photographs that were taken of the night airglow from a rocket (ref. 2). In the comparison, the faint layer is difficult to explain when the apertures, the exposure time, and the film are considered. The photographs shown in figure 3 were analyzed to determine whether the exposure was effectively less than f/2.8. The bright cloud just to the right of the center was believed to have been illuminated by lightning. Certain new experiments or modifications and additions to the experiments already scheduled for later manned flights were proposed. Some of the experiments proposed are given as follows.

1. Photographic and spectroscopic studies of the twilight scene that would be used to study aerosol heights and composition

2. Photographic or photoelectric luminance studies of the day-sky background (related to the difficulties of seeing stars during the day) and physical observations made during the day phase; as an example, Experiment S001, planned for the Gemini VIII mission, was scheduled to include at least one photograph of the day sky

3. More studies of nocturnal cloud cover

4. Planetary spectrophotography

5. Photoelectric measurements to support both visual estimates and photographic exposures for phenomena that are too dim for detection by conventional exposure meters

Gemini XI Mission

During the postflight experiments debriefing, the crewmembers indicated that sequences 1, 2, 3, 5, and 7 were performed without difficulty. The 16-millimeter photographic film data consisted of 400 frames that showed that part of sequence 2 and most of sequence 3 were the only sequences that were recorded photographically. After evaluation of the complete film records, it was concluded that 30 percent of the available film for Experiments D015 and S030 was not exposed. Apparently, the recording camera did not function during the time of crewmember participation, except during the airglow sequence. This malfunction could have resulted from the failure of the pilot to press the photo-record button or from a malfunction of the camera recording system. The camera was checked for system failure, and postflight analyses were indicative that the camera recording cathode-ray tube shorted and failed during the final sequence.

Photographic data of the 360° sweep of the earth horizon revealed stars of the fifth and sixth magnitudes. In the airglow photographs, the top of the airglow is delineated sharply. The photographs will be useful in the determination of the height of the airglow layer at all points around the horizon. The photographs in the northwestern direction seem to show a separation of the airglow layer. To determine the reality of this separation, the original film had to be studied by the use of an isodensitracer. In approximately 20 exposures to the west, the horizon was distorted by local spacecraft phenomena. In all of the pictures, a diffuse glow appears in the center of the frame. Presumably, the glow was caused by an electronic effect in the image intensifier. The search for diffuse sources of astronomical interest was made more difficult by the glow. Also, a bright band that appeared to be a reflection or ghost produced by the bright airglow layer may be seen in the sky portion of several of the photographs.

The profile of the airglow was exposed properly in the 1/30-second photographs. The airglow (viewed from above) also was exposed properly. The correct exposure was an indication that the equipment was sensitive to illumination of approximately 50 10th-magnitude stars per 0^2 or approximately 5×10^{-9} stilb. That neither the zodiacal light nor the Milky Way could be identified was incomprehensible because of this sensitivity. Perhaps the rather bright and persistent ghost images in the system make identification of the zodiacal light or the Milky Way impossible.

CONCLUSIONS

The photographs may be used to determine the airglow geometry. Although it was sensitive, the original photographic system was unsuitable for use in the study of dim and diffuse astronomical light sources. At the same number, the system had an exposure in 1/30 second, which was equivalent to the exposure obtained in 30 seconds with Tri-X film in the Experiment S001 camera that was used on the Gemini IX mission. Therefore, the system that was used on the Gemini XI mission was approximately 1000 times faster than were the photographic techniques that were used on the Gemini IX mission.

REFERENCES

1. Dunkleman, L.; and Mercer, R. D.: Dim Light Photography and Visual Observations of Space Phenomena from Manned Spacecraft. NASA Goddard Space Flight Center, Rept. X-613-66-58.

2. Hennes, John; and Dunkleman, Lawrence: Photographic Observations of Nightglow from Rockets. J. Geophys. Res., vol. 71, no. 3, 1966, pp. 755-762.

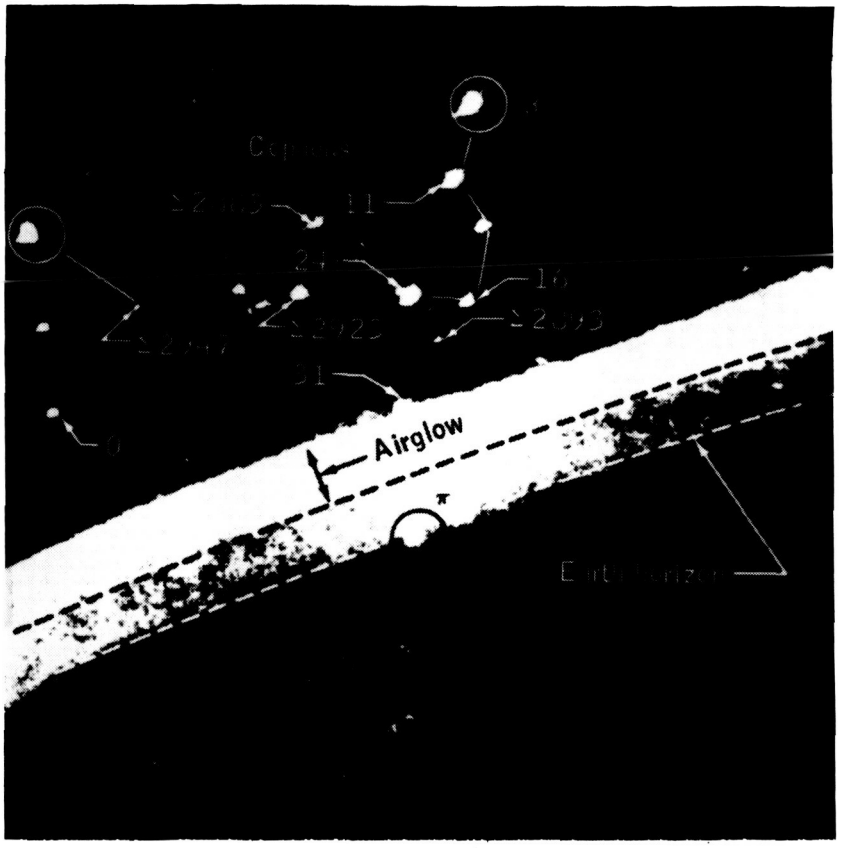

Figure 1. - A photograph of the earth airglow and star fields. This photograph was taken at night (65: 51: 27 g. e. t.) by the use of the Experiment D015 night-image-intensification tube as a sensor. It was photographed at a 1/30-sec exposure with a 16-mm camera. The earth horizon and airglow are visible clearly. Several stars between the the airglow and the earth are distinguishable easily as are stars above the airglow layer. The photograph was taken of Cepheus. The visual magnitude of O Cephei is 4. 76 and of β Cephei is 3. 23.

Figure 2. - The Gemini VII spacecraft as photographed at night by the Gemini VI crewmen.

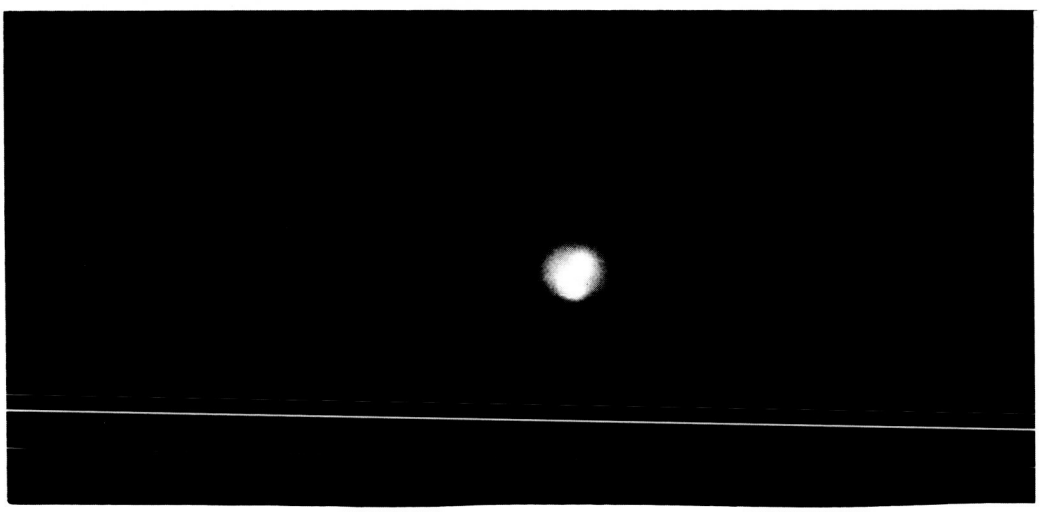

Figure 3. - The Minuteman missile entering the atmosphere, as photographed by the Gemini VII crewmen.

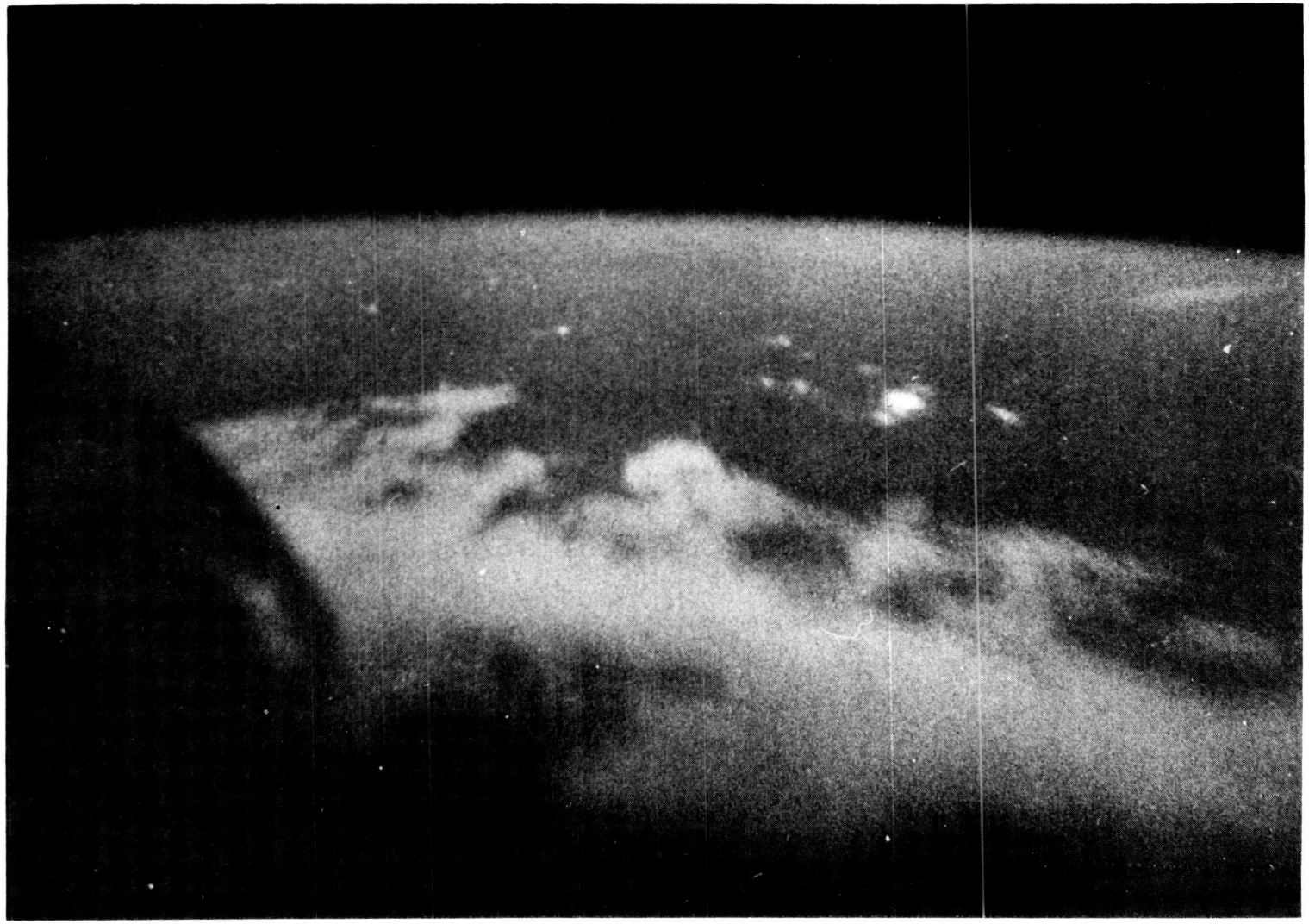

Figure 4. - Nightglow, moonlit earth and clouds, and lightning in clouds; photographed by the Gemini VII crewmen.

EXPERIMENTS D001, D002, AND D006
BASIC-OBJECT, NEARBY-OBJECT, AND SURFACE PHOTOGRAPHY

By Harold E. Geltmacher*

INTRODUCTION

The purpose of Experiments D001, D002, and D006, which were flown on the Gemini V mission, was to investigate the ability of man to acquire, track, and photograph objects in space and objects on the ground while in earth orbit. The same equipment was used on all three experiments, and the experiment numbers designate the type of object that was used as an aiming point. In Experiment D001, the aiming points were celestial bodies and the rendezvous evaluation pod (REP); the objects were at relatively long photographic range. In Experiment D002, short-range tracking and photography of the REP was the objective. In Experiment D006, aiming points were objects on the surface of the earth.

The photographic system was designed for collection of precise data on techniques of acquisition and tracking for future application to manned space flight. The equipment was selected for an evaluation of several techniques by the use of different operational modes, different film types, and lenses that had different fields of view.

EQUIPMENT

The equipment included the components shown in figure 1. The camera was a 35-millimeter Zeiss Contarex Special that had the following features.

1. Single-lens reflex
2. Focal-plane shutter
3. Lens interchangeability
4. Removable film packs

An adapter was designed to be mounted to the right-hand window of the spacecraft. Because of the limited space in the cockpit, the adapter also was a means of mounting the equipment vertically instead of horizontally. The two lenses were the 200-millimeter

*U.S. Air Force Avionics Laboratory, Wright Patterson Air Force Base, Dayton, Ohio.

Nikkor that had a field of view of 12°, and the Questar that had a field of view of 1.8° and a focal length of 56 inches (1270 millimeters) to cover the 35-millimeter-film format. The photograph-event timer was designed to activate the shutter, advance the film, and establish time correlation on the Gemini digital tape recorder.

Two types of view devices were available: a periscopic reflex viewer and a telescope. The periscopic reflex viewer was attached to the ground glass of the reflex-camera body and extended upward along the lens barrel. The telescope was attached to the adapter mount and had a magnification power of 4 and had approximately a 9° field of view. The telescope contained an inscribed crosshair and a reticle that corresponded to the 1.8° field of view of the Questar lens. The periscopic viewer was a secondary viewer for the Questar lens, and was used to test the ability of a crewman to track an object under limited (1.8°) field-of-view conditions. The three film packs contained either Type 3400 Kodak Panatomic-X Aerial film, Type 3401 Kodak Plus-X Aerial film, or Type 8443 Kodak Ektachrome Infrared Aerial film. In figure 2, the system with the 200-millimeter lens is shown attached to the right-hand window. The system with the 1270-millimeter lens is shown in figure 3. The optical sight, mounted in the left-hand window for use by the command pilot, is shown in figure 4. This sight was standard Gemini Program equipment, but also it was an integral part of these three experiments. The optical sight was alined with the longitudinal axis of the spacecraft and with the line of sight of the camera so that acquisition and tracking could be accomplished by maneuvering the spacecraft.

ACQUISITION AND TRACKING TECHNIQUES

Because investigation of acquisition and tracking techniques was the primary objective of these experiments, two acquisition modes and three tracking modes were available. The two acquisition modes were as follows.

1. Visual: In this mode, the command pilot acquired the object to be photographed by looking through the optical sight.

2. Instrument: In this mode, acquisition was accomplished by the use of pointing information from the ground-based stations and from the spacecraft attitude indicator.

The three tracking modes were as follows.

1. Visual: To evaluate this mode, the pilot sighted through the periscope or telescope and gave verbal cues to the command pilot regarding maneuvering of the spacecraft.

2. Periscope: In the periscope mode, the pilot sighted through the periscope and maneuvered the spacecraft himself to accomplish the desired tracking.

3. Telescope: In the telescope mode, the pilot maneuvered the spacecraft while sighting through the telescope.

RESULTS

On the Gemini V mission, Experiment D001 was performed by the use of celestial bodies as aiming points. However, distant photography of the REP was not possible because of spacecraft electrical-power difficulties which occurred after REP ejection. Experiment D002 close-range photography of the REP was not possible for the same reason. Experiment D006 terrestrial photography was accomplished within the limitations imposed by weather conditions and spacecraft electrical and thruster problems.

The photographs that were obtained were significant only as an element of the data to be used in technique evaluation. The other data were time-correlated position and pointing information, atmospheric conditions, sun angle, exposure settings, and the flight logs and verbal comments of the crewmembers. The photographs shown in figures 5 to 10 are representative of those that facilitated evaluation of the acquisition and tracking techniques that were used in these three experiments.

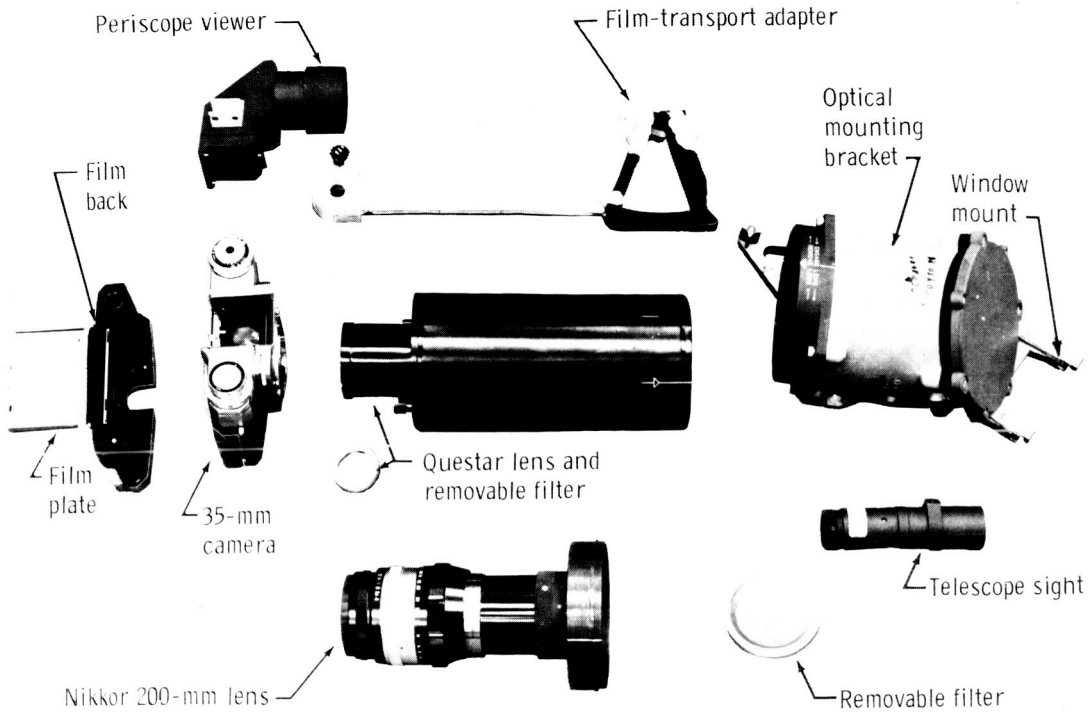

Figure 1. - The photographic equipment.

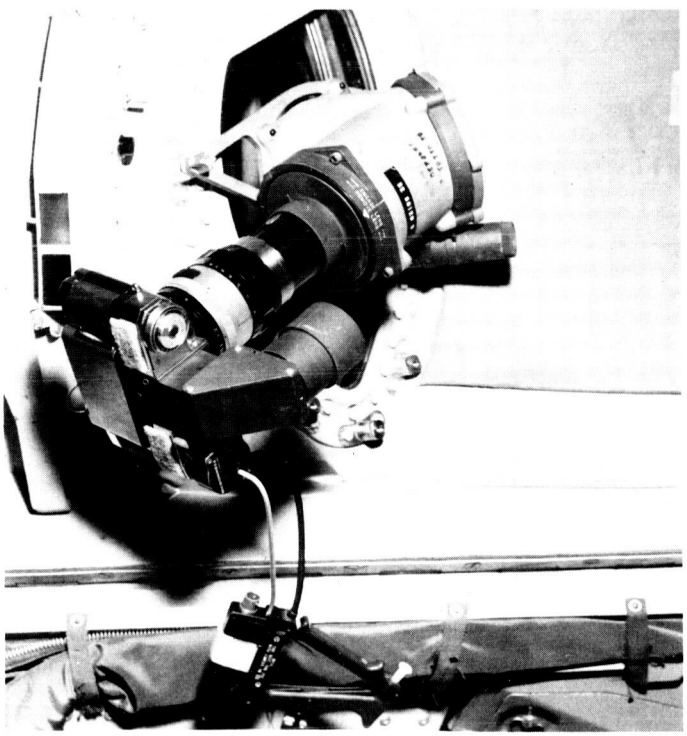

Figure 2. - The equipment installed, showing the 200-mm lens.

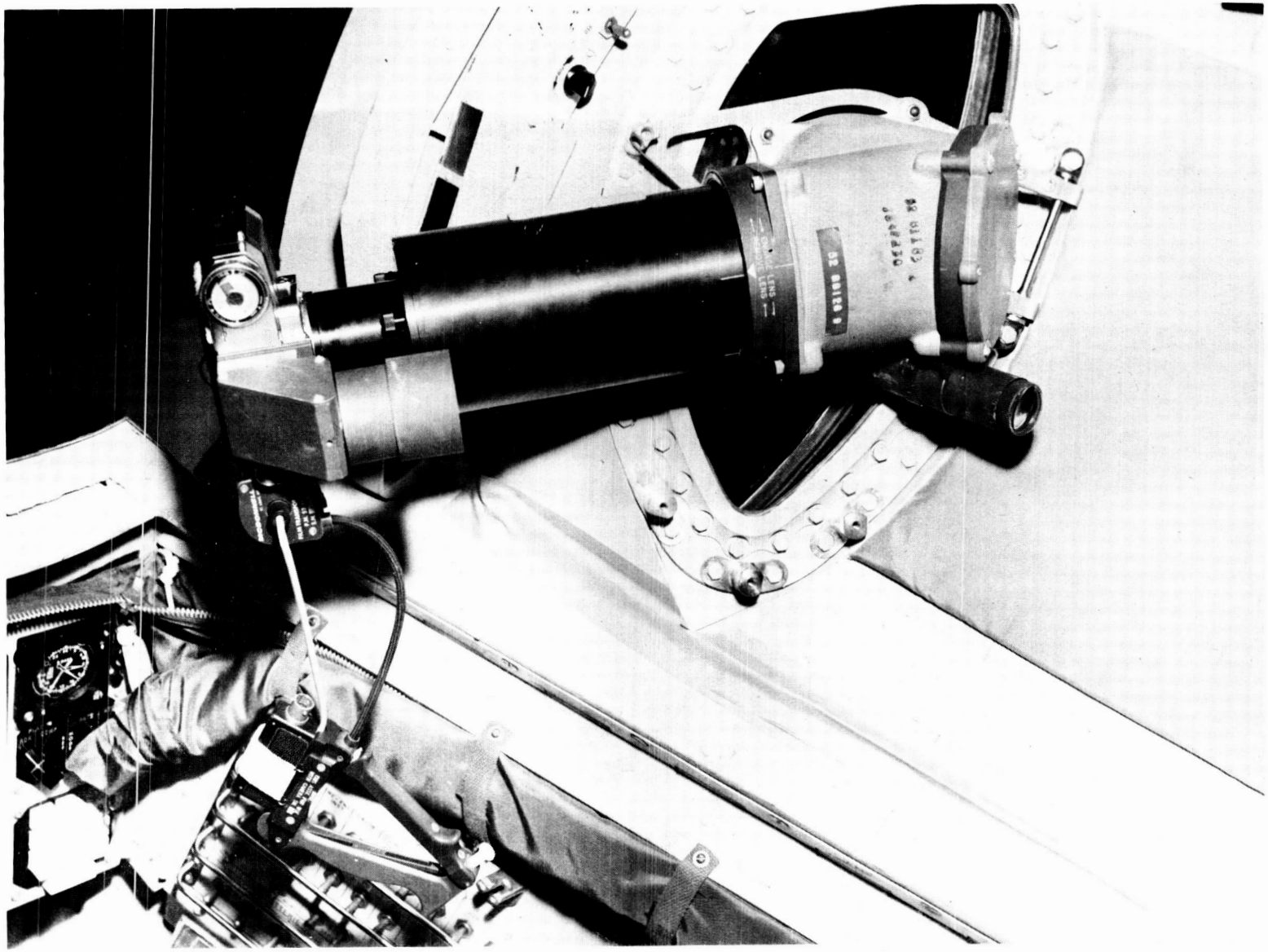

Figure 3. - The equipment installed, showing the 1270-mm lens.

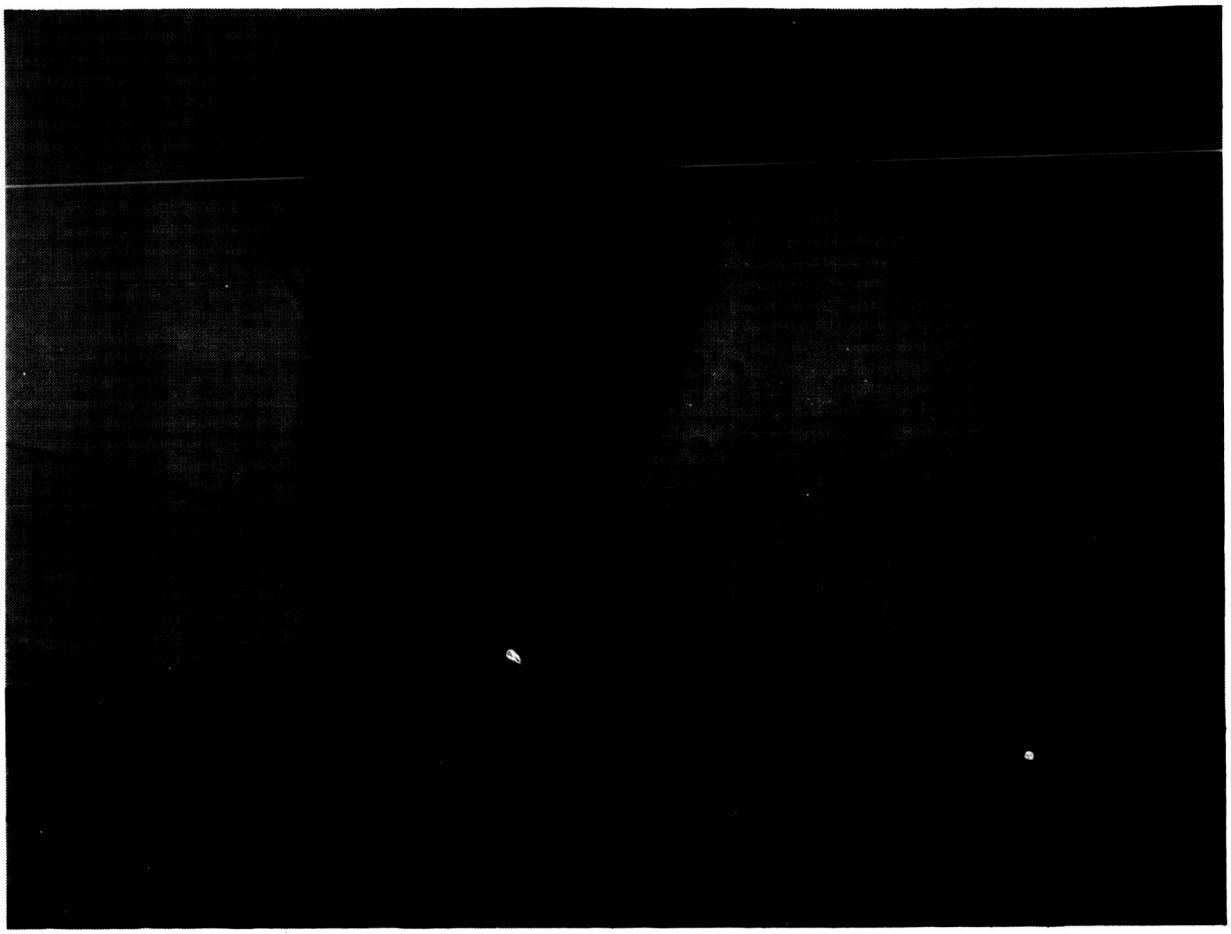

Figure 4. - The optical-sighting device.

Figure 5. - A photograph of Merritt Island, Florida.

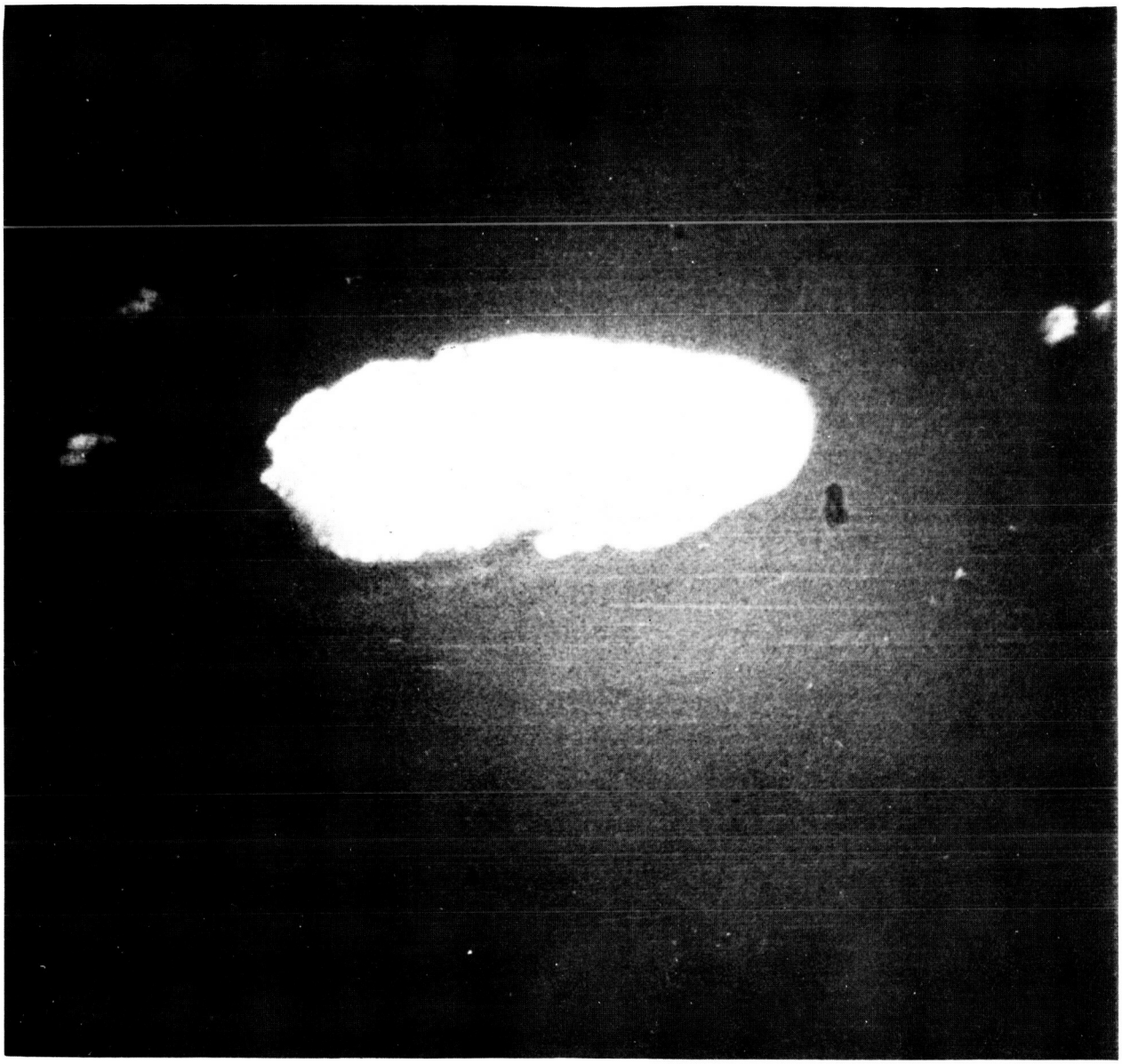

Figure 6. - A photograph of Rocas Island, Brazil.

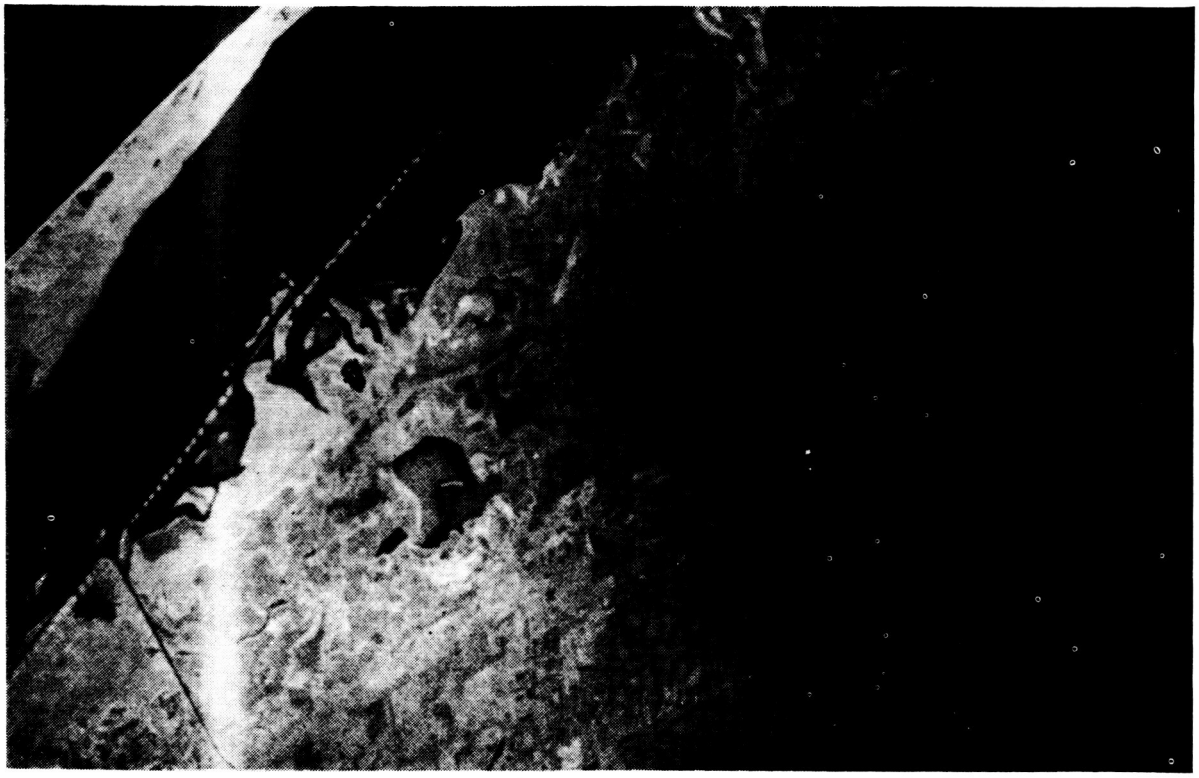

Figure 7. - A photograph of Tampico, Mexico.

Figure 8. - A photograph of the moon.

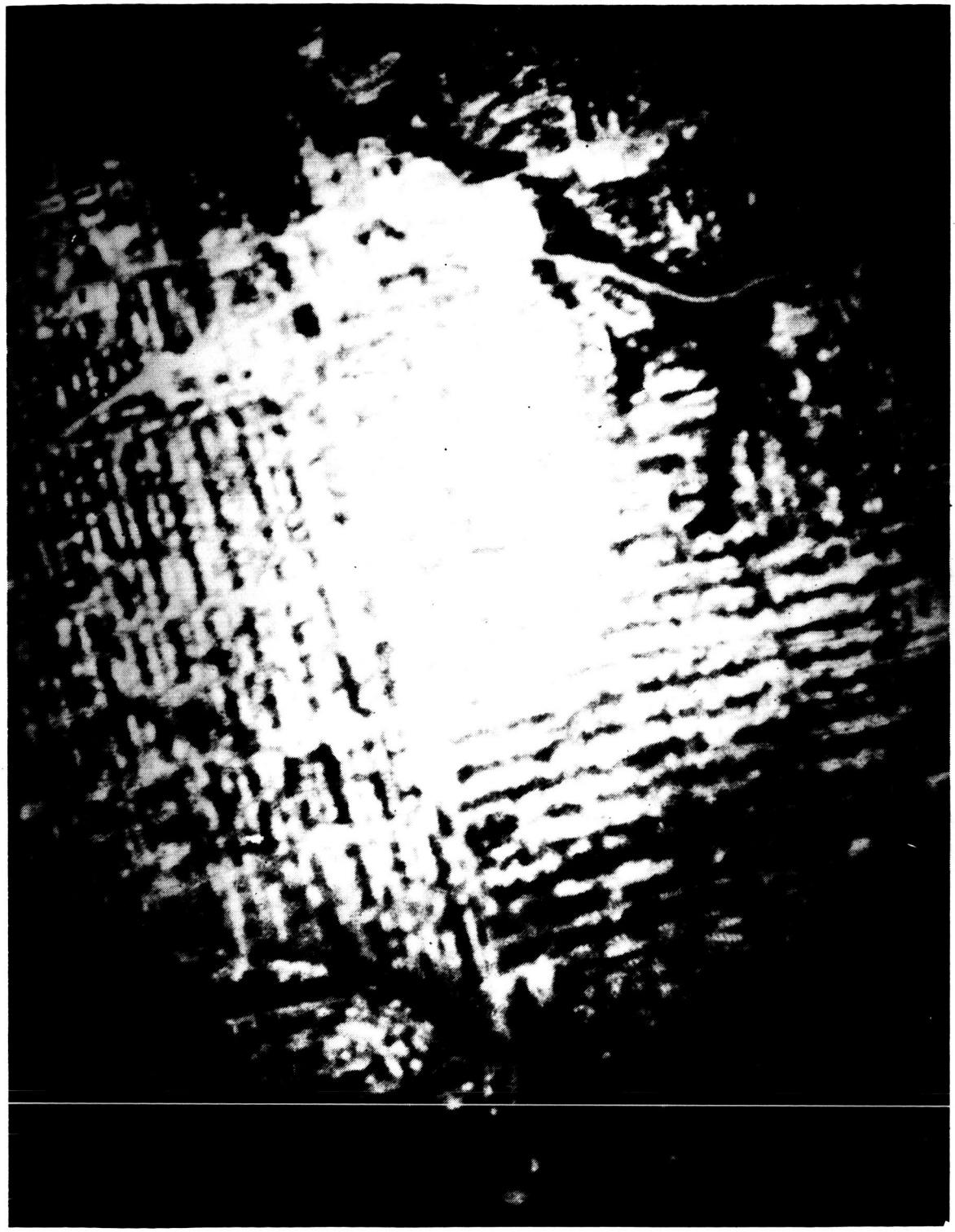

Figure 9. - A photograph of Dallas, Texas.

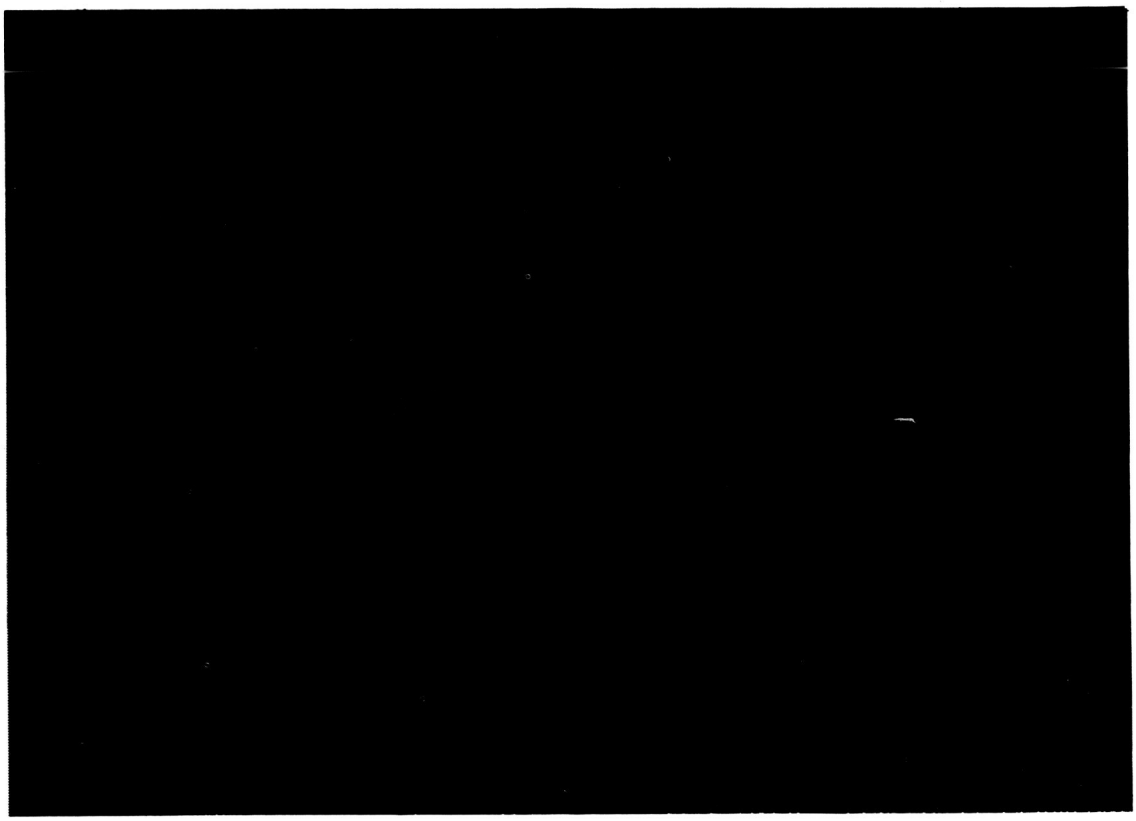

Figure 10. - A photograph of Love Field, Dallas, Texas.

EXPERIMENT M410

COLOR-PATCH PHOTOGRAPHY

By John R. Brinkmann* and Robert L. Jones*

INTRODUCTION

A slate that supported four calibrated color targets was photographed during Gemini X mission extravehicular activity (EVA) to determine if existing outdoor-type color films can reproduce colored objects accurately in the space environment. In Project Mercury and the Gemini Program, the interpretation of color by the crewmen often did not agree with that shown in the flight films. Before the performance of the color-patch experiment, the reasons for the apparent color shifts were not understood. If Apollo Program photography, particularly those films that are exposed on the lunar surface, were to be of scientific value, every effort must be made to ensure color fidelity. Most geoscientific disciplines (such as photogeology, oceanography, agricultural sciences, hydrology, air and water pollution, and meteorology) and many other possible applications necessitate a precise knowledge of true color for accurate interpretation of the results. Normal outdoor color film is balanced spectrally for a combination of sunlight and blue skylight, a condition not present in space. To determine if color film could reproduce color accurately when exposed in space environment conditions, the color-patch experiment was proposed for execution in the Gemini Program.

EQUIPMENT

The experimental equipment (fig. 1) consisted of a color-patch slate, a 3-foot extension rod, and a 70-millimeter camera. The color-patch slate was an 8- by 8- by 1/16-inch titanium plate that supported four-color targets that were composed of a ceramic material that had a matte finish. The colors were National Bureau of Standards (NBS) primary colors (red, blue, and yellow) and neutral gray. To simplify the experiment, a 3 foot-rod of four sections (each 9 inches long) of 0.5-inch-diameter aluminum was provided to hold the color patch 36 inches from the camera. The camera and color patch were attached to the rod by means of a dovetail fitting. A 70-millimeter Maurer space camera fitted with an f/2.8, 80-millimeter lens was used. To reduce the effect of ultraviolet energy on the film, an 0-52 Corning glass filter that had a cutoff at 3500 angstroms was used. The camera was equipped with 70-millimeter film that had a 2.5-mil base. This film had excellent color-reproducing qualities and had

*NASA Manned Spacecraft Center, Houston, Texas.

been used on Mercury and previous Gemini missions. Except for 2.5-mil base, the film was identical to Ektachrome MS Kodak film.

PROCEDURE

Before the Gemini X mission, the color patch was photographed under controlled lighting conditions at Kennedy Space Center (KSC) with the flight camera and film. A series of six exposures was made at 1/250 second at f/8, 1/250 second at f/11, and 1/250 second at f/16. The purpose was to obtain photographs that could be compared with similar postflight photographs taken under the same controlled conditions. Thus, determination could be made as to whether the film had undergone any changes during the mission.

During the flight, the crewmembers were to assemble the experiment, and the pilot was to photograph the color-patch slate nine times while standing in the spacecraft seat (fig. 2) and was to return the color-patch slate to the spacecraft for postflight calibration and analysis. The exposures were to be made in groups of three, beginning with 1/250 second at f/8, then 1/250 second at f/16, and finally 1/250 second at f/11. The solar-illumination angle was to be within 30° of the patch nominal.

RESULTS

Because of trouble in the spacecraft environmental control system (ECS), the standup EVA was terminated before completion of the experiment. To facilitate ingress from EVA, the color patch and rod were discarded. Before the ECS trouble occurred, the crewmen obtained four color-patch photographs at an exposure of 1/250 second at f/8. The remaining film in the magazine was used to photograph the earth weather and terrain patterns. Although the experiment was not completed, the pictures contained enough information from which certain conclusions could be drawn. The results of a subjective comparison of the flight film and the backup color patch (which was identical to the flight hardware) confirm the suitability of commercial film to record colors accurately in space.

Density measurements that were made from the gray section of the flight-film exposures resulted in the conclusion that a difference of 10 percent existed between the first and third exposures and that a difference of 17 percent existed between the lighter of the two and the second exposure (which was most dense). The density difference can be attributed either to variance in the shutter mechanism, slight changes in the incident-illumination angle, or a combination of both causes. Saturation of the four colors on the first and third exposures was almost identical, whereas the colors on the second exposure were richer because they approached more nearly the nominal exposure (1/250 second at f/11).

A preliminary analysis of the various factors that could have caused the apparent false color rendition in space photography was conducted by personnel of the NASA Manned Spacecraft Center (MSC) Photographic Laboratory and Space Science Division.

The results of the analysis were indicative that the change could have been caused by the unattenuated solar spectrum for which the film may not have been balanced.

CONCLUSIONS

The experiment resulted in the acquisition of sufficient information to confirm that objects can be photographed in space with good color fidelity by the use of existing materials. Available color film is balanced to the solar spectrum in space, and the effect of ultraviolet energy on film degradation appears to be negligible.

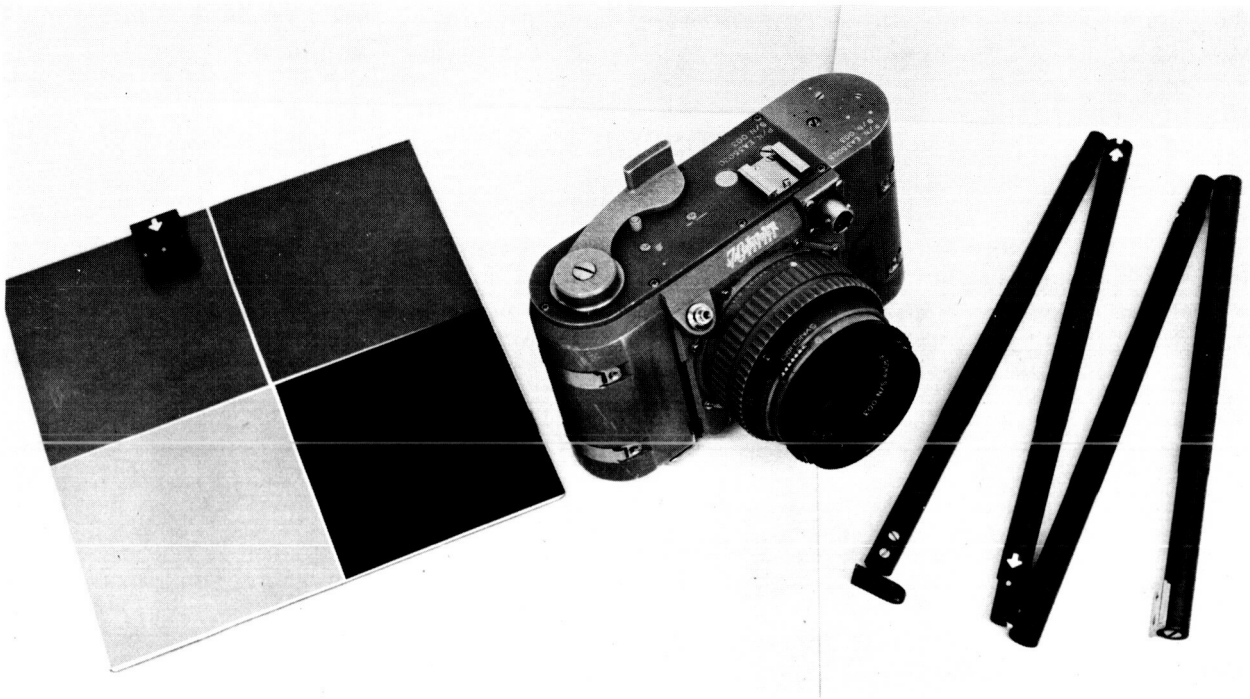

Figure 1. - The color-patch photography equipment.

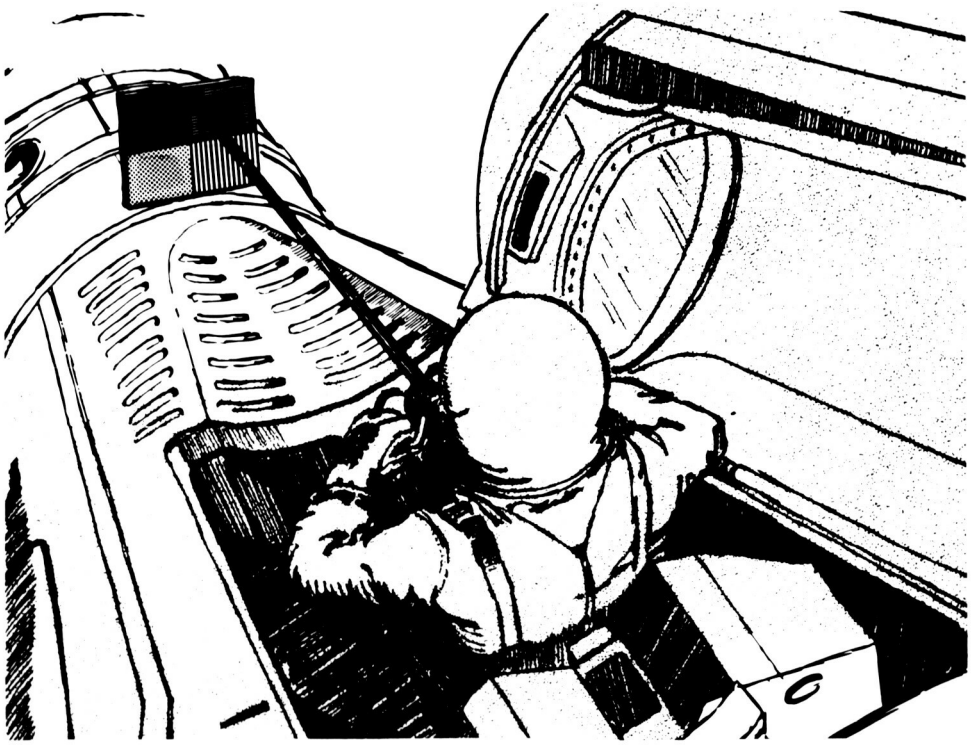

Figure 2. - The method of photography of the color patch by the spacecraft pilot.

EXPERIMENT T001

ENTRY COMMUNICATION ON THE GEMINI III MISSION

By Lyle C. Schroeder,* Theo E. Sims,* and William F. Cuddihy*

INTRODUCTION

The communications-blackout problem has been studied for several years by staff members of Project RAM (radio-attenuation measurement) at the NASA Langley Research Center (LRC), Hampton, Virginia. Initially, work was devoted to attempts to define the problem and to establish a method for prediction of radio-signal attenuation levels. Much recent work has been directed toward development of methods for the alleviation of communications blackout and for the measurement of attenuation-sensitive parameters during simulations and space-flight conditions. One of the most promising techniques that has been investigated for communications-blackout alleviation has been that involving the addition of material to the ionized flow field. The addition results in a reduction of the electron concentration in the ionized media by means of droplet-surface recombination, cooling, and electrophilic mechanisms. These methods cause a reduction in signal attenuation. Results of tests conducted on a model (1-inch nose radius) immersed in a rocket-exhaust plasma have proven that water addition causes complete restoration of the attenuated signal. Similar results were noted during a flight test of a model that had a 4-inch nose radius. In the tests cited, water injected in a sector of the flow field caused complete omnidirectional-signal recovery for moderate flow rates. This signal restoration in the tests was suggestive that the material-addition technique was feasible for a spacecraft of the shape and size of those used in the Gemini Program. Some of the advantages in testing the material-addition technique on a Gemini spacecraft were as follows.

1. The Gemini vehicle was practical because it was a manned, blunt spacecraft that has an ablative heat shield.

2. The size of the Gemini spacecraft was 10 times that of the last RAM flight-test vehicle.

3. The entry velocity of the Gemini spacecraft was approximately 7000 ft/sec greater than that of the last RAM flight-test vehicle.

4. The information was timely for application to future space entries.

*NASA Langley Research Center, Langley Station, Hampton, Virginia.

However, many conditions were not favorable for performance of the experiment on board the Gemini III spacecraft. The most important of these conditions are as follows.

1. The ultrahigh frequency (uhf) antenna was located far from the injection nozzles in the aft end of the spacecraft and was in a separated-flow region.

2. Spacecraft flight parameters, particularly roll attitude (upon which signal recovery level was dependent), were such that the water-injection window was not pointed toward ground-based receiving stations.

In any case, the experiment was an evaluation of the technique as applied to this large, blunt, ablative body. Results of the experiment, performed in such unfavorable conditions, are significant.

EXPERIMENT DESCRIPTION

System Geometry

The Gemini spacecraft began entry with the heat shield forward. The Gemini III spacecraft was banked 45° to the left at the start of entry and throughout most of the blackout period. This orientation of the spacecraft, as viewed from the south side of the flight path, is shown in figure 1. Several aspects of the geometry of the experiment can be noted from this figure. The entry uhf antenna was on the aft end of the spacecraft and the C-band antennas were on the conical portion. The experiment compartment (the right main landing-gear door) is outlined by dashed lines in the figure. As shown in figure 1, the injection nozzles were on the circumference of the conical portion, approximately 15° above the southern horizontal. Also, the anticipated distribution of the water injected is shown in figure 1. These locations are shown in more detail in figure 2. The injection nozzles were approximately 30° to the right of the bottom or windward sides. Because the spacecraft flies at an angle of attack other than 0°, it was determined that water requirements would be less if injection occurred from the windward side. As shown in the figure, the injection nozzles were pointed forward, so that the direction of injection was approximately 20° off the spacecraft surface. This arrangement was used to increase the dwell time of drops in the vicinity of the spacecraft.

The flow field on the windward side of the Gemini spacecraft was "attached" in such manner that an inviscid layer extended from the vehicle boundary layer outward to the shock. However, the air near the uhf antenna on the aft end of the spacecraft was separated from this inviscid layer, and was circulating at a relatively lower velocity. The implications that resulted from this separation of flow were considered.

Window Size

The window was defined as the volume distribution of water in the flow field. It was assumed that the attenuation mechanisms were relieved in the window, and hence the window might have been considered to be a hole in the plasma and to have free-space properties. The size of the window created by water injection was assumed initially and

subsequently was examined in wind-tunnel tests. Because the spacecraft and plasma sheath were large with respect to a uhf wavelength, it was suspected that the major radiation from the spacecraft would be beamed through the window created by water addition. Studies were performed to determine the characteristics of the beam-width pattern and to determine the signal recovery that could be expected with various assumed window sizes. The results, which confirm that beaming would occur, are presented elsewhere in this report.

Water-Injection System

The onboard experiment consisted of a water-injection system that was designed to fit into the right main landing-gear door. The installation of the equipment on the inside of this door is shown in figure 3. The electrical details of the system are presented in figure 4. The system was independent of other spacecraft interfaces except for the electrical actuation switch and the leads to the cabin. This gas-pressurized water-injection system is shown schematically in figure 5. The system was designed to be actuated by the crewman on the right side; system actuation simultaneously supplied water-expulsion pressure through the regulator to the water tank and started the mechanical timer. Once every 15 seconds, the timer opened and closed contacts to each of three solenoid valves; water was injected from the valves. This system was designed to produce alternate pulses of low, medium, and high flow rates; the pulses had durations of 0.50, 0.25, and 0.10 second. One injection cycle is shown in figure 6. The water supply was depleted after approximately 12 cycles. The planned experiment-actuation time for the Gemini III mission was 45 seconds after the beginning of uhf blackout. It was possible to update predictions for the beginning of uhf blackout after retrofire. The number of nozzles and the orifice sizes are shown in figure 2.

Frequencies Transmitted

Three frequencies were in operation during entry; these were uhf telemetry at 230.4 megahertz, uhf voice at 296.8 megahertz, and C-band at 5690 megahertz. On the uhf telemetry system, a power of 2 watts was transmitted into a quarter-wave stub antenna; a gain of 2.5 over isotropic and a voltage standing wave ratio (VSWR) of approximately 2.1:1 were used. On the uhf voice system, a power of 3 watts was transmitted into the same stub antenna with approximately the same gain and with a VSWR of approximately 2.85:1. During the injection period, the crewman was requested to key the uhf transmitter to attempt communication on this link. The C-band radar transponder operated at 1-kilowatt peak power, which was fed to three helical antennas for formation of circular roll pattern.

Ground Stations

During the experiment operational period, ground-based stations located near the entry flight path were requested to monitor signal strength on uhf telemetry, uhf voice, and C-band frequencies. The stations that were requested to monitor signal strength are listed in table I. Locations of the stations with respect to the spacecraft blackout and during the experiment are shown in figure 7.

GROUND-BASED SUPPORT STUDIES

Penetration and Flow-Rate Studies

A study was made to determine flow-rate requirements and to optimize penetration. Estimates of the water flow-rate requirement were extrapolated from the RAM B2 flight results and were calculated by use of equilibrium cooling theory. Although more accurate methods are available now, this method was the best method at the time. Three flow rates (low, medium, and high) were selected for the experiment. Under the conditions of fixed pressure and nozzle size, penetration could not be optimized throughout the blackout-altitude range. For this reason, design altitudes (at which penetration was optimized) were chosen for each flow rate. By a proper choice of nozzle size, penetration distance was chosen to extend to the shock at these altitudes. Verification of proper penetration was confirmed in wind-tunnel tests. Lateral and longitudinal penetrations also were measured to determine the size of the radio-frequency (rf) window. A plot of the variation of penetration with altitude for the conditions of the Gemini III flight is shown in figure 8. Also shown in this figure is the distance from the body to the shock and the optimum penetration distance. Penetration decreased greatly with change of altitude. It was assumed that overpenetration would result in signal recovery, but that underpenetration would not. Therefore, penetration for the actual Gemini III mission would be sufficient at altitudes greater than 240 000 feet. The Gemini III angle of attack was much lower during flight than was predicted, and, as a result, the flow field on the windward side was 25 percent thicker, and optimum penetration was reached at altitudes that were higher than had been predicted.

Antenna-Pattern Studies

Because the size of the spacecraft and the associated flow field was large relative to a uhf wavelength, it was expected that transmission through an aperture in a plasma would cause the signal to be beamed. A directive signal would cause the experiment to be dependent upon vehicle roll attitude for signal acquisition. Also, the injection nozzles would be pointed upward during flight at a normal spacecraft attitude; therefore, the signal would be beamed away from ground-based stations. As a result, a series of tests was conducted at LRC to determine the extent of recovery and the antenna pattern produced when a slot is opened in the ionized flow field. In these tests, a transmitting model was immersed in lossy-medium shrouds to simulate the Gemini equipment in a plasma sheath. Slots of various aperture size were cut in the shrouds, and the corresponding antenna patterns were recorded.

The antenna pattern for a slot size that corresponded to the anticipated distribution of droplets, as determined by wind-tunnel tests, is shown in figure 9. However, the beam-width characteristics did not depend greatly on slot size, as long as the window extended lengthwise beyond the uhf antenna. As shown in the plot of roll angle compared with signal strength, beaming occurred in the direction of injection. Therefore, for the Gemini III mission, receivers tracking the spacecraft at roll-aspect angles greater than approximately 50° (around from the rf window) would not have been expected to receive much signal.

RESULTS

Entry Events

The variation of altitude with time change is shown in figure 10; the entry flight path was shown in figure 7. In both figures, special reference is made to times important in the experiment. Blackout of uhf began at 04:39:59 g. e. t. and at an altitude of approximately 318 000 feet. At approximately 04:36:26 g. e. t. (03:33:00 before blackout), the spacecraft banked 45° to the left; thus, the injection nozzles were approximately 75° south of straight up, or approximately 15° above the horizontal. The experiment was actuated at 04:41:16 (01:17:00 after blackout initiation) and at an altitude of approximately 272 000 feet; the experiment ended after 3 minutes and at an altitude of 160 000 feet. Blackout ended at 04:45:00 and at an altitude of approximately 134 000 feet.

Water-Flow Rates

The flow rate of the water-injection system was determined by means of preflight calibration and was not monitored in real time. Twelve cycles of three different flow rates were used during the data collection period. The flow-rate sequence is shown in figure 6. The mission times during which flow-rate pulses occurred are shown in table II. Pulse times during the first 45 seconds and during the last minute of the injection period were verified by means of signal strength pulses; the remaining pulse times were determined by means of extrapolation.

Signal-Strength Measurements

Signal-strength records from all ground-based stations have been analyzed. The signal-strength records from Key West, Homestead, aircraft 3, aircraft 4, and Grand Bahama Island (GBI) are indicative that significant levels of signal recovery were observed on uhf telemetry and uhf voice frequencies, which corresponded to the early portion of the water-injection sequence. The latitude, longitude, and altitude when pulses were noted are shown in figures 7 and 10. Plots of signal strength compared with time for the Key West station are shown in figure 11. The plots contain two well-defined signal-recovery pulses and a third (less definitive) pulse. Each pulse corresponded to the high water-flow rate. Aircraft 3, aircraft 4, and Grand Bahama Island stations did not receive the third signal-recovery pulse. No signal recovery was achieved from the low and medium flow rates.

Function records from Merritt Island Launch Area (MILA) and GBI C-band radars contain signal-strength enhancement pulses that corresponded to the latter portion of the injection sequence. A tracing of the C-band signal-strength oscillograph record is shown in figure 12. The record was broken so that each line is one injection period long. The time during which injection occurred has been indicated. Pulses of significant level, which correspond to the medium and high flow rates, may be noted. The stations at GBI and MILA were tracking in the beacon mode. The other Cape Kennedy radar was tracking in the skin-track mode, and, consequently, did not record any enhancement pulses. The C-band radar records made at Eglin Air Force Base did not contain these enhancement pulses. Data from Anclote Point were inconclusive.

DISCUSSION OF RESULTS

Ultrahigh Frequency

The Gemini uhf signal, which had been blacked out completely, was increased to a high level above receiver noise by water addition. The significance of these results was that the material-addition technique of radio-signal attenuation alleviation has been shown to work for a body the size and shape of the Gemini spacecraft. Of added significance were the facts that signal recovery was noted even though aspect angles to the ground-based stations were far from optimum, and even though the predictions were based on a flow field that was not well defined. Improvement can be made in application of the technique if the experiment can be performed under more suitable conditions.

No stations north of the flight path received uhf signal-recovery pulses except GBI, where the aspect angle at the time of signal recovery was almost directly forward. On the south side of the flight path, four stations (not including GBI) received the uhf signal-recovery pulses. These results were in agreement with LRC studies of pattern beam width, which had resulted in the prediction that the signal would be beamed toward the south side of the flight plan.

Recovery was recorded for the first three high flow-rate pulses between altitudes of 275 000 and 245 000 feet. The recovered signal was very strong, but became marginal on the third pulse, and afterward was lost. This aspect of reduced effectiveness during the latter part of the data period was analyzed thoroughly from a fluid mechanics standpoint, but several factors appeared to be involved. These factors are as follows. The injection sites were a long distance from the uhf antenna. The decrease of effectiveness (on attenuation) of material addition with distance aft was noted on the RAM B2 flight test. In this test, three antennas were located from approximately 2 to 10 feet downstream from the injection site. The forward antenna recovered almost completely; the middle-antenna effect was less, and the antenna farthest downstream was less effective. Although the fact was conceded that these antennas were of different design, the decreasing recovery effect with distance downstream may have been significant to the Gemini case, because the uhf antenna was approximately 8 feet downstream from the injection site. Penetration was less than had been predicted. Because the angle of attack during flight was less than that predicted, the flow field on the windward side was almost 25 percent thicker than was expected. As a result, penetration would have decreased below required levels at higher altitudes than were predicted. The penetration requirements were recomputed to account for the lower angle of attack. These calculations prove that penetration decreased below required levels at the altitude where signal recovery terminated (for the high flow rate). Also, the calculations are proof that the medium and low flow rates could not achieve sufficient penetration to cause signal recovery at the altitudes experienced during flight.

There were unknowns in the Gemini flow field. The addition of ablative products that contained sodium and potassium was known to have caused the electron concentration of the flow field to increase. The location of the uhf antenna in a separated-flow wake region (where assumptions such as simple flow-field cooling and distribution were not applicable) conceivably could have contributed to recovery levels that were

lower than those predicted. The aspect angle was unfavorable. Because signal recovery was dependent upon aspect angle, minor deviations in aspect, caused by flight, conceivably could have been contributory factors. For the Key West and Homestead stations, as examples, roll-aspect angle increased from approximately 20° (during the second large flow-rate pulse) to approximately 30° (during the third large flow-rate pulse).

C-Band

Signal recovery on the C-band frequency was not anticipated, because the onboard antenna locations were not favorable. However, signal-strength-enhancement pulses were noted for both medium and high flow rates on Cape Kennedy and GBI radars for the portion of the experiment from 100 to 175 seconds after experiment initiation. These pulses were not received at the Eglin station; this beacon tracked during the early portion of the entry. Anclote Point data were inconclusive. Possibly, these C-band results may be linked with pattern and penetration parameters.

CONCLUSIONS

Experiment T001 was performed during the Gemini III mission to determine whether water addition was effective in the establishment of communication links during the entry portion of the flight. Attenuation levels were measured with and without water injection at uhf frequencies of 230.4 and 296.8 megahertz and at the C-band frequency of 5690 megahertz. Ultrahigh frequency signals that had been blacked out were restored to significant levels, during early portions of the water-injection sequence, by the high flow-rate injection. The C-band signal was enhanced by medium and high flow-rate injections during the latter portion of the injection period. The uhf signal recovered during water injection resulted in an antenna pattern that was beamed in the radial direction of injection from the spacecraft. The minimum flow rate required was not determined, because penetration and the antenna location were not optimum. Postflight analysis showed that the uhf recovery data were consistent with injection-penetration theory.

Although the experimental data resulted in verification of the fact that signal recovery from Gemini blackout could be achieved, much can be done to improve the technique. Future experiments are under consideration for Apollo missions that involve more ideal antenna locations and injection sites, and that will be designed to minimize the problem of signal directionality. These experiments could result in a more efficient use of water and could lead to use of operational systems to eliminate communications blackout on manned space flight.

TABLE I. - MONITORING STATIONS

Station	Frequencies monitored		
	uhf telemetry	uhf voice	C-band
Eglin Air Force Base	X	X	X
Mission Control Center at Cape Kennedy	X	X	
Telemetry Site II at Cape Kennedy	X	X	
Merritt Island (Cape Kennedy)			X
Patrick Air Force Base			X
Grand Bahama Island	X		X
Grand Turk Island	X		X
Anclote Point (Eglin AFB)	X	X	X
Key West (LRC van)	X	X	
Homestead (LRC van)	X	X	
Aircraft 4	X	X	

TABLE II. - STARTING TIMES OF FLOW-RATE PULSES

[Times are after launch]

Cycle	Small flow rate,[a] hr:min:sec	Medium flow rate,[a] hr:min:sec	High flow rate,[a] hr:min:sec
1	04:41:15.9	04:41:19.9	04:41:24.6
2	04:41:31.2	04:41:35.2	04:41:39.9
3	04:41:46.5	04:41:50.5	04:41:55.2
4	04:42:01.8	04:42:05.8	04:42:10.5
5	04:42:17.1	04:42:21.1	04:42:25.8
6	04:42:32.4	04:42:36.4	04:42:41.1
7	04:42:47.7	04:42:51.7	04:42:56.4
8	04:43:03.0	04:43:07.0	04:43:11.7
9	04:43:18.3	04:43:22.3	04:43:27.0
10	04:43:33.6	04:43:37.6	04:43:42.3
11	04:43:48.9	04:43:52.9	04:43:57.6
12	04:44:04.2	04:44:08.2	04:44:12.9

[a]Duration of pulses: small, 0.46 sec; medium, 0.21 sec; high, 0.10 sec.

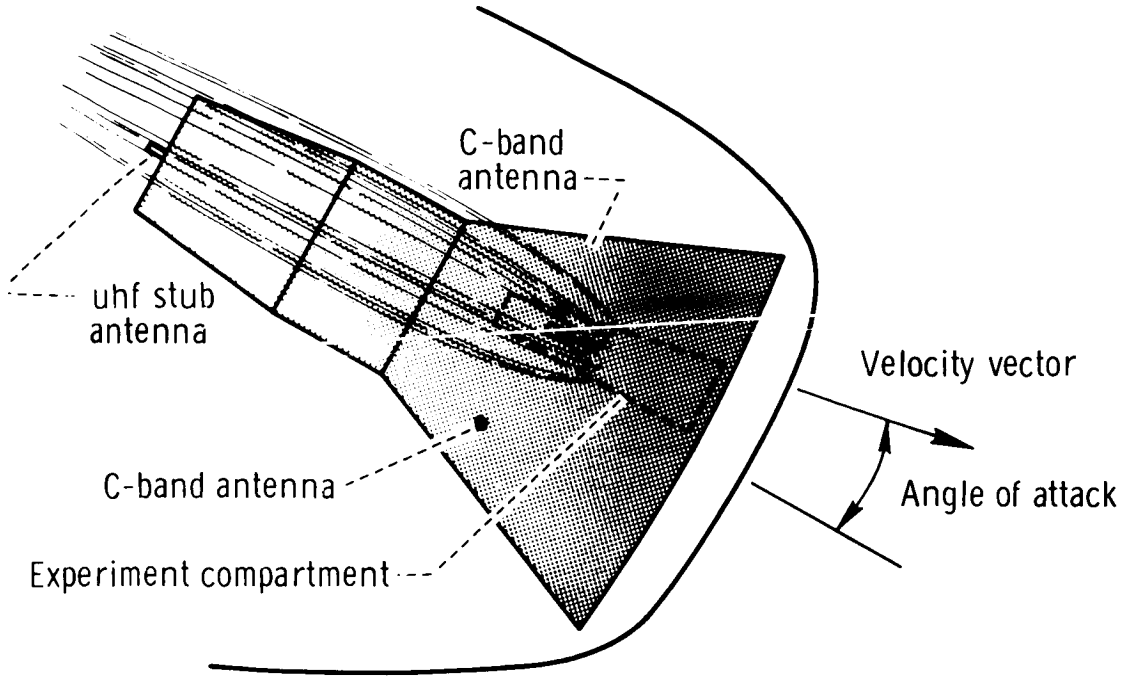

Figure 1.- The location of the experiment package.

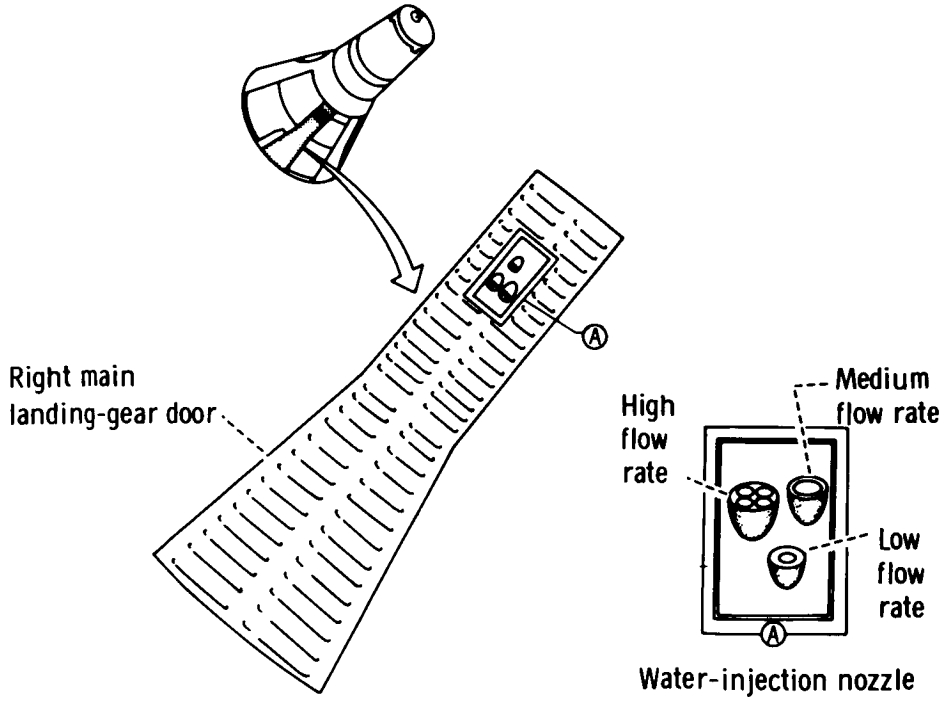

Figure 2.- A detailed view of the equipment location.

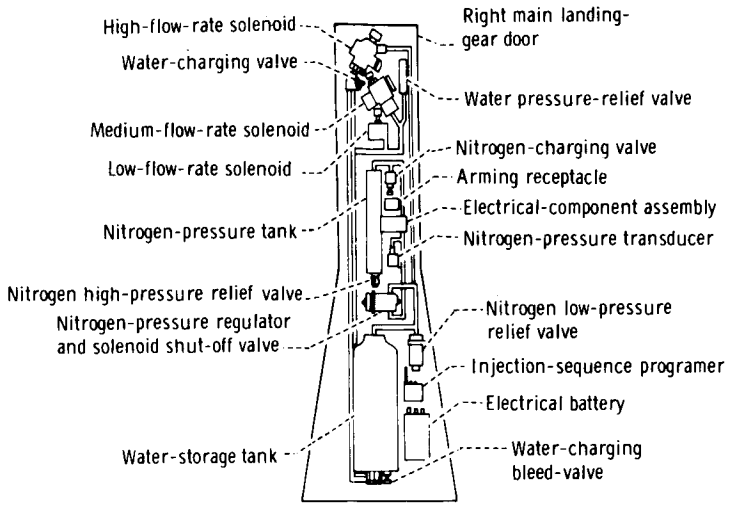

Figure 3. - The equipment installation inside the right-hand main-landing-gear door.

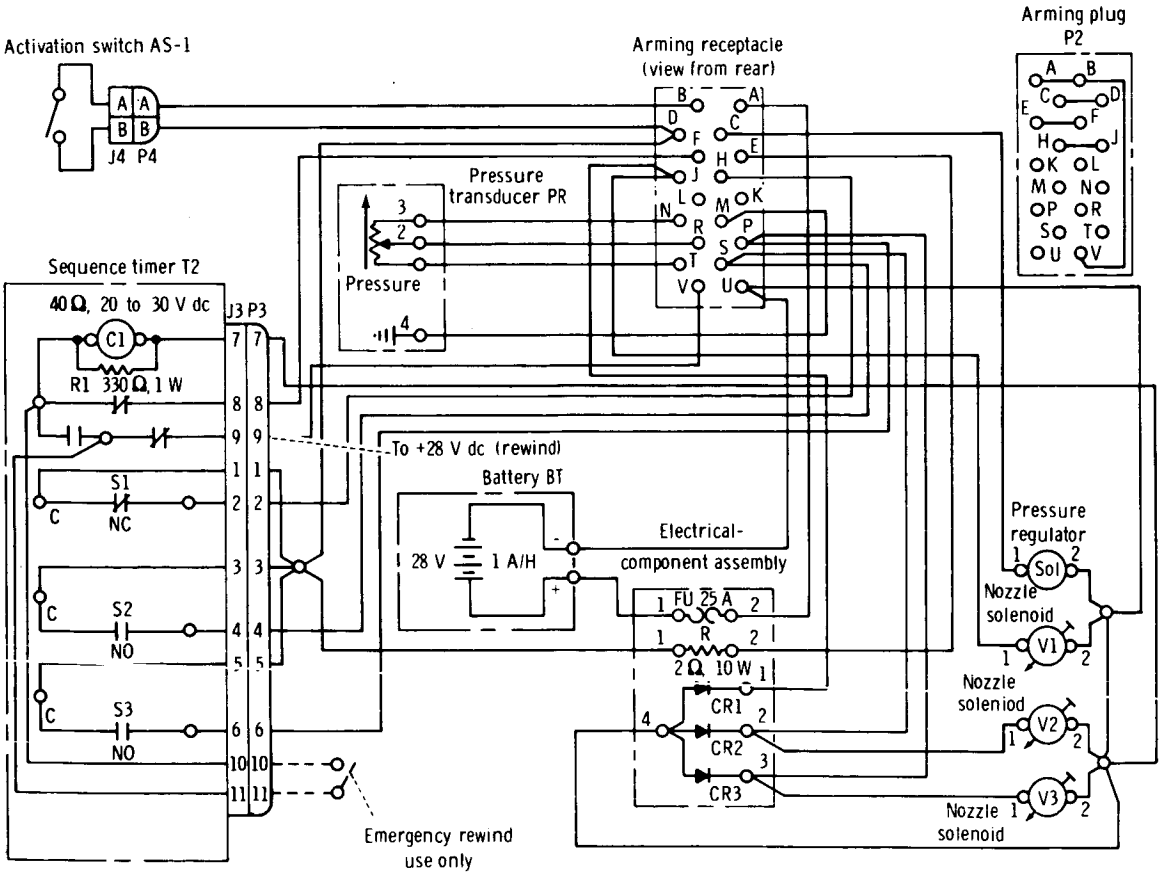

Figure 4. - A wiring diagram of the experimental equipment.

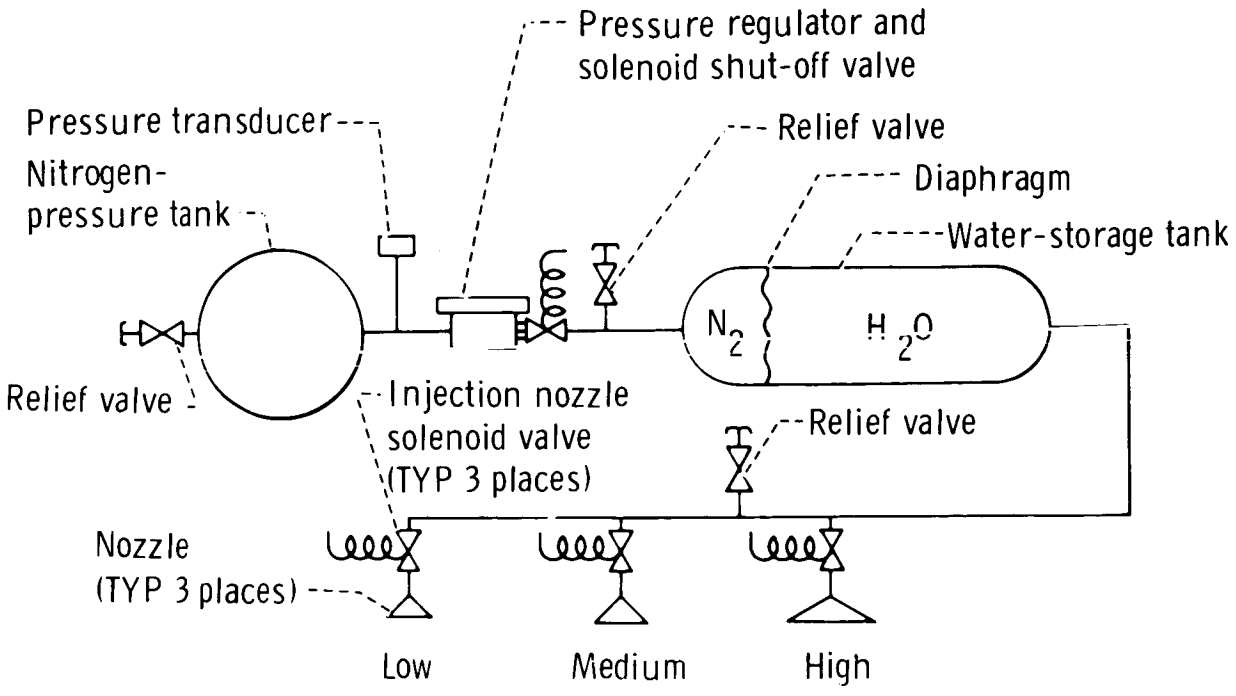

Figure 5.- A schematic of the experimental equipment.

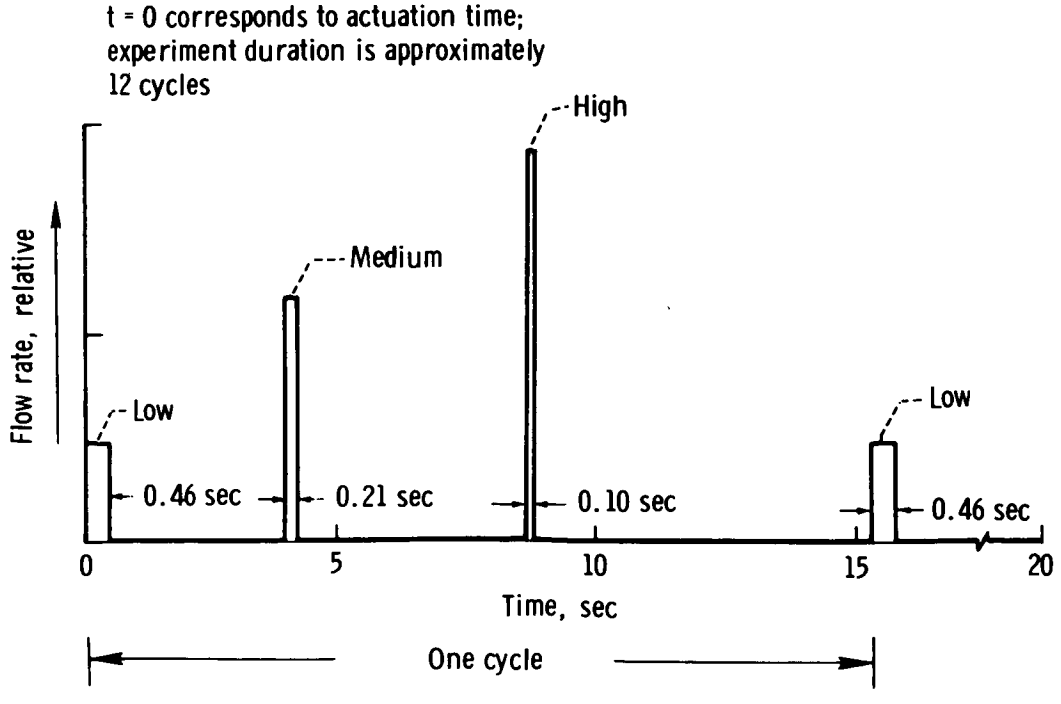

Figure 6.- The flow-rate cycle for the entry-communications experiment.

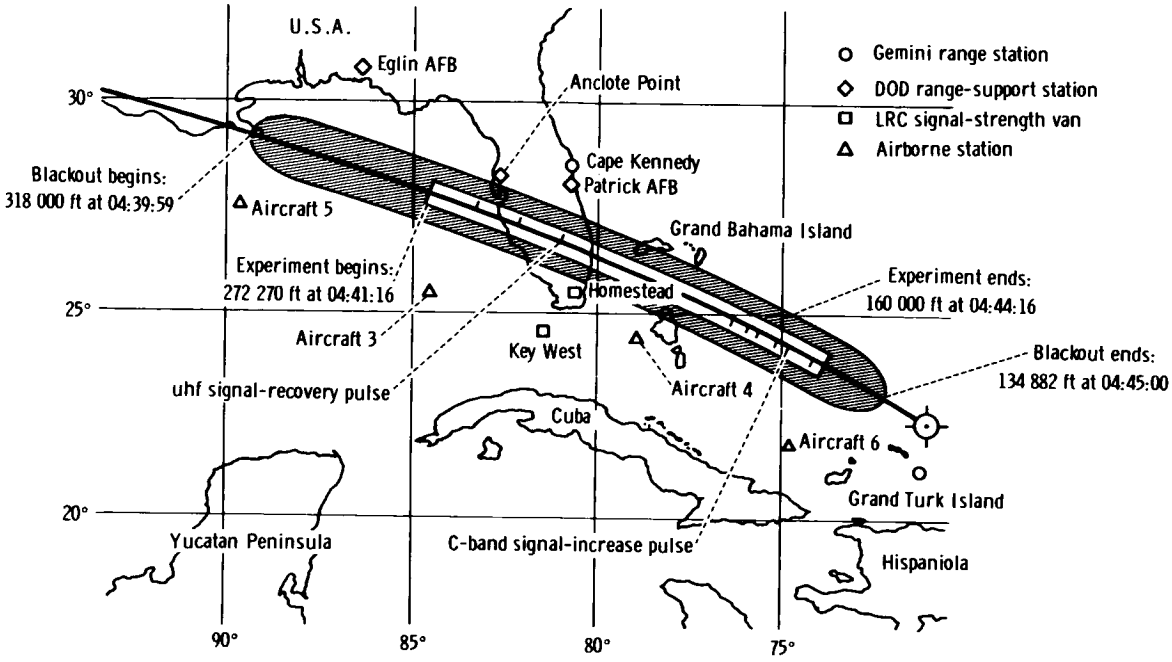

Figure 7.- The ground-based-station locations for Experiment T001.

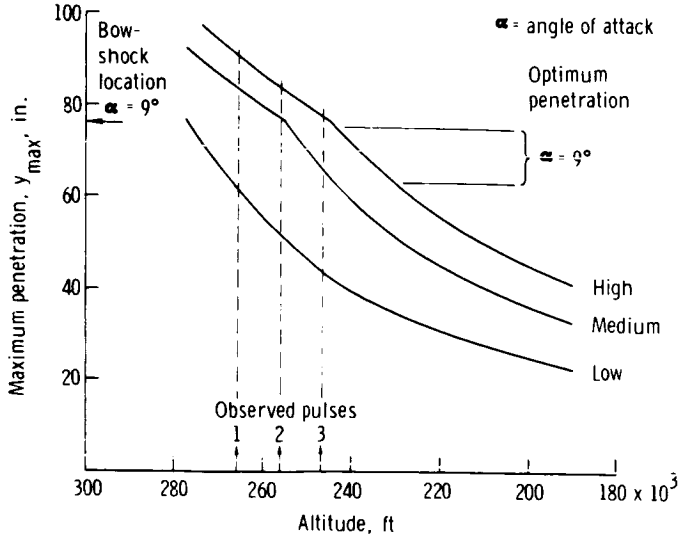

Figure 8.- A plot of the required penetration.

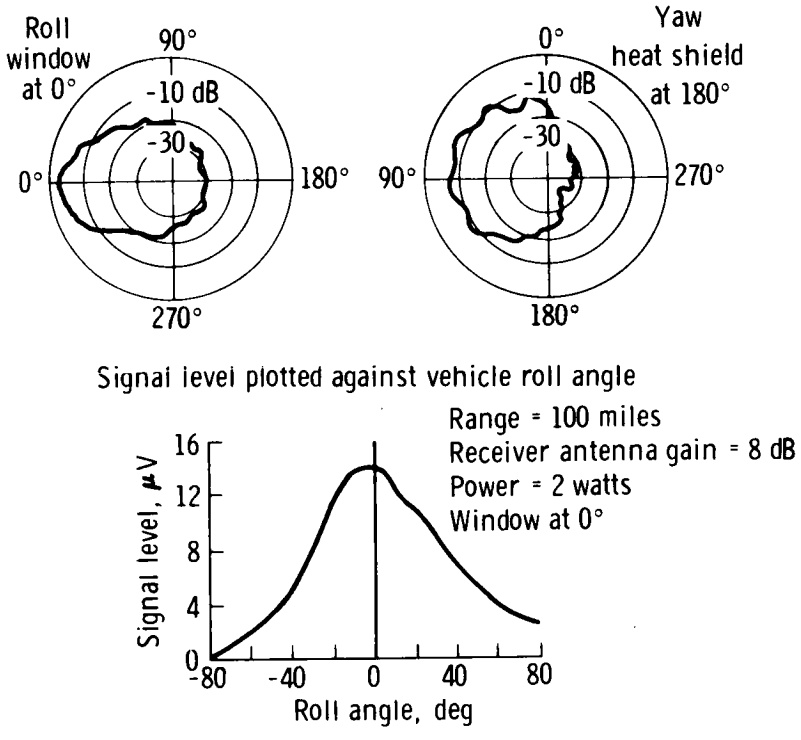

Figure 9. - Simulated antenna patterns.

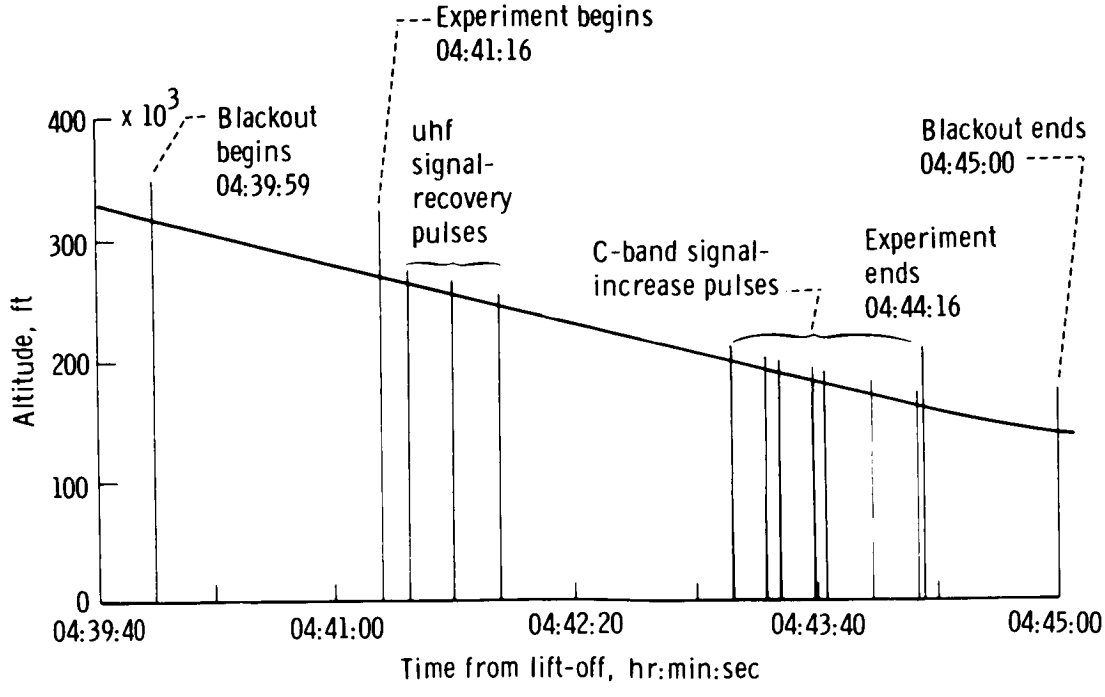

Figure 10. - A plot of entry altitude/time change.

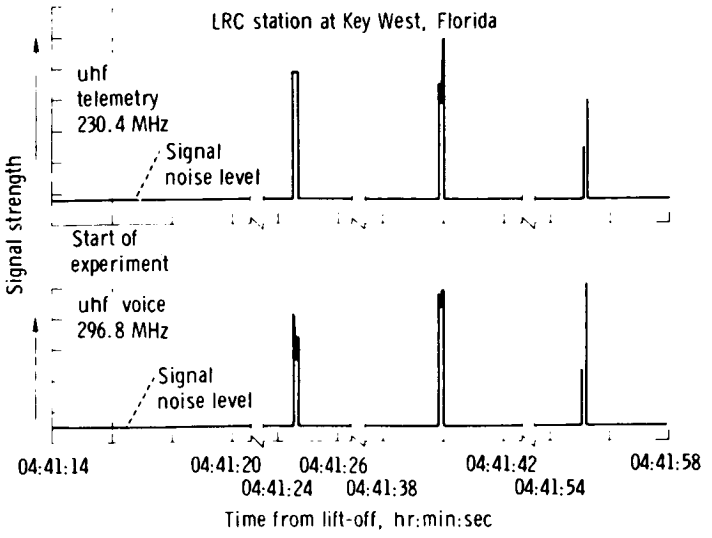

Figure 11.- A plot of signal strength.

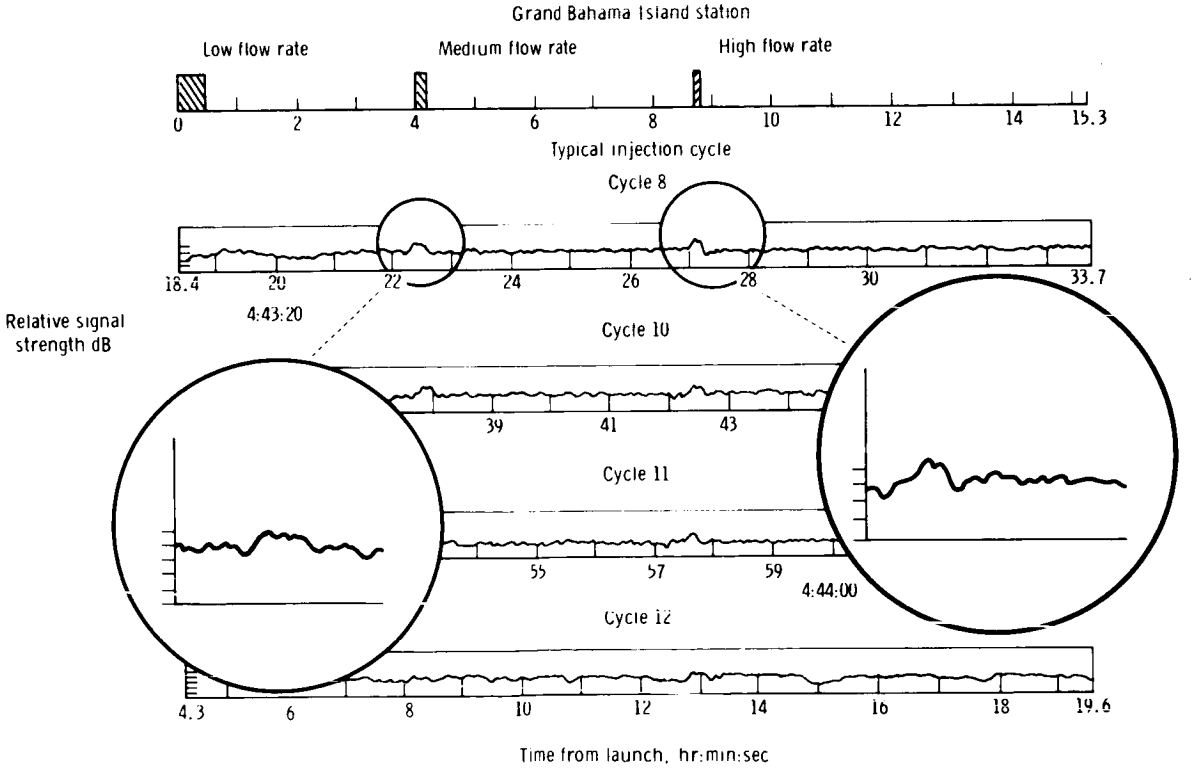

Figure 12.- The time history of C-band strength.

EXPERIMENT D014

ULTRAHIGH AND VERY HIGH FREQUENCY POLARIZATION

By Robert E. Ellis*

INTRODUCTION

Experiment D014 was flown on the Gemini VIII and IX missions. Because of early termination of the Gemini VIII mission, no results were obtained on the experiment. The purpose of Experiment D014 was the measurement of the inhomogeneities in the electron content along the orbital path of the spacecraft. Such measurements would facilitate insight into the structure of the lower ionosphere and its temporal variations. The experiment was performed by transmission of two continuous-wave (cw) signals from the spacecraft and reception of the signals at special ground-based receiving stations. Two receiving stations, one at Kauai, Hawaii, and the other at at Antigua, British West Indies, were used in the measurement of the amount of rotation (caused by the Faraday effect) that was introduced into the signals along the transmission path. The rotation angle was recorded as a function of time when the spacecraft passed over each receiving station. The rotation angles were entered into a computer program that was used to calculate the electron content.

BACKGROUND INFORMATION

Source of Experiment D014

The concept of this experiment evolved out of ionospheric measurements conducted by the staff of the U.S. Naval Research Laboratory (NRL), Washington, D.C. The 150-foot-diameter dish radar system (at Randall Cliffs, Maryland) was used. These measurements involved radar-signal returns from the moon and satellite signal transmissions.

The Scientific Need for Experiment D014

Free electrons in the ionosphere result in the fading of radio signals that transverse all or part of the ionosphere. There are three types of fading: absorption, scattering, and the Faraday effect. At frequencies of 40 megahertz or lower, radio signals (under increased solar activity) can be absorbed completely, resulting in a complete

*U.S. Naval Research Laboratory, Washington, D.C.

loss of signal. Scattering by the inhomogeneities in the electron distribution results in scintillation or rapid fluctuation of the signal level. The Faraday effect (rotation of the plane of polarization of a linearly polarized radio wave in the presence of electrons in a magnetic field) may cause either regular or irregular fading, depending upon the condition of the ionosphere. An increased understanding of the forms of radio-wave perturbation is of fundamental importance to communication engineers and physicists. The size of the inhomogeneities in the electron distribution is of special importance because inhomogeneities cause irregular fading of radio waves. Also, the altitude dependence of the irregularities in electron distribution is of interest in a study of the origin of perturbations.

The Military Need for Experiment D014

The electron content of the ionosphere will have a direct effect upon any radio signal originating in, received in, or passing through the ionosphere. Therefore, knowledge of the nature and perturbation of the electron content is of military importance because it will be related directly to the behavior of signals, communications, radar, and so forth used by the military. Several methods have been used to measure the irregularities in the electron distribution. One method involves radioastronomic techniques (two antennas and a suitable correlation analysis). By the use of this method, it is not possible to distinguish between large irregularities with slow motion and small irregularities with rapid motion. Signals from radio sources in the cosmos and signals or radar returns from superionospheric satellites, are used in another method that results in an integrated picture of ionospheric irregularities along the line of sight. From the military applications point of view, much interest is concentrated on the inhomogeneities in the lower regions of the ionosphere. Data from these lower regions are sparse. The Gemini spacecraft orbited in the lower ionosphere and moved rapidly; thus, the spacecraft was an ideal platform for use in the determination of a rapid cross section of the region of interest.

THEORY

The theory that is involved in the Faraday-effect method of determination of the electron content of the ionosphere is relatively simple and has been used regularly in ionospheric investigations. The Faraday effect may be defined as the rotation of the plane of polarization of a linearly polarized radio wave. The rotation of the electric vector of the radio wave is directly proportional to the electron content along the path of propagation and to the component of the magnetic field of the earth parallel to the path, and the rotation is inversely proportional to the square of the radio frequency.

Under conditions of quasi-longitudinal propagation and at frequencies greater than 100 megahertz (at which the plasma frequency and gyro frequency are relatively small), the Faraday rotation is defined in equation (1).

$$\Omega = 2.97 \times 10^{-2} f^{-2} \int_0^S (H \cos \theta) N \, ds \qquad (1)$$

where: Ω = rotation angle, radians

f = radio frequency, hertz

S = distance from the ground antenna to the spacecraft, meters

H = total magnetic-field intensity, ampere-turns per meter

θ = angle between the ray path and the magnetic-field vector, degrees

N = electron density, electron/m^3

s = distance measured along the ray path, meters

At frequencies below 100 megahertz, equation (1) is invalid because of the high-frequency approximation used in its derivation. Also, at frequencies less than 100 megahertz and at low-elevation angles, extreme refraction and path-splitting effects introduce additional complications. At lower frequencies, the Faraday rotation may exceed a complete revolution, resulting in an ambiguity $M\pi$ in the number of revolutions. One method for removal of this ambiguity is the use of two frequencies, one at very high frequency (vhf) and one at ultrahigh frequency (uhf); one frequency should be high enough that the total rotation angle cannot be ambiguous. For this experiment, using a spacecraft altitude of 160 nautical miles, the rotation angle always should be less than 180° at a frequency of approximately 400 megahertz. By the use of a second frequency in the 100-megahertz range, accurate measurements without ambiguity can be made.

Selection of the exact radio frequencies was influenced by several factors, in addition to frequency-spectrum availability. The first factor, variations in the predicted subsatellite electron content, was a function of sunspot activity, solar zenith angle, and spacecraft altitude. The second factor, variations in the effective magnetic-field parameter, was a function of the field-station location and spacecraft orbital paths. The third factor, total angular-orientation error, was a function of the spacecraft antenna orientation, the purity of polarization of the transmitted signals, and the measurement errors. The first two factors could be estimated readily and adequately, but the third factor was more difficult to assess. With the selected frequencies of 133.9 and 401.7 megahertz, and with an assumed error of 5° root mean square, it was determined that a subsatellite electron-content error of from 3.5×10^{14} to 7.0×10^{14} electrons/m^2 would be obtained. Because the anticipated subsatellite electron content was approximately 1.5×10^{17} electrons/m^2, an error of approximately 0.2 to 0.4 percent was expected. The accuracies were somewhat less during nighttime measurements because the total subsatellite electron content (approximately 5×10^{15} electrons/m^2) was anticipated.

EQUIPMENT

Description and Design

For convenience, this aspect of the discussion of the experimental equipment is divided into several topics.

Nomenclature and function. - The equipment used for Experiment D014 was divided into two categories: equipment located in the spacecraft and equipment located on the ground. The spacecraft equipment was as follows.

1. A dual-frequency transmitter, which generated the two harmonically related coherent cw signals requisite for the experiment

2. A diplexer, which combined the two outputs of the transmitter into a single output so that both frequencies could be transmitted (through a single coaxial line) to a single antenna without interaction between the two transmitter outputs

3. A colinear dipole antenna, which functioned as a means of transmission of the two frequencies with linear polarization from the spacecraft to the ground

4. An antenna boom assembly, which functioned as antenna storage inside the spacecraft prior to launch and functioned as a means of extension of the antenna to the proper distance outside the spacecraft during orbit

The ground-based equipment for the receiving system was as follows.

1. A 28-foot-diameter dish antenna, with feed and pedestal, which received the cw signals transmitted from the spacecraft and separated each frequency into vertical-polarization and horizontal-polarization components

2. A dual-channel receiver, which was used to amplify and heterodyne the horizontal and vertical components of the 133.9-megahertz signal to a frequency of 120 kilohertz for display (also used to detect the envelope of the 120 kilohertz signals for display)

3. A dual-channel receiver, which served the same function as the other receiver, except that it operated at the 401.7-megahertz frequency

4. An X-Y scope, which was used to display the Faraday rotation angle of the two signals

5. A 35-millimeter frame-by-frame camera, which was used to record photographically (at the rate of 2 frames per second) the Faraday rotation angle displayed on the X-Y scope

6. A tape recorder, which was used to record the 120-kilohertz intermediate frequency (i.f.) signals out of the dual-channel receivers

7. A chart recorder, which was used to record the envelope of the 120-kilohertz signals out of the receiver

8. Camera control units, which were used to control electronically the frame rate and exposure time of the 35-millimeter frame-by-frame cameras

9. An attenuator control, used to reduce the input signal level into the receivers if this level became too high, which generated tones for recording attenuator setting on the magnetic tape, and which controlled attenuator-indicator lights in the recording cameras

Physical description of equipment. - The dual-frequency transmitter was constructed of all solid-state circuitry and was housed in a rugged 6- by 7- by 3.5-inch chassis. The chassis was composed of two units, one of which contained the voltage regulator, filters, and dc-to-dc converter and the other of which contained the radio-frequency (rf) circuits. These rf circuits were encapsulated in a foam epoxy so that, after two units were assembled as a complete transmitter, they were essentially a solid unit. The total weight of the transmitter was 6 pounds. Photographs of the transmitter are shown in figures 1 to 3, and circuit diagrams of the power supply and rf portions of the transmitter are shown in figures 4 and 5, respectively. The diplexer used in this experiment had dimensions of 2.7 by 4.5 by 4.1 inches and weighed 1.2 pounds.

The colinear dipole antenna consisted of two colinear sections. One section, which served as a choke to keep the rf radiator off the boom mount, was 2 inches in diameter and 14 inches long; the other section was five-sixteenths of an inch in diameter and 31 inches long. The small-diameter section was hinged at two points: at the junction to the choke section and at its midpoint. To facilitate mounting in the spacecraft, these hinged joints were spring loaded so that the thin-diameter section could be folded to a length of 15.7 inches. During orbit, the antenna was unfolded automatically by the spring loading when it was extended outside the spacecraft. Photographs of the antenna are shown in figures 6 and 7. The total weight of the antenna was 2 pounds. The extendable antenna boom could extend the colinear dipole antenna 120 inches from the stowed position. The overall dimensions of the boom mechanism were 13.25 by 7 by 5.40 inches, and the weight of the unit was 11 pounds. A photograph of the antenna boom assembly with the antenna mounted is shown in figure 8.

Because the equipment that was used in the ground-based receiving station was predominantly standard commercial equipment, only the dual-channel receivers will be described. The physical characteristics of the two dual-channel receivers were the same. The overall dimensions were 19 by 17 by 5.25 inches; the total weight of one unit was 36 pounds.

System description and operation. - Experiment D014 involved a transmission system that was mounted in the spacecraft, and a reception system and two recording systems that were located on the ground. A block diagram of the transmitter system mounted in the spacecraft is shown in figure 9. In the spacecraft system, two cw signals, one at 133.9 megahertz and the other at 401.7 megahertz, were generated from a common crystal-controlled oscillator that fed separate channels of the appropriate multiplying and amplifying stages. The two signals out of the transmitter were fed into a diplexer in which they were combined to supply a single common output. The output

of the diplexer was connected to the colinear dipole antenna through the coaxial cable in the extendable antenna boom. The two cw signals were radiated with a linear polarization mode from the antenna.

Before beginning the experiment, the crewmembers were required to extend the dipole antenna outside the spacecraft. This was accomplished by positioning the antenna control switch to the EXTEND position, energizing the boom mechanism, and causing the boom to extend. When the experiment was performed while flying over either of the two receiving stations, the crewmembers turned on the transmitter and positioned the spacecraft to point the antenna toward the center of the earth. This maneuver required a 158° roll to the right and a 17° nosedown pitch, based on the assumptions that the spacecraft was in position and that the crewmembers were sitting upright in what might be considered as normal aircraft attitude. The spacecraft yaw had to be controlled so that its longitudinal axis was perpendicular to the orbit path, with the nose of the spacecraft pointing away from the ground-based station. While the spacecraft was over the ground-based station, this attitude had to be maintained from radio horizon to radio horizon. After the spacecraft passed beyond the line of sight of the station, the transmitter was turned off, and any spacecraft attitude could be maintained or assumed.

A block diagram of one of the ground-based receiving stations (which were identical) is shown in figure 10; a composite photograph of the station equipment is shown in figure 11. The receiving antenna was a 28-foot parabolic dish and had a special cross-dipole feed system that separated the signals into vertical and horizontal components. When the spacecraft was operating for the experiment during any station overflight, the receiving antenna was slaved from nearby tracking radar so that it pointed at the spacecraft. As the two cw signals were received from the spacecraft transmission, the antenna feed separated each signal into vertical and horizontal components. The vertical components of each frequency were fed down a single coaxial line to a frequency-separating filter. The filter had two outputs, one of which was the vertical component of the 133.9-megahertz signal, and the other was the vertical component of the 401.7-megahertz signal. The horizontal components of the two frequencies were separated in a similar manner in an identical filter. The vertical and horizontal components of the 133.9-megahertz signal were fed into the two channels of the 133.9-megahertz receiver, and the 401.7-megahertz signal components were fed into the 401.7-megahertz receiver. In each receiver, common local oscillators were used to maintain similar phase characteristics between the two channels. After conversion to 120 kilohertz in the 133.9-megahertz receiver, the vertical and horizontal signal components were fed into the vertical and horizontal amplifiers of the X-Y scope. In this manner, the Faraday rotation angle was reproduced. For example, if the rotation angle was 45°, both the horizontal and the vertical signal components out of the receiver would be equal, and a 45°-angle line would be traced on the face of the scope. The 120-kilohertz i.f. signals from the 401.7-megahertz receiver were displayed in the same manner on a second X-Y scope. Both of the scope displays, a clock, and the attenuator-position-indicator lights were photographed at a rate of approximately 2.5 frames per second. At the same time that the 120-kilohertz i.f. signals were displayed on the X-Y scopes, they were recorded on magnetic tape. In this manner, the tape could be played back into an X-Y scope, and the original display could be examined and reexamined as desired. Also, time and rf-attenuator settings were recorded simultaneously on the magnetic tape. The four i.f. signals (two in each receiver) also

were detected, and their envelopes were recorded on a four-channel chart recorder. The vertical and horizontal component envelopes of each signal fluctuated roughly as simultaneous sine and cosine plots. These records could be examined later, and information regarding the perturbation in electron content along the spacecraft path could be extracted from the short time fluctuation in the envelopes. Only time information was recorded directly by the chart recorder; the attenuator setting was entered manually.

Development

Testing, technical problems, and quality assurance were component aspects of the equipment development effort. Each of these topics is discussed separately.

Testing. - Both the diplexer and the extendable antenna boom were modifications of equipment that was used on other spacecraft. The diplexer was a minor modification of the diplexer that was used in the Gemini communications system, and the boom mechanism was similar to the high-frequency recovery-antenna boom. Therefore, only the dual-frequency transmitter and the colinear dipole antenna will be discussed. Experience with solid-state circuitry was indicative that proper operation over a wide range of temperature environments was one of the more difficult problems. As a result, all transmitter circuits, the power-supply regulator, the dc-to-dc converter, and the rf circuits were subjected to temperature tests at all stages of development. The primary objective was to develop circuits that would have the desired frequency and output-power stability and that would have a supply-voltage variation of 20 to 33 volts over a temperature range of -60° to +160° F without the use of a cold plate. This objective was achieved for the 133.9-megahertz output, but could be achieved only over a temperature range of -40° to +160° F for the 401.7-megahertz output. The major problem in the development of the colinear dipole antenna was operation at both frequencies with a minimum amount of cross-polarized signal at either frequency. Difficulty was encountered in the development of a pattern measurement range that would result in a true indication of the direct and cross-polarized signals. In this effort, 1/5- and 1/10-scale models were used, and both indoor and outdoor pattern ranges were used. The pattern measurement range that was devised finally and that was used for the final measurements was outside, and it involved a 1/10-scale model of the spacecraft and antenna.

The qualification models of both the transmitter and the antenna were subjected to environmental tests (performed by the contractor) regarding temperature, pressure, humidity, acceleration, random vibration, acoustic noise, and radio interference. No problems were encountered during these environmental tests, and both the transmitter and the antenna were qualified for space operation. Before the final models of the transmitter were delivered to the contractor, each model was subjected to a random-vibration test. Also, each transmitter was subjected to a modified temperature test, in which a scale time of only 8 hours was used at each of the temperature extremes of -60° and +160° F, instead of a 24-hour scale period. All transmitter units functioned properly during the predelivery acceptance (PDA) tests. The antennas were subjected to modified random-vibration tests that were identical to the tests described for the transmitters. These tests were made before application of the white radiator paint. Because this paint surface was damaged easily, only a voltage standing-wave ratio (VSWR) test was made on the antennas immediately before shipment. No problems

were encountered in the PDA tests. During the preinstallation acceptance (PIA) tests, it was observed that the power output from all three transmitters was less than the power measured before shipment. It was determined that this power reduction was caused by a difference in the terminating impedance of the 133.9-megahertz coaxial line out of the transmitter during the two measurements. At the NRL, the line was fed into a band-pass filter and then into the 50-ohm attenuator for power measurements. The line was terminated in the diplexer and then fed into the 50-ohm attenuators. In one case, the band-pass filter appeared to be a resistive load, whereas the diplexer appeared to be a reactive load. This problem was resolved by adjustment of the transmitter output networks after the transmitter had been mounted in the spacecraft. After the transmitters were adjusted under these conditions, the proper power outputs were obtained at the proper frequencies. During the PIA tests of the antenna, it was discovered that the coaxial cable in the prototype antenna boom contained a bad VSWR. As a result, the tests had to be performed with the antenna mounted on a ground plane, instead of mounted on a boom above a ground plane. Similar measurements had been made at the NRL, so the slight changes in VSWR that resulted from this measurement setup were predicted. As a result, the VSWR measurements were acceptable, and no further problems were encountered during the performance of PIA testing.

Technical problems. - Only minor difficulties were encountered with the 133.9-megahertz channel of the transmitter during the development program. Very little work was required in order to get this channel to operate over the temperature range of -60° to +160° F without the use of a cold plate. In the development program, only one serious problem was encountered in the 401.7-megahertz channel. This problem concerned the 200- to 400-megahertz doubling circuit, which would not operate properly at temperatures below -20° F. Changes in transistor type and circuit configuration resulted in some improvement, but did not result in satisfactory operation. After a cold soak at -60° F, this channel required 3 or 4 minutes of warmup before the proper power output and stable frequency conditions were obtained. It was decided to replace the transistor-doubler stage with a varactor-diode doubler. This modification solved the problem, and satisfactory performance was obtained after the proper alinement technique was developed. Basically, this technique consisted of a readjustment of capacitive reactance of the circuits to match the varactor impedance to that of the final amplifier, after the unit had stabilized at -35° F.

Development of the colinear dipole antenna was a problem. Spacecraft space limitations necessitated the use of a single antenna for both frequencies and limited the size of the antenna. These two factors caused difficulties in the establishment of good direct-illumination patterns at both frequencies with low cross-polarization patterns and in simultaneously obtaining a good 50-ohm match at both frequencies. In general, the solution to the antenna problem was empirical. That is, a unit was designed for both the dipole-element length and the impedance-matching transformer. This unit was constructed and tested, and the design was modified, on the basis of the results obtained from the first model, until a satisfactory unit was obtained.

Measurement of the antenna cross-polarized signal, a measurement not of interest ordinarily, presented difficulties throughout the development program. Variations in these measurements were indicative that much of a cross-polarized pattern was contributed by surrounding objects rather than by the antenna. An outdoor measurement range, in which both the spacecraft model with scale antenna and the pattern-range antenna were mounted high above the building roof, was proven to be

satisfactory. In this arrangement, the pattern-measurement antenna was mounted as close to the model antenna as possible, yet remained in the far field.

Quality assurance. - Before the requirement for Government-source inspection of all component parts was made known to the NRL, all component parts had been purchased for the transmitters and antennas. It was considered too costly and the time schedule was too short to scrap all these component parts and reorder. However, all parts were of the highest quality and were of the type that had been used in other projects that involved space-type environmental operation. Also, all parts were inspected carefully and were tested before being used in the equipment. During the construction of the transmitters, regular inspections were made for proper wiring, soldering, and cleaning. After wiring was complete and before final encapsulation and assembly, the units were inspected again. Also, the antenna was inspected carefully for mechanical assembly and structure.

Equipment Integration

The integration of equipment into the spacecraft is discussed conveniently on the basis of schedule, testing, and technical problems.

Schedule. - This experiment was relatively simple regarding integration of the equipment into the spacecraft; only three pieces of equipment were involved: the transmitter, the diplexer, and the antenna. The transmitter and diplexer only had to be mounted to a cold plate and a bracket, respectively, in the equipment module and the necessary supply and signal cables had to be installed. More care was required in the integration of the antenna and its boom assembly into the spacecraft. The boom assembly had to be alined to facilitate accurate positioning of the antenna in the extended configuration. Also, guide blocks were needed to support and guide the upper portion of the antenna when it was folded and retracted into the spacecraft. Some difficulty was encountered in obtaining the proper fit and alinement of the guide blocks. In the process of adjusting these blocks, several upper elements of the antenna were damaged. Even after proper adjustment of the guide blocks, it was necessary to hand-guide the folded element into the lower set of guide blocks to prevent damage to the antenna. The integration problems encountered in this experiment were simple enough that the spacecraft schedule did not constrain the equipment-integration schedule.

Testing. - After the equipment was installed in the spacecraft at the contractor facility, no further tests were performed on the antenna. Immediately before shipment of the spacecraft to Kennedy Space Center (KSC), half of the workstand was removed, and the antenna boom was extended to its full length. The transmitter power output and frequency were measured before shipment of the spacecraft. During the "Plan X" test on the timber tower at KSC, the antenna was extended, and signals from the transmitter were radiated. These radiated signals were monitored at the communications hangar, and the frequency and relative signal strength were measured. Also, the spectrum of the transmitter signals was tested for spurious radiation. During the Service Engineering Department tests on the launch pad, the antenna boom was energized momentarily to extend the antenna a few inches. The boom was then energized to retract the antenna to the fully retracted position. The cable from the diplexer was disconnected, and a power meter was connected to the output of the diplexer, after which the total output power of the transmitter was measured. After the power measurement was completed, an

antenna mounted external to the launch pad white room was connected to the output of the diplexer. When the transmitter was turned on, the radiated signals were monitored at the communications hangar; and the frequency, spectrum, and relative signal levels were measured. After the completion of this test, all cables were reconnected and no further tests were made on the equipment.

Technical problems. - The major problem encountered during equipment integration was the mechanical fit of the antenna in its launch housing. Guidance of the antenna into the housing during retraction was difficult without damage to the small-diameter portion of the antenna. This problem was solved by careful adjustment of the guide block. During "Plan X," some spurious radiation was observed on both sides of the cw carrier frequencies. These responses were eliminated by means of a slight readjustment of the circuits in the transmitter.

FLIGHT TEST

For convenience, the discussion of the flight test is divided into four topics regarding the planned mission, training, the actual mission, and the equipment performance.

Mission as Planned

The procedure necessary to operate the equipment for this experiment was quite simple and required a minimum of effort on the part of the crewmembers. The operation of the equipment involved only the activation of two switches, the ANTENNA EXTEND switch and the TRANSMITTER ON switch. The primary effort on the part of the crewmembers was expended in maintenance of the attitude of the spacecraft to point the antenna toward the center of the earth. Primarily, integration of the operational procedures into the flight plan concerned the method of spacecraft-attitude control. Three modes of spacecraft control were detailed and written into the procedures. The first mode involved the use of the stable platform and the computer; therefore, it was the most accurate mode and the mode that would be preferred, even though it resulted in the greatest power consumption. The next most desirable mode also involved the use of the platform, but not the computer. Pitch and yaw were to be maintained by reference to the eight ball. The least desirable mode of operation did not involve the use of either the platform or the computer; attitude was to be maintained by use of a reticle mounted on the window and referenced to the horizon.

Another problem in integrating the operational procedure into the flight plan involved the antenna. Because the small-diameter end of the antenna was folded and was spring loaded to deploy the first time it was extended, the antenna could not be retracted fully. When the antenna boom was retracted, after having been extended the first time, approximately 26 inches of the small-diameter portion of the antenna remained beyond the surface of the spacecraft. In addition to being a possible extravehicular-activity (EVA) hazard under such conditions, the antenna was subject to being bent during EVA. A bent antenna would have destroyed the necessary linear polarization, negating the experiment. As a result, it was decided not to deploy the antenna until after EVA was completed.

The only problem encountered in the integration of the experiment into the mission plan concerned the number of times the experiment was to be conducted. Because the experiment was statistical in nature (hence, the more data the better), and because no data were obtained from the Gemini VIII mission, a minimum of 10 experiment operations over each of the two ground-based stations was requested. Because of other mission operations, only four operations over each of the ground-based stations were scheduled in the final flight plan. This plan involved performance of the experiment during orbits 26, 27, 30, and 42 over the Antigua station and during orbits 30, 32, 33, and 34 over the Kauai station.

Crewmember Training

The crewmembers were given a formal briefing on the objectives of the experiment and on the anticipated procedures and problems. Because the operational procedures for this experiment were quite simple, it was concluded that no special training would be required. Crewmembers were of the opinion that any training needed to maintain spacecraft attitude would be covered adequately by the normal flight-simulator training.

Gemini IX Mission

There were no deviations from the planned operational procedure for the experiment insofar as the operation of the experimental equipment was concerned. However, the experiment operation did not conform to the planned mission because the entire mission was modified after the first rendezvous operation. Because of the change in mission plan, Experiment D014 was conducted before EVA. Six operations of the experiment was executed, one over Antigua during orbit 18 and five over Kauai during orbits 17, 18, 19, 20, and 21. Three more operations had been scheduled over the Kauai station during orbits 34, 35, and 36, but the experiment antenna was damaged during EVA.

Equipment Performance

During each of the operations over both ground-based sites, the received signals were about 30 decibels lower than had been planned. Tests were indicative that both ground-based stations were operating properly. Therefore, it was concluded that some of the equipment in the spacecraft was not operating normally. Because there was no telemetry and because all equipment was mounted in adapter sections (which were not recovered), there was no way to determine where the malfunction occurred. Although the signals were approximately 30 decibels below the expected levels, the experiment was designed to produce signals approximately 50 decibels above noise, so that usable results were obtained. The main effect of the lower signals was to reduce the accuracy of the results.

During EVA, the pilot drifted into the antenna, and the antenna broke instead of bending. The reason for the breakage of the 0.25-inch-diameter aluminum tube was

not understood. This member of the antenna was constructed of type 6061T6 aluminum alloy, which was one of the most ductile aluminum alloys; the tube should have bent, not fractured.

RESULTS

The ambiguity-removal and lower-ionospheric slab-thickness determinations for five Kauai transits were accomplished by the use of five-point plots of local azimuth and elevation, which were made available before each transit. The Antigua five-point plot (for revolution 18) was not available. Consequently, only the Kauai transits (which corresponded to revolutions 17, 18, 19, 20, and 21 of the Gemini IX spacecraft) are discussed in this report.

The first step was to determine if the direction and magnitude of the observed Faraday fading were compatible with that which would be predicted on the basis of the theory. Based on the assumption that the subsatellite electron content was invariant, the magnetic-field parameter functions were assumed to be in direct proportion to their respective Faraday rotation functions. Because, without exception, the vhf records were indicative that $\overline{\psi}$ was approximately proportional to Ω_{vhf}, it was concluded that Ω_{vhf} was indeed controlled by changes in $\overline{\psi}$, rather than by changes in electron content C. The subsatellite electron content may be written

$$C = 1.24 \times 10^{13} f_o F_2^{\,2} t \tag{2}$$

where $f_o F_2$ = the F_2-region peak plasma frequency, megahertz

t = the effective subsatellite slab thickness, kilometers

The largest plausible value for the amount of uhf rotation may be estimated by the use of equation (2), the relation

$$\Omega_{uhf} = 2.97 \times 10^{-2} f_{uhf}^{\,-2} \overline{\psi} C \tag{3}$$

and upper limits for the parameters t, $\overline{\psi}$, and $f_o F_2$. A list of $f_o F_2$ and $M(3000)F_2$ for June 4, 1966, over Maui, Hawaii, is shown in table I. By inspection, the maximum value for $f_o F_2$ is noted to be 14 megahertz. Because the Gemini IX satellite orbited at the normal altitude of the F_2 maximum (based upon the approximation of Shimazaki, $hF_2 = [1490/M(3000)F_2] - 176$), it may be shown that the maximum value for $f_o F_2$ is

certainly less than 200 kilometers for a subsatellite Chapman profile of electron density. By the use of $\overline{\psi}$ = 25 ampere-turns per meter, it may be proven that the estimated upper limit for Ω_{uhf} is less than 180° for those points at which $\overline{\psi} \leq 25$ ampere-turns per meter. In fact, four transits of Gemini IX, which occurred on June 4 over Kauai, passed through the quasi-transverse region in which $\overline{\psi}$ is similar to zero; and the remaining transit was such that the minimum value of $\overline{\psi}$ was, at most, 15 ampere-turns per meter. Clearly, Ω_{uhf} was resolvable. As a consequence, estimates of the vhf Faraday rotation were obtained conveniently from the relation

$$\Omega_{vhf} = 9\Omega_{uhf} \tag{4}$$

which may be proven from the fact that the amount of Faraday rotation is inversely proportional to the square of the radio frequency. This relation was strictly applicable only for the quasi-longitudinal mode of propagation and for the mode in which the vhf and uhf radio waves traversed identical paths. However, for the purpose of ambiguity removal, the simple relationship expressed by equation (4) is approximately true.

For all spacecraft transits over Kauai, values of $9\Omega_{uhf}$ were computed and were compared with the measured values of Ω_{vhf}. Except for an expected uhf-data-point scatter, the agreement was sufficient. The scatter of points that corresponded to the uhf data was caused by the fact that the naturally larger reading errors that were associated with the uhf polarization had been magnified nine times. To determine the subsatellite electron content and mean subsatellite ionospheric-slab thickness, values of Ω_{vhf} and $\overline{\psi}$ were determined at the closest point of approach. Values of the content and the slab thickness for those transits in which the closest point of approach did not coincide with the region of quasi-transverse propagation were computed by means of equations (5) and (6).

$$C = 1.04 \times 10^{16}\left(\frac{\Omega_{vhf}}{\overline{\psi}}\right) \tag{5}$$

$$t = \frac{C}{\left(1.24 \times 10^{13}\right)\left(f_o F_2^{\,2}\right)} \tag{6}$$

The term C is expressed in electrons/m^2-column and t is expressed in kilometers. The values of content and slab thickness for transits 18, 19, and 21 are listed in table II.

CONCLUSIONS

Because the tracking information was not available, the primary objective of the experiment (that is, the measurement of inhomogeneities) was not accomplished as of this writing. The use of ultrahigh frequency radio transmission was the primary factor in the successful removal of very high frequency Faraday rotation ambiguity; but, as was expected, this was not very useful for fine-scale polarization studies. Ionosonde data (from Maui, Hawaii) were useful in the computation of the slab thickness at the closest point of approach of the spacecraft. At 08:15 H.s.t., the slab thickness was approximately 146 kilometers, and the content was $7.63 \times 10^{16} m^{-2}$. At 09:50 H.s.t., the slab thickness had decreased to approximately 85 kilometers, and the total content had increased to $7.81 \times 10^{16} m^{-2}$. By 13:01 H.s.t., the slab thickness was approximately 40 kilometers and the content was $6.47 \times 10^{16} m^{-2}$.

TABLE I. - IONOSPHERIC SOUNDING DATA COLLECTED OVER MAUI, HAWAII[a]

[Date: June 4, 1966]

Hour	f_0F_2	$M(3000)F_2$	Hour	f_0F_2	$M(3000)F_2$
0	7.5	2.90	12	10.5	2.70
1	7.8	3.20	13	11.4	2.80
2	7.0	3.20	14	11.9	2.85
3	6.2	3.30	15	12.2	2.90
4	4.5	3.70	16	12.9	2.90
5	3.2	3.00	17	12.7	3.05
6	4.3	3.40	18	14.0	3.25
7	5.6	3.15	19	13.7	3.35
8	6.1	2.45	20	10.0	3.20
9	7.6	2.50	21	8.4	3.10
10	8.9	2.60	22	7.1	2.95
11	9.8	2.70	23	7.8	2.80

[a]Courtesy of the Institute for Telecommunication Sciences and Aeronomy, Environmental Science Services Administration.

TABLE II. - CONTENT AND SLAB THICKNESS FOR TRANSITS 18, 19, AND 21

Transit	Content, C, m^2	Slab thickness, t, km
18	7.63×10^{16}	~146
19	7.81	~85
21	6.47	~40

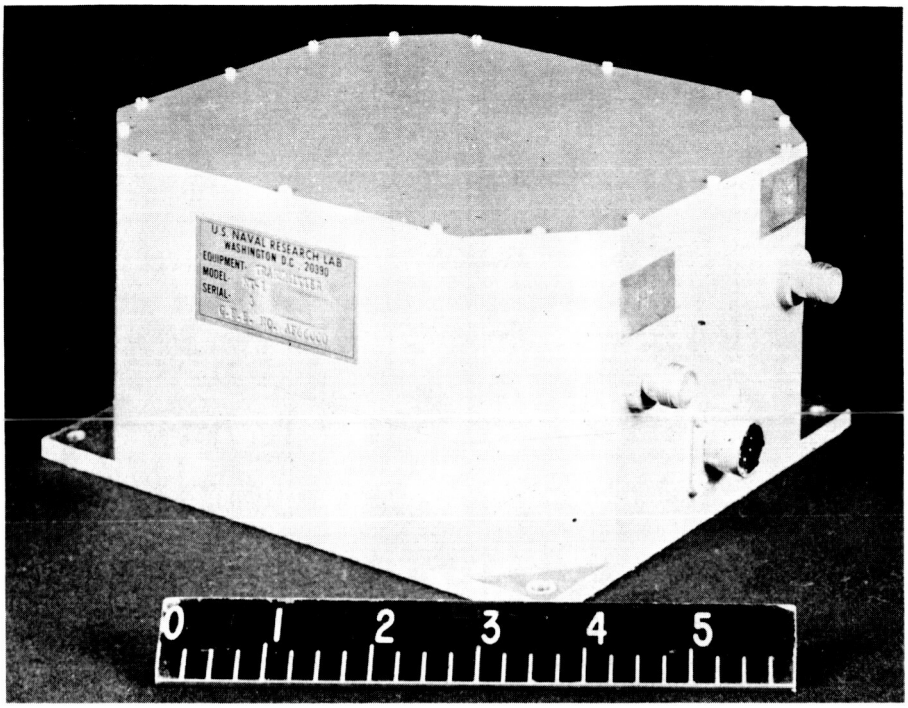

Figure 1. - The transmitter assembly.

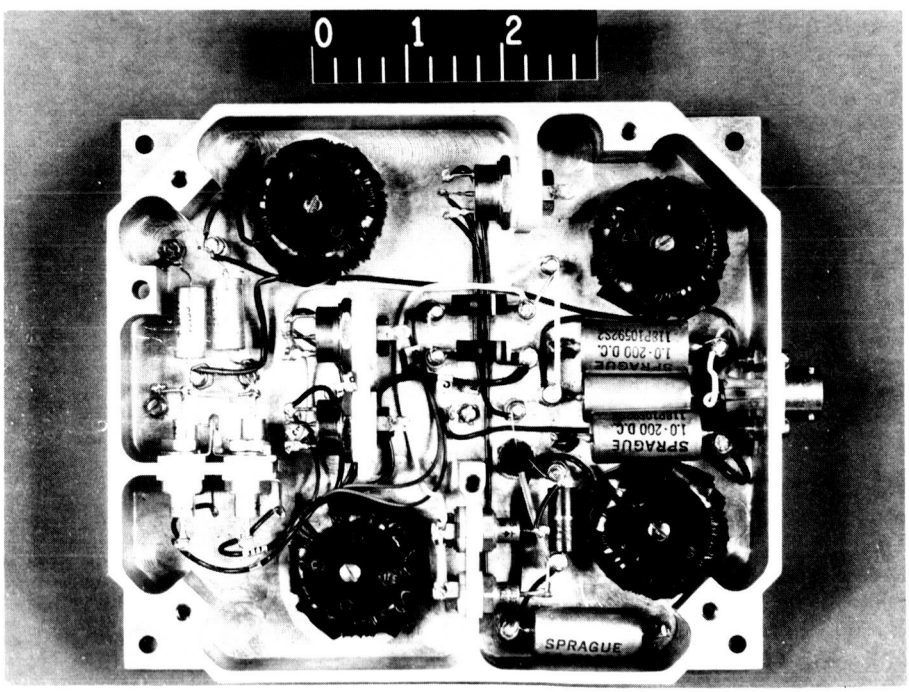

Figure 2. - The transmitter power-supply unit.

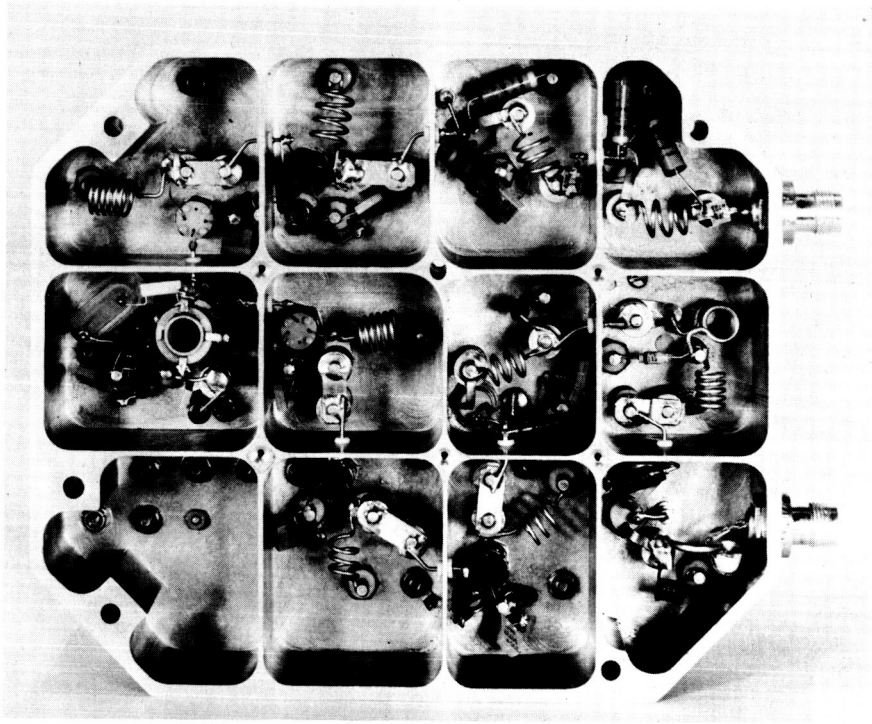

Figure 3. - The transmitter radio-frequency unit.

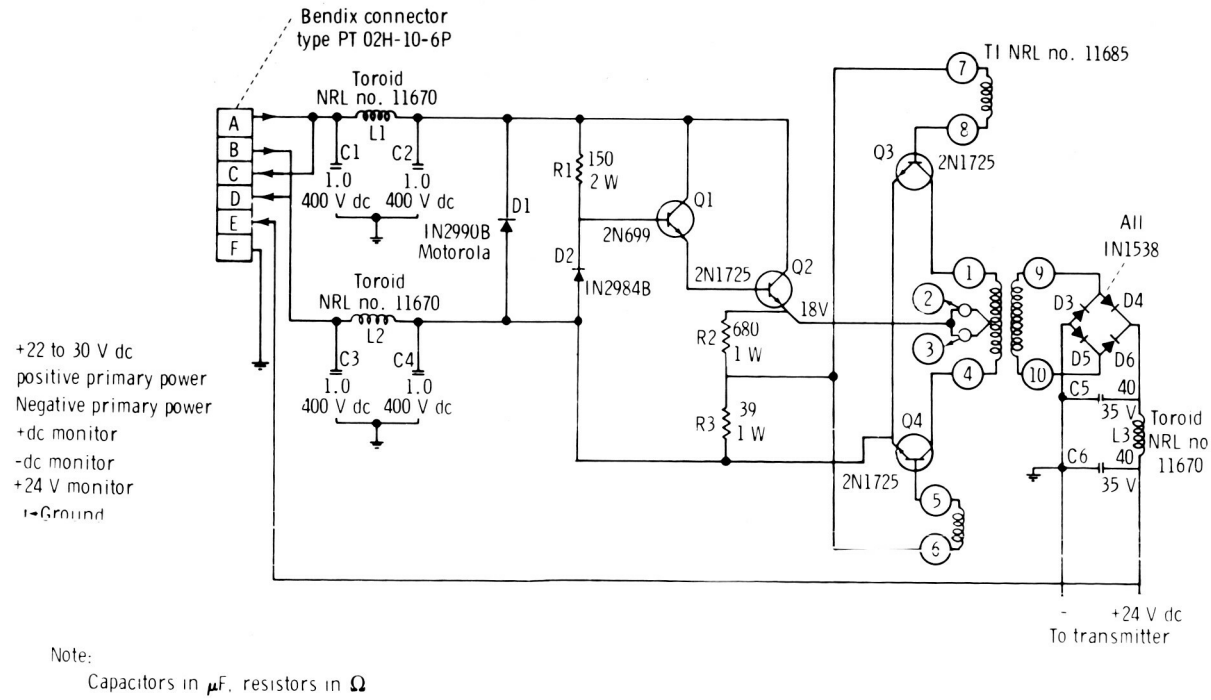

Figure 4. - A circuit diagram of the power-supply unit.

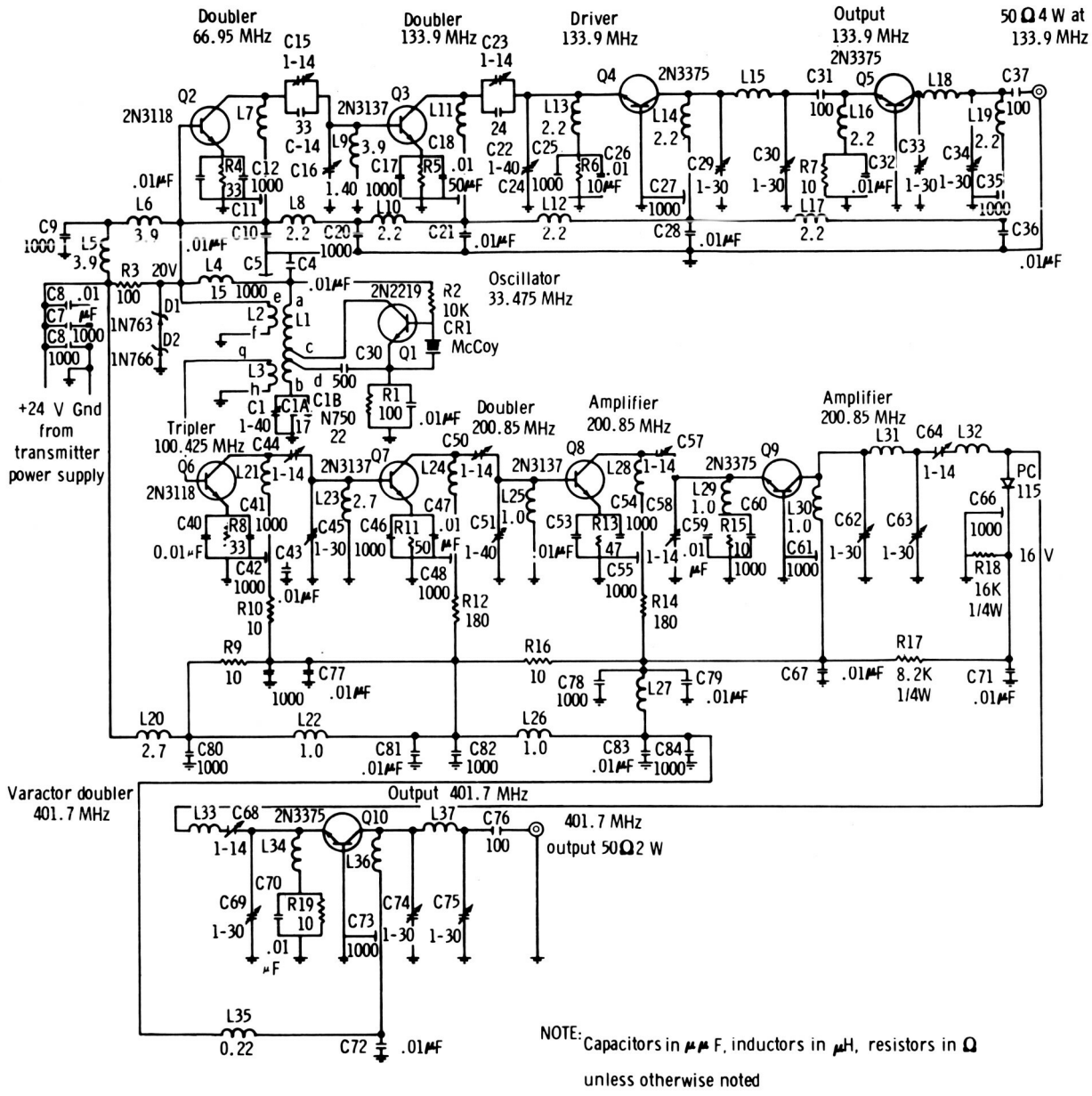

Figure 5. - A circuit diagram of the radio-frequency unit.

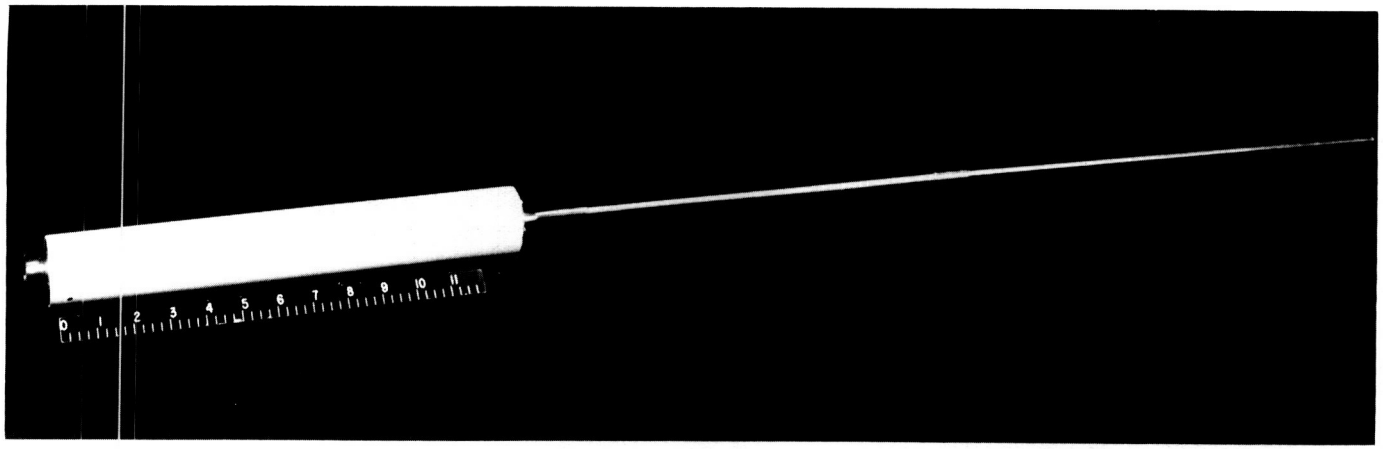

Figure 6. - The erected antenna.

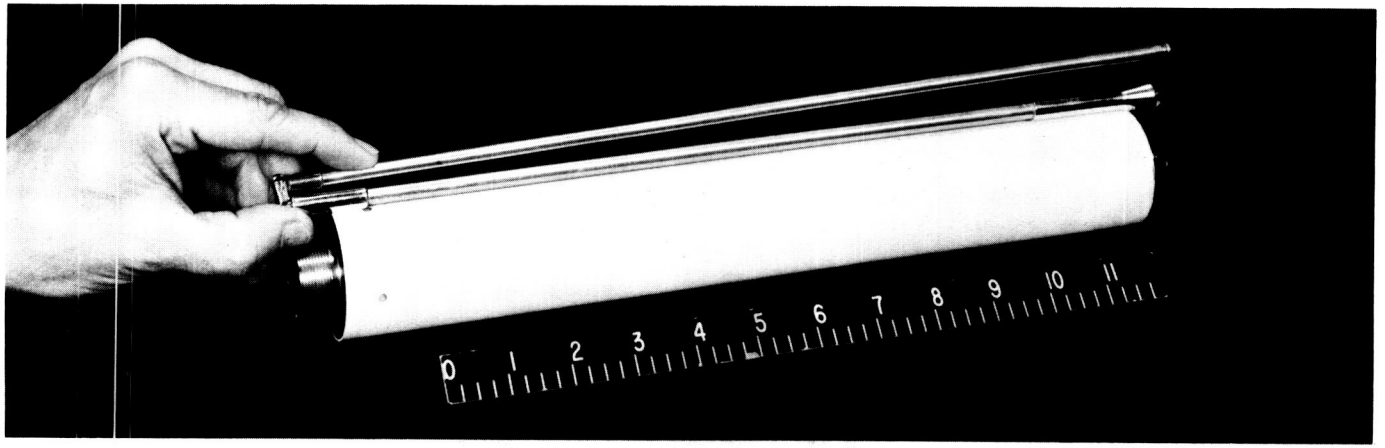

Figure 7. - The folded antenna.

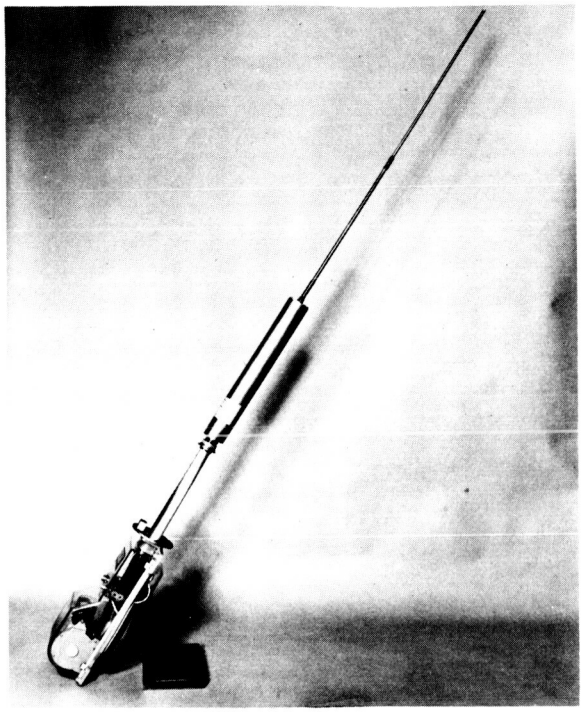

Figure 8. - The antenna boom assembly with the antenna.

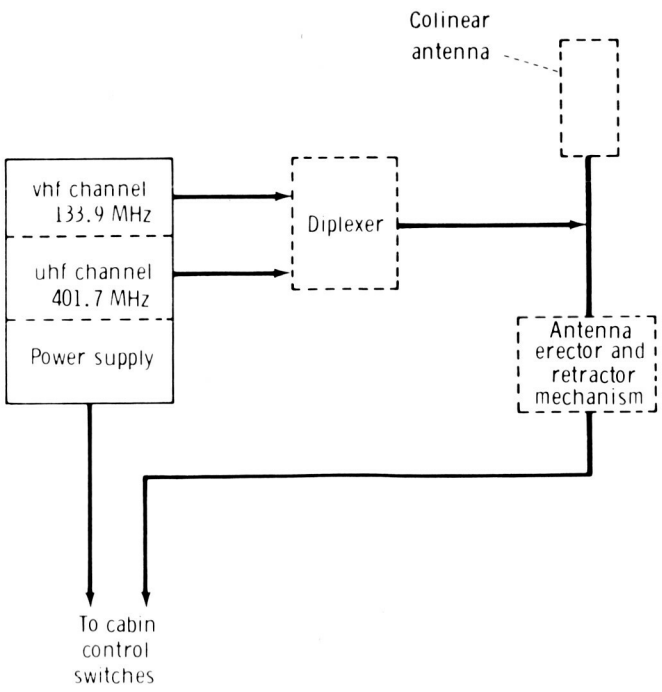

Figure 9. - A block diagram of the transmitter system.

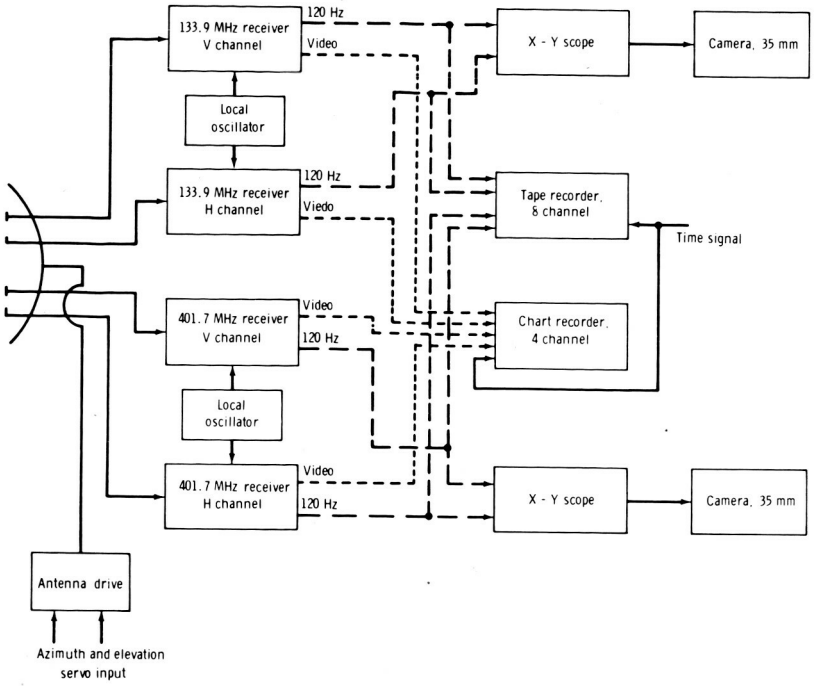

Figure 10. - A block diagram of the receiving system.

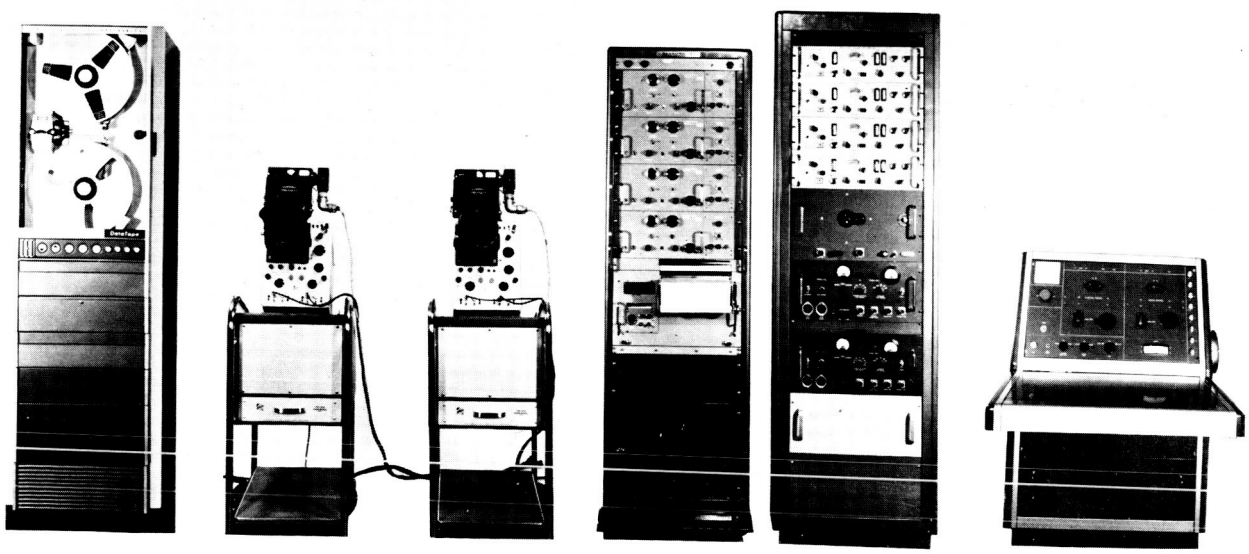

Figure 11. - The ground-based receiving equipment.

EXPERIMENT M406

OPTICAL COMMUNICATIONS

Douglas S. Lilly*

INTRODUCTION

The objectives of Experiment M406, which was flown on the Gemini VII mission, were evaluation of an optical communications system, evaluation of the crewmembers as a pointing element, and exploration of the atmosphere by use of an optical coherent radiator outside the atmosphere.

EQUIPMENT

The experimental equipment consisted of a gallium arsenide laser transmitter (flight hardware) and three instrumented ground sites. Each ground site was equipped with a flashing beacon and was capable of collection and demodulation of coded optical signals. The laser transmitted was a small, self-contained unit (8.5 by 5 by 3 inches). It produced 16 watts of optical coherent power in short bursts that were coded in such a manner that information could be transmitted. Special infrared safety (spectral) glasses and a microphone were attached to the unit. A 6-power telescope (to augment tracking) was integral to the unit, and a 400-angstrom filter was used for background discrimination.

The ground sites that were instrumented for this experiment were the White Sands Missile Range, New Mexico; Kauai Island, Hawaii; and Ascension Island in the southern Atlantic Ocean. Each site was operated in the same manner. At each site, an argon laser was used as an optical beacon, large collecting telescopes were used, and each telescope mount was slaved to an orbital-track radar. The sites had adequate instrumentation for voice processing and determination of high-frequency atmospheric effects.

PROCEDURE

Both crewmembers were given preflight beacon-tracking instruction in the docking simulator room; also, they were trained in sighting the unit in a field situation. Data, to be recorded on the spacecraft test, were complemented with static and aircraft flyby

*NASA Manned Spacecraft Center, Houston, Texas.

field tests in an attempt to isolate all deleterious parameters that affected the data and to determine a method for the elimination of these parameters. The ultimate goal was to identify atmospheric properties that affected the equipment and to establish mathematical models for use in future design efforts.

RESULTS

Unfavorable cloud conditions hampered the performance of the experiment throughout the Gemini VII mission and resulted in cancellation of all but four attempts. The ground beacon was observed only twice by the crewmen during these four attempts, and these observations were of short duration. No solid track could be accomplished by the crewmen in these short intervals, and no data were recorded. The four attempts are described as follows.

During revolution 79 over Hawaii, even though cloud cover in the general vicinity was favorable, the beacon site was obscured by clouds.

During revolution 105 over Hawaii, the crewmen saw the beacon for approximately 20 seconds. However, the beacon came in and out of view. After the pass, it was determined that a slaving data-corrector package at the ground site was not operating properly and did not facilitate close tracking of the spacecraft.

During revolution 104 over White Sands, equipment failure and complications with safety procedures delayed boresighting of the beacon with the radar; only a coarse boresight was accomplished. After the pass, it was determined that the boresight was off by three beam widths.

During revolution 119 over White Sands, the crewmen observed the beacon twice for 2 or 3 seconds. After the pass, it was determined that reversed stator leads on the ground-based equipment prevented a tight track; consequently, the beacon oscillated through the boresight.

The argon lasers that were used as ground beacons caused severe problems at the Hawaii and Ascension Island stations. The same type of laser had operated properly at White Sands during the Gemini V and VII missions. The Ascension Island laser could not be made to operate beyond boresighting. The problems encountered in this experiment, except for the argon laser deterioration, were corrected immediately after occurrence. The argon laser problem has been corrected partially by implementation of equipment modifications.

CONCLUSIONS

None of the experiment objectives were obtained. However, the information acquired is indicative of the following facts.

1. Beacon lasers that have greater survivability in field environments are needed.

2. A 1-watt argon laser is visible at orbital altitudes.

3. The green filter in front of the spacecraft acquisition and tracking telescope is a hindrance to acquisition of the beacon by an observer (crew debriefing); the filter reduces contrast of terrain features.

4. Close inspection of the beacon-telescope mount and tracking-radar mechanism must be maintained on a day-to-day basis to ensure the necessary close tracking of the spacecraft.

The Gemini VII crewmembers suggested that a laser site be established in a region that could be more easily acquired by crewmembers, such as at Cape Kennedy, Florida.

EXPERIMENT D016

POWER-TOOL EVALUATION

By Victor L. Ettredge*

INTRODUCTION

Experiment D016 was not attempted during the Gemini XI mission because of the premature termination of the on-umbilical extravehicular activity (EVA). The experiment had been scheduled for the Gemini VIII mission, but early mission termination prevented completion of the experiment. However, the objective, equipment description, and experimental procedures are described briefly in this report.

OBJECTIVE

The primary objective of Experiment D016 was the evaluation of the capability of man to perform work in the space environment. The following items were the specific objectives.

1. Determination of the ability of a crewmember to perform a controlled work task

2. Comparison of the ability of a crewmember to perform work under tethered and untethered conditions

3. Determination of the performance of the minimum-reaction power tool relative to output and reactive torques

EQUIPMENT

The experiment equipment consisted of a minimum-reaction power tool, a tool-restraint box, a conventional hand wrench, a work-task plate, and a tether that was to have been attached to the knee region of the space suit. This equipment is shown in figure 1. The general arrangement of components within the power tool is illustrated in figure 2. Direct-current power was to have been supplied to the motor through the

*U. S. Air Force Space Systems Division, NASA Manned Spacecraft Center, Houston, Texas.

electrical slipring assembly shown on the left side of figure 2. Simplified internal views are shown in figure 3. For reference, the directions of rotation of the impactor assembly are shown from the rear of the tool, and these are the directions that are involved when the tool is used for tightening fasteners.

When direct-current power of the proper polarity is applied to the motor, its armature rotates clockwise, driving the planetary gear train that causes the impactor drive shaft to be rotated clockwise. As cam A is rotated initially, cam B is forced to move rearward while a steel balls moves up an inclined plane (view A of fig. 3). The impactor barrel assembly is restrained from rotation at this time because of the engagement of the hammer lugs and the anvil lugs of the output shaft. The output shaft is prevented from rotation by the frictional forces of the controlled internal restraint (CIR) collar. The sliding-sleeve linkage holds the CIR stationary with respect to the tool barrel. As cam A is rotated approximately 59°, the impactor barrel assembly is moved sufficiently rearward to disengage the hammer lugs from the anvil lugs (view B of fig. 3). The impactor barrel assembly is then free to rotate. The energy stored in the springs causes the cams to move toward an alined configuration, thereby accelerating the impacting barrel in a clockwise direction. Continual drive-shaft rotation also contributes to acceleration of the barrel. As the barrel rotates and the cams begin to come into alinement, the barrel assembly moves forward (view C of fig. 3). After 180° of rotation, the hammer lugs on the face of the impactor barrel strike the anvil lugs. The relatively large torque value developed on the anvil-output shaft assembly exceeds the static-friction coefficient of the CIR collar, and the output shaft rotates, tightening the bolt.

The relatively small amount of power delivered by the motor gear-train assembly is stored gradually (over a relatively long time period) in the tool barrel assembly, and is delivered in the form of a high-energy, short-duration pulse to the anvil-output shaft assembly. Reaction to torque on the bolt is transferred through the output shaft and anvil-lug assembly to the hammer-lug assembly on the impactor barrel, causing the barrel to rebound. The rebound force is integrated by the spring (in the impactor assembly), which reflects the force backward through the drive-shaft assembly and divides the force at the planetary-gear train. Part of the reactive force is transferred through the gearcase assembly directly to the tool barrel, and part of the force is reflected through the armature, through the magnetic fields, to the motor field ring, and in turn to the tool barrel. Both reactive forces are in phase when they arrive at the tool housing, causing the tool barrel to rotate counterclockwise. The rotation rate of the tool barrel is restrained because of the drag-brake action of the CIR. The tool barrel is supported by large-diameter ring bearings, the inner race of which is pressed over the tool barrel; the outer race is supported by the tool housing. The only reactive force that is transferred to the tool housing is that which results from the friction of the ring bearings. The physical and operating characteristics of the tool are given in table I.

PROCEDURES

The experiment was to be performed during EVA at approximately 24:30 g. e. t. A sketch of the experiment activities is shown in figure 4. The procedural event sequence for the EVA pilot is given in the following list.

1. Grasp handrail and position self for knee-tether attachment.

2. Attach right-knee tether to handrail.

3. Grasp toolbox handle, release lock, and extend toolbox until positive lock is engaged.

4. Open toolbox, extend power-tool handle, check that the light switch is on, that the forward-reverse switch is in the forward position, and that the tool is in the impact mode.

5. Grasp power tool, tighten instrumented bolt for 5 seconds.

6. Reverse switch and loosen instrumented bolt until "just loose."

7. Unscrew, in succession, four worksite bolts.

8. Stow power tool, turn over worksite plate, and hand-start three bolts.

9. Unstow power tool, reverse switch, tighten three bolts.

10. Stow power tool on toolbox lid and remove handtool.

11. Tighten instrumented bolt for 5 seconds and loosen instrumented bolt.

12. Stow handtool in toolbox.

13. Detach knee tether from handrail.

14. Remove power tool, check that the light is on and that the tool is in the impact mode.

15. Using power tool, tighten instrumented bolt for 5 seconds.

16. Reverse switch, loosen instrumented bolt until "just loose."

17. Stow power tool in toolbox, fold handle.

18. Remove handtool.

19. Tighten instrumented bolt for 5 seconds and loosen instrumented bolt.

20. Stow handtool in toolbox.

21. Close toolbox lid.

22. Release latch on worksite and stow toolbox in adapter section.

TABLE I. - PHYSICAL CHARACTERISTICS OF SPACE POWER TOOL

Weight, lb	7.62
Length:	
Handle erected, in.	10-7/8
Handle folded, in.	10-13/16
Height:	
Handle erected, in.	9-1/16
Handle folded, in.	4-1/2
Width, in.	5
Center of gravity:	
From output shaft end, in.	6-5/32
Output shaft, in^2	0.5
Power supply	Self-contained, rechargeable, Ni-Cd battery
Speed:	
CIR on, full load, beats/min	1550 to 1650
CIR off, no load, drilling mode, beats/min	1250
Operating voltage, V	6 to 7
Current:	
CIR on, full load, A	13 to 16
CIR off, no load, drilling mode, A	3
Open-circuit voltage, V dc	7.6 to 8.2
Output torque, ft-lb	>45, developed on 0.5-in. NF AN-type bolt
Work capacity per battery charge:	
Impacting, 3-sec burst	100
Drilling, running time, min	8 to 10

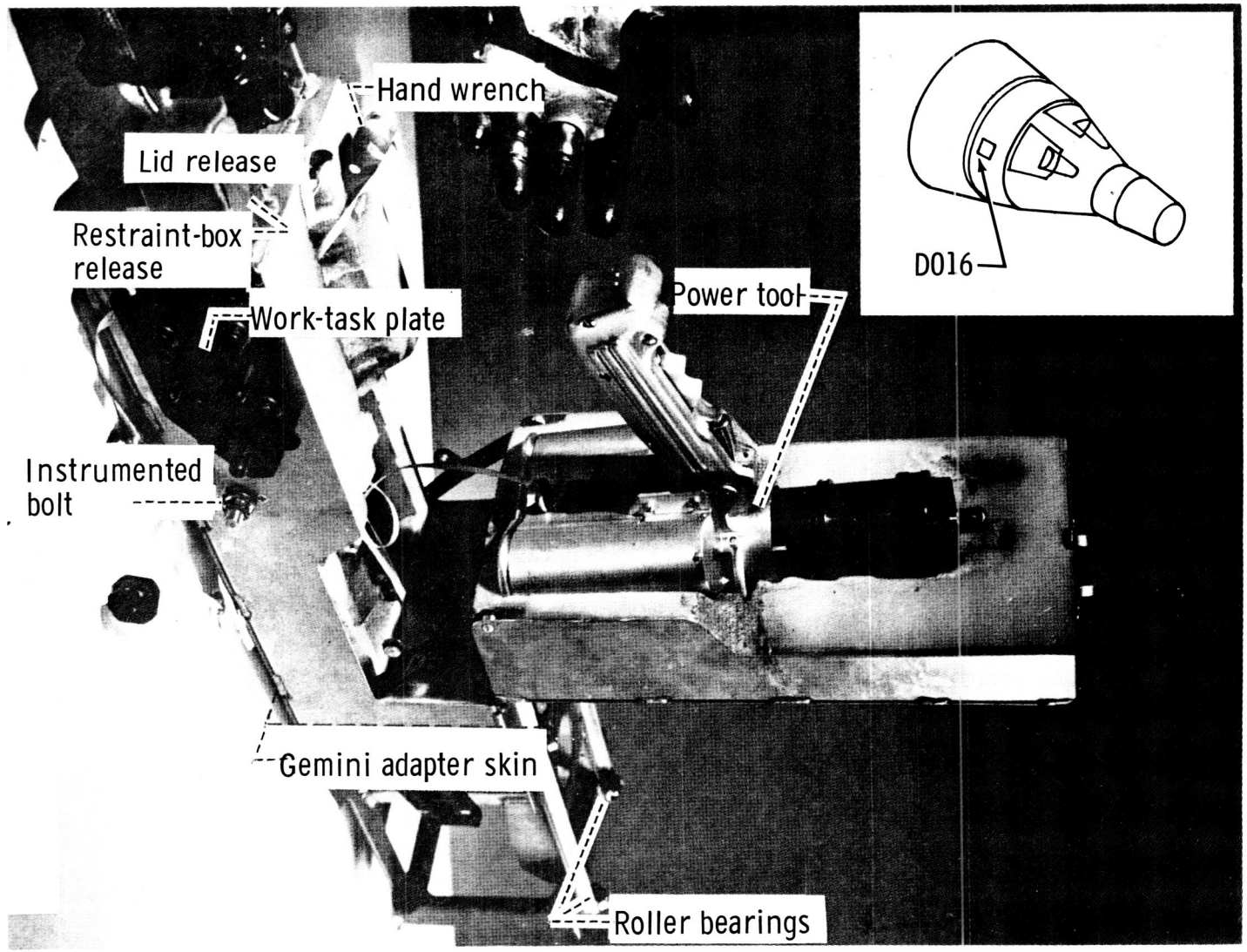

Figure 1. - The power tool and associated equipment.

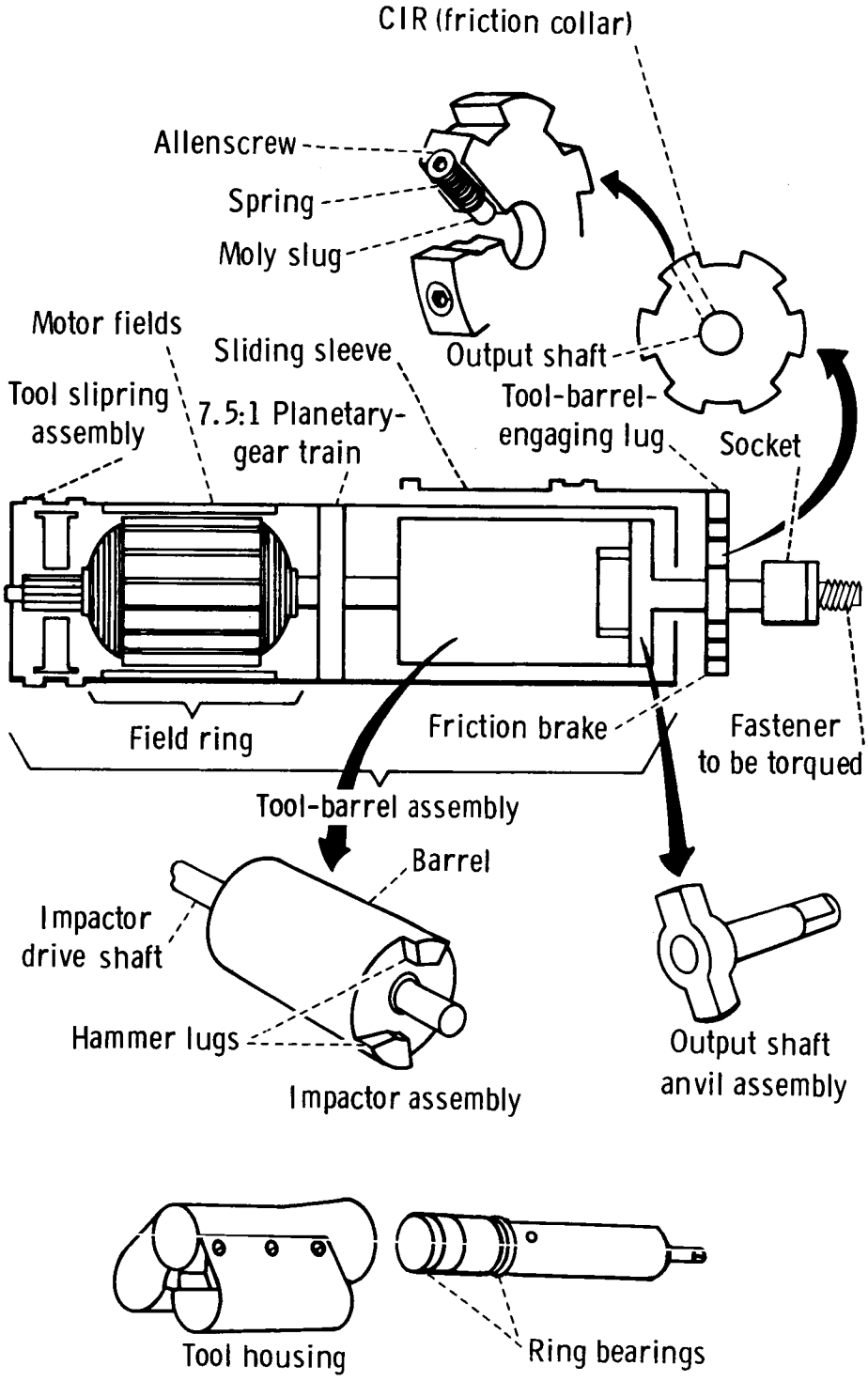

Figure 2. - An internal view of the power tool.

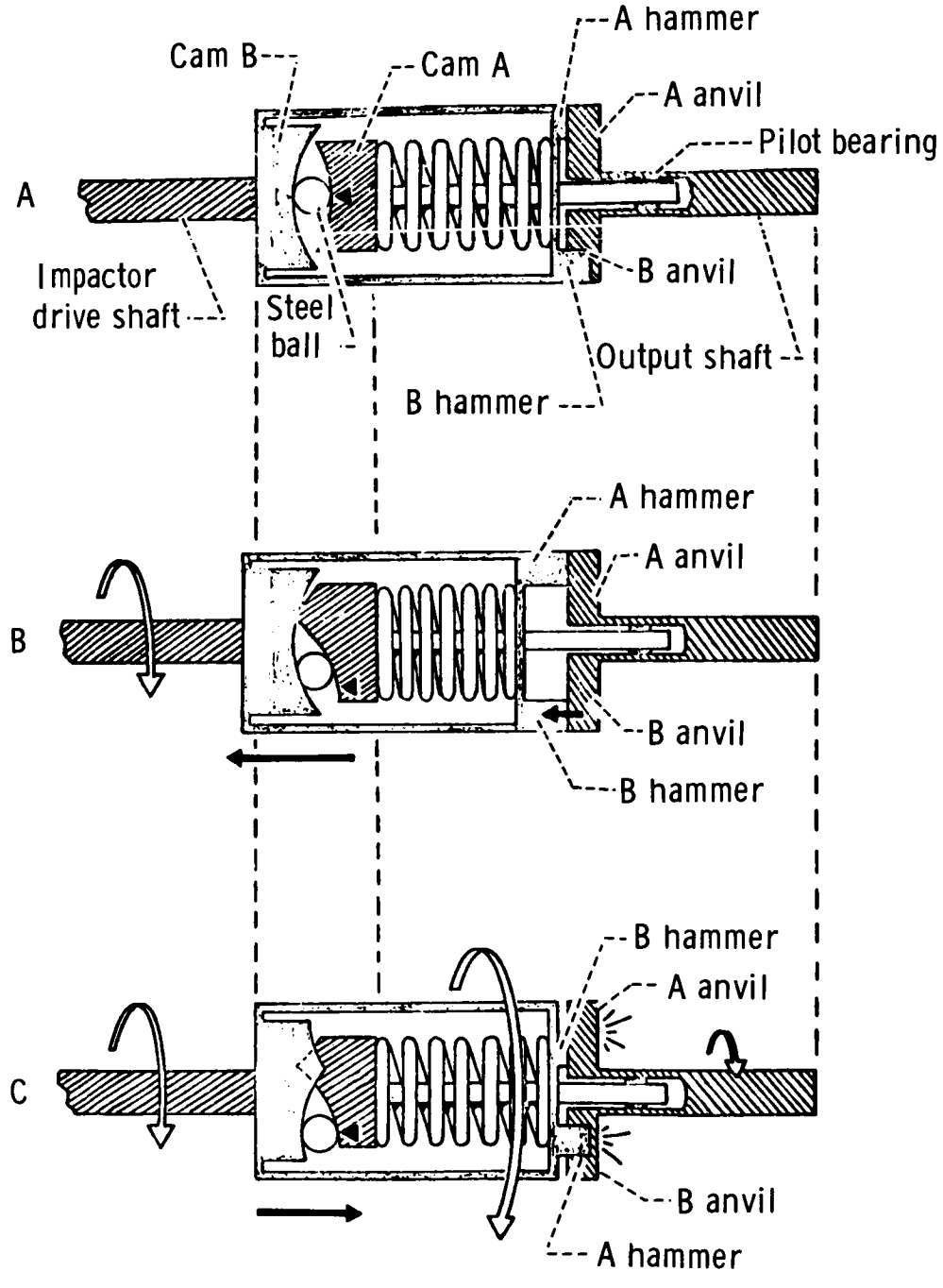

Figure 3. - The impactor-assembly operation.

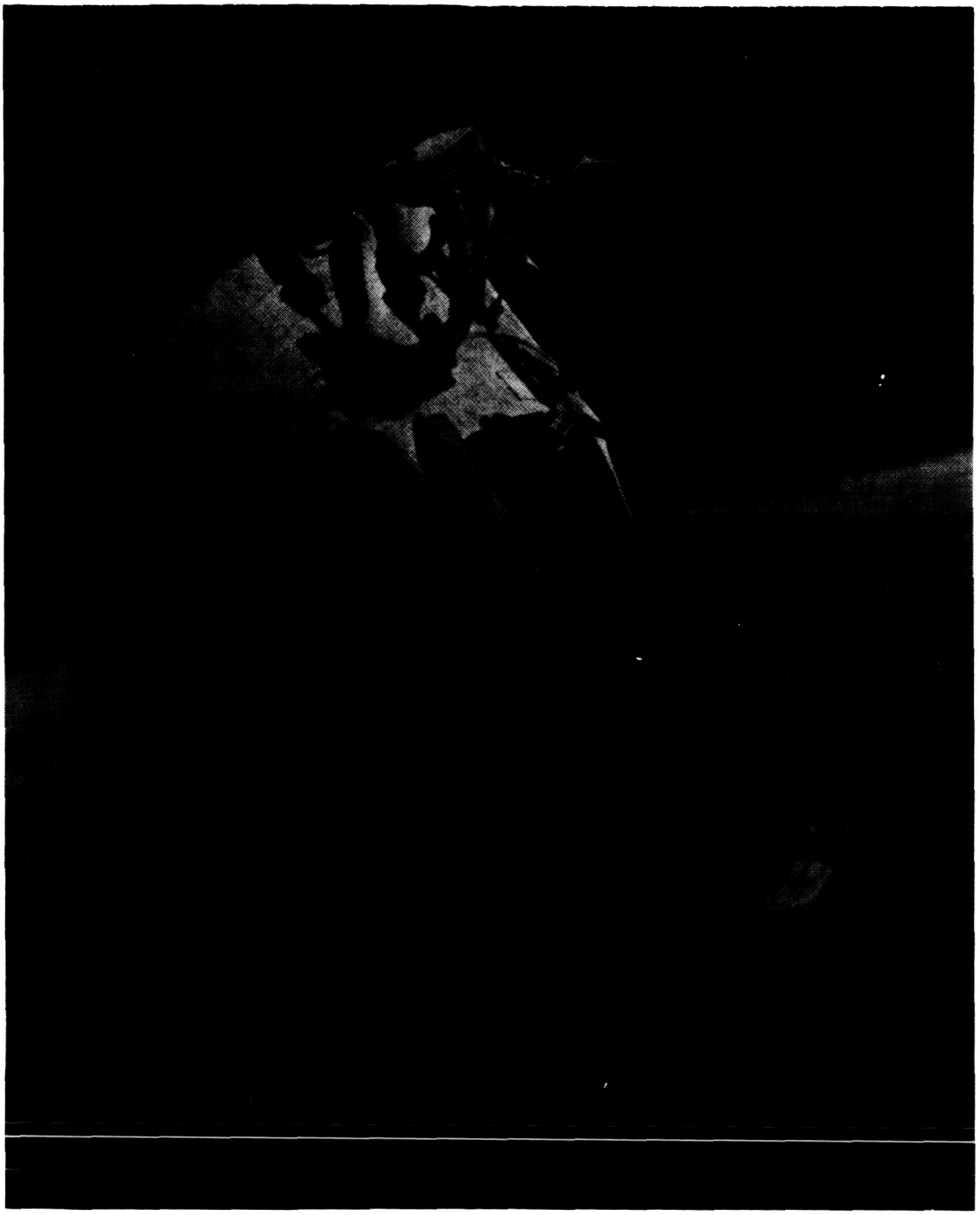

Figure 4. - An operational concept of the power tool in use.

EXPERIMENT D012
ASTRONAUT MANEUVERING UNIT

By P. N. van Schaik*

INTRODUCTION

Maintenance, repair, resupply, crewmember transfer, rescue, satellite inspection, and assembly of structures in space are operations that may be performed by men on space-station systems of the future. Many of these operations will involve extravehicular activity (EVA) and will require man to maneuver for short distances in free space. The astronaut maneuvering unit (AMU) experiment was a fundamental step toward the determination of the basic hardware and operational criteria for EVA. Experiment D012 was designed for the acquisition of experience in extravehicular maneuvering operations on the Gemini IX mission. It was planned that the experiment would result in basic information that was needed to establish the extent to which extravehicular operations may be used on future space flights.

The Gemini spacecraft configuration and environment were major factors in the establishment of the AMU packaging configuration. The modular concept was mandatory because stowage volume in the Gemini cabin was inadequate for the entire system and because the extravehicular life-support system (ELSS) was needed for egress operations. The division of systems into the two basic modules (fig. 1) was done to utilize maximally the ELSS chestpack. The chestpack contained the life-support systems, emergency oxygen supply, and all of the AMU systems-status displays and malfunction displays. The externally stored module (the backpack) contained the propulsion system, flight-control system, oxygen-supply system (OSS), malfunction-detection system, and communications system. These two modules and the Gemini pressure suit comprised the AMU, which was essentially a system that was a miniature manned spacecraft.

The AMU experiment on the Gemini IX mission was planned for the duration of one complete revolution around the earth. The nightside operation was used for checkout and equipment donning activities. Maneuvering evaluations were planned for the dayside pass. The donning phase of the AMU experiment consisted of inspection and preparation of the equipment and the actual donning of the equipment. The backpack was inspected first because it had been subjected to the launch environment. In the preparation of the backpack for donning, valves and switches were positioned to activate the AMU systems. The AMU 125-foot tether was attached, and umbilicals, harnesses, and controllers were positioned for easy access when the crewman backed

*U. S. Air Force Systems Command Field Office, NASA Manned Spacecraft Center, Houston, Texas.

into the unit. The equipment donning consisted of changeover from the spacecraft to the backpack life-support and electrical systems, checkout of the interfaces of these systems with the ELSS and the suit, and separation of the AMU from its spacecraft mounting.

According to the flight plan, the crewman was to leave the adapter and move to the nose of the spacecraft. While limited by 25 feet of AMU tether and the ELSS umbilical, the maneuvering and control capabilities of the AMU were to be evaluated. If these tests were satisfactory, the entire tether length was to be deployed and evaluation maneuvers were to be performed by the EVA pilot, by the use of the augmented target docking adapter (ATDA) and the spacecraft as references. Upon completion of these activities, the backpack was to be removed and discarded.

The AMU activities during the Gemini IX mission were terminated before equipment donning was completed. More effort was needed by the EVA pilot than had been anticipated to maintain his position in preparation of the AMU for flight. Despite this positioning problem, the EVA pilot completed the preparation tasks. After backing into the AMU, the pilot reported that the suit visor was fogged completely. At this point, the AMU experiment was terminated, and the EVA pilot returned to the cabin.

EQUIPMENT

The backpack was a highly compact unit that consisted of a basic structure and six major systems (the propulsion, flight-control, oxygen-supply, power-supply, malfunction-detection, and communication systems). The external features of the pack are shown in figure 2, and the internal equipment arrangement is shown in figure 3. The structure consisted of a backpack shell, two folding sidearm controllers, and folding nozzle extensions. The shell was a box-like structure that consisted of three main beams and support shelves on which the components were mounted. The thrusters were in the corners of the structure in order to provide controlling forces around the center of gravity of the AMU. The remainder of the components were located in the available spaces inside the pack. The total volume and shape were determined somewhat by the stowage location in the Gemini IX spacecraft equipment-adapter section. This constraint necessitated the folding features of the nozzle extensions and sidearm flight controllers. The sidearm controllers contained the controller heads, by which the pilot commanded translation and attitude. This configuration ensured accessibility of the control handles for use with the pressure suit. The nozzle extensions aimed the exhaust plume from the hydrogen peroxide thrusters away from the helmet and shoulders of the suit. A weight composition of the backpack is given in the following table.

Item	Weight, lb
Structure	34.4
Propulsion system	62.6
Reaction-control system (RCS)	12.7
Oxygen-supply system	26.9
Power-supply system	21.9
Abort-alarm system	.7
Communications system	9.7
Total	168.9

Propulsion System

The propulsion system was a conventional monopropellant system, and 90 percent hydrogen peroxide was the propellant. The propellant had a total impulse of 3000 to 3500 pound-seconds, and the pressurant gas was nitrogen. The major components of the propulsion system are shown in figure 4. A functional schematic of the propulsion system is shown in figure 5. The nitrogen tank contained high-pressure gaseous nitrogen that was supplied to a regulator, which, in turn, supplied regulated nitrogen at a nominal pressure of 455 psia to a bladder in the hydrogen peroxide tank. The selection of materials for this bladder represented one of the design problems that was encountered in the development of the AMU. Because of the storage requirement (as many as 10 days), a material was required that was practically inert to hydrogen peroxide. Also, the bladder had to have the capability of several fill and expulsion cycles. The material selected proved to be satisfactory for these applications.

The flow of propellant to the thrust-chamber assemblies was controlled by the manually operated valves, and the electrical signals to the individual thruster valves were controlled by the use of these valves. Two manually operated valves were provided, one valve for the primary control system and one valve for the alternate control system. There were 12 thrust chambers and 16 control valves. As shown in figure 6, the primary control system had eight thrusters: two forward, two aft, two up, and two down. The fore-firing and aft-firing thrusters were used in various combinations to translate fore and aft, and for pitch and yaw control. The up-firing and down-firing thrusters were used for vertical movement and for roll control. The alternate-control system involved the use of entirely separate fore-firing and aft-firing thrusters, but involved the use of the same thrust chambers for vertical translation and for roll control. However, separate control valves were used in the alternate system for the up, down, and roll commands. As a safety feature, relief valves were incorporated in the nitrogen and hydrogen peroxide lines. These valves were vented into thrust-neutralizing overboard vents.

Flight-Control System

The flight-control system was used for automatic three-axis attitude control and stabilization and for manually controlled translation in two axes. Lateral translation could have been accomplished by a 90° roll or yaw, succeeded by translation in one of the available modes. The major components of the flight-control system are shown in

figure 7. A functional block diagram is shown in figure 8. Completely redundant systems were available. Manual-control commands were made through the controller heads on the sidearm controllers.

The left hand of the EVA pilot controlled translation commands in the vertical (up and down) and horizontal (fore and aft) directions. The controller-knob movement was direction oriented; that is, the knob was rotated forward to translate forward or up to translate up. The mode-selection switch, a voice-communication volume control, and a communications selector switch were located on the left-hand controller assembly. The mode-selection switch was used for selection of either automatic or manual attitude control and for stabilization. The three-position communication selector switch made it possible for the EVA pilot to select the most desirable mode of operation with respect to the voice-operated switches in the AMU transceiver. The right-hand controller governed pitch, yaw, and roll. Also, these commands were directional; to yaw right, the knob was rotated clockwise. When the knobs were released, they returned to the "OFF" position.

While stabilized automatically, a fixed-rate command (18° per second in pitch and yaw and 26° per second in roll) was entered into the control system when the knob was rotated. The system then went into a hold position at the attitude where the knob was released. The automatic mode enabled the EVA pilot to park in space in a stabilized position and to fire the thrusters as required to maintain this position within a dead band of ±2.4°. In the absence of the external torques, the period of limit-cycle operation within the dead band was in excess of 20 seconds around all three axes. In the manual-control mode the gyros were out of the loop, and a direct fly-by-wire system resulted. While in the manual-control mode, the thrusters would have fired only in response to a manual command.

Oxygen-Supply System

The OSS supplied expendable oxygen to the chestpack ELSS at closely regulated temperature and pressure. The OSS components are shown in figure 9 and a functional schematic is shown in figure 10. A total of 7.3 pounds of oxygen was stored in the supply tank at 7500 psia. A minimum of 5.1 pounds of oxygen could have been delivered to the chestpack at 97 ± 10 psia and 65° ± 10° F. Peak design flow was 8.4 pounds per hour and normal flow was 5.0 ± 0.2 pounds per hour. The delivered-gas pressure could have been maintained at the desired value until the tank pressure dropped to less than 200 psia. A low-level switch illuminated a warning light on the chestpack when the tank pressure was 800 ± 160 psia.

Power-Supply System

The power-supply system supplied electrical power to the AMU systems for the planned duration of the mission; a 100-percent reserve capacity was used. Electrical power was supplied by two batteries that had silver-zinc cells which were enclosed in a sealed cylindrical can (fig. 11). Two cans were mounted on the backpack to ensure the requisite redundancy. One battery supplied power for the RCS. A block diagram of the arrangement is shown in figure 12. One set of taps on this battery supplied ±16.5 volts for operation of control-logic circuitry; a separate set of taps supplied

±15 volts for operation of the rate gyros and the valve amplifiers. An entirely separate battery in the can supplied 28 volts of direct current for the other systems. The 28 volts supplied from each can were fed into a common bus, but were isolated electrically by diodes for prevention of a short circuit of one battery from draining the other battery. This system is shown as a block diagram in figure 13. The batteries were installed as one of the last operations before mating the spacecraft adapter section to the launch vehicle, because the backpack was inaccessible subsequent to mating. The batteries were isolated from the AMU systems by the main power switch; the EVA pilot closed this switch as part of the predonning procedure.

The power-distribution unit contained mechanical fuses in all power circuits for protection of the lightweight wires and cables that were used in the AMU electrical systems. Dual fuses were used to ensure redundant control in case of mechanical failure. That is, two fuses were used in parallel so that if one fuse was blown for some reason other than an overload, the other fuse would maintain circuit integrity. Also, the power-distribution unit included the diodes that electrically separated the two 28-volt systems.

Malfunction-Detection System

A malfunction-detection system warned the crewmembers when certain critical out-of-tolerance conditions existed. Low fuel pressure, low oxygen supply, low fuel quantity, and those conditions indicative of certain control-system anomalies were the critical parameters that were monitored. A schematic of the system is shown in figure 14. The warning was given both as an intermittent tone in the headset and as a warning light on the chestpack display panel. Individual warning lights on the upper surface of the chestpack identified the out-of-tolerance system. A manual switch was provided so that the pilot could silence the audio tone, but the warning light would remain on as long as the out-of-tolerance condition existed. However, if a new alarm condition occurred, the tone would come on again and the appropriate warning light on the chestpack would be illuminated.

Communications System

The communications system consisted of a telemetry system and a voice system. The major components of these systems and the power-supply and malfunction-detection systems are shown in figure 15. The telemetry system monitored certain backpack parameters and biomedical parameters. The information was transmitted over a radio-frequency (rf) link to a tape recorder in the spacecraft. The data were available for postflight analysis only. A functional schematic is shown in figure 16. The AMU telemetry parameters are shown in table I. The voice-communications transceiver was an ultrahigh-frequency (uhf) transmitter-receiver that was controlled by redundant voice-operated switches. The transceiver was designed for compatibility with the basic spacecraft onboard communications system, and it utilized the microphone and earphones in the suit. A three-position switch, mounted on the translator controller and located electrically in the microphone circuit, established the following functions.

1. Continuity of the microphone leads for normal voice-operated switch (VOX) mode of operation

2. Opening of the microphone leads or "LISTEN" mode

3. Momentary closing of the leads for transmission

A schematic of this system is shown in figure 17. The signals, both from the telemetry transmitter and from the transceiver, were diplexed and radiated from a common antenna that was mounted on top of the backpack. While the AMU was stored in the spacecraft, certain parameters were put into the spacecraft telemetry system and were transmitted to ground-based stations. The hydrogen peroxide pressure and temperature were displayed on a panel inside the spacecraft.

Astronaut Maneuvering Unit Tether

The AMU tether (fig. 18) consisted of 125 feet of 3/8-inch nylon webbing, two hooks (H_3 and H_4), a single ring (R_2), and a stowage bag. At one end, a hook (H_4) was used for attachment to the spacecraft-ELSS umbilical tether. This hook made possible transversal 125 feet from the umbilical. The other hook (H_3) was located 100 feet from the first hook. When attached to the umbilical tether, hook H_3 limited the tether length to 25 feet. The ring (R_2) on the opposite end of the tether was attached to a hook (H_2) on the space suit harness.

ASTRONAUT MANEUVERING UNIT INTERFACES

Gemini Spacecraft

The AMU backpack was installed in the spacecraft equipment adapter before mating the spacecraft to the launch vehicle. The location of the AMU and the associated spacecraft hardware is shown in figure 19. Mating to the spacecraft was accomplished by the attachment of a four-legged structure (claw assembly) to the backpack and by the use of a tension bolt to pull the claw firmly against a sheet-metal structure (torque-box assembly). The torque box then was hard-mounted to the blast-shield door. The bolt was severed by an electrically detonated pyrotechnically operated guillotine. The guillotine was actuated from the cockpit after the AMU had been donned. A pull-away electrical connector was used to establish instrumentation and power leads for in-cabin monitoring and for ground-based servicing and testing.

Servicing provisions. - A service line was installed from the external surface of the adapter to the AMU hydrogen peroxide fill port for use in filling the AMU tanks with hydrogen peroxide after mating the spacecraft to the launch vehicle. Another (parallel) line to the AMU regulated-nitrogen port was installed for use in reservice of the system in the event an unstable condition in the hydrogen peroxide was detected or if launch was delayed indefinitely. If, for some reason, the hydrogen peroxide had become unstable and the system pressure had risen to a pressure greater than 575 psia, the AMU relief valve would have opened and the hydrogen peroxide would have been vented through another (third) line to the adapter skin. The fill and reservice lines were severed by the

same guillotine that released the AMU. The vent line was routed through a spring-loaded pulloff housing that was separated when the AMU was released.

Thermal interface. - Because of the 40° to 100° F temperature limitations for various AMU components, a cover assembly was placed over the AMU for passive thermal control. This cover rested against the aerospace ground-equipment attachment points on the front of the AMU. A line held the cover in this position. This line passed through the center of the AMU to a hard-mounting point on the torque-box assembly. The line was severed and the cover was jettisoned by operation of the cockpit "EVA BARS EXT" switch.

Donning hardware. - The equipment, provided in the adapter, was of benefit to the EVA pilot in donning the AMU. This hardware (fig. 20) consisted of a footrail, two handbars, an umbilical guide, and two floodlights for use during nightside operation. This equipment was deployed and properly positioned for AMU donning simultaneous with release of the thermal cover.

Instrumentation and communications. - To collect AMU performance data, a telemetry receiver, capable of acceptance of the diphase pulse-code-modulation (PCM) format that was transmitted from the AMU, was installed on the electronics module in the spacecraft adapter. The receiver demodulated the 433-MHz received signal and supplied a 5120-bps diphase signal to the spacecraft PCM recorder. These data were recorded and stored for postflight analysis. Two whip antennas were mounted on the adapter surface for receipt of the AMU telemetry transmissions. However, only one antenna was used at a time. The proper antenna was selected by coaxial switching from a signal from the telemetry receiver. The receiver exerted automatic control over the coaxial switch to change antennas when the rf signal on the antenna in use decreased below a preset level. Although propellant status was monitored in the cockpit, the same pressures and temperatures could have been monitored through the usual spacecraft telemetry to the ground-based stations. A 0- to 715-psia transducer and a thermistor in the AMU propellant tank were powered by the spacecraft for spacecraft telemetry channel RA01 (hydrogen peroxide pressure) and channel RA02 (hydrogen peroxide temperature). Hydrogen peroxide pressure readings were available until the AMU telemetry switch was placed in the "BACKPACK" position during the donning phase of the EVA. Hydrogen peroxide temperature could be read until separation of the AMU from the spacecraft. During the Gemini IX mission, the spacecraft uhf transceiver was used to maintain communication between the EVA pilot and the command pilot. This transceiver was voice operated at 296.8 MHz.

Crewmember station displays. - The five crewmember station displays and controls (fig. 21) are discussed as follows.

1. The propellant temperature- and pressure-indicator gage indicated the pressure and temperature of the hydrogen peroxide propellant stowed in the AMU.

2. The warning light for hydrogen peroxide pressure was illuminated when the pressure was as much as 575 ± 20 psia.

3. The "BUS ARM" switch, located on the Agena control panel, had to be in the "EXP" position to energize experiment squib circuits before AMU-cover release, footrail extension, telemetry-antenna deployment, and AMU release.

4. The "MMU" switch performed several functions. In the spring-loaded "DEPLOY" position, the AMU was released by guillotine severance of the hollow retention bolt and service lines. In the telemetry switch "ON" position, the telemetry receiver and its associated antenna coaxial switch were powered. The tape recorder was activated also.

5. The "INDEX BARS/EVA BARS EXT" switch, if placed in the "EVA BARS EXT" position, caused release of the AMU thermal cover and deployment of the footbar and handrails to the operational position. Also, the AMU telemetry antennas were deployed for reception of telemetry signals.

Extravehicular Life-Support System

The ELSS became an integral part of the AMU system during the donning phase of EVA. The ELSS functioned as electrical, mechanical, and life-support connections between the EVA pilot and the AMU. Through an umbilical from the AMU oxygen-supply system, oxygen was delivered to the ELSS environmental-control system at 97 ± 10 psia and 65° ± 10° F. To facilitate oxygen flow, a quick-disconnect fitting on the umbilical was attached to a mating connector on the ELSS. The OSS interface has already been discussed. Other AMU-ELSS interfaces are discussed as follows.

Restraint-harness interface. - An AMU restraint harness was installed as part of the backpack. The harness held the backpack to the space suit by pressure exerted on the forward surface of the ELSS.

Malfunction-detection-system interface. - Four alarm lights, that were visible to the EVA pilot, were installed on the ELSS to indicate out-of-tolerance conditions in the backpack propulsion system (fuel quantity and pressurization), oxygen-supply system, and reaction-control system. The lights were activated by electrical signals from the backpack through the AMU electrical umbilical. The signals were continuous as long as an alarm condition existed. Light arrangement and function are described as follows.

1. The oxygen warning light illuminated when the tank pressure was 800 ± 160 psia or when the oxygen temperature decreased to less than 5° ± 5° F.

2. The fuel quantity warning light illuminated when 30 percent of the total fuel remained.

3. The fuel low-pressure warning light illuminated at a nitrogen pressure of 650 ± 100 psia or at a hydrogen peroxide pressure of 350 ± 50 psia.

4. Certain critical functions of the RCS were monitored, and the failure of any one of the functions would have resulted in illumination of the warning light.

A switch was installed on the ELSS to test the operation of the alarm lights and portions of the backpack abort-alarm subsystem. The test signal to the backpack was supplied through the electrical umbilical. The ELSS supplied a 1700-Hz audio signal to the backpack radio receiver-transmitter upon receipt of a signal through the electrical umbilical from the AMU alarm subsystem. The signal to the backpack was continuous until the

reset switch (located on the top of the ELSS) was actuated. Switch reset generated a signal to the backpack, through the electrical umbilical, to reset the alarm trigger in the backpack.

Telemetry interface. - The following parameters, received from the space suit and ELSS through the electrical umbilical, were telemetered from the backpack.

1. Electrocardiogram
2. Respiration rate
3. Suit pressure

Hydrogen peroxide quantity-indication interface. - A meter was installed on the ELSS to indicate the quantity of hydrogen peroxide in the backpack. This meter was visible to the EVA pilot. Signals were supplied to the meter from the backpack through the electrical umbilical.

Gemini Space Suit

The results of an exhaust-plume-heating analysis were indicative that the Gemini thermal-coverall materials would be heated beyond acceptable limits during an in-space evaluation of the AMU. Consequently, the decision was made to add extensions to the upper forward thrusters and to modify the leg portion of the basic Gemini coverall. Eleven layers of superinsulation (a woven fabric, a superinsulation spacer material of fiber glass, and an aluminized reflective material) were used. The nozzle extensions were evaluated to determine the effect on performance, system design, and predonning activitites. Performance tests on extension configurations were indicative that extensions could be added without significant effect on thruster performance. Thermal analysis of the selected design resulted in verification of this solution of the heating problem that was associated with the upper forward-firing thrusters.

Prior to the Gemini IX mission, the Gemini VIII EVA glove had been adopted because its mobility and tactility characteristics were superior to the glove that had been developed for use with the AMU. The Gemini VIII glove afforded very little thermal protection from the AMU exhaust plume, and protective shields were installed on the AMU controllers. Although temperatures on the gloves were lower (significantly) than those that were predicted for the leg regions, the shields involved the same materials and layup as did the modified extravehicular coverall.

THE AMU-GEMINI IX FLIGHT PLAN

The AMU task on the Gemini IX mission was planned for the time that was available during one complete revolution around the earth. The nightside pass was to be used for checkout and donning activities, and the dayside pass was to be used for maneuvering evaluation. Electrical power and oxygen and propellant supplies limited the maneuvering or independent-operation capability of the AMU to approximately 1 hour.

At dark, the EVA pilot was to move along the handholds over the surface of the retro-adapters and equipment adapters to the interior of the equipment adapter where the backpack was to be checked and donned. After establishing a position on the footrail, the EVA pilot was to proceed with the predonning checkout of the AMU; checkout consisted of the following activities.

1. Visual check of the oxygen-supply system and nitrogen-tank pressures to verify adequate supply

2. Manual opening of the oxygen and nitrogen supply tank shutoff valves

3. Turning on the master electrical-power switch

4. Unstowage of the sidearm controllers and arrangement of the restraint strap, electrical umbilical, and oxygen umbilical in the donning positions

If the systems were satisfactory, the EVA pilot then would back into the AMU by the use of the handholds and footbars for support. Attachment of the single restraint strap across the front of the chestpack would unite the chestpack and backpack. The backpack OSS would be connected to the chestpack ELSS through a separate connector; thus, the external (to the chestpack) oxygen supply would be uninterrupted. To verify satisfactory operation, the command pilot would manually shut off the external supply before the spacecraft oxygen umbilical was disconnected. The spacecraft umbilical electrical connector and the backpack electrical connector were both attached to the same chestpack connector. Voice communications would be interrupted briefly during the changeover operation because communications were carried through the chestpack connector.

After completion of the verification, donning, and changeover operations, the backpack would be released from the adapter mounting by the command pilot who severs the attachment bolt and propellant-service lines. The propellant vent line and the electrical cable were equipped with pull-away connections. After release, the EVA pilot would return to the vicinity of the cabin by the use of the handrails and would detach the spacecraft umbilical and complete the attachment of the AMU tether. The command pilot would keep the EVA pilot in sight while the EVA pilot performed the initial flight check on the 25-foot section of the tether. The EVA pilot would make short translations and rotations around all three axes by the use of both the primary and alternate propulsion systems both in stabilized and in manual control modes. After these checks and the performance of a sufficient number of familiarization maneuvers for pilot confidence in the AMU, the 25-foot tether hook would be detached to permit full use of the tether. Maneuvers would be performed to evaluate control capability, fuel usage (both in stabilized and in manual control modes), station keeping, and rendezvous. After evaluation of the AMU, the EVA pilot would return to the region of the spacecraft nose to retrieve the spacecraft umbilical. The reverse of the donning changeover, release of the backpack into space, and a normal ingress would be performed. If retrieval of the spacecraft umbilical were not practical, the emergency oxygen supply in the chestpack could be used during ingress.

RESULTS

The AMU was serviced before the planned launch date (May 17, 1966). Evaluation of the propellant (hydrogen peroxide) status after launch cancellation was indicative of a stable pressure increase of 0.2 psia per hour caused by normal active oxygen loss. This loss was significantly less than the allowable loss (0.6 psia per hour). The decision was made not to reservice the propellant. At launch (June 3, 1966), the pressure had increased to approximately 87 psia, a nominal launch condition.

The oxygen and nitrogen systems were monitored through special ground-based equipment and evidenced no leakage. Fresh batteries were installed in the flight unit on May 25, 1966. A telemetry check of the AMU was indicative that all systems were operating normally. Immediately after launch, the propellant-tank pressure increased to 90.7 psia (normal) and remained at that value until donning checkout. The propellant temperatures were normal (72° to 77° F).

When the EVA pilot began the AMU experiment, the left adapter handhold and the umbilical guide were not extended fully, and the AMU-adapter thermal cover was not released completely. Also, the left adapter EVA light was not operative. When the EVA pilot pulled on the handhold to enter the adapter, the handhold and umbilical guide moved to the fully deployed position which released the thermal cover. Donning activities and AMU inspection were completed to the point of connecting the AMU electrical umbilical. These activities included attachment of portable penlights, opening the nitrogen and oxygen shutoff valves, read-out of oxygen and nitrogen pressures, positioning the sidearm controllers, positioning the umbilicals and the AMU restraint harness, attachment of the AMU tether, activation of the AMU electrical power, and changeover to the AMU electrical umbilical. Oxygen pressure was 7500 psia (normal) and nitrogen pressure was approximately 3000 psia (normal). The propulsion-system pressure after nitrogen-valve opening was 455 psia (normal for AMU operation). Because of difficulty in the maintenance of position in the adapter, donning activities necessitated much more time to complete than was predicted. The EVA pilot tended to drift away from the work region in the adapter. Position could not be maintained because the use of both hands was required to extend the sidearm controllers and to attach the AMU tether. Communications from the AMU to the command pilot were garbled, but were considered acceptable by both crewmembers.

Because of the loss of visibility (caused by visor fogging), the command pilot decided that the AMU experiment could not be completed. The EVA pilot disconnected the AMU umbilical, connected the ELSS umbilical, and returned to the cockpit for ingress. The AMU power remained on, and the AMU, with the systems activated for flight, remained in the adapter until retrofire. Termination of EVA precluded an evaluation of most of the AMU performance capabilities. However, the backpack successfully underwent a Gemini launch and a 2-day exposure to the space environment. Most of the functions of checkout and donning were performed before mission abort. Although the AMU was transmitting telemetry data after power-up (during the predonning activity), failure of the data recorder precluded a quantitative analysis of AMU performance. Therefore, analysis of the AMU systems was based primarily on debriefing comments of the crewmembers.

Prelaunch

Stored gaseous expendables, oxygen and nitrogen, were serviced only prior to May 6, 1966. Both tank pressures were indicative of a full charge when checked on May 29, 1966. The AMU was serviced with hydrogen peroxide on May 15, 1966. Ullage pressure increased from 19.7 to 87.9 psia (at launch time). The final prelaunch pressure could not be determined precisely because of a slow leak in the ground-based servicing and monitoring equipment. Hydrogen peroxide temperature was comparable to that of the spacecraft during the prelaunch period. Both batteries were replaced on May 21, 1966, because of the proximity of the end of the known lifetime. The batteries had been activated on May 5, 1966, and were considered good for the rated load until June 13, 1966. No major problems were encountered in the installation of the AMU in the adapter. Some interference was encountered in the installation of the AMU thermal cover because of the AMU sidearm-controller thermal shields. After evaluation, the interference was judged acceptable for flight.

Readings on the cockpit hydrogen peroxide pressure gage were approximately equivalent to telemetry readings throughout the prelaunch period. However, the cockpit temperature-gage reading was 6° F less than were the telemetry readings. The range of the cockpit hydrogen peroxide pressure gage was 0 to 500 psia, and the range of the cockpit temperature gage was -100° to +200° F. Both gages had small dial faces; such instruments are difficult to read more accurately than ±10 psia and ±10° F, respectively.

Launch

The only AMU parameters that were available during launch were hydrogen peroxide pressure and temperature. No change in either parameter was detected by the crewmen, and both parameters were monitored periodically during the launch. No temperature change was noted by telemetry during launch. An increase of two PCM counts in hydrogen peroxide pressure (approximately 6 psia) was recorded by telemetry at lift-off. No change in hydrogen peroxide pressure was noted during launch.

Orbit

During a pre-EVA period of approximately 2 days, hydrogen peroxide pressure and temperature were monitored. These parameters were monitored (by telemetry) at least once per orbit. Low activity of both parameters resulted in few cockpit readouts. During the pre-EVA period, the predicted increase in active oxygen loss (AOL) was computed continuously and was plotted against the recorded AOL increase. The actual AOL pressure increase was much lower than had been predicted; an 8.5-psia increase had been predicted. During the 50 hours 37 minutes before the backpack telemetry switch was changed to "BACKPACK" (during AMU donning), the total pressure increase was less than one PCM count (equivalent to 3 psia). It was predicted that the hydrogen peroxide temperature would decrease. During the pre-EVA period, the temperature varied from 69° to 78° F. Readings on the cockpit gages during this period were 69° F and 90 psia.

Detailed Extravehicular Activity

On this mission, ingress to the spacecraft adapter was accomplished at 50:09:00 g. e. t. Dangling lines, or lanyards, (as had been seen on the Gemini VI and VII missions) were not encountered. The thermal cover and left handhold did not deploy fully. The EVA pilot grasped the handhold while entering the adapter. Both the handhold and the thermal cover deployed normally at this time. The EVA pilot, while standing on the footbar, pulled some of the slack out of the umbilical. The umbilical guide restricted some movement in the cockpit direction, but the pilot reported that enough umbilical slack existed for AMU donning.

The adapter floodlight to the left of the predonning position was not on. The pilot removed the two penlights from the tether bag and turned them on. One of the lights did not work. The operating penlight was mounted on the side opposite the functioning floodlight. This lighting arrangement was considered marginal for nightside donning activities. The mirrors were unstowed and positioned. The AMU was found in the prelaunch configuration when it was examined by the pilot.

At 50:19:00 g. e. t., the black hook on the tether jumper was attached to the ring on the AMU tether. A short piece of tether was secured to the AMU seat; this established a three-point support (both feet and the tether) and freed one hand of the EVA pilot to snap the hook over the ring. Next, the tether bag was unstowed from the AMU, and the EVA pilot tried to attach the small AMU tether hook (the 125-foot portion) to the ring on the tether jumper. This operation was very difficult; the EVA pilot was unable to connect the small hook to the ring. The decision was made either to connect the small hook after donning or to operate only on the 125-foot tether. Meanwhile, the EVA pilot changed the setting on the ELSS to high flow because of a hot spot on his back.

At 50:28:00 g. e. t., the EVA pilot unstowed and examined the sidearm flight controllers. Unstowing the attitude controller was difficult under both one-hand and two-hand operations. The feet of the EVA pilot slipped out of the footbar stirrups during this task. This tendency to slip was noted earlier during the tether hookup and was the principal difficulty encountered in the adapter. Unstowing was accomplished finally by the use of both hands and a quick, hard pull. Also, fogging on the suit faceplate was noted at this time. The oxygen umbilical, electrical umbilical, and restraint harness were unstowed by the EVA pilot without difficulty at 50:31:00 g. e. t. The VOX switch was difficult to reach and check with the controller in the down (donning) position.

At approximately 50:33:00 g. e. t., the nitrogen and oxygen shutoff valves were opened. The nitrogen valves opened easily, but more than one try was needed to open the oxygen valve. The EVA pilot reported that the control was tighter than it was during any simulation. Finally, the valve opened easily until it hit the stop. The pilot read both pressure gages on the front of the backpack. Readings of 7500 psia on the oxygen gage (normal) and approximately 3000 psia on the nitrogen gage (normal was 2775 psia) were reported. The oxygen gage was fairly easy to read, but reading the nitrogen gage involved some difficulty. The command pilot reported that the hydrogen peroxide pressure increased to 450 psia immediately after the nitrogen valve was opened; the pressure then slowly increased to 455 psia, which was the nominal regulated pressure.

At 50:37:00 g. e. t., the EVA pilot deployed the nozzle extensions, switched the hydrogen peroxide transducer from spacecraft to backpack telemetry, and turned on the main power switch. The upper position lights were illuminated. Again, fogging of the visor and of the suit pressure gage was reported. At 50:39:00 g. e. t., the EVA pilot backed into the AMU. After turning and positioning himself in the AMU with his feet on the footbar, he had no difficulty maintaining position.

At 50:42:00 g. e. t., the pilot changed to the AMU electrical umbilical. No difficulty was encountered in making this change. The RCS warning light came on, and the warning tone was heard by both the EVA pilot and the command pilot. The EVA pilot reset the tone and the light remained on. At this point, the spacecraft onboard voice tape ran out. The pilot and command pilot communicated by rf until the AMU mission was terminated. The EVA pilot reported that reception was clear, but it was of slightly low volume and had background noise. The EVA pilot reported no anomalies in the side tone from transmissions. The command pilot reported that transmissions by the EVA pilot were abnormal after the first syllables. This anomaly was described as wavering noise superimposed on the transmission. The command pilot considered it marginally acceptable, but noted that extensive training in donning exercise permitted him to construct the messages of the EVA pilot based on less than complete transmissions. The EVA pilot used both AMU switch positions (normal VOX and listen mode) during the transmissions, and the command pilot used both the VOX and push-to-talk (PTT) mode of the spacecraft voice-control center.

The pilot checked the displays and warning lights on the ELSS and determined that the status was normal. The hydrogen peroxide quantity reading was reported at 85 percent (normal for a full load of hydrogen peroxide). The EVA pilot located the restraint harness and established the fact that it could be hooked, but hookup was delayed until the EVA pilot could see adequately to check the connections. Complete visor fogging was noted by the EVA pilot at this point. The crewmembers decided to forego complete donning until the fogging problem was corrected. While resting and awaiting sunrise, the EVA pilot raised both sidearm controllers and locked them in the flight position. The orientation of the plume shields on the attitude controller did not appear to be correct, but the control head was extended to approximately the correct length. The controller head could not be turned with one hand to check its position. When the EVA pilot later left the donning station, the control head was twisted and the EVA pilot thought a further extension of the arm occurred. Sunrise occurred at 50:56:00 g. e. t., and the pilot attempted to use the donning mirrors to check his configuration with the AMU. At 51:00:00 g. e. t., the visor was completely fogged and the EVA pilot was unable to use the mirrors.

At 51:03:00 g. e. t., the command pilot declared a no-go condition for the AMU evaluation. In the postflight debriefing, the EVA pilot reported that the AMU was acceptable for flight in all respects. The decision to abort was based on the uncertainty that was associated with the visor fogging problem and the fact that the visor fogging caused a behind-schedule condition. The EVA pilot changed to the spacecraft electrical umbilical and egressed from the adapter without incident.

After Extravehicular Activity

There were no established procedures for conditioning a backpack that was to be left in the adapter section subsequent to an abort. After the EVA pilot returned to the cockpit and the cockpit was repressurized, the backpack condition was as follows.

Portion	Position
Main power switch	On
RCS handles	Off
Telemetry switch	Backpack
Nitrogen valve	Open
Oxygen valve	Open
Altitude controller	Flight position, horizontal
Translation controller	Down position
Electrical umbilical	Stowed on translation controller
Oxygen umbilical	Probably stowed on translation controller
Restraint straps	Stowed on translation controller

The AMU was left in the adapter because of the uncertainty associated with jettisoning it in its postdonning configuration. There was no potentially hazardous condition in the backpack, with the possible exception of the propulsion system, as had been proven through tests. An unsafe condition could occur only if the hydrogen peroxide pressure increased significantly. Adequate instrumentation was available for detection of an impending unsafe condition in the hydrogen peroxide (telemetry, cockpit gages, and cockpit warning light). Previous flight data had been indicative that the hydrogen peroxide was extremely stable. The hydrogen peroxide pressure increase, from EVA through retrofire, was no greater than was predicted; it was not necessary to jettison the backpack.

CONCLUSIONS

All AMU systems used during the Gemini IX mission were in an acceptable condition for flight when the AMU evaluation was terminated. Some difficulty was experienced with reception of the AMU voice signal by the command pilot. All of the donning provisions are apparently practical in the orbital environment; however, the donning activities were more difficult to perform than had been experienced in the one-g and zero-g training exercises. Lighting was marginal because of the failure of one adapter floodlight and one penlight. The crewmembers reported a tendency for the EVA pilot and any loose equipment to move outward from the earth relative to the spacecraft. This tendency affected activities at a work station and may exert some effect on maneuvering in an extravehicular environment. This tendency must be understood and considered when planning future extravehicular missions. Night retrieval of the propulsion device from the adapter will be satisfactory if artificial lighting is adequate. The following general guidelines are recommended for future EVA.

1. The propulsion device should be retrieved and used as early in the mission as practical. The propulsion unit should be used to maneuver from the adapter. Based

on the report by the crewmembers, the use of handholds and an umbilical is not recommended after the propulsion unit has been retrieved.

2. Positive body restraint should be provided to minimize the work required to maintain position at a work station. The restraint hardware should facilitate two-handed operations.

3. Hardware such as hooks, rings, fittings, and so forth should be constructed for easier handling by crewmen wearing pressure-suit gloves.

TABLE I. - TELEMETRY PARAMETERS

System	Parameter	Range	Number of channels	Type of channel
Pilot	Electrocardiogram	--	1	Analog
	Respiration rate	--	1	Analog
	Suit exhaust pressure	0 to 15 psia	1	Analog
Propulsion	Nitrogen-tank pressure	0 to 4000 psia	1	Analog
	Hydrogen peroxide pressure	0 to 715 psia	1	Analog
	Hydrogen peroxide temperature	0° to 160° F	1	Analog
	Hydrogen peroxide fuel remaining	0 to 100 percent	1	Analog
Flight control	Rate gyro	0.01 to 45 deg/sec	3	Analog
	Control valve	On to off	8	Bilevel (event)
	Control-system valve	On to off	2	Bilevel (event)
	Manual switch position	Manual to automatic	1	Bilevel (event)
	Control switch position	On to off	10	Bilevel (event)
Oxygen	Oxygen tank pressure	0 to 8000 psia	1	Analog
Power	28 V dc	0 to 28 V dc	1	Analog
	Primary, +16 V dc	0 to +16 V dc	1	Analog
	Primary, -16 V dc	0 to -16 V dc	1	Analog
	Alternate, +16 V dc	0 to +16 V dc	1	Analog
	Alternate, -16 V dc	0 to -16 V dc	1	Analog
	Transducer excitation	0 to 10 V dc	1	Analog
	Signal-conditioner reference	0 to 5 V dc	1	Analog
Abort alarm	Alarm signals	On to off	4	Bilevel (event)
Communications	Voice-transceiver AGC[a]	0 to 8 V dc	1	Analog
	Signal-conditioner temperature	0° to 160° F	1	Analog

[a]Apollo guidance computer.

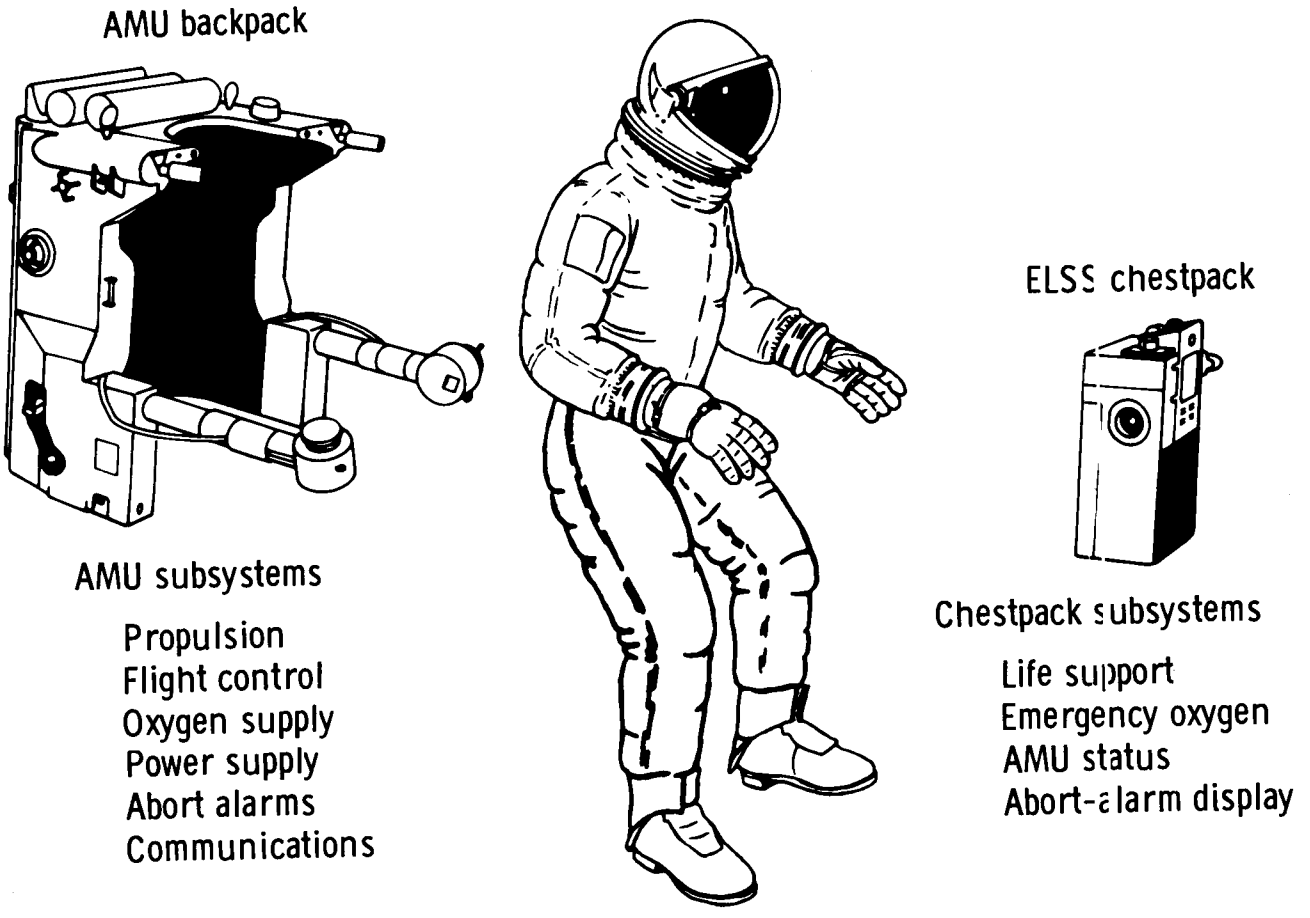

Figure 1. - The configuration of the AMU.

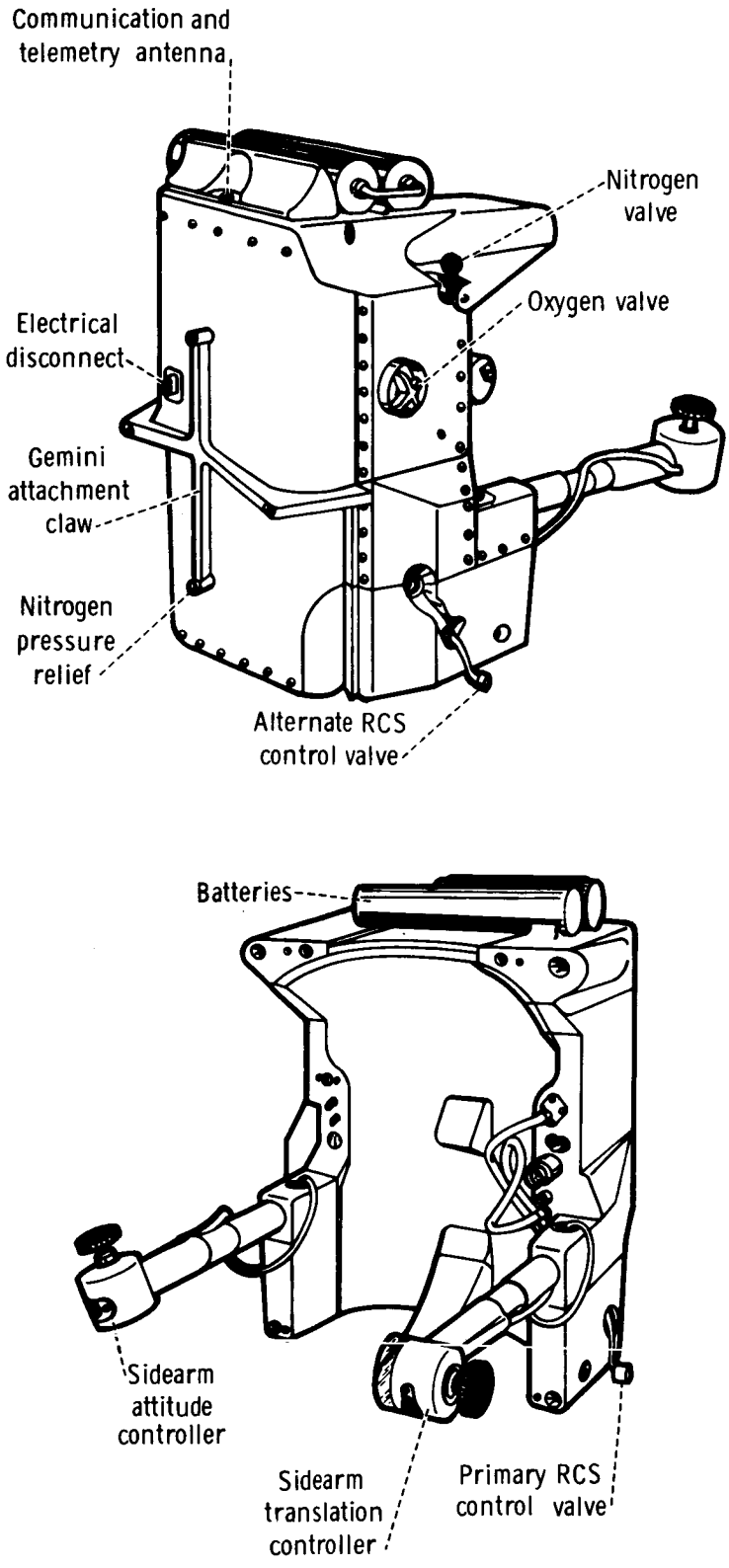

Figure 2. - The external structure of the AMU.

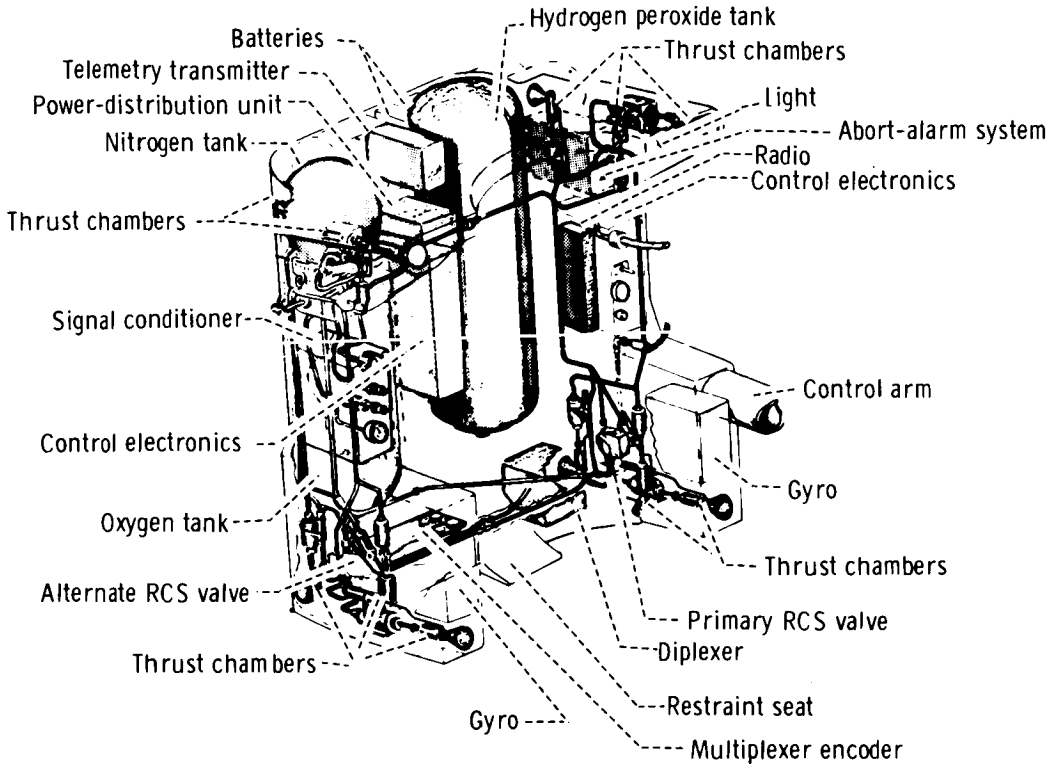

Figure 3. - The internal structure of the AMU.

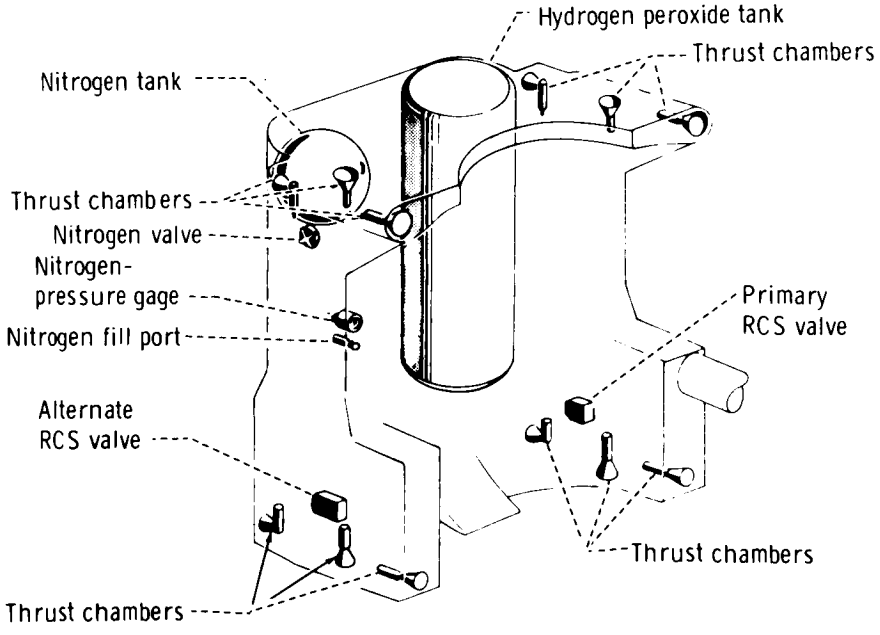

Figure 4. - The propulsion system of the AMU.

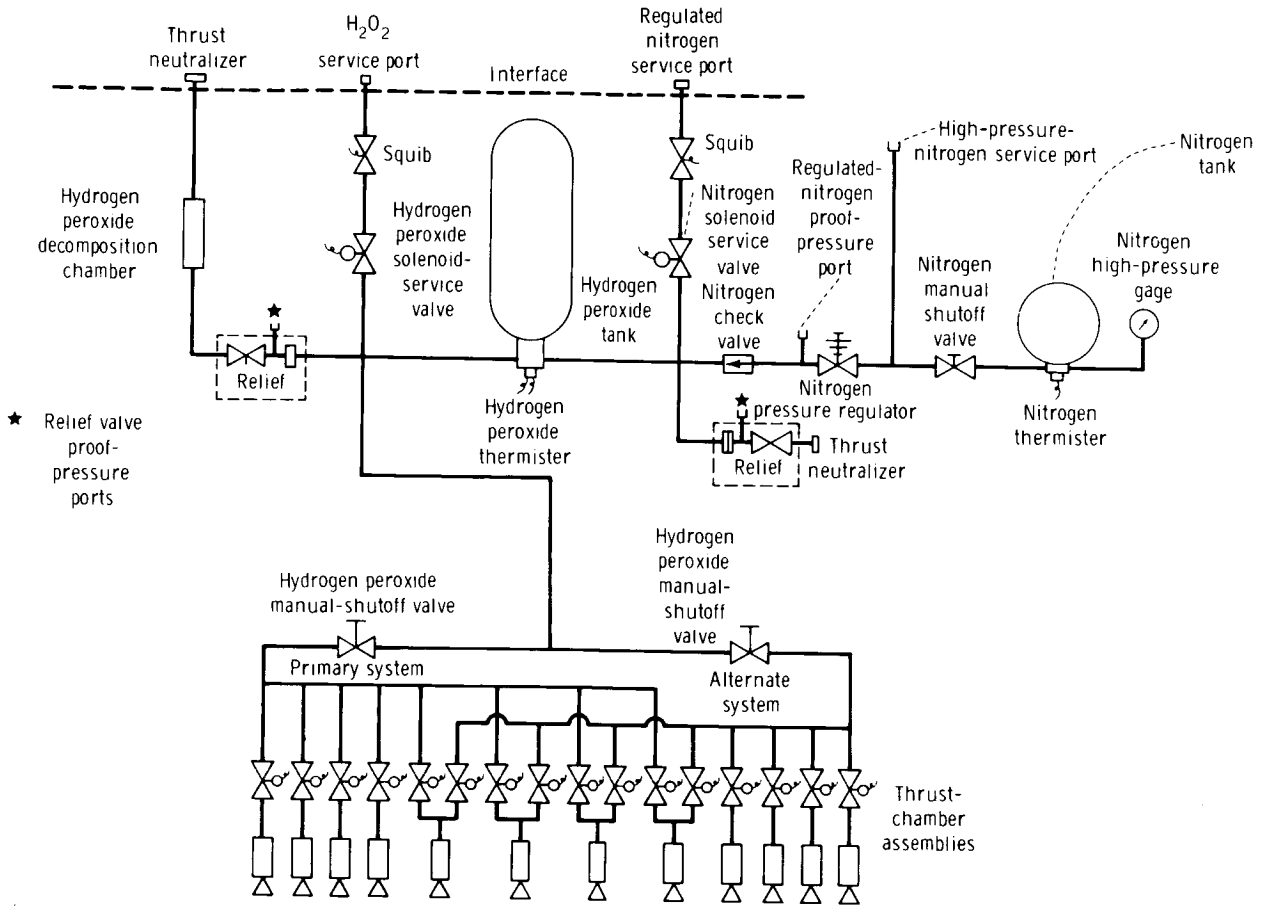

Figure 5. - A schematic of the AMU propulsion system.

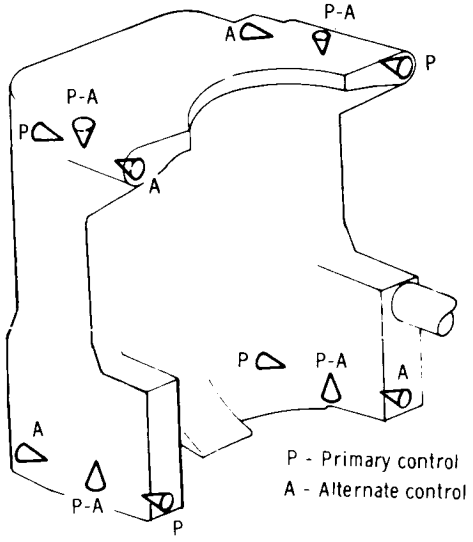

Figure 6. - The thruster arrangement of the AMU.

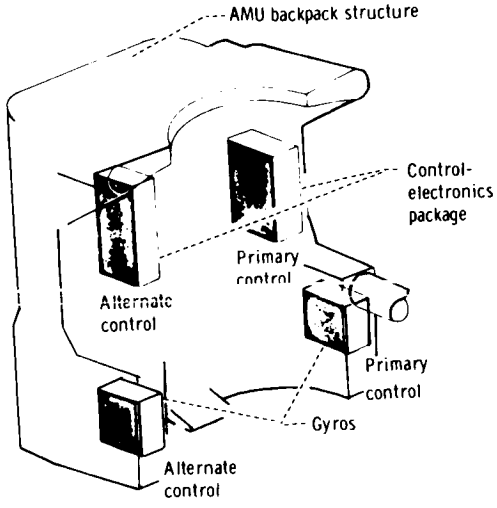

Figure 7. - The stabilization and control system of the AMU.

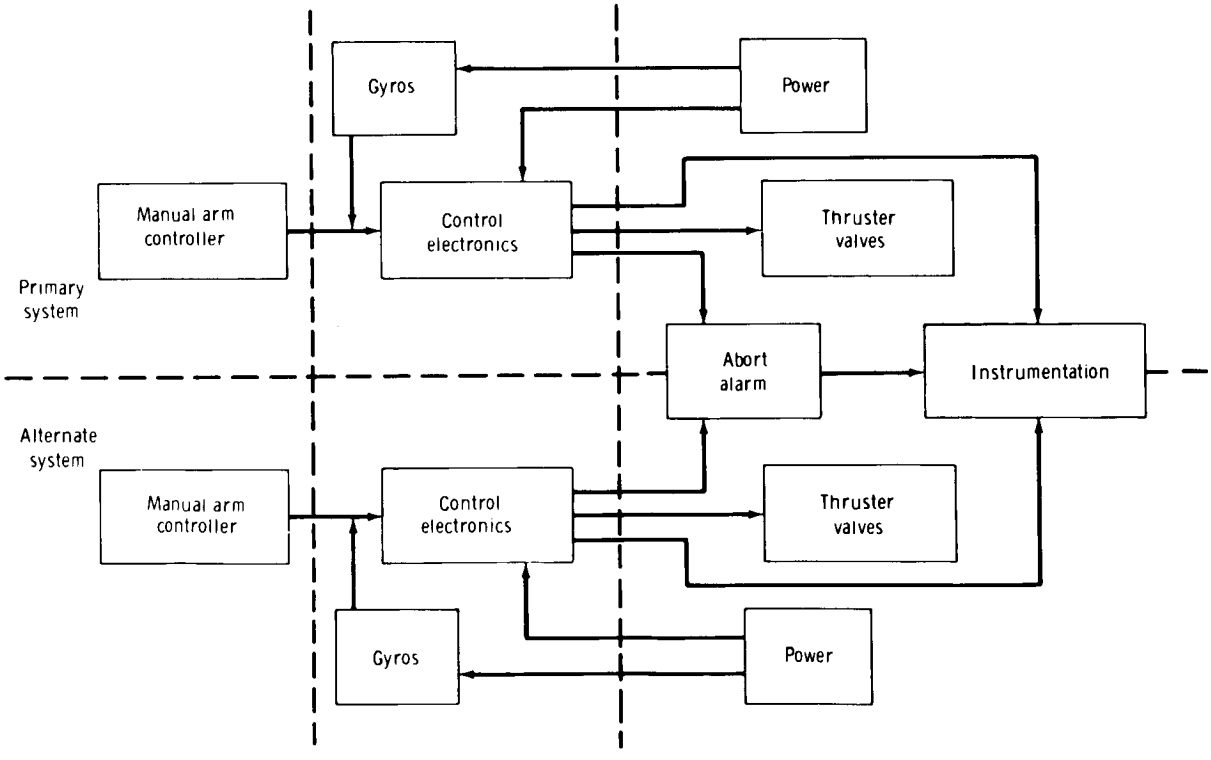

Figure 8. - The inflight control system of the AMU.

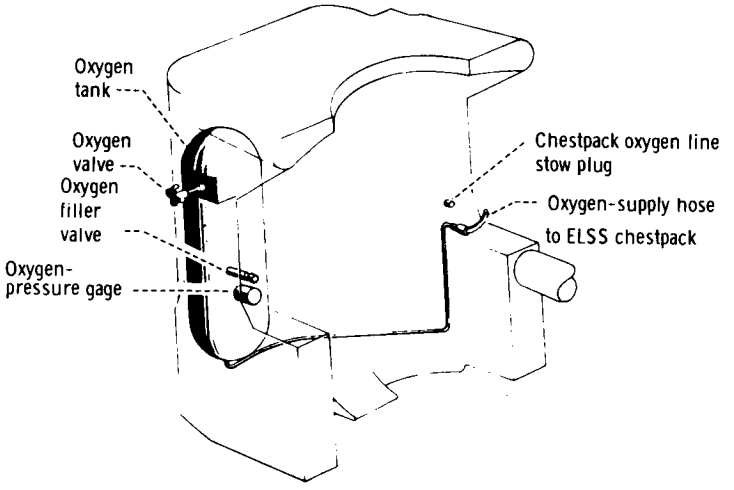

Figure 9. - The oxygen-supply system of the ELSS.

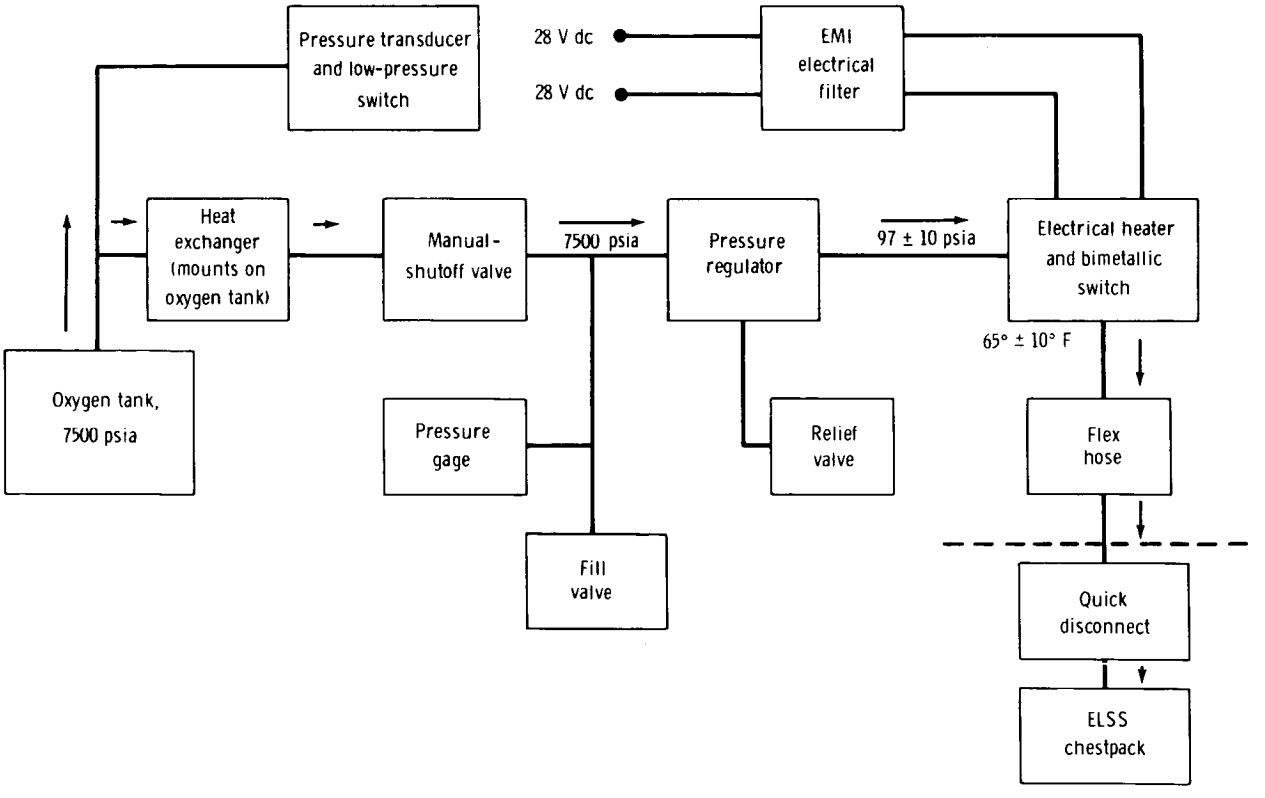

Figure 10. - A diagram of the oxygen-supply system.

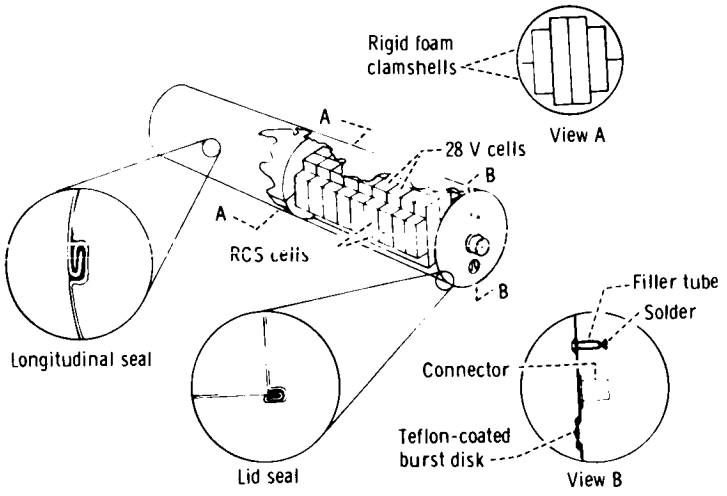

Figure 11. - The battery-pack assembly.

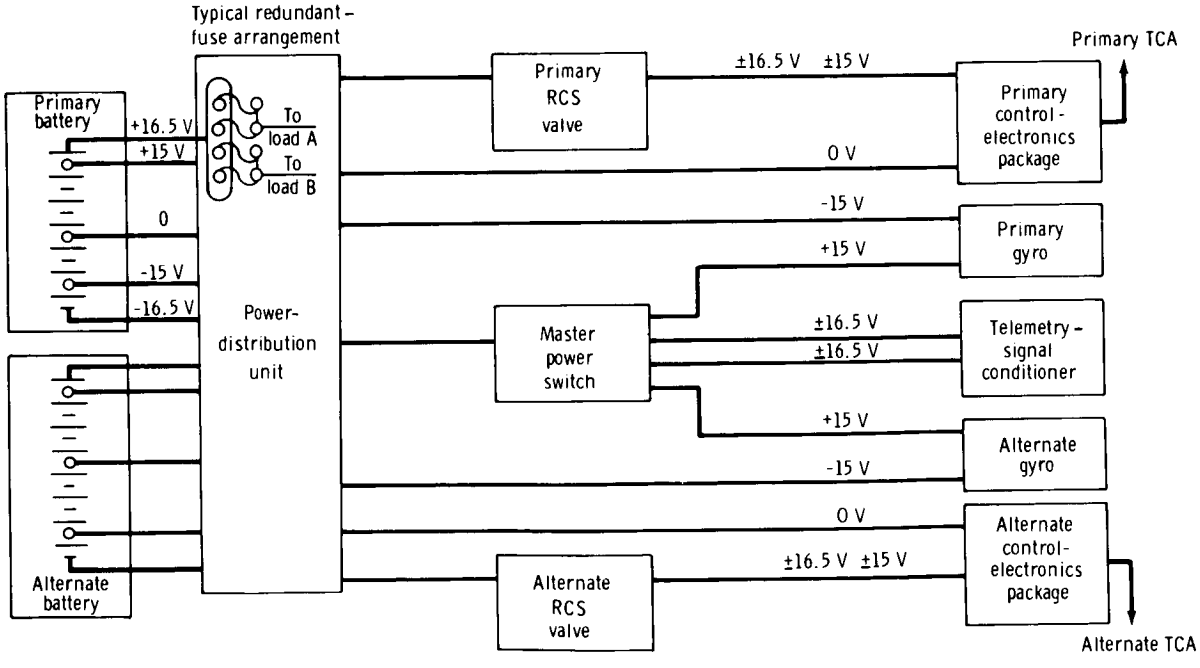

Figure 12. - The RCS electrical system.

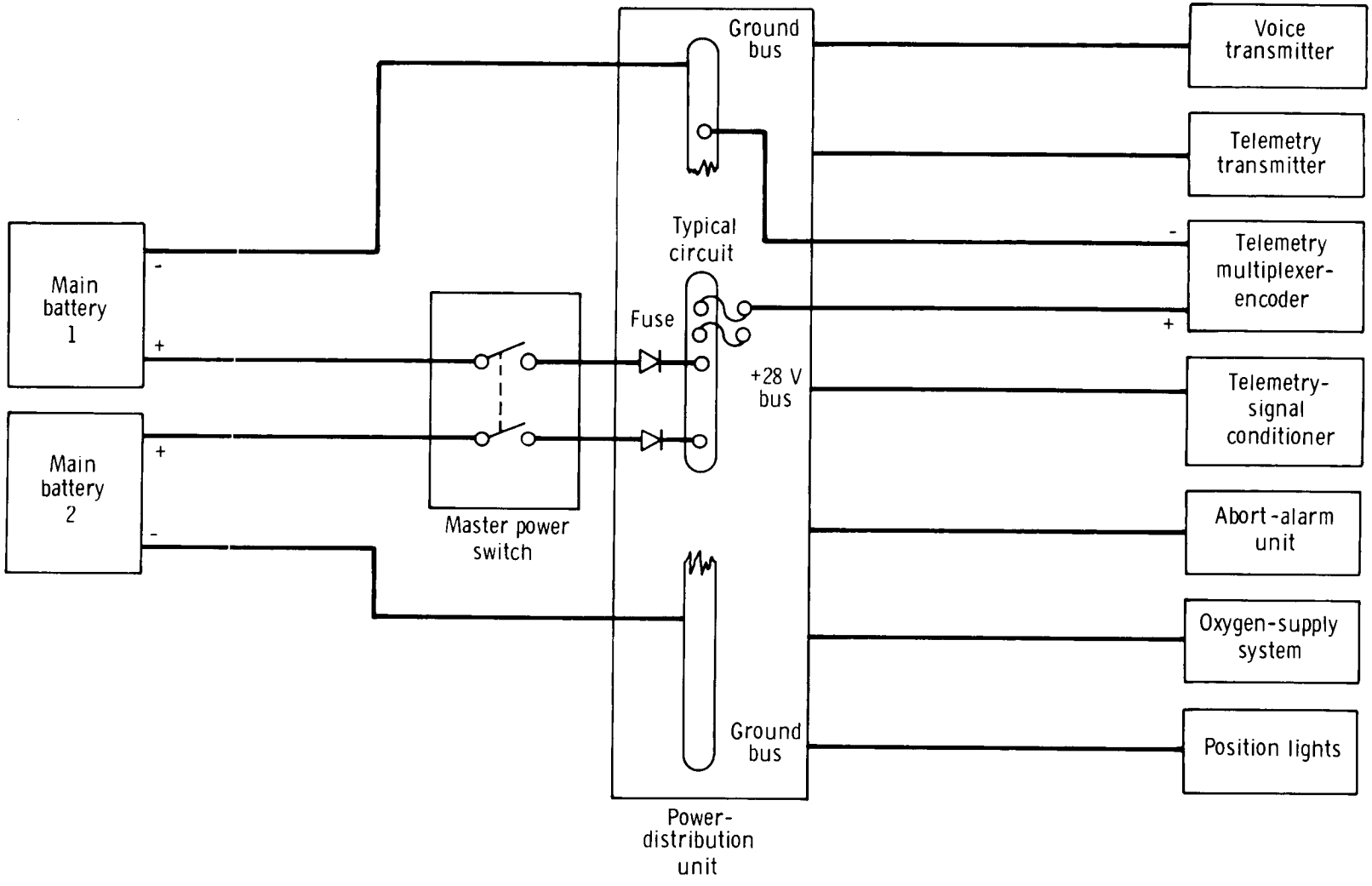

Figure 13. - The power supply (28 V).

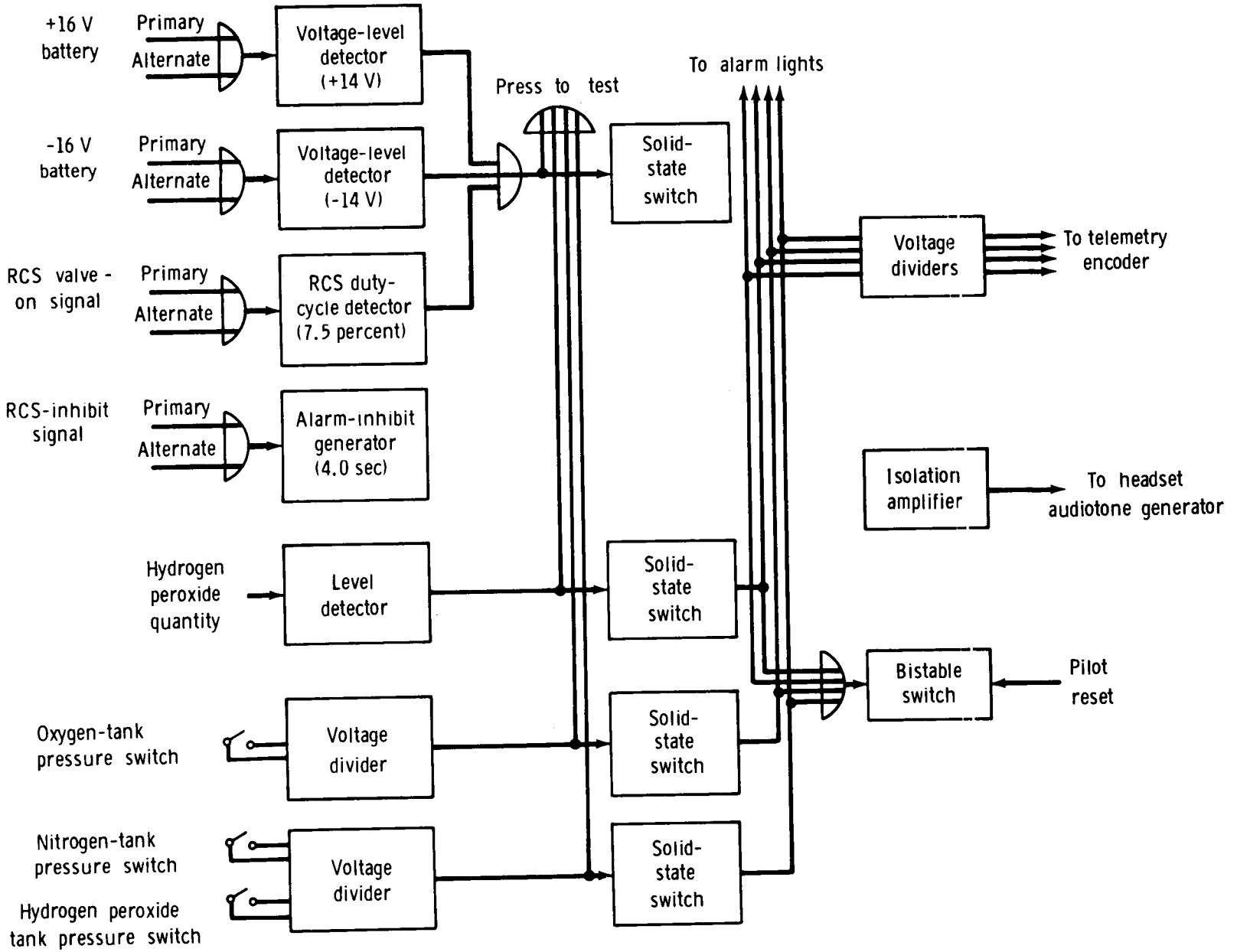

Figure 14. - The malfunction-detection system.

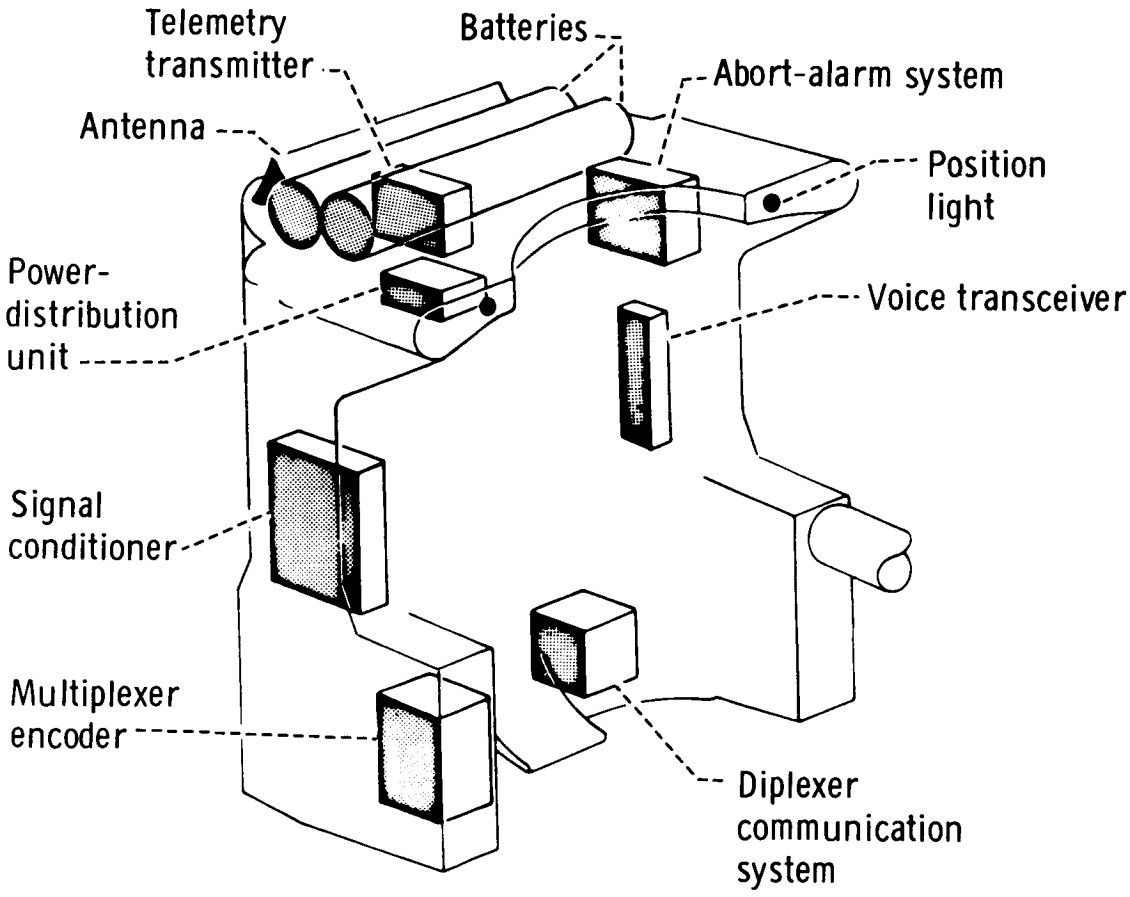

Figure 15. - The communications, telemetry, and electrical systems.

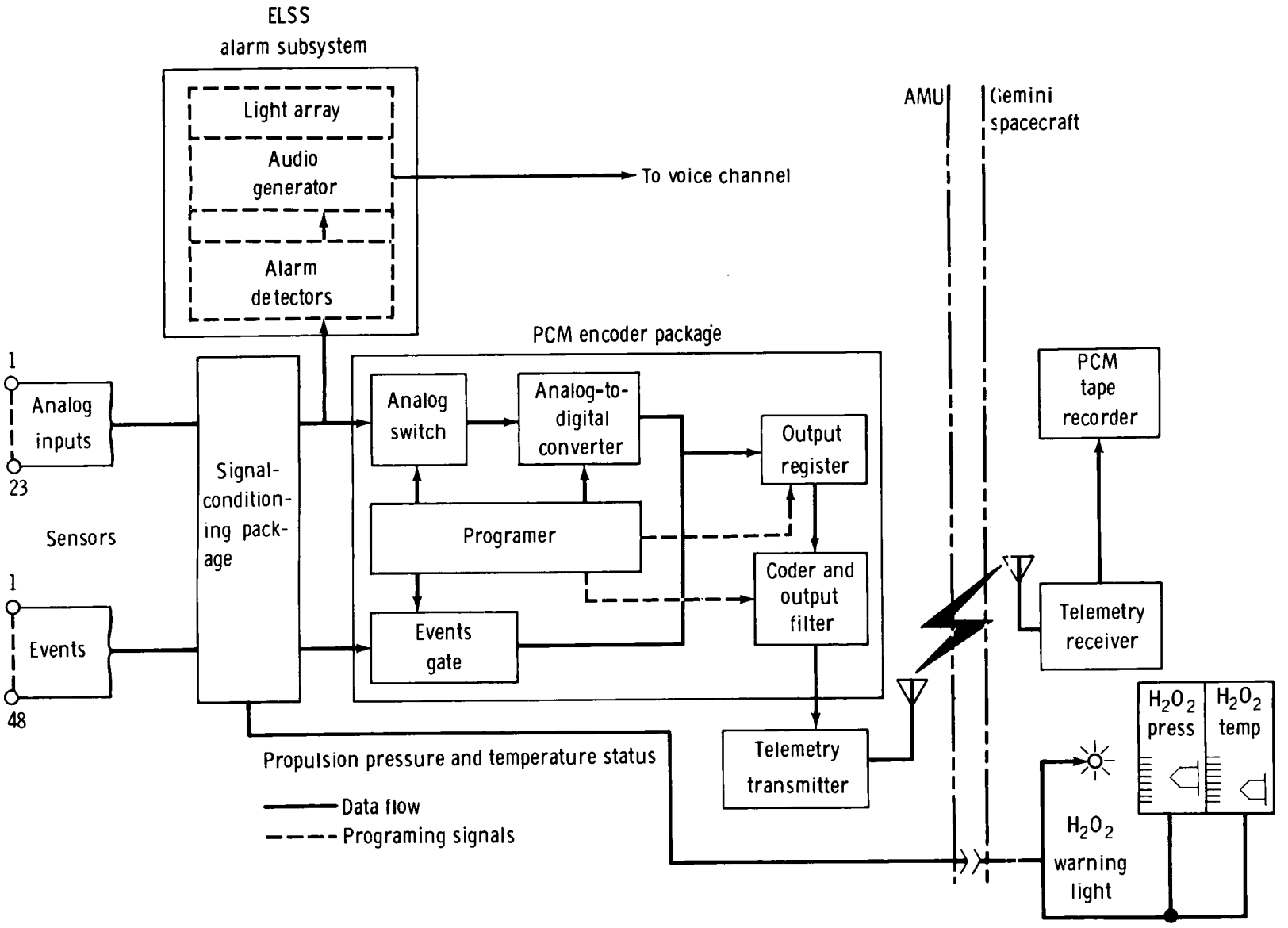

Figure 16. - The telemetry system of the AMU.

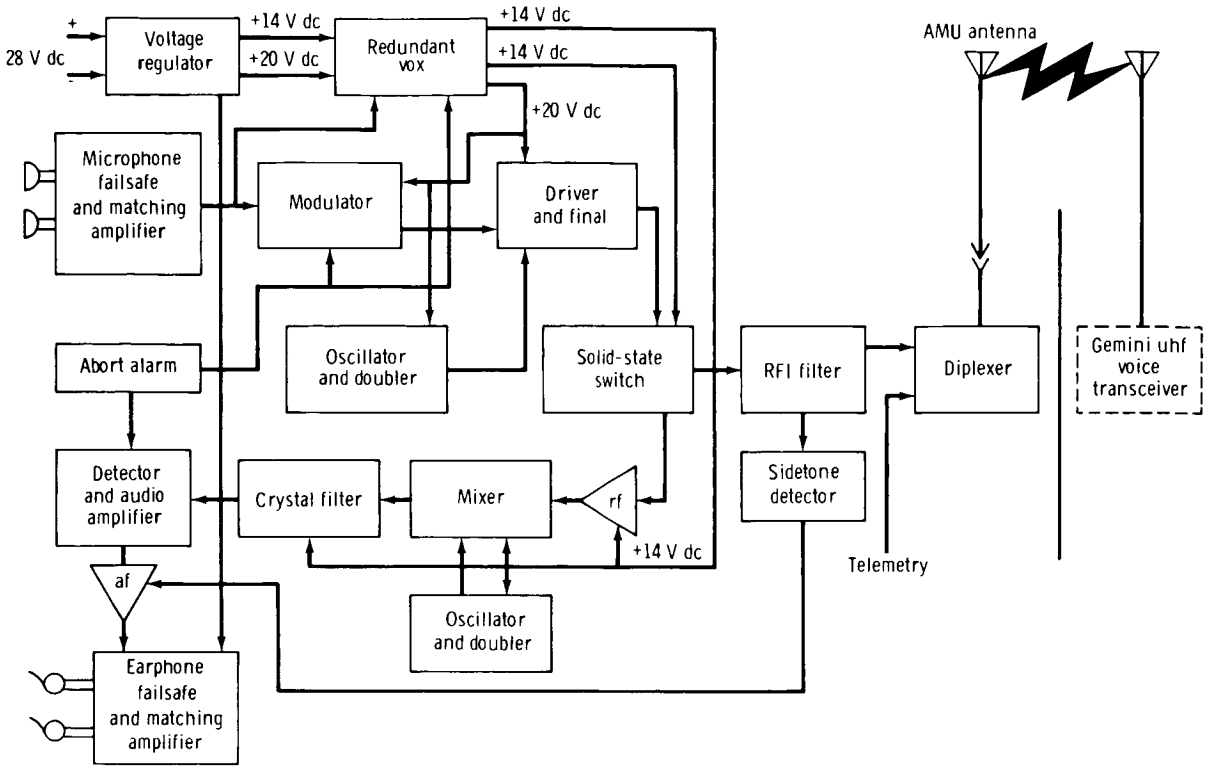

Figure 17. - The voice-communication system.

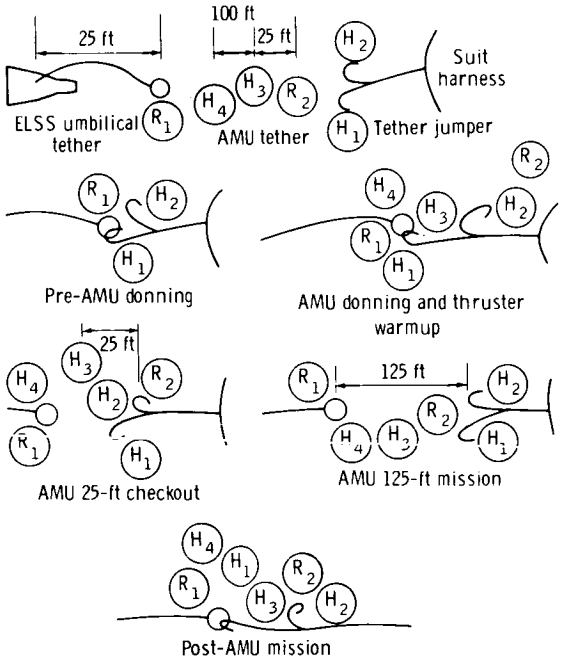

Figure 18. - Tether operations of the AMU.

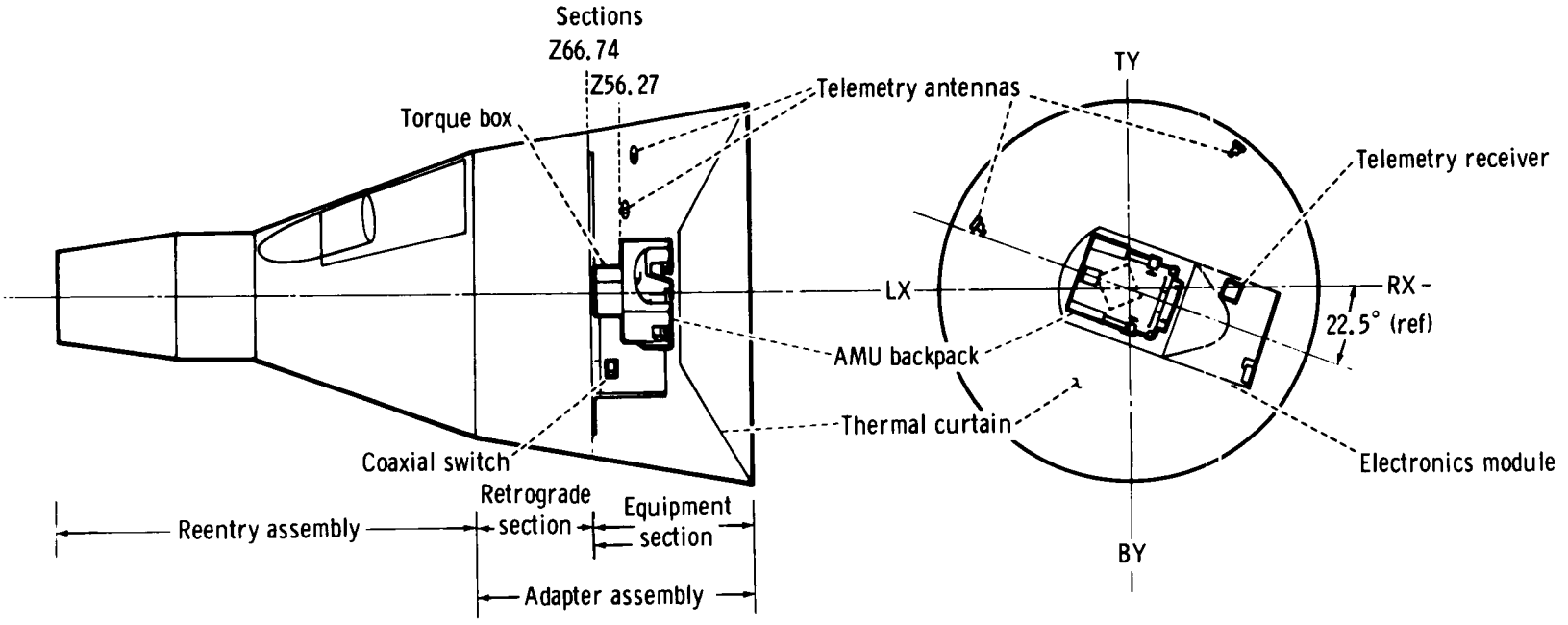

Figure 19. - Stowage location of the AMU in the adapter assembly.

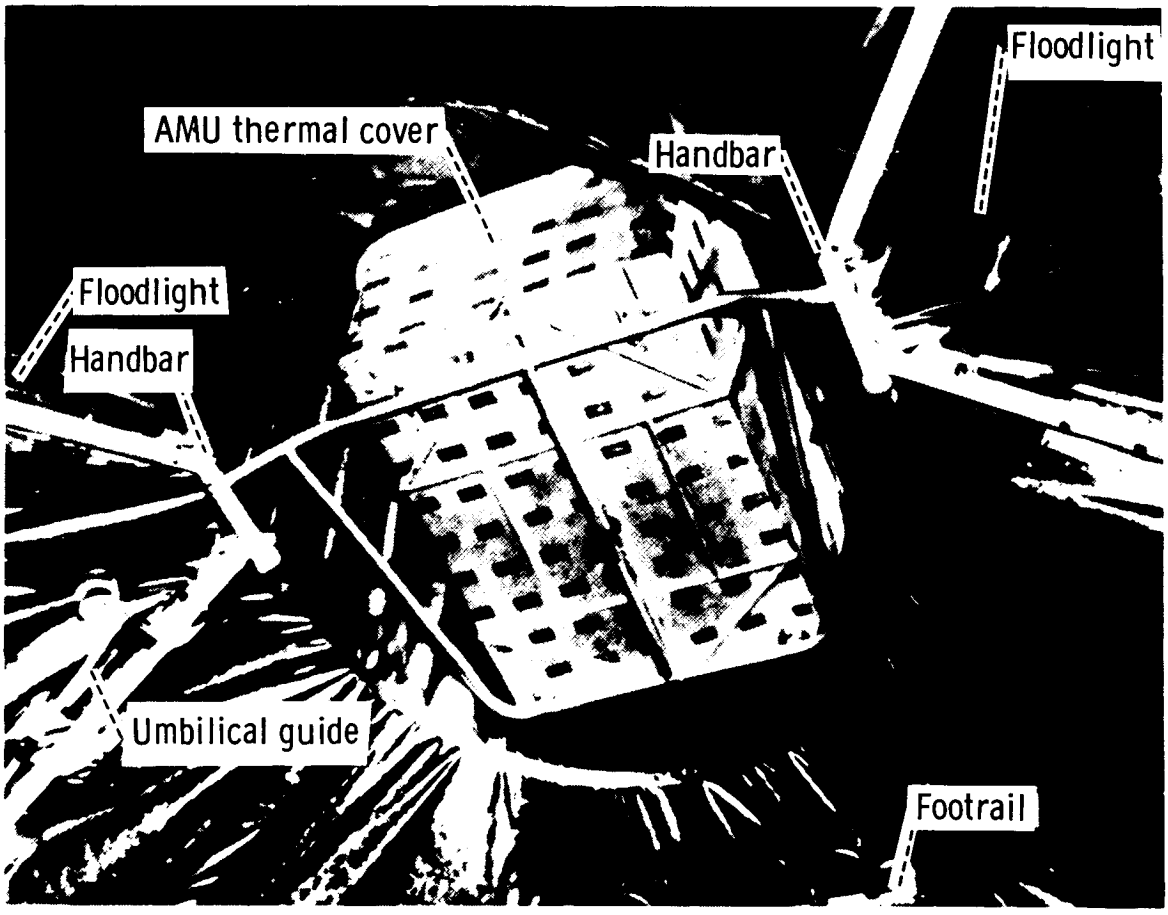

Figure 20. - The donning hardware.

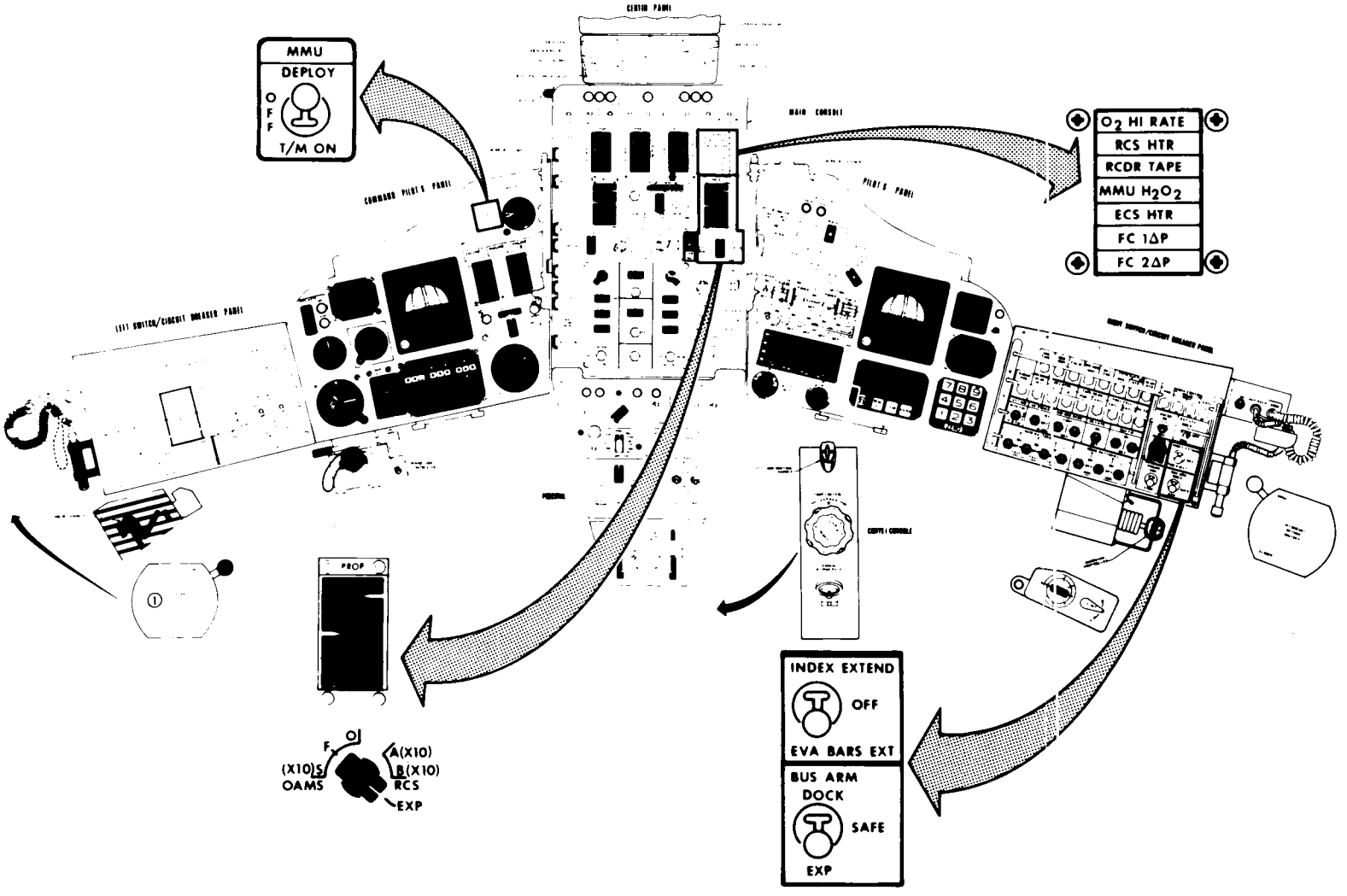

Figure 21. - The controls and indicators of the AMU.

EXPERIMENT D003

MASS DETERMINATION

By Rudolph J. Hamborsky*

OBJECTIVE

The objective of Experiment D003, which was performed on the Gemini XI mission, was the evaluation of the accuracy of a direct-contact method with a spacecraft to determine the mass of an orbiting object. The procedure involved acceleration of the Gemini Agena target vehicle (GATV) by the use of the Gemini XI spacecraft propulsion system. The GATV mass was calculated by the use of the resultant acceleration, updated Gemini spacecraft mass, and calibrated thrust level of the aft-firing thrusters of the orbital attitude and maneuver system (OAMS) of the Gemini spacecraft.

EQUIPMENT

Special equipment was not required for Experiment D003. However, the following is a list of spacecraft equipment that was used.

1. Computer: Computed velocity change ΔV during the thrusting periods

2. Manual data-insertion unit: Displayed ΔV data

3. Time-reference system: Indicated to the crewmen and recorded (through telemetry) the event time in ground elapsed time (g. e. t.)

4. OAMS: Performed required spacecraft maneuvers

5. Instrumentation system: Facilitated standard telemetry measurements

6. Voice tape recorder: Used by the crewmen to record experimental data

*Department of the Air Force, Detachment 2, NASA Manned Spacecraft Center, Houston, Texas.

PROCEDURES

Experiment D003 was performed by the use of standard spacecraft procedures; therefore, additional crewmember training was not required. A calibration acceleration of the spacecraft was required first so that the thrust of the aft-firing thrusters could be determined accurately. A mass-determination acceleration with the Gemini XI spacecraft and the GATV in the docked configuration then was required to complete the experiment. Because of operational considerations, the mass determination was performed early in the mission (01:55:29.3 g.e.t.) after the first docking. The calibration maneuver was accomplished later (54:37:28.1 g.e.t.) after the spacecraft had been separated from the GATV.

The planned procedure is given as follows. After docking, the spacecraft-GATV combination was to be thrusted for 25 seconds by the use of the aft-firing OAMS thrusters. The first 18 seconds of the thrust ensured that a minimum GATV-fuel motion would occur during the subsequent 7-second measurement period. The average acceleration was to be determined for this 7-second period and was to be derived by measurement of ΔV and thrust-time intervals Δt. The mass of the GATV was to be computed from equation (1)

$$M_{A_c} = \frac{F_c(\Delta t)}{\Delta V} - M_{G_c} \tag{1}$$

where M_{A_c} = GATV mass, slugs

F_c = maneuvering thrust of the spacecraft, pounds

Δt = measured thrust time, seconds

ΔV = measured incremental velocity, feet/second

M_{G_c} = Gemini XI spacecraft mass, slugs

The greatest error in the evaluation normally would have arisen from variable or unknown thruster output. Therefore, inflight crewmember evaluation of the spacecraft OAMS thrust was required prior to docking. This value for F_c was used in the GATV mass computations.

Two methods for calculation of the mass of the GATV were to be employed. The astronaut method was to be accomplished by the crewmen in real time by the use of data that were collected on board. The telemetry method was to be accomplished after the flight by the use of telemetry data. The results of both methods of calculation were to be compared with the mass of the GATV that was determined from the known insertion

weight and the consumption of expendables. Because of time constraints on the crewmen during the mission, calculations for both methods were performed postflight.

Astronaut Method

The manual data-insertion unit (MDIU) in the spacecraft was used to obtain ΔV, and the event timer was used for the Δt measurement. The ΔV data were available with a resolution of 0.1 foot/second, and the Δt data contained errors of less than 0.2 second. The crewmen computed the thrust, the mass, and the updated mass by the use of these inflight data. The crewmen performed the predocking part of the experiment by thrusting the spacecraft for 7 seconds with the aft-firing thrusters, by measurement of ΔV and Δt, and then by computation of the maneuvering thrust based on the updated spacecraft mass and the measured parameters. After docking and rigidifying the spacecraft-GATV combination, the crewmen thrusted by the use of the OAMS and activated the event timer to begin the mass-determination phase of the experiment. The crewmembers monitored a countdown to 7 seconds and then activated the computer for the ΔV calculation during the 7-second period. When the timer reached zero, the crewmen stopped the thrust. Then the crewmembers computed an updated spacecraft mass and used this value, with the computed predocking value of maneuvering thrust and the measured ΔV and Δt values, for calculation of the GATV mass.

Telemetry Method

An independent analysis was performed after the mission, by the use of telemetry data (fig. 1). This method involved the use of the same equation as did the astronaut method, but the ΔV data were obtained from computer telemetry data, and the Δt data were obtained through the time-reference system (TRS). The values of ΔV and Δt were available with resolutions of 0.1 foot/second and 0.125 second, respectively. By use of these data systems, the values of ΔV and Δt were obtained for the undocked configuration and the mass-determination methods were shown to be feasible.

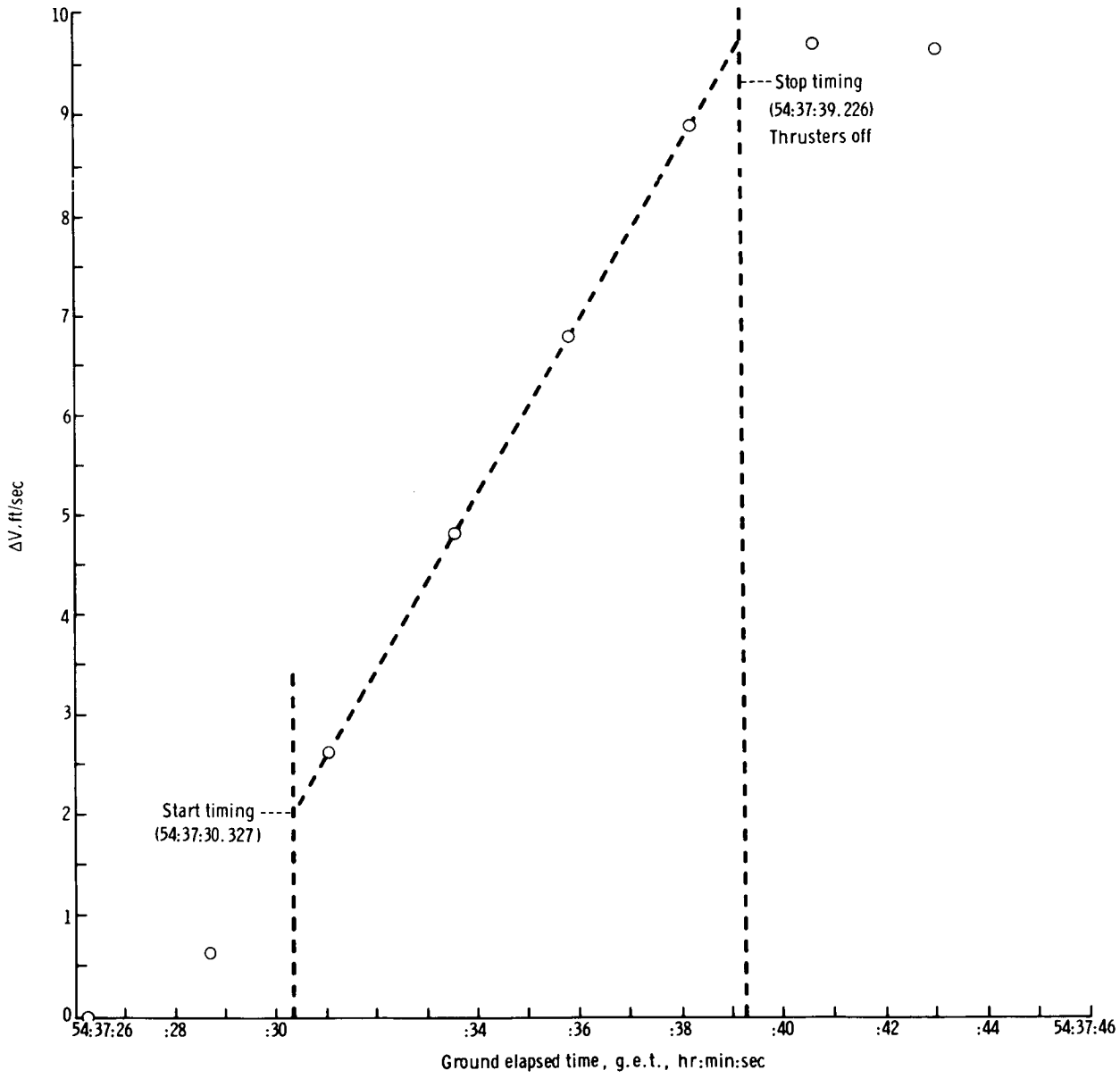

(a) Calibration maneuver.

Figure 1. - Mass determination by the use of the telemetry method.

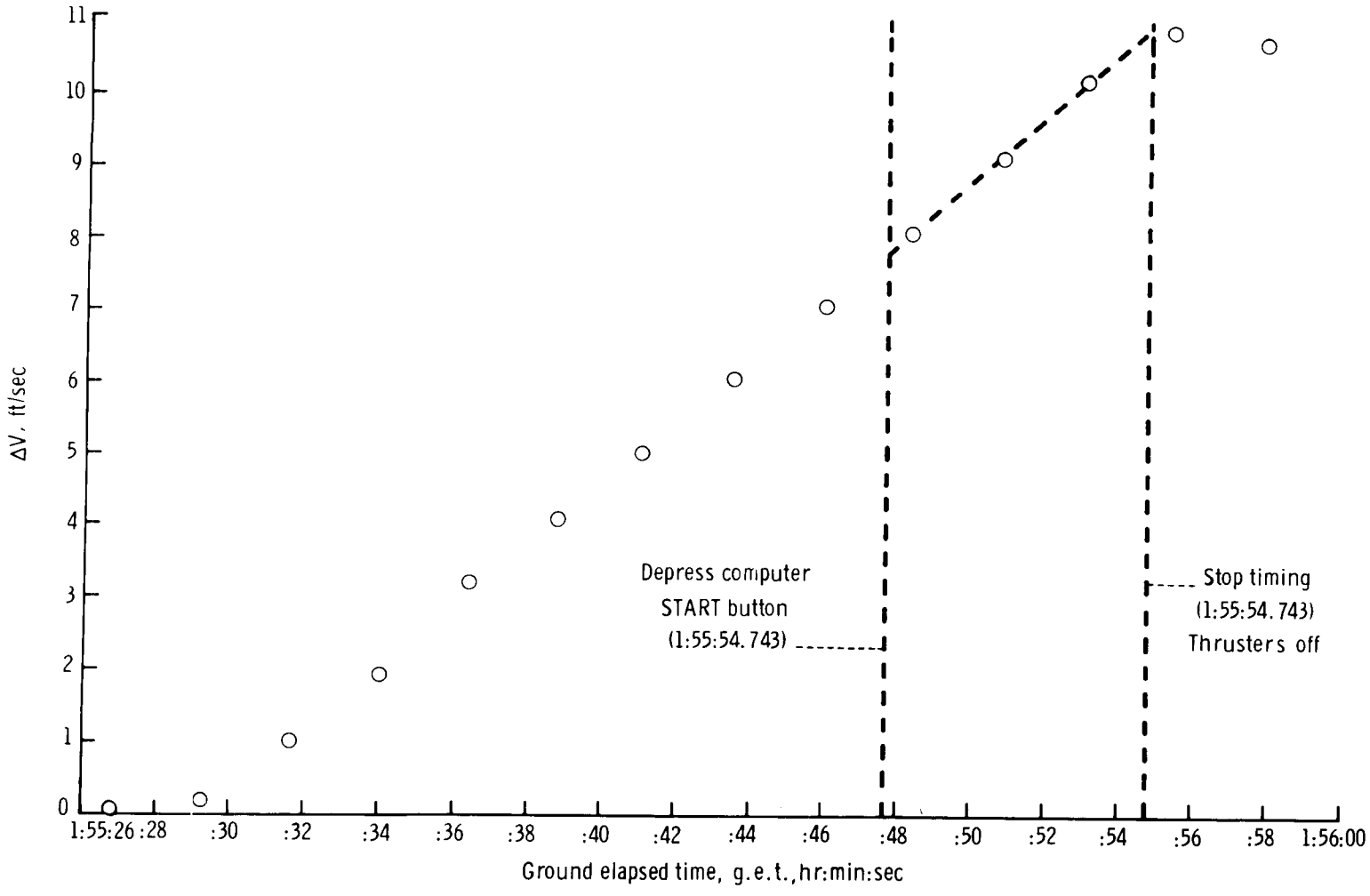

(b) Mass-determination maneuver.

Figure 1. - Concluded.